ARISTOTLE UNIVERSITY OF THESSALONIKI
SCHOOL OF GEOLOGY
DEPARTMENT OF MINERALOGY-PETROLOGY-ECONOMIC GEOLOGY

PIPERA K. KYRIAKI

Graduate of Geology
MSc of Petrology-Geochemistry

STUDY OF THE HIGH POTASSIUM MAGMATISM IN NORTHERN GREECE. IMPLICATIONS FOR THE MANTLE GEOCHEMISTRY AND THE GEODYNAMIC EVOLUTION OF THE AREA

Doctoral Thesis

Thessaloniki
2015

ARISTOTLE UNIVERSITY OF THESSALONIKI
SCHOOL OF GEOLOGY
DEPARTMENT OF MINERALOGY-PETROLOGY-ECONOMIC GEOLOGY

PIPERA K. KYRIAKI

Graduate of Geology
MSc of Petrology-Geochemistry

STUDY OF THE HIGH POTASSIUM MAGMATISM IN NORTHERN GREECE. IMPLICATIONS FOR THE MANTLE GEOCHEMISTRY AND THE GEODYNAMIC EVOLUTION OF THE AREA

Doctoral Thesis

Thessaloniki

2015

This research has been co-financed by the European Union (European Social Fund – ESF) and Greek national funds through the Operational Program "Education and Lifelong Learning" of the National Strategic Reference Framework (NSRF) - Research Funding Program: Heracleitus II. Investing in knowledge society through the European Social Fund.

PIPERA K. KYRIAKI

Graduate of Geology

MSc of Petrology-Geochemistry

STUDY OF THE HIGH PORASSIUM MAGMATISM IN NORTHERN GREECE. IMPLICATIONS FOR THE MANTLE GEOCHEMISTRY AND THE GEODYNAMIC EVOLUTION OF THE AREA.

Submitted to the School of Geology

Department of Mineralogy-Petrology-Economic Geology

Date of Oral Presentation: 16/10/2015

Supervising Committee

Associate Professor Koroneos Antonios, Supervisor

Associate Professor Soldatos Triantafyllos, Member of the Supervising Committee

Researcher Perugini Diego, Member of the Supervising Committee

Committee of Inquiry

Professor Koroneos Antonios

Associate Professor Soldatos Triantafyllos

Researcher Perugini Diego

Professor Kilias Adamantios

Professor Magganas Andreas

Professor Kyriakopoulos Konstantinos

Assistant Professor Papadopoulou Lambrini

Annex Number of the Scientific Yearbook of Geology N °

STUDY OF THE HIGH POTASSIUM MAGMATISM IN NORTHERN GREECE. IMPLICATIONS FOR THE MANTLE GEOCHEMISTRY AND THE GEODYNAMIC EVOLUTION OF THE AREA.

ISBN:

Dedicated to my family

and my friends

Βέλτιστοι γιγνόμεθα πρὸς τοὺς θεοὺς βαδίζοντες

Πυθαγόρας, 580-490 π.α.χ.χ.

PREFACE

The present study is the outcome of the combination of new and lots of previous research made on the Greek part of the Rhodope Massif and is based significantly on the latter. It deals with the geochemistry of the magmatic products of the Rhodope Massif and tries to conclude on the magmatic and geodynamic evolution of the area during the magmatic activity. The geological complexity of the Rhodope Massif itself, its debatable metamorphic evolution as well as the numerous and various magmatic products not only in the Greek part but in the Bulgarian part also, makes the study of the area complicated. Nevertheless, the author tried to combine most of the magmatic and geotectonic Rhodopian data in order to contribute to the study of the area. Below, I would like to thank all the people who helped, contributed and supported me in many different ways for the completion of the present thesis.

Emeritus Professor Christofides Georgios, for the assignment of the thesis and for supervising me the first years, for his valuable support and guidance and his insistence to apply for the "Heracletus II" funding program. He also provided many unpublished data from the Xanthi and Evros areas for the present thesis.

Professor Poli Giampiero from the University of Perugia, one of the first members of the supervising committee who kept providing so far his valuable assistance and significant schientific guidance. Moreover, I would like to thank him and his family for their hospitality while I was in Perugia for geochemical analyses.

My supervisor, Professor Koroneos Antonios for all these years of cooperation and his contribution to the present thesis. He had been a valuable tutor when I was a geology student, supervisor during my MSc thesis and the second supervisor of the present thesis.

Asc. Professor Soldatos Triantafyllos for his support, help and contribution to this thesis especially for the Elatia and Vrontou plutons by providing information and samples.

Researcher Perugini Diego of the University of Perugia, for worthily taking over the place of Professor Poli Giampiero as a member of the supervising committee and for his valuable scientific guidance.

Ass. Professor Papadopoulou Lambrini for her valuable help on the Maronia pluton by providing samples, the constructive discussions we had and her support and friendship during all of these years.

Emeritus Professor Eleftheriades Georgios, although he couldn't be in the university to watch the progress of my thesis, his many years of field work provided me with volcanic samples and his support during my MSc thesis provided me with much of technical knowledge.

Professor Kilias Adamantios for his support, the faith he showed to me and the discussions on the geology of the Rhodope Massif.

Asc. Professor Tranos Markos for this support, the faith he showed to me and the time we spent discussing on the geology of the Rhodope Massif.

Professor Georgia Pe-Piper from the St Mary's University of Canada for the major and trace elements of some samples she provided and her support.

Professor Daflos Theodoros from the University of Vienna for the valuable discussions and his valuable help.

Professors Magganas Andreas and Kyriakopoulos Konstantinos from the University of Athens for the constructive discussions on the present thesis.

My family, for their patience and for all these years of support.

My friends, Dr. Bourliva Anna and Dr. Theodosoglou Eleni for their help, their friendship and support during all these years in the university.

Mousallam Gattas-Konstantinos for his immeasurable support and patience all of these years, and his assistance on sampling.

The PhD candidate of petrology Kipouros Nikolaos for the time we spent discussing the geology of the Rhodope Massif.

The MSc students Stamatiadis Aris, Papaspyrou Marianna and Wilelmini Karantoni for their assistance during my lecturing in the laboratory courses.

Last but not least, all my friends who supported me all these years.

Table of Contents

INTRODUCTION

The Rhodope Massif (RM) is defined as a key area for understanding the evolution of the Tethyan systems. Due to the complexity of the area many researchers have focused on its tectonic and magmatic evolution separately and some efforts have been made to combine petrology and tectonics. The Rhodope Massif is considered today as a metamorphic complex, with a large scale nappe tectonics, interrupted by magmatic products, formed during the closure of the Tethys Ocean. The present thesis deals with the magmatic products of the Hellenic Rhodope Massif (HRM). Although this research is dedicated to Greece, it is impossible to ignore the work that has been carried out in the Bulgarian part of Rhodope as both parts constitute an interrelated system. A lot of work has been made regarding the magmatic evolution of the HRM magmatic rocks as well as their origin, and many geochemical data have been published (e.g *Del Moro et al., 1988; Eleftheriadis et al., 1989; Mavroudchiev et al., 1993; Jones et al., 1992; Pe-Piper et al., 1998; Christofides et al., 1998, 2004; Soldatos et al., 2008; Papadopoulou et al., 2004; Vlahou et al., 2006*).

The Tertiary magmatism of Rhodope is considered as the result of crust-mantle interaction during a convergent magin geotectonic event; however the nature of the mantle component is controversial as well as the geodynamic processes in the mantle that led to magma generation. The contribution of the continental crust in the geochemical character of these rocks is also controversial. Postcollisonal mafic igneous rocks above continental subduction zones are an analog to arc volcanics above oceanic subduction zones, providing an additional for the study of mantle geochemistry and crust-mantle interaction at convergent plate margins (*Zhao et al., 2013*).

In order to address the nature of the mantle source and the processes of their formation during the Tertiary tectonic events in Rhodope Massif the few basic members of the magmatic rocks are studied. The geochemical character of the less differentiated rocks, the basic rocks, is considered crucial to address the mantle source and the geodynamic processes. Crustal contamination plays a major role in the geochemical character of the rhodopian tertiary magmatism and felsic magmatism dominates the Rhodope Massif. Felsic rocks are studied in order to address the nature of the crustal contaminant and/or mixing component of the magmatic rocks as well as to understand the evolutionary processes that took place in the crust.

Most of the magmatic products of the HRM have been studied individually with few efforts to give interpretation for the geodynamic evolution of the area. This is mainly due to the lack of geochemical data and especially isotopic data and further the study of the basic members of the magmatic products which are few in the HRM. The aim of the present study is to provide geochemical and isotopic data which are considered very important in order to examine the nature of the mantle component of these rocks and the geodynamic evolution during their formation.

The present study combines the previous research with new geochemical and isotopic data for these rocks. All new and previous published data are reported in Appendices A and B.

The software Geochemical Data Toolokit (GCDKit, *Janoušek et al., 2006*), Petrograph 2 Beta (*Petrelli et al., 2005*) were used for the geochemical processing of the data.

More specifically, the structure of the present thesis is comprised of a **preface** an **introduction**, **seven chapters, references** two **apendices** with the geochemical data, a **summary in English** and **a summary in Greek**.

In the **first chapter** a brief description of the geological setting of the study area is presented. The study area (RM) is a geologically complexed area being studied for many years, still researcers debate on its evolution. In this chapter we shall present all the available views so far regardings its structure and evolution.

In the **second chapter**, the analytical methods used in this study are described.

The **third chapter** is an extended chapter presenting the petrological data of the rocks studied here. Since this study compiles lots of old and new data a brief bibliographic description of each area was avoided, instead each paragraph presents bibliographic data coupled with the new data.

The **fourth chapter** provides a comparison among the mafic rocks of all areas presented and compares the geochemical characteristics of the HRM magmatic rocks with the Bulgarian RM magmatic rocks, since the magmatic rocks of Bulgaria intrude the same basement. Mafic rocks with low Si_2O, high MgO and mg# were selected as the more representative samples for each area. The mafic rocks give evidence for the origin of the rocks as they represent the less differentiated rocks.

The **fifth chapter** gives evidence for the nature of the crustal and mantle component that gave genesis to the HRM magmatic rocks using the geochemical data of the mafic rocks.

The **sixth chapter** infers for geotectonic and geodynamic implications based on previous geochemical and geophysical research coupled with the new geochemical data of the present thesis.

The **seventh chapter** summarises and cites the conclusions resulting from all the previous chapters.

1. GEOLOGICAL SETTING

1.1 The Rhodope Massif

1.1.1 Historical Perspective

Rhodope in ancient Greek means "reddish view". There are many versions for the origin of the name Rhodope. According to mythology she was daughter of Ocean and Tethys or a Naiad Nymph daugther of Strymon and the wife of King Haemus with whom she gave birth to Hebros. They compared their selves to Hera and Zeus and the mighty gods changed them into mountains as a punishment. Another version of the myth refers to her as a Thracian girl who was sold in Egypt at the 6th b.c century. Her reddish beauty charmed the Egyptian king Psammetichus Amasis who married her and named her homeland Rhodope.

The name "Massif de Rhodope" was first given by *Viquesnel (1853)*. Rhodope Massif was considered in the early years as a pre-Alpine basement. Later this consideration was brought into dispute (*Meyer, 1968; Ivanov, 1988; in Burg 2012*) and the alternative was that the Rhodope is a complex of synmetamorphic nappes formed during the closure of the Tethys (*Burg et al., 1990; Koukouvelas & Doutsos, 1990*).

1.1.2 General Structure, tectonics and kinematics

The Rhodope Massif (RM) is located between the Balkan belt to the north and the Dinarides–Hellenides to the south–southwest extending over large areas of northern Greece and southern Bulgaria (***Fig. 1.1 & 1.2***). A small part of RM continues in the northwestern Turkey. It comprises mostly continental rocks with intercalations of oceanic material and represents the northernmost part of a southwest vergent Alpine nappe stack that developed during convergence between Africa and Europe from Jurassic to Neogene times (e.g *Papanikolaou & Panagopoulos, 1981; Burg et al., 1990, 1996; Ricou et al., 1998; Barr et al. 1999*).

The borders of the RM (***Fig. 1.2***) are defined by the west-northwestern-striking Maritsa fault to the north in Bulgaria, which is composed of a series of subparallel, mainly dextral strike-slip faults (*Burg et al. 1996, Georgiev et al., 2010*). To the west the top-to-the-SW Tertiary Strymon detachment (*Dinter & Royden, 1993; Sokoutis et al. 1993; Dinter et al. 1995; Lips et al. 2000*) separates the RM from the Serbomacedonian

Massif. Both the RM and the Serbomacedonian Massif are situated east of the Vardar (Axios) zone and were considered by some authors as a single tectonic zone (e.g., *Burg et al., 1995; Ricou et al. 1998; Himmercus et al., 2007*). To the east, the RM is structurally overlain by the Circum Rhodope Belt (*Kauffmann et al., 1976; Kockel et al., 1977; Meinhold et al., 2010)*, comprising greenschist-facies rocks and ophiolites.

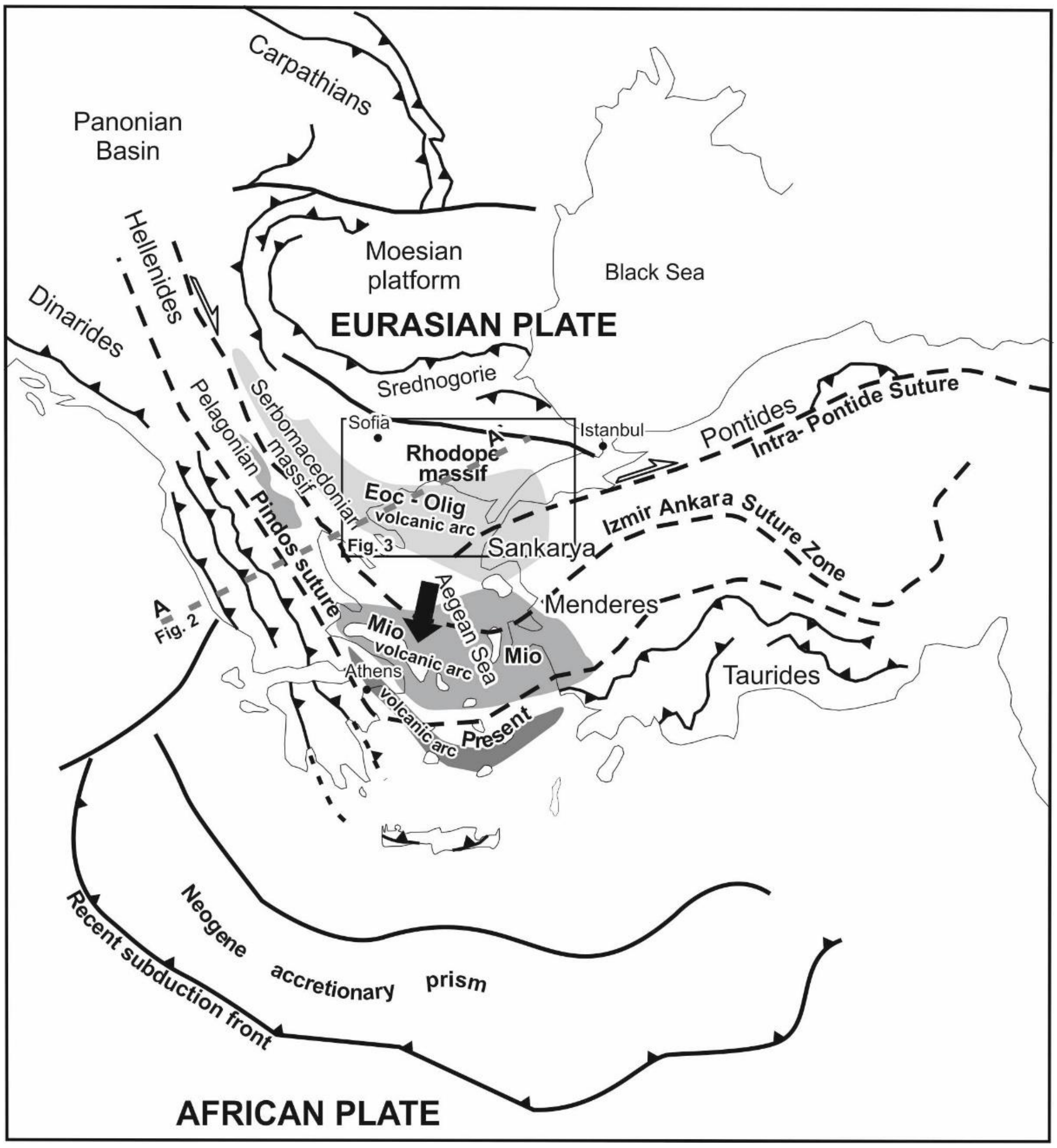

Figure 1.1 Position of the Rhodope Massif after *Kilias et al. (2011)*

Various authors have proposed several basic schemes for the subdivision of RM into different units (e.g., *Papanikolaou & Panagopoulos 1981; Mposkos, 1989; Kilias & Mountrakis, 1990; Dinter et al., 1995; Burg et al., 1996; Krohe & Mposkos, 2002; Bonev et al., 2006; Turpaud, 2006; Bonev & Stampfli, 2008; Georgiev et al., 2010;*). The subdivision schemes are based on structural criteria (e.g. *Burg et al., 1996*), on metamorphic facies distinction (e.g. *Krohe & Mposkos, 2002*) and on geochronological data. (*Turpaud, 2006; Turpaud & Reischmann, 2010*). In a simplified scheme, two major tectonic units can be distinguished in the HRM, consisting mainly of varying amounts of ortho- and paragneisses, mica schists, marbles, calc-silicate rocks, amphibolites and eclogites (*Papanikolaou & Panagopoulos, 1981; Mposkos, 1989; Burg et al., 1996; Barr et al., 1999; Turpaud, 2006; Cornelius, 2008*). A commonly used scheme for the HRM (central and western), based both on geological and petrological criteria, is the one proposed by *Papanikolaou and Panagopoulos (1981)*, with an upper tectonic unit (UTU, also known as Sidironero unit) and a lower tectonic unit (LTU, also known as Pangaion unit), separated by a SSE–NNW striking, northeast-dipping, thrust fault zone (Nestos thrust). *Turpaud (2006) and Turpaud & Reischmann (2010)* identified two crustal units for the central HRM on the basis of distinct intrusion ages. The Thracian Terrane which records a Permo-Carboniferous igneous activity and the Rhodope Terrane, a Late-Jurassic magmatic complex. Those Terranes corresponds in general to the LTU and the UTU respectively of *Papanikolaou & Panagopoulos (1981)* and are separated by the Nestos thrust, which was recently interpreted as a suture zone (Nestos Suture Zone of *Turpaud, 2006*). The Nestos Suture Zone, is a strongly sheared mélange zone between the two metamorphic Terrains with a top-to-the-southwest shear sense including HP/UHP metamorphic rocks. This subdivision scheme was argued by *Liati et al. (2011)*.

Structural and petrologic investigations have shown that the HRM experienced multiphase deformation up to high-pressure (HP) conditions (e.g., *Mposkos, 1989; Burg et al., 1996; Liati et al., 2002; Liati, 2005; Bauer et al., 2007*) and locally (in Central and Eastern RM) up to ultrahigh-pressure (UHP) conditions (e.g., *Mposkos & Kostopoulos, 2001; Liati et al., 2002; Perraki et al., 2006; Cornelius, 2008*).

The extensional deformation of RM resulted in strong crustal thinning which started in Eocene (*Kilias et al., 1999; Burchfiel et al., 2003; Brun & Sokutis, 2007*) or earlier in Early Paleocene (*Bonev et al, 2006*). A strong crustal thinning in back-arc areas is usually associated with magmatism. Post – collisional magmatism (plutonic and volcanic) variable in composition, space, and time dominates the RM

(*Christofides et al., 1977; 1998; 2004; Kyriakopoulos, 1987, Del Moro et al., 1988; Harkoversuska et al., 1989; Koukouvelas & Pe-Piper, 1991; Jones et al., 1992; Eleftheriadis, 1995; Yanev, 2003; Marchev et al., 2004, Soldatos et al., 2008*).

RM was assumed to have been formed from the closure of one subduction-exhumation cycle, the closure of the Paleo Tethys ocean. Due to many different (U)HP metamorphic events in many different regions of RM, *Liati (2005)* suggests the former existence of different fragments (microcontinents), rifted off from thinned continental margins of Godwana, within a long-term compressional environment with multiple subduction and collision cycles of the fragments. *Jahn-Awe et al. (2010)* support that the variety of HP/UHP ages along the Nestos Shear Zone (NSZ) is explained by a subduction polarity change. *Turpaud (2006)* recognizes the UHP relics only within the mélange zone, a part of the NSZ which he delineates in the central RM between the Thracia and the Rhodope terrane. He proposes that despite the wide age range one single Jurassic subduction (of Nestos ocean) explains the UHP stage. Observed differences in petrography and lithologies suggest a subdivision of the Rhodope Suture Zone (RSZ) into a lower and upper part, which, due to their differing position in the exhuming wedge, experienced different metamorphic conditions and followed different exhumation paths. *Krenn et al., (2010*) and *Nagel et al. (2011)* support that the NSZ is the base of an Eocene age southwestward thrust wedge which included not only the structurally higher parts of the Rhodope Metamorphic Province but also the entire Internal Hellenides. They also support that the UHP Rocks are unrelated to the tectonic processes in the NSZ and probably represent slivers of a higher tectonic unit captured by thrusting along the NSZ. *Jahn-Awe et al. (2011)* support that the Thracia Terrane (Pangeon-Pirin Complex) represents the eastern prolongation of the Apulian (External Hellenides) carbonate platform and the Rhodope Terrane a part of the Vardar Zone subducted toward NE in the Paleogene.

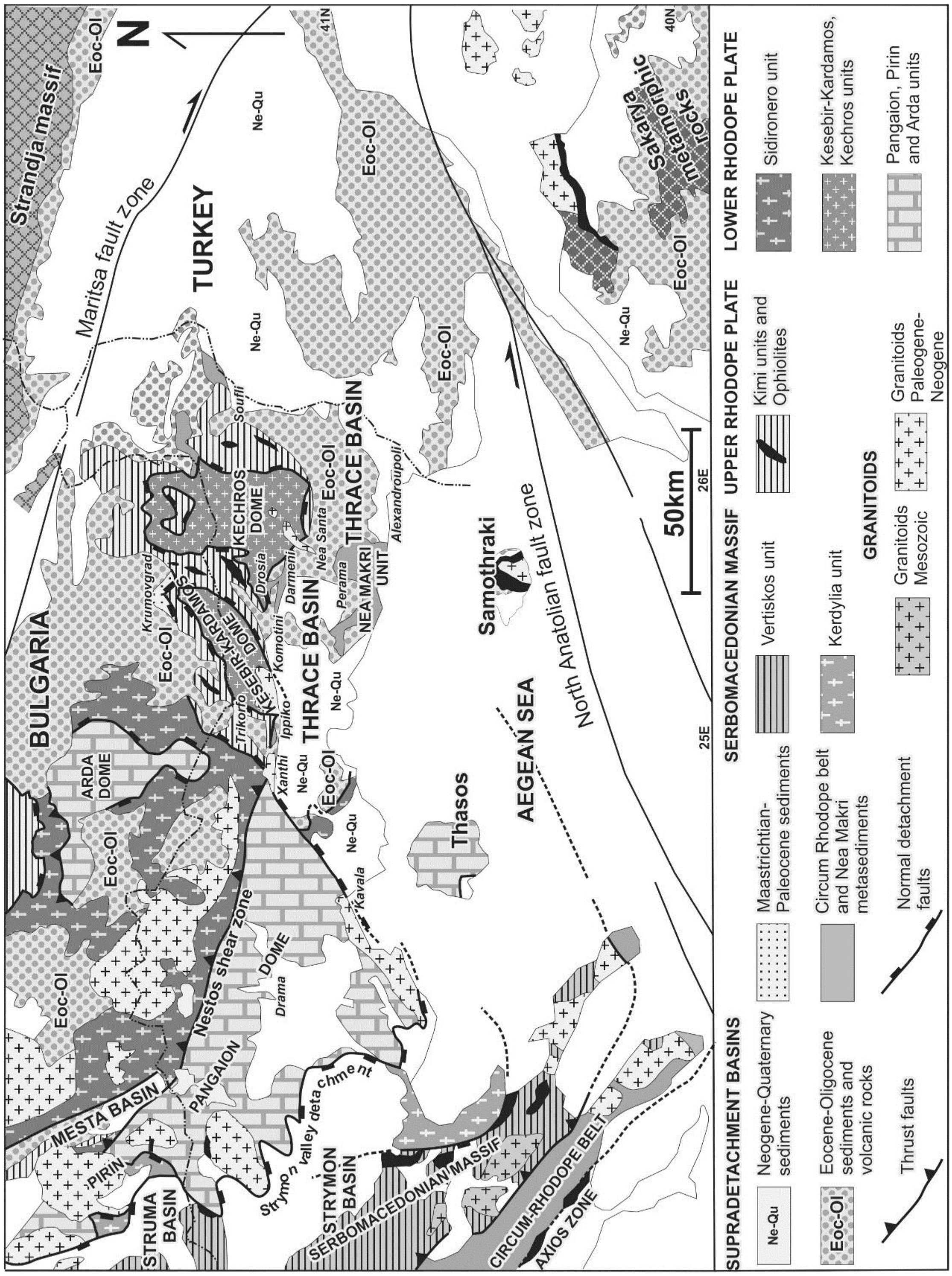

Figure 1.2 General structure of the Rhodope Massif modified after *Kilias et al. (2011)*

1.1.3 Metamorphism

Deformation and metamorphism of the RM is quite complicated and not yet completely clarified. However, a lot of research has been carried out the last twenty years which contributed greatly to unravel the metamorphic history of it. Based on a compilation of radiometric data, predominantly SHRIMP, on numerous metamorphic rocks of the RM, the metamorphic history of the latter could be in general interpreted by at least four distinct metamorphic events during Alpine times (e.g. *Liati et al., 2011; Burg, 2012* and references therein): Late Jurassic (close to ca. 150 Ma), Late Cretaceous (ca. 73 Ma), Early Eocene (ca. 51 Ma), and Late Eocene (ca. 42 Ma).

Ultra high-pressure (UHP) and high-pressure (HP) metamorphism had probably started during the Early Jurassic (e.g *Reischmann & Kostopoulos, 2002; Liati, 2005; Bauer et al., 2007*)

Amphibolite-facies (U)HP metamorphism with locally granulite-facies metamorphism and relic eclogite-facies metamorphism is widespread in the RM basement lithologies (e.g *Liati, 1986; Mposkos et al., 1990; Mposkos & Liati, 1993*). Ar-Ar mica studies (*Lips et al., 2000, Wawrzenitz & Mposkos 1997*) and K-Ar, Rb-Sr micas and hornblende studies (*Papadopoulos & Kilias, 1985*) conclude that this amphibolite and greenschist-facies metamorphism is related to an early Cretaceous or older metamorphic episode.

The Eo-Oligocene ages measured in the same samples of the previous metamorphism are interpreted as cooling ages during the exhumation of rocks to shallow crustal levels (e.g. *Turpaud & Reischmann, 2010*). Other studies interpret the Eo-Oligocene ages as an Upper Eocene metamorphic event which reached HP at least in the northern part of central RM and affected also rocks of the West RM (*Liati & Gebauer, 1999, Liati et al., 2004*). The Ar-Ar studies as well as the zircon SHRIMP studies revealed the preservation of a Late Permian to Jurassic metamorphic HP eclogite episode (*Liati, 1986; Kolceva et al. 1986; Lips et al., 2000; Wawrzenitz & Mposkos, 1997*).

The low-grade to non-metamorphic Mesozoic sequence of Rhodope corresponding to the Circum-Rhodope belt, interpreted as island arc-accretionary complex, escaped the overprint of the Cretaceous compressional tectonic and metamorphic processes remaining in the upper plate highest metamorphic pile when subduction reversal occurred towards the north of the remnant Vardar Ocean (*Bonev & Stampfli, 2011*).

1.1.4 Magmatic activity

Magmatism in the RM is the result of the convergence between the Eurasian and the African plates. This magmatism varies from basic to acid in composition, space and time over the RM since the Late Cretaceous. During Late Eocene- Oligocene, the magmatic activity extends NW into the North Aegean-Rhodope-Serbia region and to the SE into the Thracian Basin and western Anatolia (e.g. *Aldanmaz et al., 2000*). Three distinctive magmatic events related with subduction can be recognised in the RM, a Late Cretaceous subduction related, an Early-Middle Eocene post-collisional adakitic (*Harkoversuska et al., 2004; Marchev et al., 2013*) and a later Eocene-Early Oligocene extensional.

Late Cretaceous magmatic rocks were recognised in the Balkan Zone, the Late Cretaceous Srednogorie Magmatic Zone (*e.g Popov, 1987*) but this magmatism is not geologically restricted to the Srednogorie Tectonic Zone. The Late Cretaceous magmatic products occur also in the Bulgarian part of the RM between the RM and the Strendogorie Zone, and in the Pirin Mts (e.g *von Quadt, 2005; Marchev et al., 2006; Georgiev et al., 2009* and references therein), but do not occur in the HRM. *Marchev et al. (2013)* designated this magmatism as Late Cretaceous Magmatic Belts (LCMB). Magmatism within the belt has highly variable composition, represented by tholeiitic, calc-alkaline, shoshonitic and ultra-K extrusive and intrusive rocks with low $^{87}Sr/^{86}Sr_{(i)}$ and high $^{143}Nd/^{144}Nd_{(i)}$ isotopes. *Von Quadt et al. (2005)* and *Georgiev et al. (2009)* proposed models of slab rollback and rifting to explain the observed younging from north (~90 Ma) to south (~67 Ma) and variations of mantle and crustal input with time in the Srednogorie segment.

The Early-Middle Eocene (~56 to ~40 Ma) magmatic activity is distinctly different from the preceding subduction-related Late Cretaceous magmatism and the later Late Eocene–Late Oligocene extensional magmatism. *Harkoversuska et al. (2004)* were the first to separate the rocks from the Kraishte from the Late Cretaceous and Late Eocene–Lower Oligocene rocks. *Marchev et al. (2013)* defined a separate Early-

Middle Eocene Magmatic Belt with adakitic affinity, which can be traced for 250 km from Eastern Serbia, through the Kraishte Zone, SW Srednogorie and the RM. To the east, this magmatic belt continues in NW and further east into the Eastern Pontides. Post-collisional adakitic magmatism in the HRM is represented by the plutons of Elatia and Sithonia. These plutons from HRM along with rocks of the same age from the Bulgarian RM (Spanchevo, Dolno, Pripek, Topolovo Drangovo, Smilyan, Kaiser-Rohrmeier, Yugovo, Dolen plutons and Kraishte volcanics) differ significantly in composition, demonstrating a strong dependence on the present thickness of the crust and decreasing crustal input from NW to SE (*Harkoversuska et al., 1998; Marchev et al., 2013*).

The late Eocene-Oligocene magmatic event is the result of the back-arc extensional event and the collapse of the Rhodopian orogeny (e.g *Burg et al., 1990; Jones et al., 1992; Kilias et al., 2002; Tranos et al., 2014*). During the early Oligocene massive acid to basic and calc-alkaline to shoshonitic volcanism accompanied sedimentation in fault bounded basins. The products (plutonic and volcanic) of this magmatic event are widespread all over the RM. Mafic magmas are rare in the HRM while they are rather common in the eastern RM in the Bulgarian part. Many suggestions have been made on the petrogenesis, the nature of the sources and the role of crustal contamination controlling these magmas. Many workers consider this magmatism as originated from enriched lithospheric mantle (e.g. *Pe-Piper et al., 1998; Christofides et al., 1998; Yanev et al., 1998*) and others (*Marchev et al., 1998a*) from contamination of asthenospheric-derived melts. This magmatic activity ends with the within-plate (OIB-Type) magmatic products of Krumovgrad (*Marchev et al., 1998b*).

In the present thesis the rocks studied (***Fig. 1.3***) belong to the late Eocene-Oligocene magmatic event apart from the Elatia pluton which belongs to the Early-Middle Eocene magmatic activity.

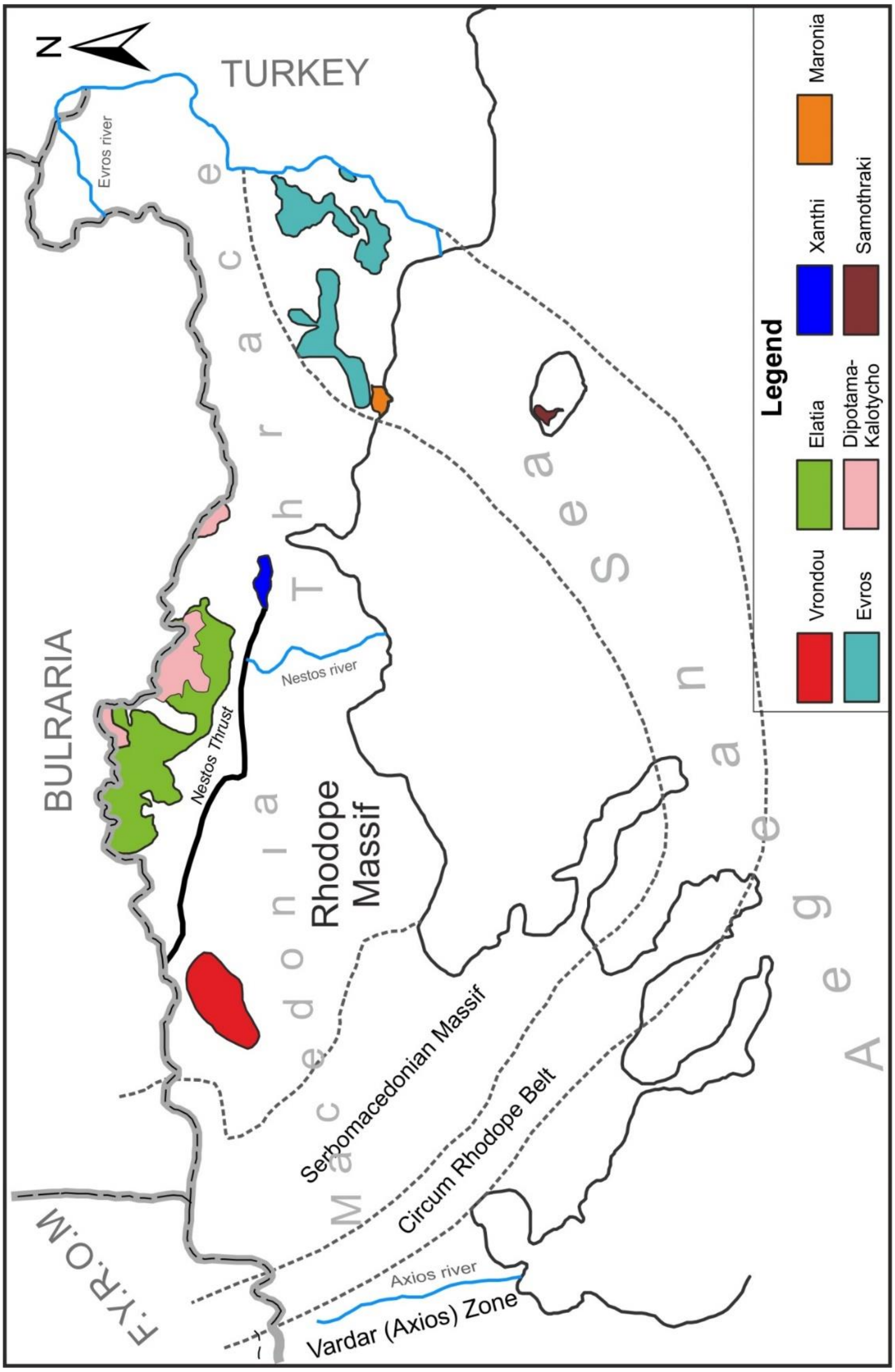

Figure 1.3 Magmatic rocks of the HRM of the present thesis

1.2 The Circum-Rhodope Belt

The Circum-Rhodope Belt (CRB) sensu stricto comprises low-grade metamorphosed Triassic and Jurassic sedimentary rocks fringing the high-grade metamorphic rocks of the Serbo-Macedonian and Rhodope massifs in northern Greece (***Fig. 1.3***). Main outcrops occur in the easternmost part of the Vardar suture zone in the Chalkidiki peninsula (Melissochori Formation; formerly Svoula flysch) and in Thrace (Makri unit and Melia Formation). The tectonostratigraphic relationship between the CRB and the high-grade metamorphics has been the subject of long discussions. Older interpretations maintain that the CRB represents the original Mesozoic stratigraphic cover of the Serbo-Macedonian crystalline basement, whereas later revisions propose the existence of two distinct greenschist-facies Mesozoic metasedimentary units: an eastern unit related to the development of a Jurassic black shale basin north of the Rhodope, and a western unit related to the development of an olistostromic flysch in the Cretaceous.

The term CRB was coined by *Kauffmann et al. (1976)* to describe low-grade Triassic and Jurassic metasedimentary rocks fringing the unified high-grade metamorphic mass of the Hellenic hinterland (i.e. Rhodope plus Serbo-Macedonian massifs), thought of as representing the original Mesozoic stratigraphic cover of the crystalline basement (Model 1). However, the concept of a CRB was rejected by *Ricou et al. (1998)* who proposed the existence of two distinct greenschist-facies Mesozoic metasedimentary units: an eastern unit (fringing the Rhodope Massif to the southeast in the Thrace area) related to the development of a Jurassic black shale basin north of the Rhodope, and a western unit (fringing the Serbo-Macedonian Massif to the west) related to the development of olistostromic flysch in the Cretaceous.

On the Chalkidiki peninsula, the CRB mainly consists of Mesozoic sedimentary and igneous rocks, various types of metamorphic rocks and ophiolites (*Mercier, 1968; Kockel et al., 1971, 1977; Kauffmann et al., 1976; De Wet, 1989; Ricou & Godfriaux, 1994; Michard et al., 1998; Ricou et al., 1998*). The CRB sensu lato includes the Examili Formation, Pirghoto Formation, Svoula Limestone, Melissochori Formation (former Svoula flysch), Aspri Vrisi Serie, the Chortiatis unit, the adjacent ophiolite complexes and the Prinochori Formation. Further details can be found, for example, in *Kockel et al. (1977)*, *De Wet (1989)*, *Ricou et al. (1998), Meinhold et al. (2009)* and *Meinhold & Kostopoulos (2013)*.

In northeastern Greece, substantial parts are occupied by the Rhodope Massif. The CRB includes the Makri unit, the Melia formation and the Evros ophiolites. Further details can be found, for example, in *von Braun (1968)*, *Papadopoulos et al. (1989), Magganas et al. (1991)*, *Meinhold et al. (2010)*.

2. METHODS OF ANALYSIS

2.1 X-Ray Fluorescence (XRF)

Major and some trace element analysis (Cr, Ni, Sc, V, Pb, Zr, Rb, Ba, Sr, Nb) element analysis were performed at the Saint Mary's University (Halifax, Canada) on a Philips (Panalytical) PW2400 X-ray spectrometer with the Philips PW2510 102 position sample changer.

The PW2400 is a wavelength-dispersive sequential spectrometer, which utilizes a 3kW Rh anode to produce a continuum of primary X-rays used to excite the sample. The fluorescing wavelengths from the sample are separated using natural and synthetic crystals and the photons captured by either a flow detector or a scintillation counter.

The major elements were measured on fused glass beads. Beads are prepared by mixing 5 g lithium tetraborate, 300 mg lithium fluoride and 35 mg lithium bromide with 1 g sample and fusing the mixture in a platinum crucible using the Claisse Fluxy at a temperature of approximately 1050 °C. The melts are molded into 30 mm disks and analysed.

Trace elements are determined on pressed pellets. These are prepared by mixing 10 g sample with 1.5 g powdered Bakelite (a phenol-formaldehyde co-polymer) and pressing the mixture into a disk approximately 5 mm thick and 40 mm diameter using the Herzog press at 20 tonnes for 10 seconds. The pellets are heated to 180 °C for 15 min and cooled to produce a sample for analysis.

All data are corrected either using theoretically determined alpha coefficients (e.g. major elements) or by using Compton scatter (e.g. trace elements).

Accuracy for this method for silica is within 0.5%. The error is less than 1% for the other major elements. For trace elements, the accuracy is within 5%.

Instrument precision, as defined by repeated analysis of a single sample is within 0.6% relative. Sample precision, as defined by measurement of different samples taken from the same aliquot is within 1% elements done on fused beads and 0.7% for those done on pressed pellets.

2.2 Inductively Coupled Plasma Mass Spectrometry (ICP-MS)

Trace Elements and REE analysis were performed by a Laser Ablation-Inductively Coupled Plasma-Mass Spectrometer (LA-ICP-MS) system installed at the Earth Sciences Department of Perugia University [belonging to Scientific Methodologies Applied to Archaeology and Art (SMAArt) Centre] is composed by a commercial New Wave UP213 (New Wave, UK) LA system coupled with a Thermo Electron X7 (Thermo Electron Corporation, Waltham, USA) ICP-MS.

The laser ablation system is a frequency quintupled Nd:YAG laser, whose fundamental wavelength of 1064 nm is converted into 213 nm by means of three harmonic generators. The commercial ablation cell (New Wave, UK), capable to support both thin sections and cylindrical resin chips, has been modified in order to mount together both reference materials and unknown samples. In addition, special adjustments have been developed on the ablation cell for the lodging of 'large' samples (up to c.a. 5 cm). Helium is preferred over argon as a carrier gas to enhance the transport efficiency of ablated aerosol (*Eggins et al., 1998*). The helium carrier gas exiting the ablation cell is mixed with argon make-up gas before entering the ICP torch; this configuration permits the maintenance of stable and optimum excitation condition. LA-ICP-MS measurements are carried out using time resolved analysis operating in a peak jumping mode. The laser repetition rate and the laser energy density are fixed to 10 Hz and ~10 J/cm^2, respectively.

The LA-ICP-MS system is optimized for dry plasma conditions prior to each analytical session on a continuous linear ablation of NIST SRM 612 glass standard by maximizing the signals for selected masses (La^+ and Th^+) and reducing oxide formation by minimizing the ThO^+/Th^+ ratio.

Data are collected in discrete runs of 15-24 analyses, each run comprising 6-15 unknowns and 1 quality control standard analysed as an unknown, bracketed by 8 analyses of the external standard. External calibration is performed using NIST SRM 610 and 612 glass standards in conjunction with internal standardization using a major element, generally 29Si or 42Ca (*Fryer et al., 1995*), previously determined by an independent technique (e.g. EPMA or XRF) following the method proposed by *Longerich et al. (1996)*.

Unknown samples are mounted together with standards in order to avoid changes in instrumental conditions due to continuous opening of the ablation cell interface. A typical analysis consists of acquiring 60 s of background followed by 60 s of the signal produced by the ablated aerosol. Data reduction is performed on the time-resolved signals by carefully selecting homogeneous portion of background and signal intensity. Data reduction is performed by using the Glitter software (*van Achterbergh et al., 2001*) and in-house written codes.

2.3 Thermal Ionization Mass Spectrometry (TIMS)

The Sr and Nd isotope analytical work was performed at the Laboratory of Geochronology, Department of Lithospheric Research, University of Vienna. Results are based on the TIMS procedure.

Powders of selected samples (c. 100-200 mg) were digested in tightly screwed Savillex beakers using an ultra pure mixture of HF: HClO4 (5:1) for 2 weeks at 100-110 °C on a hot plate. After acid evaporation repeated treatment of the residue using 5.8 N HCl resulted in clear solutions. Element extraction (Sr, REE) was performed using AG 50W-X8 (200-400 mesh, Bio-Rad) resin and 2.5 N and 4.0 N HCl as eluants. Nd was separated from the REE group using teflon-coated HdEHP and 0.18 N HCl as eluant. Maximum total procedural blanks were < 1 ng for Sr and 50 pg for Nd, and were taken as negligible. The pure element fractions were evaporated using a Re double filament assembly and run in static mode on a Thermo-Finnigan Triton TI TIMS machine. A mean $^{87}Sr/^{86}Sr$ ratio of 0.710268 ± 0.000006 (n = 4) was determined for the NBS987 (Sr) and a mean $^{143}Nd/^{144}Nd$ ratio of 0.511844 ± 0.000003 (n = 4) for the La Jolla (Nd) international standards during the period of investigation. Within-run mass fractionation was corrected for

$^{88}Sr/^{86}Sr = 8.3752$, and $^{146}Nd/^{144}Nd = 0.7219$, respectively. Errors quoted represent 2s errors of the mean. For Nd, a continuous depletion of the upper mantle is assumed throughout geological time, and the following Depleted Mantle (DM) model parameters were used: $^{147}Sm/^{144}Nd = 0.222$, $^{143}Nd/^{144}Nd = 0.513114$ (*Michard et al., 1985*).

2.4 Multicollector Inductively Coupled Plasma Mass Spectrometry (MC-ICP-MS)

The whole rock Pb isotope analysis were performed at the Laboratory of Geochronology, Department of Lithospheric Research, University of Vienna. The chemical procedures which were used are from *Kamber & Cladu (2009)*. 50 mg of whole rock powder were digested over 96 hours in 30 ml Teflon beakers at 170 °C on a hotplate in a mixture of 2 ml ultra-pure HF (48%) and 1 ml ultra-pure HNO_3 (65%). After evaporation to dryness, residues were converted with 3 ml ultra-pure HNO3 (65%) and then taken up in 10 ml of ultra-pure HNO_3 (25%). This solution was transferred to a 12 ml test tube, centrifuged and inspected for insoluble fluorides. If present, these were attacked with additional HNO_3 until full dissolution was reached.

In exchange procedures were made in 2 ml Teflon columns using ion exchange resin BioRad AGX-1x8 (200-400 mesh). Pb purification was made using the HCl-technique (*Kamber & Cladu, 2009*).

The Pb isotopic compositions of the whole rock samples were determined on a NU Plasma Plus MC-ICP-MS using standard procedures. Instrumental mass bias was corrected offline using correction factors derived from repeated measurements of the reference material BCR-2a using a standard-bracketing procedure. In order to estimated the overall reproducibility of the analytical procedures, every 5 sample was analyzed in duplicate. Overall reproducibility on the Pb isotope ratios were always better than 0.1% at the 2-sigma level.

3. PETROLOGY

3.1 Introduction

The igneous rocks studied in the present thesis have been subjects of investigation for many years by many researchers. The detailed petrological study is beyond the scope of the present thesis. Moreover, it is already presented by previous authors. However, it is related with the geochemical proccesses that took place in the mantle and crust during the formation of the Tertiary igneous rocks of the HRM. Therefore, it is considered necessary that the new geochemical and isotopic data here should be presented and combined to the previous work that has been made. For each area studied here, a brief description from the bibliography combined with the new data will follow. The samples collected for the present study were examined in terms of petrography and geochemistry, and they combined and incorporated to the already published data. In some areas some petrographic types will not be all presented due to their ambiguous relation to the other types of the same area. In some cases, the geochemical data of the present study gave new insights on the evolution and origin of the study rocks and will be presented accordingly.

3.2 The Elatia Pluton

3.2.1 General

The Elatia pluton is located north of the Drama city and constitutes the main part of the Elatia-Skaloti-Paranesti complex, which together with the Barutin-Buynovo pluton in SW Bulgaria consist one of the largest batholiths of the Rhodope Massif. The Elatia pluton intrudes the metamorphic rocks of the upper tectonic unit (UTU) of the HRM with limited contact metamorphism effects. It consists of four main rock types (***Fig. 3.2.1***); a (hornblende)-biotite granodiorite (GRD) in the central part, which becomes porphyritic biotite granodiorite (PGRD) in the outer northern and central-west part which passes locally into quartz-diorite or monzogranite in the Bulgarian part, a two-mica granite to leucogranite (TMG) in the eastern part and biotite granite (GR) to leucogranite which cuts the GRD through the whole outcrop in the form of non-mappable dykes that vary in thickness from several centimetres to several meters (*Soldatos et al., 2008* and references therein). Scarce enclaves occur in some areas in the GRD. The contact between the GRD and the TMG is indistinct (*Jones et al., 1992*). The foliations in GRD, are variably developed, the strongest foliations being near, and aligned parallel to, the southern lower contact with partially migmatised and gneissic basement rocks. At this basal contact, shallow northward-dipping, meter-scale, sheet-like layers reflect the larger structure of the intrusion. The western margin is also foliated. Both layering and foliation are sub-parallel to the penetrative foliation in the bordering country rocks; locally there are large bodies of country rock at the base of the granite sheets, and here the granite and country rock foliations are broadly concordant. Biotitic xenoliths are locally abundant, especially towards the southern part of the intrusion. Several generations of pegmatites and aplites occur around contact-zones. Scarce enclaves also occur in the Elatia pluton, but so far no author has given geochemical data.

The age of the Elatia pluton was debatable for many years. Biotite K-Ar datings from both the Greek and Bulgarian parts of the batholith gave ages of 29.1±1.2 to 45.0±2.0 Ma (*Kamenov et al. 1974; Palshin et al. 1974; Sklavounos, 1981*). *Kotopouli (1981)* reported a possible intrusion age of Upper Cretaceous or Lower Tertiary on the ground of geological data in the Skaloti area. *Soldatos et al (2001b)* based on Rb-Sr geochronology suggests an age older than 48 Ma. The age of the Elatia pluton was finally clarified with the U-Pb method on GRD zircons at about 56 Ma (*Soldatos et al., 2008*).

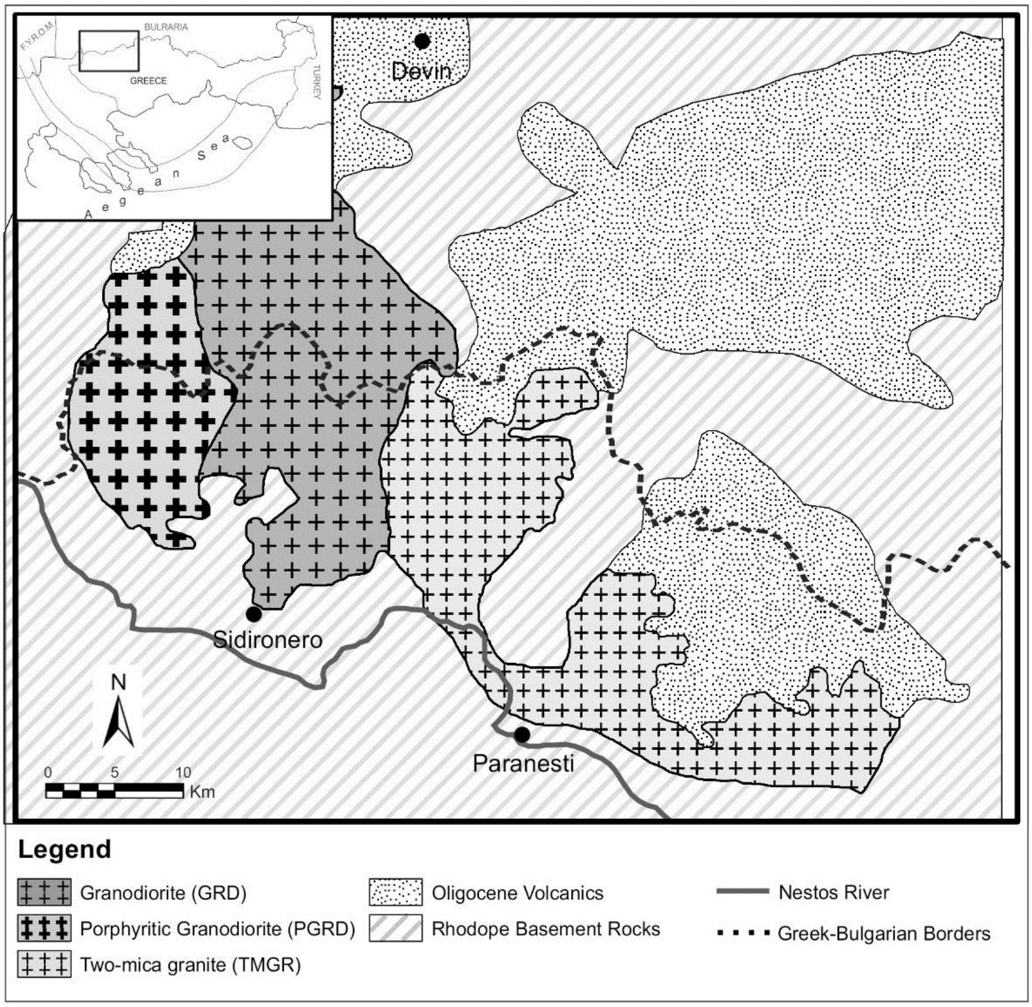

Figure 3.2 Simplified map of the Elatia pluton. Modified after *Soldatos et al. (2008)*

Regarding the evolution of the Elatia pluton *Soldatos et al. (2001a)* suggest that GRD (and PGRD), GR and TMG comprise three distinct rock groups. The existence of a genetic relation between GRD and GR seems at first sight possible as indicated by the major and most of the trace element variation diagrams, but is ruled out by the Zr, Ba, Th and REE behaviour as well as by the Sr isotopes. A genetic relation between GR and TMG is ruled out, since they have always cross-cutting trends, although a genetic relation is supported by their REE patterns and Sr isotopes.

Several authors have discussed the geotectonic setting of the Elatia pluton. *Jones et al. (1992)* based on the R1-R2 diagram of *Batchelor & Bowden (1985)* suggested a post-collision uplift tectonic setting for the Greek part of the batholith although their data plot also in the pre-plate collision granites and late-orogenic granite fields and in the late-orogenic granites and syn-collision granites field. For the same part of the batholith *Soldatos et al. (2001a)* suggested that the magma genesis is related to a subduction tectonic environment most likely prior to the collision. The geochemical discrimination diagrams (*Soldatos et al. 2001a, b*) suggest different tectonic setting for the GRD, PGRD and TMG. On the R1-R2 diagram of *Batchelor & Bowden (1985)*, the GRD samples plot in the pre-plate collision granites field, the TMG samples plot in the syn-collision granites field while the GR samples straddle the above two fields.

Previous authors have compared the Elatia pluton with the Sithonia Pluton which intrudes the Serbomacedonian Massif. The plutons have similar characteristics in terms of age, mineralogy, petrographic types, geochemistry and crystallization pressure. *Christofides et al. (2001)*, investigated and compared the Elatia pluton with the Sithonia pluton and suggested a pre-collision origin for both of them. On the other hand, *Marchev et al. (2013)* suggested that the Elatia pluton along with the Sithonia Pluton belong to a series of Early-Middle Eocene post-collisional Magmatic Zone.

In the present study we report new petrological and geochemical data for the Elatia pluton and the so far not studied mafic enclaves in conjunction with previous research. Moreover, we provide re-evaluation of the evolution and geotectonic setting.

3.2.2 Petrography and Mineralogy

The petrography and the mineralogy of the Elatia pluton has been discussed by *Kotopouli (1981)* and *Soldatos (1985, 2001a)*. Enclave petrological characteristics are studied in the present study.

Granodiorite (GRD): It consists mainly of (hornblende)-biotite granodiorite that varies locally from quartz diorite through quartz monzodiorite and tonalite to granite (GR). It is a medium- to coarse-grained grey to dark grey rock. In the central-west part of the pluton, GRD becomes porphyritic (PGRD; ***Fig. 3.2.1***) with large K-feldspar megacrysts and displays some sort of foliation. No compositional and mineralogical differences exist between the porphyritic and the non-porphyritic types. The main rock-forming constituents are plagioclase (33-67 vol.%), K-feldspar (7-35 vol.%), quartz (12-32 vol.%) and biotite (5-22 vol.%). Hornblende (<4 vol.%) appears in subordinate proportion in the less evolved rocks. Accessory minerals (1-6 vol.%) comprise primary epidote, titanite, allanite, apatite, zircon, opaque minerals. Plagioclase shows oscillatory zoning with composition 21-48 % An. K-feldspar is perthitic microcline (66-84 % Or) with relatively high triclinity. Biotite is greenish-brown in colour with $Fe^{2+}/(Fe^{2+}+Mg^{2+})$ = 0.44-0.53, TiO_2 = 1.4-2.7 wt.% and Al_2O_3 = 15.2-17.0 wt.% Amphibole has optical characteristics of common hornblende with $Mg^{2+}/(Mg^{2+}+Fe^{2+})$ =0.48-0.56.

Biotite granite (GR): It consists of biotite granite to leucogranite. It is less abundant and cuts the GRD throughout the whole outcrop in the form of non-mapable dykes that vary in thickness from several centimetres to several metres. It is a fine- to medium- grained light grey to grey rock. Its mineral constituents are plagioclase (30-38 vol.%), K-feldspar (23-34 vol.%), quartz (28-32 vol.%) and biotite (3-14 vol.%). As accessory minerals (<4 vol.%) occur allanite, zircon, opaque minerals (haematite and some pyrite) and very few secondary chlorite and muscovite. Plagioclase is slightly zoned and more acid in composition (16-26% An) than in the GRD. K-feldspar is also perthitic microcline (80% Or). Biotite is brown to reddish brown in colour with higher $Fe^{2+}/(Fe^{2+}+Mg^{2+})$ =0.60-0.66, higher TiO_2 = 2.8-3.9 wt.% and slightly higher Al_2O_3 =16.1-17.1 wt.% than the GRD biotite.

Two-mica granite (TMG): The eastern part of the Elatia pluton is occupied by a two-mica granite, which intrudes the GRD and represents the Paranesti pluton (*Kotopouli, 1981; Sklavounos, 1981*). It resembles the GR with the only difference being the presence of white mica. It consists of plagioclase (28-37 vol.%), K-feldspar (25-36 vol.%), quartz (26-33 vol.%), biotite (2-4 vol.%), white mica (1-5 vol.%) and the same accessories (<3 vol.%) as in the GR. Plagioclase is acid in composition (9-19% An), K-feldspar is also perthitic microcline, biotite is brown in colour and similar in composition with that of the GR $Fe^{2+}/(Fe^{2+}+Mg^{2+})$ =0.72, TiO_2 = 3.5 wt.%, Al_2O_3 = 16.8 wt.%). White mica has optical features and chemistry favouring a primary origin. Its Si content is 6.3 (based on 22O) indicating that it is a phengite.

Beside the above major rock-types there are also scarse minor enclaves in the GRD. Their mineral constituents are the same as in the GRD, but they have a more mafic appearance due to the greater amount of ferromagnesian minerals. Pegmatitic and aplitic dykes (APL) are also common in the Elatia pluton.

Enclaves & Diorite: There are scarce enclaves usually altered in the GRD. Morover a diorite septa found in the GRD with moderately sharp contacts. Both the enclaves and the diorite sample also exhibits the same mineralogy with the GRD. They consist mainly of plagioclase (~50%) which displays oscillatory zoning, biotite (15-17% vol.%) and hornblende (10-13% vol.%), minor orthoclase (2-3 vol.%), minor quartz (2-3%) and accessory minerals as primary epidote (6-8 vol.%) with often allanite core, apatite and zircon(<4%). Titanite has not been observed in any of the enclaves. Although they present the same mineralogy their texture differs with some displaying a microgranular texture with subhedral biotites while others a medium-grained granitic texture. The diorite exhibits typical granitic texture.

3.2.3 Major Element Geochemistry

Here, only the geochemistry of the GRD, the enclaves and the diorite will be presented since the relationship with the GR and TMG is ambiguous and there are no mafic members in the other petrographic types.

The geochemical data used for the Elatia pluton is a compilation of new data and published data of *Soldatos et al. (2001)* and *Jones et al. (1992)* and are presented in Appendix A**.** Some, but not all of the previous published data are used here due to the differences between the several analytical methods and the problems that arise. New geochemical analyses on the same previous analysed samples from previous workers were compared in order to test their reliability.

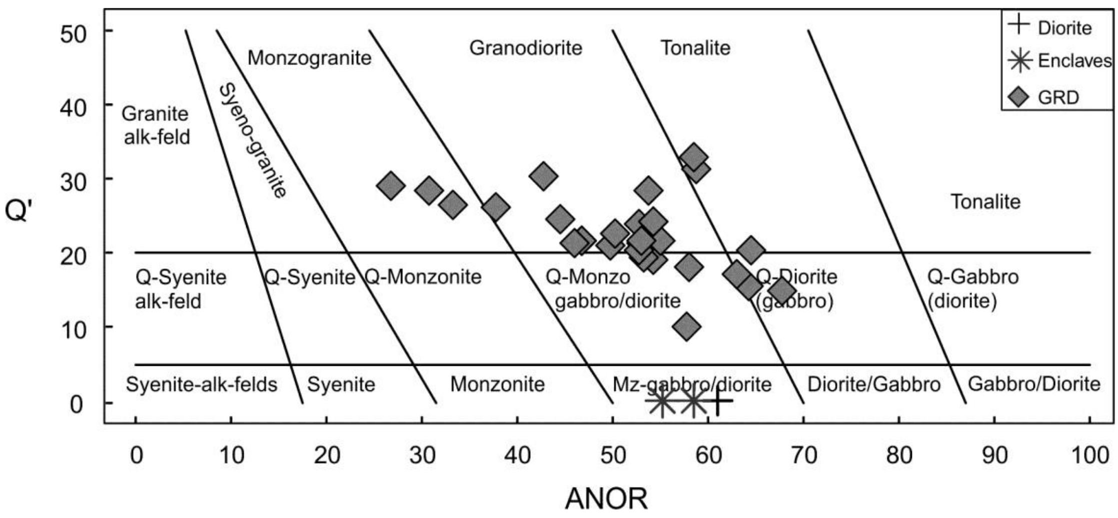

Figure 3.2.2 Q-ANOR classification diagram after *Streckeisen & Le Maitre (1979)*

On ***Fig. 3.2.2*** samples used in the present study are presented on the Q-ANOR diagram after *Streckeisen & Le Maitre (1979)*. Most GRD samples are plotted in and around the granodiorite field while the enclaves and the diorite are plotted in the Monzogabbro (diorite) field.

On the SiO_2 versus K_2O diagram (***Fig. 3.2.3***) of *Peccerillo & Taylor (1976)* most samples are plotted on the High-K calc-alkaline series with few samples on the calc-alkaline series while the enclaves and diorite are plotted on the shoshonite series field.

On the SiO_2 versus K_2O+ Na_2O diagram (***Fig. 3.2.4***) of *Irvine & Baragar (1971),* the enclaves and diorite are plotted on the alkaline field. There is a gap on SiO_2 between the enclaves and the GRD samples of more than 7%.

Variation diagrams for the major elements are presented in ***Fig. 3.2.5***. Most major elements decrease with differentiation with well-defined trends apart from the K_2O which increases and Na_2O which is rather constant with a tendency to decrease for the GRD. There is not any good correlation for the mg# but it is worthy to note the enclaves and few GRD samples have high mg# >50.

Regarding the enclaves and the diorite they display a rather good trend with the GRD samples apart from K_2O though, due to the SiO_2 gap between the basic enclaves and diorite and the granitic samples it is not clear whether they are wellcorellated. The variation of all the major elements, at least for the GRD, is attributed to the fractionation of hornblende, biotite, plagioclase and apatite.

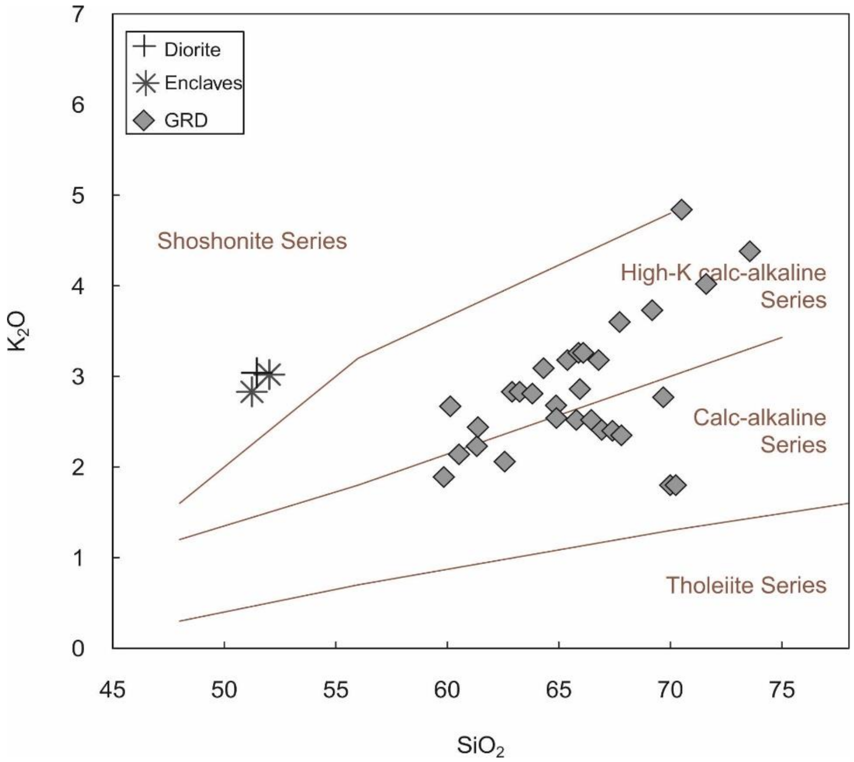

Figure 3.2.3 SiO_2 versus K_2O diagram after *Peccerillo & Taylor (1976)*

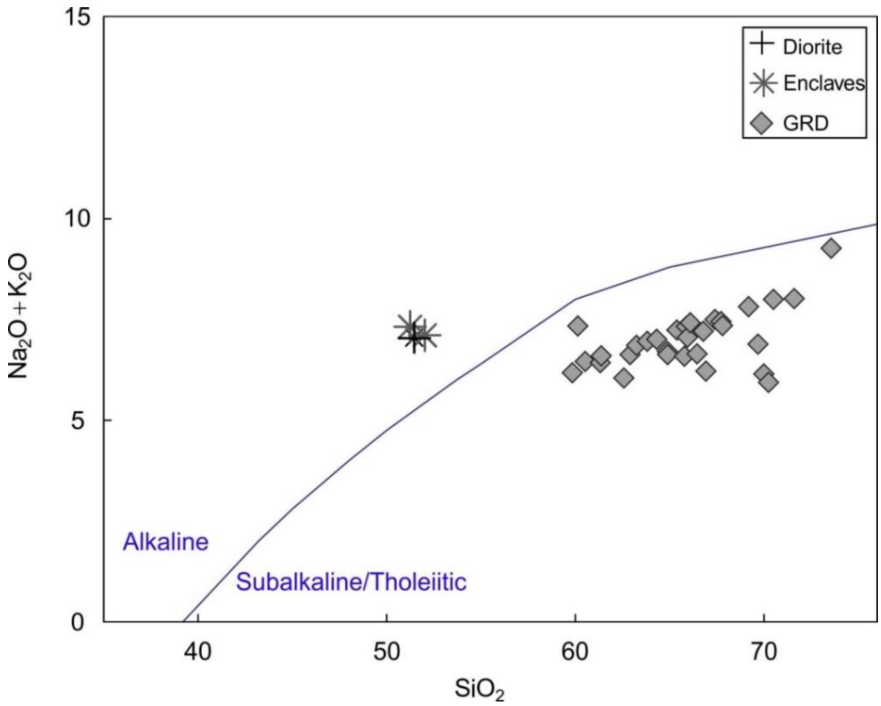

Figure 3.2.4 SiO_2 versus K_2O diagram. Discrimination line of alkaline and subalkaline rocks after *Irvine & Baragar (1971)*

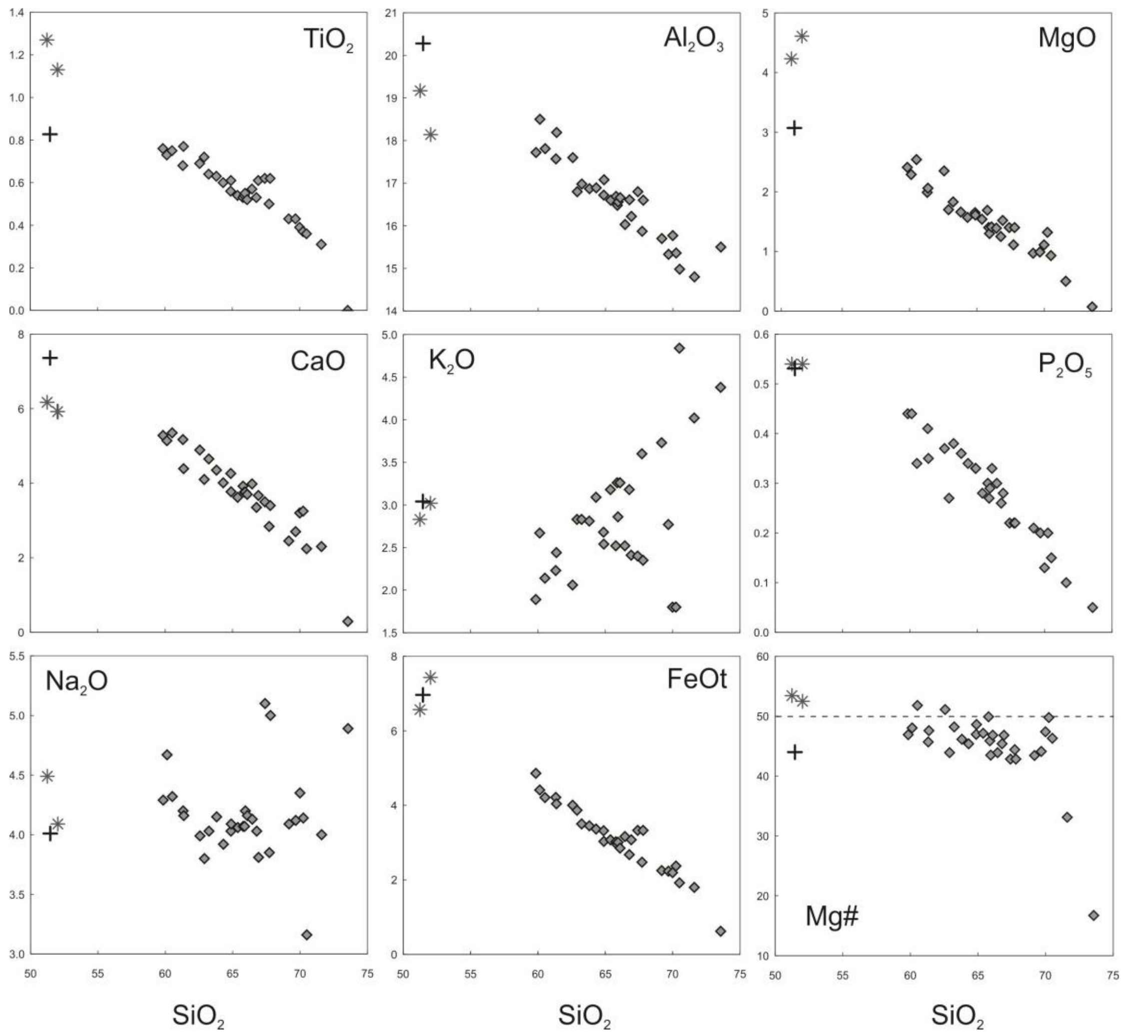

Figure 3.2.5 Variation diagrams for major elements. Symbols as in Fig. 3.2.2

3.2.4 Trace Element Geochemistry

Trace element variation diagrams for selected trace elements are presented on ***Fig. 3.2.6***.

The GRD samples display good correlation on the Sr, V, Zr, and less for Rb and La diagrams with a decreasing trend with differentiation. Pb displays good correlation and increases with differentiation. For the Ba, Y, Nb and Cr variation the samples are scattered with a tendency to decrease with differentiation. Th and U are highly scattered with U tending to increase while Th is rather constant tending to decrease at higher SiO_2. Especially the decrease in Y is attributed in hornblende fractionation.

On **Fig. 3.2.7** the primitive mantle normalised diagrams for the three rock types are presented. All types exhibit typical features of convergent margin generated magmas· variable enrichment in LILE (Large-Ion Lithophile Elements), depletion in HFSE (High Field Strength Elements), the TNT (Ta,Nb,Ti) and P negative anomalies and Pb and K positive anomaly. Sr displays variable negative trends. A Ba negative anomaly is presented for GRD and enclaves but is absent for the diorite. This, in relation to the negligible Sr anomaly is probably the result of no or minor plagioclase fractionation on earlier fractionation stages. A Th-U positive anomaly is also displayed by the GRD, whereas diorite displays a negative Th anomaly. The enclaves show similar patterns with the GRD apart from the P and Ti anomaly which is smaller for the enclaves than the GRD which probably implies lesser crustal input.

On ***Fig. 3.2.8*** the REE chondrite normalised patterns for the three rock types are presented. Eu negative anomaly is present from negligible for the enclaves and diorite to significant for the GRD. Enrichment of the LREE is present in all types with minor variation though the diorite displays smaller enrichment than the other types. The enclaves and diorite are more enriched in HREE than the GRD but all show similar HREE patterns with Tb_{cn}/Lu_{cn} >1 suggesting residual garnet in their source. The significant MREE enrichment that all types present, implies the role of hornblende fractionation in these rocks though it occurs in small proportion in the rocks.

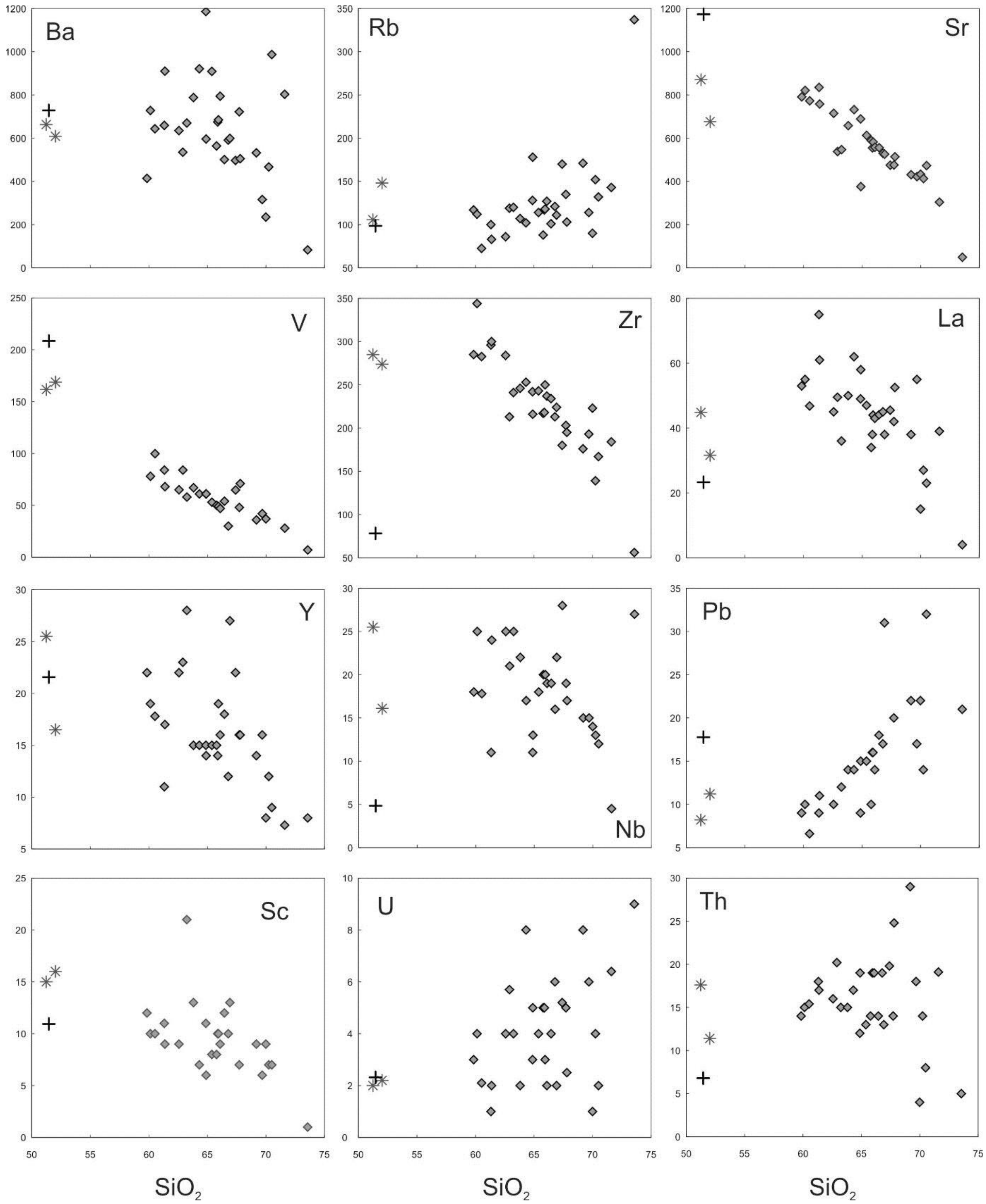

Figure 3.2.6 Variation diagrams for selected trace elements. Symbols as in Fig. 3.2.2

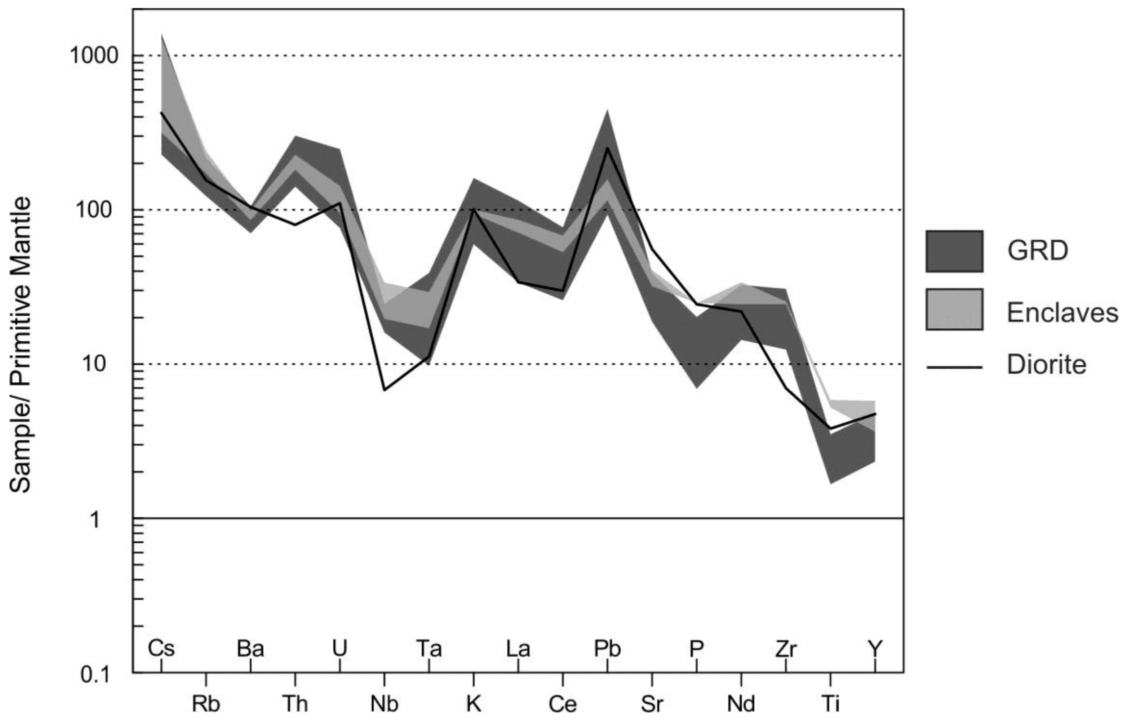

Figure 3.2.7 Multi-element spider diagram patterns. Normalisation values from *Sun & McDonough (1989)*.

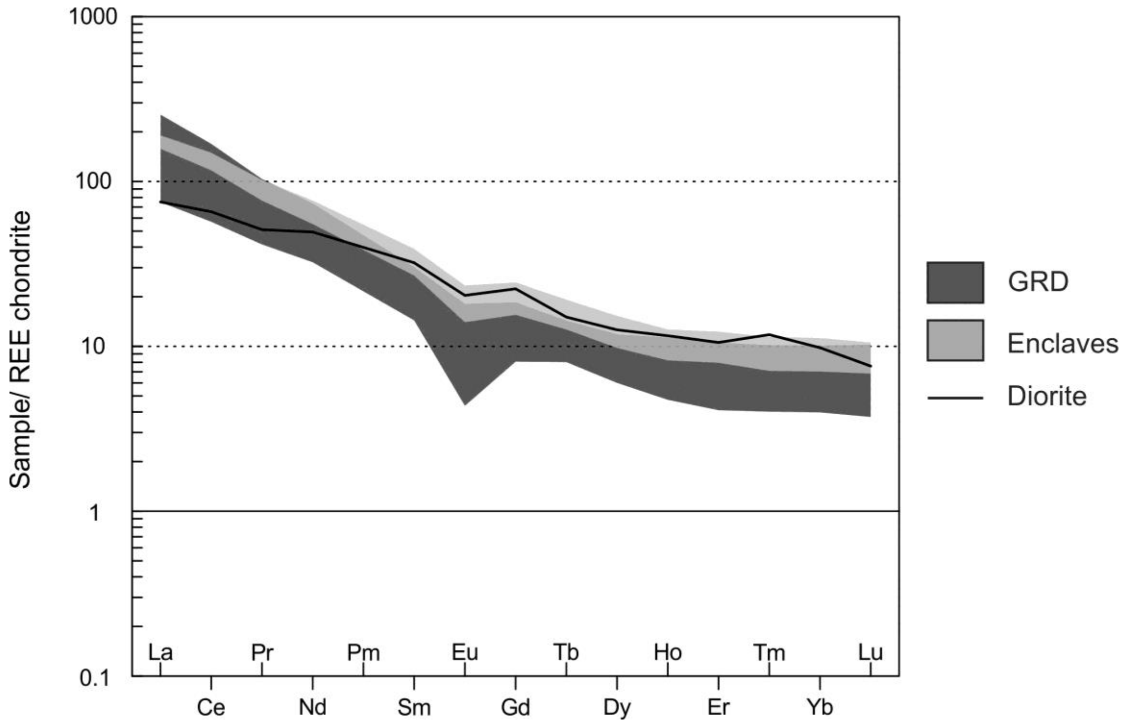

Figure 3.2.8 REE spider diagram patterns. Normalisation values from *Boynton (1984)*.

3.2.5 Sr and Nd bulk rock isotope composition

The Sr and Nd bulk rock isotopic composition of the Elatia pluton of previously published data along with new ones are given in Appendix B. The initial Sr and Nd compositions of the enclaves and GRD are similar but the diorite exhibits comparatively low Sr_i and high Nd_i ratios (***Fig. 3.2.9***).

According to its isotopic composition the diorite sample displays an origin from a more depleted source which tends towards the DM or EAR. The rest of the samples display typical isotopic compositions of rocks which originate from mixed source. This is the result from a "depleted" (mantle?) and an "enriched" component (crust?). Taking into account that the enclaves are mafic rocks of similar mineral composition with the diorite it appears that the enclaves are the outcome of a mixing between a depleted component (which may be represented by diorite) and high Sr_i low Nd_i component which probably is the jurassic metamorphic rocks of the Rhodopian crust.

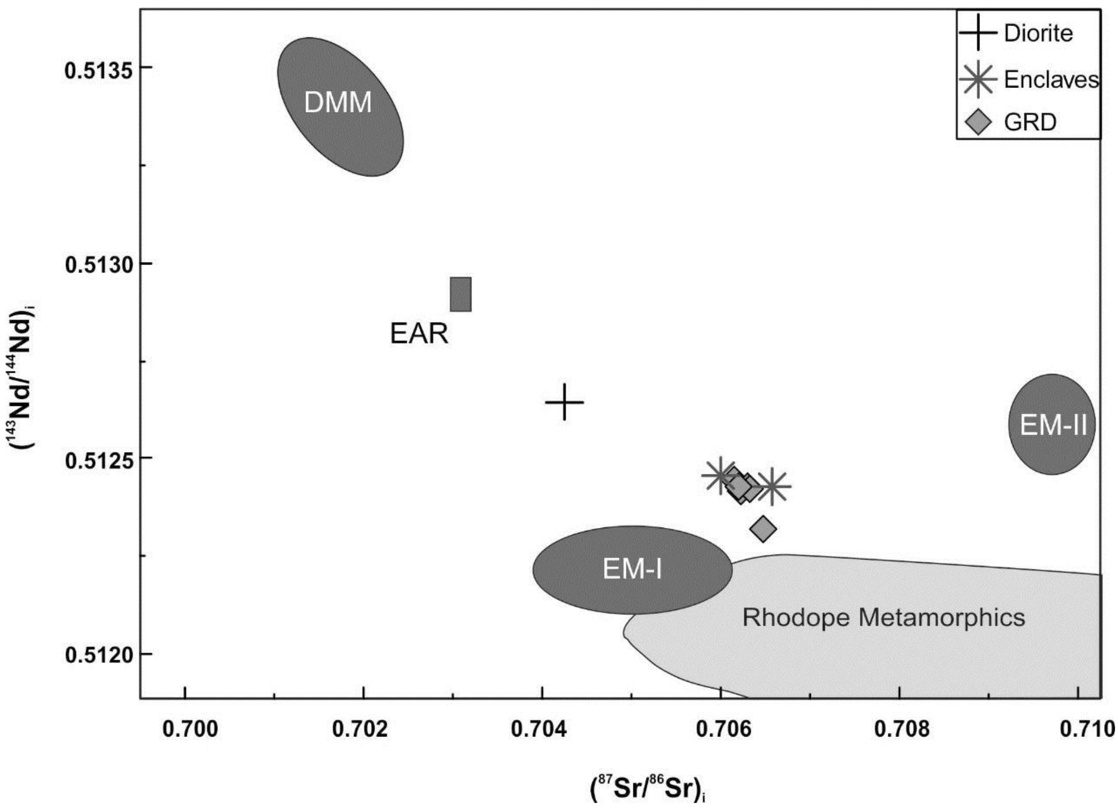

Figure 3.2.9 $(^{87}Sr/^{86}Sr)_i$ versus $(^{143}Nd/^{144}Nd)_i$. The fields illustrated are; DMM=Depleted Morb Mantle, EM-I=Enriched Mantle I, EM-II=Enriched Mantle II after *Zindler & Hart (1986)*. EAR=European Asthenospheric Reservoir

after *Cebria & Wilson (1995),* Rhodope metamorphics after *Cornelius (2008)* and *Castorina et al. (2014)*

3.2.6 Petrogenetic Implications

Origin and Evolution

Previous workers on the Elatia pluton using geochemical models have discussed on the evolutionary processes and the relation between the GRD, the GR and the TMG *(Jones et al., 1992; Soldatos et al., 2001b).* For the enclaves and diorite there are no previous data. Their mineralogy (paragraph 3.1.2) is similar to the GRD though the enclaves texturally present variation. The mineral chemistry shows that there are no differences between the GRD and the enclaves and diorite (paragraph 3.2.2). Their major element variation implies relationship with the GRD but their trace element variation is ambiguous especially for the diorite sample. The trace element and REE spider diagrams however, imply a strong relation between the enclaves and GRD. The diorite displays differences but a strong connection among them is supported but the continuous depletion with differentiation of their HREE, the similar HREE patterns they display and their constant shift on the MREE which implies amphibole fractionation.

So far, assimilation and fractional crystallization (AFC) was proposed to be the main differentiation process between the less differentiated GRD samples and the more differentiated GRD samples (*Soldatos et al., 2001a*) but the presence of several enclaves indicate a mixing process rather than assimilation.

The role of the mafic members and especially of the diorite is a key to better understand the origin of the Elatia pluton. The Sr_i and Nd_i isotopic composition of the enclaves from the Elatia pluton is similar to the GRD revealing extensive mixing.

Nonetheless, the diorite sample with more depleted REE and trace element patterns and the very low Sr_i and high Nd_i ratios may represent the most primitive magma composition in the area. However, the more enriched compatible elements, its depletion in some compatible elements (see ***Fig. 3.2.6***) and the low mg#, that it presents relative to the enclaves implies that this sample has probably been subjected through a complex differentiation process. This is probably related with the cummulitic diorite outcrops (*Soldatos* unpb. data) in the area, but needs further study. Nevertheless its isotopic contents can be attributed as realiable since they can not be depleted from differentiation processes. It should be mentioned here that there are several cummulitic rocks in the Elatia area consisting mainly of amphibole (*Soldatos* unpb. data) with very low SiO_2, low Al_2O_3, high mg# and enriched in compatible elements. If a link between the diorite and these rocks could be assumed then the answer for the selective depletion of the diorite could be given. Unfortunately there are only few poor data for these rocks and there diorite septa sample found is unique. Nevertheless, the enclaves of the Elatia pluton demonstrate a rather mantle derived origin thought they have been subjected to mixing with a crustal component they maintain high MgO and mg#.

For the origin of the Early-Middle Eocene magmatic rocks of RM *Marchev et al. (2013)* proposed melts derived from an enriched mantle source accompanied with different degrees of crustal contamination from the metamorphic rocks of the Middle Allochthon of RM. *Christofides et al. (2007)* studying the 50 Ma Sithonia Plutonic Complex were enclaves were found suggested an Upper Mantle origin component for this magmatism. The mafic enclaves of the Sithonia Plutonic Complex, according to *Perugini et al. (2003)* have been subjected to extensive mixing limiting the source information.

Based on the study of *Rohrmeier et al. (2013)* from the Yugovo and Smilyan plutons *Marchev et al. (2013)* argue for the possibility of a Variscan component. Some authors due to the limited data from mafic rocks for the Early-Middle Eocene magmatism attribute the depleted isotopic character to a Variscan component.

Regarding the Elatia pluton the isotopic characteristics of the felsic rocks and the enclaves are in favour of mixing between a mantle and a crustal component while the very low Sr_i and high Nd_i of the diorite could be interpreted as of mantle origin.

A Variscan component is highly unlikely here as indicated by the high εNd (+1.5) and the young T_{DM} age (~0.8).

Adakitic affinity

Recently, *Marchev et al. (2013)* revealed the adakitic signature of the Elatia pluton studying and re-evaluating the Early-Middle Eocene magmatic activity in RM, Kraisthe zone and Srendogorie zone. Both plutonic and volcanic rocks of these zones share common mineralogical, geochemical and isotopic characteristics. In ***Fig. 3.2.10*** and ***Fig. 3.2.11*** the Sr/Y versus Y and La/Yb versus Yb discrimination diagrams of adakitic rocks for the old and new geochemical data of the Elatia pluton are presented. According to *Moyen (2009)* the so-called "adakitic" signature is a composite one. It can reflect a range of situations and processes such as high Sr/Y sources, garnet-present melting or interactions with the mantle (also in the garnet stability field), or even garnet fractionation. However, in many cases the difference between these processes can be made with a careful petrogenetical study, one that is not restricted to pointing to "high Sr/Y". For the Elatia pluton and the rest of the mentioned Early-Middle Eocene plutons the adakitic signature is generated by the amphibole ± epidote ± allanite fractionation which produces adakitic signatures (*Marchev et al., 2013*). Such "adakites" are, certainly, high pressure melts (i.e., more than 10 kbar), of different sources; this can occur in a range of situations, encompassing under-plated mafic rocks (in a continental arc), delaminated crust (in a collision) or lower collisional crust, etc; this does not make them "adakites" (*Moyen, 2009*).

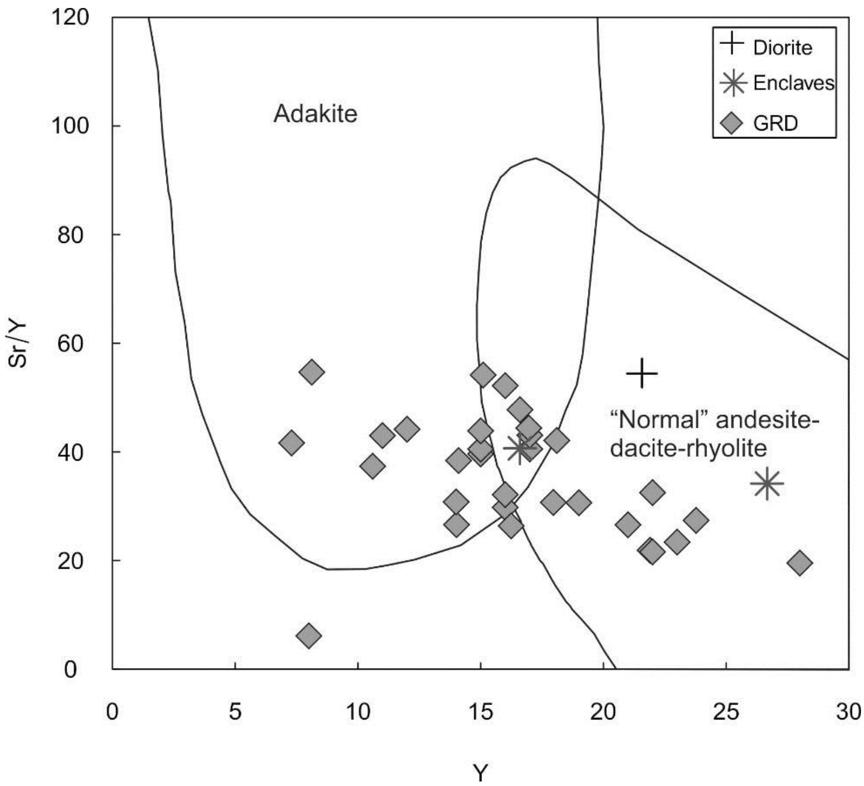

Figure 3.2.10 Discrimination diagram Sr/Y versus Y for adakites. Fields of adakite and calc-alkaline lavas are from *Richards and Kerrich (2007)*

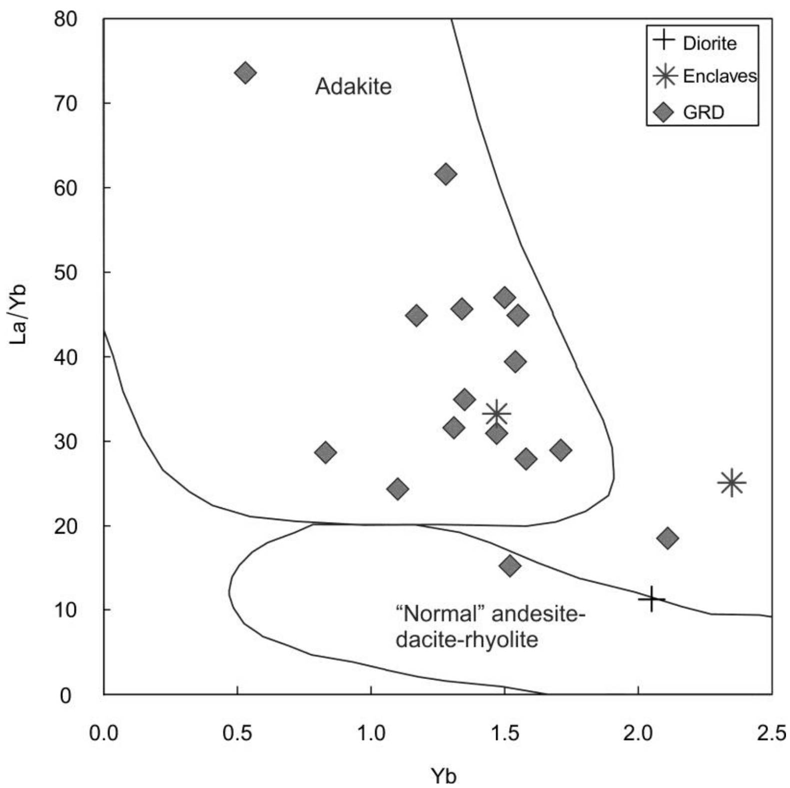

Figure 3.2.11 Discrimination diagram La/Yb versus Yb for adakites. Fields of adakite and calc-alkaline lavas are from *Richards and Kerrich (2007)*

3.2.7 Revaluation of the geotectonic setting of the Elatia pluton

Several authors have discussed the geotectonic setting of the Elatia pluton (paragraph 3.2.1). All of them support a subduction related environment based on several geotectonic discrimination diagrams with some supporting a pre-colission environment (e.g. *Soldatos et al., 2001a*) and others supporting a post-colission environment (e.g *Jones et al., 1992; Marchev et al., 2013*).

The last years the validity of previously used discrimination diagrams are under dispute since the decision boundaries of most tectonic discrimination diagrams are drawn by eye *(Vermeesch, 2006).* Pearce himself revised his key diagram of Rb/Y+Nb (*Pearce et al., 1984*) adding a post-collision field (*Pearce, 1996*). This discrimination diagram has been used for the Elatia pluton along with others to conclude for the geotectonic setting of the pluton. In ***Fig. 3.2.18 the*** Rb/Y+Nb revised discrimination diagram of *Pearce (1996*) is presented.

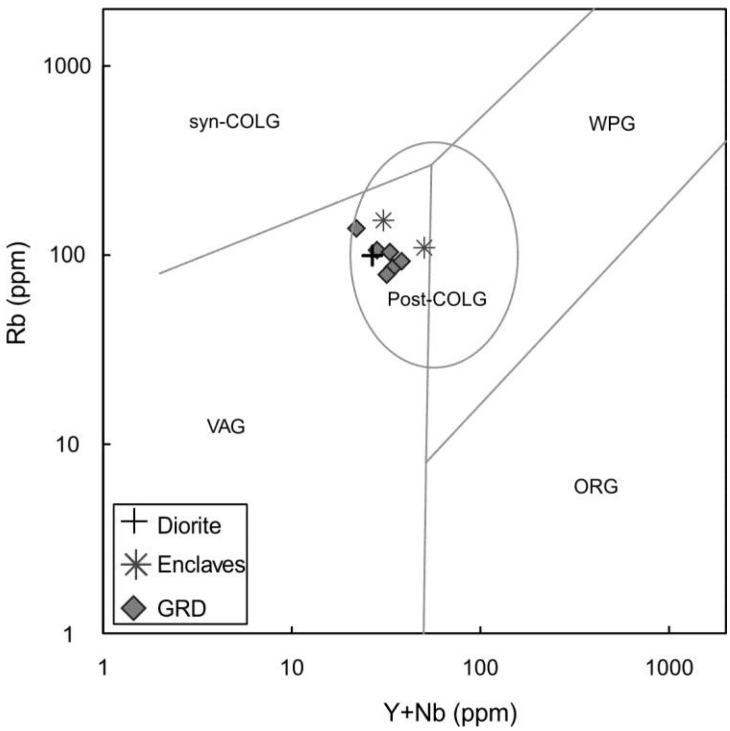

Figure 3.2.12 Rb versus Y+Nb discrimination diagram of geotectonic settings (*Pearce et al., 1984* modified by *Pearce, 1996*)

A lot of effort has been made by many authors to revisit the old discrimination diagrams and used discrimination analysis which is more rigorous for the decision boundaries with very good probabilities. *Verma & Verma (2013)* presented three sets of discrimination diagrams obtained from the correct statistical methodology of $\log_e$-ratio transformation and linear discriminant analysis. These sets of diagram were attributed for the Elatia pluton in ***Figs. 3.2.13-15***. All the samples are plotted in the “Col” field which is actually discriminated using samples from post-colissional tectonic environments. Thus, a post-collisional setting is suggested for the Elatia pluton rather than a pre-collision one.

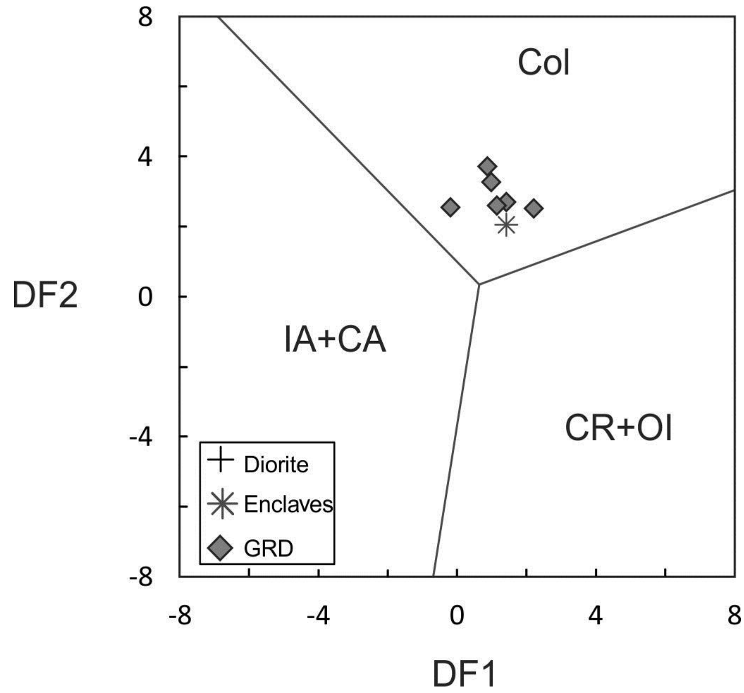

Figure 3.2.13 Tectonic discrimination diagrams for intermediate magmas according to Verma & Verma (2013). Col=Colissional Settings; IA+CA= Island Arc & Continental Arc; CR=Continental Rift & Oceanic Islands.
DF1=(-0.1672589*ln(La/Yb))+(-1.2542899*ln(Ce/Yb))+(1.295171*ln(Sm/Yb))+(1.3318361*ln(Nb/Yb))+(0.2698636*ln(Th/Yb))+(1.9286976*ln(Y/Yb))+(0.18097357*ln(Zr/Yb))-3.815745639.
DF2=(-0.2426713*ln(La/Yb))+(1.7265475*ln(Ce/Yb))+(0.4902224*ln(Sm/Yb))+(-1.2755648*ln(Nb/Yb))+(0.9602491*ln(Th/Yb))+(0.8511852*ln(Y/Yb))+(-0.4894082*ln(Zr/Yb)) - 3.305510646

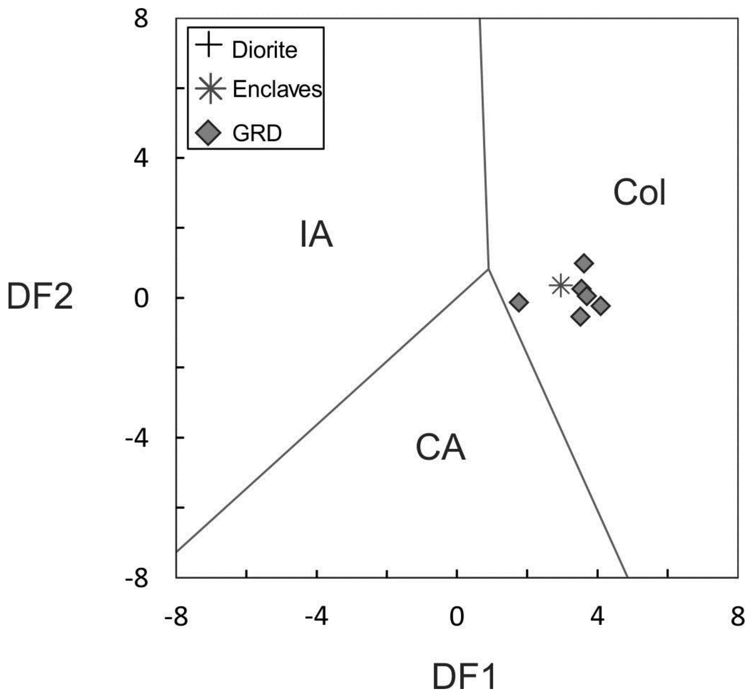

Figure 3.2.14 Tectonic discrimination diagrams for intermediate magmas according to Verma & Verma (2013). Col=Colissional Settings; IA = Island Arc; CA=Continental Arc.

DF1=(0.092724*ln(La/Yb))+(0.752143*ln(Ce/Yb))+(0.9296053*ln(Sm/Yb))+(0.1235102*ln(Nb/Yb))+(0.347945*ln(Th/Yb))+(1.472513*ln(Y/Yb))+(-0.0339674*ln(Zr/Yb))-5.801482381.

DF2=(-2.038286*ln(La/Yb))+(-0.073322*ln(Ce/Yb))+(-1.36043*ln(Sm/Yb))+(-0.0782899*ln(Nb/Yb))+(1.8248761*ln(Th/Yb))+(2.7738488*ln(Y/Yb))+(0.44440139*ln(Zr/Yb)) - 3.684349292

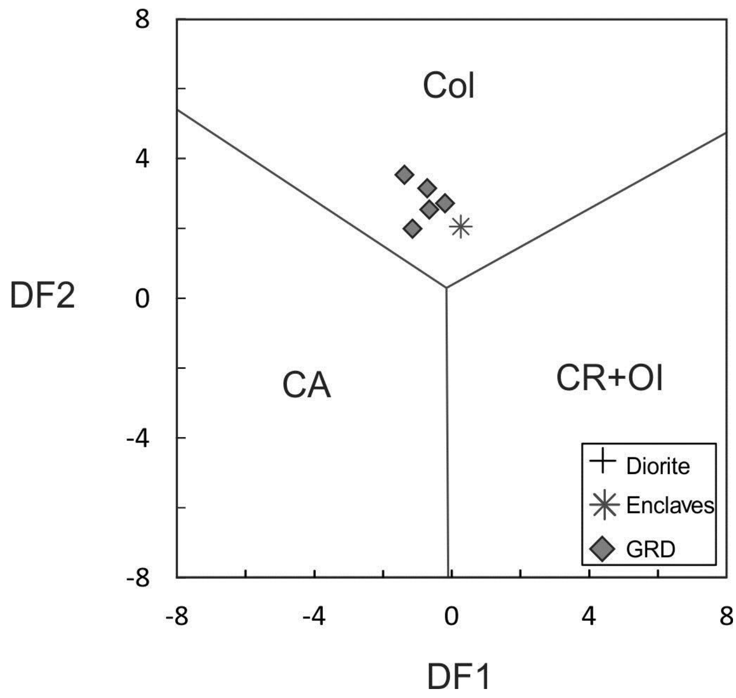

Figure 3.2.15 Tectonic discrimination diagrams for intermediate magmas according to Verma & Verma (2013). Col=Colissional Settings; CA= Continental Arc; CR=Continental Rift & Oceanic Island.
DF1=(-0.977026*ln(La/Yb))+(-1.3886489*ln(Ce/Yb))+(1.36560*ln(Sm/Yb))+(1.8999127*ln(Nb/Yb))+(0.5690460*ln(Th/Yb))+(1.65772638*ln(Y/Yb))+(-0.30523813*ln(Zr/Yb))-0.87680549008.
DF2=(-0.086967*ln(La/Yb))+(1.1636159*ln(Ce/Yb))+(0.3635930*ln(Sm/Yb))+(-0.90127239*ln(Nb/Yb))+(1.1257989*ln(Th/Yb))+(1.19149068*ln(Y/Yb))+(-0.39964298*ln(Zr/Yb)) - 3.915383182

3.3 The Xanthi Plutonic Complex

3.3.1 General

The Xanthi Plutonic Complex (XPC) intrudes the southern part of the Rhodope metamorphic complex of Northern Greece. The exposed area (about 40km^2) is an elongated body of nearly E-W direction starting from the Xanthi town to the west and ending west of the Filia village to the east (***Fig 3.3.1***). Geophysical data suggest a laccolith-like, truncated pyramid-shaped intrusion based at an approximate depth of 4.5 (*Maltezou & Brooks, 1989*) to 7 km (*Tsokas et al., 1996*) which extends several kilometers southwards. The southern edge of the exposed body is marked by a major fault. *Koukouvelas & Pe-Piper (1991)* suggested that the emplacement of the Xanthi intrusion had been controlled by major faults and that it took place along a listric fault of the Kavala-Komotini fault zone during regional extension.

The western and northwestern margins of XPC are in magmatic contact with marbles and gneisses of the Rhodope Massif. There is a contact metamorphic aureole typically a few hundred meters wide (*Christofides, 1977; Liati, 1986*).The eastern end of the pluton cuts Eocene-Oligocene sedimentary rocks (dominantly flysch) which are intruded by andesitic dykes.

The western and central part is occupied by the Grandiorite, having hornblende and biotite which makes up about 75% of the outcrop area. The eastern part of the pluton consists of monzonite, quartz monzodiorite, quartz monzonite porphyry, gabbro, monzogabbro and sparse quartz gabbro and quartz diorite. Mafic microgranular enclaves of quartz dioritic composition are present in the granodiorite. Aplitic-pegmatitic veins and lamprophyric dykes are found throughout the complex.

Christofides (1977) investigated the XPC in the framework of his doctoral thesis and based on major element geochemistry supported the hypothesis that the gabbroic and monzonitic rocks probably originated from a magma which was different from the one that gave the granodioritic rocks. On the other hand *Kotopouli and Pe-Piper (1989)*, based also on major element geochemistry suggested that the XPC rocks may all be products of the same differentiation process. They also supported a significant amount of crustal contribution to the magma.

Jones et al (1992) suggested that although some northern Greece granites could be the consequence of evolutionary processes such as crustal assimilation or crystal settling, the majority have compositions which are inconsistent with crustal involvement. *Sergi (1997)* investigated the petrogenesis of the granodioritic rocks of the XPC and their mafic microgranular enclaves. Based on field evidence, as well as petrographic and geochemical data, she concluded that the Xanthi pluton could represent ascent of a zoned magma body, with a silicic cap (granodiorite, tonalite, quartz diorite) having intruded first, followed by the deeper more mafic

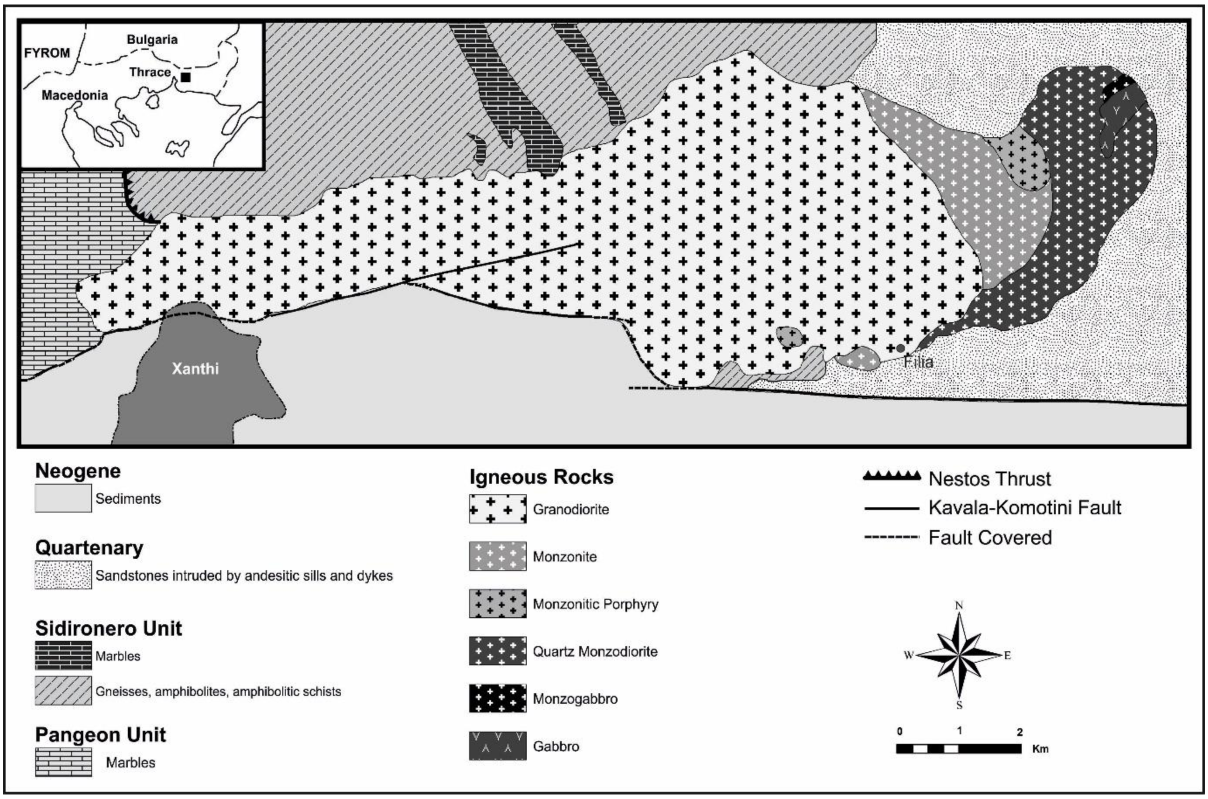

Figure 3.3.1 Simplified Map of the XPC, modified after *Christofides (1977)*

levels as syn-intrusive dykes. The enclaves derived from disruption of syn-plutonic intrusions of co-genetic mafic magma. In their comparative study of the most important Tertiary plutons of the Hellenic Rhodope Massif, including XPC, *Christofides et al. (1998)* distinguished two groups of magmas, a basic group and an acid one. The basic magma derived as a consequence of a multistage mantle-crust process whereas the acid magmas were considered as crustal melts.

Meyer (1968), studying the geology of Rhodope between the Nestos and Strymon rivers gave an 27.1±0.4, 27.9±0.9 Ma for the granodiorite. *Liati (1986)* studied the metamorphic rocks into which the XPC was emplaced as well as the contact metamorphic aureole. She gave an Oligocene age for the granodiorite (hornblende K/Ar age of 28.8±0.3 to 30.4±0.6 Ma). Whole-rock/Bi Rb/Sr isochron of the Xanthi granodiorite, obtained by *Kyriakopoulos (1987)*, gave 28.8 ± 0.7 Ma and 26.3 ± 0.1 Ma. Mineral separates Ar/Ar data gave ages from 29.4±2.7 to 30.6±2.3 Ma (on hornblende) and from 25.1±0.5 to 25.3±0.4 Ma (on biotite) for the granodiorite, 25.8 ± 0.4 Ma for the monzonite and 26.5 ± 0.6 Ma for the leucomonzogrbbro (*Christofides et al., 2012*). Slightly younger ages (26.0 ± 1.8 Ma and 25.5 ± 1.2 Ma) for the monzonite were obtained from two apatite fission-track datings by *Bigazzi et al. (1994)*.

Kyriakopoulos (1987) based on the discrimination diagrams of *Pearce et al. (1984)* suggests a Syn-COLG origin for the XPC. A post-collision origin related to extension is given by *Jones et al. (1992)* and *Christofides et al. (1998).*

3.3.2 Petrography and Mineralogy

The petrography and mineralogy of the XPC was mainly and extensively studied by *Christofides (1977)*. The XPC is a composite plutonic body with great compositional variation. Its dominant component is granodiorite followed by gabbro, monzogabbro, monzonite/quartz-monzonite (hereafter monzonite), quartz-monzodiorite/ monzodiorite (hereafter quartz monzodiorite), and quartz monzonite porphyry. Quartz gabbro and quartz diorite were found locally (***Fig. 3.3.2***). The complex, mainly the granodiorite, is intruded by aplites and rarely pegmatites. A few lamprophyric veins are intruding the granodiorite. Granodiorite, encloses mafic microgranular enclaves (MME) of quartz diorite to tonalite in composition. *Christofides (1977)* distinguished three major groups; the "Acid" group composed of the granodiorites, the "Basic" group composed of the gabbros, monzogabbros, monzonites/quartz-monzonites, quartz-monzodiorites/monzodiorites, and quartz monzonites porphyry and the MME. The description of each group will follow, but the major groups will be used further for the purpose of the present study.

Granodiorite (GRD): is a medium-grained rock with typical granitic texture. The main mineral constituents are plagioclase, orthoclase, quartz, biotite and hornblende. Augite, apatite, titanite, zircon, and opaques, mainly magnetite, are among the common accessories. The content of quartz, orthoclase and plagioclase is 17-24 vol.%, 13-24 vol.% and 43-58 vol.% respectively. At some places (not mappable) the granodiorite is richer in orthoclase and passes gradually into monzogranite. In places, at the peripheral of the granodiorite margins there is a transition to porphyritic granodiorite and monzogranite with limited augite component. Aplitic mainly, pegmatitic and lamprophyric veins cross all over the granodiorite with their thickness ranging from some centimeters up to 20 meters.

Quartz occurs as interstitial unhedral to subhedral crystals often displaying wavy extinction. Plagioclase is sub- to euhedral, and usually displays zoning normal and discontinuous. Their composition ranges between oligoclase (An_{25}) and andesine (An_{50}) but usually there is a labradoric core intensively altered. The Or content is 0.7-7 %. It often contains microcrystals of other minerals. Orthoclase is perthitic with albite component 11-20%, sub- to anhedral and occurs interstitially. It is sometimes slightly altered to kaolinite and rarely to sericite. It displays limited myrmikitic intergrowth in contact with the plagioclase. Biotite and hornblende are found in all samples and their abundance ranges between 3-8.5% and 0.7-8.0% respectively. Therefore, the granodiorite is sometimes biotite-hornblende and sometimes hornblende-biotite. Biotite is yellow-brownish to brownish with a constant ratio $Mg^{2+}/Mg^{2+}+Fe^{2+}$~0.6 and usually altered to chlorite. Hornblende is yellow-brownish to olive-greenish and usually altered to chlorite.

Monzonites (Mz): are medium- to coarse-grained, massive and unaltered rocks. They display monzonitic texture with euhedral plagioclases surrounded by anhedral K-feldspar. They consist mainly of plagioclase orthoclase, pyroxenes, biotite and subordinary hornblende, quartz, apatite, titanite and opaque minerals.

Orthoclase content ranges between 23.4 to 42.7 usually found in large crystals with Carlsbad twinning. It surrounds euhedral plagioclases and microcrystals of pyroxenes and biotite and is often perthitic. In most cases it is full of opaque yellow-brownish or black microcrystals which are oriented in two or three directions. Its albite component is 23-33%. Plagioclase content ranges between 25.7 and 47.6 and has plate shape. There is a wide range in anorthite from An_{38} to An_{71}. They usually display zoning but with small chemical variation from core to rim. Sometimes they have labradoritic core. Pyroxene is mainly augite and less hypersthene and their content ranges between 3.2 to 18.5% with a constant $100Mg^{2+}/Mg^{2+}Fe^{2+}Fe^{3+}Mn^{2+}$ ratio of ~57. Their colour is white or slightly pink. They contain opaque minerals and small crystals of biotite. Hypersthene is in most cases altered. Biotite content ranges between 5.2 to 12.3% and displays strong colours from yellow to brown-red with intense pleochroism with a constant $Mg^{2+}/(Mg^{2+}+Fe^{2+}$ ~0.6. It is enclosed in pyroxenes and sometimes it contains plagioclases. Hornblende is yellow-greenish found in small percentages in the rock in most cases at the rim of augite replacing it. Sometimes it can be found in the middle of the pyroxene. It displays a constant $Mg^{2+}/Mg^{2+}+Fe^{2+}$ ~0.6. Quartz content ranges between 1.5 to 4.2% found between the other minerals. Magnetite and ilmenite are usually found in biotite. Apatite also is included in biotite or in feldspars and usually in large crystals. There is another monzonitic occurrence at the NE part of the pluton which have the same mineralogical composition but are richer in hornblende and orthopyroxene.

Quartz monzodiorites (QMzd): are medium to fine-grained, massive and unaltered rocks. Plagioclases usually display zoning with composition ranging between andesine (An_{41}) to labradorite (An_{62}). Orthoclase is always anhedral, fills the space between the other minerals and surrounds the plagioclases and its albite component is 15-20%. Pyroxene content ranges between 11.2 to 19.8%, they are white to pink and are mainly augites with a constant $100Mg^{2+}/Mg^{2+}+Fe^{2+}+Fe^{3+}+Mn^{2+}$ ratio ~60. Hypersthene is up to 2% and is almost always altered and usually it is surrounded by augite. Biotite (6.7 - 12.2%) in leafy form and less in prismatic, is found usually with pyroxene or in the pyroxene. It has yellow, brown and brown-red colour. It has a constant ratio of $Mg^{2+}/Mg^{2+}+Fe^{2+}$ ~6. Quartz content is up to 7.3% and is found in angular form among the other minerals. All the other minerals, opaque, hornblende, apatite and titanite are found in very low contents.

Leucomonzogabbros (LMzG): are coarse-grained rocks easily distinguished among the gabbros and the quartz monzodiorites. They consist mainly of plagioclases, orthoclases, augite and biotite. In lesser amounts there are hypersthene, olivine, quartz, chlorite, calcite, apatite, Iddingsite, talc and opaque minerals. Plagioclases are in large twin crystals which sometimes display zoning. Their composition ranges from andesine to felsic labradorite, usually between 37 and 67% of An and the Or component is about 30%. They usually display the anti-perthite phenomenon. Often, they surrounded by orthoclase and sometimes orthoclase replaces the plagioclase.

Orthoclase usually is anhedral. It is altered to kaolinite. Augite is white to pink coloured with enclaves of biotite, opaque minerals and quartz.

Hypersthene content is very low in the rock, is almost always altered, displays pleochroism and is surrounded or crossed by iddingsite and other products of alteration. Biotite is usually leafy, yellow-redish to brown-redish and sometimes altered to chlorite. It surrounds large crystals of opaque minerals and sometimes forms a shell around them. Apatite occurs in large crystals in orthoclases.

Olivine gabbro (Gb): these rocks occupy a small area 600m in length and 200m in width. They are medium-grained rocks and their boundaries with the quartz monzodiorite are clear. Olivine gabbros mainly contain plagioclases, augite, olivine and biotite while the hypersthene, orthoclase, apatite, minerals from alteration and opaque minerals are minor.

Plagioclases are always above 60% and they are plate-like. Sometimes they are full of microcrystals of epidote, calcite and opaque minerals. Their composition in An is An_{29} to An_{50}, so they are considered acid enough for gabbroic rocks.

Orthoclase is rare and occurs only in a limited number of samples. Augite is anhedral in rounded crystals with slightly pink or slightly greenish colour, but usually is colourless. Many times it appears full of opaque grains or needles that consist of biotite, opaque minerals and olivine. Its 100Mg/(Mg+Fe^{2}+Fe3+Mn) ratio is between ~71-76. Hypersthene is always minor at the edges of augite and olivine in single crystals and altered with $100Mg^{2+}/Mg^{2+}+Fe^{2+}+Fe^{3+}+Mn^{2+}$ ratio ~64-74. Olivine is anhedral and white with cracks filled with iddingsite and opaque minerals. It is usually enclosed in augite or partly surrounded by it. The content of olivine ranges from 3.8 to 8.6%. Its composition ranges between 58.47 to 66.75 in Fo and its $100Mg^{2+}/Mg^{2+}+Fe^{2+}$ component ~65-70.

Microgabbros (MGb): at the contact of the olivine gabbro with the monzodiorite fine grained rocks are formed. They contain small plagioclase, pyroxene, olivine and biotite crystals.

Plagioclases are small, elongated and the An content ranges from An_{45} to An_{66}.

Olivine is anhedral with cracks filled with iddingsite and opaque mineral. Its $100Mg^{2+}/Mg^{2+}+Fe^{2+}$ component has a constant value of ~59. Augite is the main pyroxene of microgabbros and is usually anhedral. Its ranges from very fine to fine –grained. Its $100Mg^{2+}/Mg^{2+}+Fe^{2+}+Fe^{3+}+Mn^{2+}$ ranges from 64 to 75. Hypersthene is minor in microgabbros with very fine –grained anhedral crystals. Its $100Mg^{2+}/Mg^{2+}+Fe^{2+}+Fe^{3+}+Mn^{2+}$ ranges is 54-67. Biotite has an orange-red colour with anhedral crystals and usually encloses pyroxene or coexists with pyroxene crystals. Its $Mg^{2+}/Mg^{2+}+Fe^{2+}$ ranges is between 0.5-0.7. Hornblene is minor and its $Mg^{2+}/Mg^{2+}+Fe^{2+}$ ranges between 0.6-0.7.

Quartz gabbro and quartz diorite: These rocks are studied together due to their small size of occurrence and the mineralogical similarities. They occur near the Fillia village close to the boundary between the granodiorite and quartz monzodiorite. They consist mainly of plagioclases, hornblende, biotite, augite, quartz and secondarily of orthoclase, chlorite, apatite, titanite, epidote and opaque minerals. Plagioclases are of plate form and display zoning from basic andesine to acid bytownite for the quartz gabbro, and andesine (sometimes up to 52% of An) for the quartz diorite. The core is usually assimilated so is missing. Quartz, mostly in the quartz diorite as well as orthoclase, occupy the space among the rest of the minerals. In quartz gabbro quartz is usually secondary close to altered mafic minerals. On the upper rocks there is a complex of hornblende and biotite observed that gives a diablastic texture on the rock.

Porphyritic quartz leucomonzonite (PLMz): it appears like a vein body and microscopically has monzonitic texture. It consists mainly of plagioclase, orthoclase, biotite, pyroxene and rarely hornblende megacrystals. The smaller crystals are feldspars, quartz and mafic minerals mainly pyroxene and biotite.

Plagioclases are almost always surrounded by orthoclase which displaces them, often up to their complete disappearance. They are zoned with composition ranging from 26 to 78% An. They enclose opaque minerals and biotite. Opaque minerals and pyroxenes are accumulated between the boundaries of orthoclase-plagioclase.

Biotite is the most abundant mafic mineral in leafy form with yellow to brown-red colour and usually bears enclaves of apatite and opaque minerals. Often, it exist with pyroxene, totally surrounding pyroxene or filling its cracks. Pyroxene (orth- and clino-) is usually altered. It is surrounded by yellow-greenish amphibole or exists inside the amphibole forming islets. This amphibole seems to have a secondary origin. Apatite is usually filled with small grains of opaque minerals.

Mafic Microgranular Enclaves (MME): are mostly found in the granodiorites and are limited at the periphery of the rock. Their size varies from some millimeters up to 25 cm. Their shape is usually rounded but often they are found with prismatic shape. Macroscopically they are fine-grained rocks similar to the fine-grained quartz monzodiorites with a pseudo-ophitic texture.

Mineralogically they consist of plagioclases, quartz, orthoclase, hornblende, biotite, pyroxene, chlorite, titanite, apatite, zircon and opaque minerals. They can be characterized as (biotite)-hornblende quartz diorites. Plagioclases are often zoned and their composition is andesine. They enclose biotite, opaque minerals and apatite and often display zonal alteration. Orthoclase is much less in content than plagioclase and rarely its megacrysts enclose minerals. Quartz is anhedral and as the orthoclase fills the space among the other minerals. Hornblende is the most abundant mineral and is found in two forms either as prismatic elongated crystals or as simple prismatic, displays strong pleochroism with olive-green, green and brown-yellow colours. Usually encloses opaque minerals, biotite, titanite and apatite. Also contains pyroxene relics and sometimes it is altered to chlorite. Biotite is a minor mineral usually altered to chlorite, it is leafy or has board form. Pyroxenes are few and appear as relics or as single crystals. Apatite is usually found in needle form.

3.3.3 Major Element Geochemistry

The geochemical data used for the study of the XPC are mainly a combination of *Christofides (1977, 1989)* and *Christofides et al. (2014),* unpublished data of the same author, and some MME data of *Sergi (1997)*. All geochemical data are presented on Appendix A. There are many gabbroic rocks in the XPC of cumulitic origin (**CGb**) that will not be presented here since they do not represent magmas and will be used only for their initial Sr, Nd and Pb isotopic ratios. Four basic groups will be used here; a) the “Acid” group of *Christofides (1989)* which consists of the GRD, b) the “Basic” group of *Christofides (1989)* which consists of the rest monzonites and monzodiorites c) the MGb from the “Basic” group separately and d) the MME. Athough the MGb are part of the basic group they need to be separated here for the purpose of the present study.

In ***Fig. 3.3.2*** all samples used in the present study are presented on a Q-ANOR classification diagram. The “Acid group” is crearly separated from the “Basic” group and the MME.

In ***Fig. 3.3.3*** the MGb and most of the MME belong to the calc-alkaline series, while the ”Basic group” rocks are strongly enriched in K_2O and are plotted mainly to the Shoshonite and High-K calk-alkaline series while the “Acid” group rocks belong to the High-K calc-alkaline series. In this figure the groups are clearly separated and different evolutionary trends for the XPC “Acid” and “Basic” groups are implied with the MME holding an intermediate position. These trends are not so obvious in the rest major element variation diagrams (***Fig. 3.3.4***) apart from Na_2O and P_2O_5 where the for “Basic” group increase with differentiation, for the “Acid” group decrease while the MME for the Na_2O exhibit very high contents. In the rest major element variation diagrams there is a continuous well correlated decreasing trend. MgO content is moderately high for the MGb group and some rocks of the Basic group which both also display high mg# (>50).

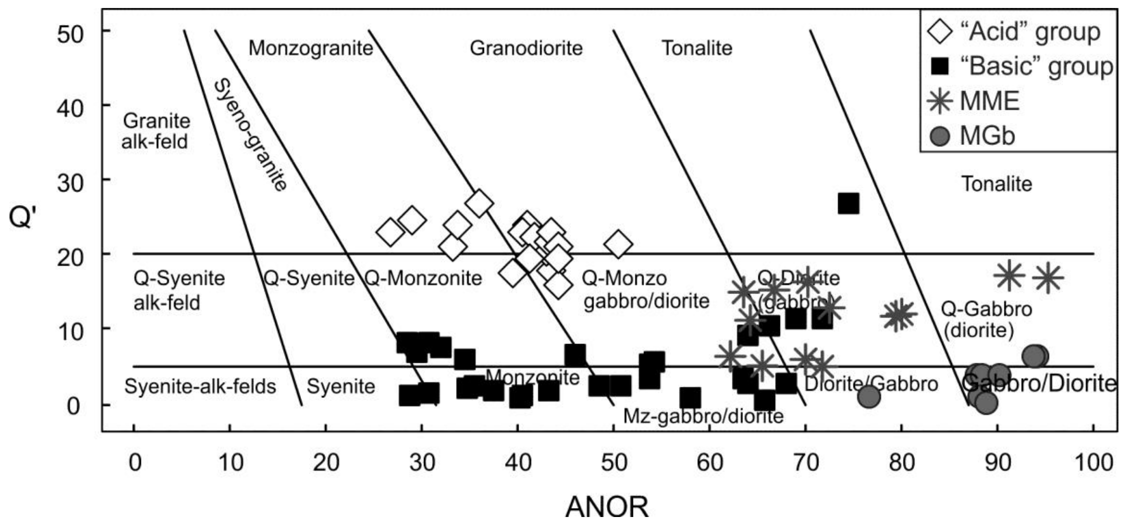

Figure 3.3.2 Q-ANOR classification diagram after *Streckeisen & Le Maitre (1979)*

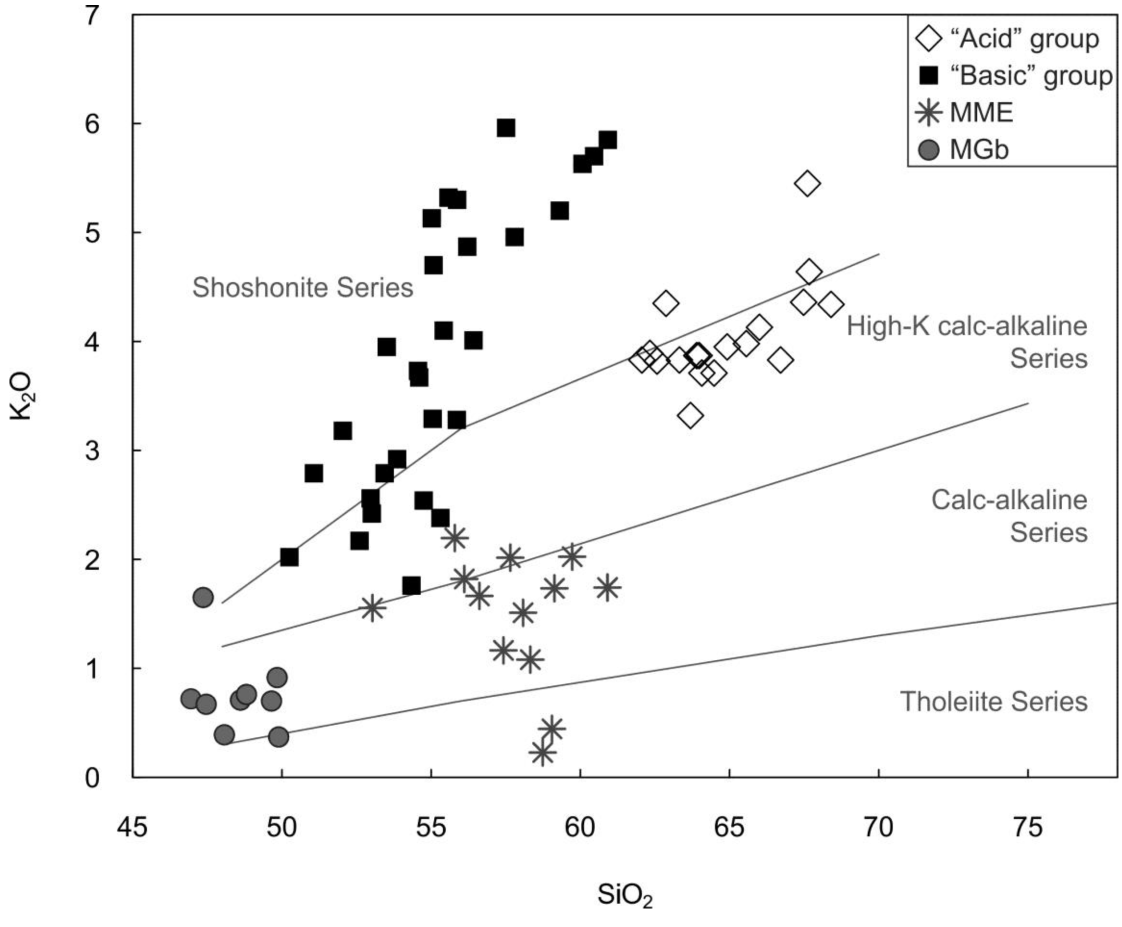

Figure 3.3.3 SiO_2 versus K_2O diagram after *Peccerillo & Taylor (1976)*

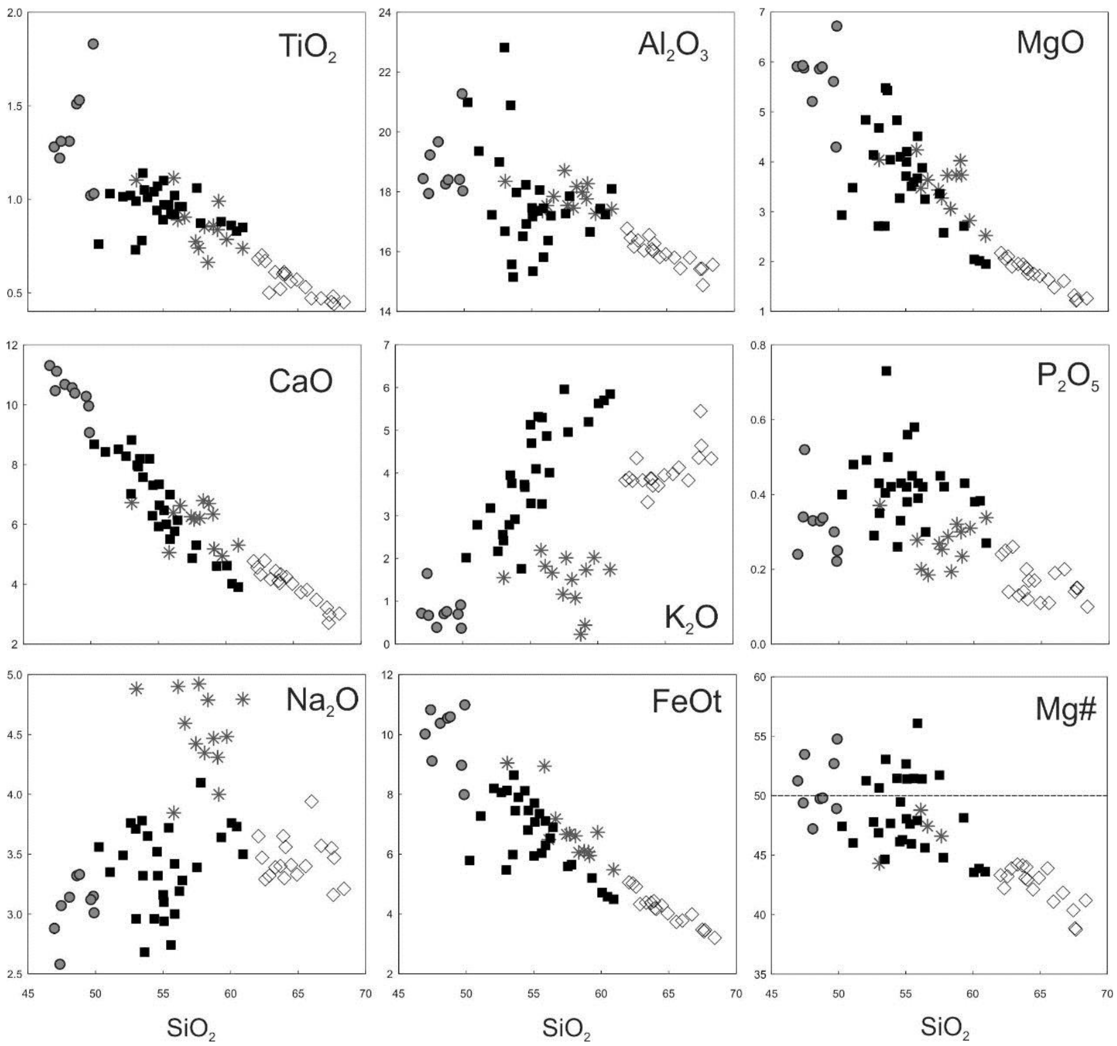

Figure 3.3.4 Variation diagrams for major elements. Symbols as in Fig. 3.3.2

3.3.4 Trace Element geochemistry

In most trace element variation diagrams (***Fig. 3.3.5***, e.g. Rb, , Ba, Nb, Y, La, Zr;) the trace elements behave as incompatible in the "Basic" group and MGb and then become compatible dropping in the "Acid" group. MME hold an intermediate position without displaying any variation for some trace elements (e.g. Ba, Sr, Zr, Th), for other trace elements they follow the "Acid group" trend (e.g. Rb, Y) and in some cases they follow the "Basic" group trends (e.g. Nb, U, V). The MGb rocks unlike the MME for the majority of the trace elements follow the trends of the "Basic group". Mineral fractionation cannot explain these variations for the trace elements. Therefore a mixing proccess has been proposed from previous authors and is supported here.

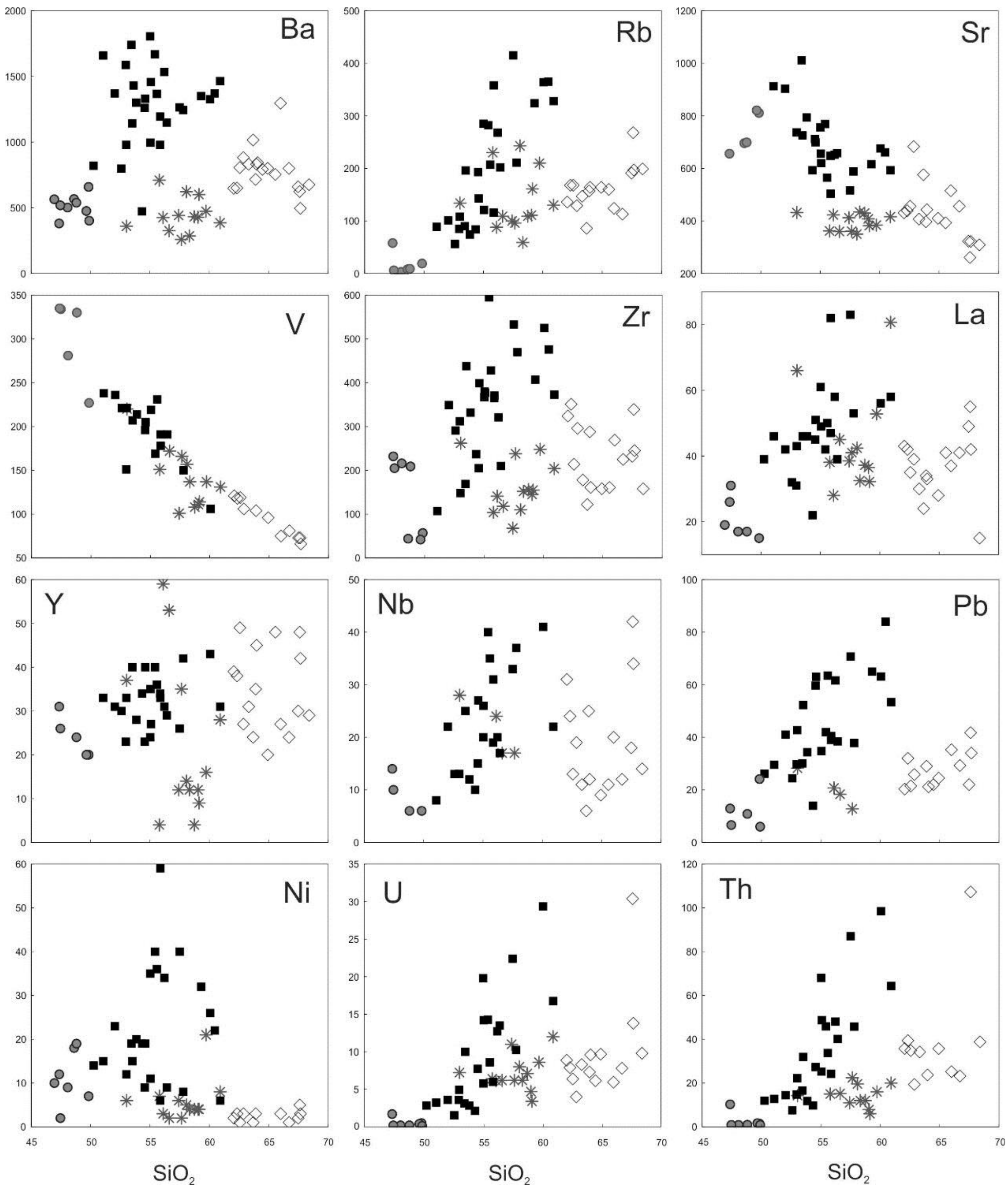

Figure 3.3.5 Variation diagrams for selected trace elements. Symbols as in Fig. 3.3.2

Trace element patterns (***Fi.g 3.3.6***) show LILE enrichment for the "Basic", "Acid" and MME, minor enrichment for the MGb and characteristic anomalies for such geotectonic environments with TNT (Ta,Nb,Ti) and P negative anomalies, , and Pb and K positive anomalies. All groups display an U-Th positive anomaly. The MGb does not display negative Ti, no positive Y anomaly displayed by the other groups and has a intense Rb negative anomaly which does not exists to the other groups. MME do not display positive K anomaly. The MGb group differs from the other groups also in terms of no Ba negative anomaly, a Zr negative anomaly. The patterns of the "Basic" and "Acid" groups are similar. MME patterns are similar to the "Basic" and "Acid" group apart from the K positive anomaly. GBds show many differences from the other groups.

REE patterns are presented on ***Fig. 3.3.7***. All groups display variable enrichment in LREE in relation to the HREE and flat HREE patterns. GBd displays more flat REE patterns and no Eu anomaly. The other groups present begative Eu anomaly. The flat REE patterns regarding the GBd are consistent with early olivine and pyroxene fractionation but inconsistent with residual garnet in the source.

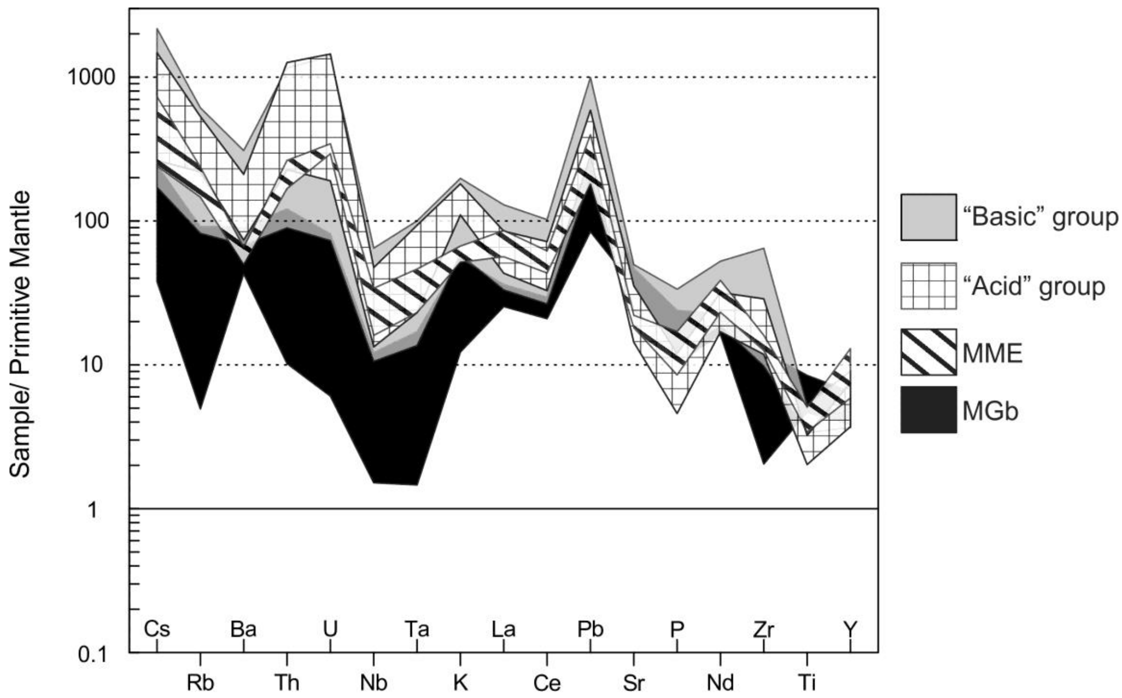

Figure 3.3.6 Multi-element spider diagram patterns of all petrographic types. Normalisation values from *Sun & McDonough (1989)*

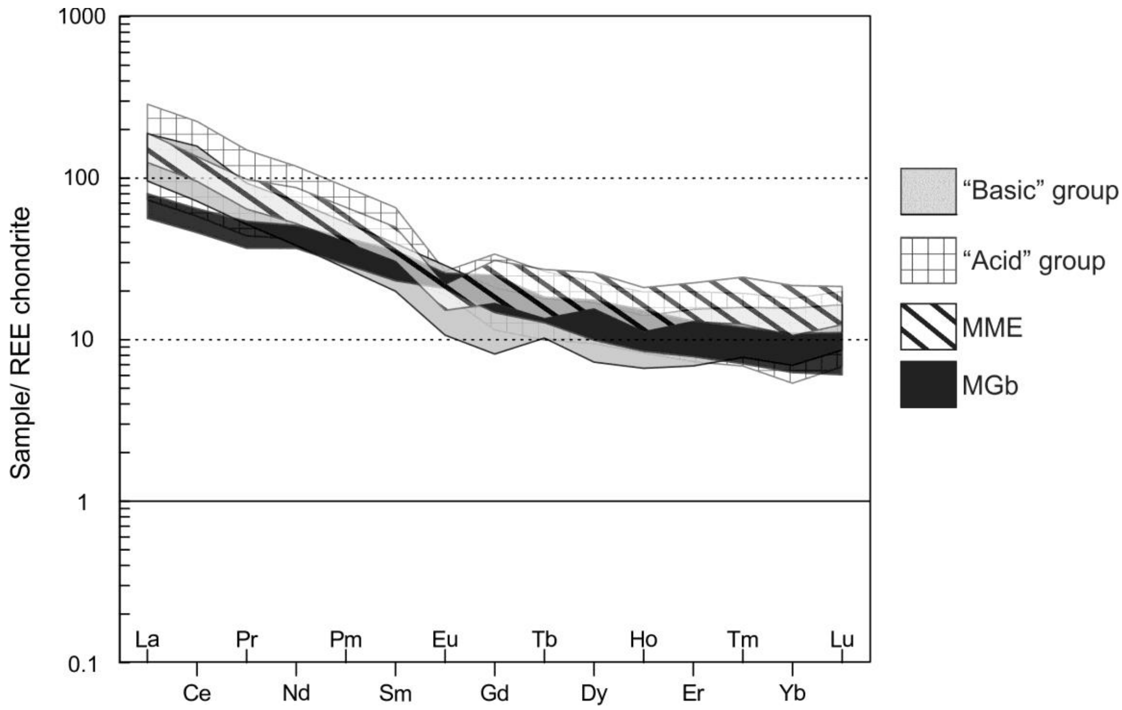

Figure 3.3.7 REE spider diagram patterns of all petrographic types. Normalisation values from *Boynton (1984)*

3.3.5 Sr, Nd and Pb bulk rock isotope composition

The Sr, Nd and Pb bulk rock isotope composition for the rock groups of XPC is given in Appendix B. All isotopic data for Sr, Nd and $^{207}Pb/^{206}Pb$ $^{206}Pb/^{204}Pb$ are from *Christofides et al. (2012, 2014)* and have been presented only graphically while the $^{208}Pb/^{204}Pb$ are unpublished and are presented here for the first time.

In ***Fig. 3.3.8*** the initial Sr ratio versus initial Nd ratio is presented. Both "Basic" and "Acid" group display similar Sr and Nd isotopic ratios and plot between the EM-I and EM-II mantle reservoirs on a mixing line between a depleted mantle component and an enriched crustal one. The MGb rocks show the most depleted isotopic composition. MME isotopic ratios resemble the "Acid" group ratios. It is worthy to note that the "Acid" group displays similar isotopic ratios with the more mafic members of XPC. In general, all samples show rather depleted isotopic contents towards the DMM and/or EAR reservoirs implying mixed reservoir origin.

Pb bulk rock isotope data can provide further information on the origin of the rocks. As shown in ***Fig. 3.3.9***, the MGb rocks show the lowest $^{207}Pb/^{206}Pb$,

$^{208}Pb/^{206}Pb$ and $^{206}Pb/^{204}Pb$ of all XPC rocks while the "Basic" the "Acid" group and the MME share similar $^{207}Pb/^{206}Pb$ and $^{208}Pb/^{206}Pb$ ratios. However there is a thin distinction between the "Acid" and the "Basic" group with the MME holding an intermediate position. The rocks of the "Acid" group show slightly lower $^{207}Pb/^{206}Pb$ and $^{208}Pb/^{206}Pb$. All samples roughly lie on a mixing trend line between a depleted component and a more enriched component. It is safe here to be refered to a straight mixing line since the Pb isotopes both are divided with the ^{204}Pb isotope.

Fig. 3.3.10 for ^{208}Pb isotope is better clarifying the nature of the depleted component since the ^{208}Pb isotope is a good tracer especially for the asthenospheric contribution. As it is indicated the depleted reservoir is probably the DMM and is unlikely to be the EAR.

The upward trend and increase in the $^{207}Pb/^{204}Pb$ and $^{208}Pb/^{204}Pb$ ratios indicates involvement of crustal material. Unfortunately there are no Pb isotope data available for the RM metamorphics to compare. Nevertheless, this is essential information regarding the less differentiated rocks and their origin and as for the more felsic rocks regarding the degree of crustal contamination. The Pb isotopic composition of the mafic rocks coupled with the Sr and Nd isotopic composition indicate an origin of both depleted (mantle) and enriched (crust) component. However, due to the Sr and Nd isotopic composition the enriched crustal material from the RM metamorphics should be excluded for most of the mafic members and the most possible crustal component candidates should be the slab subducted sediments. However, in ***Fig. 3.3.9*** it appears that the enclcaves and the "Acid" group, with few samples from the "Basic" group which appear to be separated from the other mafic rocks, show a cross-cutting trend with the other rocks and in ***Fig. 3.3.10*** they show parallel rends. This probably implies a different source material or either a different crustal component evolving in the genesis and evolution of these groups

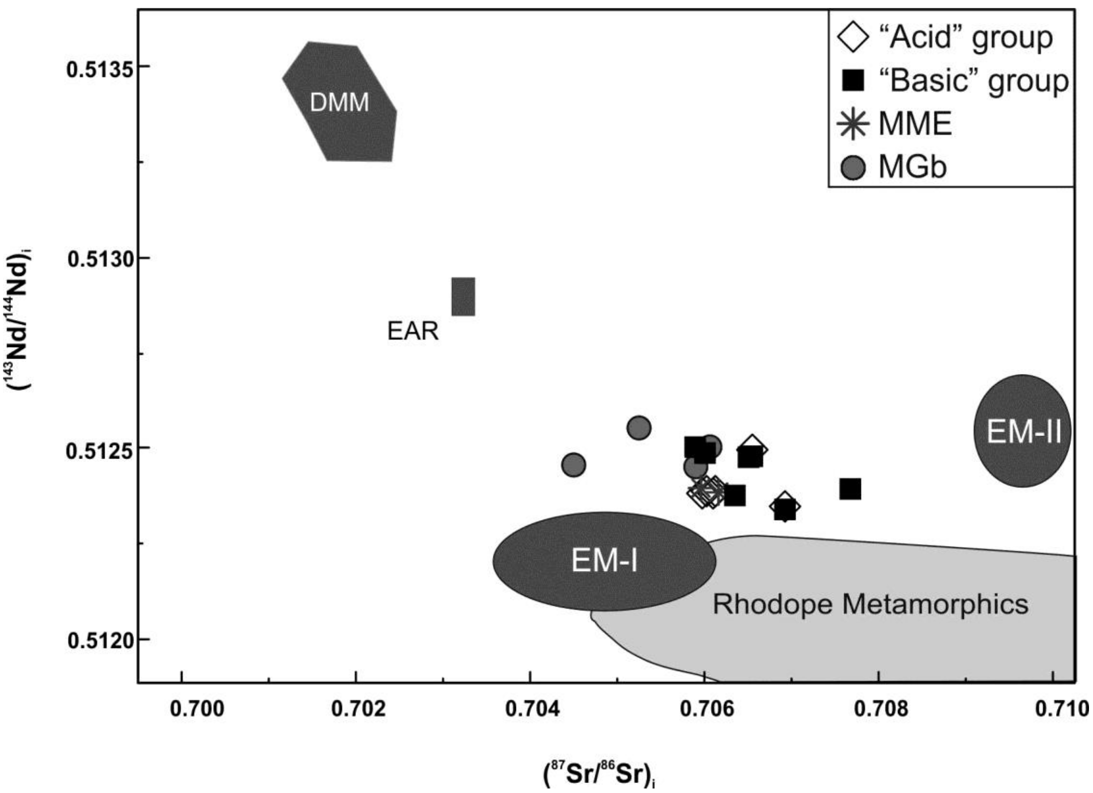

Figure 3.3.8 ($^{87}Sr/^{86}Sr)_i$ versus ($^{143}Nd/^{144}Nd)_i$. The fields illustrated are; DMM=Depleted Morb Mantle, EM-I=Enriched Mantle I, EM-II=Enriched Mantle II after *Zindler & Hart (1986*). EAR=European Asthenospheric Reservoir after *Cebria & Wilson (1995),* Rhodope metamorphics after *Cornelius (2008) and Castorina et al. (2014)*

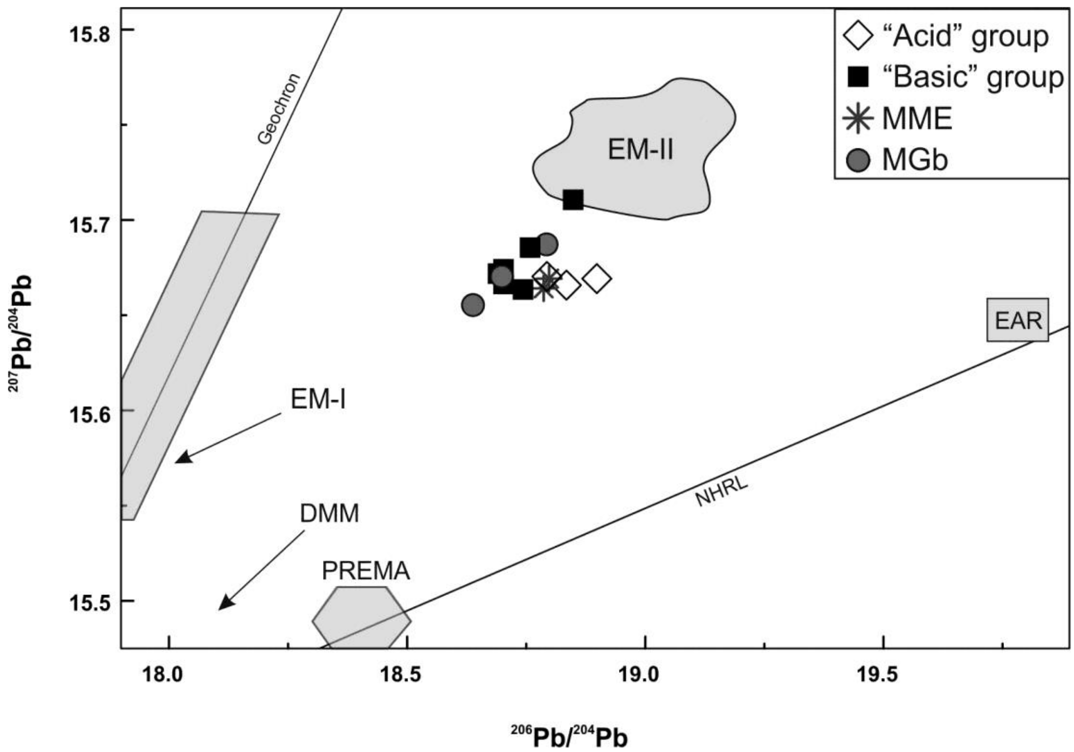

Figure 3.3.9 $^{207}Pb/^{204}Pb$ versus $^{206}Pb/^{204}Pb$. The fields illustrated are; The fields illustrated are; DMM=Depleted Morb Mantle, EM-I=Enriched Mantle I, EM-II=Enriched Mantle II after *Wilson (1989)*. EAR=European Asthenospheric Reservoir after *Cebria & Wilson (1995)*. NHRL after *Hart (1984)*

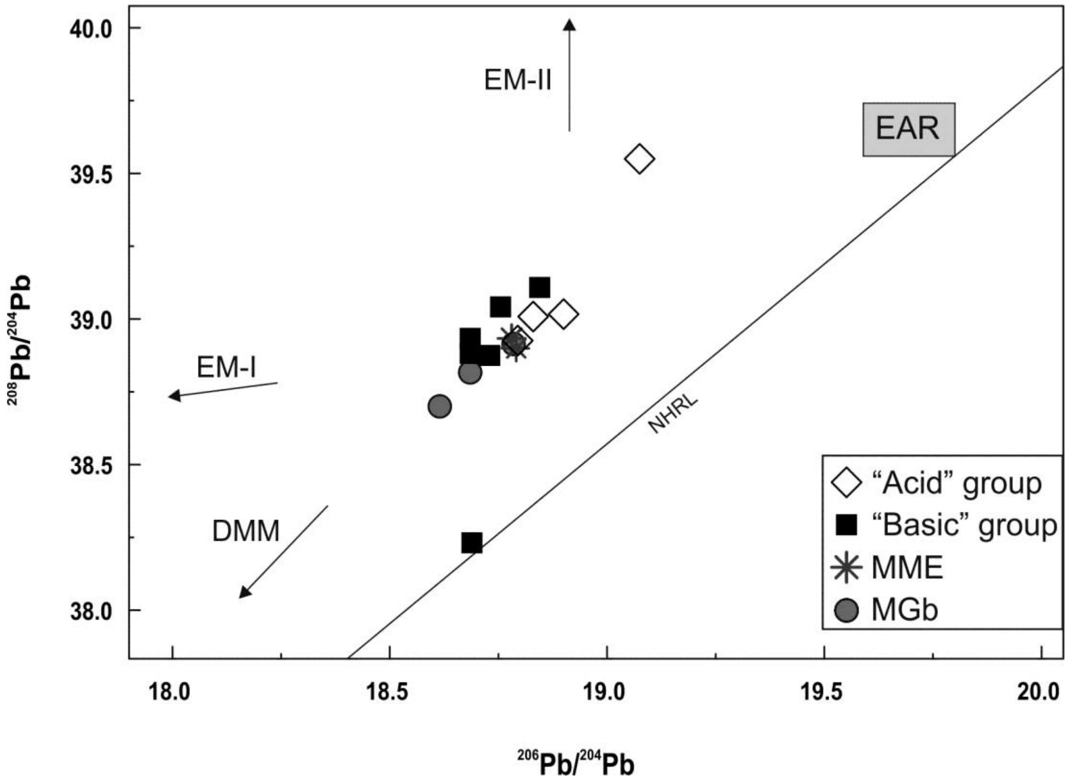

Figure 3.3.10 $^{208}Pb/^{204}Pb$ versus $^{206}Pb/^{204}Pb$. The fields illustrated are; The fields illustrated are; DMM=Depleted Morb Mantle, EM-I=Enriched Mantle I, EM-II=Enriched Mantle II after *Wilson (1989)*. EAR=European Asthenospheric Reservoir after *Cebria & Wilson (1995)*. NHRL after *Hart (1984)*

3.3.6 Petrogenetic implications

Mixing seems to play a major role in the evolution of XPC rocks although a specific mixing model has not been defined yet from previous authors and is beyond the scope of the present study. MGb plays a key role in the evolution of the XPC rocks and seems to be related with the "Basic" group. They are the most mafic members of the XPC, apart from the cumulitic gabbros, and present a mantle derived character taking into account their incompatible element depletion, the lack of Eu anomaly, the isotopic ratios depletion and the high mg#. They have probably been subjected to a differentiation process either during the formation of the cumulitic gabbros or fractionation during the ascendance of their magma. The "Basic" group presents a strongly differentiated picture and in most cases its more felsic members display strong enrichment in incomptatible elements even stronger than the "Acid" group. The MME follow the trends of the "Acid" group in most cases but they are depleted in K. They sometimes stand in the middle between the "Acid" group and the more mafic members of the "Basic" group for trace as well as for isotopes. Whether the MME are the mixing result between the MGb and the "Acid" group it can not be clarified. Although mixing is definitely a process which leads the evolution of the XPC, the exact process can not be estimated. The evolution of some monzonite rocks of the "Basic" group seems ambiguous for they display different trends from the rest fo the "Basic" group rocks.

The isotopic composition of the XPC rocks provide very important information regarding the origin as well as the evolution of the XPC. It is important to note here that the MGb rocks are the less differentiated rocks of the XPC with high mg# and are suitable indicators for the origin of the XPC. Most of the rocks show origin from mixed reservoirs regarding their Sr_i, Nd_i and Pb isotopic composition. Some MGb rocks especially, display highly depleted isotopic composition which indicates the involvement of a depleted reservoir either the DMM or the EAR. Pb isotopes give a more detailed picture. The ^{207}Pb isotope indicates a DMM component rather than a EAR mixed with a crustal one. Pb isotopes also indicate two different trends probably related to different sources or crustal material evolved. One scenario could be two different mantle derived mafic magmas originated from unhomogenized metasomatized mantle, one depleted in LILE and LREE represented by the MGb group and one more enriched represented by the most mafic rocks of the "Basic" group to be the source of the XPC. It's unlikely that all rocks from the "Basic" group to have been evolved from the GBd group since trace element patterns and trace element cross-cutting trends do not suggest this. Further evolution into the Rhodopian crust and interaction with it could give genesis to the more felsic members of the XPC. However, this probably comprises a composite evolution and its beyond the scope of this study.

3.4 The Vrondou Pluton

3.4.1 General

The Vrondou complex (***Fig. 3.4.1***) is located close to the Greek-Bulgarian borders, north of Serres in Central Macedonia, Northern Greece. It is a north-eastwards elongated composite pluton (covering more than 250 Km^2) intruding gneisses, amphibolites and marbles of the LTU of the Western Rhodope massif (*Soldatos et al., 1998* and references therein). Small and large pockets of the crystalline basement, ranging up to several tens of meters, are found within the pluton, especially in the southern part. To the eastern and north-eastern margins of the pluton a clear contact aureole has been developed (*Kolocotroni, 1992* and references therein). The pluton is, in general, undeformed. However, the southern and western parts are slightly to intensively deformed by a flat-lying shear system, which has led to mylonitic foliation and SW-plunging stretching lineation (*Kolocotroni, 1992*). The resulting gneissic texture becomes progressively clearer towards the southern margins. Recrystallized quartz, feldspars and mafic minerals are a common feature of the more deformed rocks. The field relations of the various rock-types are rather obscure, apart one case in the eastern part of the pluton where a sharp contact between a medium-grained granodiorite and a coarse-grained quartz monzonite was found. Leucocratic dykes, mainly aplitic and occasionally pegmatitic, are encountered throughout the entire plutonic body. In contrast, microgranular enclaves with ellipsoidal or irregular shapes, up to 30 cm in diameter, are present only in the north-eastern part of the pluton. A small elongated gabbro-dioritic body with sharp contacts with the granodiorite outcrops in the south-eastern part of the pluton. Rounded to angular blocks of diorite are enclosed in the granodiorite with a similar aspect to magmatic breccia. In some cases gabbro shows clear cumulate features. Finally, hornblende-rich lamprophyric dykes occur in the southern margins of the pluton (*Kolocotroni, 1992*). *Papadakis (1965)* measured 54.9 ± 4.2 Ma with K-Ar dating on a hornblende separate, whereas an Oligocene age was obtained at 34±2 to 30±1 Ma with the same K/Ar method on hornblende by *Marakis, (1969)* and biotite at 30 ± 3 Ma by *Dürr et al. (1978)*. A similar age (30.82 ± 14.8 Ma) based on

Rb-Sr whole-rock data was accepted by *Kolocotroni (1992)*, although the error is considered high. It must be noted here that *Meyer & Pilger (1963)* suggested an older age for the western part of the Vrondou pluton, thus supporting a non-simultaneous formation. In contrast, *Kaufman (1976)* suggested a mid-Oligocene emplacement age for the eastern undeformed part of the Vrondou pluton, while the strongly mylonitic western part may have been emplaced in earliest Miocene time.

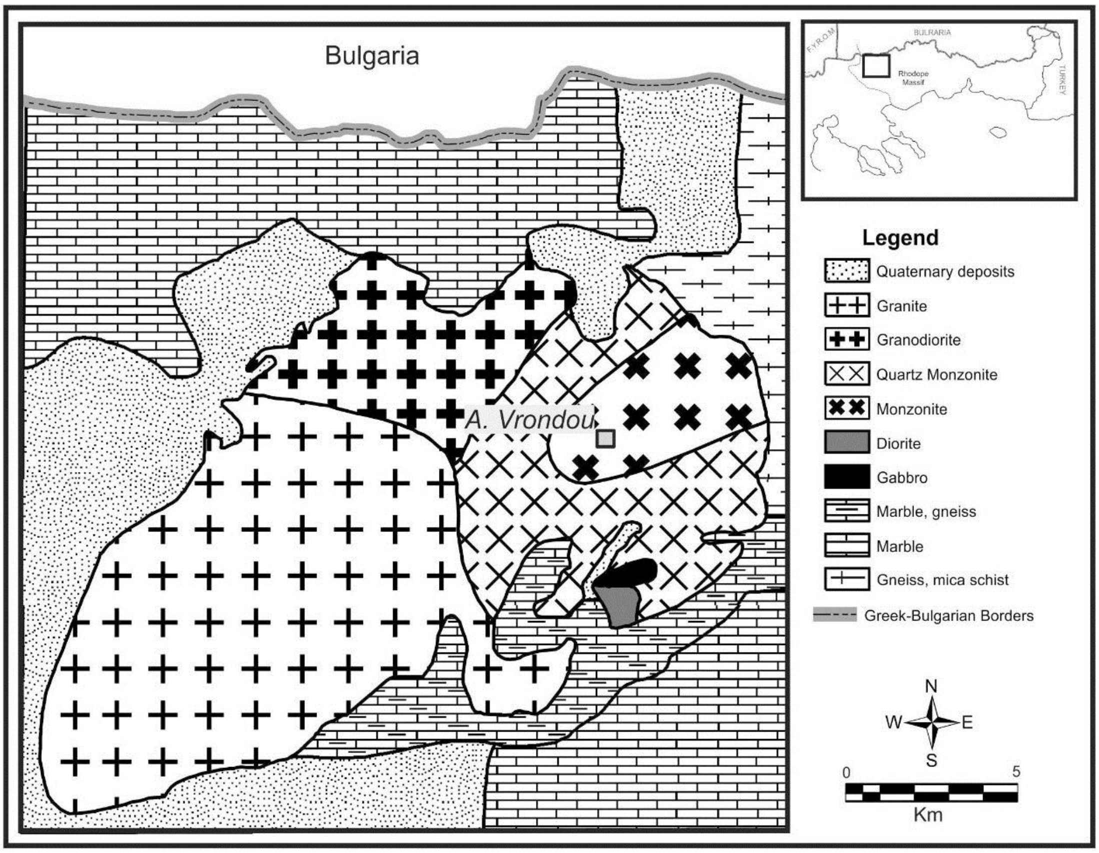

Figure 3.4.1 Simplified Map of the Vrontou pluton, modified after *Soldatos et al. (1998)*

3.4.2 Petrography and Mineralogy

On the normative Q-ANOR classification diagram (***Fig. 3.4.2*** the rocks are classified as quartz monzonite, granite (granite + monzogranite), granodiorite, monzonite, quartz monzodiorite, quartz syenite, diorite and gabbro. The petrographic and mineralogical description is given by *Soldatos et al. (1998* and references therein*)*. In the present study the majority of the rocks collected are mafic microgranular enclaves, gabbros and diorites and few monzonites and quartz-monzonites.

Based on petrographical and geochemical data of the previous authors the above rock-types are mainly grouped and will be used from now on in the following groups: 1) **GBDR**: gabbros and diorites; 2) **MZ**: monzonites; 3) **QMZ**: quartz monzonites and granodiorites; 4) **QSY-GR**: quartz syenites; 5) **Low-K MME**; 6) **High-K MME**

GBDR: medium- to coarse-grained gabbros and fine- to medium-grained diorites. Gabbros bear plagioclase, hornblende, clinopyroxene, and rare olivine and orthopyroxene; Diorites bear plagioclase, hornblende and biotite. Olivine and orthopyroxene appear auhedral to anhedral and in symplectitic intergrowths with opaque oxides. Orthopyroxene is enstantite. Clinopyroxene is of diopsidic composition coexisting with hornblende. It appears as euhedral to anhedral crystals or as irregular relics of variable size in hornblende and is often altered to actinolitic amphibole along cleaveages or margins. Hornblende is euhedral to subhedral of green-brown colour and is classified mainly as magnesio-hornblende. Plagioclase in unzoned, euhedral to subhedral with oligoclase to labradorite in composition. The accessory phases are titanite, apatite, zircon, opaques and spinel in gabbros.

MZ: coarse-grained monzonites, coarse-grained clinopyroxene-bearing quartz monzonites, and coarse-grained quartz monzodiorites with clinopyroxene + hornblende ± biotite; Clinopyroxene is euhedral to abhedral of diopsidic composition coexisting with hornblende. Hornblende is euhedral to subhedral with green-brown colour and is classified mainly as magnesio-hornblende and less as tschermakitic, edenitic and magnesian hastingsitic hornblende and it sometimes preserves clinopyroxene cores. Plagioclase is euhedral to subhedral and exhibits slight to extensive normal and oscillatory zoning, and not rarely patchy cores. Fine-grained, euhedral plagioclase occurs as inclusion in K-feldspars. Biotite exhibits euhedral to subhedral crystals, brown to straw yellow in colour. In some samples, biotite occurs as very fine rounded inclusions. It is often partly altered to chlorite. Compositionally biotite from clinopyroxene-bearing monzonite is more Ti and Mg richer (Mg#>60) than that from other rock-types (Mg#<60). K-feldspar is orthoclase, often twinned after the Carlsbad law and occurs as a groundmass mineral and as megacrysts in the porphyritic rocks. It appears in euhedral to subhedral crystals, but also as big irregular crystals poikilitically including all other phases. The accessory phase are titanite, apatite, zircon and opaques

QMZ: clinopyroxene-free coarse-grained quartz monzonites showing often porphyritic texture and medium- to coarse-grained granodiorites occurring mainly in the central-northern part of the studied area, and as small masses in other places. Hornblende is euhedral to subhedral with green-brown colour and is classified mainly as magnesio-hornblende and less as tschermakitic, edenitic and magnesian hastingsitic hornblende and it sometimes preserves clinopyroxene cores. Plagioclase is euhedral to subhedral of oligoclase to labradorite composition. K-feldspar is microcline and occurs as a groundmass mineral and as megacrysts in the porphyritic rocks. It appears in euhedral to subhedral crystals, but also as big irregular crystals poikilitically including all other phases. Not uncommonly, K-feldspar contains inclusions of plagioclase and mafic minerals and often is twinned after the Carlsbad law. The accessory phases are titanite, apatite, zircon and opaques

QSY-GR: coarse-grained quartz syenites and medium- to coarse-grainedgranites. Quartz syenites have the same mineralogy with granite except that hornblende is the main or the only ferromagnesian mineral. Hornblende is euhedral to subhedral of green-brown colour and is classified mainly as magnesio-hornblende and less as tschermakitic, edenitic and magnesian hastingsitic hornblende. Plagioclase is euhedral to subhedral and exhibits slight to extensive normal and oscillatory zoning, and not rarely patchy cores. Fine-grained, euhedral plagioclase occurs as inclusion in K-feldspars. Biotite (Mg#<60) exhibits euhedral to subhedral crystals brown to straw yellow in colour. It is often partly altered to chlorite. K-feldspar is microcline and occurs as a groundmass mineral and as megacrysts in the porphyritic rocks. It appears in euhedral to subhedral crystals, but also as big irregular crystals poikilitically including all other phases. The accessory minerals are titanite, apatite, zircon and opaques

Low- and High-K Mafic Microgranular Enclaves (Low- and High-K MME): Abundant mafic microgranular enclaves occur in the plutonic rocks of the eastern and northern part. The enclaves have mostly the same mineral assemblage present in the host rock and are more fine-grained holocrystalline rocks with equigranular subophitic matrix. They mainly classify as diorite and monzodiorite consisting of plagioclase + hornblende ± clinopyroxene ± biotite ± K-feldspar + accessories (the accessory phases are titanite, apatite, zircon, opaques). There are two types of enclaves; the first type (Low-K MME) contains abundant hornblende and subordinate biotite, while the second type (High-K MME) consists of hornblende and clinopyroxene with clinopyroxene occurring as independent crystals and/or relics in hornblende cores. This group is also characterised by the presence of abundant K-Feldspar which poikiltically includes the other phases.

3.4.3 Major Element Geochemistry

The geochemical data used here are a combination of *Soldatos et al. (1998)* data, *Soldatos unpublished* data provided for the present study and the new data of the present study. They are all presented in Appendix A**.** For the needs of the present study the six groups referred above will be used. In ***Fig. 3.4.2*** the QANOR diagram is presented with all new and old data.

It is noteworthy that the Low-K MME and the GBDR groups show similar behavior on the QANOR diagram while the High-K MME show simiral behavior with the MZ. The GBDR group of Vrondou pluton shows variable cumulitic affinity but will not be excluded here since it is the most mafic groups of the Vrondou and if treated with caution can give important evidence for the Vrondou pluton. Moreover its cummulitic affinity does not seem to remarkably affect the major element variation.

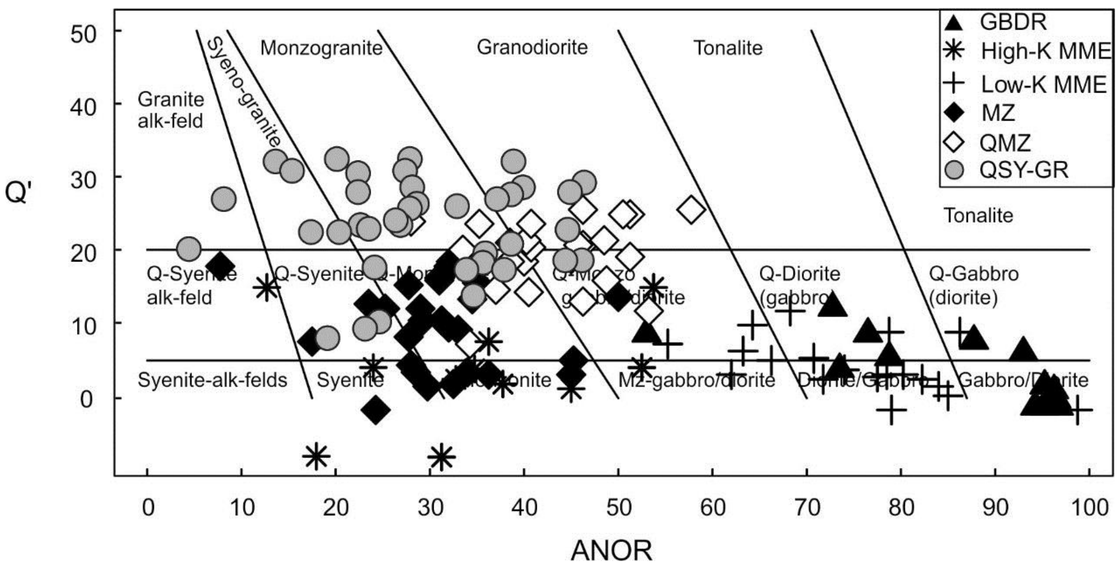

Figure 3.4.2 Q-ANOR classification diagram after *Streckeisen & Le Maitre (1979)*

The same picture is displayed in ***Fig. 3.4.3***. Most of the Low-K MME follow the GBDR in Calc-alcaline series while the High-K MME follow the MZ in Shoshonitic series. However there are few GBDR rocks which show shoshonitic character. The QMZ rocks show High-K calc-alkalline character and the QSY-GR rocks straddle between the High-K calc-alkaline series and the Shoshonite series. The MME are clearly distinguished here with the Low-K MEE belonging to the Calc-alkaline and High-K series, while the High-K MME to the Shoshonite series. In ***Fig. 3.4.4*** the variation diagrams of the major elements are presented. In all variation diagrams, apart from the K_2O, Na_2O and P_2O_5, the groups display good negative correlation with SiO_2. On the K_2O diagram though, the groups define two distinct trends, the first with the low-K MME, part of GBDR, the QMZ and the QSY-GR and a parallel second trend with part of the GBDR, the High-K MME and the MZ. The High-K MME present higher K_2O but lower Na_2O contents than the low-K enclaves. The GBDR, High-K and Low-K MME show increase P_2O_5 with SiO_2 while the rest groups decrease. Many GBDR, Low-K MME, hi-K MME and monzonites display high mg# (>50%) and there is especially one High-K MME (SB-38X) which displays the highest mg# of all rocks despite the higher SiO_2 content . This sample displays also remarkably high TiO_2, MgO, CaO, and P_2O_5 content but low Al_2O_3 and Na_2O and appears significantly less differentiated than the majority of the GBDR rocks, at least for the major elements apart from SiO_2.

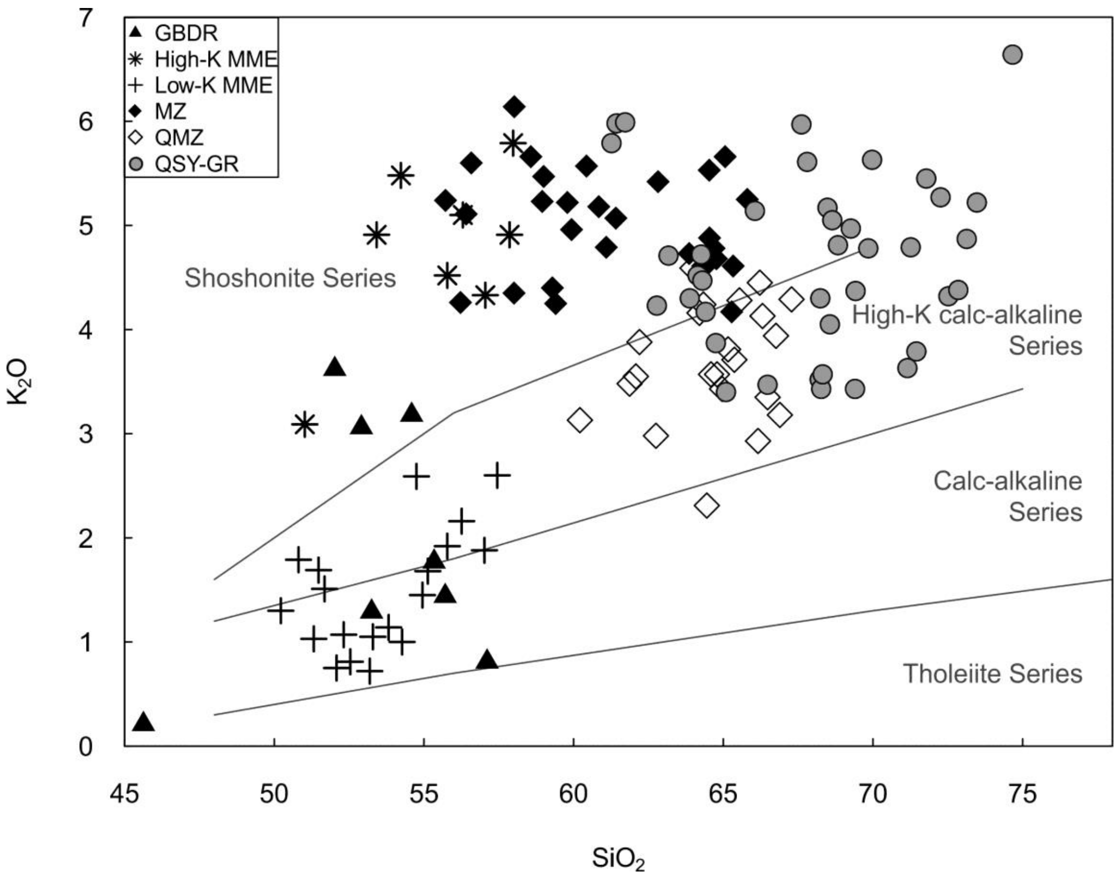

Figure 3.4.3 SiO_2 versus K_2O diagram after *Peccerillo & Taylor (1976)*

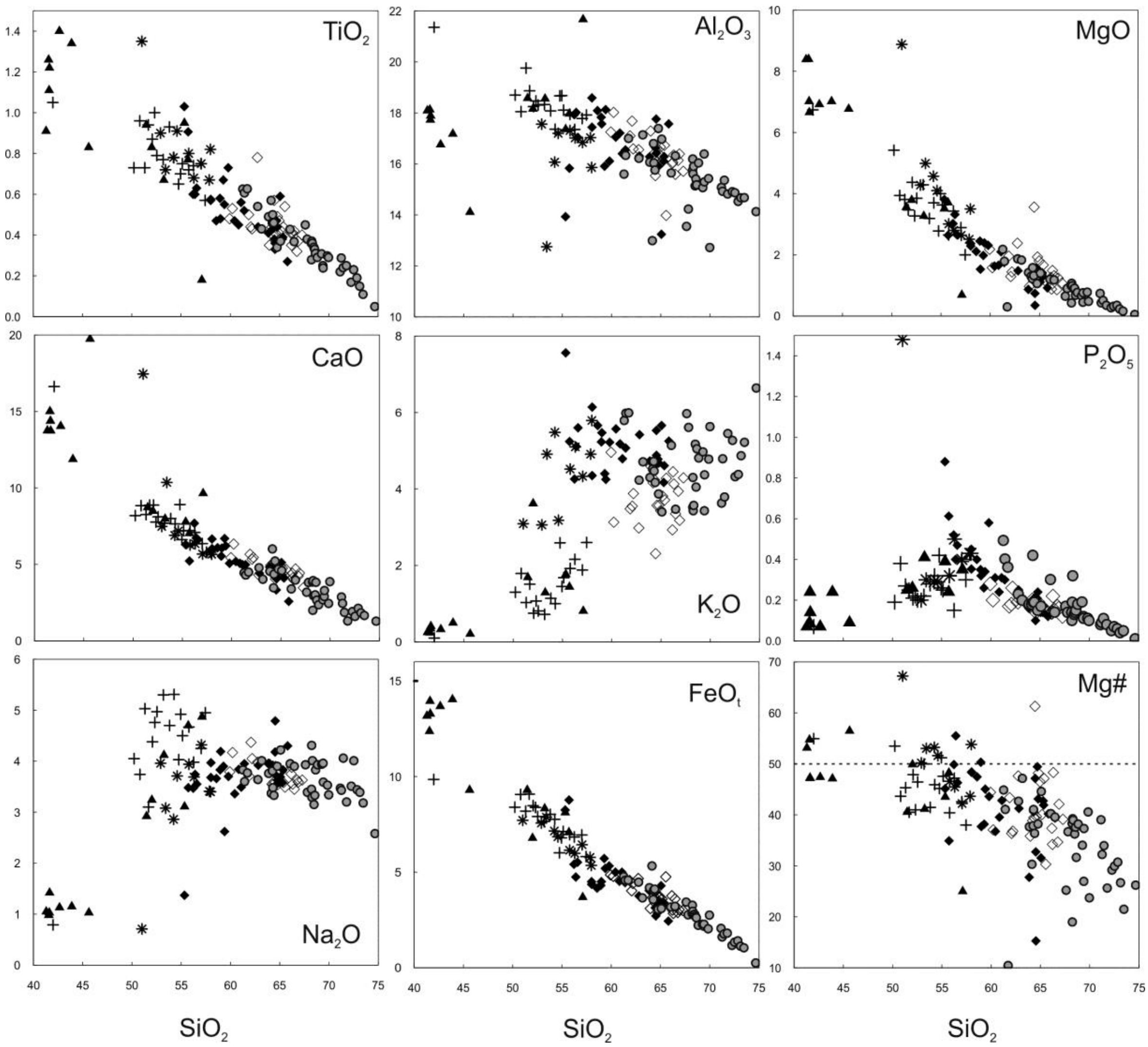

Figure 3.4.4 Variation diagrams for major elements. Symbols as in Fig. 3.4.2

3.4.4 Trace Element Geochemistry

In the trace element variation diagrams (***Fig. 3.4.5***) the trends of the different grups are roughly distinguished. For the GBDR, the High-K and Low-K MME groups Ba, Zr, Y, Nb behave incompatibly while behave compatibly for the rest of the groups. Sr behaves incompatibly for the QSY-GR and the QMZ group but is scattered for the other groups. Rb behaves incompatibly for the MME groups, but not clear trends are displayed for the other groups. V behaves comtatibly for all groups while Pb, U and Th behave for all groups incompatibly. La and Ni are scattered but there are some MZ and High-K samples that display high Ni contents.

The High-K MME sample mentioned in the previous paragraph displays remarkable high contents also in trace elements such as Y, Ni, Th, Nb and La.

The trace multi-element primitive mantle normalised patterns fo the MZ, QMZ, High-K and Low-K MME are presented in ***Fig. 3.4.6***. Therefore, the MME groups are presented with the host group they are found with. The QSY-GR group is not presented here due to its lack in mafic rocks that are the main subject of this study. The GBDR group was considered better not to be presented here due to its cumulitic character that, contrary to the major elements, affects mainly the trace element and REE patterns. The MZ trace element patterns display typical features of convergent boundaries geotectonic settings such as the TNT (Ta, Nb, Ti) negative anomalies (***Fig. 3.4.6***). On the other hand the High-K MME patterns display differences. The Nb-Ta negative anomaly becomes slighter and there is one sample (SB-38X) which does not display a clear Nb-Ta anomaly but rather a slight positive Ta anomaly. The same sample does not display either Pb positive anomaly and has positive P anomaly. The REE chondrite normalised patterns of the same groups are presented in ***Fig. 3.4.7***. All groups display LREE enrichment, all High-K MME display Eu negative anomaly but MZ display negligible Eu anomaly. The QMZ and Low-K MEE display similar patterns but Low-K MME are more depleted in LILE and have negligible K positive anomaly and Ti negative anomaly (***Fig. 3.4.6***). On the other hand their host rock (QMZ) displays negative Eu anomaly, but the Low-K MME do not (***Fig. 3.4.7***). The HREE horizontal patterns of the Low-K MME ($Tb_{cn}/Lu_{cn}<1$) show a garnet-free source for these rocks if we assume that the more mafic members of these rocks are not remarkably differentiated magmas while all the other groups show a garnet bearing source.

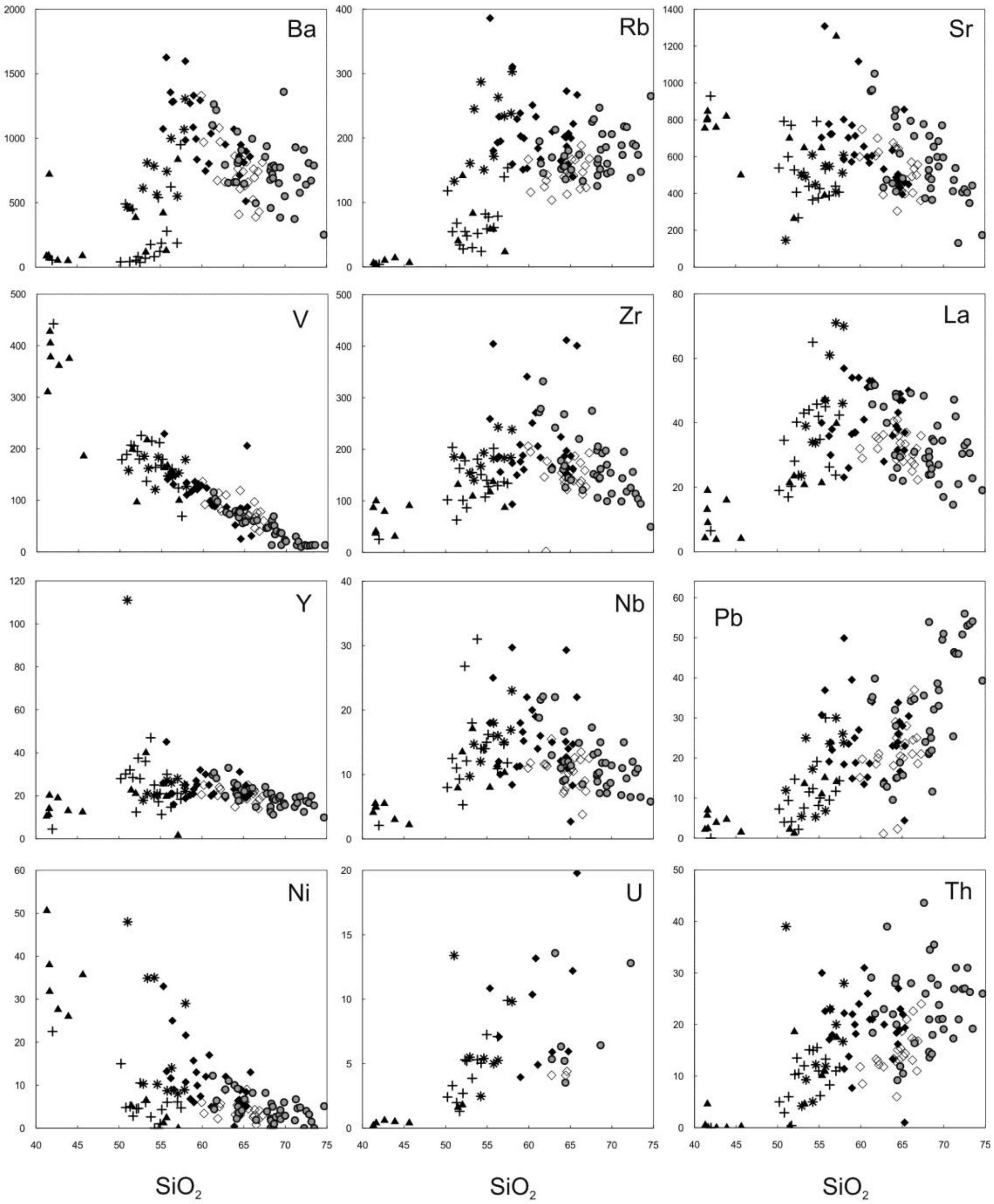

Figure 3.4.5 Variation diagrams for selected trace elements. Symbols as in Fig. 3.4.2

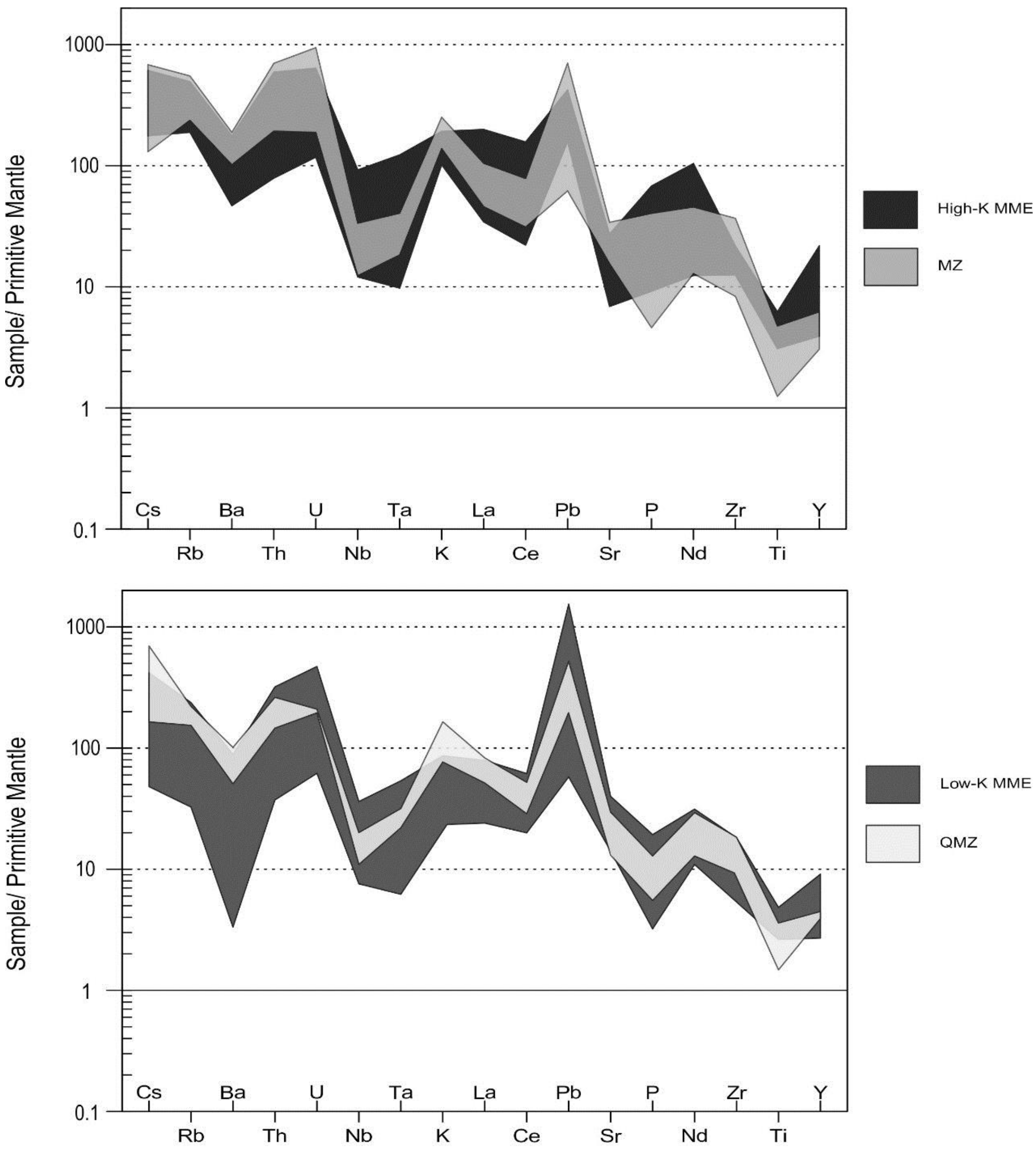

Figure 3.4.6 Multi-element spider diagram patterns. Normalisation values from *Sun & McDonough (1989).*

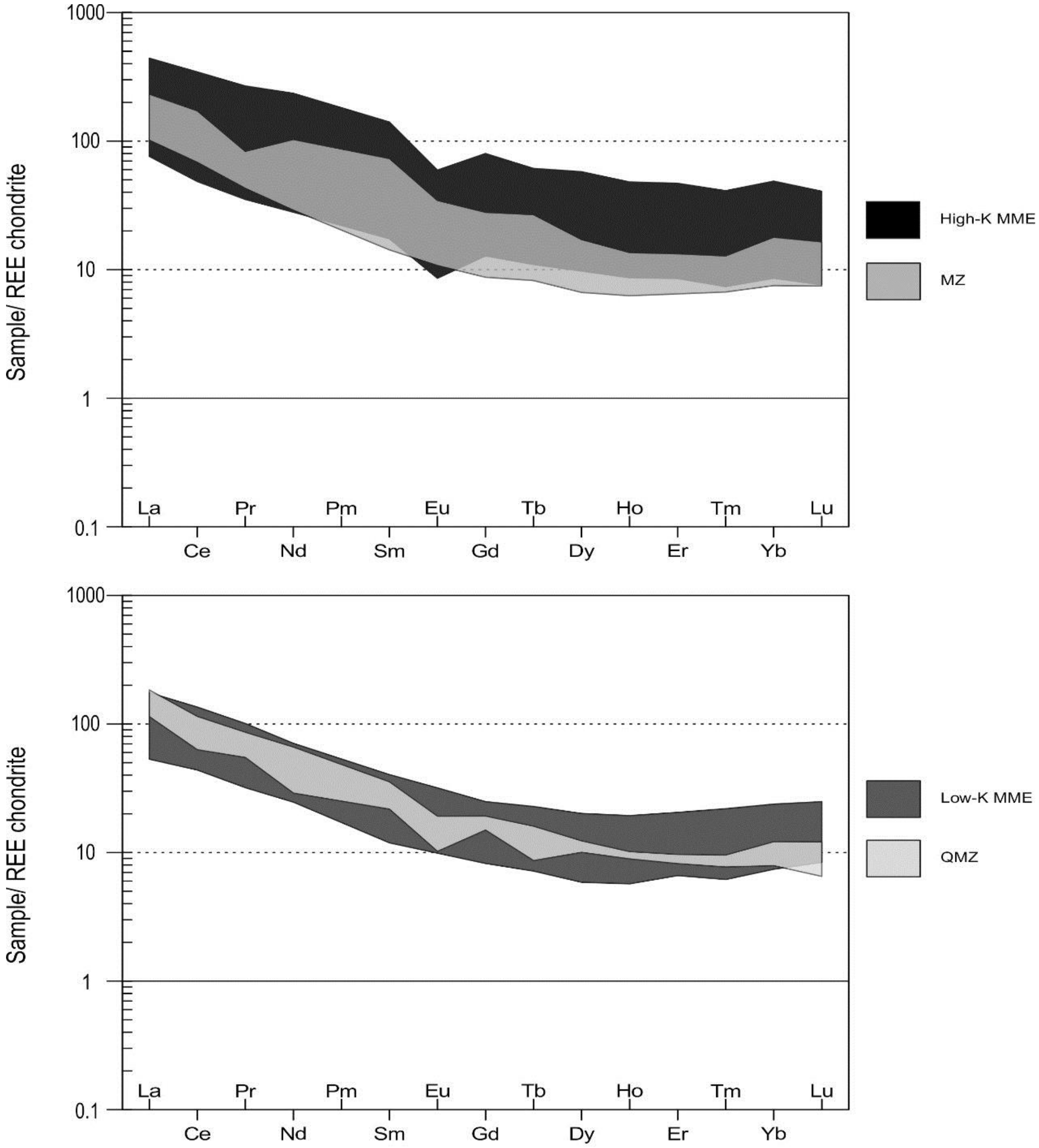

Figure 3.4.7 REE spider diagram patterns. Normalisation values from *Boynton (1984)*.

3.4.5 Sr and Nd bulk rock isotopic composition

The bulk rock Sr and Nd isotopic composition of the Vrondou pluton are presented in ***Fig. 3.4.8***. The isotopic composition is given in Appendix B. The initial isotopic Sr and Nd ratios of the GBDR have more depleted isotopic characteristics relative to the other groups. Although these rocks have cumulitic character, the Sr and Nd isotopic compositions are not affected during the cumulitic process and can be safely used here. More enriched relative to the GBDR are the MME groups. MZ, QMZ and QSY-GR groups display stronger enrichment in Sr_i and depletion in Nd_i with one QMZ showing crustal isotopic ratios. Nevertheless, all groups display mixed sources most probably between the DMM and/or EAR and an enriched crustal component.

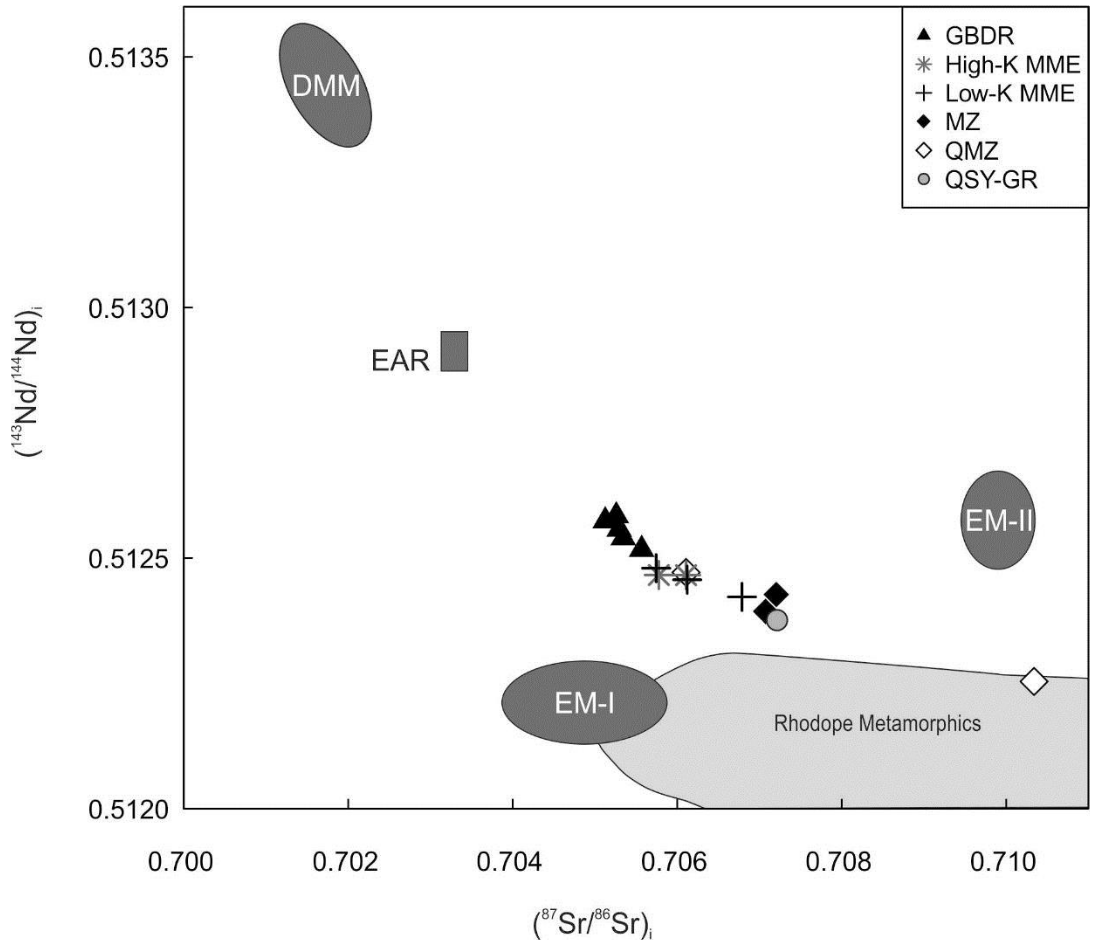

Figure 3.4.8 $(^{87}Sr/^{86}Sr)_i$ versus $(^{143}Nd/^{144}Nd)_i$. The fields illustrated are; DMM=Depleted Morb Mantle, EM-I=Enriched Mantle I, EM-II=Enriched Mantle II after *Zindler & Hart (1986)*. EAR=European Asthenospheric Reservoir after *Cebria & Wilson (1995)*, Rhodope metamorphics after *Cornelius (2008) and Castorina et al. (2014)*

3.4.6 Petrogenetic Implications

The basic lithogeochemistry of some rocks of the Vrondou favour for mantle-derived melts. However, they present enriched LILE and LREE implying that they were subjected in differentiation during their ascend from the mantle in the Rhodopian crust. The isotopic characteristics of the more felsic rocks coupled with their major and trace element characteristics and the presence of numerous enclaves favour for a mixing process in the Rhodopian crust between a mantle derived end-member similar to the Vrondou enclaves and a felsic component like the crustal rocks of the RM.

Soldatos et al. (1998) proposed at least four different parental magmas in the genesis of the Vrondou complex: the more basic rocks of the QSY-GR group outcropping in the southwestern area; the shoshonitic lamprophyres outcropping in the southern area, and believed to be the precursor of the High-K MME; the gabbro-dioritic rocks outcropping in the south-eastern area, and believed to be the precursor of the Low-K enclaves; the two acid magmas that have undergone processes of mixing with the latter two to give the range of the MZ group and QMZ group rocks.

All geochemical data presented above indicate that the High-K MME are slightly differentiated rocks with one MME (SB-38X) displaying primitive features such as high MgO (8.88 wt. %), mg# (67.2%), Ta positive anomaly, P positive anomaly and high Ni, Cr, Y, Nb and Ce/Pb (23.4) contents. On the other hand it displays also evolved features. *Soldatos et al. (1998)* suggested that the High-K MME are slightly evolved magmas from lamprophyric parental sources. The presence of lamprophyres in the area, with which this sample shares common features, implies that crystal fractionation had taken place prior to its genesis and resulted in the more evolved High-K MME magma. The enriched features of these rocks couldn't have been the result of mixing with crustal material, otherwise the primitive features would have been overprinted, but most possibly was inherited from an enriched lithospheric mantle source which is the same source of lamprophyres. *Soldatos et al. (1998)* proposed a garnet bearing source which is consistent with the HREE patterns of all the groups apart from the Low-K MME. The MZ group rocks as indicated from the previous authors can be derived from the mixing between the High-K MME and anatectic magmas of the lower-middle continental crust.

The Low-K MME display different features from the High-K MME. In most variation diagrams they are clearly separated from the High-K MME. They have typical tarce element and REE patterns of convergent boundaries magmas but small positive K anomaly and do not display Eu anomaly. Many of these rocks display the least enriched LILE relative to HSFE among all the other groups. *Soldatos et al. (1998)* proposed different parental magmas for the the MME groups and related the Low-K MME with the GBDR. These evidence infer two variably enriched mantle sources for the Vrondou mafic rocks. Melts from these sources evolved through interaction with crustal rocks of the RM and gave genesis to the wide spectrum of the Vrondou pluton rocks.

3.5 The Maronia Pluton

3.5.1 General

The Maronia pluton is situated south of the Komotini town, in Southwest Thrace intruding the CRB. It intrudes marbles of the metasedimentary series of the Makri unit causing a rather wide zone of contact metamorphism (skarn). Eastwards it intrudes a metamorphic sequence of phyllites, greenschists and gneisses of the overlying metavolcanosedimentary series of the same unit (***Fig. 3.5.1***) causing intense thermal metamorphism to the surrounding rocks (hornfelses), while southwards the pluton itself is intruded by a small body of porphyritic micro-granite (*Papadopoulou et al., 2004* and references therein). The age of the Maronia pluton, based on Rb-Sr whole rock-biotite isochrones, has been determined as Oligocene (29 Ma) and is considered to be the youngest of the Tertiary plutons that intrude Thrace (*Del Moro et al., 1988; Papadopoulou, 2003*).

The rocks compose the Maronia pluton are gabbros, monzonites, quartz monzonites, monzogabbro, quartz monzogabbros, mafic microgranular enclaves. *Papadopoulou (2003)* distinguished three main rock groups: a) the Basic group which is composed of gabbros b) the Intermediate wich is composed of monzonites, quartz monzonites, monzogabbro, quartz monzogabbros and mafic microgranular enclaves and c) the Acid group which consists of granite porphyry micro-granite and aplitic veins. The porphyry micro-granite is differentiated from the other Maronia rocks. The field relationship of the rock types are not clear. Few small exposures of gabbro have been found near the center of the plutonic body. There is no clear relation of the gabbro and the rocks of the intermediate group. The granite and the aplitic dykes intrude the rocks of the intermediate group and scattered basement blocks are enclosed by the rocks of the intermediate group.

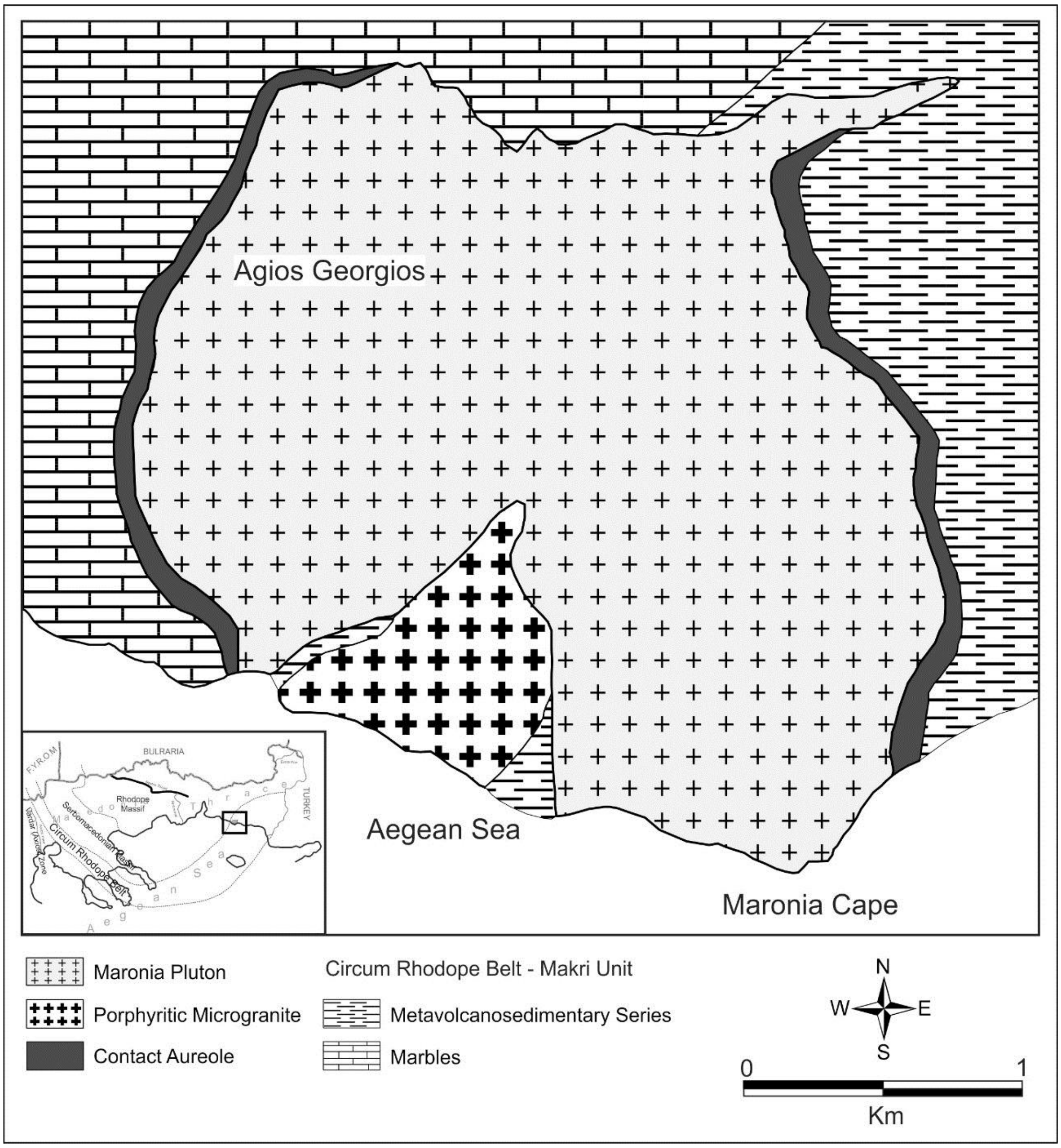

Figure 3.5.1 Simplified Map of the Maronia pluton, modified after *Papadopoulou et. al (2004)*

3.5.2 Petrography and Mineralogy

The petrography and mineralogy of the Maronia pluton has been mainly described by *Papadopoulou et al. (2001)* who distinguished three main rock groups; a)the Basic, b)the Intermediate and c)the Acid group.

The **Basic group** is composed of gabbro, a dark-coloured, medium-grained rock, having plagioclase, clinopyroxene, red-brown biotite and Fe-Ti oxides and apatite as accessory minerals. Orthopyroxene and olivine are very rare. Interstitial feldspar is also present. Orthopyroxene, is a Mg-rich enstatite and clinopyroxene is augite. Plagioclase appears in zoned crystals with the core composition ranging from An_{54} to An_{78} whereas in the unzoned antiperthitic crystals the overall composition ranges from An_{35} to An_{48}. Actinolite, resulting from the breakdown of pyroxene also exists. Biotite has a $Fe^{2+}/Fe^{2+}+ Mg^{2+}$ ratio from 0.123 to 0.501.

The **Intermediate group** is composed of monzonite, quartz monzonite, monzogabbro , quartz monzogabbro and mafic microgranular enclaves. monzonite shifts to quartz monzonite with an increase of interstitial quartz up to 6 vol%. These rocks are fine- to medium-grained with monzonitic texture. They consist of plagioclase, clinopyroxene, orthopyroxene, hornblende, redbrown biotite, orthoclase and Fe-Ti oxides and apatite as accessory minerals. Non-perthitic orthoclase encloses poikilitic ally plagioclase, biotite, orthopyroxene, clinopyroxene and Fe-Ti oxides. Patches of a second generation of K-feldspar is often recognised in the poikilitic K-feldspar. Biotite often encloses grains of accessory minerals as well as orthopyroxene and clinopyroxene. The latter is the most abundant pyroxene. Pinkish orthopyroxene is often altered to uralite. Hornblende, wherever present, occurs both as primary crystals and as an alteration product of pyroxenes. Monzogabbro grades into quartz monzogabbro with a small increase of interstitial quartz. Both rocks are coarse- to medium-grained and contain the same mineral phases as in the case of monzonite. In this rock type, the K-feldspar occupies the interstitial space between plagioclase and the ferromagnesian minerals, whereas the previously described second K-feldspar generation is missing. Orthopyroxene is more abundant than in the other rock types. Hornblende exists in smaller amounts. From monzogabbro to monzonite, an antipathetic relation seems to exist between orthopyroxene and amphibole and orthoclase. The mafic microgranular enclaves, classified as monzogabbro, are fine-grained, consisting of zoned plagioclase phenocrysts, biotite, amphibole, quartz and a few remnants of clinopyroxene phenocrysts, with smaller crystals of orthoclase, epidote and magnetite.

Orthopyroxene, is a Mg-rich enstatite and clinopyroxene is augite. Plagioclase appears in zoned crystals with the core to rim composition ranging from An_{54} to An_{78} whereas in the unzoned antiperthitic crystals the overall composition ranges from An_{35} to An_{48}. Zoning is either normal or oscillatory. Actinolite, resulting from the breakdown of pyroxene also exists. Biotite has a decreasing $Mg^{2+}/Mg^{2+}+Fe^{2+}$ ratio relative to the gabbros and is Ti rich. Amphibole is a magnesiohornblende with $Mg^{2+}/Mg^{2+}+Fe^{2+}=0.69$ to 0.91 occurring as a primary phase in a few samples of monzonite and monzogabbro. K-feldspar ranges in composition from Or_{70} to Or_{85}. The non-perthitic major K-feldspar phase contains small amounts of BaO (<1wt%). The other phase occurring as patches in the previous one, contains BaO up to 3.5 wt%.

The **Acid group** consists of granite, aplitic dykes and porphyritic micro-granite. Granite in the form of dykes , (0.5 m to a few metres thick) is a fine-grained rock having quartz, K-feldspar, plagioclase, biotite and a few accessory minerals (epidote, allanite, apatite and zircon). Porphyritic micro-granite consists mainly of quartz and perthit ic K-feldspar phenocrysts, few plagioclase phenocrysts and few microphenocrysts of biotite set in a medium-grained groundmass of quartz, K-feldspar and plagioclase. It is strongly altered, tectonised and is related with porphyry copper mineralization. Biotite has a $Fe^{2+}/Fe^{2+}+ Mg^{2+} = 0.271$ and TiO_2 reaches the content of 3.6wt%. Plagioclase has a composition of oligoclase. The K-feldspar in the Acid group has a composition of $Or_{90}Ab_{10}An_{0}$.

3.5.3 Major Element Geochemistry

The geochemical data used for the study of the Maronia pluton are a combination of *Papadopoulou et al (2004)* and new data of the present study. They are all presented in Appendix A. The three rock groups of *Papadopoulou (2003)* will be used here with the one mafic microgranular enclave treated seperately. All old and new samples are presented on a Q-ANOR classification diagram in ***Fig. 4.5.2***. The new samples of the present study belong to the Basic and Intermediate group.

All rocks show shoshonitic character apart from the mafic microgranular enclave having high-K calc-akaline character. There is an significant compositional gap of

SiO_2 between the Acid and the Intermediate group of about 7%, except one sample between them.

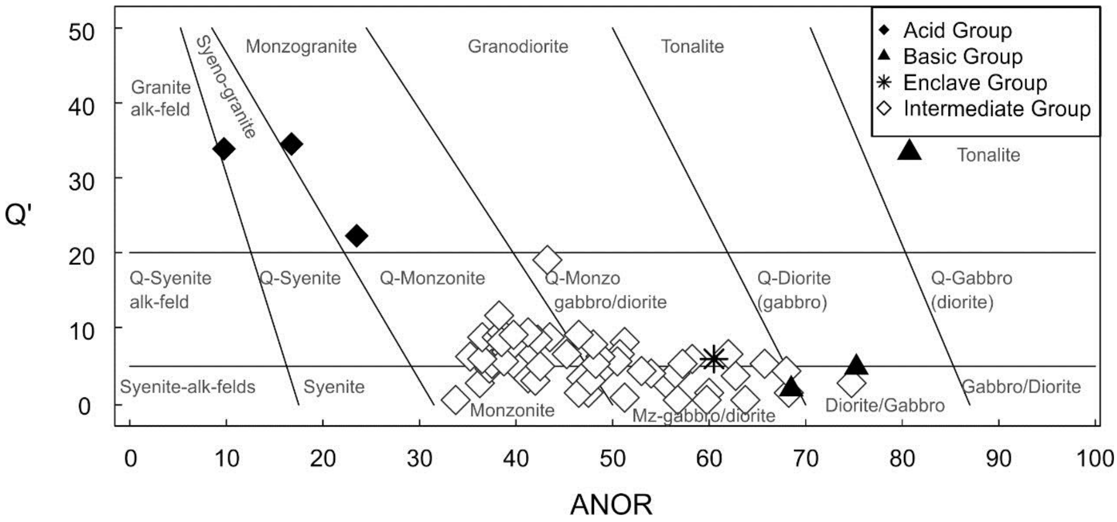

Figure 3.5.2 Q-ANOR classification diagram after *Streckeisen & Le Maitre (1979)*

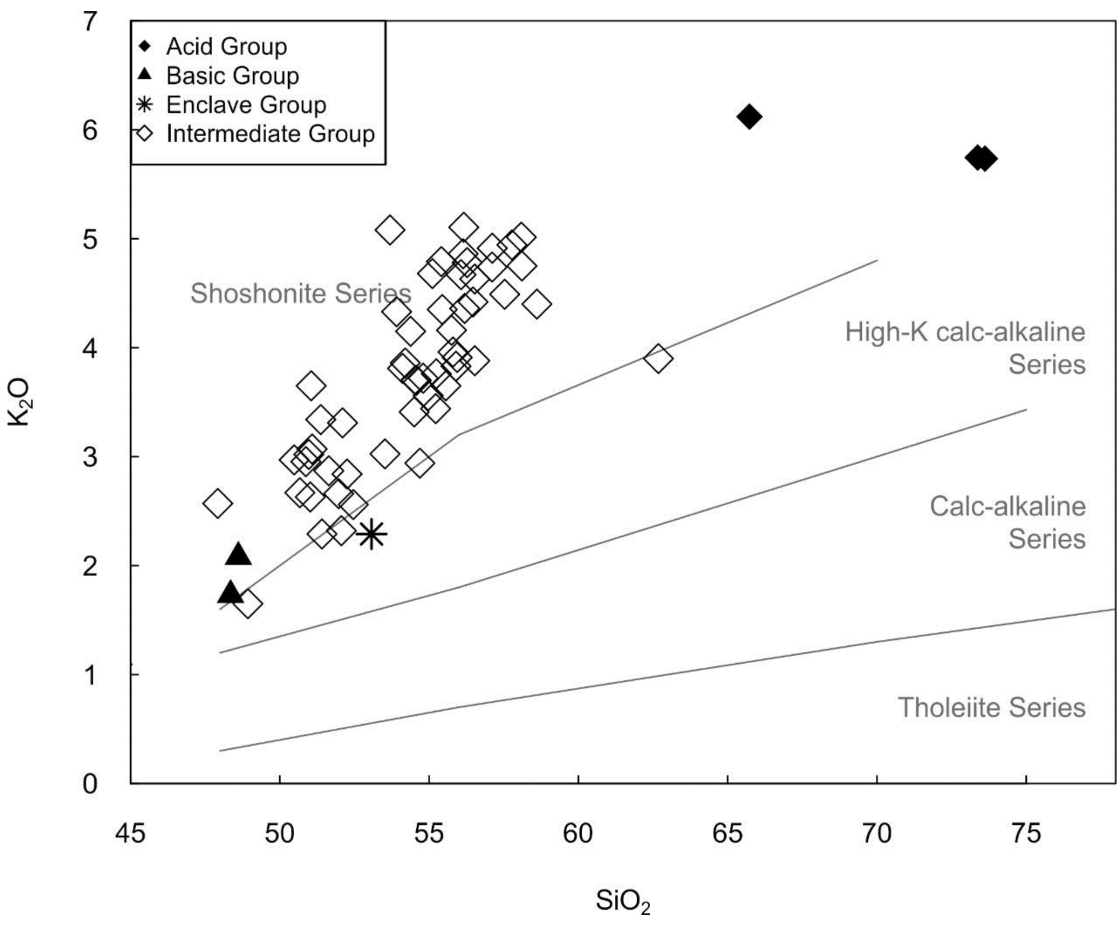

Figure 3.5.3 SiO_2 versus K_2O diagram after *Peccerillo & Taylor (1976)*

The major element variation diagrams are presented in ***Fig. 3.4.5***. For the TiO_2, MgO, CaO, P_2O_5, FeO_t and for the mg# the rocks show negative correlation with SiO_2, while a positive correlation of K_2O and N_2O with SiO_2. In the Basic group the Al_2O_3 is increased with SiO_2 but it is rather scattered in the Intermediate group and decreases in the Acid group. In the K_2O and N_2O versus SiO_2 diagram the acid group is separated from th other two groups. MgO content is rather high for the rocks of the Basic group and most of the Intermediate group rocks have high mg# (>50). The mafic microgranular enclave in most diagrams follows the trend of the Intermediate group apart from the Na_2O.

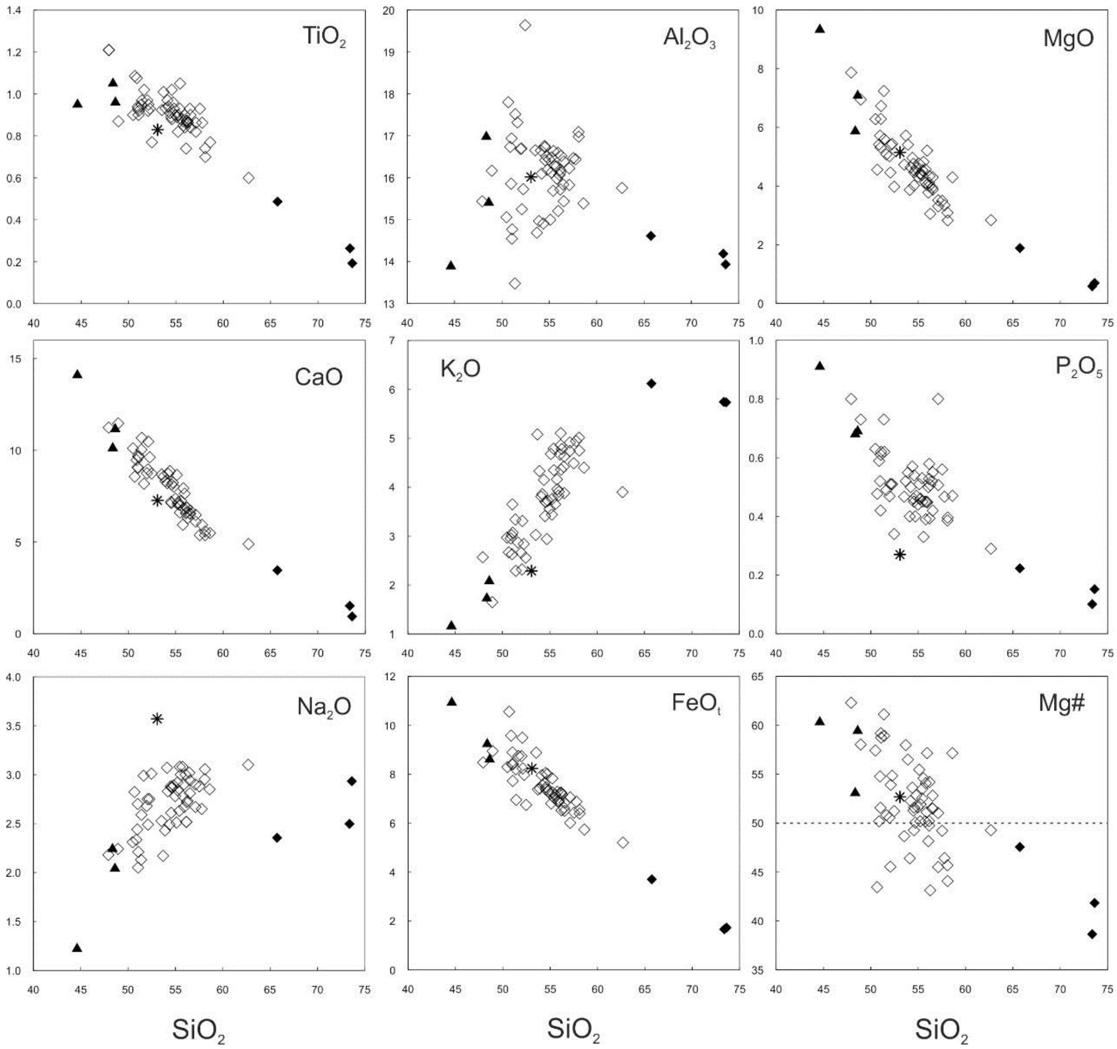

Figure 3.5.4 Variation diagrams for major elements. Symbols as in Fig. 3.5.2

3.5.4 Trace Element Geochemistry

Selected trace element variation diagrams are presented in ***Fig. 3.5.5***. The Intermediate group shows a wide range in the Zr, La, Nb and Cr and increases sharply with SiO_2. The Ba, Rb, Pb, U and Th behave incompatibly for the Basic group and the Intermediate group but in the Basic group Zr, La and Nb are rather stable while in intermediate group displays a wide range. The mafic microgranular enclave in most diagrams apart from Y follows the intermediate group trends. The Acid group has different behavior than the other groups in most variation diagrams wich probably indicates the weak genetic relashionship of this group with the others.

The trace element patterns of the Maronia rocks are presented in ***Fig. 3.5.6***. Since there are few and incomplete available data for the acid group and due its ambiguous relashionship with the other groups, it is not presented here. In general, all groups display LILE enrichment relative to the HSFE but there are some remarkable differences. All groups show typical characteristics of convergent boundaries magmas with TNT (Ta, Nb, Ti) and Pb positive anomalies. The Basic group follows the mafic microgranular enclave pattern except a positive P anomaly and a slighter Sr negative anomaly. It also displays slighter K and Pb positive anomalies. Few rocks of the intermediate group exhibit positive Ba, negative Th and negligible negative P anomalies. In all groups depletion in Zr is observed.

The REE patterns of the Maronia pluton are presented in ***Fig. 3.5.7***. All groups display LREE enrichment relative to the HREE. The enclave shows horizontal HREE pattern and has high HREE content. All groups show Eu negative anomaly which is slighter for the Basic group. Steep HREE patterns indicate residual garnet in their source (Tb_{cn}/Lu_{cn} = 1.3-2.3).

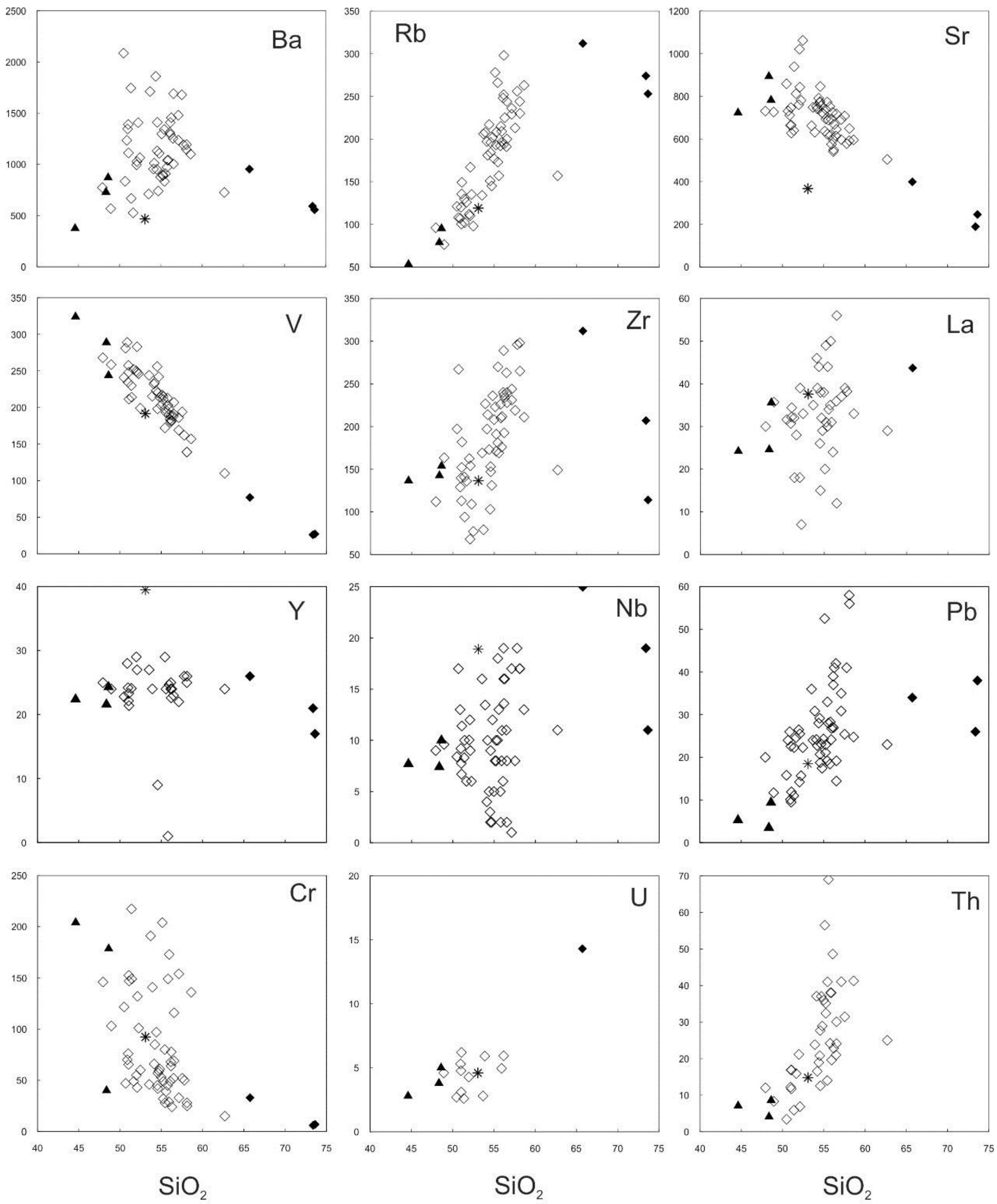

Figure 3.5.5 Variation diagrams for selected trace elements. Symbols as in Fig. 3.5.2

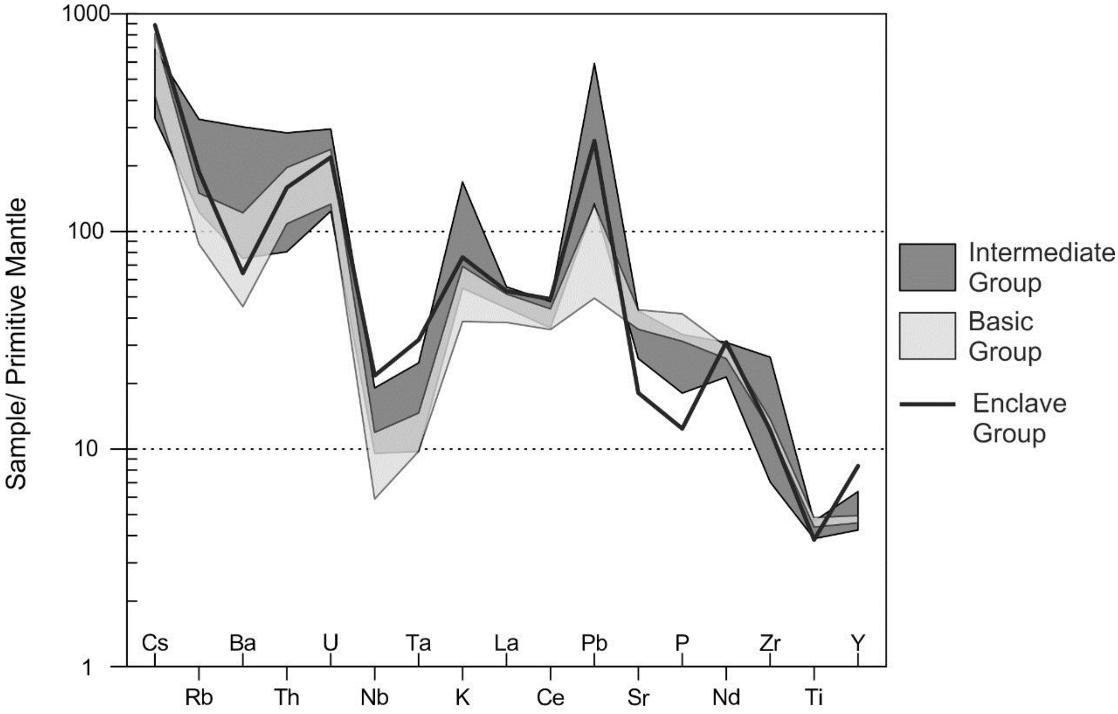

Figure 3.5.6 Multi-element spider diagram patterns. Normalisation values from *Sun & McDonough (1989)*.

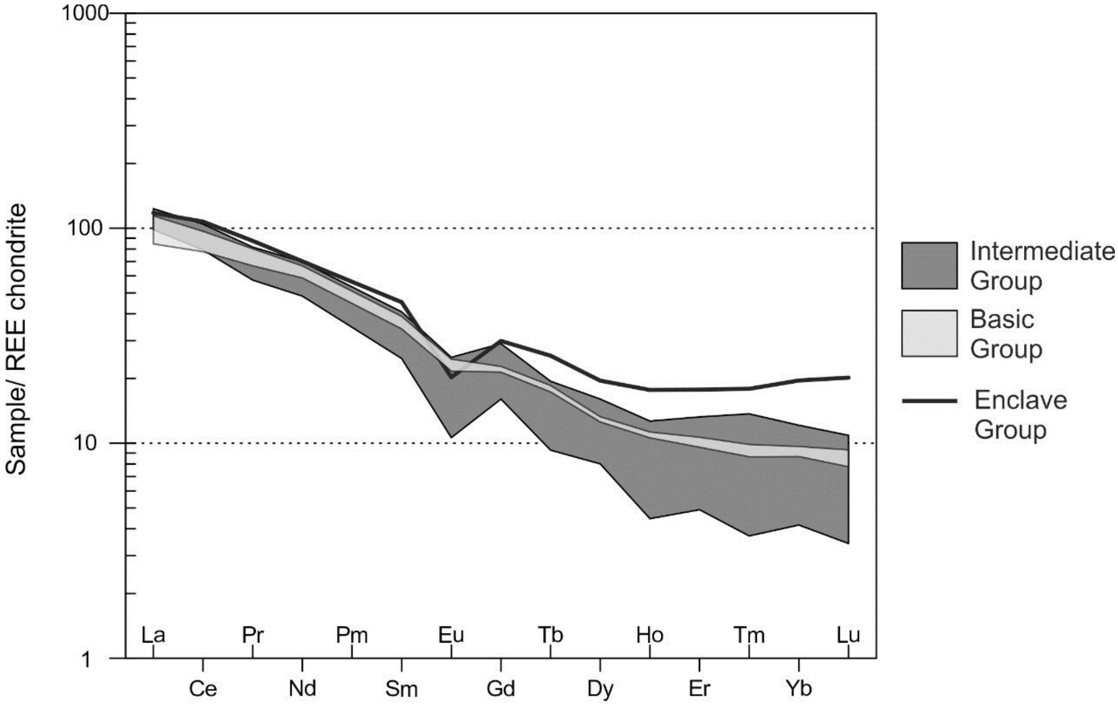

Figure 3.5.7 REE spider diagram patterns of all petrographic types. Normalisation values from *Boynton (1984)*.

3.5.5 Sr and Nd bulk rock isotopic composition

$(^{87}Sr/^{86}Sr)_i$ versus $(^{143}Nd/^{144}Nd)_i$ of the Maronia pluton are presented in ***Fig. 3.5.8***. The isotopic compositions are given in Appendix B. The mafic microgranular enclave displays the most depleted isotopic ratios, the Intermediate group has a wide range and the Basic group has more enriched isotopic ratios than the intermediate group. Nevertheless, their isotopic ratios show a depleted mantle and/or an asthenospheric component assimilated with crustal material. Regarding the Acid group, although it was assumed from previous authors that it is a crustal anatectic melt, its isotopic ratios do not favour for this since they are more depleted than any metamorphic basement rock. The rocks of the Acid group are probably the evolved members of a mafic melt, similar to the mafic microgranular enclave, or the mafic rocks of the Intermediate group that differentiated in the Rhodopian crust.

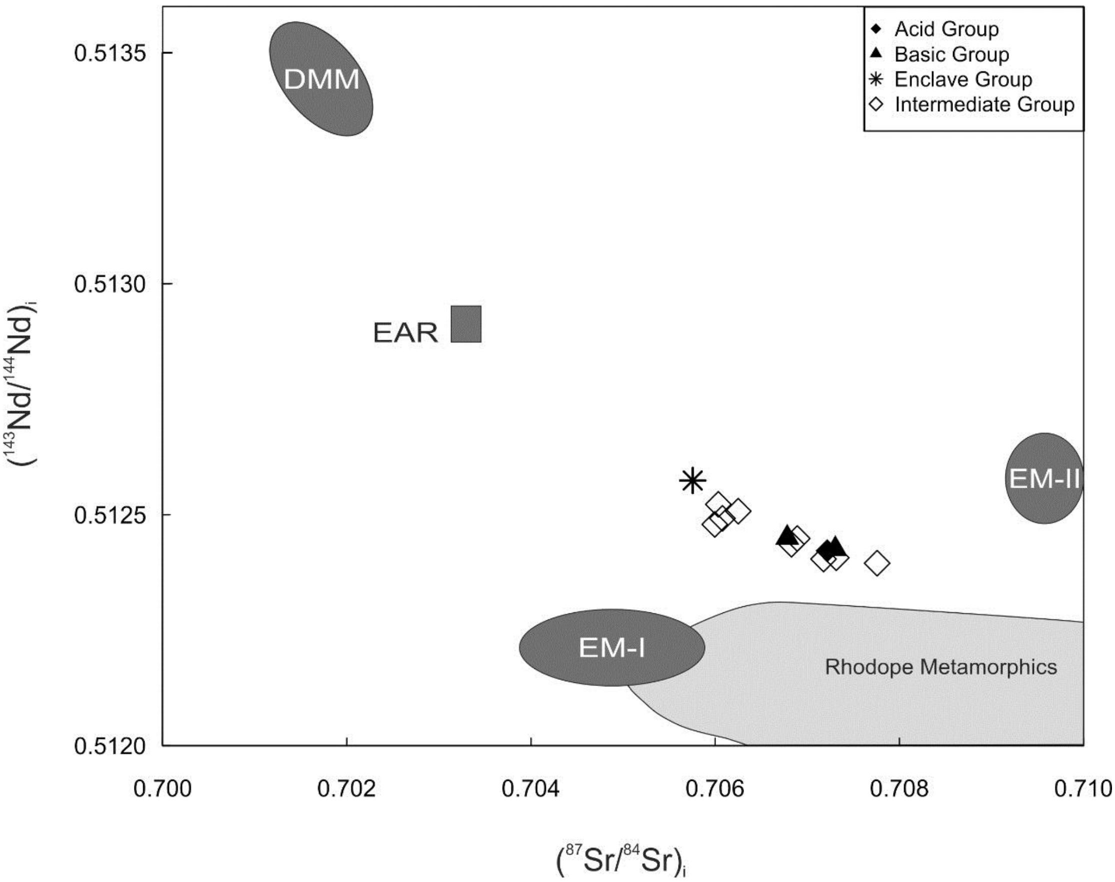

Figure 3.5.8 $(^{87}Sr/^{86}Sr)_i$ versus $(^{143}Nd/^{144}Nd)_i$. The fields illustrated are; DMM=Depleted Morb Mantle, EM-I=Enriched Mantle I, EM-II=Enriched Mantle II after *Zindler & Hart (1986)*. EAR=European Asthenospheric Reservoir

after *Cebria & Wilson (1995)*, Rhodope metamorphics after *Cornelius (2008)* and *Castorina et al. (2014)*

3.5.6 Petrogenetic implications

For the evolution and the relation of the Maronia rock groups little can be told and according to *Papadopoulou (2004)* its evolution is a rather composite history. Although the Basic group has the lowest silica content, slighter LILE enrichment, higher content in some compatible trace elements, slighter K positive anomaly and a positive P anomaly, it displays more enriched isotopic ratios than the more basic rocks of the Intermediate group. In other words, the Basic group displays the more depleted characeristics in terms of major and trace elements than the Intermediate group, however it has more evolved isotopic ratios. On the other hand, the mafic micrigranular enclave displays the most depleted isotopic composition among the other groups, high HREE content but more enriched trace element patterns. Of course more rocks from the Basic group and more mafic microgranualr enclaves would be helpful for the better understanding of the relation of these groups. In general these three groups show many common features which implies a common origin but simultaneously display features implying the opposite. We should note that geochemistry is a very important factor of a melt but the differentiation of a magmatic body is much more complicated process depending on many variables not only chemical but also physical and can generate magmas variable in composition with different trace element signatures and even initial isotopic compositions (e.g *Marsh, 2006; Bea, 2010*).

Nevertheless, all three groups display some noteworthy primitive features. The basic group and the most basic members of the intemediate group have very high MgO content (about 5-8 wt. %) and mg# (up to 61), and a positive P anomaly for the basic group. There is also a positive Ba anomaly for the intermediate group which most likely originated from crustal contamination. These rocks were clearly contaminated by crustal material but their most basic members preserve some characteristics of their source due to the minor role of assimilation. The isotopic composition and the above depleted preserved features favour for a mantle component enriched from crustal material as implied from the significant enrichment in incompatible elements.

3.6 The Evros Volcanics

3.6.1 General

The Tertiary Evros volcanic rocks (EVR) have been mainly studied from *Christofides et al. (2003 & 2004).* The EVR crop out in northeastern Greece (Thrace) mostly in central and eastern HRM and CRB (***Fig. 3.6.1***), in close association with fault-controlled sedimentary basins, formed in an extensional regime. Three volcanic areas, the Loutros-Feres-Dadia, Kirki-Esimi and Mesti-Petrota, after the corresponding basins, could be distinguished (***Fig. 3.6.1***).

Based on K/Ar geochronology two main periods of volcanic activity, an Oligocene (33.5-25.4 Ma) and a Lower Miocene (22.0-19.6 Ma) could be broadly distinguished.

In each area both intermediate and acid lavas are present in association with pyroclastics. The younger lower Miocene activity occurs only in the Loutros-Feres-Dadia basin. In the northeastern and southwestern parts of the Loutros–Feres–Dadia area the acid rocks, mostly rhyolites, dominate while in the middle part andesite and in a lesser extend dacite are the prevailing rock-types. Lava flows and domes, in some cases exhibiting columnar jointing, are very often associated with pyroclastics. The latter, in most cases, are intruded or covered by the former. In the Kirki-Esimi area the most widespread rock is andesite, often with columnar jointing. Rhyolites are present in the form of a dense net of NW-SE trending dykes at the northeastern part of the area. The overall width of the dykes varies from a few tens of centimetres to hundreds of meters whereas their length extends from tens of metres to some kilometres. Dacites occur mostly at the eastern part of it, west of Esimi village. In the Mesti-Petrota area, andesite is again the prevailing rock followed by dacite and rhyolite. Rhyolitic ignimbrites, strongly welded, tuffs and lahars are widespread. Two groups of rocks, based on their mineralogy, could be distinguished. The first group, the PxBt group, consists of basaltic andesites, pyroxene andesites, trachyandesites and trachydacites, and it is characterized by the presence of pyroxenes ± biotite. The second group, the HblBt group, comprises the biotite-hornblende andesites, the dacites and the rhyolites and it is characterized by the presence of Hornblende ± biotite.

3.6.2 Petrography and Mineralogy

Petrography and mineralogy of the EVR have been mainly studied from *Christofides et al. (2003 & 2004* and references therein). The EVR comprise intermediate and acid rocks, basaltic andesites, andesites, trachyandesites, dacites, trachydacites, and rhyolites. Trachyandesites are further subdivided in latites and benmoreites according to Na_2O and K_2O contents. *Christofides et al. (2003)* used the general term trachyandesites. All rocks show porphyritic texture with groundmass ranging between 40 and 80 vol.%. Phenocrysts are more abundant (20 to 60 vol.%) in basaltic andesites and andesites than in dacites and rhyolites (30 to 50 vol.%). Andesites are distinguished into two groups namely the pyroxene andesites and the biotite-hornblende andesites. Hornblende-biotite andesites are found mainly in the Kirki-Esimi and Loutros-Feres-Dadia areas.

Basaltic andesites contain plagioclase and clino- and orthopyroxene subhedral to auhedral phenocrysts, set in a semicrystalline to hollocrystalline groundmass. Plagioclase is mainly bytownite (An_{70}-An_{80}) and shows oscillatory zoning. Clinopyroxene is augite while orthopyroxene is hypersthene.

Pyroxene andesites contain plagioclase and clino- and orthopyroxene subhedral to auhedral phenocrysts set in a hypocrystalline to holocrystalline groundmass and in some samples subhedral biotite crystals are also present as well as secondary calcite. Plagioclase is mainly labradorite (An_{54}–An_{69}) and shows normal oscillatory zoning. Clinopyroxene is augite while orthopyroxene is hypersthene. In few clinopyroxene crystals observed, the core is occupied by hypersthene.

Biotite-hornblende andesites contain plagioclase, subhedral to euhedral biotite, subhedral hornblende subordinate quartz and few samples contain small clino- and orthpyroxene crystals. Plagioclase is labradorite showing oscillatory zoning. Quartz usually appears with magmatic erosion. Hornblende is mainly magnesio-hornblende with high $Mg^{2+}/Mg^{2+}+Fe^{2+}$ ratio (>0.8).

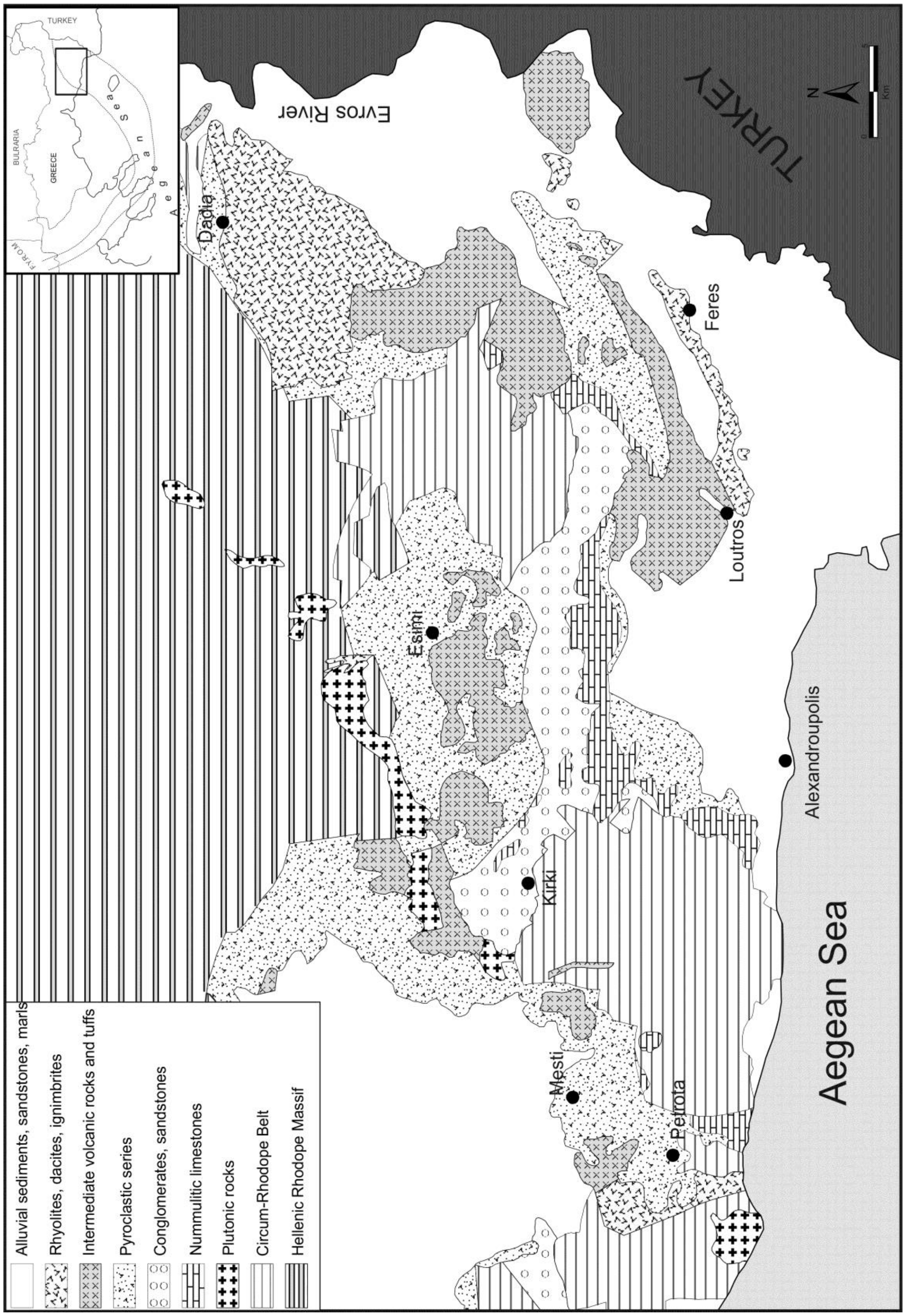

Figure 3.6.1 Simplified map of the EVR modified after *Christofides et al. (2004)*

Trachyandesites and trachydacites contain plagioclase, subhedral to auhedral clino- and orthopyroxenes and subhedral to auhedral biotite set in a mainly hypocrystalline groundmass. Pyroxenes are often altered to uralite. Plagioclase is andesine to labradorite (An_{34}-An_{60}) showing oscillatory zoning. Clinopyroxene is augite while orthopyroxene is hypersthene. Hornblende relics are also present in some samples.

Dacites and rhyolites consist of plagioclase, sanidine, quartz, subhedral biotite and subordinate sunhedral hornblende set in a glassy or semiglassy matrix, which very often exhibits very nice perlitic and sphaerolitic textures. Plagioclase is oligoclase to labradorite (An_{20}-An_{60}) showing oscillatory zoning. The $Mg^{2+}/Mg^{2+}+Fe^{2+}$ of biotite ranges between 0.58-0.69. Sanidine (Or_{75-65}) is usually twinned after in the Carlsbad Law. Quartz often appears with magmatic erosion.

Apatite, titanite and zircon are accessories in all rocks.

3.6.3 Major Element Geochemistry

The geochemical data for the EVR used here are published data of *Christofides et al. (2004)*, unpublished data of *Christofides* and new data. They are all presented in Appendix A. The two main groups (PxBt and HblBt) subdivided by *Christofides et al. (2004)*, will be used hitherto.

In ***Fig. 3.6.2*** the old and new data are presented on a TAS classification diagram of *Le Bas et al. (1986)*. Only andesites of both main rock groups are plotted in the same field but there is difference on the silica content which is higher for the HblBt group. Both groups show calc-alkaline and high-K calk alkaline character with few samples displaying shoshonitic character (***Fig. 3.6.3***).

In ***Fig. 3.6.4*** major element variation diagrams are presented. The two groups show good corelletion in some variation diagram but in TiO_2, MgO and P_2O_5 there are clearly two distinct trends. All oxides increase in the two groups with differentiation apart from K_2O which increases and N_2O and mg# where samples are rather scattered. Both groups display moderate MgO contents but rather high mg# (>50) which are especially high for the HblBt group even for the more felsic members.

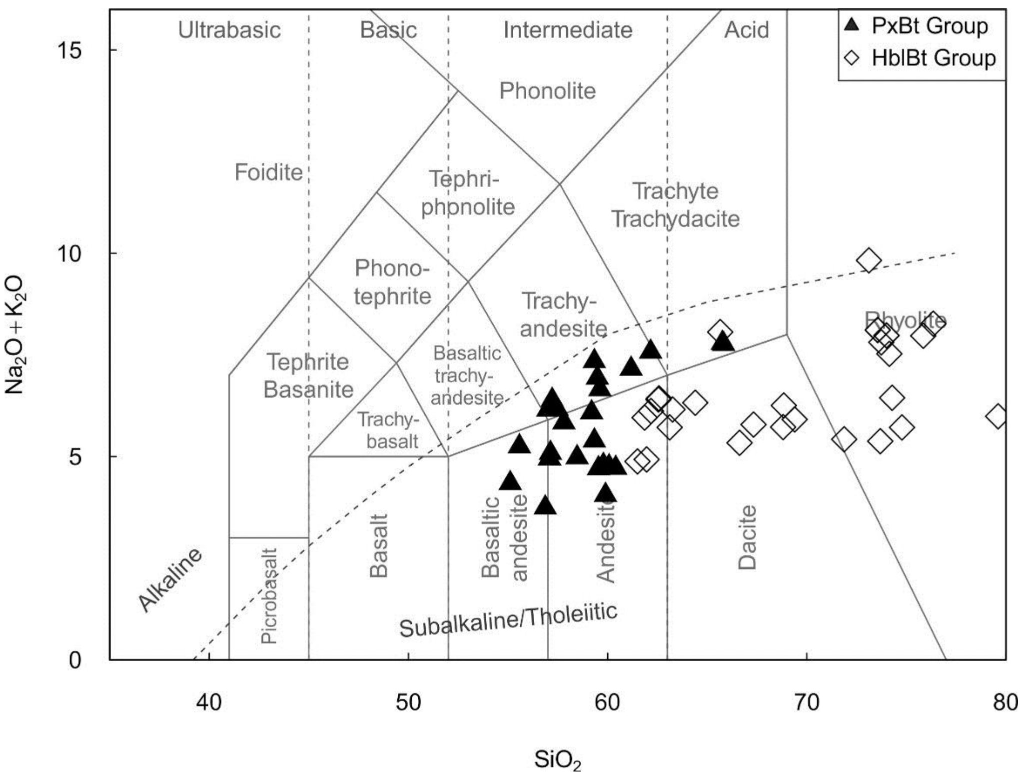

Figure 3.6.2 TAS (Total Alkalies-Silica) classification diagram after *Le Bas et al. (1986)*. Discrimination alkaline-subalkaline line after *Irvine & Baragar (1971)*

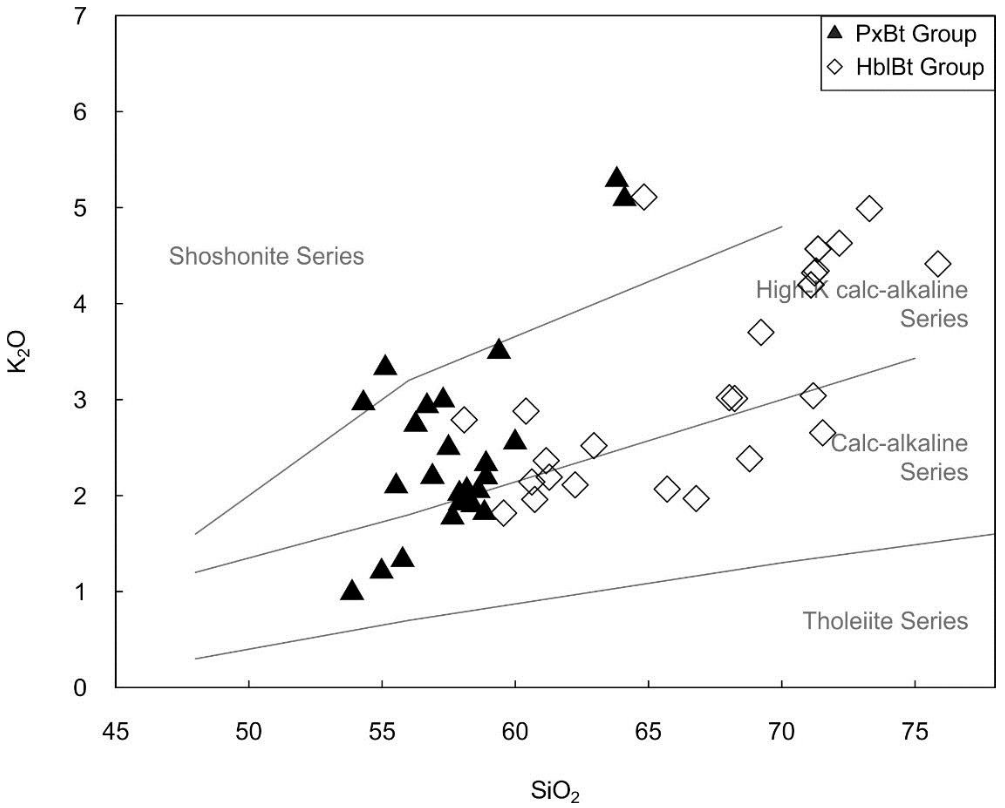

Figure 3.6.3 SiO_2 versus K_2O diagram after *Peccerillo & Taylor (1976)*

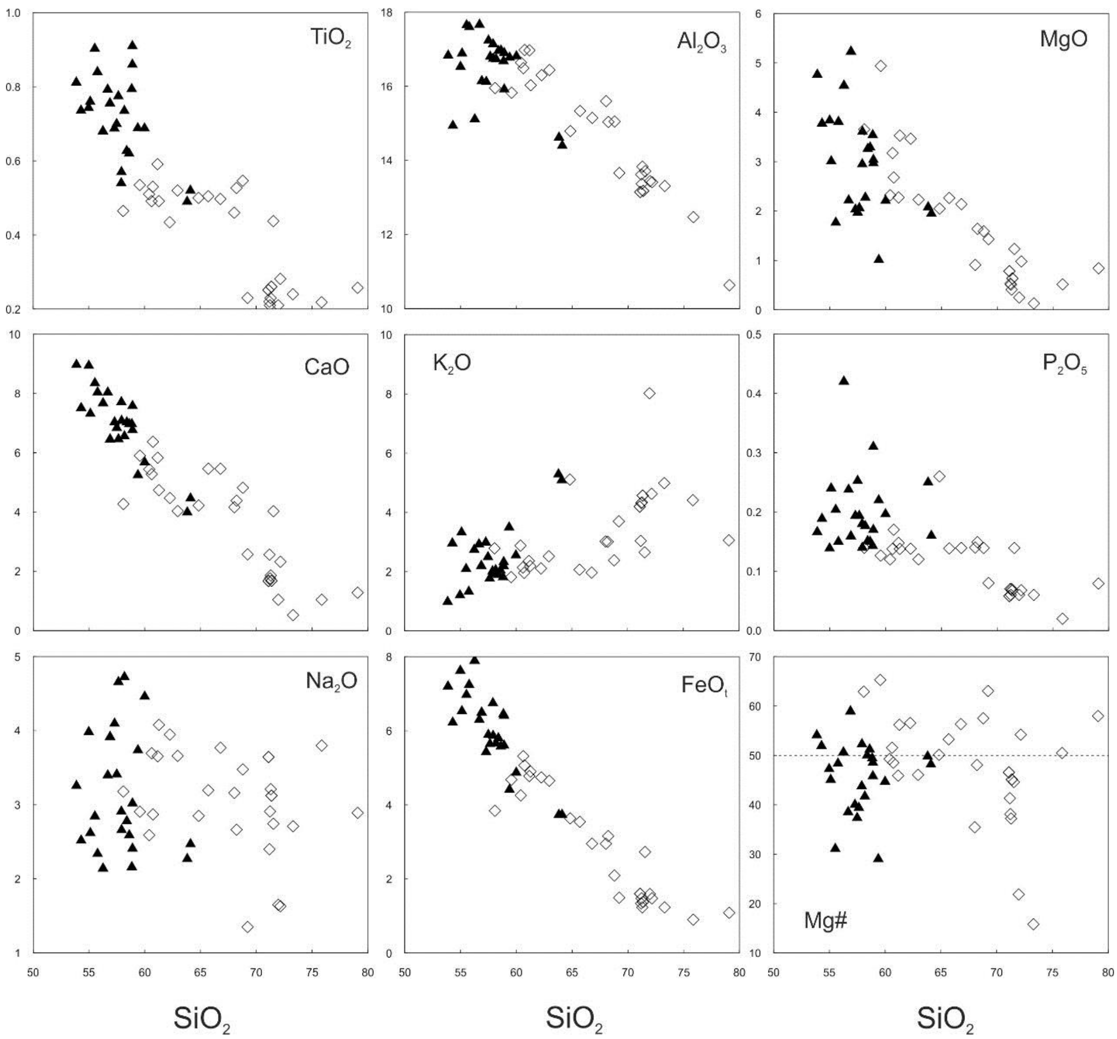

Figure 3.6.4 Variation diagrams for major elements. Symbols as in Fig. 3.6.2

3.6.4 Trace Element Geochemistry

In ***Fig. 3.6.5***, selected trace element variation diagrams are shown. In some variation diagrams the distinction between the two groups is clear (Rb, La, Nb, Y, Pb U, Th) due to the parallel trends they exhibit. Samples are generally rather scattered especially for the HblBt group. In some compatible element variation diagrams (V, Cr) both groups display negative correlation with silica but the PxBt group shows steeper trends. In Ba, Zr PxBt group seems to increase for the PxBt group but remains rather constant for the HblBt group.

In the multi-element spider diagram (***Fig. 3.6.6***) both groups display common patterns characteristic for convergent boundaries geotectonic environments, with LILE enrichment relative to the HSFE, TNT (Ta, Nb, Ti) negative anomalies and

Pb positive anomalies. Despite the restricted SiO_2 content of the PxBt group, it displays wider trace element range and slighterr P and Ti negative anomalies than the HblBt group.

In ***Fig. 3.6.6*** the REE patterns of both groups are shown. Both groups show LREE enrichment relative to the HREE and Eu negative anomaly, however the HblBt group shows higher enrichment in LREE and more depleted MREE probably due to residual hornblende in the source. They both display almost horizontal HREE patterns but the Tb/Yb_{cn} (up to 1.6) shows residual garnet in the source.

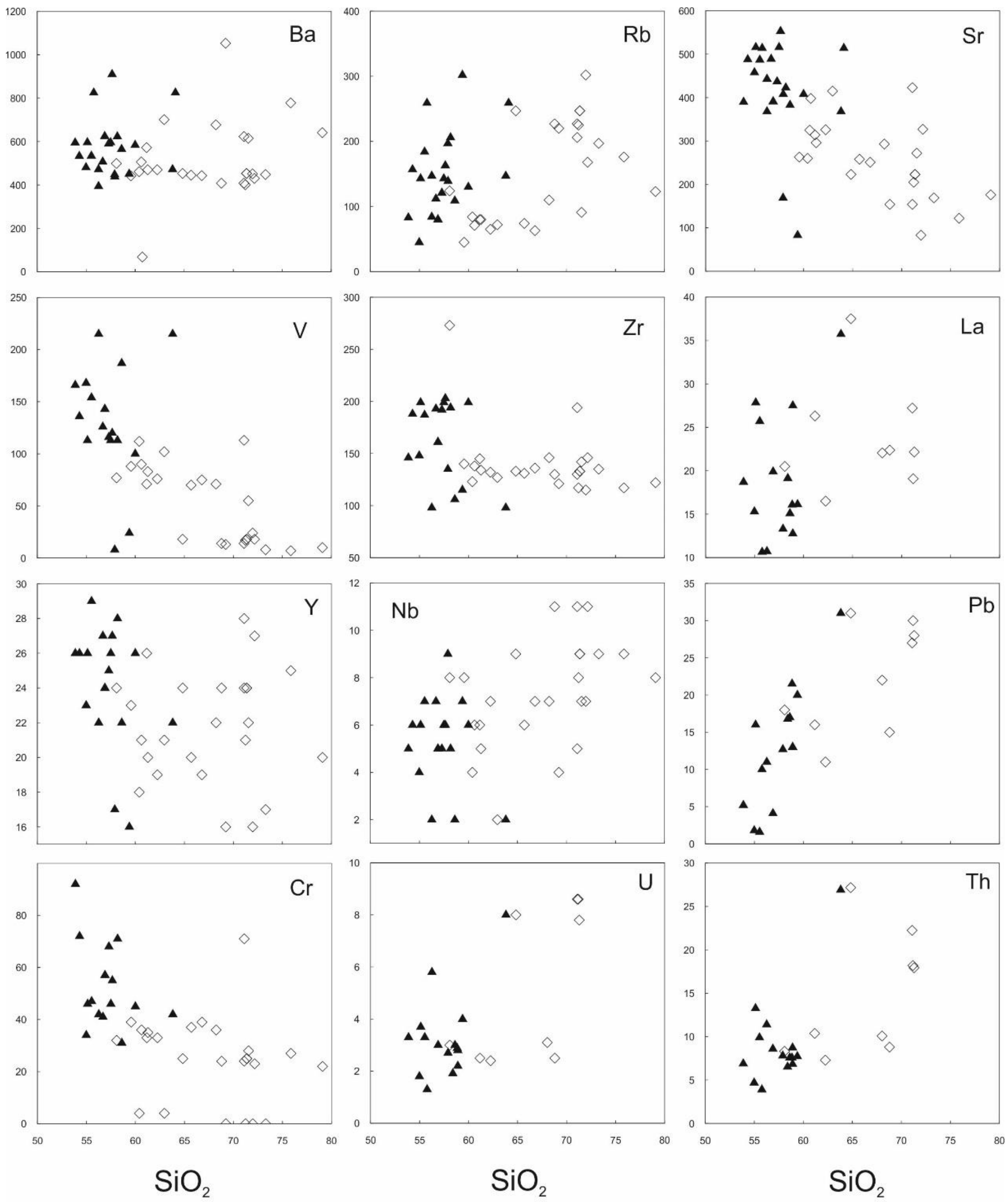

Figure 3.6.5 Variation diagrams for selected trace elements. Symbols as in Fig. 3.6.2

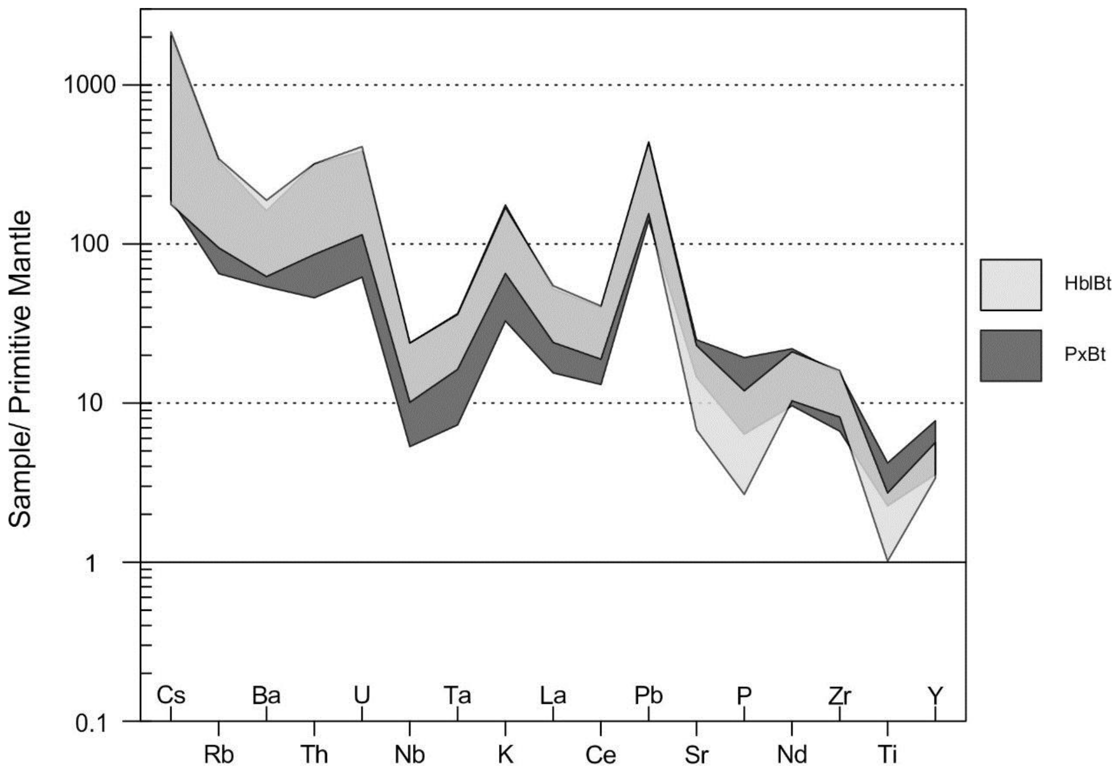

Figure 3.6.6 Multi-element spider diagram patterns of the two groups. Normalisation values from *Sun & McDonough (1989)*.

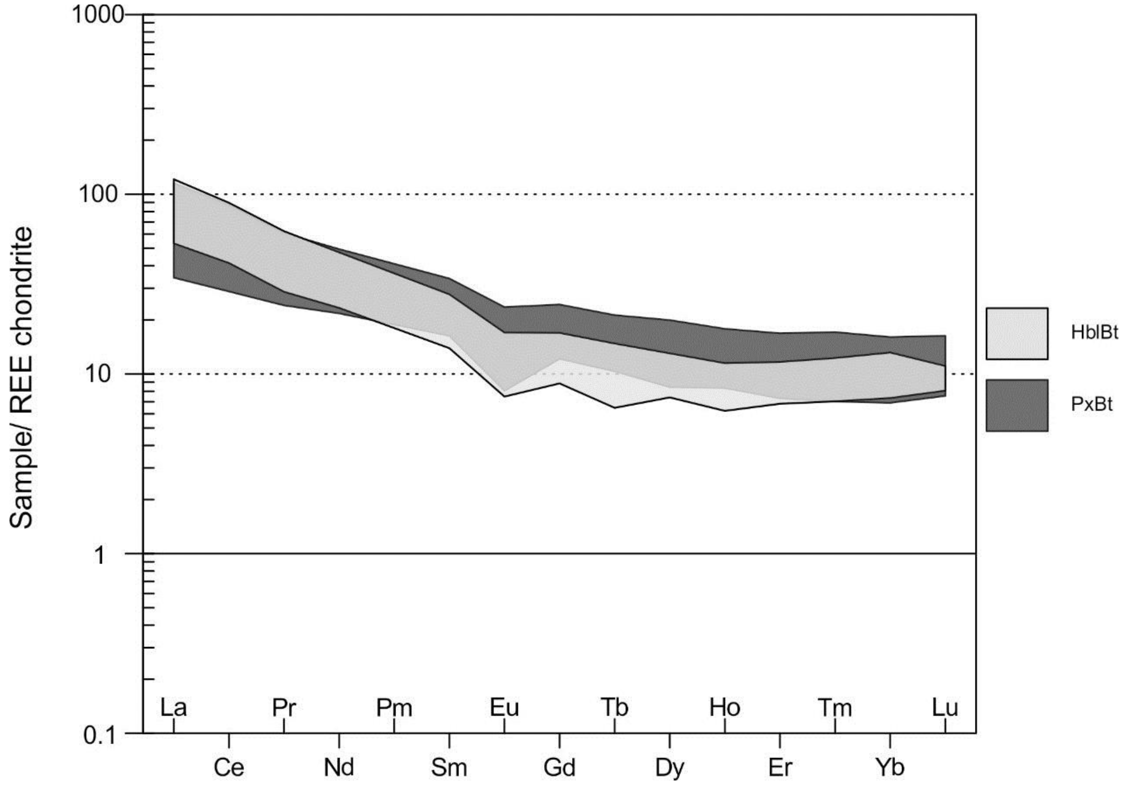

Figure 3.6.7 REE spider diagram patterns of the two groups. Normalisation values from *Boynton (1984)*.

3.6.5 Sr, Nd and Pb bulk isotopic composition

The Sr and Nd initial isotopic composition of the rocks imply strong mantle component for their genesis. There are limited initial isotopic ratios for the HblBt group due to lack of Nd elemental data. The isotopic composition of the EVR is given in Appendix B. It should be noted here that there are limited number of samples for the HblBt group. The PxBt group appears more depleted is Sr and Nd initial isotopic ratios than the HblBt group. The trend of the rocks implies origin from a mantle component (DMM or EAR) and variable crustal enrichment. In ***Fig. 3.6.9*** the Pb isotopic composition shows a DMM component enriched with crustal material especially implied from the steep upward trend of the HblBt group rocks. On the other hand in ***Fig. 3.6.10*** the EAR reservoir cannot be excluded from the origin of these rocks since there might be a trend of the PxBt group towards the NHRL. It is noteworthy that the HblBt group displays a wider range in isotopic composition regarding Pb which may imply different source or highly unhomogenised source from the PxBt group or variable crustal contamination.

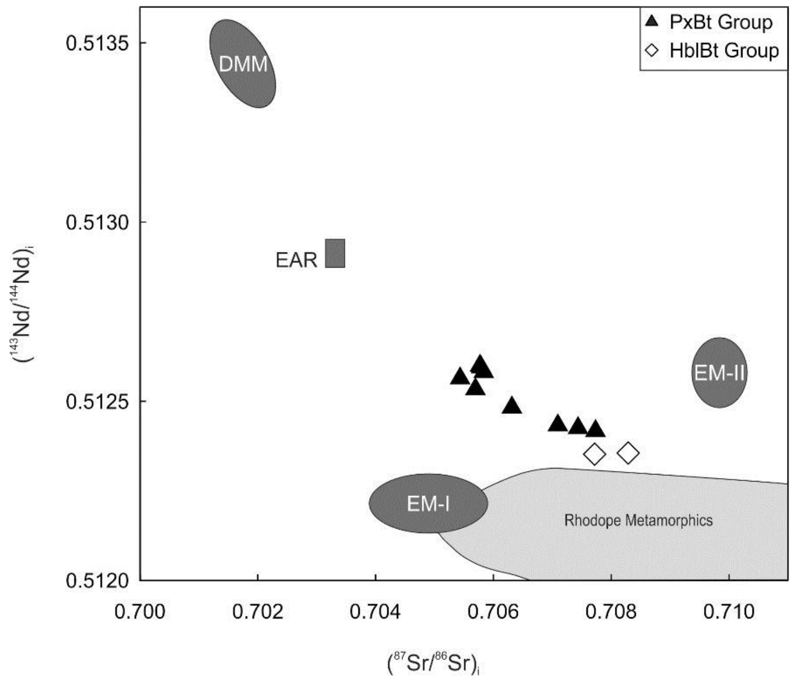

Figure 3.6.8 $(^{87}Sr/^{86}Sr)_i$ versus $(^{143}Nd/^{144}Nd)_i$. The fields illustrated are; DMM=Depleted Morb Mantle, EM-I=Enriched Mantle I, EM-II=Enriched Mantle II after *Zindler & Hart (1986*). EAR=European Asthenospheric Reservoir after *Cebria & Wilson (1995),* Rhodope metamorphics after *Cornelius (2008) and Castorina et al. (2014)*

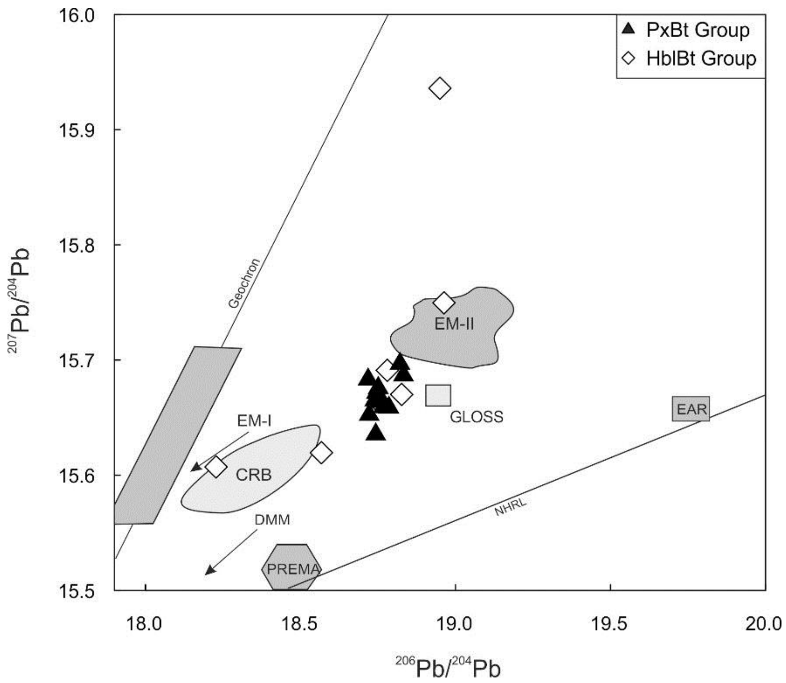

Figure 3.6.9 ^{207}Pb/^{204}Pb versus ^{206}Pb/^{204}Pb. The fields illustrated are; DMM=Depleted Morb Mantle, EM-I=Enriched Mantle I, EM-II=Enriched Mantle II after *Wilson (1989)*. EAR=European Asthenospheric Reservoir after *Cebria & Wilson (1995)*. GLOSS after *Plank & Langmuir (1998)*. NHRL= North Hemisphere Reference Line after *Hart (1984)*

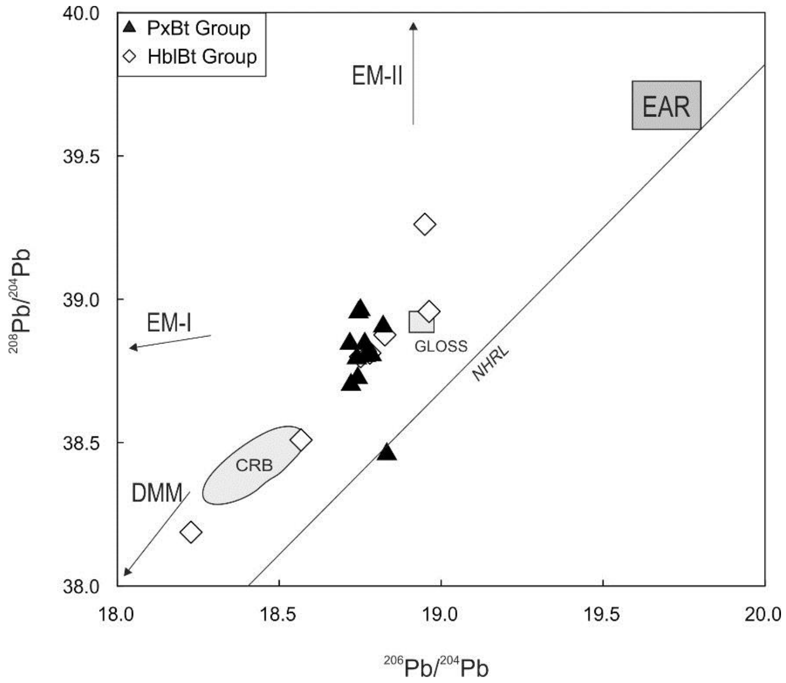

Figure 3.6.10 ^{208}Pb/^{204}Pb versus ^{206}Pb/^{204}Pb. The fields illustrated are; DMM=Depleted Morb Mantle, EM-I=Enriched Mantle I, EM-II=Enriched Mantle II after *Wilson (1989)*. EAR=European Asthenospheric Reservoir after *Cebria & Wilson (1995)*. GLOSS after *Plank & Langmuir (1998)*. NHRL= North Hemisphere Reference Line after *Hart (1984)*

3.6.6 Petrogenetic implications

In the EVR volcanics there are no true basic rocks found. There are some basalts in the Petrota area but they are extremely altered to be analysed. However, the basic members of the two groups show high mg# and depleted isotopic ratios which probably implies minor or no crustal contribution from the rhodope metamorphics. Both groups show typical orogenic characteristics. The two groups display different evolutionary paths as shown from the major and trace element variations, the differences in isotopic composition and the different trends in inter-element variation diagrams as *Christofides et al. (2004)* have already shown. The same authors propose an MFC process for both groups between a basic end-member and an acid end-member. The new data presented here do not add any difference in the evolutionary history already proposed.

Regarding the origin of the parental magmas of these rocks the same authors proposed partial melting of a strongly metasomatised mantle for the PxBt group and a hybrid magma of the PxBt group as the parental magma of the HblBt group. They also suggest crustal melting for the origin of the evolved Rhyolites but do not exclude the mantle origin. One rhyolite sample displays a rather low initial Sr ratio (0.7054) as well as depleted Pb isotopic composition which implies that it can' t be originated from pure crustal melting. Pb isotopes for the HblBt group exhibit higher variation than the PxBt group but they also show in some cases more depleted ratios than the PxBt group. This probably suggests variable crustal contribution for the origin of the HblBt group higher than the PxBt.

As a whole, both groups originate from an enriched mantle-derived parental magmas which evolved through MFC process, hybridized from Rhodopian crustal melts with variable crustal contribution which seems more intense for the HblBt group.

3.7 The Samothraki Volcanics

3.7.1 General

The basement of the Samothraki island is believed to be part of the Circum-Rhodope belt (*Kauffmann et al., 1976*), consisting of low-grade metamorphic rocks of an Upper Jurassic to Lower Cretaceous age (***Fig. 3.7.1***). The Samothraki volcanics were mainly investigated and discussed by *Eleftheridis et al. (1993, 1994)* and *Vlahou et al. (2006)*

The Tertiary volcanic rocks of Samothraki island commonly overlie a series of tuffites composed of tuffaceous conglomerate and tuffaceous sandstone stratigraphically overlying an Eocene clastic neritic sequence. Sills of mafic volcanic rocks cut the upper part of the tuffite series. The volcanic products are found to gradually form thicker bodies, and the tuffites are topped by a well-defined lava flow. These mafic sills and lava flows are grouped as the "Agios Nectarios unit." Rocks of similar stratigraphy and geology are found in the south, around the villages of Lakoma and Dafnes and in the area of Kitada, and are also grouped in this unit. In this lowermost volcanic unit, lava domes intrude and in some cases are seen to lift up the Eocene epiclastic strata. In the area northwest of Samothraki (Hora), the domes form hills, namely Tourli, Vrehos, and numerous hills between the villages of Samothraki (Hora) and Paleapoli. Each of these domes was treated as a separate unit, because there was no geological evidence to connect them genetically, other than their geographical closeness. On the north shore of the island, at the Katsambas gully, lava flows and vents are found to intrude the tuffites but show no geological connection to the previously mentioned domes. As a result, they are considered to form the "Hora-Katsambas unit." On the south-southwest shores of the island, around the villages of Lakoma, Profitis Ilias, and Dafnes and the area of Kitada, another volcanic unit (the Lakoma unit) is found to cover the tuffites and to include in their upper part mafic sills that intrude rocks of the Agios Nectarios unit. Another outcrop of volcanic rocks is found in the northeast area of the island called Agia Paraskevi. Finally, a vein that was found to intrude the Vrehos dome was taken as a separate unit-referred to as the "younger vein" because it could not be grouped into any of the previously mentioned units. *Eleftheriadis et al. (1993, 1994)* has distinguished two series of volcanic rocks with distinct geochemical and geological characteristics: the "old" and the "young" volcanic rock series. *Vlahou et al. (2006)* distinguished further the volcanic rocks in: the "old" group (25 Ma), comprising basalts to latites; the "intermediate" group (22 Ma) of andesites to latites; and the "young" group (22-19 Ma) of latites to rhyolites. Additionally, a "younger vein" (17 Ma) was found with geochemical characteristics similar to those of the intermediate group.

The samples collected for the needs of the present study belong to the Old and Young group described by *Vlahou et al. (2003)* and one sample of the intermediate group. There is also a lamprophyre sample collected which will be described in the next paragraph.

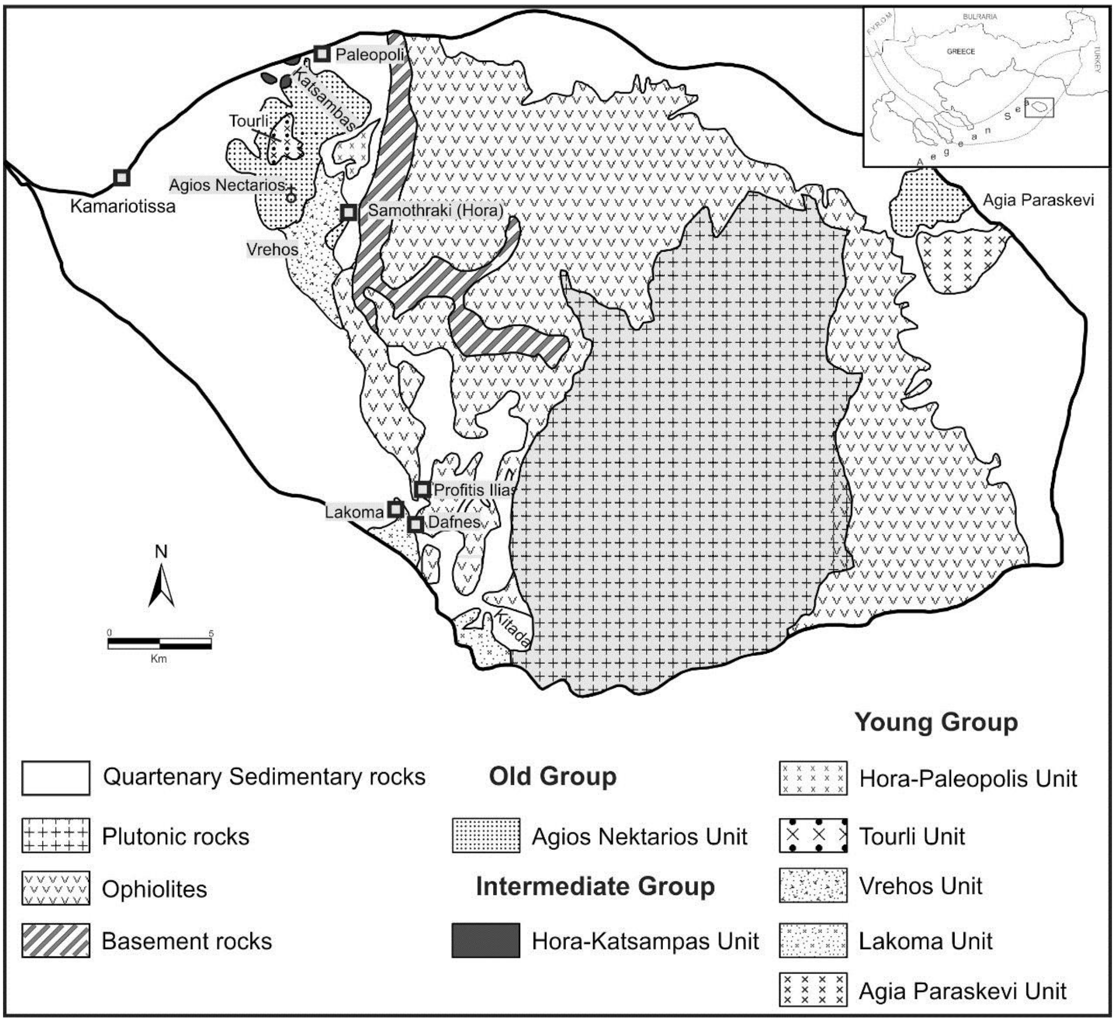

Figure 3.7.1 Simplified map of Samothraki modified after *Vlahou et al. (2006)*

3.7.2 Petrography and Mineralogy

The petrology and mineralogy of the Tertiary volcanic rocks from Samothraki island have been discussed by *Eleftheriadis et al. (1993, 1994)*, *Vlahou et al. (2001)*, and *Vlahou (2003)*. A brief summary will follow.

Old Group. **Agios Nektarios Unit**. This unit consists of basalts, basaltic trachyandesites, andesites, trachyandesites, and trachytes with calc-alkaline to high-K calc-alkaline and shoshonitic affinity. They are dark in color and slightly porphyritic to subaphyric (groundmass 56-77%). The phenocrysts consist mainly of zoned plagioclase (18.7-26.9%), ranging in composition from labradorite to oligoclase, and pyroxene (4.8-0.4%); primary magnetite and titanomagnetite are also present. In some cases, plagioclase disequilibrium textures have been identified. Completely altered biotite and hornblende were also found.

Intermediate Group. Hora-Katsampas Unit. This unit comprises veins and lava flows consisting of andesites to latites of shoshonitic and high-K calc-alkaline affinities. They show different shades of gray color, and they are porphytitic in texture (groundmass 55-70%). The phenocrysts are zoned plagioclase (16.2-21.9%), ranging from labradorite to oligoclase, pyroxene (5.2-0.5%), and magnetite, forming sizable euhedral to subhedral crystals. In some cases, apatite may be present in relatively large amounts. In addition, completely altered biotite crystals (and to a lesser extent hornblende) were found in the more evolved lava flows of the unit, whereas in the less evolved ones glomeroporphyritic clots of plagioclase and mafic minerals are present. Zeolites, forming fan-like masses, occupy cavities in the groundmass.

Young Group. The Hora-Paleapoli Unit comprises several low domes intruding the Agios Nectarios unit and the tuffites. They are light gray to greenish gray in color, and they show porphyritic texture. They are classified as trachytes, composed of plagioclase, sanidine, quartz, biotite, pyroxene, and hornblende. Accessory minerals include titanite and apatite in relatively large amounts. The volcanic rocks in these domes have been altered significantly due to the circulating fluids associated with dome formation. The products of this alteration, which in many cases has fully affected the primary minerals, are mainly carbonate minerals and oxides.

The Tourli dome consists of trachytes with euhedral crystals of quartz and characteristic idiomorphic megacrysts of sanidine, in some cases reaching 10 cm in length and showing chemical zonation. Their color is light gray to light brownish gray with a porphyritic texture (groundmass 66-71%). The phenocrysts present are andesine plagioclase (11-7.5%), sanidine (1-2%, excluding the megacrysts), quartz (1.5-2.5%), biotite (6-10%), and pyroxene (4.5-8%). The latter are found both as small phenocrysts and as groundmass constituents. The plagioclases are commonly zoned. The biotite is brown in color and appears in two distinct forms, one as phenocrysts, often with an alteration rim, and another as mostly fresh, lathlike elongated microphenocrysts. The accessory minerals found are apatite, allanite, zircon, magnetite, and titanomagnetite. Calcite occurs as a secondary mineral. Some zeolite glomerates were also found in the groundmass. Completely altered sedimentary xenoliths have also been found in these rocks. **The Vrehos dome** is situated to the west of Samothraki village and extends to the south as far as Alonia village. The rocks from this dome are classified as high-K dacites, although some trachytes and rhyolites are also found. They are white to light gray in color, and, as in the Tourli dome, idiomorphic megacrysts of sanidine as long as 10 em can be seen. They are porphyritic (groundmass 56-59%), and their main phenocrysts are andesine to oligoclase plagioclase (15-19%), sanidine (4-13%), quartz (2-7%), biotite (1.5-5%), hornblende (3-3.5%), and pyroxene (3-4%). The accessory minerals are apatite, allanite, titanite, and magnetite. Calcite can also be found replacing some minerals, mainly in the groundmass, while secondary opaque minerals are present. Biotite occurs in two forms, as described for the Tourli unit. Disequilibrium textures of plagioclase, and in some cases of ferromagnesian minerals, have also been seen. In addition, plagioclase crystal clusters as well as enclaves of igneous origin are present.

The volcanic products of the **Lakoma Unit** are classified as latites, high-K dacites, trachydacites, trachytes, and rhyolites, and they are gray, light gray, to whitish in color. They are porphyritic or hyalophyric (groundmass 52-67%), with quartz (0.5-4%), sanidine (2-10.5%), oligoclase plagioclase (8-25%), oxyhornblende (7-8.5%), and biotite (2.5-5%). The accessory minerals found include apatite, allanite, titanite, magnetite, titanomagnetite, and zircon. In the porphyritic samples, glomeroporphyritic clots of plagioclase and biotite were found.

Agia Paraskevi Unit, is a dome-like formation comprising porphyritic latites to high-K dacites. Macroscopically they are greenish to whitish gray, and they consist of quite altered feldspars, hornblende, pyroxenes, and biotite. The ferro-magnesian minerals in this case have been altered mainly to calcite, chlorite, epidote, and titanite instead of the opaque minerals found in the rest of the units. A younger porphyritic trachyte consisting of quartz (~2%), sanidine (~2%), andesine to oligoclase plagioclase (~13%), biotite (~10%), and very small amounts of hornblende seems to intrude this formation. The accessory minerals include allanite, apatite, and magnetite**.**

Younger Vein Unit is a dark-grey porphyritic high-K latite that intrudes the Vrehos dome. The phenocrystic minerals are labradorite to andesine plagioclase (26.8-28.2%) and pyroxene (9.4-11.8%). The oxides and apatite are accessories. The plagioclase shows zoning, and in some cases disequilibrium textures. Pyroxene is found as euhedral to subhedral crystals of different sizes, while some of them show slight optical zoning. Ghost crystals of olivine and orthopyroxene are also observed.

Lamprophyre is a dark-grey porphyritic vein intruding the Samothraki pluton, with large K-Feldspar crystals which appear eroded in the rims from the ground mass implying their plutonic origin. Apart from sanidine, euhedral biotite, plagioclase and phlogopite are the main phenocrysts.

3.7.3 Major element Geochemistry

The geochemical data of Samothraki volcanics used in this study are published data of *Vlahou (2003)*, in conjuction with the new data (Appendix A). The are all presented in ***Fig. 3.7.2*** on a TAS classification diagram. As mentioned above the new samples classified according to the discrimination of the three groups from *Vlahou et al. (2003)*. The lamprophyric sample is classified as trachyandesite, however its mineralogy differs from all other rocks to be grouped with, but is presented here in order to give addtional data for the geochemistry of the volcanic rocks of Samothraki.

Most of the rocks of the Old series display alkaline character due to the high Na_2O wt.% in their composition. In seven samples nepheline appears as a normative mineral but does not exist as mineral phase in any rock.

Regarding the K content of the rocks, the Young group is classified as High-K and shoshonitic, the Intermediate group as High-K and two samples as shoshonitic and the Old group displays a wide range from tholeiitic to shoshonitic (***Fig. 3.7.3***). The lamprophyre sample displays remarkable high K content and is classified as shoshonitic.

The major element variations (***Fig. 3.7.4***) show distinct trends between the Old and the Young group, while the Intermediate group overlaps both groups. In TiO_2, MgO, CaO, FeO_t and in the mg# all groups display negative correlation with the silica content and have parallel trends. Al_2O_3 seems rather stable for both groups, Na_2O and K_2O are rather stable for Intermediate and Young group while is scattered for the Old group and P_2O_5 seems to decrease in all groups with different slopes. For the lamphrophyre sample trends can't be defined since it is unique, however in some elements it displays extreme features like the low Al_2O3, high MgO, high TiO_2 and high K_2O contents. All groups display rather high mg# and despite the higher silica content for the Younger group it displays the highest mg# from the other two groups.

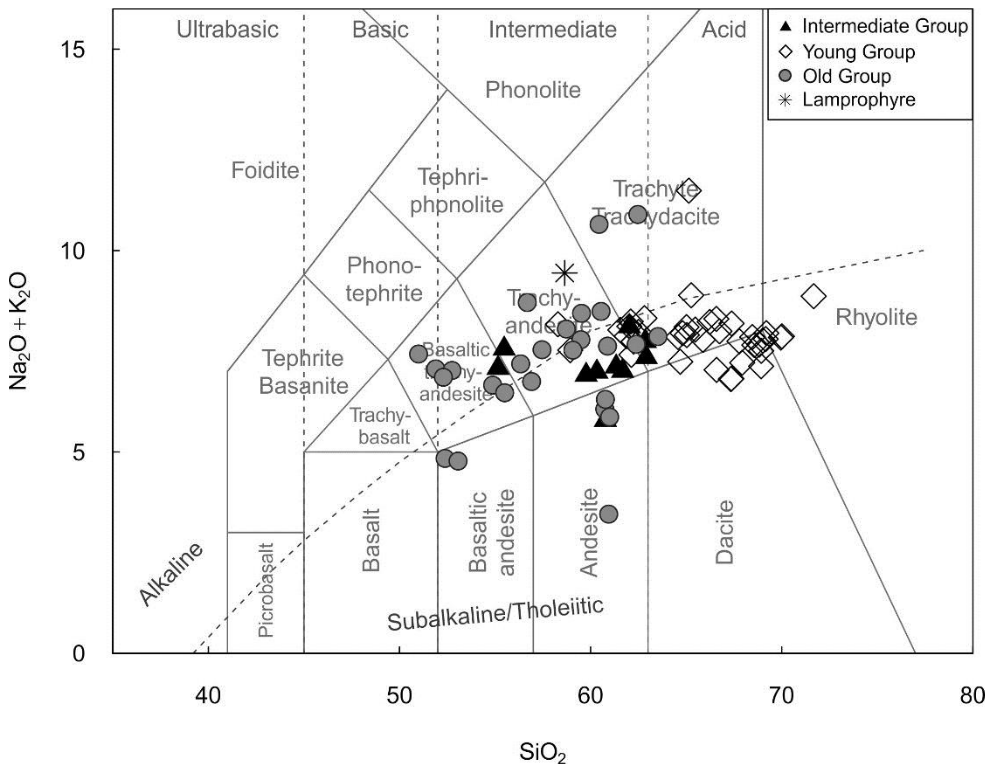

Figure 3.7.2 TAS (Total Alkali-Silica) classification diagram after *Le Bas et al. (1986)*. Discrimination alkaline-subalkaline line after *Irvine & Baragar (1971)*

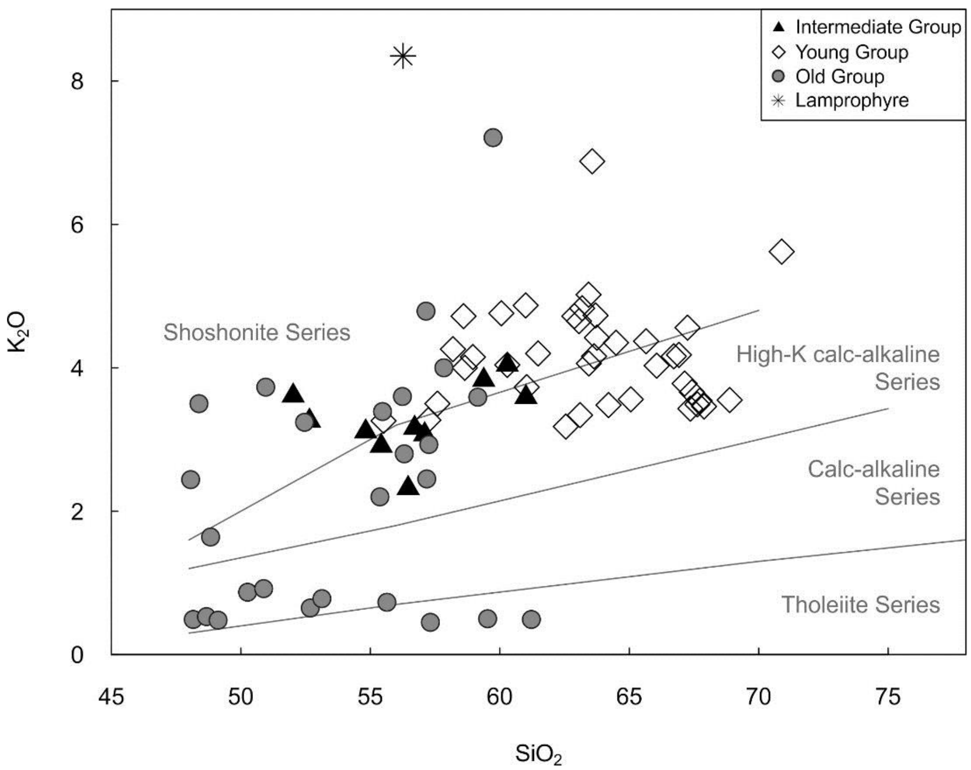

Figure 3.7.3 SiO_2 versus K_2O diagram after *Peccerillo & Taylor (1976)*

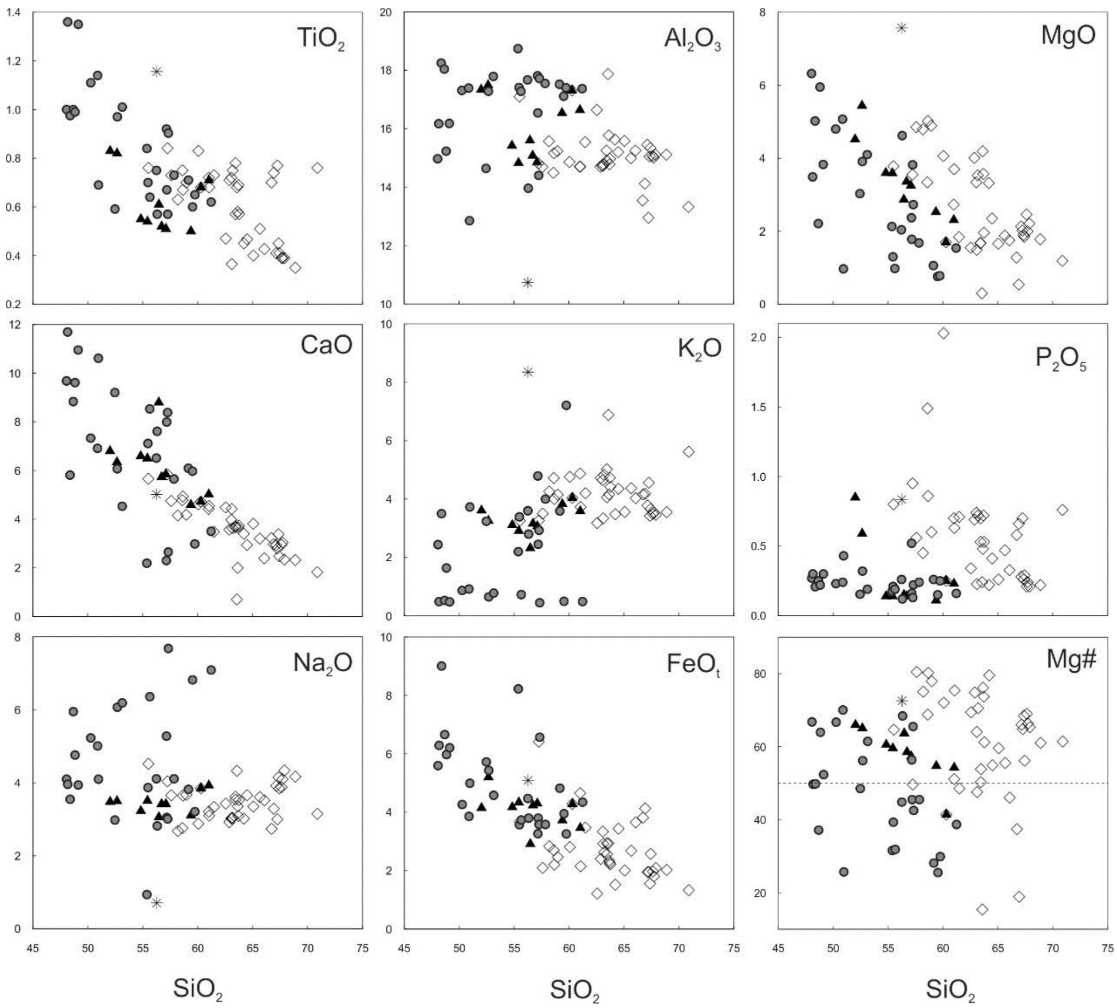

Figure 3.7.4 Variation diagrams for major elements. Symbols as in Fig. 3.7.2

3.7.4 Trace Element Geochemistry

The trace element variation trends (***Fig. 3.7.5***) exhibit significant scattering especially for the Young group. Sr, V, Y and Cr decrease with silica in all groups but in Sr the trends are parallel. There are also some Old group rocks which show a stable Cr and do not follow the decreasing trend. Ba and Nb decrease with silica for the Young group but increases for the other two groups. Zr is rather constant for the Old and Intermediate group but decreases for the Young group. Rb increases with silica for all groups except some Old group rocks which have low and constant Rb. La, Pb, U and Th increase with silica for all groups. The parallel and cross-cutting trends that the Young group displays in relation to the Old and Intermediate group shows differences in fractionating minerals in the evolution of the rocks and imply different evolutionary paths and different source.

The multi-element patterns of all three groups including the lamprophyre display typical features of convergent boundaries magmas (***Fig. 3.7.6***) with minor variations between them. LILE enrichment relative to the HSFE , TNT (T, Nb, Ti) negative anomalies and K, Pb positive anomalies are displayed by all groups. There is a negative Th anomaly for few samples of the Young group. The P negative anomaly is not displayed by the Old and Young Group but is displayed by two samples of the Intermediate group and the Lamprophyre. All groups, apart from the Intermediate for which data are missing, exhibit remarkable high Cs content which is inconsistent with magmatic procedures. The most possible explanation is the zeolites formed in this rocks which are selectively absorb Cs (*Nakamoura et al., 2013*).

Regarding the REE patterns of the Samothraki rocks some problems arise from the previous analyses of *Vlahou (2003)*. Some of the HREE analyses are problematic. This is probably due to analytical errors in specific REE as new analyses of the present study on the exact same samples which presented the same problem yielded smooth HREE patterns. All groups display LREE enrichment relative to the HREE. The Young and Intermediate groups present Eu negative anomaly which is negligible or doesn't present in the Old group and the Lamprophyre. The Old group appears more depleted than the other groups with the Young group and Lamprophyre showing the highest enrichment in LILE and ΣREE. The HREE slope of all groups (Tb_{cn}/Lu_{cn}) indicate residual garnet in the source rock.

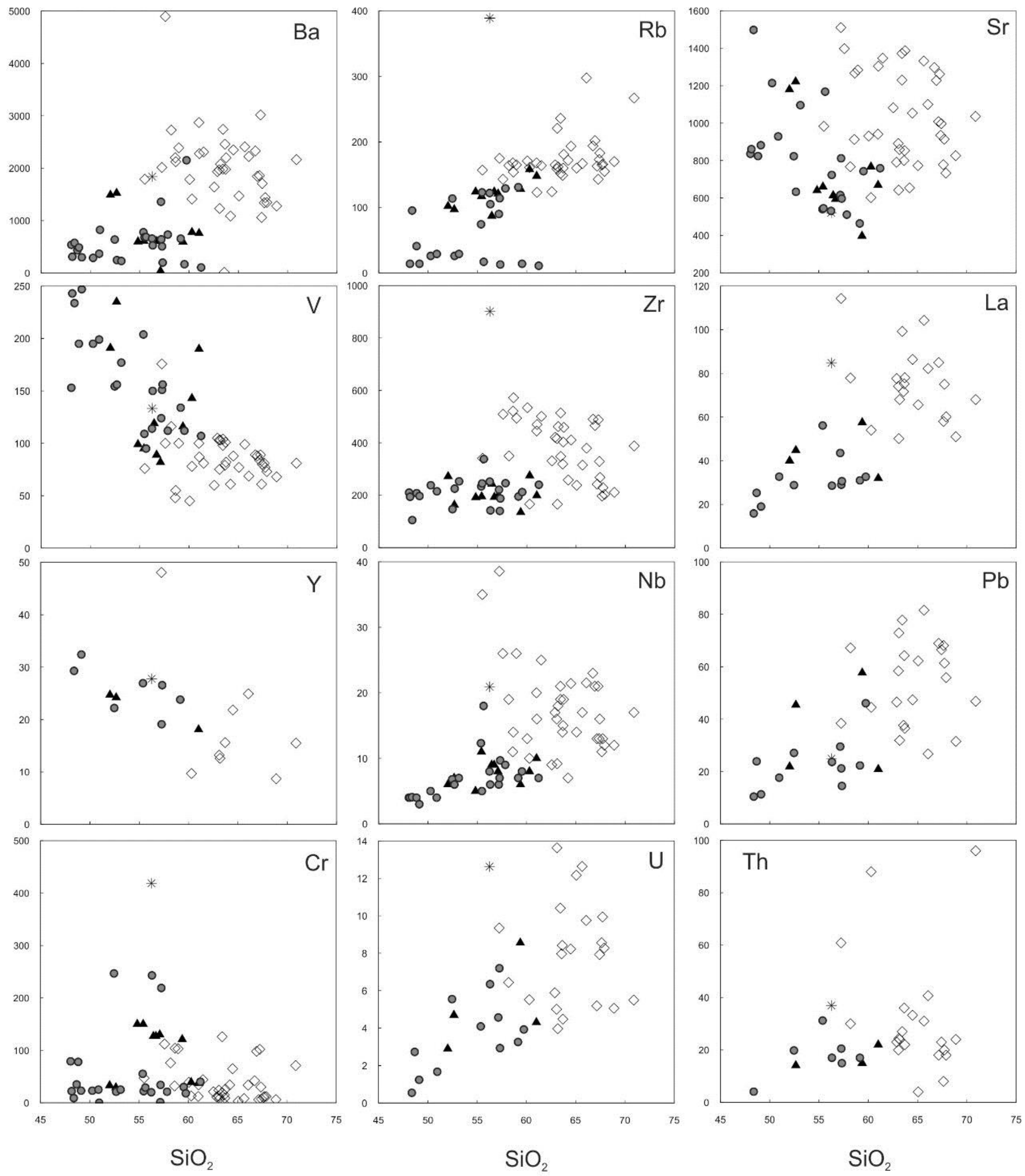

Figure 3.7.5 Variation diagrams for selected trace elements. Symbols as in Fig. 3.7.2

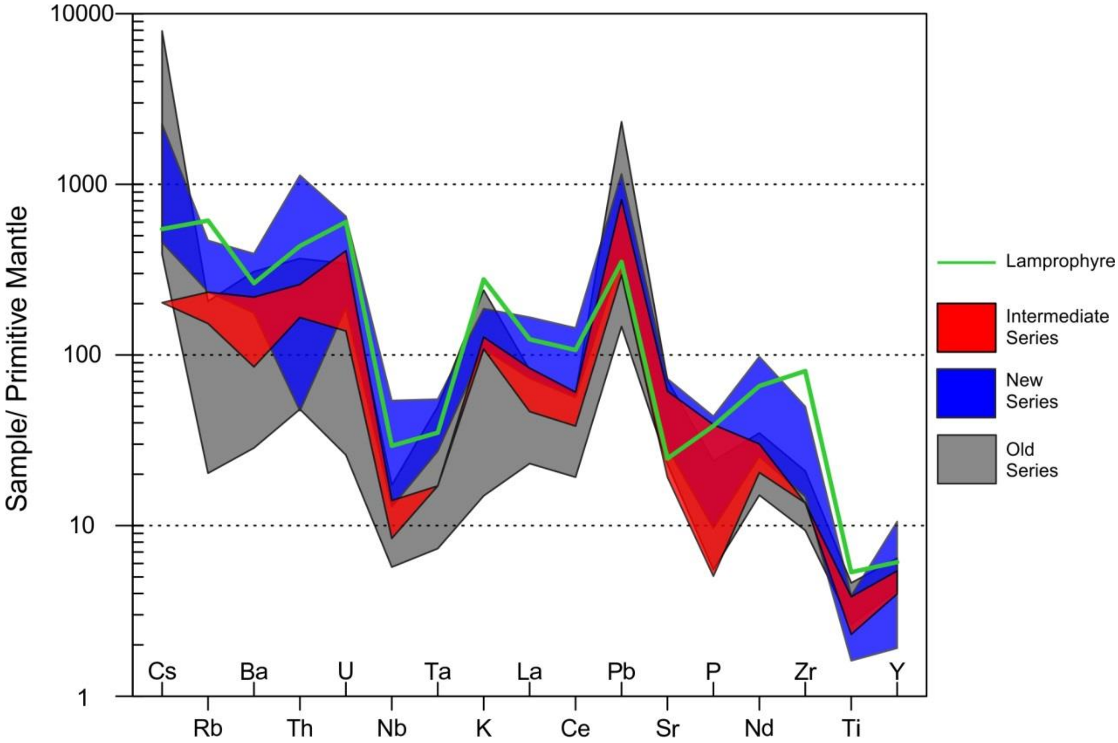

Figure 3.7.6 Multi-element spider diagram patterns. Normalisation values from *Sun & McDonough (1989).*

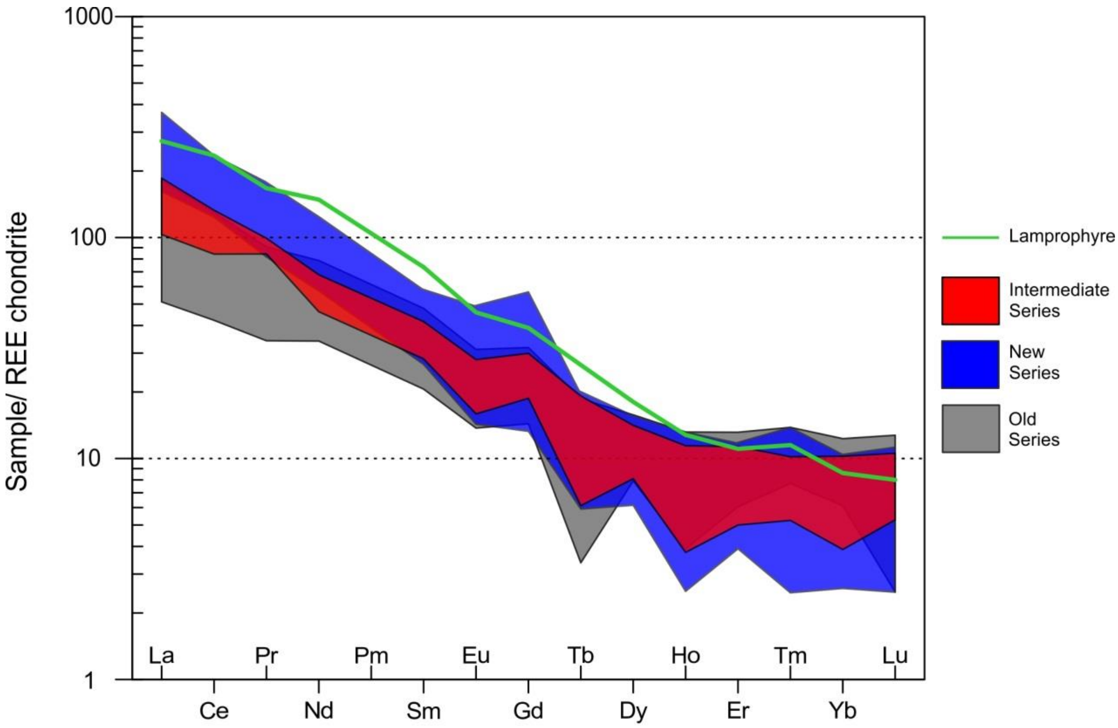

Figure 3.7.7 REE spider diagram patterns of all petrographic types. Normalisation values from *Boynton (1984)*.

3.7.5 Sr, Nd and Pb bulk isotopic composition

The Sr and Nd isotopic ratios of the Samothraki rocks clearly define three different groups (***Fig. 3.7.8***). The Sr and Nd isotopic composition is given in Appendix B. The Old group shows the more depleted isotopic raitios, the Intermediate group follows with more enriched isotopic ratios and the Young group present far more enriched isotopic ratios. Regarding the Old and Intermediate group they show typical character of mantle derived rocks with enriched isotopic ratios from a crustal component. This crustal component could be either the slab subducted sediments or the continental crust of Rhodope during their ascent. The Young group presents remarkable enriched isotopic ratios overlapping the Rhodope metamorphic complex and they are the most enriched Sr and Nd isotopes among the other Tertiary magmatic rocks of Rhodope at least for those presented here.

There are only two analysed samples for Pb isotopes provided by *Pe-Piper et al. (1998)*. Both samples are close to the EM-II and GLOSS with the Young group sample showing higher $^{207}Pb/^{204}Pb$ and $^{208}Pb/^{204}Pb$ ratio (***Figs. 3.7.9 & 3.7.10***) than the Old group sample.

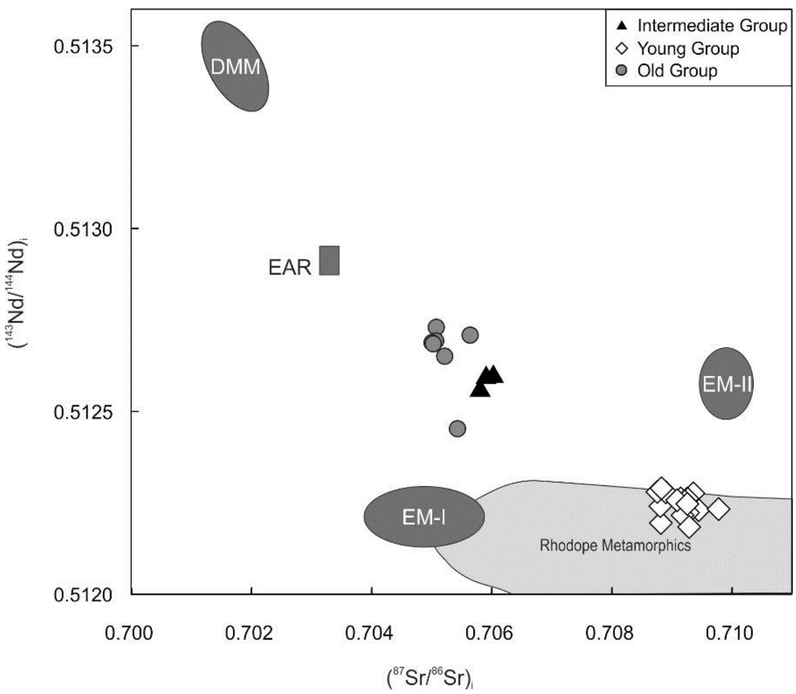

Figure 3.7.8 $(^{87}Sr/^{86}Sr)_i$ versus $(^{143}Nd/^{144}Nd)_i$. The fields illustrated are; DMM=Depleted Morb Mantle, EM-I=Enriched Mantle I, EM-II=Enriched Mantle II after *Zindler & Hart (1986)*. EAR=European Asthenospheric Reservoir after *Cebria & Wilson (1995),* Rhodope metamorphics after *Cornelius (2008) and Castorina et al. (2014)*

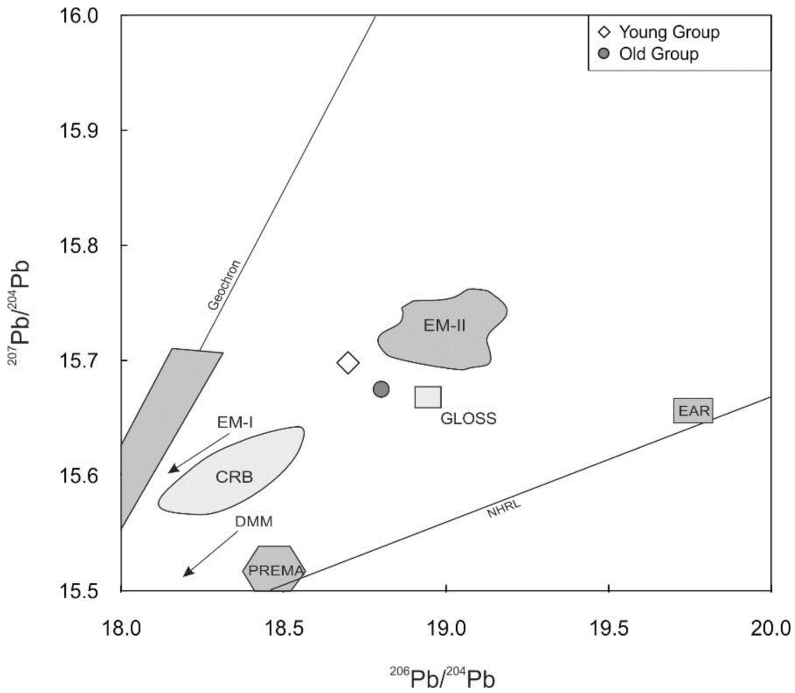

Figure 3.7.9 $^{207}Pb/^{204}Pb$ versus $^{206}Pb/^{204}Pb$. The fields illustrated are; DMM=Depleted Morb Mantle, EM-I=Enriched Mantle I, EM-II=Enriched Mantle II after *Wilson (1989)*. EAR=European Asthenospheric Reservoir after *Cebria & Wilson (1995)*. GLOSS after *Plank & Langmuir (1998)*. NHRL= North Hemisphere Reference Line after *Hart (1984)*

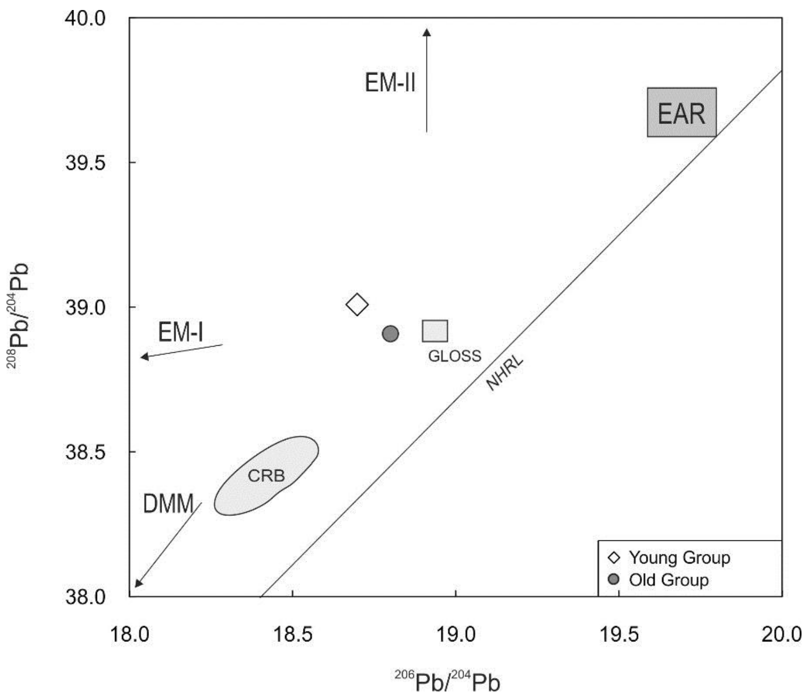

Figure 3.7.10 $^{208}Pb/^{204}Pb$ versus $^{206}Pb/^{204}Pb$. The fields illustrated are; DMM=Depleted Morb Mantle, EM-I=Enriched Mantle I, EM-II=Enriched Mantle II after *Wilson (1989)*. EAR=European Asthenospheric Reservoir after *Cebria & Wilson (1995).* GLOSS after *Plank & Langmuir (1998).* NHRL= North Hemisphere Reference Line after *Hart (1984)*

3.7.6 Petrogenetic implications

Previous workers suggest different MFC evolution processes for the Old and Young group (*Vlahou et al. 2006*). Regarding the intermediate group no evolutionary model was applied due to the high alteration of its rocks. They showed that an MFC model between a basic end-member and a more acid end-member, both with mantle signature, could explain the geochemical characteristics of the Old group. Regarding the young group they argue for a similar process though the acid end-member is lacking.

The isotopic ratios of Sr, Nd, suggest clear mantle origin for the Old and Intermediate group with minor contribution from crustal material. Whether this crustal material is of subducted sediment or continental origin is ambiguous. The Pb isotopic ratios might suggest an oceanic origin regarding that the Old group sample is closer to the average GLOSS. However, the EAR contribution can not be excluded regarding the geodynamic setting of the RM. The Sr and Nd isotopic ratios of the Young group are highly enriched and overlap the Rhodope metamorphic basement field. Nevertheless, it can't be accounted for a crustal anatectic melt (e.g high MgO, mg#, P_2O_5, Sr contents)but rather the result of mixing between a mantle derived melt and a highly enriched continental crustal component.

It should be noted here that the presence of several lamprophyric dykes is an important evidence for the mantle origin of these rocks. These lamprophyres are in some extent contaminated because they are found intruding the Samothraki granite with sharp contacts and enclose large K-Feldspar crystals from the granite. Still, the lamprophyric mass analysed here maintain extreme compositions with very high MgO (7.6 w.%), mg# (73), Cr (418 ppm), Ni (292 ppm) and simultaneously high content in some incompatible elements which could not originate from the granite contamination. This simply indicates that this rocks originated from a highly metasomatised lithospheric mantle.

3.8 The Central Rhodope Oligocene Volcanics

3.8.1 General

The volcanic rocks of the areas Kotani-Kalotycho and Dipotarna-Kotyli-Zarkadenia (***Fig. 3.8.1***) are Oligocene in age on the basis of biostratigraphic evidence and radiometric determination and are known as the Central Rhodope Oligocene Volcanics (CROV, *Eleftheriadis, 1995*) and are located at the Greek-Bulgarian borders. They belong to the Oligocene series of the Rhodopian magmatic rocks.

They range in composition from basalts to rhyolites, and belong to orogenic calc-alkaline and shoshonite series. These lavas were erupted during an extensional tectonic event, in a post-collisional setting. The eastern part of the occurance, the Kotani-Kalotycho area, includes mainly basic to intermediate rocks (basalts, basaltic andesites, high-K andesites, latites, trachytes), whereas the western part, the Dipotama-Kotyli and Zarkadenia areas, is of larger extent and consists of acid rocks only (high-K dacites, rhyolites). They cut across the crystalline basement of the RM and are structurally associated with the formation of sedimentary (extensional) basins (*Baker & Liati. 1991*). In particular, the volcanics of the Kotani-Kalotycho area were erupted in a NE-SW-trending sedimentary basin containing basal conglomerates and conglomeratic mollasse-like sandstones with layers of nummulitic limestone.

The volcanic products are usually interbedded within clastic sediments. Similarly, the Dipotama -Kotyli volcanic rocks crop out in a sedimentary basin which locally contains lignite layers and fossils of Oligocene age. Both basins are fault-controlled and belong to the Eastern Rhodope basins which were initiated during the Eocene.

They are considered to have been formed in an extensional regime. The studied rocks occur in the form of dyke-like bodies, necks and domes as well as lava flows, some of which arise from successive eruptions. Otherwise, the acid volcanic rocks of the Dipotarna-Kotyli-Zarkadenia areas form an extensive ignimbritic plateau, which continues into Bulgaria covering hundreds of km^2. The absolute ages (K-Ar dating) of the Kotani-Kalotycho basic to intermediate rocks mainly range from 35 to 29 Ma. Alike to the Dipotarna-Kotyli-Zarkadenia acid rocks, a rhyolitic rock from the same area gives an age of around 30 Ma, which coincides with that determined on similar acid volcanic rocks from the Central Bulgarian Rhodope.

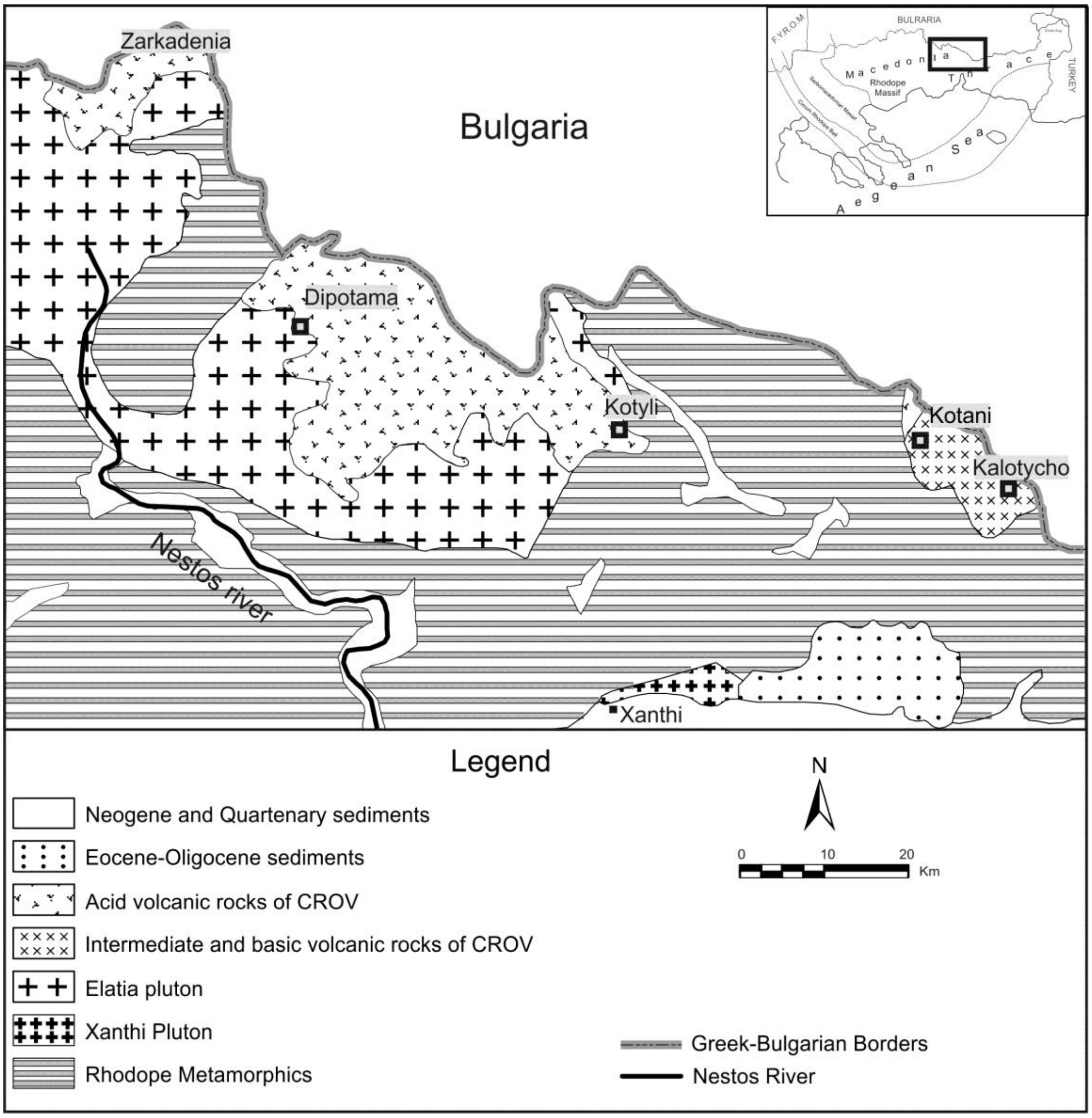

Figure 3.8.1 Simplified map of the CROV modified after *Eleftheriades (1995)*

3.8.2 Petrography and Mineralogy

The CROV were mainly studied by *Eleftheriadis (1989)* and *Eleftheriadis (1995)*. The CROV consists of basalts, basaltic andesites, andesites, high-K andesites, trachytes, high-K trachytes and rhyolites. They show an aneven geographical distribution with Kotani-Kalotycho (K-K) area containing a greater variety of rock-types than the other areas despite its smaller size. The volcanic rocks of the K-K area are mainly classified as basalts, high-K basaltic andesites, high-K andesites, latites and trachytes, whereas shoshonitcs. andesites and rhyolites occur in subordinate amounts. In addition to the volcanic rocks which have porphyritic textures, there are subvolcanic rocks (dolerites) of basaltic to high-K basaltic andesite composition showing typical ophitic texture. These subvolcanic rocks are found intruding the basement of the area but never intruding the other volcanic rocks of the CROV.

The volcanic and subvolcanic rocks with silica contents up to about 60 wt.% contain phenocrysts of plagioclase (An_{70-50}), calcic augite and subordinate amounts of hypersthene set in a crystalline to hypocrystalline groundmass. In some cases, hypersthene crystals are rimmed by clinopyroxene. Olivine phenocrysts or pseudomorphs of serpentine after olivine appear in some basaltic andesites. Minor amounts of interstitial sanidine and phlogopite occur in some dolerites whereas hornblende (magnesio-hastingsite) occurs rarely in the shoshonites and rocks with silica greater than 60 wt%. The latites and trachytes are distinguished from the other rock-types by their abundant whitish to pinkish sanidine phenocrysts up to 2 cm in length. Apart from sanidine there are also phenocrysts of plagioclase (An_{50-45}). biotite and clinopyroxene of diopsidic composition set in a crystalline groundmass. Feldspars are usually slightly to moderately kaolinized whereas biotite is almost entirely altered to chlorite and epidote. Apatite, sphene and Fe-Ti oxides occur as accessory minerals.

The volcanic rocks of the Dipotama-Kotyli and Zarkadenia (D-K-Z) areas are classified as high-K dacites and rhyolites. They have a porphyritic texture with phenocrysts and phenocrystal fragments of plagioclase (An_{40-20}), sanidine and quartz . The latter two minerals commonly show embayed margins. while some plagioclase crystals have "spongy" or "skeletal" Ca-rich cores (up to An_{75}). surrounded by normally-zoned Na-rich plagioclase. Biotite occurs in all the studied rocks while hornblende (magnesia- hornblende and very rarely, magnesian hastingsitic hornblende) appears in most of them. These two minerals are usually opaque and reverse-zoned . In the high-K dacites clinopyroxene occurs in almost equal amounts with biotite generally showing disequilihrium textures. Apatite, Zircon, sphene and titanomagnetite are the accessory minerals. The groundmass varies from entirely glassy to microcrystalline, often exhibiting linear flow structures and vitroclastic textures. Spherulites occasionally are developed due to extensive devitrification of the glassy groundmass. In some cases, rhyolitic rocks enclose xenoliths (garnet bearing two-mica gneisses) and/or isolated mineral phases derived from the crystalline basement.

3.8.3 Major element Geochemistry

The geochemical data used for the CROV are a combination of published data of *Eleftheriadis (1995)* and new data given in Appendix A. For the needs of the present study the rocks were separated in three groups, the Basic, the Intermediate and the Felsic according to their petrographical and geochemical characteristics. The Basic group comprises the basalts, the Intermediate group the high-K basaltic andesites, high-K andesites, latites and trachytes while the Felsic group the dacites and rhyolites. There is also one enclave found in a rock from the Intermediate group which has high LOI (4.4 wt.%), but it could give additional information and will be included. The three groups are presented on a TAS diagram in ***Fig. 3.8.2***.

The character of all groups is mainly High-K and shoshonitic (***Fig.3.8.3***). In each group the rocks with the higher silica content present shoshonitic character. The variation diagrams of CaO, TiO_2, FeO_t, MgO and P_2O_5 present negative correlation with SiO_2 (***Fig. 3.8.3***). For Al_2O_3 there is a good negative correlation for the Intermediate and Felsic group but the Basic group displays positive trend. For K_2O there are some samples of the Intermediate and Acid groups that do not follow the trend line. For Na_2O the Basic and Intermediate group display good positive trend but the Acid group shows negative trend probably due to sanidine fractionation.

The mg# is rather scattered for all groups. The enclave seems to follow the basic group trends in all diagrams. The Basic and Intermediate group show rather high MgO content but rocks of all three groups show rather high mg# contents.

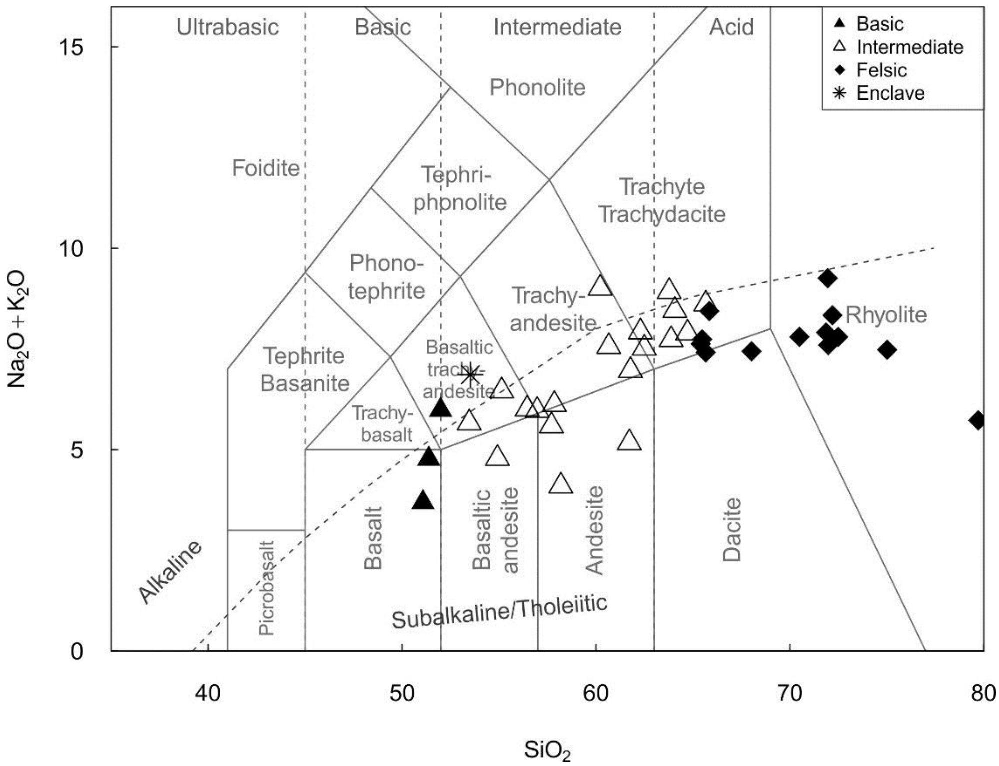

Figure 3.8.2 TAS (Total Alkali-Silica) classification diagram after *Le Bas et al. (1986)*. Discrimination alkaline-subalkaline line after *Irvine & Baragar (1971)*

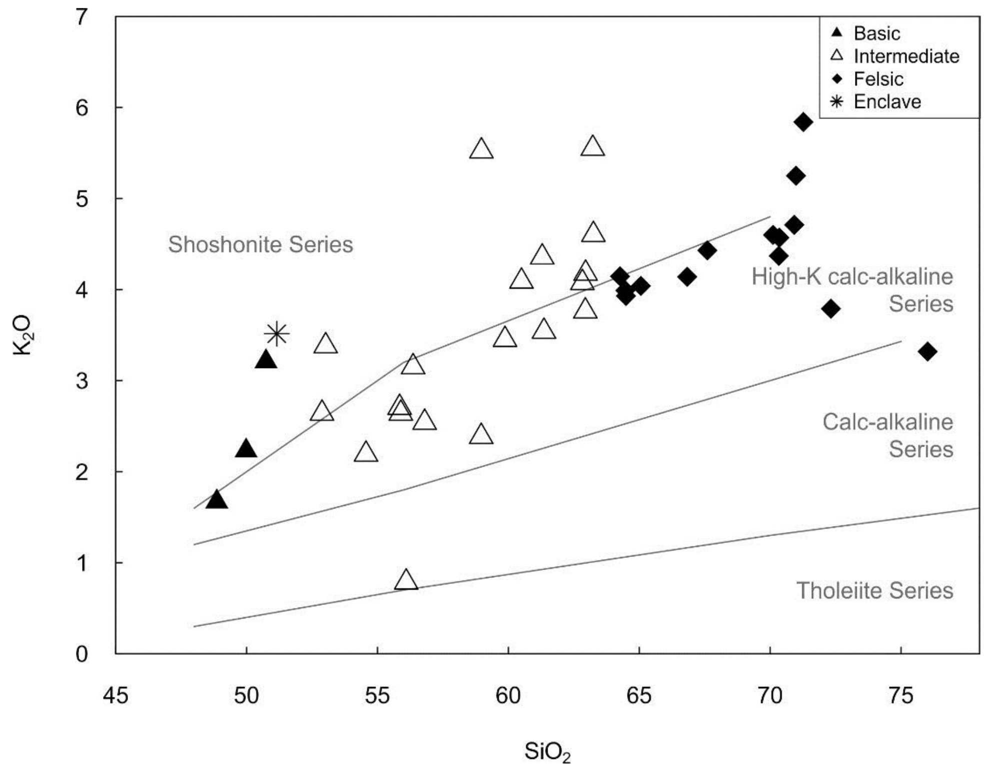

Figure 3.8.3 SiO_2 versus K_2O diagram after *Peccerillo & Taylor (1976)*

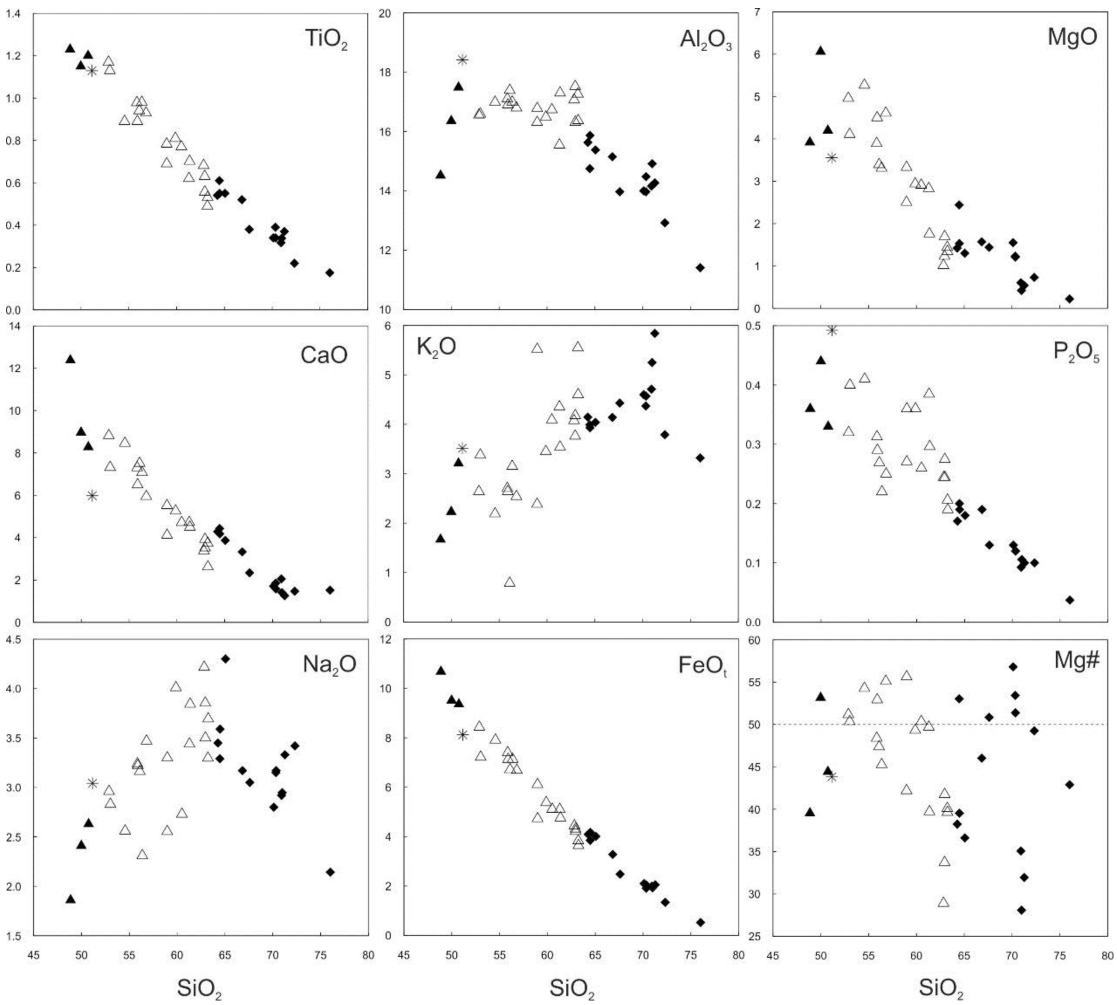

Figure 3.8.4 Variation diagrams for major elements. Symbols as in Fig. 3.8.2

3.8.4 Trace Element Geochemistry

The trace elements of Rb, Nb, Pb, U, Th display a good positive trend with differentiation (***Fig. 3.8.5***). Some trace elements like Ba, Y, and La increase with differentiation for the Basic and Intermediate group while they decrease for the Acid group probably due to different mineral fractionation. For Zr and La the trends are rather scattered for the basic group, is positive for the Intermediate group and negative for the Acid group. Sr, V and Cr show negative correlation with silica for all groups. The enclave found in the Intermediate group doesn't seem to follow the Basic or the Intermediate group trends.

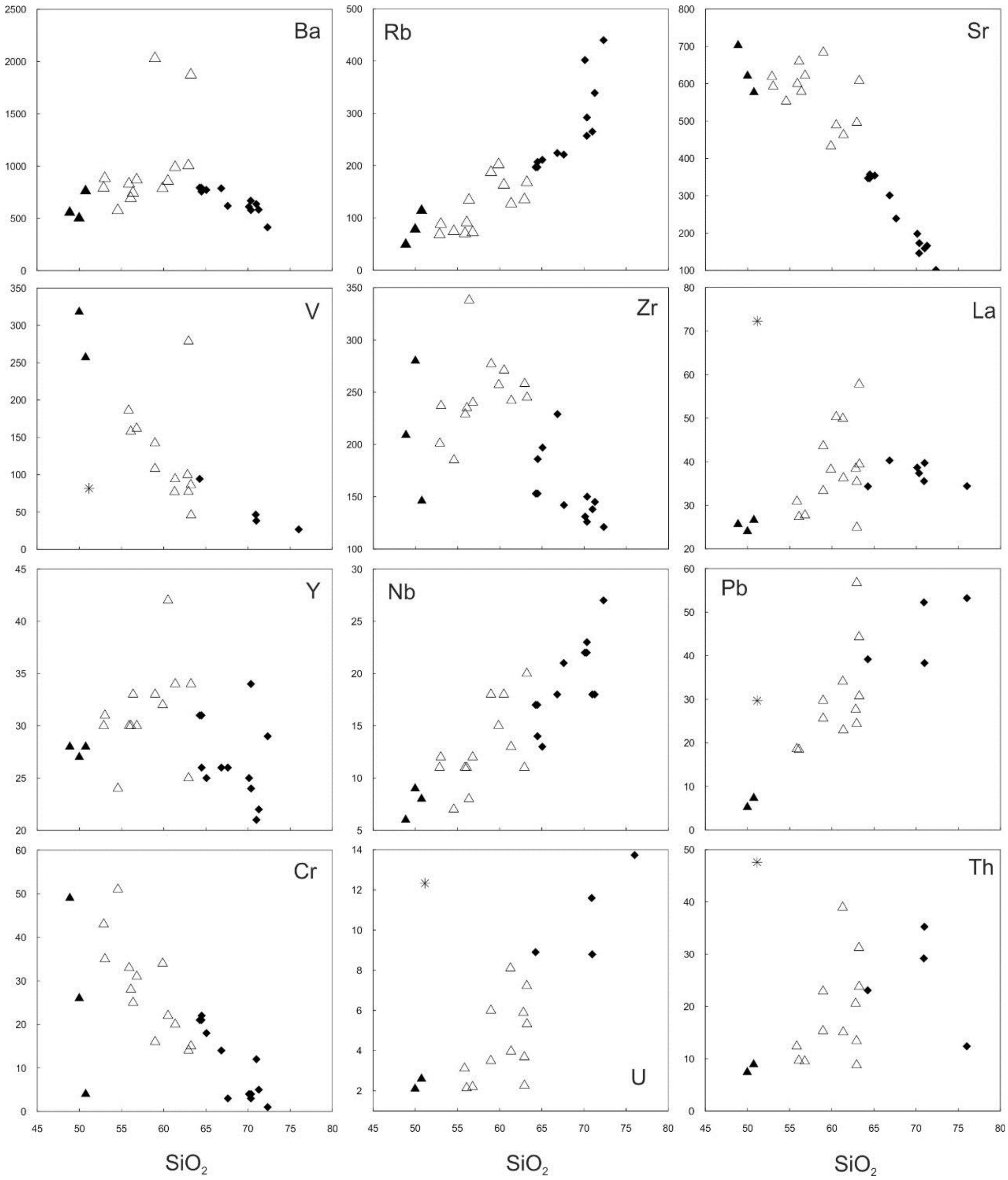

Figure 3.8.5 Variation diagrams for selected trace elements. Symbols as in Fig. 3.8.2

The trace element primitive mantle normalised patterns of the CROV rocks are typical for convergent boundaries geotectonic settings (***Fig. 3.8.6***) with LILE enrichment relative to the HSFE and TNT negative anomalies. The Basic group exhibits sligher LILE enrichment relative to the other groups and the Felsic group higher P and Ti negative anomalies. K, Pb, Th and U show positive anomalies which are also characteristics of such rocks. The Intermediate group shows a small difference regarding Ba which displays slighter negative in relation to the other groups or positive anomalies.

The REE chondrite normalised patterns of all the CROV rocks show LREE enrichment relative to the HREE and the enclave displays the highest ΣREE (***Fig. 3.8.7***). Most of the rocks display negative Eu anomaly and the Felsic group displays the highest. There are few rocks of the Intermediate group that do not display Eu anomaly.

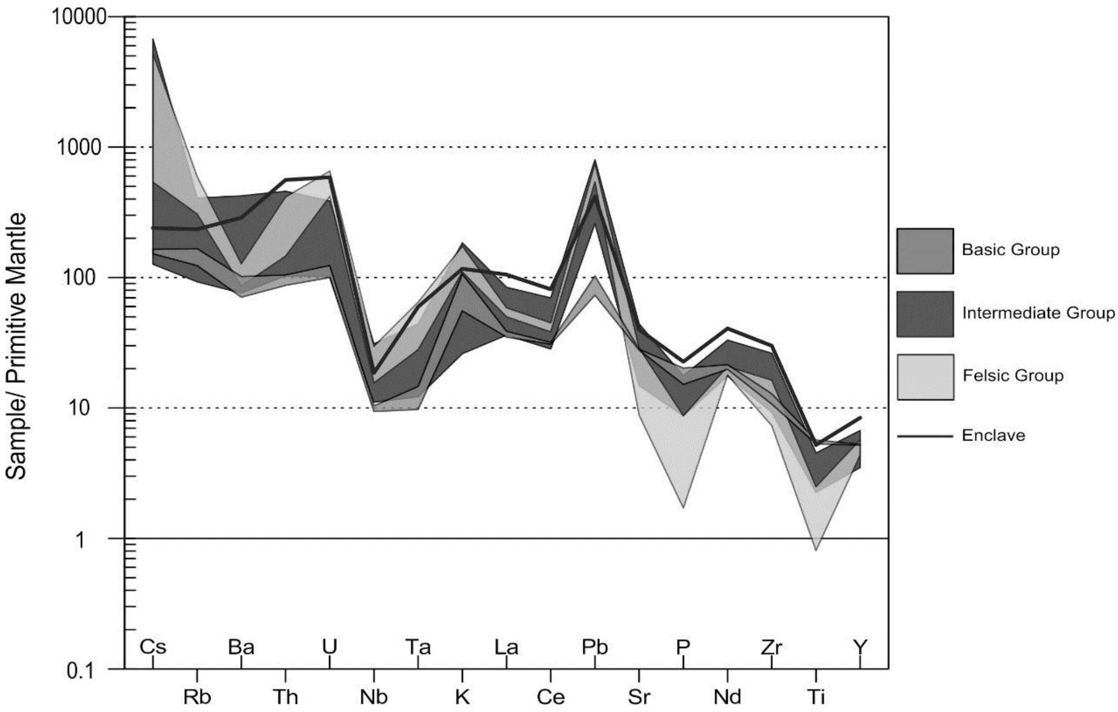

Figure 3.8.6 Multi-element spider diagram patterns. Normalisation values from *Sun & McDonough (1989)*

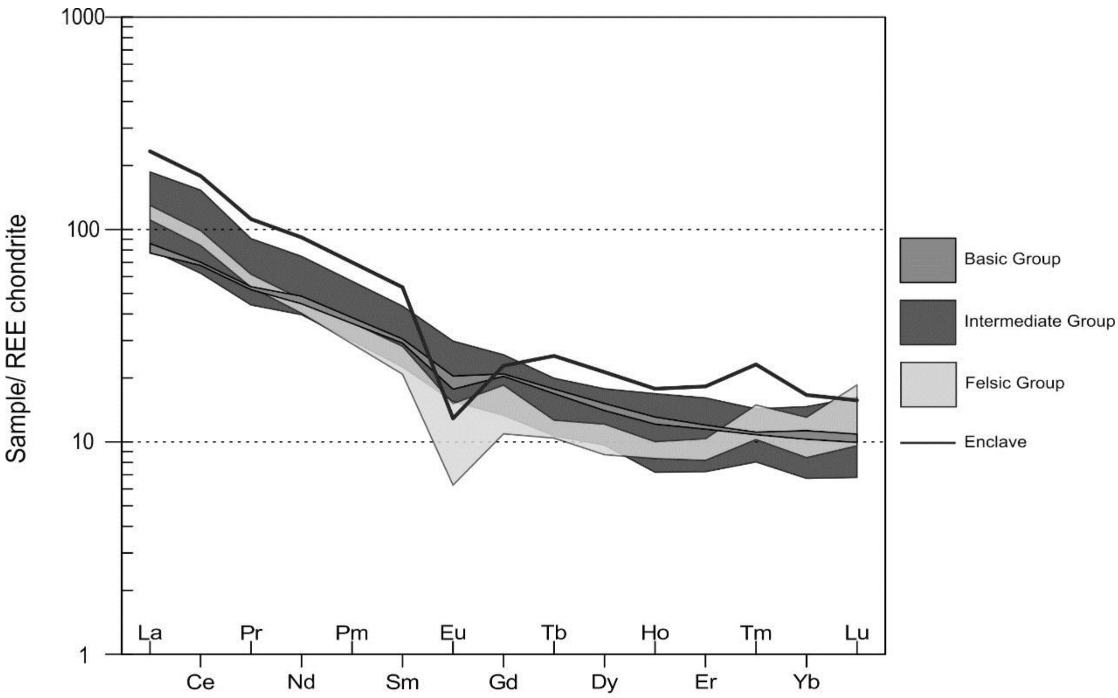

Figure 3.8.7 REE spider diagram patterns of all petrographic types. Normalisation values from *Boynton (1984)*

3.8.5 Sr and Nd bulk isotopic composition

The Basic and Intermediate groups show similar Nd_i which is rather constant at about 0.5124, but the Intermediate group shows wider range in Sr_i (***Fig. 3.8.8***). The enrichment in Sr_i of the Intermediate group could be the result of contamination of a melt with isotopic composition similar to the Basic group. On the other hand, the Sr_i and Nd_i isotopic composition of the Felsic group is rather enriched relative to the other two groups.

The initial isotopic compositions of the Basic and Intermediate group show a rather mixed origin; a mantle component (DMM of EAR) mixed with a crustal component (***Fig. 3.88***) while the Felsic group shows more enriched isotopic composition close to the Rhodope metamorphics. There are two assumptions for the origin of the Felsic group that can be made; the first is that a mafic melt similar to the Basic or the Intermediate group subjected through extensive contamination from the basement rocks of Rhodope Massif and the second that the Felsic group is a pure crustal melt.

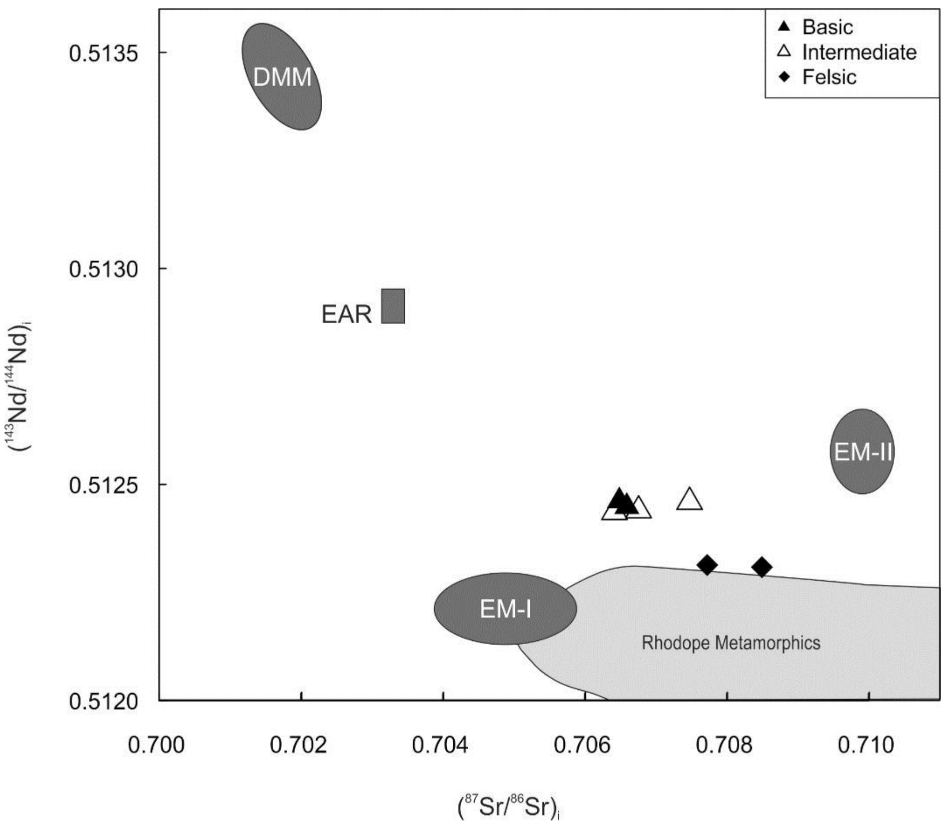

Figure 3.8.8 ($^{87}Sr/^{86}Sr)_i$ versus ($^{143}Nd/^{144}Nd)_i$. The fields illustrated are; DMM=Depleted Morb Mantle, EM-I=Enriched Mantle I, EM-II=Enriched Mantle II after *Zindler & Hart (1986*). EAR=European Asthenospheric Reservoir after *Cebria & Wilson (1995),* Rhodope metamorphics after *Cornelius (2008) and Castorina et al. (2014)*

3.8.6 Petrogenetic implications

For the evolution of the CROV *Eleftheriades (1995)* proposed thet the Felsic group is genetically related to the other two groups not through a simple FC (Fractional Crystallization) but through an MFC (Mixing and Fractional Crystallisation) proccess. Taking into account the whole rock isotopic data of the present study, it becomes clear that FC cannot be applied for these rocks since the major and trace element data show genetic relationship of the Felsic group with the Intermediate group but the Felsic group has significant different isotopic ratios from the other groups. Therefore mixing or assimilation with a highly enriched component (continental crust), as the previous author suggested, is a possible mechanism for the genesis of the Felsic group rather than crustal anatexis. The most prominent mechanism to give genesis to the Felsic group is an MFC process, since a rather high incorporation of the enriched component is necessary to increase the isotopic ratios. Regarding the Basic and the Intermediate group they display rather similar isotopic composition, but in many cases the trace element data show that the genetic relationship between these two groups is rather ambiguous since the display parallel or cross-cutting trends in some trace elements (e.g Rb, Sr, Cr). Moreover the rocks that represent the Basic group are few and both volcanic and subvolcanic and thus the relationship with the rest of the other groups in not clarified. Nevertheless, the presence of the basic enclaves (one analysed) found in the Intermediate group suggest that a mixing mechanism have played a key role for the genesis of the Intermediate group. A scenario of a mafic melt represented by the Basic group mixed with a more enriched continental crustal melt during its ascent in the RM could account for the genesis of the intermediate group.

On the basis of its geochemical and isotopic data the origin of the Basic group, which probably compises the source of the CROV is a strongly metasomatised mantle since there are no crustal lithologies that via melting could produce rocks with similar geochemistry .

4. GEOCHEMICAL CHARACTERISTICS OF THE MAFIC ROCKS

4.1 Introduction

All rocks presented in the previous chapter were formed during the same post-collisional event and the subsequent extension which took place in RM and started in Eocene (paragraph 1.4) apart from the Elatia pluton which formed before the beginning of the extension processes and intruded a thickened crust (paragraph 3.2). All previous researchers attribute the genesis of the magmatic products to mantle partial melting and contamination from products of crustal anatexis (e.g *Jones et al. 1992; Christofides et al., 1998; Pe-Piper & Piper, 1998*).

In the HRM, the mafic magmatic rocks are limited in each area and primitive mantle derived rocks have not been found. However primitive mantle rocks of unorogenic origin with mantle ultramafic cumulate xenoliths have been found only in the late stage of extension in Krumovgrad alkaline basalts (*Marchev et al., 2006, 2008*). However, these ultamafic cumulate xenoliths, according to the previous authors, have been subjected in assimilation of lower crustal material.

The source of the previous magmatic activity can only be investigated through the available mafic rocks of the RM which are accounted to be the least differentiated magmas that underwent minimum or no contamination. The rocks of each area described in the previous chapter include few or more mafic members.

Although in this study there are both plutonic and volcanic rocks, they share a common geotectonic setting and mantle origin and they will be treated as representative mafic magmas for each area regardless the differences of their formation procceses during their ascendance in the Rhodopian crust.

The rocks described in this chapter were selected due to their SiO_2, MgO and mg# content in order to eliminate the result of crustal contamination. Nonetheless, there are geochemical differences among them which may be due to different factors such as crustal thickness, source contamination, degree of source partial melting, mixing or assimilation of variable continental crustal material, crystal fractionation e.t.c. Moreover, they also present different petrographical characteristics. In some areas there are only enclaves representing the mafic members (e.g. Elatia pluton) and in other areas both basic rocks and enclaves (e.g. Xanthi). Due to the above mentioned differences a geochemical description and comparison of the mafic selected rocks is necessary. Additionaly here, the trace element patterns of a dyke (sample PD-2 with SiO_2=51.18, K_2O=0.52, MgO=6.48) from the EVR broader area is presented. This dyke bears xenolites which are composed mainly of large amphibole crystals that seem to be in disequilibrium with the dyke due to the magmatic erosion they were subjected. In this area there are numerous such dykes intruding the basement but more research should be made in the future. They are attributed to mantle derived magmas which bear lower mantle xenolites and so this dyke is used here as an example of mantle derived magma contaminated from lower crustal material (*Eleftheriades et al., 1996; Baziotis & Ntaflos* personal communication).

4.2 Major and Trace elements

Mafic rocks are generally limited in Rhodope magmatic rocks and their abundance is various among the areas. The rock samples from each area selected to represent the mafic members are presented in ***Fig. 4.2.1*** on a SiO_2 versus Na_2O+K_2O diagram. Most rocks apart from the EVR display high alkali content but none of them is a true alkaline rock since nepheline in few rocks exists only as a normative mineral (LK-17, K1X, MT-117, LK-18, MAL-113)but never as mineral phase. Regarding the silica content, the rocks of Maronia, the MGbs from Xanthi, the Samothraki Old Group, the CROV and one sample from the Vrondou Low-K MME display the lower contents (41-51 wt.%). On the other hand the EVR display the highest silica contents. The K_2O content of the rocks (***Fig. 4.2.2*** and ***4.2.3***) ranges from low (0.7 wt%) for the Vrondou Low-K MME, MGb of XPC, Samothraki Old Group and some EVR and increases to very high (3.7 wt%) for nearly the same SiO_2 contents (48-52 wt%). In ***Fig. 4.2.3*** variation diagrams of the major elements with MgO are presented. In some plots each area shows good correlation with MgO (SiO_2, Al_2O_3, CaO, Na_2O, mg#) and in other plots the picture is rather scattered. In particular, the Samothraki rocks display scattered variation in most diagrams or are separated in two groups showing different characteristics. In the same areas there are samples of calc-alkaline affinity as well as samples with shoshonitic affinity. The rocks of Elatia, Maronia, CROV and the High-K MME of Vrondou clearly display shoshonitic character. The XPC displays the highest TiO_2 and Al_2O_3 contents. The Maronia rocks display the highest CaO and P_2O_5 contents as a whole, but with one High-K enclave of Vrondou (SB-38X) holding the highest position. Na_2O is higher for the Samothraki Old Group as well as for the low-K MME of Vrondou. FeO_t is very high for the XPC and very low for the Samothraki rocks. This is probably the reason that the Samothraki rocks display the highest mg# of all areas. The Samothraki rocks displaying steeper slop exceeding all other rocks and showing the highest mg# for almost all given MgO content.

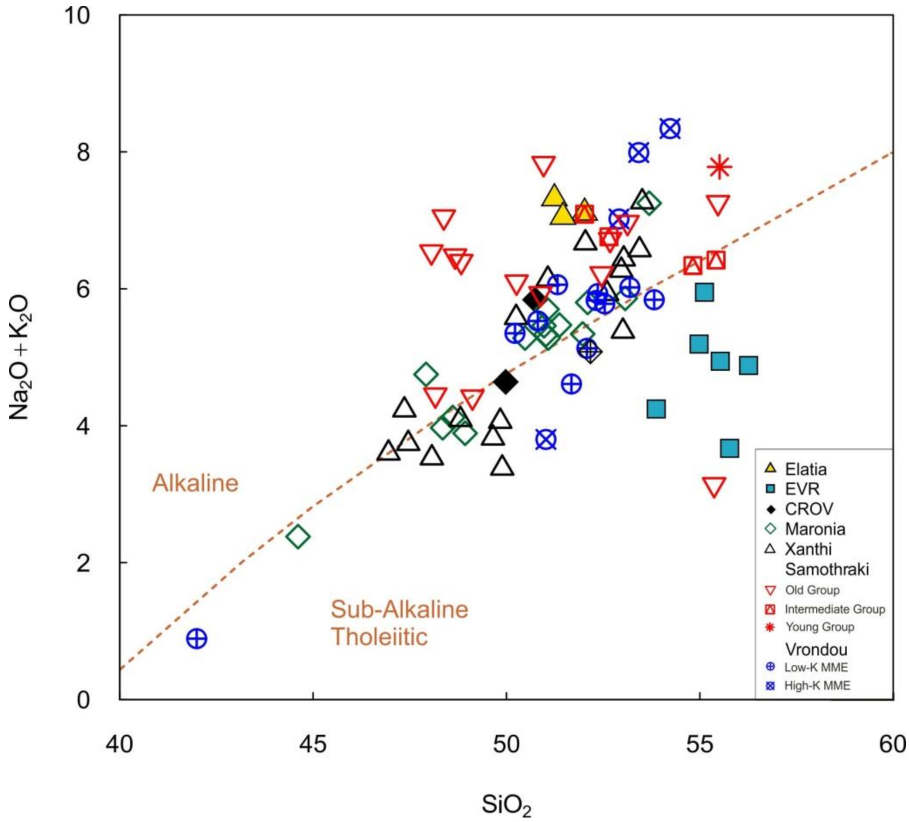

Figure 4.2.1 Discrimination of alkaline-subalkaline rocks after *Irvine & Baragar (1971)*

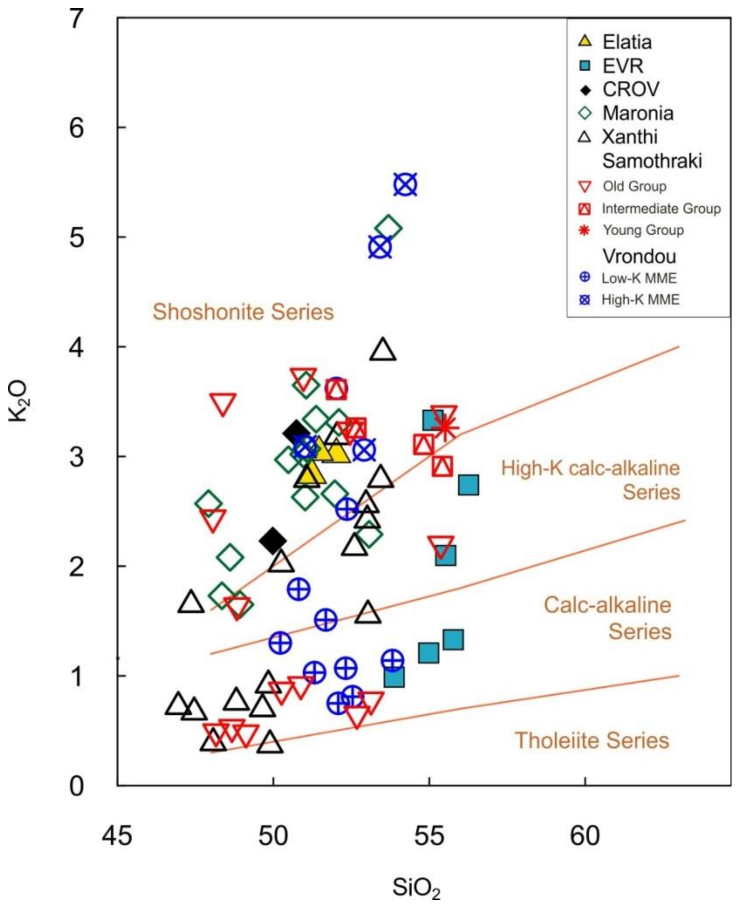

Figure 4.2.2 SiO_2 versus K_2O diagram after *Peccerillo & Taylor (1976)*

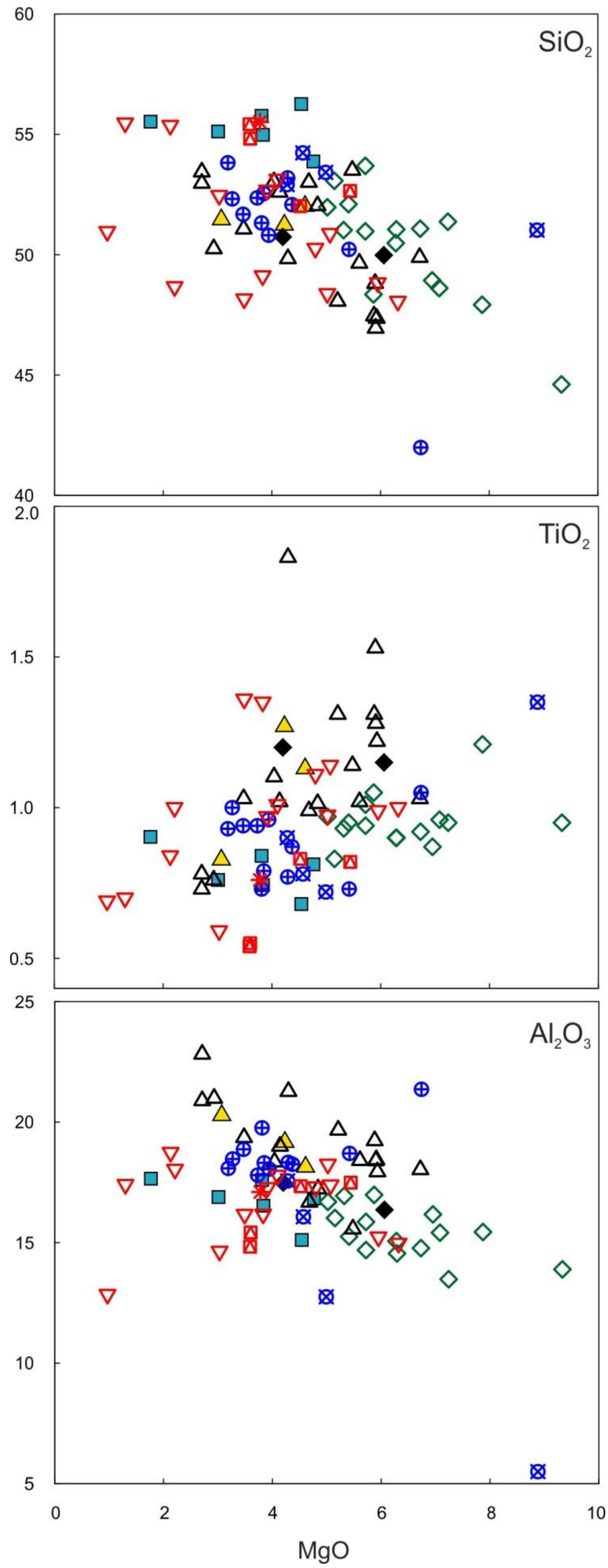

Figure 4.2.3 Variation diagrams for major elements. Symbols as in Fig. 4.2.1

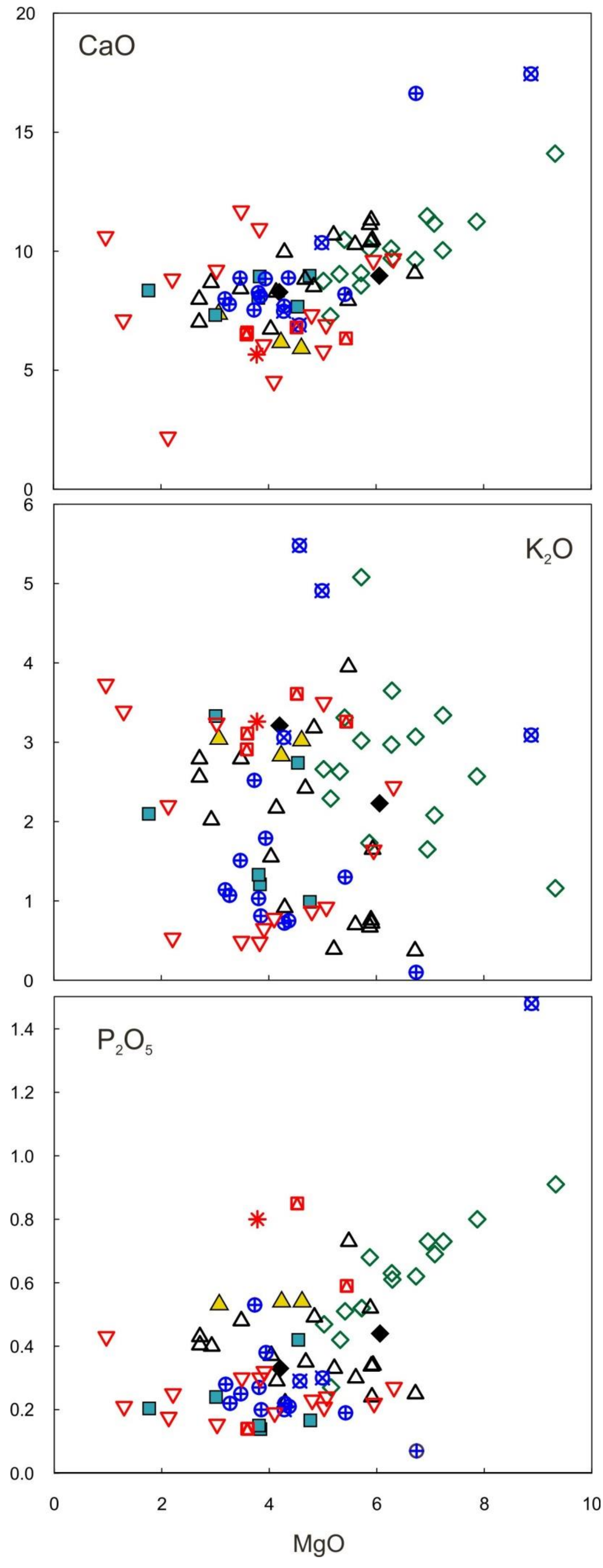
CaO
K2O
P2O5
MgO
20
15
10
5
0
6
5
4
3
2
1
0
1.4
1.2
1.0
0.8
0.6
0.4
0.2
0.0
0
2
4
6
8
10

Figure 4.2.3 (Cont.) Variation diagrams for major elements. Symbols as in Fig. 4.2.1

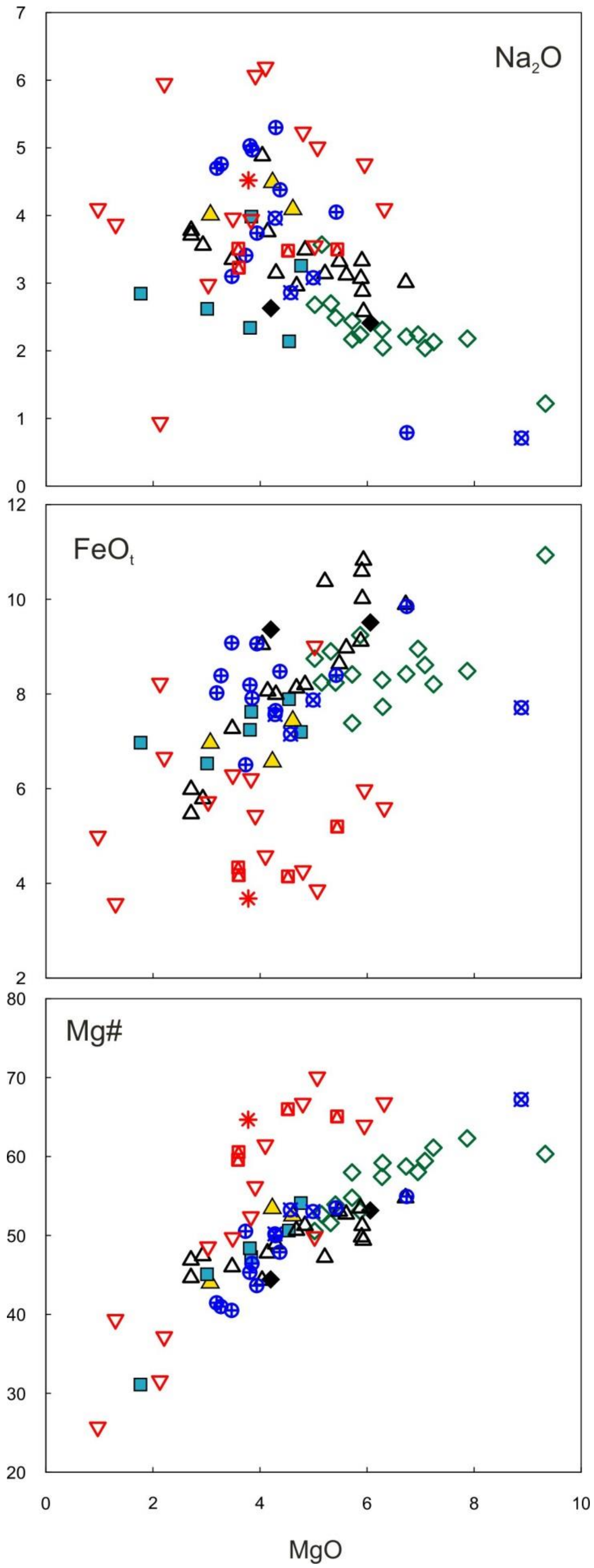

Figure 4.2.3 (Cont.) Variation diagrams for major elements. Symbols as in Fig. 4.2.1

Trace element variation diagrams of selected trace elements with MgO are presented in ***Fig, 4.2.4***. Most of the Maronia rocks display rather high Ba contents as well as few XPC and Samothraki Intermediate group rocks while the Low-K MME of Vrondou show very low contents close to zero. The High-K MME of Vrondou display the highest Rb contents while the Low-K MME of Vrondou, some XPC and Samothraki rocks show very low contents. On the opposite, both MME of Vrondou and EVR display low Sr contents while the XPC and Samothraki display the highest contents. For the compatible elements Ni and Cr the Maronia pluton has the highest contents followed by some Samothraki rocks and High-K Vrondou MME, while for V Maronia holds the highest position. Elevated Zr contents are displayed mostly from the Samothraki, Elatia and few XPC rocks and at the same time other XPC rocks display the lowest contents. The EVR has the lower La contents with the highest contents displayed by some XPC and Elatia rocks while one High-K MME displays very high La contents. Nb is relatively low for all samples apart from the SB-38X High-K Vrondou MME which displays very high contents. Pb is low in general and behaves as constant for each area with the exception of one Samothraki and one Low-K Vrondou MME with much higher contents. The SB-38X Vrondou MME displays very high Nb contents (>60 ppm), while two Low-K Vrondou MME, one of Elatia and the one Samothraki New Group rock exceed the 20 ppm. Y is rather constant for all the rocks apart from the Vrondou MME that displays good negative correlation with MgO for the Vrondou rocks, but the SB-38X sample rock displays very high contents not consistent with the rest of the Vrondou rocks. Both U and Th have a similar scattered behavior for each area. For these elements the XPC rocks display simultaneously the lowest and the highest contents. For the same elements the SB-38X MME has also very high contents (Th~50, U~13).

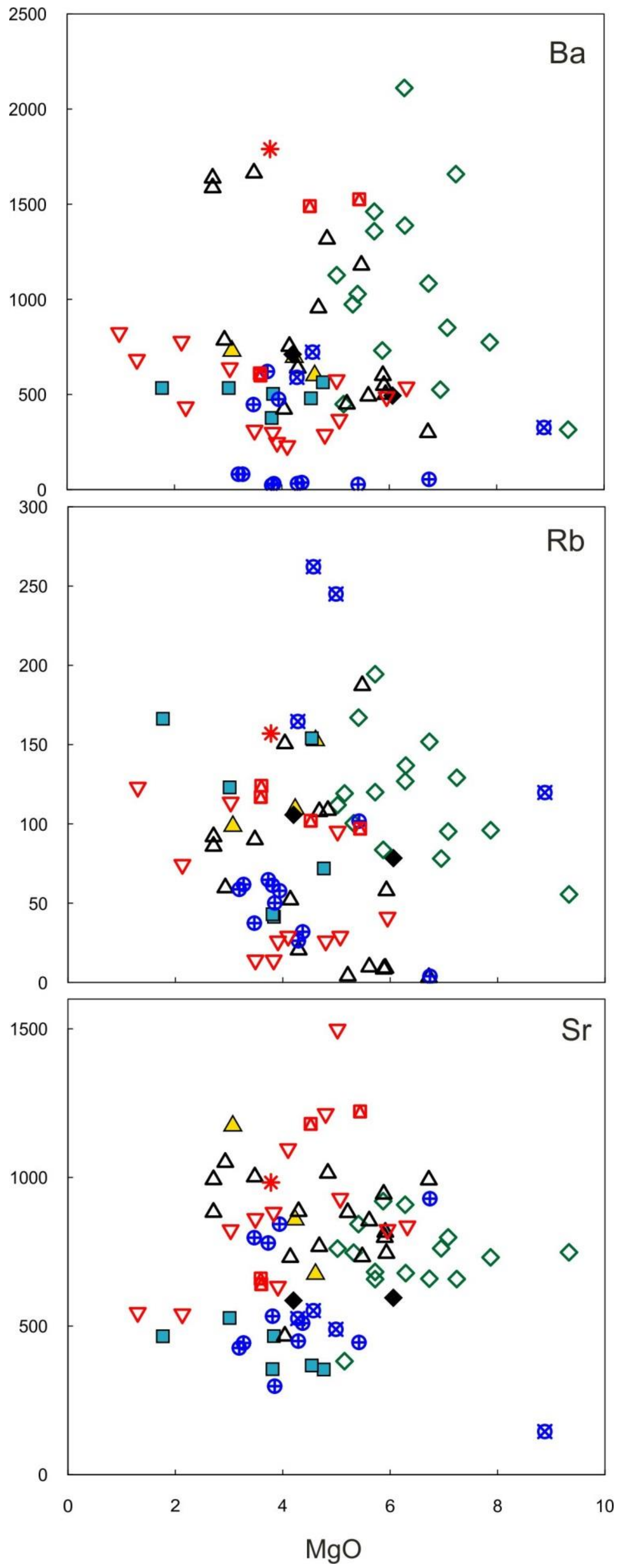

Figure 4.2.4 Variation diagrams for selected trace elements. Symbols as in Fig. 4.2.1

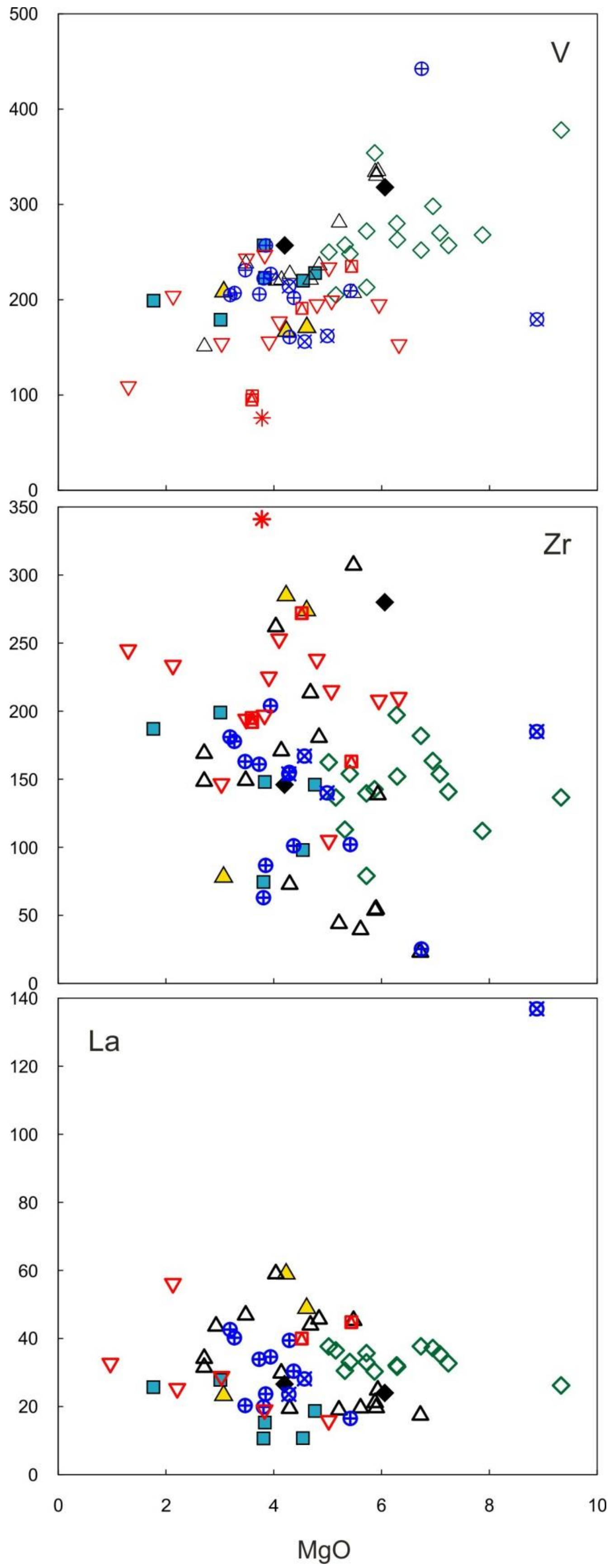

Figure 4.2.4 (Cont.) Variation diagrams for selected trace elements. Symbols as in Fig. 4.2.1

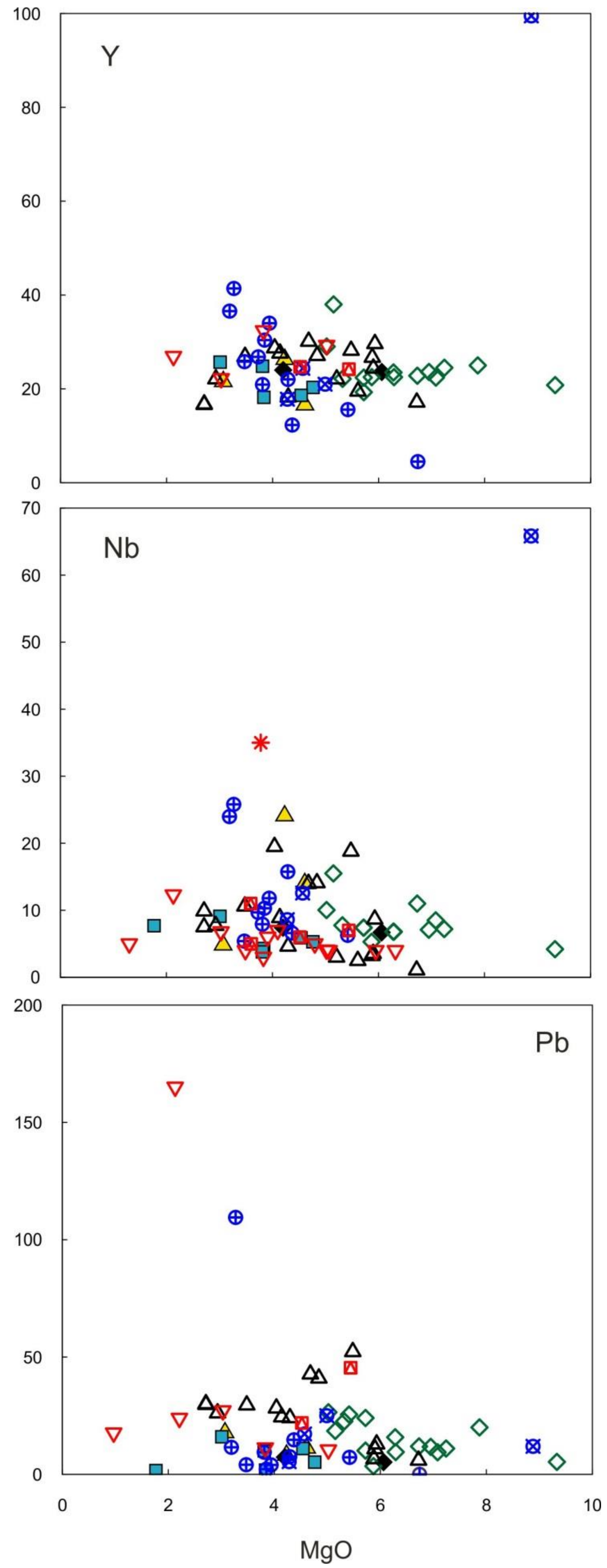

Figure 4.2.4 (Cont.) Variation diagrams for selected trace elements. Symbols as in Fig. 4.2.1

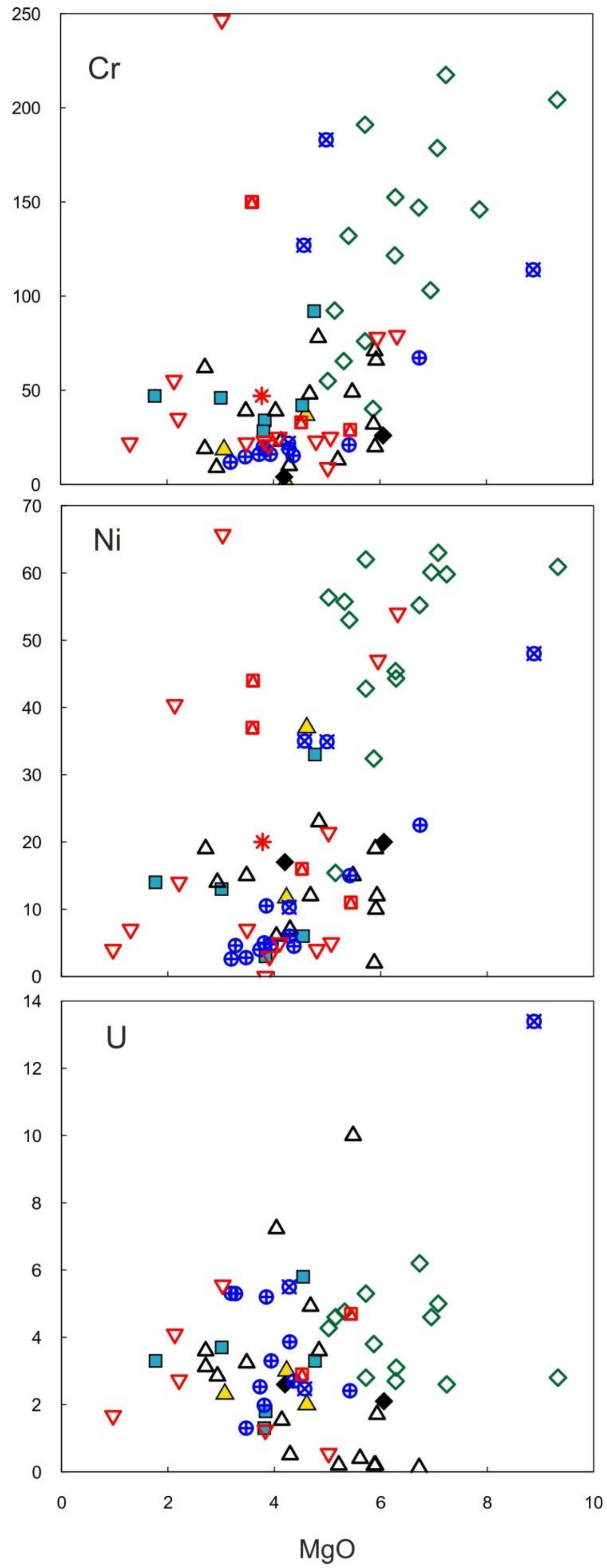

Figure 4.2.4 (Cont.) Variation diagrams for selected trace elements. Symbols as in Fig. 4.2.1

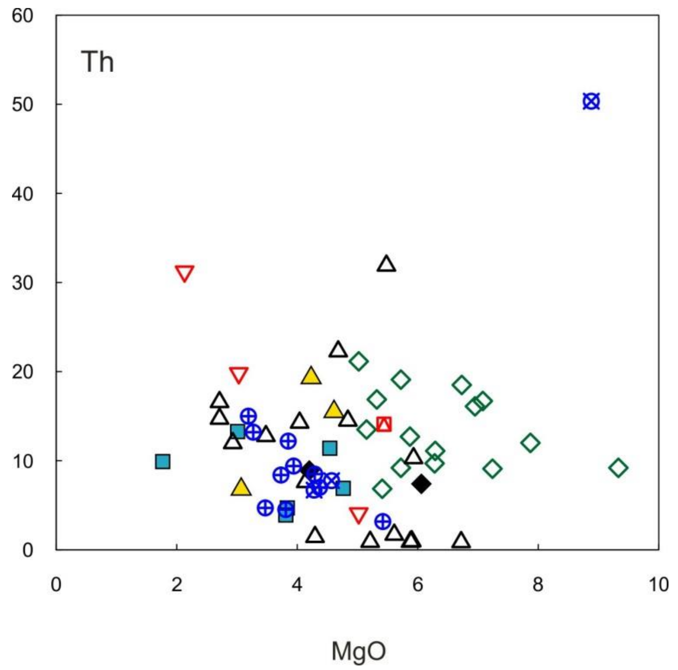

Figure 4.2.4 (Cont.) Variation diagrams for selected trace elements. Symbols as in Fig. 4.2.1

4.3 Trace Element Patterns

Trace element patterns for the mafic rocks of the study areas normalized to primitive mantle are presented in ***Fig. 4.3.1***.

All rocks present variable enrichment of LILE relative to HSFE. Most samples exhibit typical geochemical features of convergent boundaries magmas; Nb, Ti negative anomalies and Pb positive anomalies. Many rocks from Vrondou, Maronia, Xanthi, Samothraki and Elatia display a slight Ba positive anomaly or no Ba anomaly while other rocks display stronger positive anomalies (Maronia, Xanthi) while the rest rocks display negative anomalies. Th and U positive anomalies are displayed by most rocks apart from some Vrondou, Maronia, Xanthi, EVR, Samothraki Intermediate group and Elatia rocks which display negative Th anomaly. This negative Th anomaly results from the high Ba abundances and the Ba positive anomalies in these rocks. In few rocks from Vrondou Low-K MME and Samothraki Old group there is a negative K anomaly whereas all other rocks display positive K anomaly. In these cases this negative anomaly coupled with High Ta content of these rocks give, rise to a positive Ta anomaly. One more sample from

Maronia not presented in the figure due to lack of Nb and the SB-38X Vrondou High-K MME also share this positive Ta anomaly but in those cases due to high Ta contents (7.66 and 5.04 respectively). Positive Pb anomaly is presented to all samples with variable extent. P negative anomalies are generally small and in some rocks are absent or are positive (SB-38X Vrondou High-K MME, Maronia, Xanthi, EVR, Samothraki Intermediate Group). Ti negative anomalies are insignificant or are slightly positive in some rocks from Vrondou, Maronia, Xanthi, CROV and Elatia.

The REE element patterns for the mafic rocks of the study areas normalized to chondritic values are presented in ***Fig. 4.3.2***.

All rocks display LREE enrichment relative to HREE with La/Lu chondrite normalised values from 4 to 31. All rocks have Tb/Lu chondrite normalised values >1, except most of the Vrondou Low-K MME which have <1. The High-K Vrondou MME, Samothraki and CROV rocks present all negative Eu anomaly. All the other rocks do not display Eu anomaly or display positive Eu anomaly.

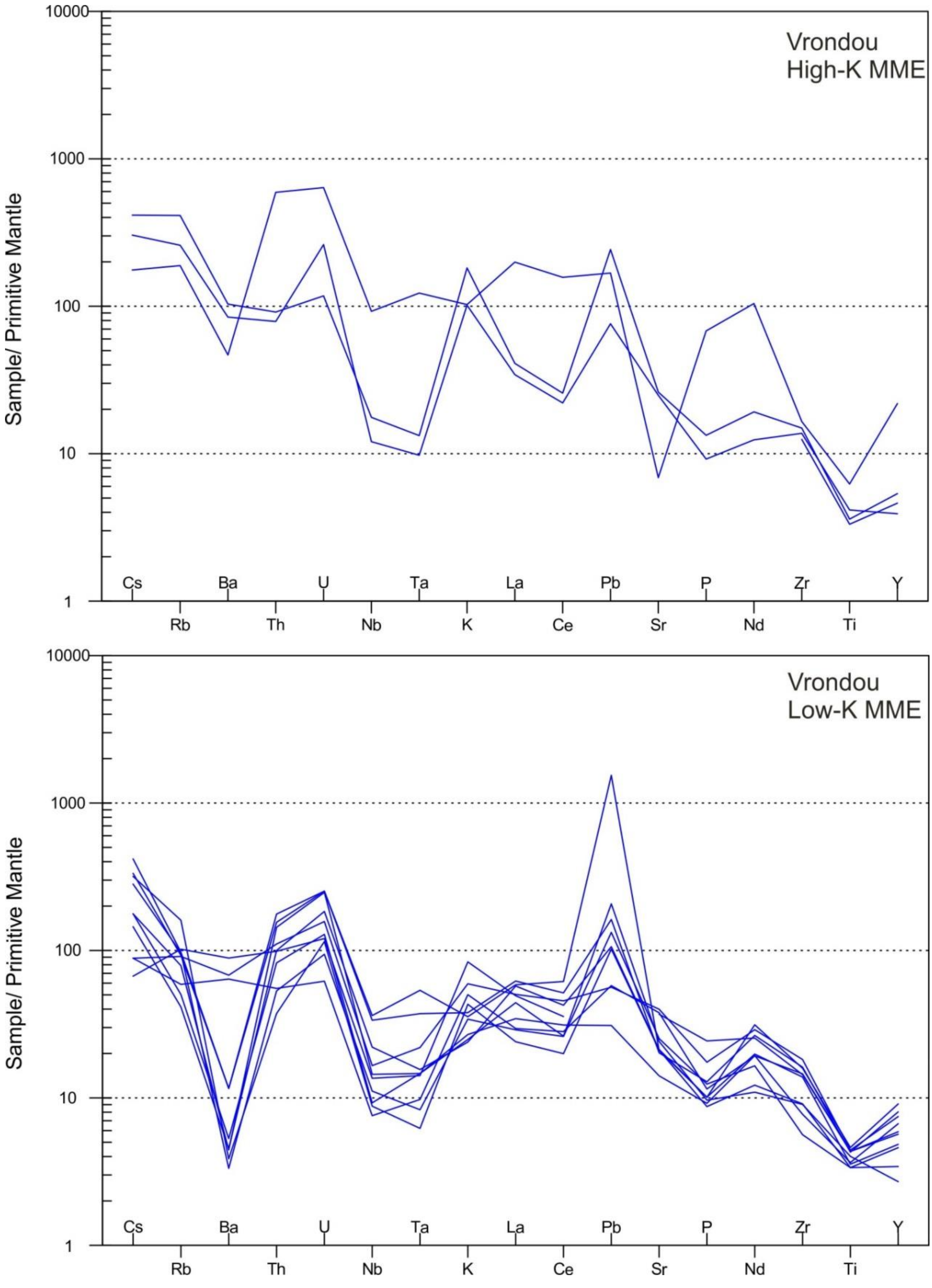

Figure 4.3.1 Multi-element spider diagram patterns. Normalisation values from *Sun & McDonough (1989)*

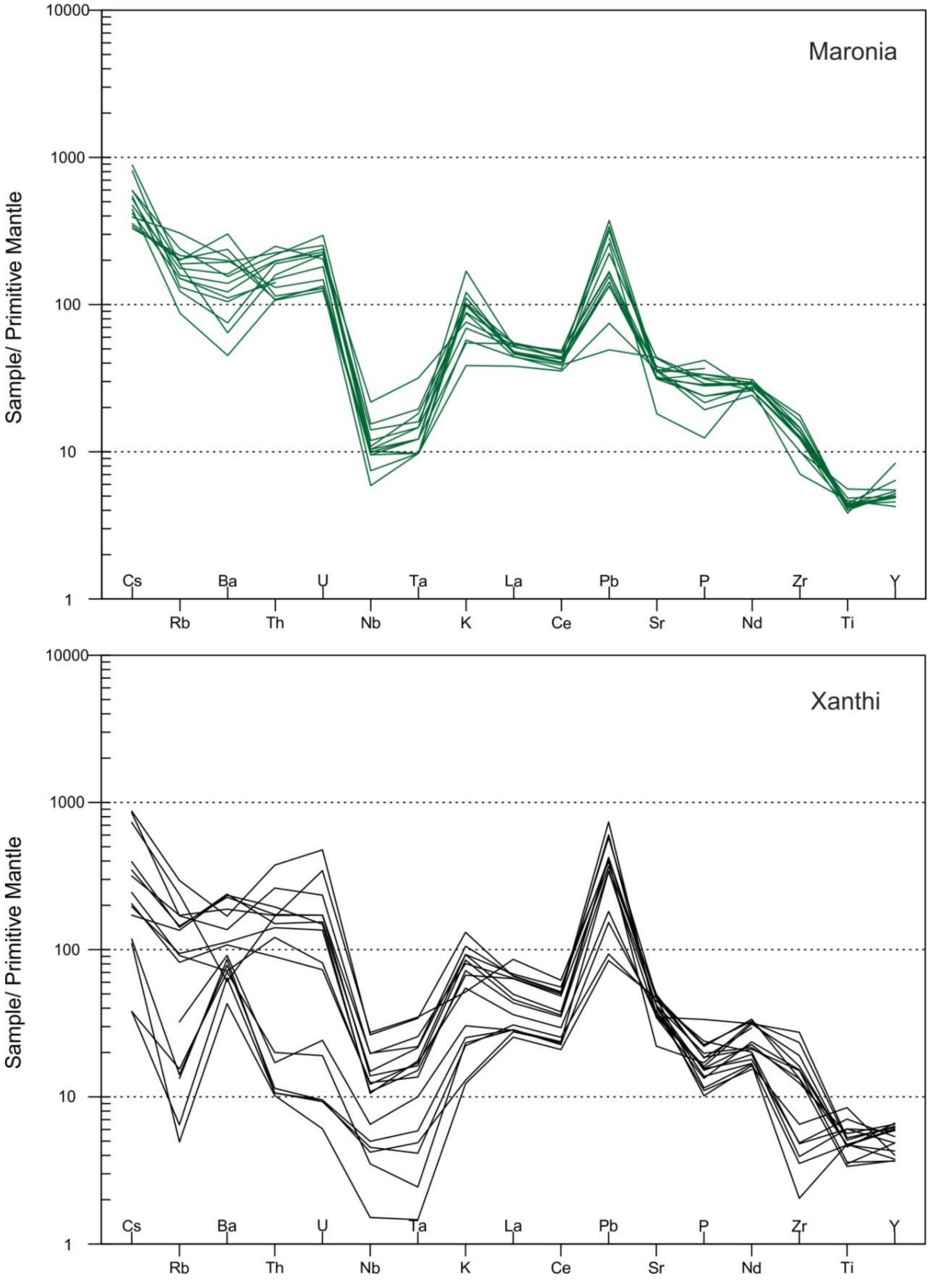

Figure 4.3.1 (Cont.) Multi-element spider diagram patterns. Normalisation values from *Sun & McDonough (1989)*

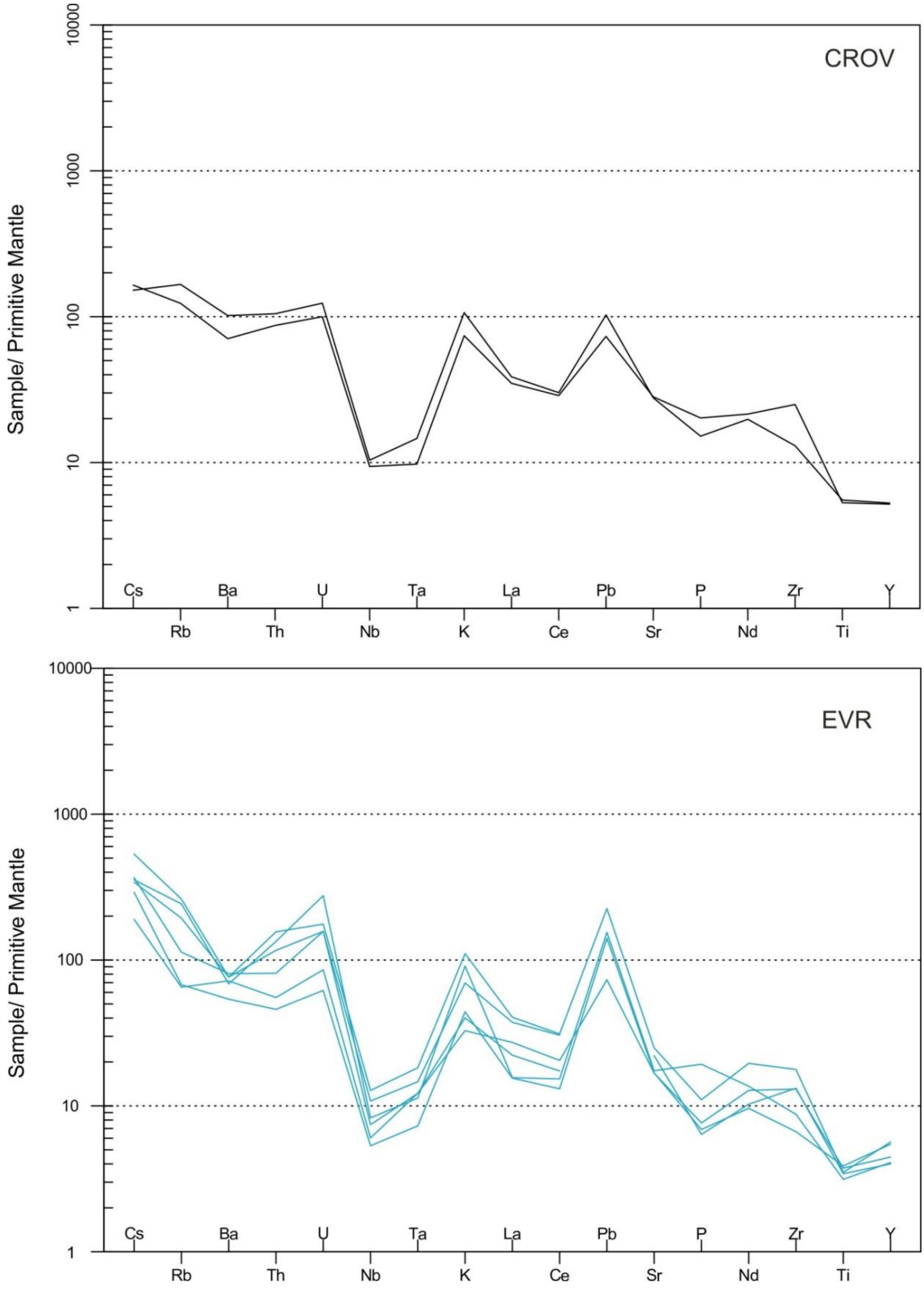

Figure 4.3.1 (Cont.) Multi-element spider diagram patterns. Normalisation values from *Sun & McDonough (1989)*

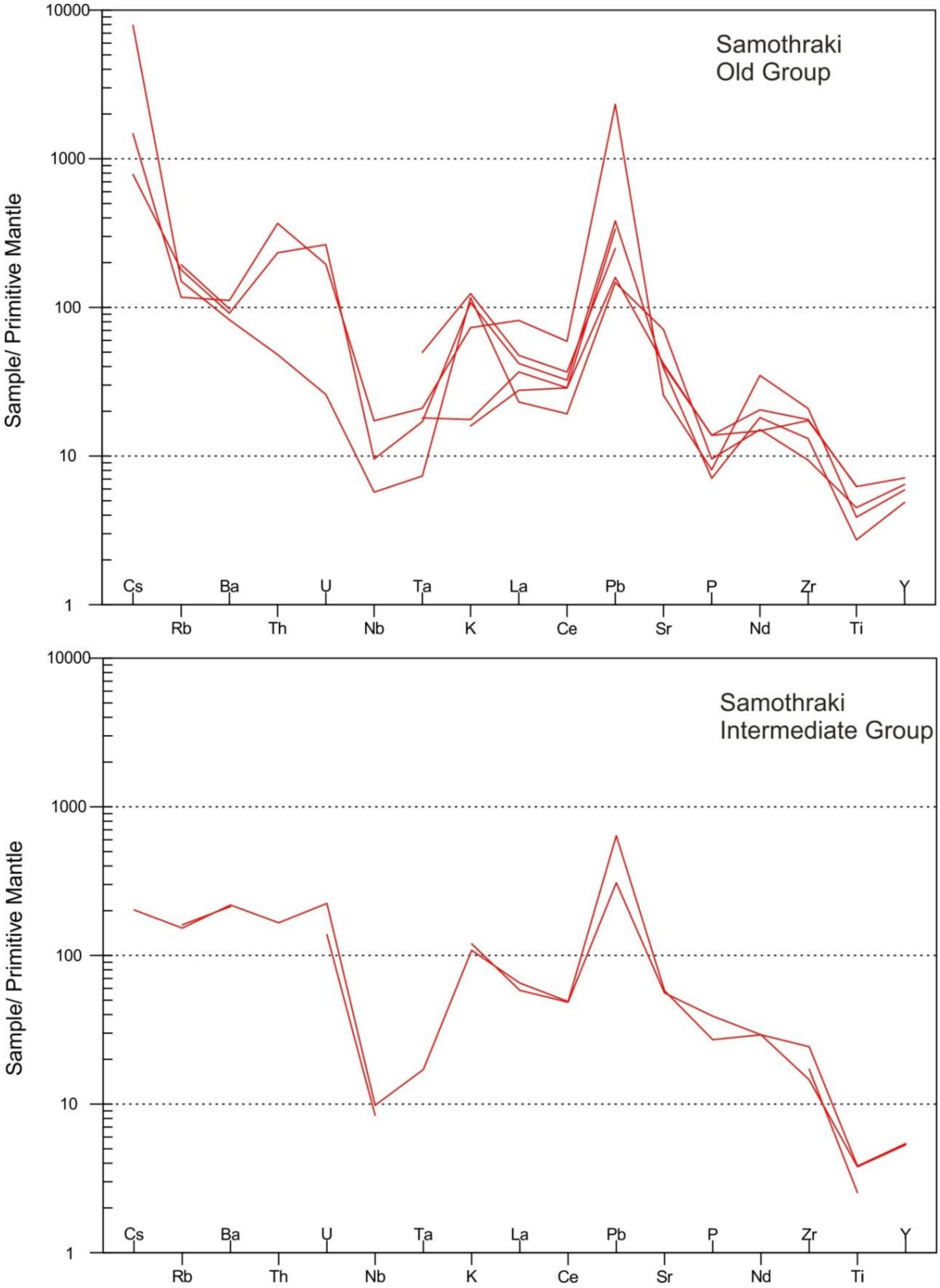

Figure 4.3.1 (Cont.) Multi-element spider diagram patterns. Normalisation values from *Sun & McDonough (1989)*

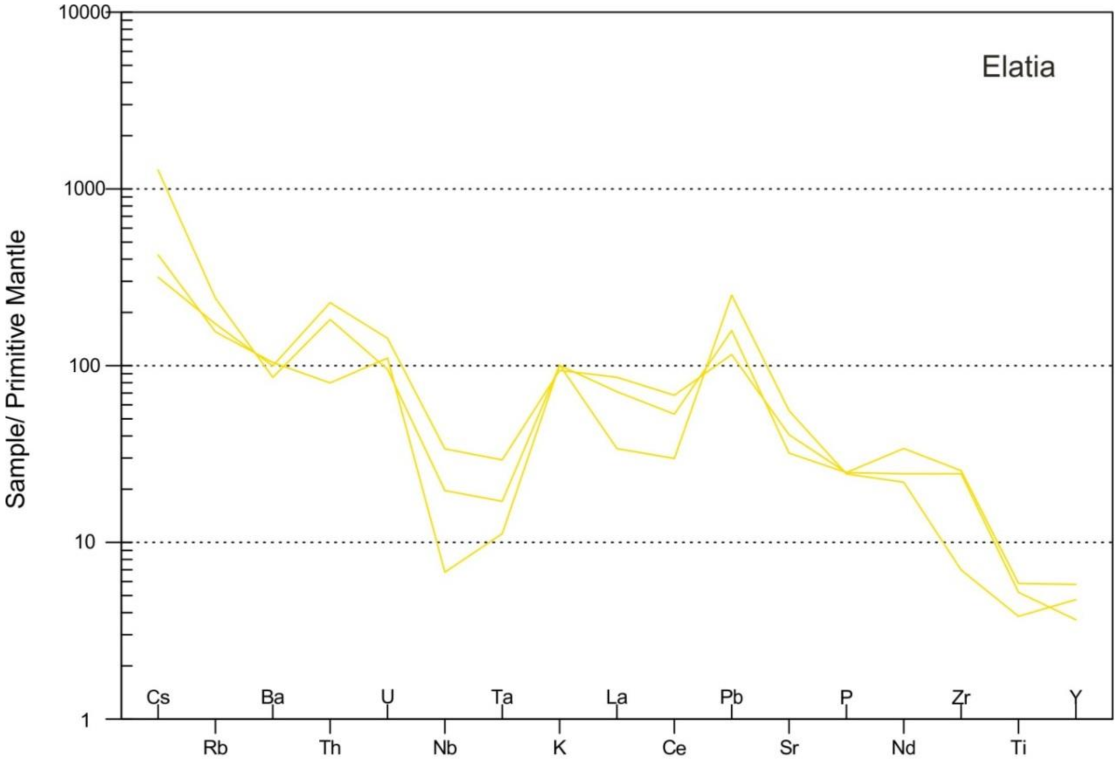

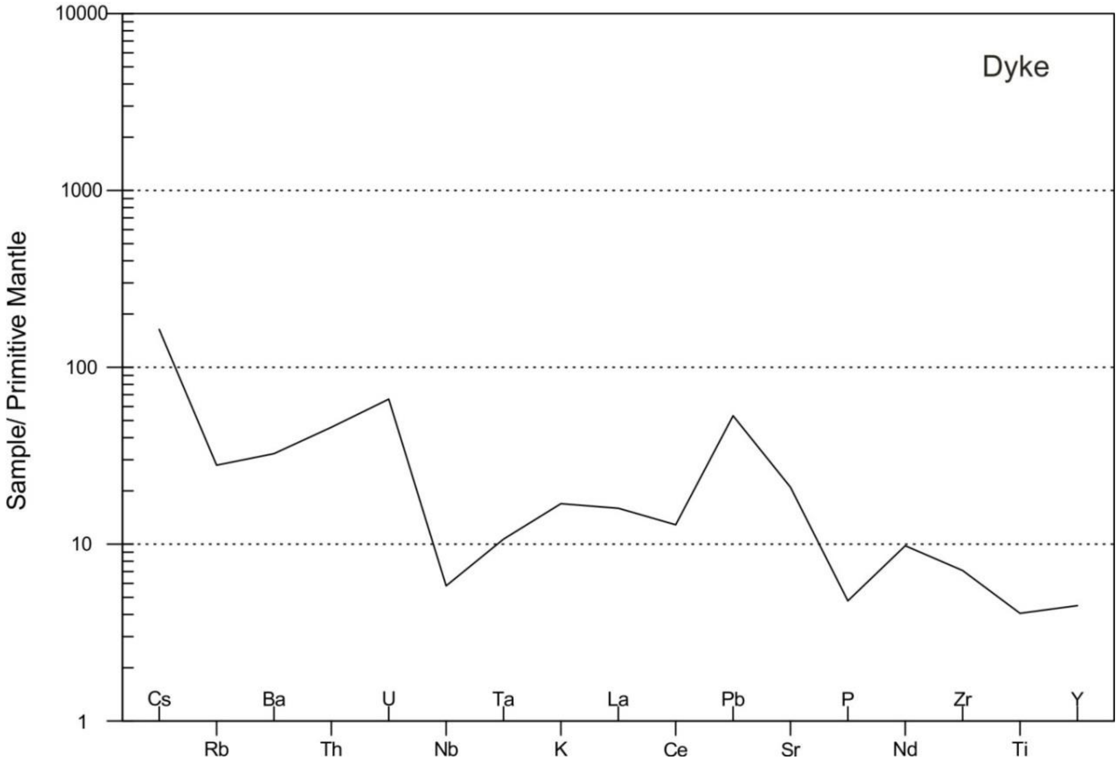

Figure 4.3.1 (Cont.) Multi-element spider diagram patterns. Normalisation values from *Sun & McDonough (1989)*

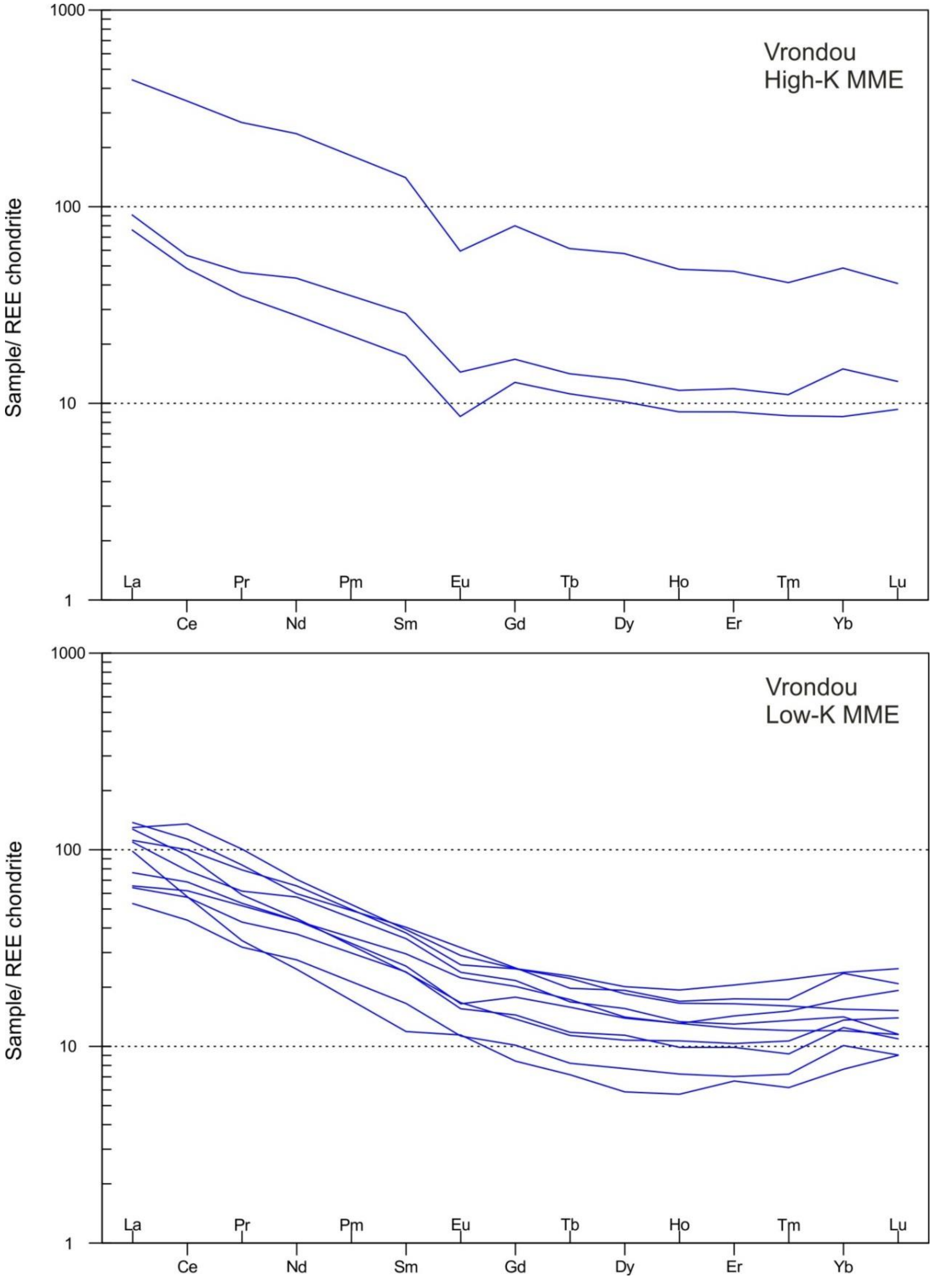

Figure 4.3.2 REE spider diagram patterns. Normalisation values from *Boynton (1984)*

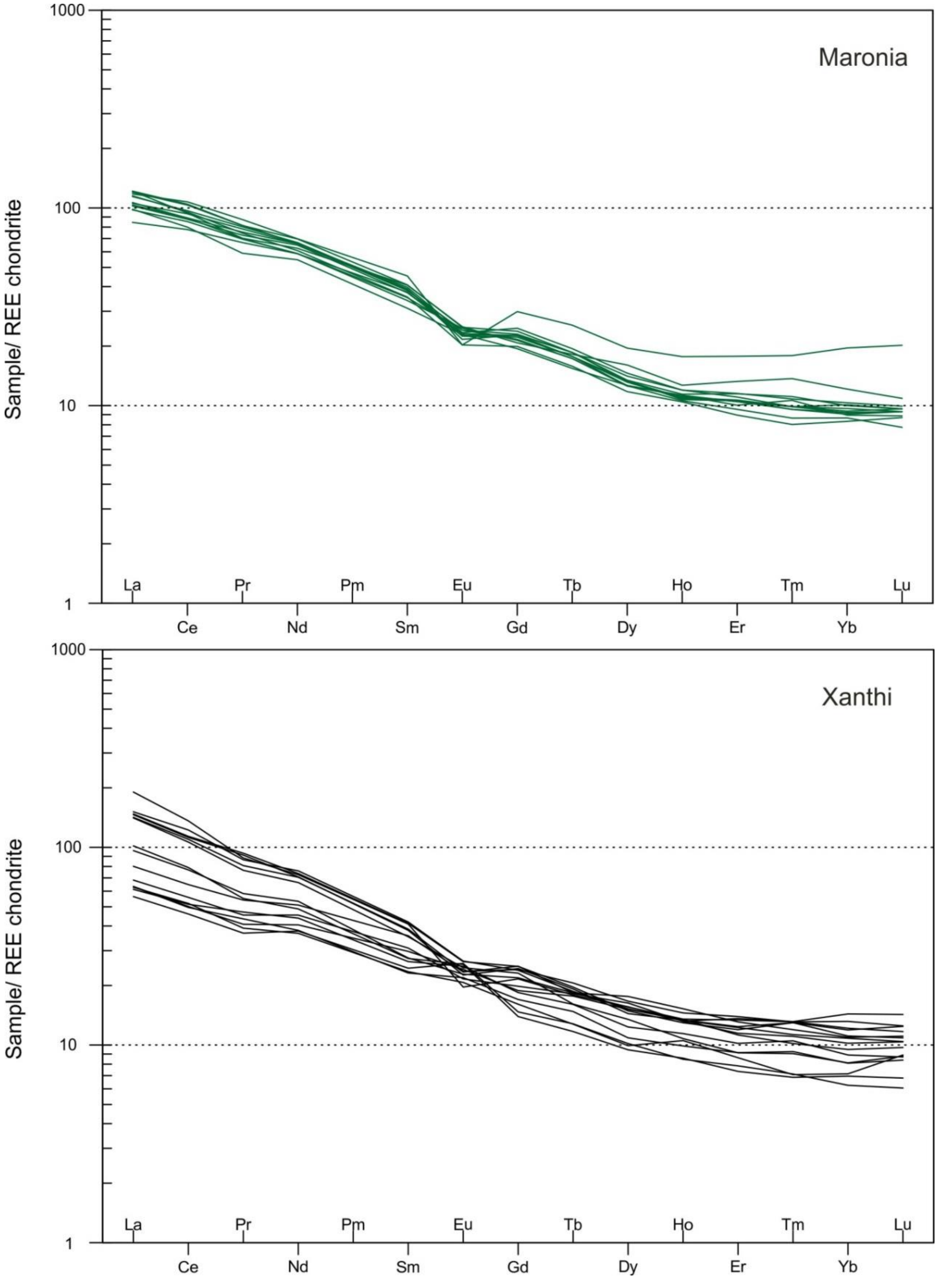

Figure 4.3.2 (Cont.) REE spider diagram patterns. Normalisation values from *Boynton (1984)*

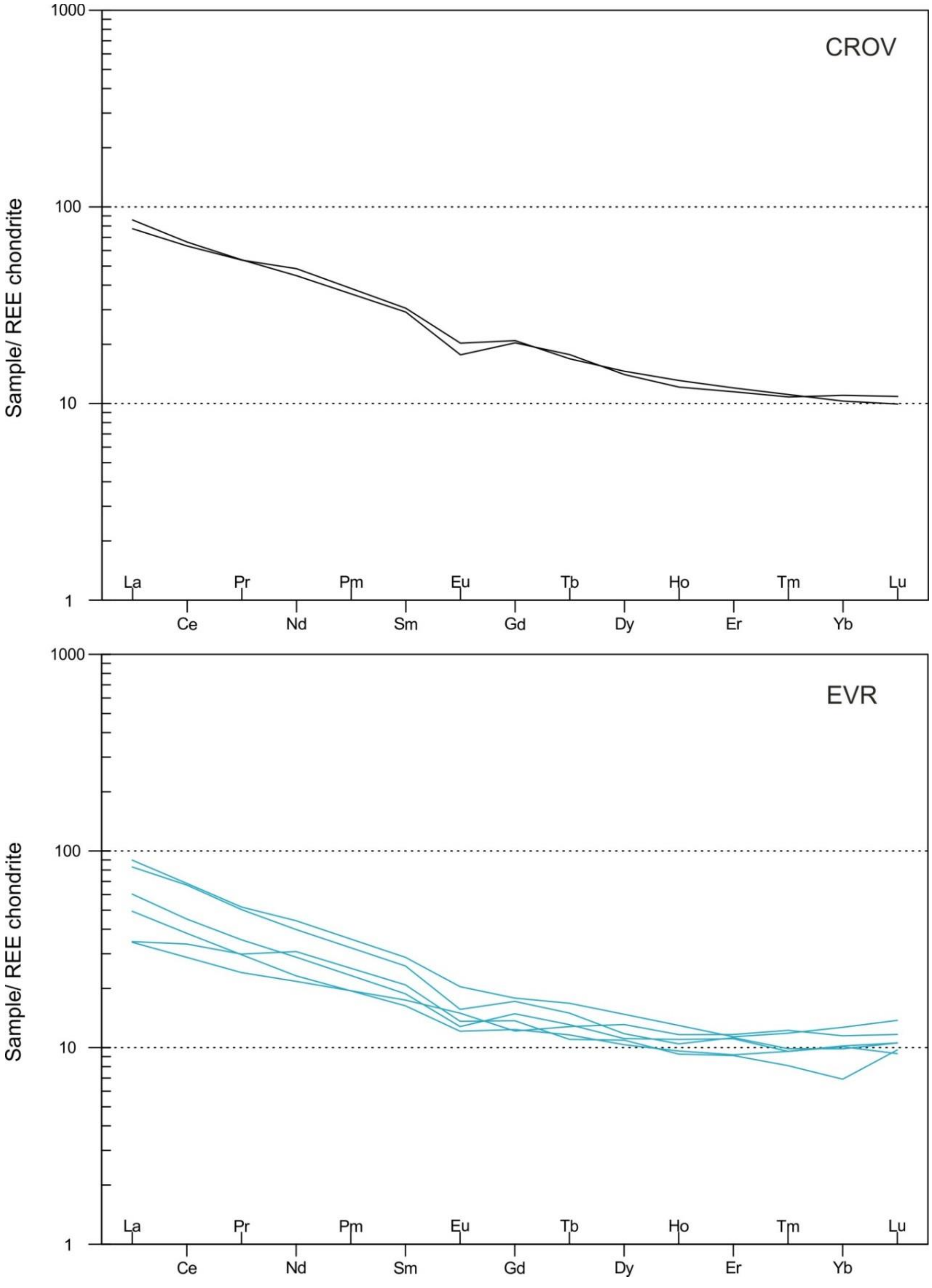

Figure 4.3.2 (Cont.) REE spider diagram patterns. Normalisation values from *Boynton (1984)*

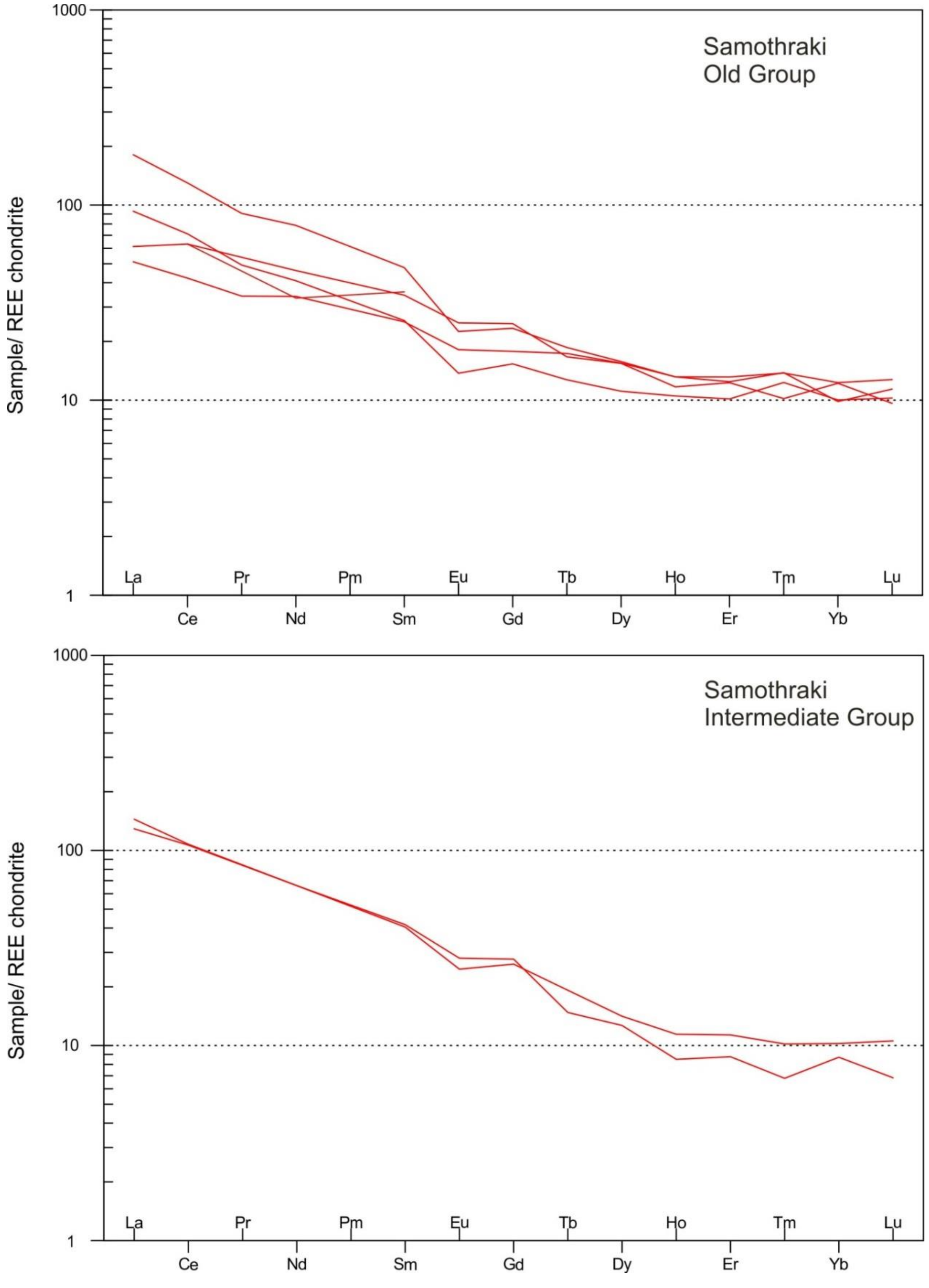

Figure 4.3.2 (Cont.) REE spider diagram patterns. Normalisation values from *Boynton (1984)*

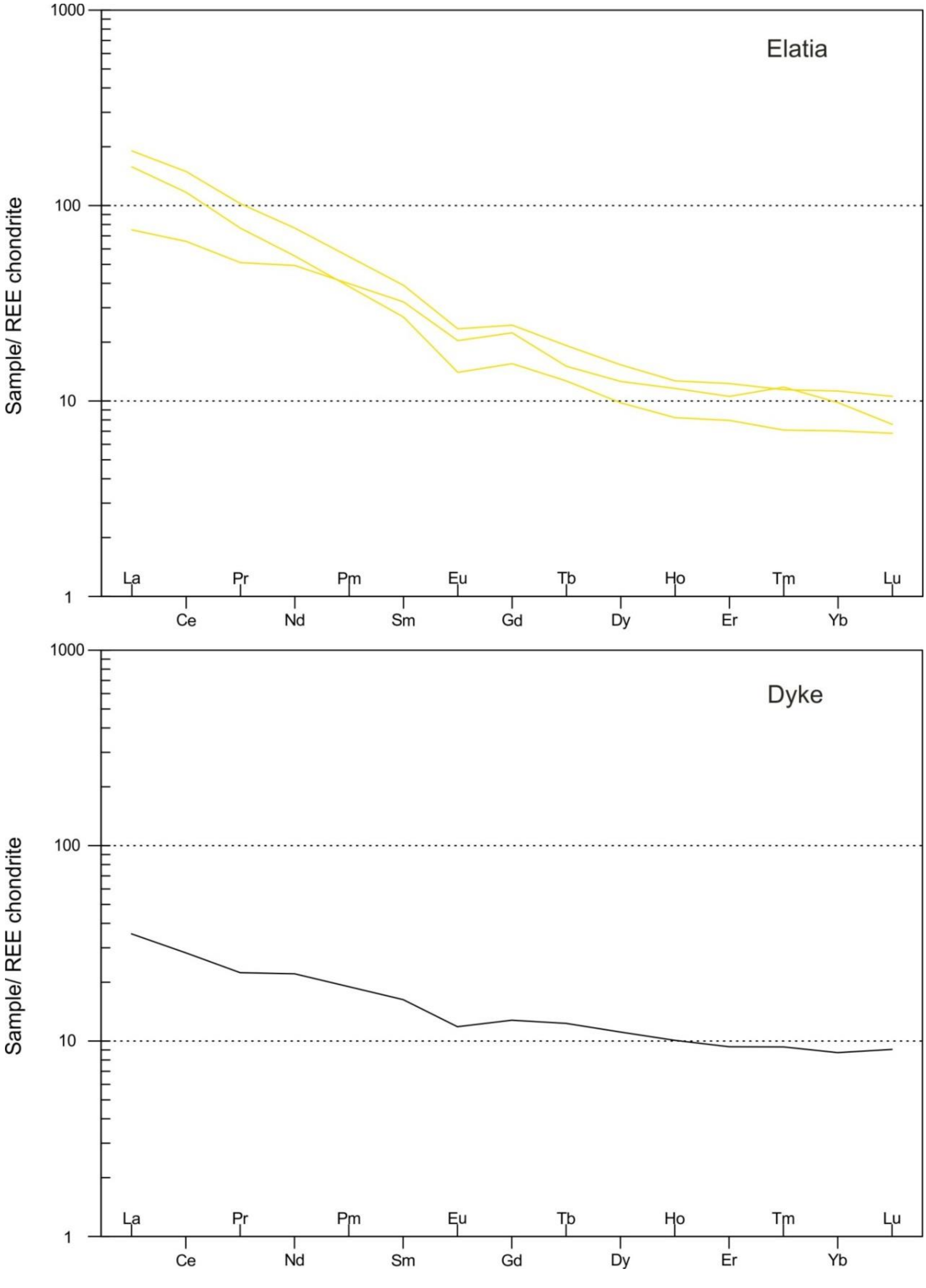

Figure 4.3.2 (Cont.) REE spider diagram patterns of all petrographic types. Normalisation values from *Boynton (1984)*

4.4 Bulk Iostopic Composition

In ***Fig. 4.4.1*** the $^{87}Sr/^{86}Sr_{(i)}$ versus εNd_i of the rocks of this study are presented. The Sr and Nd isotopic contents of the Vrondou GBDR group are also presented.

All areas display a wide isotopic range. In general, they show a good negative correlation of εNd_i with Sr_i, however there is one rock from Xanthi, which displays theless radiogenic Sr_i but low εNd_i with a large gap in Sr_i between this sample and the rest of its samples. All The Samothraki Old group rocks and the Elatia diorite sample exhibit the highest εNd_i with positive εNd_i. One EVR rock displays almost zero εNd_i (εNd_i = -0.01) but has more radiogenic Sr_i from the sample with the lowest Sr_i. The Vrondou rocks exhibit the lower Sr_i contents for given εNd_i relative to the other rocks excluding the Elatia diorite and the Samothraki Old group. The two groups of MME show similar isotopic composition, but the GBDR rocks show more depleted isotopic composition relative to the MME. The CROV rocks, although they are only two representative samples, show the lowest average isotopic composition among the other areas.

Pb available isotopic compositions of the rocks are presented in ***Fig. 4.4.2***. The sample from the Samothraki Young group exhibits the highest $^{207}Pb/^{204}Pb$ and $^{208}Pb/^{204}Pb$ contents from the Xanthi and EVR rocks but moderate $^{206}Pb/^{204}Pb$ contents. This, coupled with the lower Sr and Nd contets of the rock shows that the Young Group has a more enriched source. The rocks of Samothraki Old group displays the highest and $^{206}Pb/^{204}Pb$ contents and moderate $^{207}Pb/^{204}Pb$ and $^{208}Pb/^{204}Pb$ contents while the Samothraki Old Group sample has the highest $^{206}Pb/^{204}Pb$ among all rockspresented and moderate $^{207}Pb/^{204}Pb$ and $^{208}Pb/^{204}Pb$ contents. The isotopic composition of Xanthi rocks exhibit a wider range, from far more depleted composition to very enriched. The EVR rocks show $^{206}Pb/^{204}Pb$, $^{207}Pb/^{204}Pb$ and $^{208}Pb/^{204}Pb$ contents within the range of the other rock groups. In general, the Pb isotopic content of these three areas do not present high variation and the more depleted in $^{206}Pb/^{204}Pb$ is one Xanthi MGb rock.

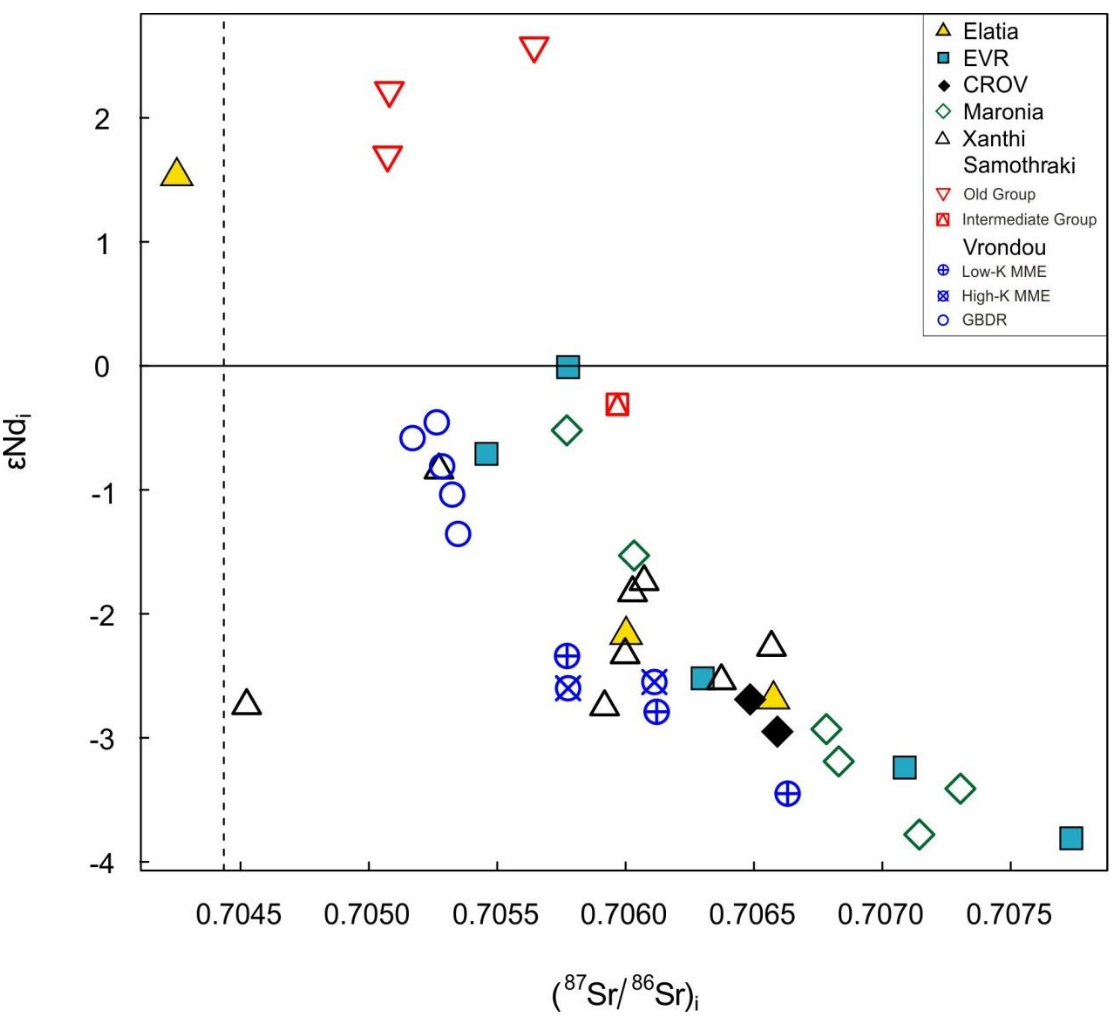

Figure 4.4.1 $(^{87}Sr/^{86}Sr)_i$ versus $εNd_i$ of the basic rocks of the present study

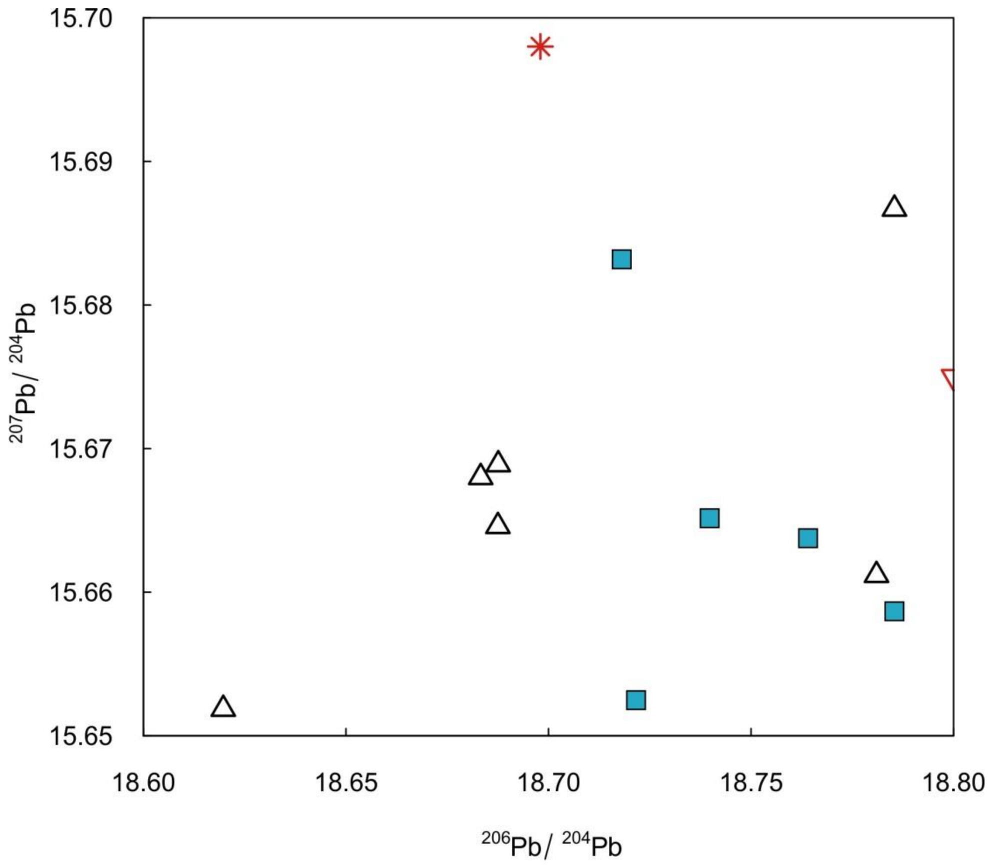

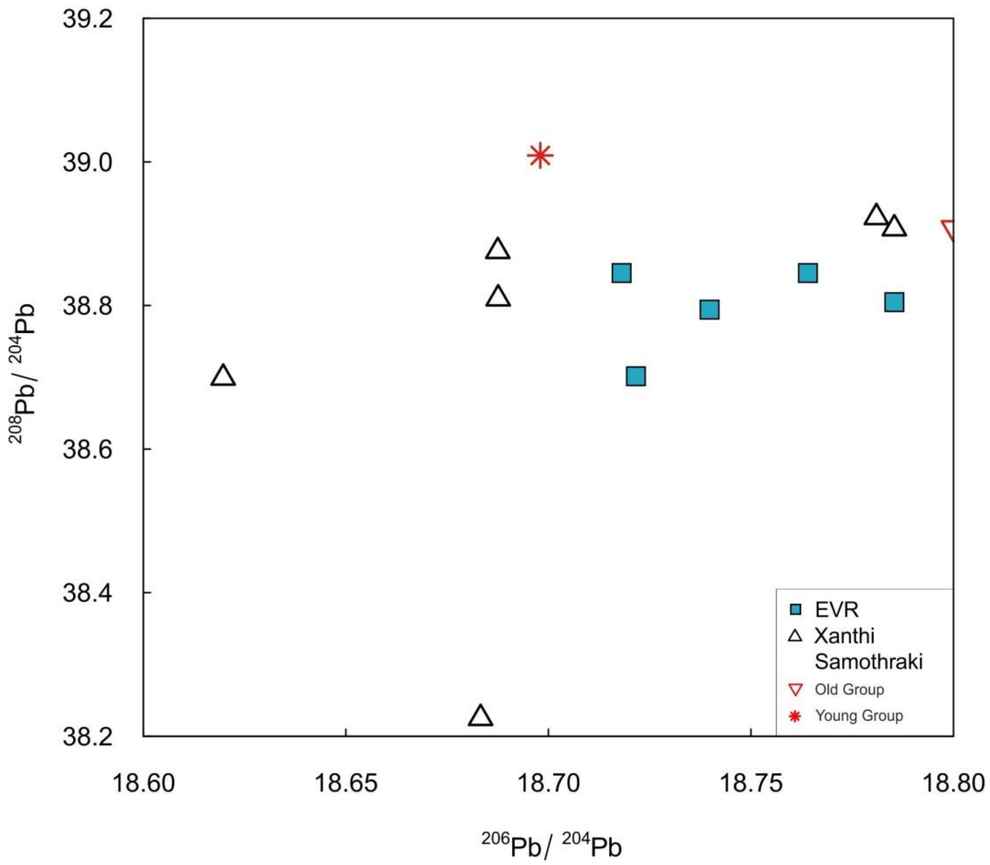

Figure 4.4.2 $^{207}Pb/^{204}Pb$ versus $^{206}Pb/^{204}Pb$ and $^{208}Pb/^{204}Pb$ versus $^{206}Pb/^{204}Pb$ of the basic rocks of the present study

4.5 Comparison of geochemical characters with the Bulgarian volcanics of Rhodope Massif

The HRM magmatic rocks are stricktly related to the Bulgarian RM magmatic rocks. They intrude the same metamorphic basement, they have similar formation ages and were formed during the same geotectonic event. Therefore, it is essential to compare the geochemical characteristics of the HRM magmatic rocks with the Bulgarian RM rocks. For the plutonic rocks of the Bulgarian RM geochemical data especially of the mafic rocks are restricted but there are enough data for the mafic volcanic rocks of eastern Rhodopes (***Fig. 4.5.1***).

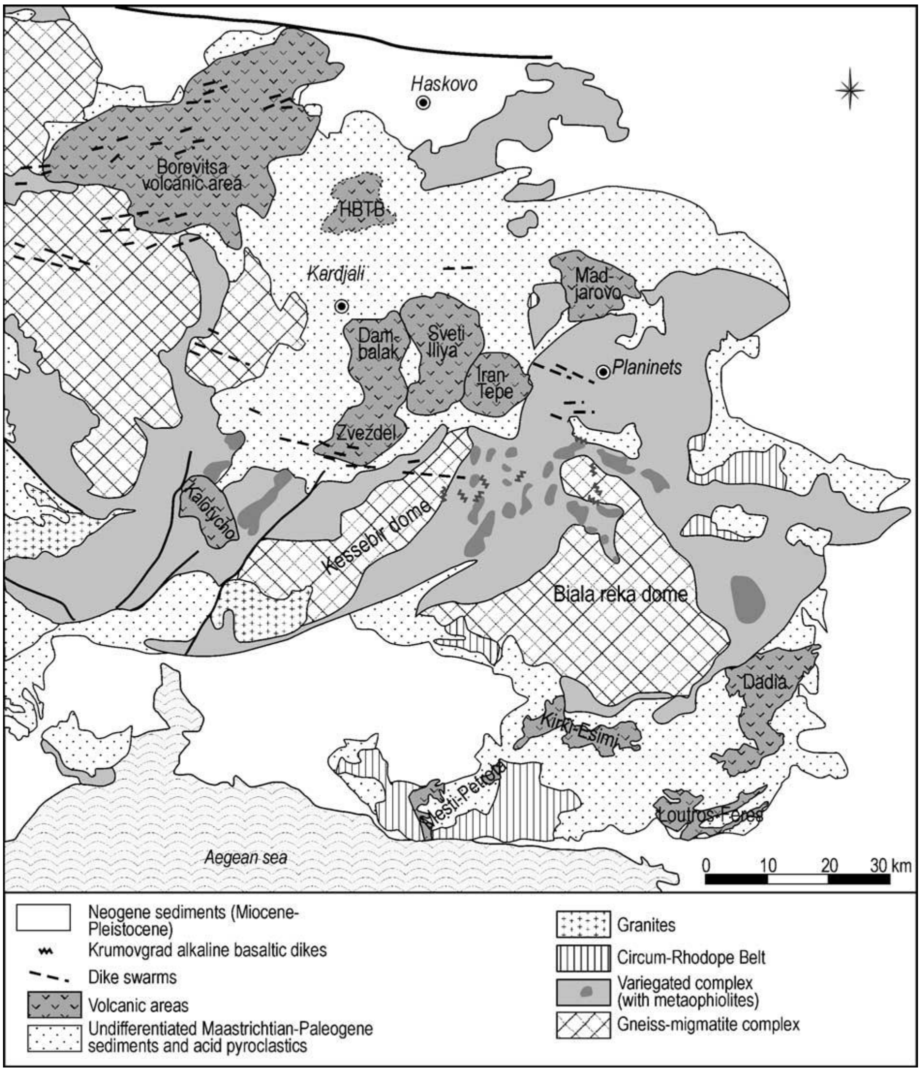

Figure 4.5.1 Simplified gological map of the eastern Rhodopes with the volcanic areas after *Marhcev et. al (2004)*

The data used here for the Bulgarian RM magmatic rocks are from *Kirchenbaur et al. (2002)* and *Marchev et. al. (2004)*. Two groups from the Bulgarian RM magmatic rocks have been distinguished for the needs of the present study, one consisting only from the KAB rocks (Krumovgrad alkaline basalts; 26-28 Ma according to *Marchev et al., 1997*) which exhibit very different geochemical characters than the other Rhodope magmatic rocks, and the other is the whole set of the Eastern Bulgarian magmatic rocks. The KAB rocks have rather anorogenic than orogenic characteristics. Their distinct differences are the high Nb, Ta and TiO_2 contents (***Fig. 4.5.2 and 4.5.3***), positive Nb anomaly on primitive mantle normalized patterns (Nb/Nb*>1, ***Fig. 4.5.4***), and asthenospheric Sr, Nd and Pb isotopic content (***Fig. 4.5.6 and 4.5.7***). The previous authors have connected the Eastern Bulgarian volcanics with the KAB through geochemical and geodynamical evolutionary procceses. So far the magmatic rocks of the HRM were supposed to be the missing evolutionary link between the Eastern Bulgarian volcanic and the KAB especially based on the published isotopic data (***Fig. 4.5.8***).

The high Al_2O_3 in all rocks suggests that the Eu/Eu* reflects the crustal contamination rather than the plagioclase fractionation. Therefore, there should be a good correlation between the Eu/Eu* and the Sr_i for rocks of common origin since they covary together (*Marchev et al., 2004*). However, there are some HRM magmatic rocks that display much higher Eu/Eu* than the KAB, as well as much lower, and most of the HRM samples do not follow the trend between the Eastern Bulgaria volcanic and the KAB(***Fig. 4.5.5***). Here the HRM magmatic rocks are not correlated with the Eastern Bulgarian volcanics and the KAB rocks implying a different history for these rocks.

In general, all the Eastern Bulgarian volcanics have major and trace element geochemical characters indistinguishable from the HRM magmatic rocks with some rocks of the latter showing more depleted characters. The differences are found in the isotopic characteristic of the HRM magmatic rocks and the Eastern Bulgarian volcanic were the HRM magmatic rocks exhibit less radiogenic Sr_i and more radiogenic Nd_i isotopic composition. Most Eastern Bulgarian volcanics display much higher $^{206}Pb/^{204}Pb$ isotopic composition towards a more asthenospheric component and some of them display higher $^{207}Pb/^{204}Pb$ and $^{208}Pb/^{204}Pb$ isotopic composition implying stronger crustal contamination (***Fig. 4.5.7***)

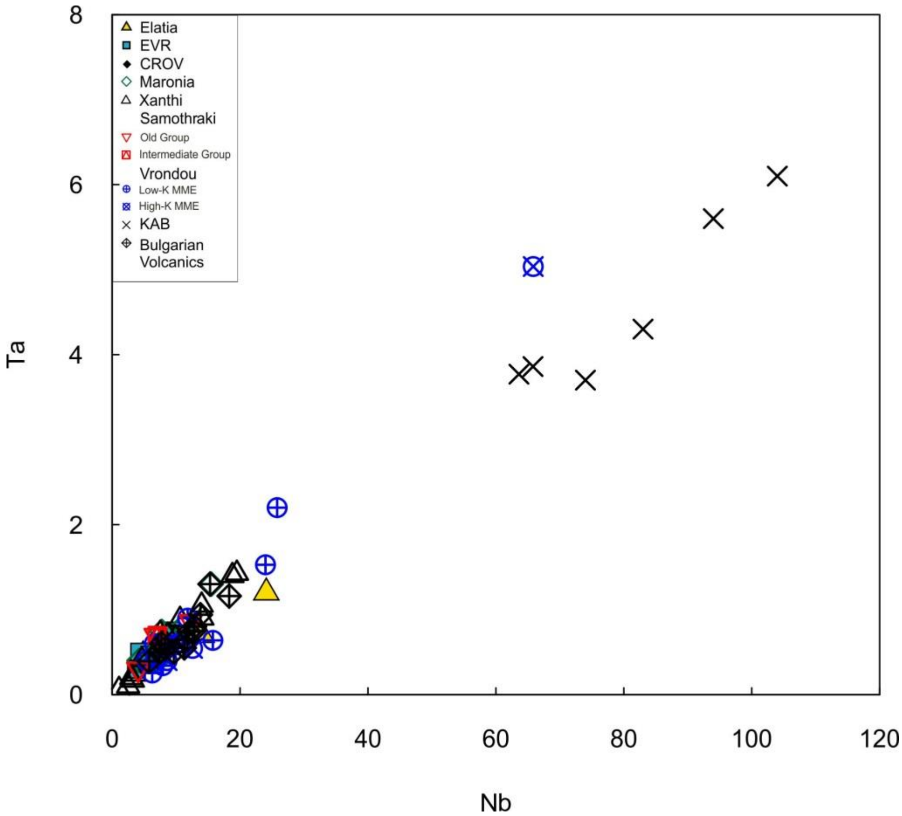

Figure 4.5.2 Nb versus Ta for the HRM and Bulgarian RM basic magmatic rocks

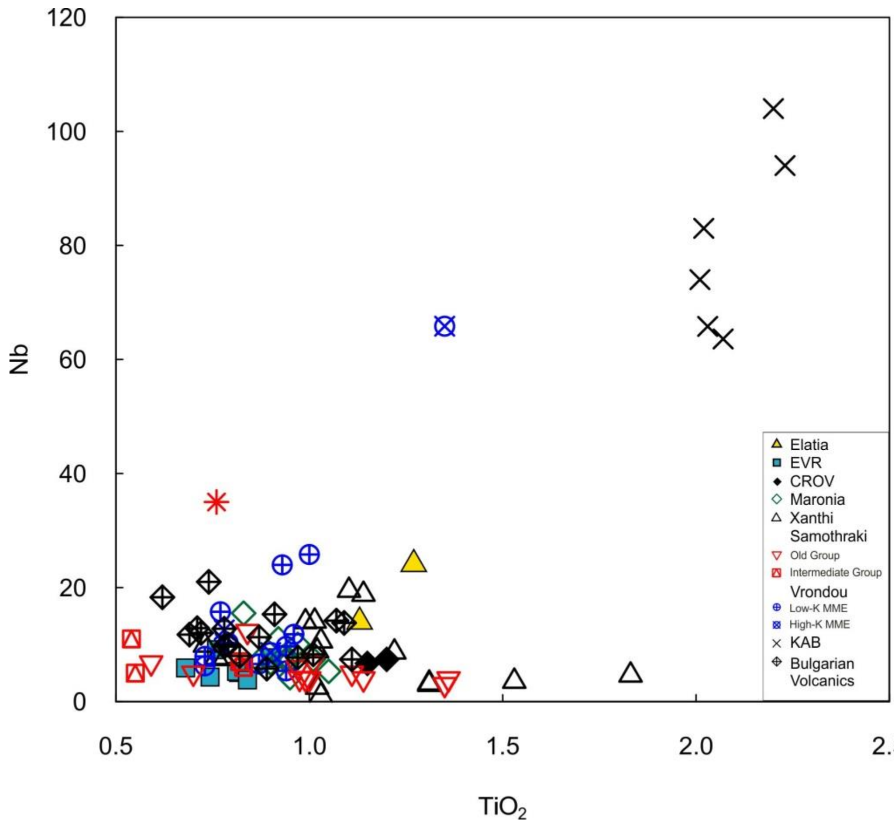

Figure 4.5.3 Ti2O versus Nb for the HRM and Bulgarian RM basic magmatic rocks

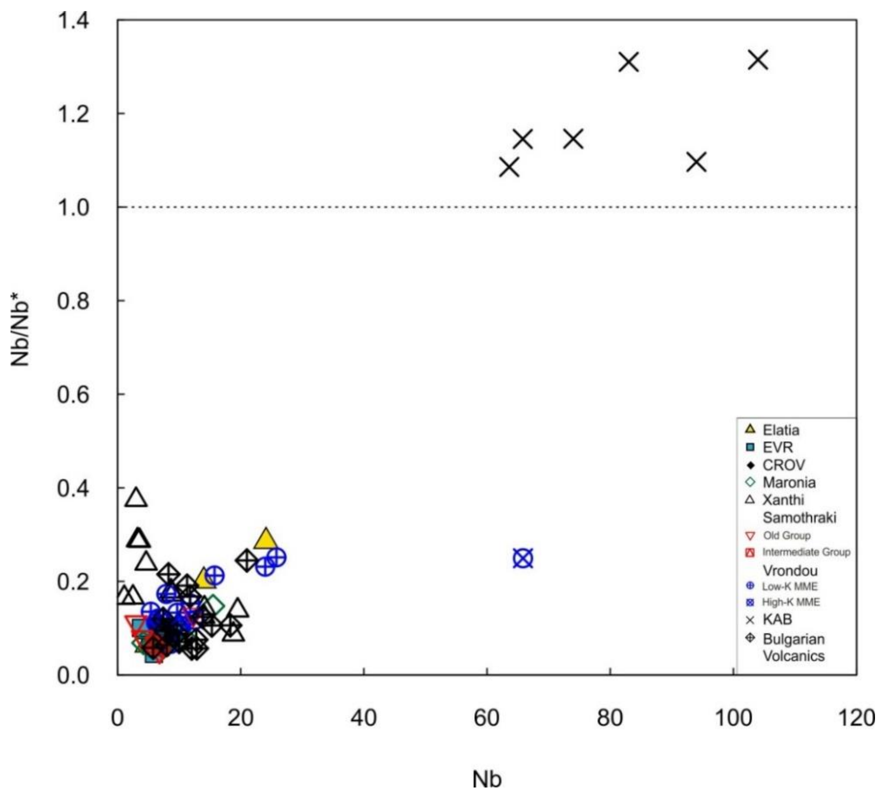

Figure 4.5.4 Nb versus Nb/Nb* for the HRM and Bulgarian RM basic magmatic rocks

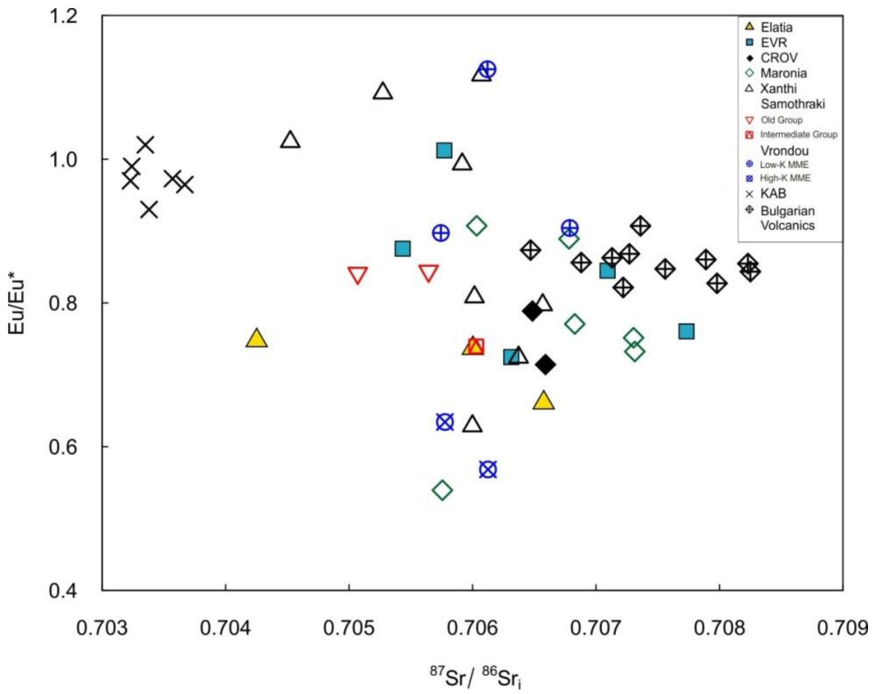

Figure 4.5.5 $(^{87}Sr/^{86}Sr)_i$ versus Eu/Eu* for the HRM and Bulgarian RM basic magmatic rocks

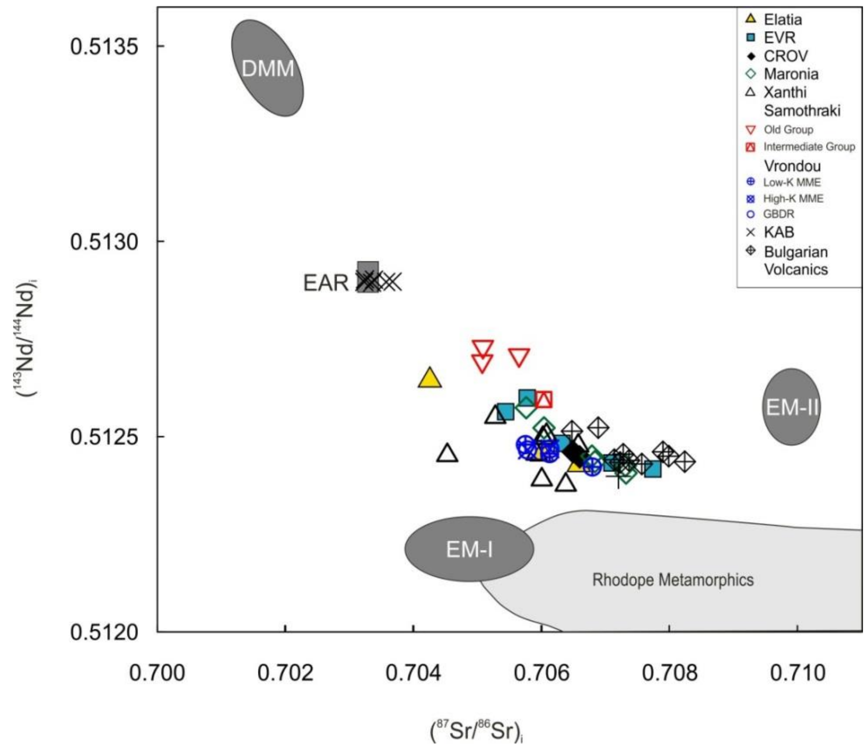

Figure 4.5.6 $(^{87}Sr/^{86}Sr)_i$ versus $(^{143}Nd/^{144}Nd)_i$ of the basic rocks. The fields illustrated are; DMM=Depleted Morb Mantle, EM-I=Enriched Mantle I, EM-II=Enriched Mantle II after *Zindler & Hart (1986)*. EAR=European Asthenospheric Reservoir after *Cebria & Wilson (1995),* Rhodope metamorphics after *Cornelius (2008) and Castorina et al. (2014)*

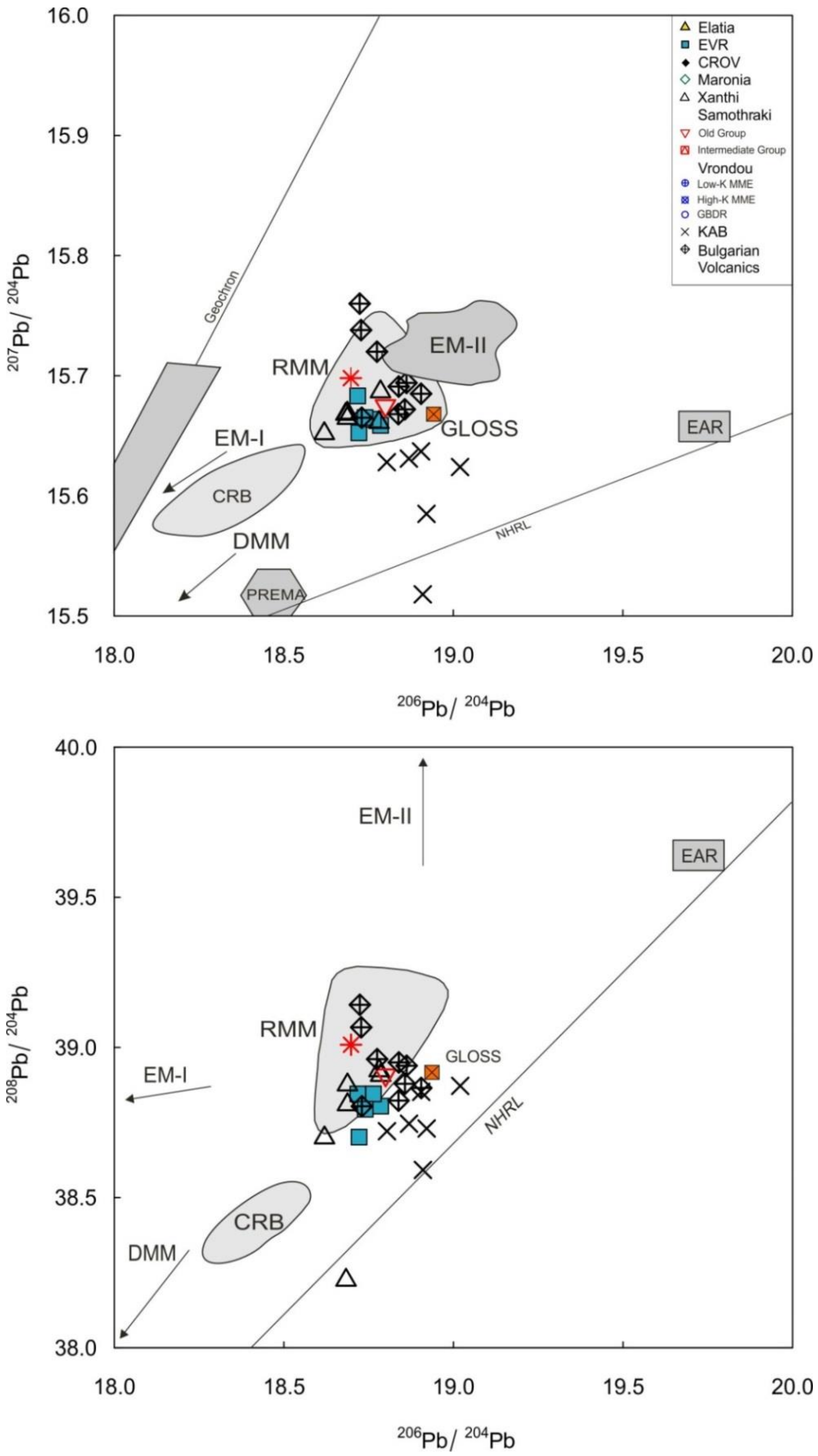

Figure 4.5.7 $^{207}Pb/^{204}Pb$ versus $^{206}Pb/^{204}Pb$ and $^{208}Pb/^{204}Pb$ versus $^{206}Pb/^{204}Pb$. The fields illustrated are; DMM=Depleted Morb Mantle, EM-I=Enriched Mantle I, EM-II=Enriched Mantle II after *Wilson (1989)*. EAR=European Asthenospheric Reservoir after *Cebria & Wilson (1995)*. GLOSS after *Plank & Langmuir (1998)*. NHRL= North Hemisphere Reference Line after *Hart (1984)*. RMM=Rhodope

Massif Metamorphics after ***Frei 1995***. CBR=Circum Rhodope Belt after *Bonev and Stampfli (2008)*

4.6 Discussion

The mafic magmatic rocks of HRM show variable enrichment in incompatible elements (e.g K, Rb, Sr, Ba) but simultaneously display depleted features like the low silica content, the high mg#, the Eu, Ti and P positive anomalies and the depleted Sr and Nd isotopic composition relative to the metamorphic basement of Rhodope. Despite the narrow range of silica content of the rocks of all the studied areas there are similarities but also significant geochemical differences among them. Some rocks are enriched or depleted in specific incompatible elements (e.g High-K Vrondou enclaves with high K_2O, Rb and low Sr contents) while others are enriched in both specific incompatible and compatible elements simultaneously (e.g Maronia with high K_2O, Cr, Ni, Ba, Rb and Sr contents). Different crystal fractionation, formation conditions and contamination factors could only explain these features in a limited extent. On the other hand, the common geotectonic origin of these rocks suggests a unhomogenized source origin rather than any other factor.

All samples of this study, except few Low-K Vrondou MME, show a common garnet bearing source. Their Sr and Nd isotopic characteristics are rather depleted relative to the Rhodope metamorphic rocks favoring for mantle and crustal component. In each area the isotopic composition is not identical among all rocks but they display parallel increased trends towards the metamorphics rocks of Rhodope. There are not Pb isotopic composition for all the study rocks but taking into account the available ones they display minor variability. Their Pb isotopic composition partially overlap the Rhodope metamorphic (not shown), but Pb is an element commonly cited as typically introduced in magma by selective contamination (*Dickin, 1981*) and thus their Pb isotopic composition could have been slightly affected these rocks during their ascent in the RM basement.

The KAB geochemistry differs from all other magmatic rocks of RM and presents anorogenic characteristics. The other Bulgarian volcanics have similar geochemical features with the HRM magmatic rocks but different isotopic features. The Sr_i and Nd_i isotopic composition of the HRM magmatic rocks are more depleted than the Eastern Bulgarian volcanics. Regarding the Pb isotopic composition there are distinct differences between them. The Bulgarian volcanics show higher $^{206}Pb/^{204}Pb$ isotopic composition towards a more asthenospheric component and some of them display higher $^{207}Pb/^{204}Pb$ and $^{208}Pb/^{204}Pb$ isotopic composition which implies stronger crustal contamination. The isotopic differences between the HRM magmatic rocks and the Bulgarian volcanics might favor in different source, different degree of crustal contamination, different nature of crustal contaminant or both of the latter. The continental crustal contamination for the HRM magmatics, in contrast with the Bulgarian magmatics, does not seem to have play significant role. The geochemical characteristics of the HRM magmatics coupled with the depleted isotopic characters indicate a different contaminant other than the RM metamorphic. Moreover, the Eastern Rhodope magmatics exhibit far more enriched isotopic characters which has been attributed from previous authors to shallow-level continental crustal contamination.

For the HRM magmatics the most prominent crustal contaminant is the slab derived sediments which succeed to import enriched geochemical characteristics into the ascending magmas formed from mantle wedge melting and maintain moderate enrichment of isotopic content.

The asthenospheric contribution for the HRM magmatics is highly unlikely since there are no rocks with asthenospheric features in the HRM and they clearly show more depleted Pb isotopic contents than the Bulgarian volcanics.

5. CRUSTAL CONTRIBUTION AND MANTLE GEOCHEMISTRY

5.1 Introduction

The felsic rocks of each area presented in this thesis and described in the third chapter of petrology, are the outcome of both crust and mantle interaction. Mantle derived melts and crustal anatectic melts through mainly mixing processes in the Rhodopian crust were interacted and gave genesis to the plutonic and volcanic rocks of the HRM. These rocks share many common petrographic and geochemical features but the differences in the geochemistry of the felsic members may attributed to various factors like the nature of the anatectic melt, the geochemistry of the basic end-member, the differentiation processes and the pressure-temperature conditions. The only studied rocks that present significant differences in terms of age and petrography are those of the Elatia pluton. The Elatia pluton in contrast with the other areas lacks of mafic rocks, is about 20 Ma older and has abundant accessory minerals and adakitic affinity.

In the the previous chapter, the geochemical and isotopic characteristics of the HRM mafic magmatic rocks as well as the differences they present relative to the Bulgarian volcanics, were described. Because of their mafic lithochemistry, they are certainly originated from partial melting of ultramafic mantle lithology (*Wyllie, 1984*). However, they present geochemical characteristics which could have originated either from contamination from continental crustal lithologies or subduction related sediments. In the convergent boundaries magmatism, the slab subducted sediments play an important role and present similar geochemical and isotopic composition with the upper continental crust (*Plank & Langmuir, 1998*). On the other hand, the preserved depleted characteristics in some HRM mafic magmatic rocks relative to the continental crust and especially their depleted isotopic composition suggest that these rocks could not have probably interacted with upper crustal lithologies. This chapter elaborates the crustal contribution that took place in the genesis of both mafic and felsic members of the rocks as well as the source component of the genesis of the more mafic members.

5.2 On the subducted sediment contribution in the mantle

The modern sinking oceanic lithosphere does not melt in most subduction zones; instead it releases aqueous fluids that trigger the mantle wedge to melt (*Tatsumi and Eggins, 1995*) and only when high temperature conditions are attained in subduction zones, then slab melting-induced magmatism would take place (e.g . *Drummond and Defant, 1990*)

Most authors favor for a mantle continually modified by mantle metasomatism (e.g. *Frey and Green, 1974; Boettcher and O'Neil, 1980; Menzies and Murthy, 1980*). The mechanism proposed for the interaction between subducted fluids or sediment melts and the mantle wedge enrichment is dissolution and reprecipitation of mantle lherzolite. The products of this reaction strongly depend on the pressure and temperature conditions as well as the geochemistry of the slab derived melts. This mechanism could resemble to an assimilation and fractional crystallization process (AFC) between the mantle rock and the fluids/melts (e.g *Ayers & Eggler, 1995; Brenan et al., 1995; Stalder et al., 1998*) and will be used later here to model trace element partitioning between the slab release fluids/sediment melts and the mantle wedge. Although the above process is not well investigated and there are still a lot to be learned some experimental efforts have been made from previous authors on the behaviour and partitioning of trace elements during the slab fluid/sediment melts and mantle wedge reaction (e.g. *Green et al., 1994; Ayers & Eggler, 1995; Brenan et al., 1995; Stalder et al., 1998, Kessel et al., 2005).*

Another issue being investigated by many researchers is whether at high pressures the slab component, which transfers such elements to the mantle, is a fluid, melt or supercritical liquid, has remained unknown. Most thermal models of mature subduction zones suggest that temperature conditions for the subducting crust are far below its solidus at subarc depths. The missing link in this controversy is the composition and nature of the fluids or melts departing from the slab, which in turn allow conditions of their formation to be constrained. A critical petrological parameter in this debate is the closure of the immiscibility gap between an aqueous fluid and a hydrous silicate melt. At typical crustal pressures, aqueous fluids contain a few per cent of solute while partial melts have 15wt% H_2O. At higher pressures, the amount of solutes in the fluid and the solubility of H_2O in silicate melts both dramatically increase, and the compositions of fluid and melt converge along a miscibility gap, which eventually disappears. The intersection of the miscibility gap's critical curve with the solidus then defines the end point of the solidus, and terms any fluid or melt beyond this point 'supercritical liquid' (*Kessel et al., 2005* and references therein). The pressure of the critical end point of the solidus is strongly dependent on bulk composition, and varies from 1.6 GPa in feldspatic systems to 10 GPa in mantle systems. In potassium and mica-rich lithologies of the subducted crust, this endpoint is situated between 5 and 6 GPa, corresponding to depths of 150–180 km of the subducting slab beneath volcanic arcs (*Schmidt et al., 2004*). It has been proposed that supercritical liquids have high trace element solubilities at relatively low temperatures. Finally, the chemical properties of supercritical liquids liberated at depths exceeding ~160 km removes the dichotomy of fluids versus melts. As a consequence, fluid-type geochemical signatures from the oceanic crust are limited to depths ≤160 km: at higher pressures, the mobile phase will inevitably add a melt-like trace element pattern to the mantle wedge (*Kessel et al., 2005*). Nevertheless, at least in part sediment melts are needed to explain trace element signatures of arc magmas (e.g. *Plank, 2005*).

5.3 Isotopic Modelling

Asthenospheric mantle contribution in the RM magmatic rocks has been suggested by previous authors. As discussed in the previous chapters, asthenospheric contribution for the HRM magmatic rocks is highly unlikely. Metasomatism of an enriched mantle by slab derived melts and/or fluids is the most prominent suggestion. However both scenarios are to be, in terms of geochemistry, tested here.

The present paragraph aims to model both scenarios in terms of isotopic composition. The most widely accepted equation to perform isotopic ratio mixing between two end-members (mantle and crust/subducted sediments) is the one developed by *Vollmer (1976)* for ratio ratio plots and applied for Sr-Nd isotopic mixing modelling from *Langmuir et al. (1978)*.

The general mixing equation is a hyperbola with the form:

$$Ax + Bxy + Cy + D = 0 \qquad (1)$$

Symbols used are

x, y = general variables along the abscissa and ordinate, respectively

xi, yi = coordinates of data point i

ai = denominator of yi (ai = 1 if y is an element)

bi = denominator of xi (bi = 1 if x is an element)

A, B, C, D = coefficients of the general variables x and y; and r = a ratio related to coefficient B which reflects the extent of hyperbolic curvature of a mixing curve. The coefficients A, B, C and D of equation (1) are a function of the type of plot. A mixing curve for each type of plot may be calculated through any two typical data points which are well separated.

When using ratio-ratio plots (e.g. K/Rb-Ba/Sr or $^{87}Sr/^{86}Sr$-$^{206}Pb/^{204}Pb$) the coefficients of equation (1) are from *Vollmer (1976)*.

$$A = a_2 b_1 y_2 - a_1 b_2 y_1$$

$$B = a_1 b_2 - a_2 b_1$$

$$C = a_2 b_1 x_1 - a_1 b_2 x_2$$

$$D = \frac{a_1 b_2 x_2 y_1}{a_2 b_1 x_1 y_2}$$

$$r = \frac{a_1 b_2}{a_2 b_1}$$

Apllying this for Sr and Nd isotopic ratios using the approximation Sr~^{86}Sr the equation takes the form

$$A\left(\frac{^{87}Sr}{^{86}Sr}\right)_{mix} + B[Nd]_{mix}\left(\frac{^{87}Sr}{^{86}Sr}\right)_{mix} + C[Nd]_{mix} + D = 0$$

$$A = [Nd]_b\,[Sr]_a - [Nd]_a[Sr]_b$$

$$B = [Sr]_b\,[Sr]_a$$

$$C = [Sr]_a\left(\frac{^{87}Sr}{^{86}Sr}\right)_a - [Sr]_b\left(\frac{^{87}Sr}{^{86}Sr}\right)_b$$

$$D = [Nd]_a\,[Sr]_b\left(\frac{^{87}Sr}{^{86}Sr}\right)_b - [Nd]_b\,[Sr]_a\left(\frac{^{87}Sr}{^{86}Sr}\right)_a$$

Tha volume fraction (f_b) of the mixing component is calculated from the equation below:

$$\left(\frac{^{87}Sr}{^{86}Sr}\right)_{mix} = \frac{f_b[Sr]_b\left[\frac{^{87}Sr}{^{86}Sr}\right]_b + (1-f_b)[Sr]_a\left[\frac{^{87}Sr}{^{86}Sr}\right]_a}{f_b[Sr]_b + (1-f_b)[Sr]_a}$$

The mixing curve resulting from this equation is a hyperbola whose curvature is controlled by the B coefficient. The numerical value of r is a function of the extent of the curvature between two points and of the overall curvature of the hyperbolic curve.

$$r = \frac{\frac{[Sr]_a}{[Sr]_b}}{\frac{[Nd]_a}{[Nd]_b}} = \frac{\frac{[Sr]_a}{[Nd]_a}}{\frac{[Sr]_b}{[Nd]_b}}$$

If r = 1, then the mixing curve is a straight line.

In ***Fig. 5.3.1*** a isotopic mixing model of Sr and Nd isotopes, following the above equation, between the lithospheric mantle and subducted sediments scenario is presented. For the slab subducted sediments which correspond to the trench sediments of the RM there are no available geochemical data therefore the GLOSS data of *Plank & Langmuir (1998)* from several areas around the world were used. More specifically, the average bulk compositions of sediment columns of each area, and not one specific sediment, though a rough choice, seems to be a suitable, since there are numerous geochemical analyses and would be inappropriate to be used on a graph. The thickness of sediments from each area is of several hundreds of meters. It is worthy to note, that one type of subducted sediment is not the only one that contributes in the enrichment of the mantle wedge, but several sediments could have contribute. Moreover, the fraction of the sediment melt is another important factor. Here, the bulk sediment melt is used, since the isotopic mixing line is not depending on any of the intermediate stages like fractional crystallization but on the composition of the end-members. The composition of the subducted sediments used in this model is mainly a combination of different kinds of clays, cherts and radiolarites. Other sediments like limestones, volcaniclastics or turbidites tested for the same model do not sufficiently match to our results.

The end-member data used for the model are presented in ***Table 5.3.1***. The subcontinetnal lithospheric mantle (SCLM) beneath the eastern Rhodopes is rather depleted according to many authors (e.g *Rosenbaum et al. 1997*; *Marchev et al., 2013*) therefore a depleted MORB mantle reservoir (DMM, *Workman & Hart, 2006*) component was selected as the depleted end-member. The original mantle beneath the arcs has been generally accepted as identical to mid-ocean ridge basalts (MORB) source mantle, because of the rather uniform chemistry of MORB's and the similarity in high field strength element ratios between the MORB's and arc lavas (e.g *Pearce, 1993; Tatsumi & Eggins, 1995*). Here, accordingly, the average MORB of *Gale et al. (2013)* for trace elements and *Workman & Hart (2006)* for isotopic composition were used as the DMM end-member representative melt. The reason why that the ultamafic cumulate xenoliths from KAB (*Marchev et al., 2006, 2008*) weren't used here as the mantle end-member is due to their continental crustal assimilation that have been subjected.

The meaning of the model mixing lines on ***Fig. 5.3.1*** is whether similar melts from the subducted sediments presented, or a combination of such subducted sediments, could have contributed and interact with the subcontinental mantle wedge beneath the HRM and result in the enriched mafic melts that intruded all over the HRM. As shown in ***Fig. 5.3.1,*** the HRM mafic rocks lie across one or more of the mixing lines which means that they could have originated from such a process. The fraction of the subducted sediments necessary for each mixing process depends on the elemental Sr and Nd and isotopic Sr and Nd composition and varies among the mixing lines between 0.1 to 0.4 at least for the genesis of the most mafic rocks of each area. The reported fractions are rather satisfying. It is noteworthy that not all HRM magmatic rocks can be explained by a single mixing line presented. This, along with the scattering of data among the different areas, suggests that each developed independently in a heterogeneous source (e.g. *Langmuir et al., 1978*).

The same mixing equation was applied for different end-members on ***Fig. 5.3.2***. In this isotopic model the mafic end-member is the pure asthenosphere derived melts of KAB (*Marchev et al., 2004*) and RM crustal lithologies from the surrounding areas. This model is aiming to test the scenario of the above authors for an asthenospheric origin with assimilation of upper crustal lithologies which they applied for the eastern Rhodopes volcanic rocks.

The parameters used for the model on ***Fig. 5.3.2*** are reported in ***Table 5.3.2***. The representative sample of KAB used is IIEG-01 (*Marchev et al., 2004*). As shown on the isotopic model on ***Fig. 5.3.2*** most the HRM rocks lie on the different mixing lines between the asthenospheric melt and the RM metamorphics. For some of the Xanthi rocks there was no metamorphic rock that could form a mixing line to account for their origin. However, in most of these mixing lines the fraction of RM metamorphic rocks necessary in order to result in the isotopic composition of the HRM mafic magmatics is rather high more than 0.4 in most cases. Asthenospheric contamination from continental crust in RM according to previous authors occured in low levels during the period of extension were the process of assimilation and fractional crystallization was the drining mechanism. High fractions of continental crust in that case are unlikely to be ssimilated. Therefore, such a geodynamic scenario cannot account for the high mixing fractions of HRM metamorphics and the asthenosphere-continental crust model is rather unlikely for the genesis of the HRM mafic magmatic rocks.

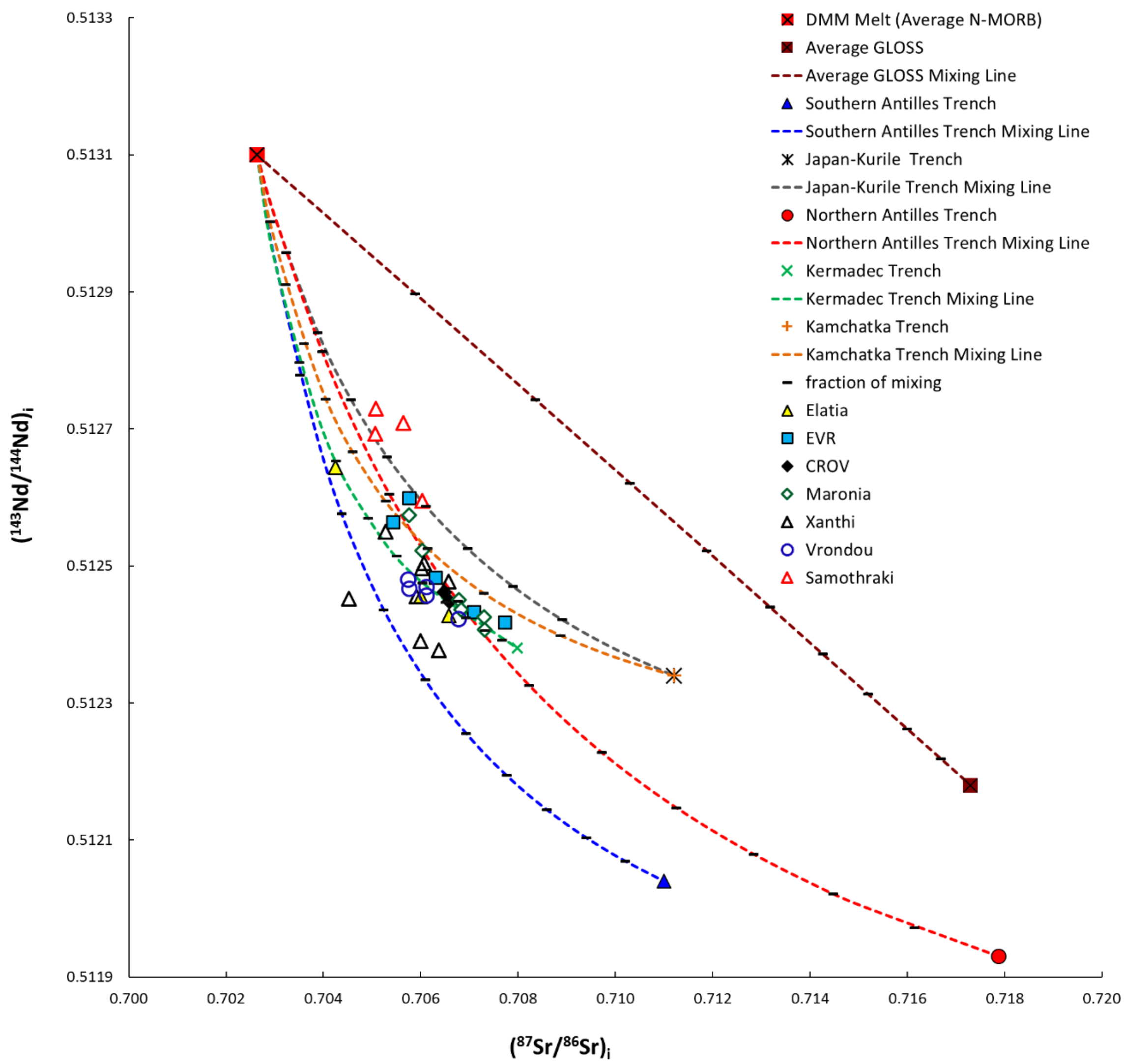

Figure 5.3.1 $(^{87}Sr/^{86}Sr)_i$ versus $(^{143}Nd/^{144}Nd)_i$ diagram of the mafic HRM magmatic rocks. Mixing lines are between average N-MORB (*Gale et al., 2013*) and selected subducted sediments (*Plank & Langmuir, 1998*). The mixing hyperbolic lines were calculated using the mixing equation of *Langmuir et al. (1978)*. Values are reported in Table 5.3.1

Table 5.3.1. Elemental Sr and Nd comporition of MORB are N-MORB average composition from *Sun & McDonough (1989)*, isotopic Sr_i and Nd_i compositions of MORB are average MORB composition far from plumes from *Su & Langmuir (2003)* and average GLOSS and average sediment composition of specific trenches around the world are from *Plank & Langmuir (1998)*

	MORB	GLOSS	Kermadec	Japan-Kurile	Kamchatca	N. Antilles	S. Antilles
Sr	128	327	222	87	38	111	135
Nd	10.66	27	69.53	22.03	14.1	31.22	41.64
Sri	0.70263	0.71730	0.70799	0.71121	0.71121	0.71788	0.711
Ndi	0.51310	0.51218	0.51238	0.51234	0.51234	0.51193	0.51204

r	0.96	0.25	0.31	0.21	0.28	0.26

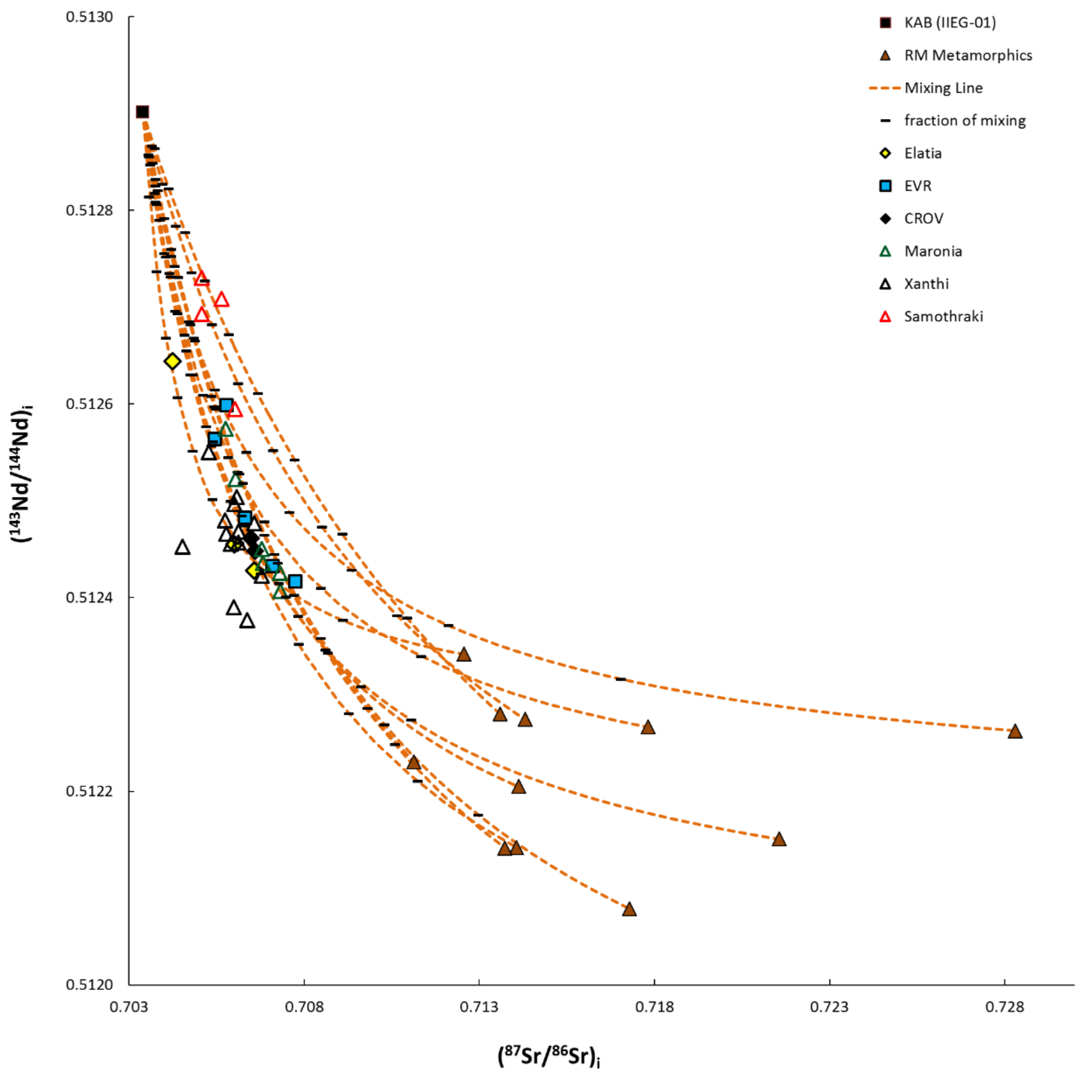

Figure 5.3.1 $(^{87}Sr/^{86}Sr)_i$ versus $(^{143}Nd/^{144}Nd)_i$ diagram of the mafic HRM magmatic rocks and selected Rhodope metamorphics (*Cornelius, 2008*). The mixing hyperbolic lines were calculated using the mixing equation of *Langmuir et al. (1978)*. Values are reported in Table 5.3.2

Table 5.3.2. Elemental Sr and Nd and isotopic Sr_i and Nd_i compositions of KAB (sample IIEG-01 from *Marchev et al. (2004)*, elemental Sr and Nd and isotopic Sr_i and Nd_i compositions of the Rhodope metamorphics are from Cornelius (2008). Initial Sr and Nd ratios for the Rhodope metamorphics were determined based on 30 Ma

	KAB	RH346	RH358	RH360	RH370	RH375	RH376	RH434	RH413	RH418	RH11	RH60
Sr	801	108.13	122.92	197.84	253.58	177.14	147.75	109.12	246.51	203.76	64.82	433.25
Nd	29.00	35.46	18.54	24.16	17.02	15.65	48.46	24.79	32.59	19.68	16.42	36.14
Sri	0.70338	0.72829	0.71412	0.71728	0.71359	0.71431	0.71255	0.71782	0.71406	0.71373	0.72156	0.71112
Ndi	0.51290	0.51226	0.51221	0.51208	0.51228	0.51227	0.51234	0.51227	0.51214	0.51214	0.51215	0.51223

r	0.11	0.24	0.30	0.54	0.41	0.11	0.16	0.27	0.37	0.14	0.43

5.4 Trace Element Modelling

This paragraph is aiming to model for both scenarios the trace element behaviour. Trace element modelling is a much more complicated procedure than the isotopic modelling since many more parameters are used and more assumptions should be made. In paragraph 5.2 some features of the subducted sediment contribution in the mantle wedge were stated. Here, following results of bulk distribution coefficients from previous experiments, will be attempted to model trace element behaviour during subducted sediment melting and interaction with the mantle wedge through an AFC equation (*DePaolo, 1981*). According to *Tatsumi (2001)* calculations, such a process has a high r (ration of assimilation over crystallization). The term aqueous melt will be used hereafter since hydrous sediment melts are needed for efficient release of LILE and LREE these elements from subducted sediments at sub-arc depth. This also implies that top of slab temperatures at sub-arc depth are likely 750-850 °C. The significant enrichment in LILE and LREE of most the HRM magmatic rocks does not allow to use aqueous fluids for this model (e.g. *Plank, 2005*).

For the first model for a lithospheric mantle enriched by subducted sediment melts the average MORB of *Su & Langmuir (2003)* will be also used here to represent the geochemistry of the mantle lherzolite under the RM. Alike the previous paragraph the the ultamafic cumulate xenoliths from KAB will not be used here.

For the subducted sediment melts some assumptions should be made here. There are melting experiments on the behaviour of trace elements during melting of such sediments in different conditions, however they are not enough to represent all the possible combinations of subducted sediments and the temperature-pressure conditions. A better approach here is considered to select a melt from or close to the subducted sediments that satisfy the isotopic model in the previous paragraph (5.3). The first step is to apply batch melting to these sediments and decide a representative melt. Bulk partition coefficients for this step are taken from *Johnson*

& Plank (1999). These authors, determined experimentally distribution coefficients across the sediment solidus within a wide range of temperatures and pressure combinations on pelagic clays. Such sediments match the trench sediments used in the previous paragraph (5.3) to model the isotopic mixing. In ***Fig. 5.4.1*** a Rb versus Sr diagram with batch melting model for all the trench samples used here is presented. The scope was to select an average sediment melt composition to use further. In the same figure a sediment melt from *Tatsumi (2001)* is also presented as reference. There are two different models based on two different sets of bulk partition coefficients. These two sets were selected among others in order to show the strong changes in trace element partitioning which is correlated with the differences in temperature and pressure conditions and mineralogy of the sediment in the top of slab mantle wedge (experiments PC38 and PC47; *Johnson & Plank,1999*). For example, Rb can act as compatible in phengite presence (phengite stability field) or as incompatible in the phengite break-down field. Taking all these in account, it is apparent that the possible melts are various and that it is hard to define an, at least, average sediment melt. Moreover, the temperature-pressure conditions that took place in the subarc mantle wedge M are completely unknown. However, in order to proceed to a manle-subducted sediment model the sediment melt from *Tatsumi (2001)* will be used as a reference melt.

A problem that arises in this paragraph is the scattering of the samples not only for the rocks among the areas but also for the rocks of the same area. Geochemical heterogeneity among the mafic rocks could be attributed to many factors like source heterogeneity or fractionation during the ascent of magmas. However, what is substantial here is not to fit all rocks in a single model but to successfully explain the origin of some of the rocks of each area from a model.

In ***Fig. 5.4.2*** the variation of Rb (b), Ba (a) and Th (c) elements versus Sr are presented, to display the relation between the MORB mantle and the subducted sediments, and the AFC model between these end-members. The bulk partition coefficients of *Gomez-Tuena et al. (2007)* and a assimilation/crystallization ratio of 0.9 were used to model this procces. However, the presented model is meaningless, since, as it was written above, the parameters and pressure-temperature conditions are variable. For example, the presented model for Sr versus Ba (a) might be correlated with the rocks of the EVR, but for the Vrondou rocks is not. However, this does not mean that this is not the case since the sediment melt which contributed in the genesis of Vrondou rocks might have originated from mica stability field and immobilized Ba. Therefore, Ba would act incompatibly and a $D_{Ba}>1$ should have been used. In other words, the chemical signature of the subducted sediments in the arc magmas, as previous authors have investigated, are strongly dependent from the sediment geochemistry and the pressure-temperature conditions, and so far researchers experiment and discuss on this process (e.g. *Ayers & Eggler, 1995; Stalder et al., 1998; Johnson and Plank, 1999; Kessel et al., 2005; Gomez-Tuena et al., 2007*).

On the other hand, the genesis of the RM magmatism from asthenospheric material with Rhodopian metamorphic rocks can be modelled better constrained since, first of all, the geochemistry of the end-members are well known and secondly the crustal conditions are also known. In ***Fig. 5.4.3*** the elements of Rb, Ba and Th elements versus Sr are presented for the AFC model. The parameters of the model are indicative and are presented in ***Table 5.4.1***.

From the ***Fig. 5.4.3*** it is suggested that the AFC process between asthenospheric derived melts and RM metamorphics is not plausible. Apart from the the AFC line, there many HRM rocks that appear more depleted than the KAB basalts. No AFC process could be applied here between these end-members to successfully model the genesis os these rocks.

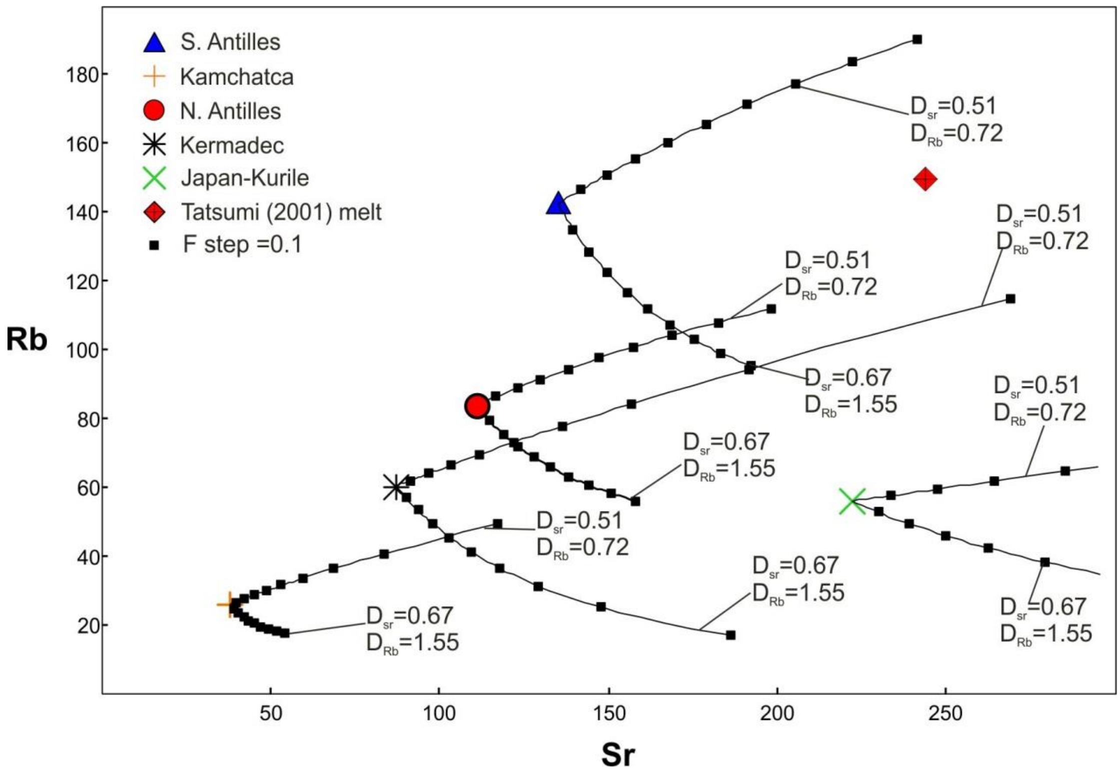

Figure 5.4.1 Rb versus Sr of selected subducted sediments with batch melting models of subducted sediments displayed. D_{Sr} and D_{Rb} values are from *Johnson and Plank (1999)*, Rb and Sr average trench sediment composition are from *Plank and Langmuir (1998)*

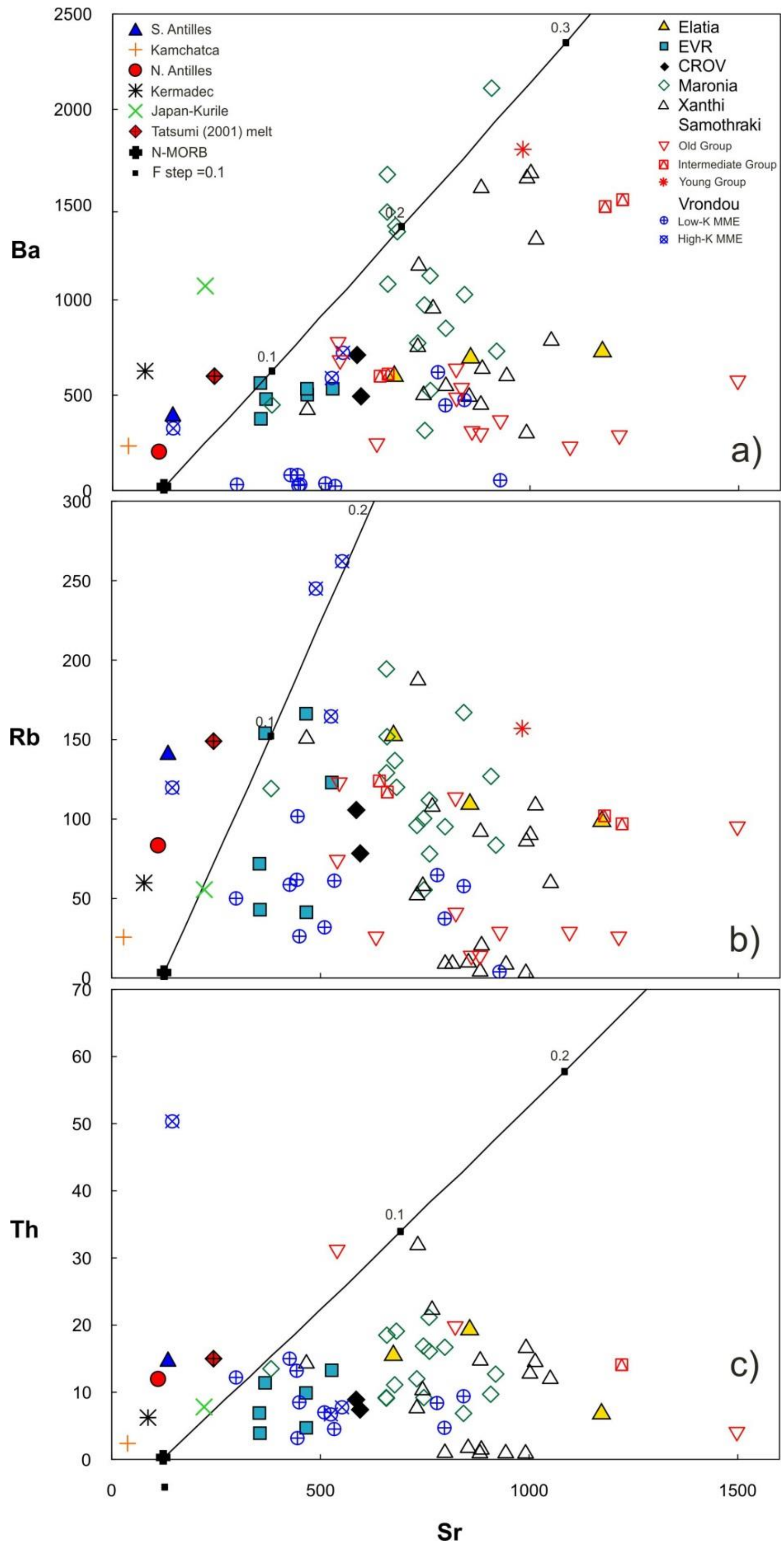

Figure 5.4.2 (a) Sr versus Ba (b) Sr versus Rb and (c) Sr versus Th diagrams displaying assimilation and fractional crystallization model between the subducted sediment melt of *Tatsumi (2001)* and MORB mantle. The bulk partition coefficients between the mantle and the melt are from *Gomez-Tuena et al. (2007)*

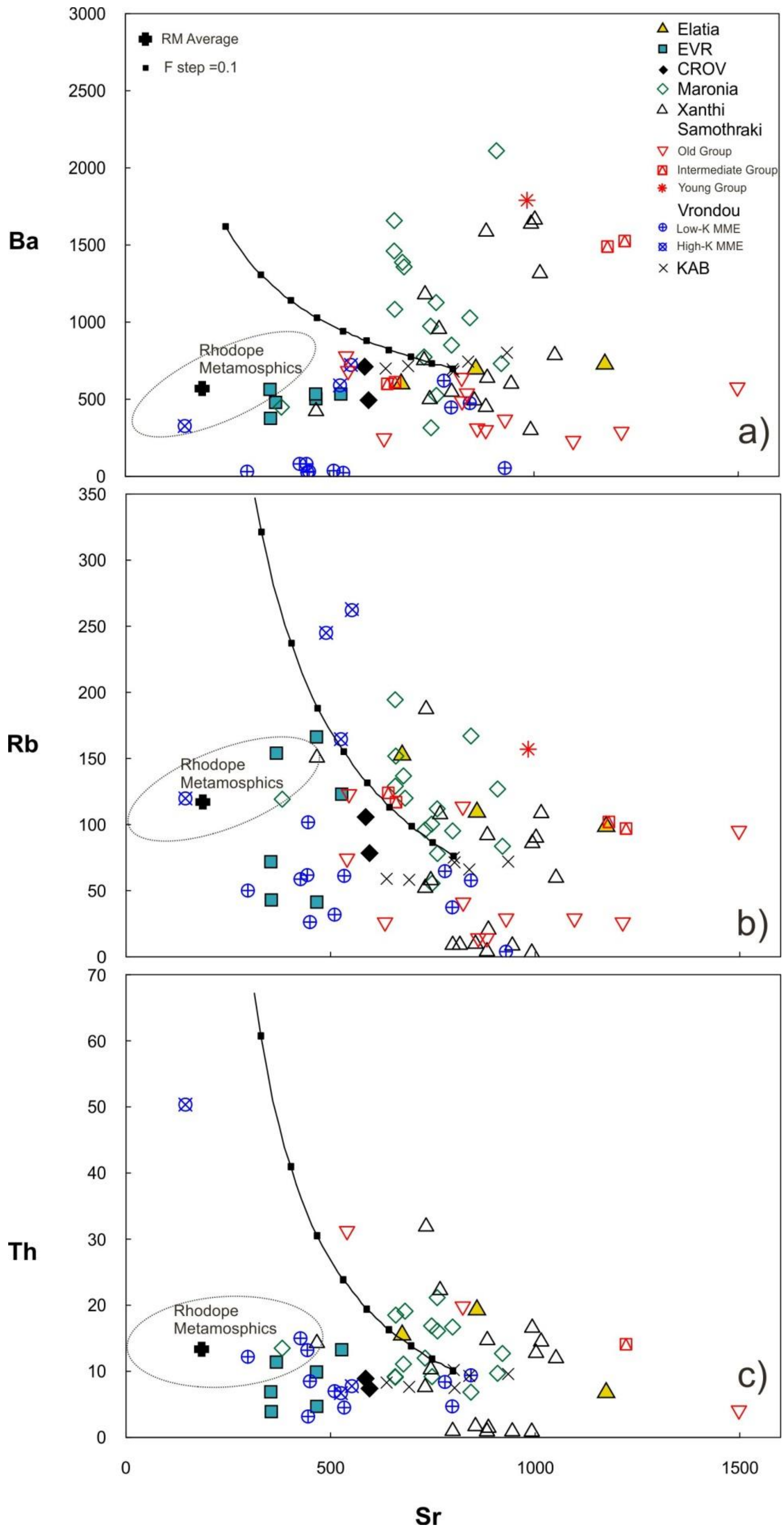

Figure 5.4.3 (a) Sr versus Ba (b) Sr versus Rb and (c) Sr versus Th diagrams displaying assimilation and fractional crystallization model between the subducted

KAB (sample (IIEG-01) and the average rhodope metamorphics (*Cornelius, 2008*). The parameters used for the model are reported in Table 5.4.1

Table 5.4.1 Composition of end-members for the model of Fig. 5.4.3 and parameters of the AFC process

	Sr (ppm)	Rb (ppm)	Ba (ppm)	Th (ppm)
IIEG-01	801	75	695	10.2
RM aver.	187.71	1170.9	569.54	13.34

D_{Sr}	D_{Rb}	D_{Ba}	D_{Th}	r
1.2	0.3	0.6	0.1	0.3

5.5 Nature of the Crustal component

5.5.1 Crustal contribution in the genesis of the felsic rocks

The genesis of the felsic and mafic plutonic and volcanic rocks of the HRM according to previous authors and the present study (chapter 3) are the outcome of mixing prosecces beetwen either mafic mantle derived melts and felsic continental crustal anatectic melts or crustal anatectic melts. The exact processes that took place during the genesis of the felsic magmas are beyond the scope of the present study and in most areas have been reported by previous authors and discussed in chapter 3.

In terms of petrography and geochemistry the felsic magmatic rocks in most areas have similar characteristics and age, apart from the Elatia pluton that has older age, and are reported in chapter 3. The Elatia pluton is the oldest pluton among the other in the present study (56 Ma) and also presents differences in petrographic and geochemical characteristics. The absence of basic rocks and the abundant accessory minerals are unique petrographic characteristics among the other areas studied here. Moreover, the high La/Yb and Sr/Y ratios, which is not presented in any of the other areas, give an "adacitic" affinity to the Elatia pluton implying amphibole ±

epidote ± allanite fractionation rather than origin from subducted oceanic crust melting. Such processes take place in deep crust in high pressure plutons (e.g. *Moyen, 2009*). *Soldatos et al. (2001b)* has reported high-pressures for the Elatia pluton genesis. All the above lead to the conclusion that during the genesis of the Elatia pluton there was a thick continental crust in the area of the HRM probably previous to the beginning of the extensional collapse of the orogene (see chapter 1).

The geochemistry of the felsic members of both plutonic and volcanic rocks show similar enriched characteristics in LILE (**Fig. 5.5.1**) and LREE (**Fig. 5.5.2**) and typical TNT anomalies (**Fig. 5.5.1**) of convergent margins rocks. Their depleted Sr_i and Nd_i isotopic characteristics relative to the continental crust of the RM (**Fig. 5.5.3**) indicate however that the magmas that generated these rocks cannot account for pure crustal anatectic melts, at least of middle-upper continental crust. Lower crust amphibolitic rocks however, could melt and give rocks with similar isotopic characteristic, but such a scenario cannot stand since amphibolitic lower crust of such composition cannot comprise the source of the enrichment mentioned above taking into account the depleted LILE of the HRM amphibolites (e.g *Castorina et al. 2014; Baziotis et al. 2014*).

Basic members are present in both plutonic and volcanic rocks and mafic enclaves are present in all plutonic and even one volcanic rock from the CROV. However, differantiation of such mafic magmas through simple fractional crystallization could not generate the felsic rocks of each area. Interaction of enriched mafic melts with RM crustal lithologies could account for the enriched characteristics of the felsic rocks and their slightly enriched isotopic composition relative to the mafic members. Besides, crustal melting is mainly induced by mantle melts providing heat in the continental crust during periods of extension (e.g *Herbert & Sparks, 1988)*.

Finally, the presence of mafic enclaves in each area strongly indicates that mixing and fractional crystallization is the major mechanism controlling the interaction of mantle and crustal melts and accounts for the genesis and the differantiation of the HRM magmatic rocks.

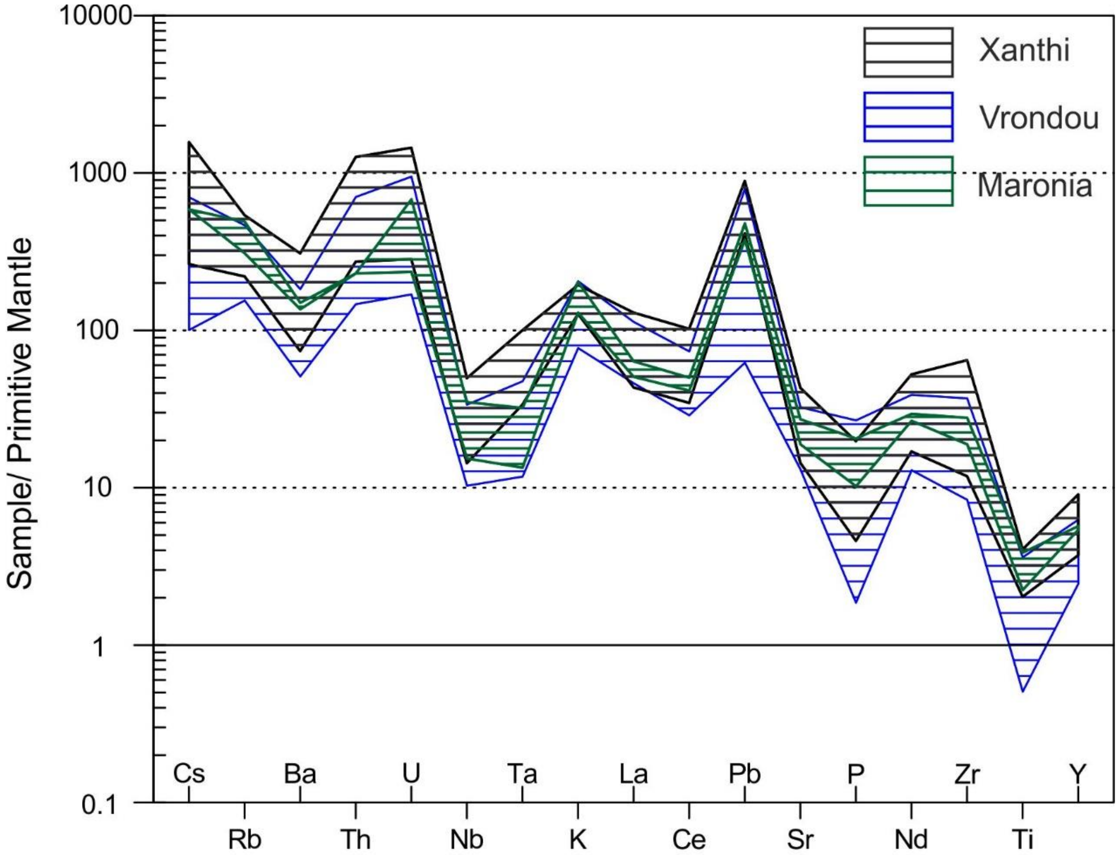

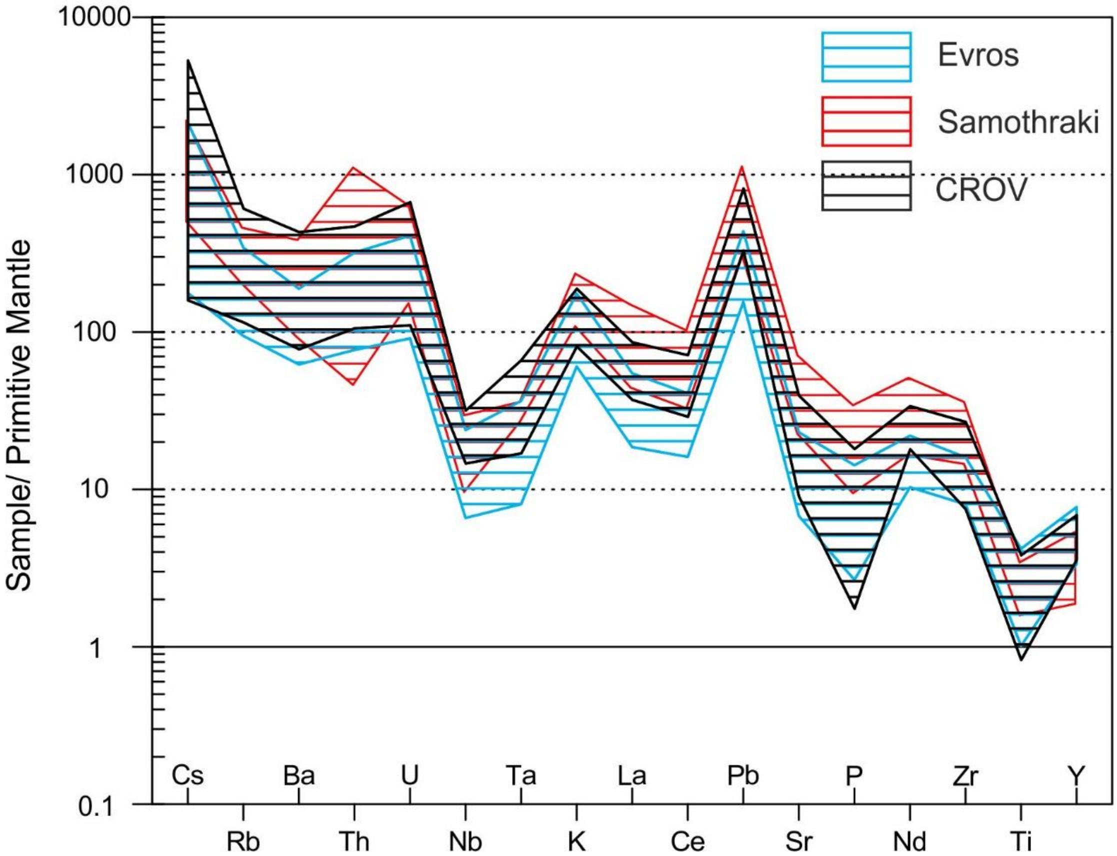

Figure 5.5.1 Trace element patterns of the felsic rocks from all the areas (apart from Elatia). Normalization values after *Sun & McDonough (1989)*

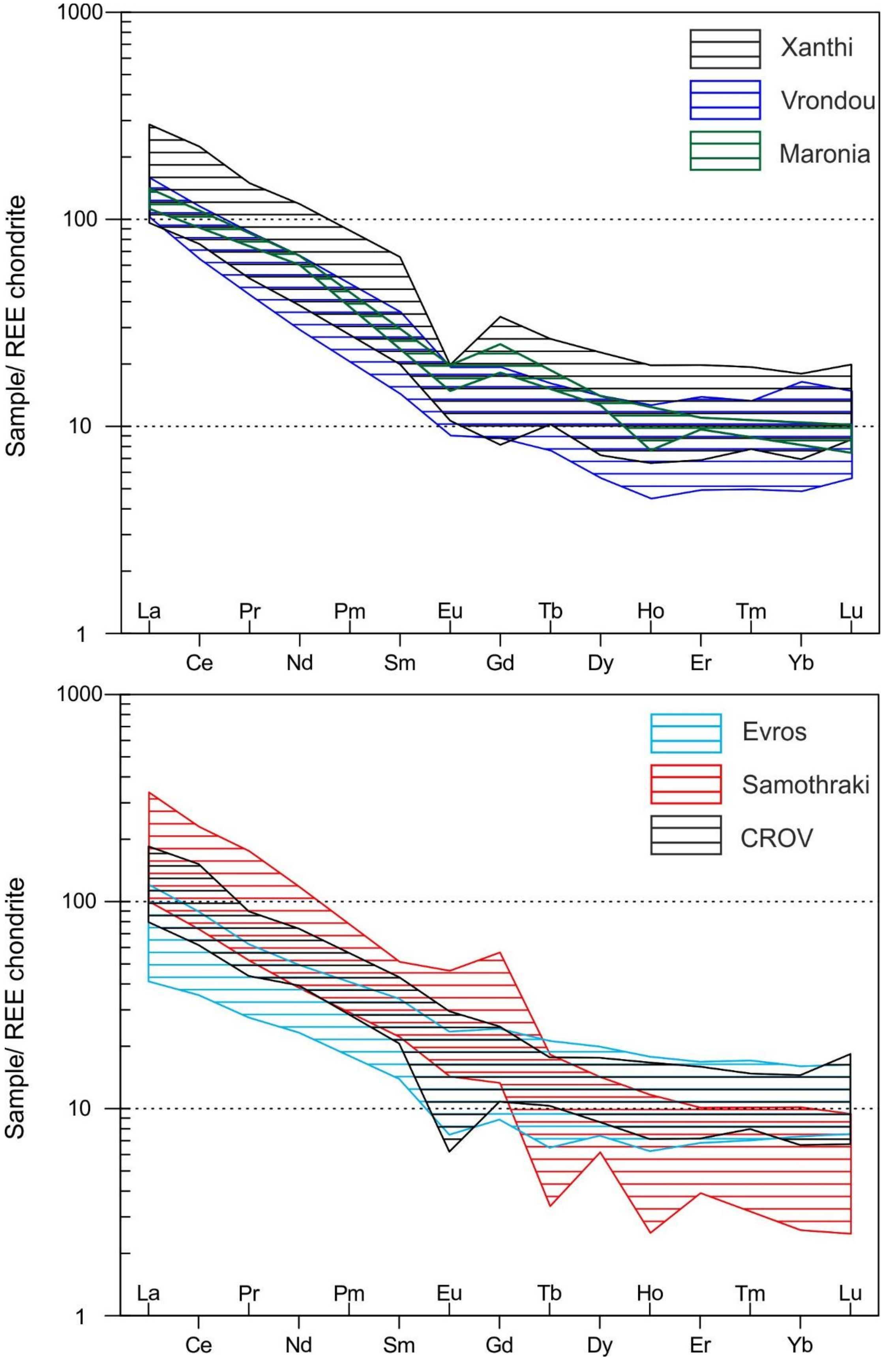

Figure 5.5.2 Trace element patterns of the felsic rocks from all the areas (apart from Elatia). Normalization values after *Sun & McDonough (1989)*

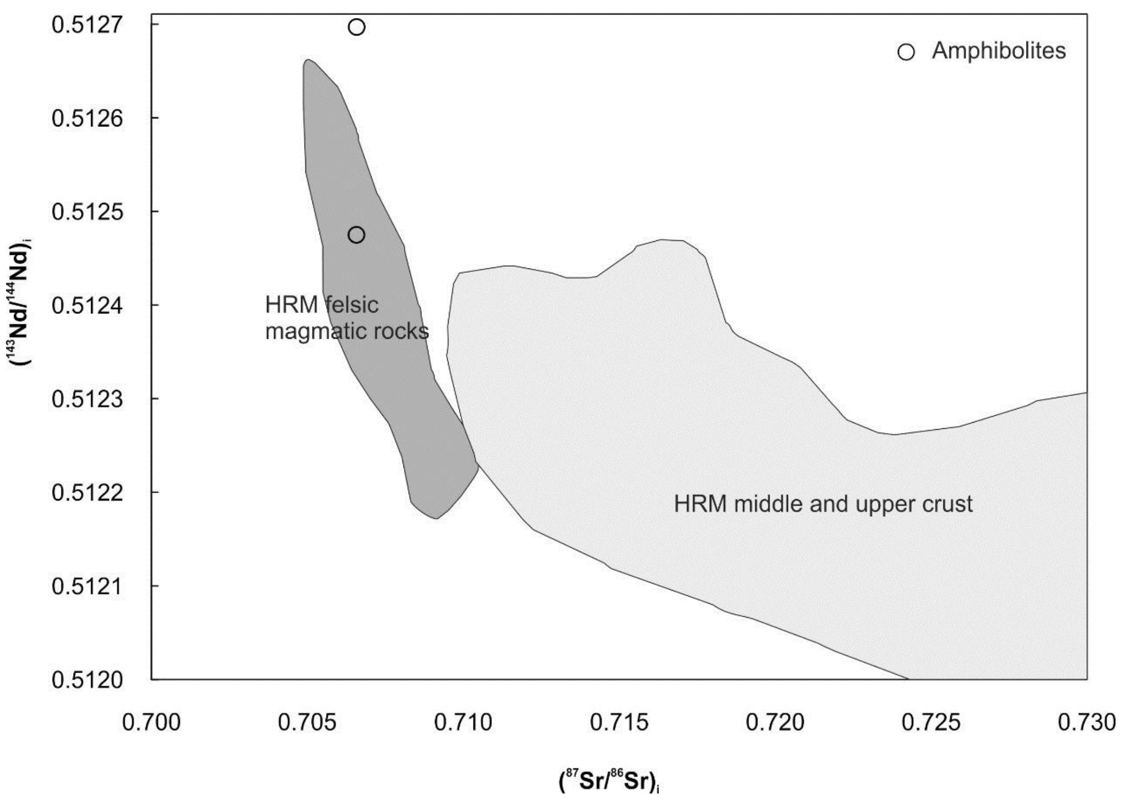

Figure 5.5.3 $(^{87}Sr/^{86}Sr)_i$ versus $(^{143}Nd/^{144}Nd)_i$ isotopic ratios. RM crust from *Cornelius (2008)* and the two amphibolites are from *Castorina et al. (2014)*

5.5.2 Crustal contribution in the genesis of the mafic rocks

The mafic rocks in such geotectonic environments are generated mainly in the mantle wedge above the subducted slab and intrude the continental crust. Subducted oceanic crust melting generating the magmas of adakites comprises also a mechanism which is not the case here. The enriched characters of the mafic rocks (high LILE and LREE) could be attributed in either; a) contamination from continental crustal material throught AFC (Assimilation and Fractional Crystallization) processes during their ascend in the continental crust (e.g *Gill, 1981*) or b) previous enrichment of the mantle wedge above the subduction through metasomatism from sediments and fluids released from the subducted oceanic sediments of the slab since the slab-derived fluid phase contains significant amounts of volatiles including water and incompatible elements, mainly large ion lithophile elements (LILE), Th, U and some light rare earth elements (LREE) (e.g *Zindler and Hart, 1986*; *Hawkesworth et al., 1993*) or c) subducted continental crustal material (e.g

Li et al., 1997; *Wang et al., 2005*). The latter two prosecces lead to genesis of mafic rocks with continental affinity.

The absence of correlations between the major elements and isotopic ratios of the rocks can rule out the contamination from middle and upper continental crust (case a). In ***Fig. 5.5.4*** SiO_2 and mg# versus initial isotopic Sr are presented depicting the trends of crustal assimilation and fractional crystallization. It is apparent in this figure that crustal assimilation could not account for the isotopic characteristics of the mafic rocks.

Ratios of Sr/Sm and Rb/Sr can determine the nature of the contamination component since the Sr/Sm ratio is usually increased from subducted sediment component while Rb/Sr from continental crustal lithologies (***Fig. 5.5.5***). In the same figure it is obvious that the HRM magmatic rocks follow the trend of the worldwide convergent margins which orininated from mantle metasomatism. In ***Fig. 5.5.5*** it is shown that most samples from all the areas except only one sample form Vrondou, have an upward trend towards subducted sediment lithologies. Moreover, the low $(La/Yb)_N$ ratio (2.9-25) implies also that continental crustal material contamination is not the case here (*Zhao et al., 2013)*. These observations indicate that not only the melts could not have interacted with middle and upper continental crust during their ascent but also rules out contamination from subducted continental crust (case c).

The presence of mafic enclaves and the mafic dykes that bear lower crustal xenolites (e.g PD-2 sample) could implie hybridization of the magmas in the lower crust. On the other hand, lower crustal lithologies are of metabasaltic-amphibolitic composition and are able to preserve the depleted characteristics in these rocks, therefore they can not comprise the source of enrichment.

All the above observations come in accordance with the isotopic modelling of paragraph 5.3 where it is implied that continental crustal contribution is probably not the case since significant amounts of continental crustal material need to be assimilated in order to produce the HRM mafic rocks melts. Therefore the most prominent suggestion for the origin of the mafic members of the HRM magmatic rocks so far is the melting of a metasomatised mantle wedge from slab subducted sediments under the RM (case b). However, the exact processes and conditions for this scenario is hard to be specified since the existed experimental data for these processes are numerous and case driven, and could not be applied for this area. Moreover, further differentiation of these magmas during their ascent like fractional crystallization or hybridization with other mantle melts in the lower crust or hybridization with lower crustal lithologies are beyong investigation.

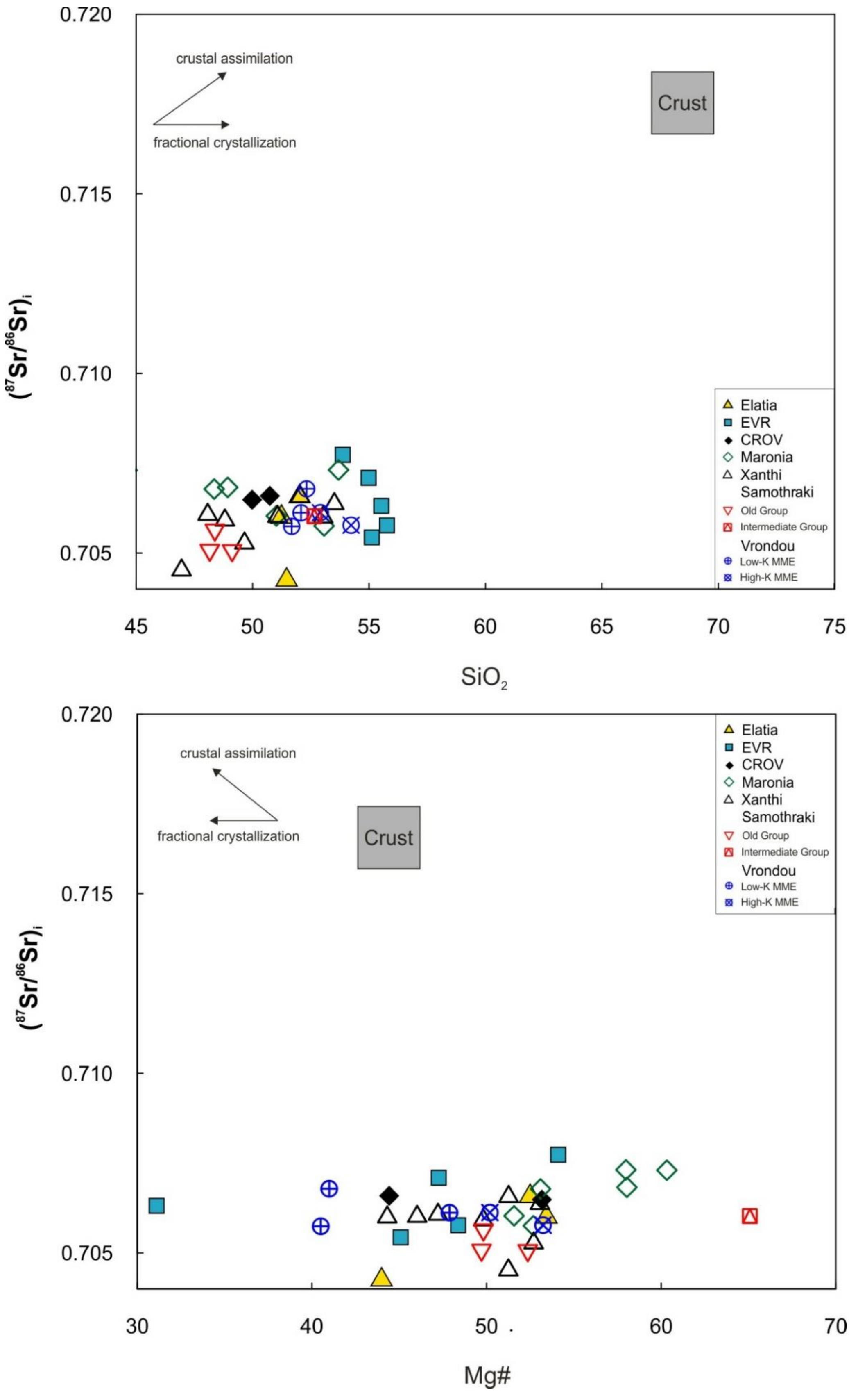

Figure 5.5.4 SiO_2 and mg# versus $(^{87}Sr/^{86}Sr)_i$ displaying the effects of continental crustal assimilation and fractional crystallization**.** The "crust" field reflects the middle and upper HRM crust

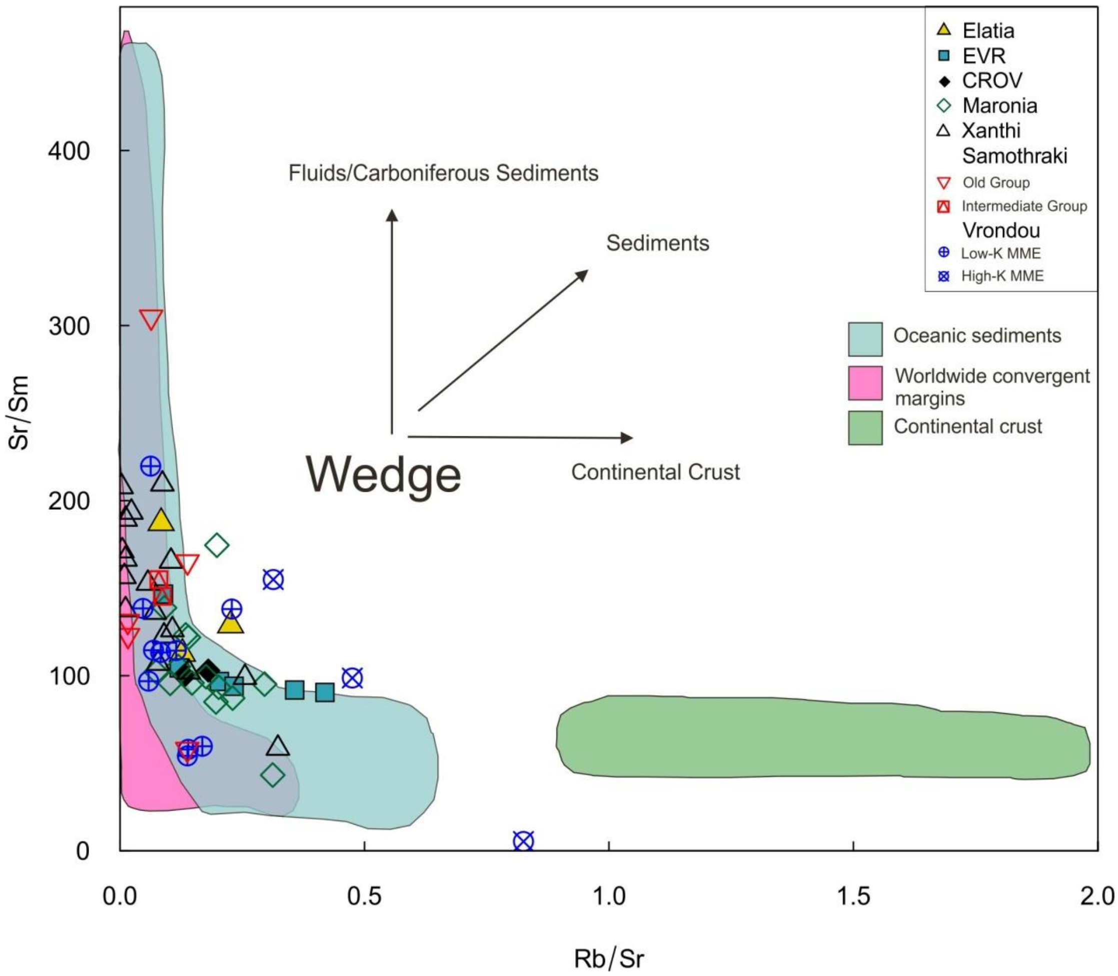

Figure 5.5.5 Sr/Sm versus Rb/Sr diagram displaying the trends towards subducted sediment contamination and continental crustal contamination. Fields illustrated are from personal communication with *Poli G*.

Many authors (e.g *Pe-Piper et al. 1998*), suggested that the Tertiary magmatic rocks of HRM were formed from a metasomatised mantle enriched during subduction. *Perugini et al. (2004)*, suggested that fluids released by the subducted slab induced metasomatic processes generating a 'leopard skin' mantle wedge able to produce mafic melts ranging from typical calc-alkaline to ultra-potassic. Subducted sediments play an important role in arc magmatism and crust-mantle recycling. The metasomatism of the mantle wedge though, is not a simple process ssince there are large variations in the chemical composition of subducted sediments which for the most part are linked to the main lithological constituents (*Plank & Langmuir, 1998*) and the differences in partition coefficients the elements present in fluid and silicate melts (e.g *Elliot et al. 1997*). Moreover, the depth and degree of partial melting in the mantle wedge additionaly contributes in the variation of mantle-wedge enrichment. Based on these observations the mantle derived melts under these circumstances could present significant variability.

The enriched characteristics of the HRM mafic rocks could only be attributed in variable mantle enrichment from the subducted slab melts. The nature of these melts can be assessed from trace elements ratios of the mafic rocks such as Ba/La (e.g. *Elliott et al., 1997*), Ba/Th and Th/Yb (e.g. *Hawkesworth et al., 1997*). Ba and Yb are fluid mobile elements and the increase of their concentration in the sediment melts is positively correlated with the amount of fluid. Th and La on the other hand are preferentially mobile in sediment melts rather than fluids. As a consequence, mantle melts that have been mainly metasomatized by fluid-like sediment component are enriched in Ba and Yb over Th and La.

In ***Fig. 5.5.7*** the role of fluid-like component from slab dehydration and sediment component from slab subducted sediments is presented. In general, subducted sediments seem to play a major role in the enrichment of these rocks and only Xanthi and Maronia rocks seem to be more affected from fluid-like components. The Xanti especially shows two totally diferent trends, one towards fluids and one towards sediment melts suggesting that this pluton has origin from two differently metasomatizes mantle wedge locations. However, there is no clear distinction for fluids and sediment melts. In paragraph 5.2, it was discussed the difference between the aqueous fluids and hydrous silicate melts. There is no clear distinction between those two, however the fluid-like character or the melt-like character they give to the resulted mantle wedge melts indicates the main contribution.

Finally, the samples in these diagrams show general trends but the samples from the different areas seem to overlap each other with no clear distinction among them suggesting that they are originated from a common source. This source seems to be variably enriched from sediment melts and fluids which depending on the pressure-temperature conditions and the nature of the sediment melts/fluids melted and gave genesis to rocks which share common characteristics and fewer differences.

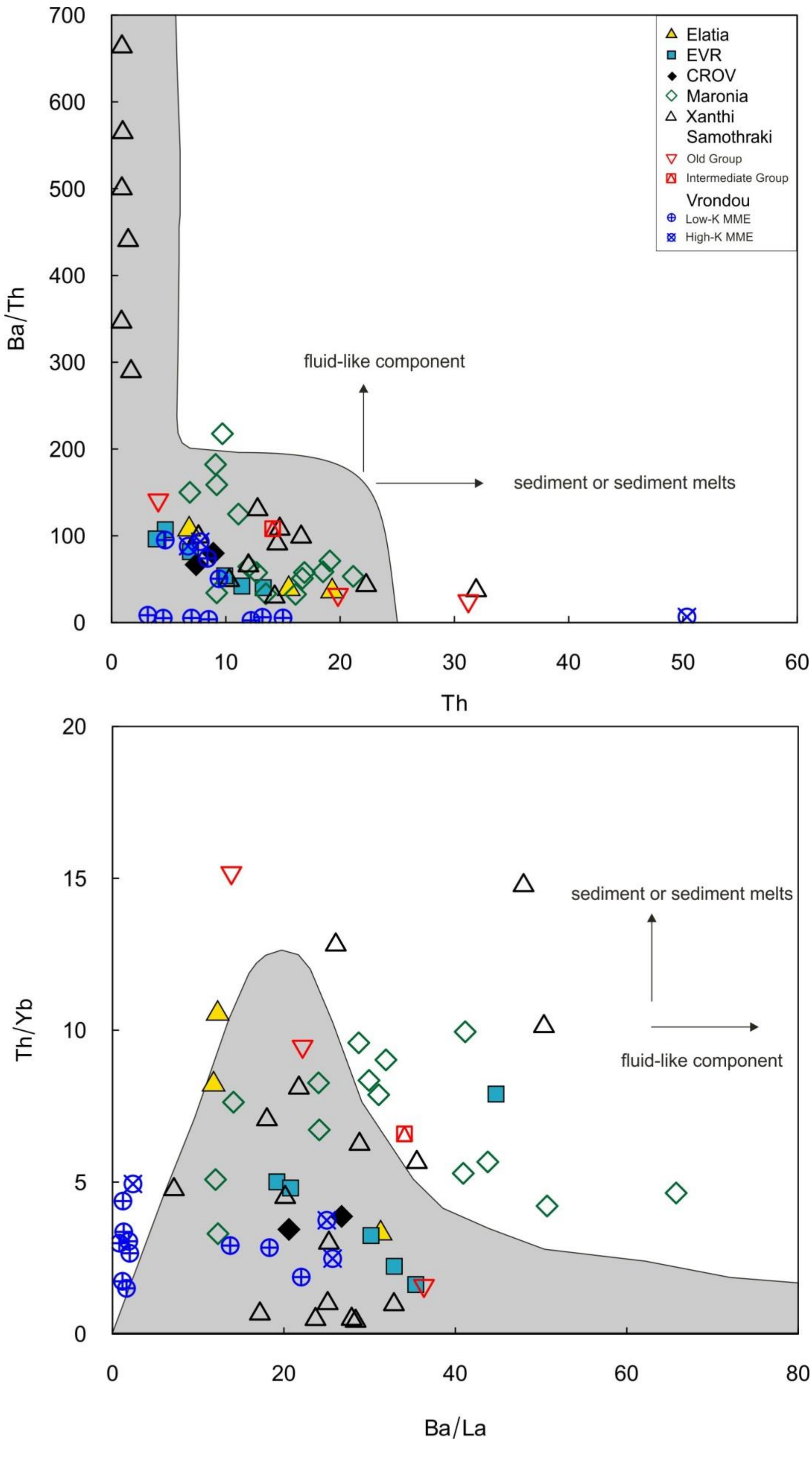

Figure 5.5.7 Th versus Ba/Th and Ba/La versus Th/Yb displaying the role of fluids and sedimentary components of the subducted slab. The grey shaded field represents a compilation of arc basalts worldwide (*Hawkesworth et al., 1997*)

5.6 Nature of the Mantle source

To estimate the extent of enrichment from subducted component among the different areas relatively the Th/La and Ce/Pb indicators are used in ***Fig. 5.6.1***. Th/La in arc magmas is inherited from subducting sediment. Variations in Th/La in most arc basalts depends strongly on variations in the composition of subducting sediment and the final Th/La in the arc magma will depend on amount the sediment component incorporated in the mantle (*Plank, 2005*). The Ce/Pb indicator is high in the mantle and can be changed only by the addition in the mantle wedge of slab derived components (*Miller et al., 1994*). The variability in Th/La of rocks from each area is attributed in differences in the mantle enrichment from the subducted fluids or sediments while the increased Ce/Pb ratio (Vrondou, Maronia, Elatia) suggests that these rocks preserve depleted characteristics. It is significant that the Xanthi rocks are separated in two different groups, one displaying higher Th/La ratio and the other low Th/La ratio. This probably suggests that the basic group of Xanthi was originated from two distinct mantle derived magmas, one enriched and one depleted. The low Th/La of the Xanthi group rocks coupled with the results of ***Fig. 5.5.7*** with high Ba/Th ratio suggests that a more fluid-like component contributed in the genesis of this melt.

Despite the differences in enrichment among the different areas, there are also differences observed among the rocks of the same area. This could probably be attributed in differentiation processes during the ascent of the mantle melts such as fractional crystallization, interaction of different mantle melts during their ascent or even multiple source melt contribution in the genesis of the rocks of a specific area.

So far, the preserved depleted characteristics of some of the HRM magmatic rocks, the comparison with asthenosphere derived Bulgarian volcanics and the isotopic and trace element models suggest that the mantle wedge under the HRM was a previously MORB depleted mantle. Previous authors also suggest a DMM mantle wedge beneath RM (e.g *Yanev et al., 2003*) However, the data here indicate re-enrichment of the mantle wedge with subducted sediment/fluids crustal material which resulted in enriched mafic mantle-derived rocks. Mantle metasomatism from subducted sediments and fluids and mantle melt trigger, is a rather complicated process depending on many factors as stated in previous paragraphs, and the result is a heterogeneously metasomatised mantle or a so-called leopard-skin mantle (*Perugini et al. 2004*), which melts and results in variably enriched melts.

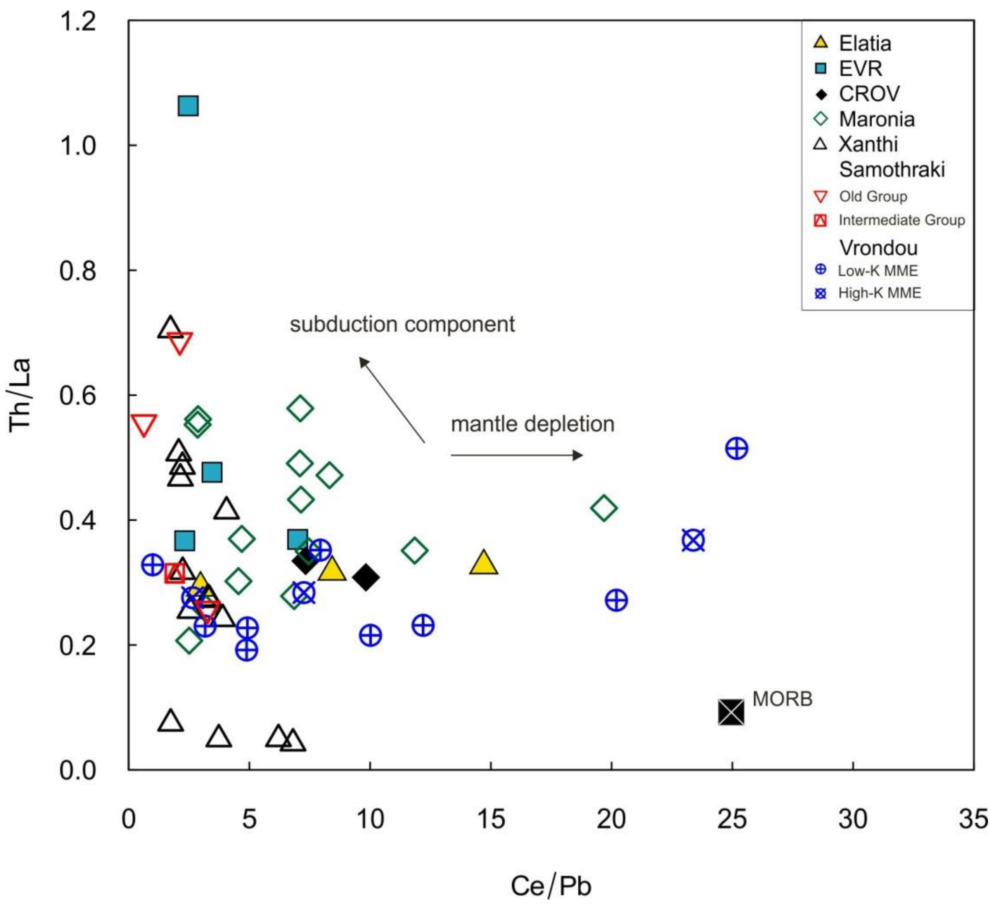

Figure 5.6.1 Ce/Pb versus Th/La displaying the contribution of component of the subducted slab in the mantle wedge

6. GEOTECTONICS AND GEOCHEMICAL GEODYNAMICS

6.1 Geotectonic Implications

The Eocene to Miocene magmatic activity of the Rhodope Massif has been attributed in convergent margin geotectonic setting and in particular in continental arc magmatism. According to *Kamenov et al. (2000)* the Rhodope is considered to be a frontal part of the Srednogorie arc. Dating in the Central Srednogorie (*Peytcheva et al., 2002*) document a southward shift of this magmatism from 92 to 78 Ma. Therefore, the 70-30 Ma Rhodope granitoid intrusions may be a continuation of the Srednogorie magmatism into the Rhodope region. The available age and geochemical data for Late Cretaceous-Early Eocene granitoid magmatism are insufficient to clarify this period. However, it is clear that an isolated subduction event can hardly explain 40 million years continuous magmatism in the Rhodopes unless the subduction process persisted. Indeed, progressive southward migration of magmatic activity in the Aegean region (*Fyticas et al., 1984*), commenced in the Rhodopes in the Late Eocene (*Yanev et al., 1998*), has been confirmed by seismic tomography (*Spakman et al., 1988; Papazachos, 1994*).

Previous authors have proposed the involvement of Pindos and Vardar-Axios subducted oceans beneath the Rhodope Massif (e.g *Boccaletti et al. 1974; Robertson and Dixon 1984; Mountrakis, 1983, 1986; Robertson et al. 1996; Pe-Piper 1998*) but so far the exact subduction mechanism has not been clarified. According to previous authors the Vardar-Axios ocean closure took place during Late Cretaceous, however the remnant of the subducted slab at the eastern margin of the Vardar–Axios ocean, that remained open into the Tertiary (*Brown and Robertson, 2004; Sharp and Robertson, 2006*) under the Internal Hellenides, could also be the driving mechanism for the Tertiary magmatic activity in the Rhodope province, simultaneously with the opening and sedimentation of the Thrace basin. Seismic tomographies (*Spakman et al. 1988; Papazachos, 1994*) show one northward dipping high-density slab beneath the north Aegean.

Dating from the Early Cretaceous, the Pindos oceanic basin appears already to have been narrower in the north than in the south. Closure resulted in continental collision in the north, prior to further south (*Degnan & Robertson, 1998* and references therein). Final closure began in the late Cretaceous, and suturing of the Pindos basin was complete by the late Eocene (e.g *Jones et al, 1992*).

The involvement of the Pindos subducted ocean in the geochemical characters of the RM magmatism is probably very restricted since several Ma (10-20) are necessary for mantle melts to ascend in the continental crust. Coupling this observation along with the post-collisional character ot the RM magmatism started at 50+ Ma where the Pindos ocean was still suturing supports the latter assumption. Moreover, the contribution of one and only subducted slab along with the composite mechanisms of mantle metasomatism could account for the RM magmatics geochemical characters.

6.2 Geochemical Geodynamic Implications

Several geodynamical models based on the geochemistry of the magmatic rocks have been proposed for the geochemical interpretation of the Rhodopian magmatism.

6.2.1 Slab rollback and slab detachment

The negative buoyancy of the subducted lithosphere with respect to the surrounding mantle (slab pull force) is thought to be one of the main driving forces of Earth's tectonic plates motion (e.g. *Forsyth and Uyeda*, 1975; *Chapple and Tullis, 1977*; *Carlson et al., 1983*).

The irregular motions of plates and the irregular distribution of plate consumption and generation require that subduction zones and descending lithospheric slabs migrate laterally. Absolute plate motions indicate that slab migration is generally retrograde; that is, it is opposite to the direction of motion of the plates to which the slabs are attached. As a result, the downward motions of slabs are generally steeper than their dips, probably because of their negative buoyancy relative to the surrounding mantle. An important consequence of lateral slab migration is the displacement of material away from one side of the slab and inward flow of an equal volume toward the other side (e.g *Garfunkel et al., 1986*) resulting in backward migration of the subducted slab and it is known as slab roll-back (***Fig. 6.2.1***).

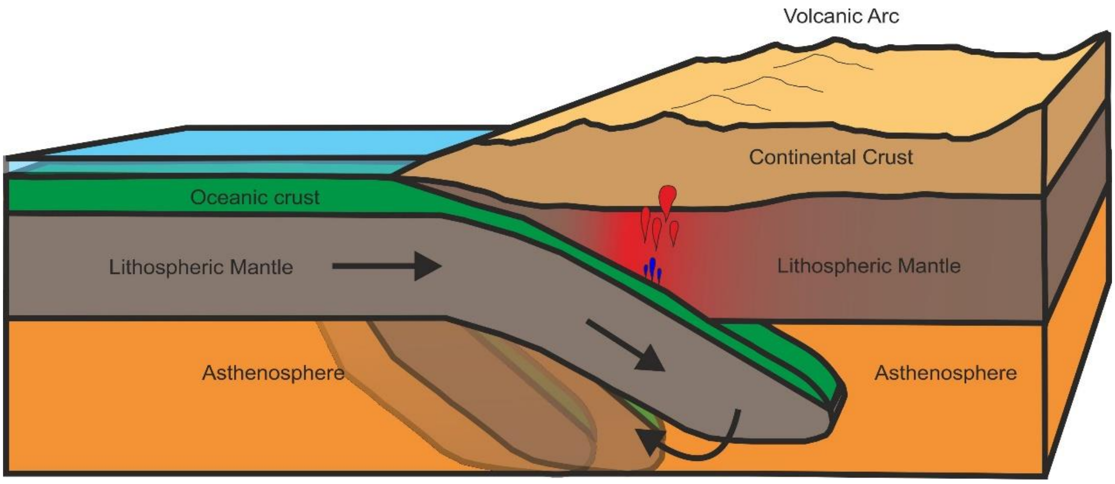

Fig. 6.2.1 Schematic figure of the backward migration of the subducted slab (slab roll-back). Figure not in scale

The downgoing slab may lead to extensional shearing in the descending plate, permitting separation of the downdip, dense oceanic lithosphere from the adjacent lighter continental lithosphere. Detachment may occur by means of a lithosphere-penetrating normal-sense shear zone or by some combination of these mechanisms (*Sacks & Secor, 1990*). Slab detachment (***Fig. 6.2.2***) is a usual process in the collision settings (e.g *Innocenti et al., 1982*; *Sacks & Secor, 1990*; *Wortel & Spakman 2000*). According to *Huw Davies & von Blanckenburgh (1995)* the continental collisions are preceded by subduction of dense oceanic lithosphere, and followed by attempted subduction of buoyant continental lithosphere. This situation of opposing buoyancy forces leads to extensional deformation in the subducted slab. A narrow rifting mode of deformation will result if there is strain localization. Slab break-off/detachment results. Slab detachment was suggested as a mechanism to explain the magmatism in the Alps and the Aegean region. It leads to heating of the overriding lithospheric mantle by upwelling asthenosphere and melting of its enriched layers. Different degrees of partial melting of the enriched lithosphere produce magmas ranging from alkaline to ultrapotassic, whereas slightly higher degrees of melting of more fertile peridotite layers produce calc-alkaline melts. According to the depth of melting, the mantle source of the magmas show different alkalinity (*Pearce et al. 1990*). Hydrous potassic phases are potential hosts for alkalis and H_2O in metasomatized mantle to depths and are likely to be source components for deep-seated generation of potassium-rich magma More alkaline magmas indicate deeper lithospheric source bearing K-richterite while more potassic magmas indicate the presence of phlogopite in the lithospheric mantle source (e.g . *Konzett & Ulmer, 1999*)

According to *Yanev et al. (1995, 1998)* slab detachment can explain the variations of the Rhodope Tertiary magmatism from more alkaline to less alkaline varieties. Rollback of the slab may lead to extension in the cold back-arc lithosphere and its replacement by hot asthenosphere to shallow mantle levels and explains the southward trench and the magmatic migration in the region from more alkaline to the northern (Bulgaria) to less in the HRM. According to *Marchev et al. (2004)*, this should promote massive crustal melting and large volumes of felsic magmas and it is probably not the case. Finally, it is obvious that at least some of the lithosphere mantle had remained to provide the source for the spinel lherzolite xenoliths in the KAB.

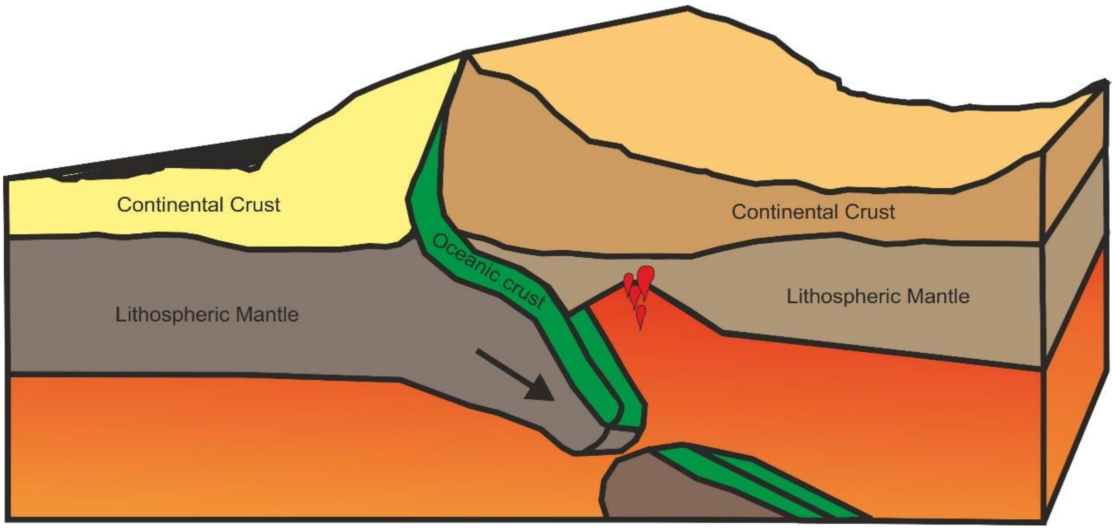

Fig. 6.2.2 Schematic figure of the slab separation (slab detachment or slab break-off). Figure not in scale

This model fails to provide sufficient explanation for the genesis of the HRM mafic magmatic rocks. The similarity in isotopic characteristic of both mafic and felsic rocks, the absence of rocks with asthenospheric geochemical character and the absence anatectic crustal rocks in the HRM suggests derivation from a common non-asthenospheric source and absence of continental crustal contribution . Moreover the significant asthenospheric contribution predicted by this model, at least at the final stages of the extension, suggests that this is not the case for the HRM magmatic rocks. Nonetheless, slab detachment is not unlikely to have occurred earlier during the persisting subduction of the oceanic crust under Rhodopes previous to the genesis of the Tertiary magmatism, however its predicted effects are not reflected in the geochemistry of the rocks.

Slab roll-back has been suggested by the previous authors to explain the southward migration of the magmatism. However, it has also been rejected from the same authors because it wouldn't satisfactorily combined with other mechanisms mainly due to the slab detachment and the asthenospheric intrusion it causes. Nevertheless, it comprises the only plausible mechanism to explain the southward migration of the RM magmatism and it is not necessarily excludes other mechanisms.

6.2.2 Delamination

Mantle convection beneath continents during subduction, may extend right up into the base of the crust. The convection that removes the chilled boundary layer of mantle lithosphere from a shield is a finite amplitude instability which starts at linear rift in the lithosphere and propagates laterally at several centimeters per year. The mantle pulls away from the crust and sinks downward leaving in its place a layer of hot asthenosphere which has risen adiabatically to replace it (*Bird, 1978*). Moreover, some authors suggest that part of lower crust may also delaminated with the lithospheric mantle (*Meissner et al., 1998*; ***Fig. 6.2.3***).

Yanev et al. (1998) had also proposed delamination of thickened crust after the Europe-Apulia continental collision in order to explain Priabonian–Oligocene magmatism in the Eastern Rhodopes. According to *Marchev et al. (2004)* this model has the same shortcomings as the previous one and in many respects it is indistinguishable from slab break off. It predicts a rapid intrusion of the asthenosphere in the place of delaminated mantle and eclogitized lower crust resulting in uplift and extensional collapse. Rapid asthenospheric uplift would produce a thermal anomaly leading to partial melting of the asthenosphere and lower lithosphere and underplating of these magmas beneath the lower crust. This would cause widespread lower crustal melting and hybridization as indicated by the bimodal volcanic compositions. The southward migration of the activity could reflect a delamination process which would have started under the Eastern Rhodopes and then migrated southward under the North Aegean region.

This model has the same shortcomings as the previous one both for the Bulgarian RM and the HRM magmatic rocks. Asthenospheric contribution and crustal anatexis predicted by such model is not reflected in the geochemistry of the rocks neither for the Bulgarian RM nor for the HRM.

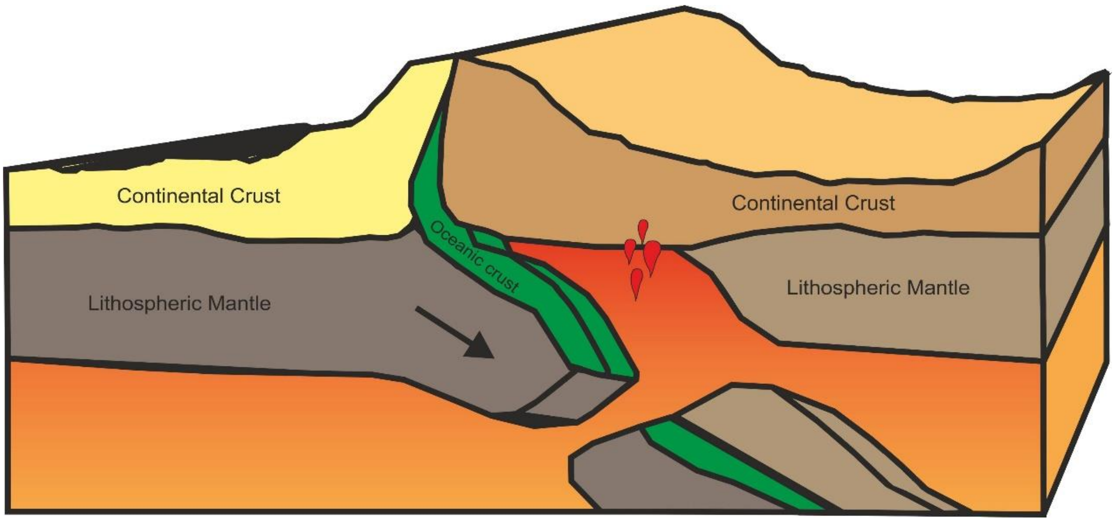

Fig. 6.2.3 Schematic figure of delamination. Figure not in scale

6.2.3 Convective removal or convective thinning

Convective removal of the lithospheric root below regions of lithospheric convergence (e.g *Platt and England, 1994; Houseman and Molnar, 1997;* ***Fig. 6.2.4***) adds potential energy to the lithosphere of these belts, thereby driving extension by normal faulting and is difficult to be distinguished from other processes leading to removal of the lithosphere (e.g. delamination). Following a period in which mountain belts are built by crustal thickening, many such belts collapse by normal faulting and horizontal crustal extension in the back-arc region . Such collapse occurs because removal of thickened mantle lithosphere adds potential energy to the lithosphere of these belts, thereby driving extension. According to some authors, convective thinning differs from delamination in symmetry of the convective thinning with no migrating delamination front and removal of the lower part of the mantle only, which excludes direct contact between the asthenosphere and the crust. This model cannot give sufficient explanations on the southward migration of the RM magmatism. *Marchev et al. (2004)* suggests that some form of convective thinning of the lithosphere and of asthenospheric mantle diapirism could be appropriate processes explaining the magmatism and extension in the Rhodope region.

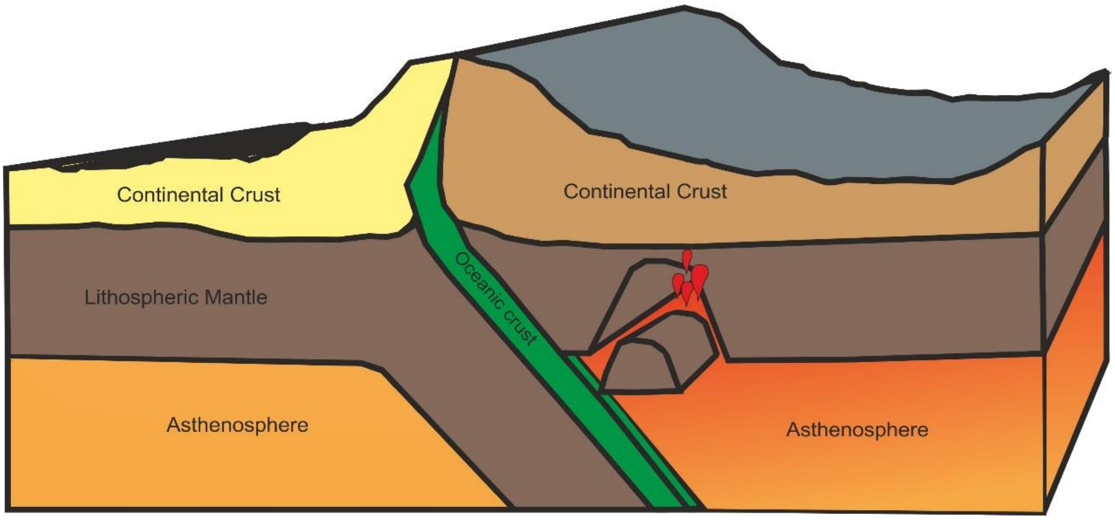

Fig. 6.2.4 Schematic figure of the separation of the lower part of the lithospheric mantle according to the convective removal process. Figure not in scale

So far, from the available geochemical and the few geophysical data, a specific integrated geodynamical model has not been suggested. In the present study the studied mafic rocks give important information for the mantle geochemistry and dynamics and can contribute to a more specific geodynamic model for the area.

Migration of the magmatism from convergent type to orogenic type with asthenospheric mantle contribution is a fact due to the mafic rocks analysed from the eastern Rhodopes (*Marchev et al., 2004*). For the HRM rocks, as shown in the previous study, seems that only melts from a metasomatised by slab-derived melts lithospheric mantle contributed in their genesis. A simple convective type removal geocynamic model can not explain the lack in asthenospheric contribution in the HRM magmatic rocks.

6.2.4 Unified geodynamical model for the RM magmatics

The geodynamic model proposed here inferred from geochemical data is a compilation of a slab roll-back mechanism followed by slab detachment and convective thinning (***Fig. 6.2.5***). After the closure of the Vardar-Axios ocean in Upper Cretaceous the subduction process persisted beneath the RM. Slab roll-back is a mechanism that sufficiently interprets the southward migration of the magmatism. Slab roll-back could have start occurring before and persisted after the continental collision of the Apulia and Rhodopes. According to *Huw Davies & von Blanckenburgh (1995)* dry asthenospheric mantle will melt only if break-off occurs at a depth shallower than ca. 50 km, which suggests that slab break off under the RM occurred at deeper mantle levels which explains the absence of abundant asthenospheric melts that this model predicts. Detachment of the subducted oceanic crust in deeper mantle levels would not affect the RM magmatism since the younger slab remnant is able to sufficiently contribute to the magma genesis.

Slab roll-back leads to back-arc extension. The backarc extension is favored for narrow slabs and near lateral slab edges and is driven by rollback induced toroidal mantle flow (*Schellart & Moresi, 2013*) in which detachment might have also contributed. Such a process could have led to lithospheric mantle convective thinning and mantle diapirism. Seismic studies in the Eastern Rhodopes of *Babuska et al. (1987)* indicate a regionally thinned lithosphere about 80 km thick. Convective thinning beneath the RM, triggered from the anomalous hot mantle, could probably gave rise to asthenospheric diapirism in a restricted area under the eastern Bulgarian RM resulting in asthenospheric derived melts with shallow level crustal contamination and finally, after advanced thinning, in the youngest pure asthenospheric OIB type melts of Krumovgrad basalts. According to *Marchev et al. (2004)* at least some of the lithosphere mantle had remained to provide the source for the spinel lherzolite xenoliths in the KAB. HRM comprised the southern part of this subduction mechanism located apparently further from the thinned lithospheric area of asthenospheric diapirism preserving enough lithospheric mantle to give genesis to the HRM magmatic rocks.

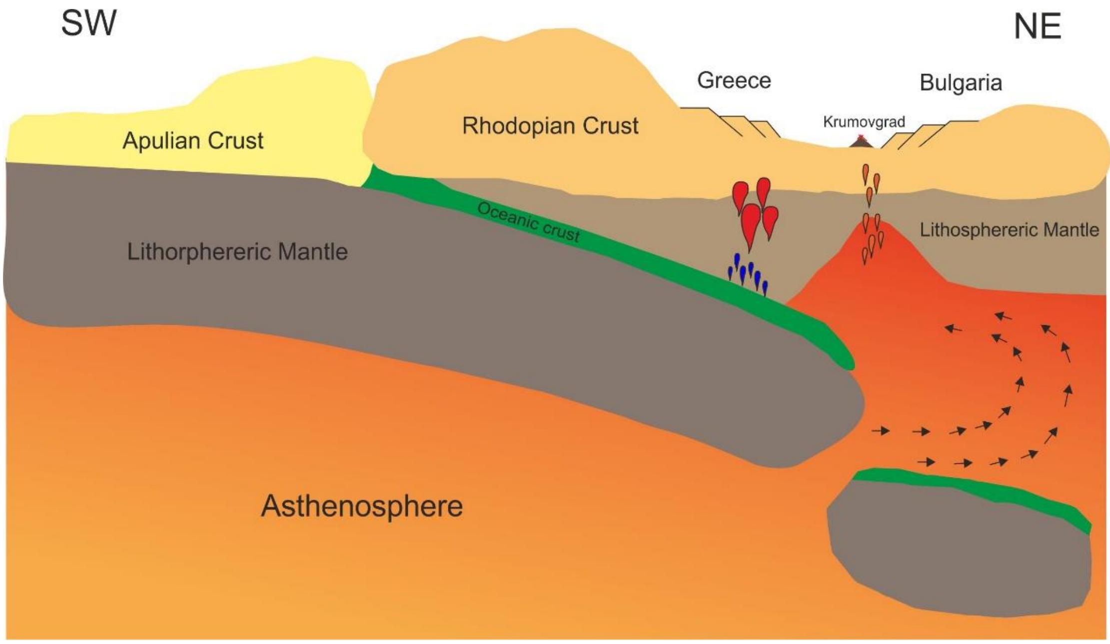

Fig. 6.2.5 Schematic figure of the geodynamical model proposed in the present thesis. The model combines slab break-off (>50 km depth) and and convective thinning of the overlying lithospheric mantle and ashtenospheric mantle diapirism. Figure not in scale

7. CONCLUSIONS

The Tertiary magmatism of the Hellenic Rhodope Massif was formed after the collision of the Rhodope Massif with the Apulia plate and the closure probably of the Axios-Vardar ocean.

After the convergence and the thickening of the orogeny, post-collision plutonic rocks (~50 Ma) are reported all over Rhodope Massif characterized by adakitic affinity. The Elatia pluton belongs to this group of plutonic rocks and presents different characteristics from the other HRM magmatic rocks excluding its mafic enclaves which cpmrise its only mafic member. The following upper Oligocene-lower Miocene extensional deformation in the back-arc is accompanied by the intrusion of plutonic and volcanic rocks which share similar geochemical features. The geochemistry of the mafic members of these rocks present similar characteristics and indicate derivation from a lithospheric heterogeously enriched mantle (leopard-skin mantle) metasomatised from slab subducted released sediment melts and fluids. Mafic mantle melts intruding the Rhodopian crust provided heat which coupled with the decompression of the crust triggered melting of the Rhodope metamorphic rocks. Mixing between the mafic and the Rhodopian crustal anatectic melts resulted in the genesis of lagre volumes of magmas that gave genesis to the plutonic and volcanic magmatic rocks.

The geodynamic setting suggested was induced by combining the origin of the HRM magmatic rocks in comparison with the origin of the magmatic rocks of the Bulgarian RM and the previous geotectonic and geophysical studies in the area. Slab roll-back and detachment could be the driving forces triggering toroidal mantle flow and mantle upwelling. Slab detachment however, could have occurred in deeper mantle and eliminated the asthenospheric contribution, at least in the geochemistry of the HRM magmatic rocks. Persisting extension and mantle upwelling resulted in progressive thinning of the upper lithospheric mantle. Finally, asthenospheric diapirism have occurred at some extent in the thin lithospheric mantle and resulted in the orogenic asthenospheric derived melts of the Bulgarian RM at the end of the magmatic activity in lower Miocene.

ABSTRACT

The Rhodope Massif is extending over large areas of northern Greece and southern Bulgaria. It is defined as a key area for understanding the evolution of the Tethyan systems. It is considered today as a metamorphic complex, with a large scale nappe tectonics, interrupted by magmatic products, formed during the closure of the Tethys Ocean. Due to the complexity of the area many researchers have focused on its tectonic and magmatic evolution separately and few efforts have been made to combine petrology and tectonics. The present study combines all previous research carried out for the Tertiary magmatic products of the Hellenic part of the Rhodope Massif with new geochemical and isotopic data. It focuses both on the mafic and the felsic magmatic rocks, aiming to conclude on the nature of the mantle source, the role of the RM continental crust and to suggest a unified geodynamical model for the area. Although this research is dedicated to Greece, it is impossible to ignore the research that has been carried out in the Bulgarian part of the Rhodope Massif as both parts constitute an interrelated system.

After the convergence and the thickening of the orogen, post-collision plutonic rocks (~50 Ma) are reported all over Rhodope Massif characterized by adakitic affinity. According to new data and new discrimination analysis applied here, the Elatia pluton belongs to this group of plutonic rocks and presents different characteristics from the other magmatic rocks of the Hellenic Rhodope Massif. The following upper Oligocene-lower Miocene extensional deformation in the back-arc, is accompanied by the intrusion of plutonic and volcanic rocks which share almost similar geochemical features. The geochemistry of the mafic members of these rocks, present similar geochemical and isotopic characteristics and indicates derivation from a lithospheric enriched mantle source metasomatised from slab subducted released sediment melts and fluids. Additionally, limited deviations observed in the geochemistry of the mafic rocks suggest variable enrichment of the mantle source from the slab subducted released sediment melts and fluids resulting in a so-called a leopard-skin mantle. Subsequently, the mafic mantle-derived melts

intruded the Rhodopian crust and provided heat which, coupled with the decompression of the crust caused by the mantle upwelling, triggered melting of the Rhodope metamorphic rocks. Mixing and fractional crystallization process, as inferred from the presence of mafic enclaves to most of the studied areas, seems to be the driving mechanism between the mantle-derived mafic melts and the Rhodopian crustal anatectic melts. This interaction resulted in the genesis of the large volumes of magmas that gave genesis to the Tertiary plutonic and volcanic magmatic rocks intruding the Hellenic Rhodope Massif.

The geodynamic setting suggested here, was induced by combining the origin of the magmatic rocks of the present study in comparison with the origin of the magmatic rocks of the Bulgarian RM and the previous geotectonic and geophysical studies in the area. Slab roll-back and detachment could be the driving forces toroidal mantle flow and mantle upwelling. Slab detachment however, could have occurred in deeper mantle (>50 Km) and eliminated the asthenospheric mantle contribution at least in the geochemistry of the magmatic rocks of the Hellenic Rhodope Massif. Persisting extension and mantle upwelling resulted in progressive thinning of upper lithospheric mantle and continental crust. Finally, asthenospheric diapirism occurred at some extent and resulted in the orogenic asthenospheric derived melts of the Bulgarian Rhodope Massif at the latest stages of the magmatic activity in lower Miocene.

ΠΕΡΙΛΗΨΗ

Η Μάζα της Ροδόπης καταλαμβάνει ένα μεγάλο μέρος της βόρειας Ελλάδας και της νότιας Βουλγαρίας. Αποτελεί πολύ σημαντική περιοχή για την κατανόηση και την εξέλιξη των συστημάτων του ωκεανού της Τυθήος. Σήμερα θεωρείται ένα μεταμορφικό σύμπλεγμα με μεγάλα τεκτονικά καλύμματα τα οποία διακόπτονται από διεισδύσεις μαγματικών προϊόντων που δημιουργήθηκαν κατά το κλείσιμο του ωκεανού της Τηθύος. Λόγω της πολυπλοκότητας της περιοχής, πολλοί ερευνητές επικεντρώθηκαν ξεχωριστά στην τεκτονική και στη μαγματική εξέλιξη και λίγες είναι οι προσπάθειες που έγιναν να συνδυαστούν η πετρολογία μαζί με την τεκτονική. Η παρούσα μελέτη συνδυάζει όλη την έρευνα που προηγήθηκε για τα Τριτογενή μαγματικά προϊόντα του ελληνικού μέρους της Μάζας της Ροδόπης με νέα γεωχημικά και ισοτοπικά στοιχεία. Επικεντρώνεται στα βασικά και στα όξινα μαγματικά πετρώματα με σκοπό να δώσει στοιχεία για την σύσταση του μανδύα, το ρόλο που έπαιξε ο ηπειρωτικός φλοιός της Μάζας της Ροδόπης και προτείνει ένα ολοκληρωμένο γεωδυναμικό μοντέλο για την περιοχή. Παρότι η έρευνα αυτή αφορά τον ελληνικό χώρο είναι αδύνατο να αγνοηθεί η έρευνα που έχει γίνει για τη Βουλγαρική Μάζα της Ροδόπης καθώς και τα δύο μέρη αποτελούν ένα ενιαίο σύστημα.

Μετά τη σύγκλιση των ηπειρωτικών πλακών και την πάχυνση του ορογενούς, δημιουργήθηκαν μαγματικά πετρώματα που διεισδύουν σε όλη τη Μάζα της Ροδόπης και χαρακτηρίζονται από αδακιτικό χαρακτήρα. Σύμφωνα με νέα στοιχεία και μία νέα ανάλυση διάκρισης ο πλουτωνίτης της Ελατιάς φαίνεται πως ανήκει σε αυτήν την ομάδα πλουτωνικών πετρωμάτων της Μάζας της Ροδόπης και παρουσιάζει χαρακτηριστικά που διαφέρουν από τα υπόλοιπα πετρώματα της Ελληνικής Μάζας της Ροδόπης. Το επικείμενο ολιγοκαινικό-κάτω μειοκαινικό εκτατικό παραμορφωτικό γεγονός που ακολούθησε πίσω από το τόξο της σύγκρουσης συνοδεύεται από την διείσδυση πλουτωνικών και ηφαιστειακών πετρωμάτων τα οποία παρουσιάζουν σχεδόν παρόμοια χαρακτηριστικά. Τα γεωχημικά και ισοτοπικά χαρακτηριστικά αυτών των πετρωμάτων καταδεικνύουν ότι προήλθαν από εμπλουτισμένη λιθοσφαιρική μανδυακή πηγή η οποία εμπλουτίστηκε από τήγματα ιζημάτων και ρευστών της καταδυόμενης

ωκεάνιας λιθόσφαιρας. Επιπλέον, κάποιες περιορισμένες γεωχημικές διαφορές που παρουσιάζουν τα βασικά πετρώματα δείχνουν μεταβαλλόμενο εμπλουτισμό της μανδυακής πηγής από τα τήγματα και τα ρευστά της καταδυόμενης ωκεάνιας λιθόσφαιρας με αποτέλεσμα τη δημιουργία ενός λεγόμενου "leopard-skin" μανδύα, δηλαδή ενός ανομοιογενώς εμπλουτισμένου μανδύα. Στη συνέχεια τα βασικά τήγματα διείσδυσαν στον φλοιό της Ροδόπης προσφέροντας θερμότητα, κάτι το οποίο σε συνδυασμό με την αποσυμπίεση του φλοιού που προκλήθηκε από την αναθόλωση του μανδύα προκάλεσαν τήξη των μεταμορφωμένων πετρωμάτων της Μάζας της Ροδόπης. Η διαδικασία της μίξη με ταυτόχρονη κλασματική κρυστάλλωση, όπως δείχνει η παρουσία εγκλεισμάτων στα περισσότερα πετρώματα των υπό μελέτη περιοχών, φαίνεται να αποτελεί τον κύριο μηχανισμό αλληλεπίδρασης μεταξύ των μανδυακής προέλευσης βασικών τηγμάτων και των ανατηκτικών φλοιικών τηγμάτων της Ελληνικής Μάζας της Ροδόπης.

Το γεωδυναμικό καθεστώς που προτείνεται στην παρούσα μελέτη είναι το αποτέλεσμα του συνδυασμού της προέλευσης των μαγματικών πετρωμάτων της παρούσας μελέτης σε σύγκριση με την προέλευση των μαγματικών πετρωμάτων της Βουλγαρικής Ροδόπης καθώς και των προηγούμενων γεωτεκτονικών και γεωδυναμικών μελετών. Η αντίθετη, ως προς την κατεύθυνση της κατάδυσης, κίνηση του καταδυόμενου ωκεάνιου φλοιού (roll-back) και η αποκόλληση του (detachment) θα μπορούσαν να αποτελούν τις κινητήριες δυνάμεις που προκάλεσαν ροή επιστροφής (return flow) και αναθόλωση (upwelling) του μανδύα. Η αποκόλληση της καταδυόμενης ωκεάνιας λιθοσφαιρικής πλάκας θα έπρεπε να έχει λάβει χώρα σε βαθύτερα σημεία του μανδύα (>50 χλμ) ώστε να εμπόδισε τη συμβολή ασθενοσφαιρικού μανδυακού υλικού τουλάχιστον στα μαγματικά πετρωμάτα της Ελληνικής Μάζας της Ροδόπης. Η συνεχής έκταση στην περιοχή και η αναθόλωση του μανδύα είχαν σαν αποτέλεσμα στην προοδευτική λέπτυνση του λιθοσφαιρικού μανδύα και του ηπειρωτικού φλοιού. Τελικά, ασθενοσφαιρική διείσδυση θα πρέπει να έλαβε χώρα σε κάποιο χρόνο στα τελικά στάδια της μαγματικής δραστηριότητας, μετά από εκτεταμένη λέπτυνση, στο κάτω Μειόκαινο και συνέβαλε στη δημιουργία των πετρωμάτων με ορογενετικά ασθενοσφαιρικά χαρακτηριστικά της Ανατολικής Βουλγαρίας.

REFERENCES

Aldanmaz, E., Pearce, J. A., Thirlwall, M. F., & Mitchell, J. G. (2000). Petrogenetic evolution of late Cenozoic, post-collision volcanism in western Anatolia, Turkey. Journal of Volcanology and Geothermal Research, 102(1), 67-95.

Ayers, J. C., & Eggler, D. H. (1995). Partitioning of elements between silicate melt and H_2O-NaCl fluids at 1.5 and 2.0 GPa pressure: Implications for mantle metasomatism. Geochimica et Cosmochimica Acta, 59(20), 4237-4246.

Babuska, V., Plomerova, J., Spasov, E., 1987. Deep structure of the lithosphere beneath the territory of Bulgaria. Stud. Geophys. Geod. 31, 266-283.

Baker, J. H., & Liati, A. (1991). The Oligocene Volcano-Sedimentary Sequence of the Dipotama Basin, N. Greece - Temporal Relationships Between Tertiary Granites and Volcanics, and Implications for the Regional Tectonic Evolution. Geologie en Mijnbouw, 70(1), 75-83.

Barr, S. R., Temperley, S., & Tarney, J. (1999). Lateral growth of the continental crust through deep level subduction-accretion: a re-evaluation of central Greek Rhodope. Lithos, 46(1), 69-94.

Bauer, C., Rubatto D., Krenn K., Proyer A. & Hoinkes G. (2007). A zircon study from the Rhodope metamorphic complex, N-Greece: time record of a multistage evolution. Lithos 99:207-228.

Baziotis, I., Mposkos, E., & Asimow, P. D. (2014). Continental rift and oceanic protoliths of mafic–ultramafic rocks from the Kechros Complex, NE Rhodope (Greece): implications from petrography, major and trace-element systematics, and MELTS modeling. International Journal of Earth Sciences, 103(4), 981-1003.

Bea, F., (2010). Crystallization dynamics of granite magma chambers in the absence of regional stress: multiphysics modeling with natural examples.Journal of Petrology, 51(7), 1541-1569.

Bird, P. (1979). Continental delamination and the Colorado Plateau. J. geophys. Res, 84(B13), 7561-7.

Boccaletti, M., Gocev, P. & Manetti, P. (1974). Meoszoic isotopic zones in the Black Sea region: Societa Geologica Italiana, Bollettino, v. 93, p. 547-565.

Boettcher, A. L., & O'neil, J. R. (1980). Stable isotope, chemical, and petrographic studies of high-pressure amphiboles and micas: evidence for metasomatism in the mantle source regions of alkali basalts and kimberlites. Am J Sci, 280, 594-621.

Bonev, N., Burg J.-P. & Ivanov Z. (2006). Mesozoic-Tertiary structural evolution of an extensional gneiss dome-the Kesebir-Kardamos dome, E. Rhodope, Bulgaria-Greece. International Journal of Earth Sciences 95, 318-340.

Bonev, N. & Beccaletto, L. (2007). From syn- to post-orogenic Tertiary extension in the north Aegean region: constraints on the kinematics in the eastern Rhodope-Thrace, Bulgaria- Greece and the Biga Peninsula northwest Turkey. In: Taymaz, T., Yilmaz, Y., Dilek, Y. (Eds.), The Geodynamics of the Aegean and Anatolia. Geological Society, London0 Special Publications 29, 113-142.

Bonev, N. & Stampfli, G. (2008). Petrology, geochemistry and geodynamic implications of Jurassic island arc magmatism as revealed by mafic volcanic rocks in the Mesozoic low-grade sequence, Eastern Rhodope, Bulgaria. Lithos 100, 210-233.

Bonev, N. & Stampfli, G. (2011). Alpine tectonic evolution of a Jurassic subduction-accretionary complex: Deformation, kinematics and $^{40}Ar/^{39}Ar$ age constraints on the Mesozoic low-grade schists of the Circum-Rhodope Belt in the eastern Rhodope-Thrace region, Bulgaria-Greece. Journal of Geodynamics 52, 143-167.

Boynton, W. V. (1984). Cosmochemistry of the rare earth elements: meteorite studies. In: Rare earth element geochemistry. In: Developments in geochemistry. Enderson, P. (ed.) (British Museum of Natural History), London (UK) v. 2, 522 p.

Brenan, J. M., Shaw, H. F., Ryerson, F. J., & Phinney, D. L. (1995). Mineral-aqueous fluid partitioning of trace elements at 900 C and 2.0 GPa: Constraints on the trace element chemistry of mantle and deep crustal fluids. Geochimica et Cosmochimica Acta, 59(16), 3331-3350.

Brown, S. A., & Robertson, A. H. (2004). Evidence for Neotethys rooted within the Vardar suture zone from the Voras Massif, northernmost Greece.Tectonophysics, 381(1), 143-173.

Brun, J.P. & Sokoutis D. (2007). Kinematics of the Southern Rhodope Core Complex (North Greece). International Journal of Earth Sciences 99(1), 109-138.

Burchfiel, B.C., Nakov, R. & Tzankov, T. (2003). Evidence from the Mesta half-graben, SW Bulgaria, for the Late Eocene beginning of Aegean extension in the Central Balkan Peninsula. Tectonophysics 375(1), 61-76.

Burg, J. P., Ivanov, Z., Ricou, L. E., Dimor, D. & Klain, L. (1990). Implications of shear-sense criteria for the tectonic evolution of the Central Rhodope massif, southern Bulgaria. Geology, 18(5), 451-454.

Burg, J-P, Ricou, L-E, Ivanov, Z., Godfriaux, I., Dimov, D. & Klain, L. (1996). Syn-metamorphic nappe complex in the Rhodope Massif. Structure and kinematics. Terra Nova 8, 6-15.

Burg, J. (2012). Rhodope: From Mesozoic convergence to Cenozoic extension. Review of petro-structural data in the geochronological frame. In: (Ed.) Emmanuel Skourtsos, and Gordon S. Lister, The Geology of Greece, Journal of the Virtual Explorer, Electronic Edition, ISSN 1441-8142, volume 42, paper 1.

Carlson, R.L., Hilde, T.W.C., Uyeda, S. (1983). The driving mechanism of plate tectonics: Relation to age of the lithosphere at trench. Geophys. Res. Lett. 10, 297-300.

Castorina, F., Koroneos, A., Masi, U., & Eleftheriadis, G. (2014). Geochemical and Sr-Nd isotopic evidence for origin and evolution of the Miocene Pangeon granitoids, Southern Rhodope, Greece. International Geology Review, 56(5), 622-652.

Cebria, J. M., & Wilson, M. (1995). Cenozoic mafic magmatism in Western/Central Europe: a common European asthenospheric reservoir. Terra Nova, 7, 162.

Chapple, W.M., Tullis, T.E. (1977). Evaluation of the forces that drive the plates. J. Geophys. Res. 82.

Christofides, G. (1977). A contribution to the study of the plutonic rocks of Xanthi area. Ph.D. thesis, Thessaloniki Univ., Greece, Thessaloniki, 249.

Christofides, G. (1989). Evolution of the Xanthi pluton, N. Greece. In Proc. XIV Congress CBGA, Sofia (pp. 168-169).

Christofides, G., Koroneos A., Pe-Piper G., Katirtzoglou K. & Chatzikirkou A. (1999). Pre-Tertiary A-Type magmatism in the Serbomacedonian massif (N. Greece): Kerkini granitic complex. Bulletin of the Geological Society, Greece 33, 131-48.

Christofides, G., Koroneos., A, Pipera, K., Poli, G. and Soldatos, T. (2012). The Oligocene Xanthi plutonic complex (N. Greece): Petrogenetic implications inferred from major and trace element and Sr, Nd and Pb isotope geochemistry. 7th Hutton Symposium on the Origin of Granites and Related Rocks, Avila, Spain, July 2011. Abstracts, 39.

Christofides, G., Koroneos, A., Pipera, K., Poli, G., Soldatos, T. (2014). Geochemical constraints on the origin and evolution of the Xanthi Plutonic Complex (Rhodope Massif, N. Greece). XX International Congress of the Carpathian Balkan Geological Association, Tirana (Albania), September 24-26, Special Issue 1, 428-431.

Christofides, G., Koroneos, A., Soldatos, T., Eleftheriadis, G., & Kilias A. (2001). Eocene magmatism (Sithonia and Elatia plutons) in the Internal Hellenides and implications for Eocene-Miocene geological evolution of the Rhodope massif (Northern Greece). Acta Vulcanologica 13, 73-89.

Christofides, G., Pecskay, Z., Eleftheriadis, G., Soldatos, T. & Koroneos, A. (2004). The Tertiary Evros volcanic rocks (Thrace, Northeastern Greece): petrology and K/Ar geochronology. Geologica Carpathica 55, 397-409.

Christofides, G., Perugini, D., Koroneos, A., Soldatos, T., Poli, G., Eleftheriadis, G.,& Neiva, A. M. (2007). Interplay between geochemistry and magma dynamics during magma interaction: An example from the Sithonia Plutonic Complex (NE Greece). Lithos, 95(3), 243-266.

Christofides, G., Pipera, K., Koroneos, A. & Papadopoulos, A. (2012). New geochronological data from the Xanthi pluton: Constraints on the Nestos thrust dating. Proceedings of International Conference: "The Geological schools of Bulgaria, the school of Prof. Zhivko Ivanov", 49-52.

Christofides, G., Soldatos, T., Eleftheriadis, G., & Koroneos, A. (1998). Chemical and isotopic evidence for source contamination and crustal assimilation in the Hellenic Rhodope plutonic rocks.Acta Vulcanologica, 10, 305-318.

Chung, S. L., Chu, M. F., Ji, J., O'Reilly, S. Y., Pearson, N. J., Liu, D., Lee, T.Y & Lo, C. H. (2009). The nature and timing of crustal thickening in Southern Tibet: geochemical and zircon Hf isotopic constraints from postcollisional adakites. Tectonophysics, 477(1), 36-48.

Cornelius, N. K. (2008). UHP metamorphic rocks of the Eastern Rhodope Massif, NE Greece: new constraints from petrology, geochemistry and zircon ages. Unpub. PhD Thesis Johannes-Gutenberg Universität, Mainz.

Cox, K. G., Bell, J. D., & Pankhurst, R. J. (1979). The interpretation of igneous rocks. Springer Science & Business Media, London. Allen & Unwin (Ed), 450 pp.

Huw Davies, J., & von Blanckenburg, F. (1995). Slab breakoff: a model of lithosphere detachment and its test in the magmatism and deformation of collisional orogens. Earth and Planetary Science Letters, 129(1), 85-102.

De Wet, A.P. (1989). Geology of a part of the Chalkidiki peninsula, Northern Greece. Ph.D. thesis, University of Cambridge, United Kingdom.

Del Moro, A., Innocenti, F., Kyriakopoulos C., Manetti P. & Papadopoulos P., (1988). Tertiary granitoids from Thrace (Northern Greece): Sr isotopic and petrochemical data. Neues Jahrb. Mineral. Abh. 159, 113-135.

Dickin, A. P. (1981). Isotope geochemistry of Tertiary igneous rocks from the Isle of Skye, NW Scotland. Journal of Petrology, 22(2), 155-189.

Dinter, D.A. & Royden, L. (1993). Late Cenozoic extension in northeastern Greece: Strymon valley detachment system and Rhodope metamorphic core complex. Geology 21, 45-48.

Dinter, D. A., Macfarlane, A., Hames, W., Isachsen, C., Bowring, S., & Royden, L. (1995). U/Pb and 40Ar/39Ar geochronology of the Symvolon granodiorite: Implications for the thermal and structural evolution of the Rhodope metamorphic core complex, northeastern Greece. Tectonics, 14(4), 886-908.

Drummond, M.S., and Defant, M.J., (1990). A model for trondhjemite-tonalitedacite genesis and crustal growth via slab melting: Archean to modern comparisons: Journal of Geophysical Research, v. 95, p. 21 503-21 521.

Dürr, S., Altherr, R., Keller, J., Okrusch, M. & Seidel, E. (1978): The median Aegean crystalline belt: stratigraphy, structure, metamorphism, magmatism. In: "Alps, Appenines, Hellenides –Geodynarnic investigation along geotraverses by an international group of geoscientists", H. Cloos, D. Hoeder & K. Schmidt (Eds.), I.U.G.S. Rep. 38, Stuttgart, 445-477.

Eggins, S. M. (2003). Laser Ablation ICP-MS Analysis of Geological Materials Prepared as Lithium Borate Glasses. Geostandards Newsletter, 27(2), 147-162.

Eleftheriadis, G. (1995). Petrogenesis of the Oligocene volcanics from the Central Rhodope massif (N. Greece). Eur. J. Miner. 7, 1169 -1182.

Eleftheriadis, G., Christofides, G., Esson, J., Soldatos, T. & Koroneos, A. (1996). Petrology and geochemistry of the vocanic dykes from the Santorini caldera walls. The European Laboratory Volcanoes: 2nd Workshop, Santorini, Greece, May 1996. Proceedings, 137-155.

Eleftheriadis, G., Esson, J., Soldatos, T, and Christofides, G. (1993). Magmatic evolution of the Tertiary volcanic rocks of Samothraki island (Thrace, N. Greece), in Honorary publication for Ath. Panagos, AEM Polytechnical School, Athens, p. 330-348 (in Greek).

Eleftheriadis, G., Pe-Piper, G., Christofides, G., Soldatos, T., and Esson, L. (1994). K-Ar dating of the Samothraki volcanic rocks, Thrace, northeastern Aegean (Greece), in Proceedings of the 4th International Congress of the Geological Society of Greece, Patras: Bulletin of the Geological Society of Greece, 30 (1), 205-212.

Elliott, T., Plank, T., Zindler, A., White, W., & Bourdon, B. (1997). Element transport from slab to volcanic front at the Mariana arc. Journal of Geophysical Research: Solid Earth (1978-2012), 102(B7), 14991-15019.

Forsyth, D.W., Uyeda, S. (1975). On the relative importance of the driving forces of plate motion. Geophys. J. Royal Astronomical Soc. 43, 163-200.

Frey, F. A., & Green, D. H. (1974). The mineralogy, geochemistry and origin of Iherzolite inclusions in Victorian basanites. Geochimica et cosmochimica acta,38(7), 1023-1059.

Fryer, B. J., Jackson, S.E. & Longerich, H. P. (1995) . The design, operation and role of the Laser-Ablation Microprobe coupled with an Inductively Coupled Plasma - Mass Spectrometer (LAM-ICP-MS) in the Erath Sciences. Canad. Mineral., 3333, 303-312.

Fyticas, M., Innocenti, F., Manetti, P., Mazzuoli, R., Peccerillo, A., Villari, L. (1984). Tertiary to Quaternary evolution of the volcanism in the Aegean Region. In: Dixon, J.E., Robertson, A.H.F. (Eds.), The Geological Evolution of the Eastern Mediterranean. Geol. Soc. London Spec. Publ. vol. 17, pp. 687-699.

Gale, A., Dalton, C. A., Langmuir, C. H., Su, Y., & Schilling, J. G. (2013). The mean composition of ocean ridge basalts. Geochemistry, Geophysics, Geosystems, 14(3), 489-518.

Garfunkel, Z., C. A. Anderson, and G. Schubert (1986). Mantle circulation and the lateral migration of subducted slabs. J. Geophys. Res., 91, 7205-7223.

Gómez-Tuena, A., Langmuir, C. H., Goldstein, S. L., Straub, S. M., & Ortega-Gutiérrez, F. (2007). Geochemical evidence for slab melting in the Trans-Mexican Volcanic Belt. Journal of Petrology, 48(3), 537-562.

Georgiev, S., Marchev, P., Heinrich, C., von Quadt, A., Peytcheva & I.,Manetti, P. (2009). Origin of nepheline-normative high-K ankaramites and the evolution of Eastern Srednogorie Arc in Southeastern Europe. Journal of Petrology, 50, 1899-1933.

Georgiev, N., Pleuger, J., Froitzheim, N., Sarov, S., Jahn-Awe, S., & Nagel, T. J. (2010). Separate Eocene–Early Oligocene and Miocene stages of extension and core complex formation in the Western Rhodopes, Mesta Basin, and Pirin Mountains (Bulgaria). Tectonophysics, 487(1), 59-84.

Gill, J. B. (1981). Orogenic andesites and plate tectonics(Vol. 390). Berlin, Springer-Verlag, 390 pp.

Green, T.H. (1994). Experimental studies of trace-element partitioning applicable to igneous petrogenesis - Sedona 16 years later: Chemical Geology, v. 117, p. 1-36.

Houseman, G. A., & Molnar, P. (1997). Gravitational (Rayleigh–Taylor) instability of a layer with non-linear viscosity and convective thinning of continental lithosphere. Geophysical Journal International, 128(1), 125-150.

Hawkesworth, C.J., Gallagher, K., Herget, J.M., McDermott, F. (1993). Mantle and slab contributions in arc magmas. Annual Review of Earth and Planetary Sciences 21, 175-204.

Hawkesworth, C., Turner, S., Peate, D., McDermott, F. & van Calsteren, P. (1997). Elemental U and Th variations in island arc rocks: implications for U-series isotopes. Chemical Geology 139, 207-221.

Harkoversuska, A., Marchev, P., Machev, Ph. & Pecskay, Z., (1998). Paleogene magmatism in the Central Rhodope area, Bulgaria-a review and new data. Acta Vulcanologica 10 (2), 199-216.

Harkoversuska, A., Pecskay, Z. & Popov,M., (2004). The Kraishtemagmato-tectonic zone (Western Bulgaria). Geologica Balcanica 34 (3-4), 3-19.

Harkoversuska, A., Yanev, Y. & Marchev, P. (1989): General features of the Paleogene orogenic magmatism in Bulgaria. Geologica Balc. 19 (1), 37-72.

Hart, S.R. (1984). A large scale isotope anomaly in the southern hemisphere mantle. Nature 309, 753-757.

Herbert, E. H., & Sparks, R. S. J. (1988). The generation of granitic magmas by intrusion of basalt into continental crust. Journal of Petrology, 29, 599-624.

Hermann, J., & Rubatto, D. (2009). Accessory phase control on the trace element signature of sediment melts in subduction zones. Chemical Geology, 265(3), 512-526.

Himmerkus, F., Anders, B., Reischmann, T. & Kostopoulos, D. (2007). Gondwana-derived terranes in the northern Hellenides. In: Hatcher Jr., R.D., Carlson, M.P., McBride, J.H., Martínez Catalán, J.R. (Eds.), 4-D Framework of Continental Crust: Geological Society of America, Memoir 200, 379-390.

Himmerkus, F., Reischmann, T. & Kostopoulos, D., (2009). Triassic rift-related metagranites in the Internal Hellenides, Greece. Geological Magazine 146:252-265.

Innocenti, F., Mazzuoli, R., Pasquare, G., Radicati di Brozolo, F. & Villari, L. (1982). Tertiary and Quaternary volcanism of the Erzurum–Kars area (Eastern Turkey): geochronological data and geodynamic evolution. Journal of Volcanology and Geothermal Research 13, 223-240.

Jahn-Awe S., Froitzheim N., Nagel T.J., Frei D., Georgiev N. & Pleuger J. (2010). Structural and geochronological evidence for Paleogene thrusting in the Western Rhodopes (SW Bulgaria), subm. Tectonics 29:TC3008.

Jahn-Awe, S., Pleuger, J., Frei, D., Georgiev, N., Froitzheim, N., & Nagel, T. J. (2012). Time constraints for low-angle shear zones in the Central Rhodopes (Bulgaria) and their significance for the exhumation of high-pressure rocks. International Journal of Earth Sciences, 101(7), 1971-2004.

Janoušek, V., Farrow, C. M., & Erban, V. (2006). Interpretation of whole-rock geochemical data in igneous geochemistry: introducing Geochemical Data Toolkit (GCDkit). Journal of Petrology, 47(6), 1255-1259.

Johnson, M. C., & Plank, T. (2000). Dehydration and melting experiments constrain the fate of subducted sediments. Geochemistry, Geophysics, Geosystems, 1(12).

Jones, C.E., Tarney, J., Baker, J.H. & Gerouki, F. (1992). Tertiary granitoids of Rhodope, Northern Greece: magmatism related to extensional collapse of the Hellenic orogen?. Tectonophysics 210, 295-314.

Irvine, T. N. & Baragar, W. R. A. (1971). A guide to the chemical classification of the common volcanic rocks. Canadian Journal of Earth Sciences 8, 523-548.

Ivanov, Z. (1988). Apercu general sur revolution geologique et structural des Rhodopes dans le cadre des Balkanides. Bulletin de la Societe geologique de France, 4(2), 227-240.

Kamber, B. S., & Gladu, A. H. (2009). Comparison of Pb Purification by Anion-Exchange Resin Methods and Assessment of Long-Term Reproducibility of Th/U/Pb Ratio Measurements by Quadrupole ICP-MS. Geostandards and Geoanalytical Research, 33(2), 169-181.

Kamenov, B., Daboversuski, C., Harkoversuska, A., Maneva, B., Mavroudchiev, B., Stanisheva-Vassileva, G., Vassilev, L., Yanev, Y. (2000). Late Cretaceous and Tertiary magmatism and related metallogeny in Bulgaria: review and problems. Abstracts of ABCD-GEODE workshop, Borovets, Bulgaria, pp. 33.

Kamenov, BK., Philipova, M. & Shumliansky, V. (1974). Petrochemical peculiarities and formation of the Barutin-Buynovo pluton. Annuaire de l' Universite de Sofia, 66, 219-244, (in Russian with English abstract).

Kauffmann, G., Kockel, F. & Mollat, H. (1976). Notes on the stratigraphic and palaeogeographic position of the Svoula Formation in the Innermost Zone of the Hellenides (Northern Greece). BulIetin de la Société Géologique de France, 18, 225-230.

Kessel, R., Schmidt, M. W., Ulmer, P., & Pettke, T. (2005). Trace element signature of subduction-zone fluids, melts and supercritical liquids at 120-180 km depth. Nature, 437(7059), 724-727.

Kilias A., Falalakis, G. & Mountrakis, D. (1999). Cretaceous-Tertiary structures and kinematics of the Serbomacedonian metamorphic rocks and their relation to the exhumation of the Hellenic hinterland (Macedonia, Greece). International Journal of Earth Sciences, 88(3):513-531.

Kilias, A., Falalakis G., Sfeikos, A., Papadimitriou, E., Vamvaka, A. & Gkarlaouni, Ch. (2011). Architecture of Kinematics and Deformation History of the Tertiary Supradetachment Thrace Basin: Rhodope Province (NE Greece). In: New Frontiers in Tectonic Research - At the Midst of Plate Convergence. InTech pp. 241-268.

Kilias, A. & Mountrakis, D. (1990). Kinematics of the crystalline sequences in the western Rhodope massif. Geologica Rhodopica 2, 100-116.

Kilias, A. A., & Mountrakis, D. M. (1998). Tertiary extension of the Rhodope massif associated with granite emplacement (Northern Greece). Acta Vulcanologica, 10, 331-338.

Kockel, F., Mollat, H. & Walther, H. W. (1977), Erläuterungen zur geologischen Karte der Chalkidhiki und angrenzender Gebiete 1 : 100,000 (Nord-Griechenland), Bundesanstalt für Geowissenschaften und Rohstoffe, Hannover, 119 p.

Kockel, F. & Walther, H.W. (1965). Die Strymon Linie als Grenze zwischen Serbo-Mazedonischem und Rila-Rhodope Massiv in Ost Mazedonien. Geol. Jahrb. 83, 575- 602.

Kolceva, K., Zeljaskova-Panajotova, M., Bobrecov, N.L. & Stojanova, V. (1986). Eclogites in Central Rhodope metamorphic group and their retrograde metamorphism. Geochem Mineral Petrol (Sofia) 20(21), 130-144.

Kostopoulos, D., Gerdjikov, I., Gautier, P., Reischmann, T. & Cherneva Z. (2003). First evidence of UHP metamorphism in the Central Rhodope Massif of southern Bulgaria. Geophys Res Abstr 5, 08327.

Kotopouli, C.N. (1981). The magmatic rocks in the area of Skaloti-Paranesti, Greek Rhodope. Ph.D. Thesis, University of Patras, Greece, 255 p. (in Greek with English abstract).

Kotopouli, C. N. & Pe-Piper, G. (1989). Chemical composition of pargasite and hornblende in low to high grade metamorphic rocks of the Rhodope Zone, Xanthi, Greece. Mineralogy and Petrology, 40(4), 275-288.

Kolokotroni, C. (1992): The emplacement and petrogenesis of the Vrondou granitoid pluton, Rhodope Massif, NE Greece. PhD Thesis, University of Edinburgh, 425 pp.

Koukouvelas, I. & Doutsos, T. (1990). Tectonic stages along a traverse cross cutting the Rhodopian zone (Greece). Geologische Rundschau, 79(3), 753-776.

KoukouveIas, L. & Pe-Piper, G. (1991). The Oligocene Xanthi pluton, northern Greece: a granodiorite emplaced during regional extension. J Geol Soc Lond 148:749-758.

Konzett, J., & Ulmer, P. (1999). The stability of hydrous potassic phases in lherzolitic mantle-an experimental study to 9.5 GPa in simplified and natural bulk compositions.Journal of Petrology,40(4), 629-652.

Krohe, A., & Mposkos, E. (2002). Multiple generations of extensional detachments in the Rhodope Mountains (northern Greece): evidence of episodic exhumation of high-pressure rocks. Special Publication-Geological Society Of London, 204, 151-178.

Krenn, K., Bauer, C., Proyer, C., Klötzli, U. & Hoinkes G. (2010). Tectonometamorphic evolution of the Rhodope orogen. Tectonics 29(4).

Kyriakopoulos, G.K. (1987). Geochronological, geochemical, mineralogical and isotopic studies of the Tertiary plutonic rocks of the Rhodope. Ph.D. thesis, University of Athens, 343 pp.

Langmuir, C. H., R. D. Vocke Jr., N. H. Gilbert, & R. H. Stanley (1978). A general mixing equation with applications to Icelandic basalts, Earth Planet. Sci. Lett., 37, 380-392.

Le Bas, M. J., Le Maitre, R. W., Streckeisen, A., & Zanettin, B. (1986). A chemical classification of volcanic rocks based on the total alkali-silica diagram. Journal of petrology, 27(3), 745-750.

Li, S.-G., Nie, Y.H., Xiao, Y.L., Zheng, Y.F. (1997). Geochemical evidence for the recycling of subducted continental crust from Dabie orogen, eastern China. Sci. China, Ser. D: Earth Sci. 27, 412-418 (in Chinese).

Liati, A. (1986). Regional metamorphism and overprinting contact metamorphism of the Rhodope zone, near Xanthi, N. Greece: petrology, geochemistry, geochronology. Dissertation, Techn Univ Braunschweig, pp 186.

Liati, A., (2005). Identification of repeated Alpine (ultra) high-pressure metamorphic events by U–Pb SHRIMP geochronology and REE geochemistry of zircon: the Rhodope zone of Northern Greece. Contributions to Mineralogy and Petrology 150:608-630.

Liati, A. & Gebauer D (1999) Constraining the prograde and retrograde P–T–t path of Eocene HP-rocks by SHRIMP dating of different zircon domains: inferred rates of heating, burial, cooling and exhumation for central Rhodope, northern Greece. Contrib Mineral Petrol 135:340-354.

Liati, A., Gebauer D. & Fanning C.M. (2004). The duration of exhumation processes in (U)HP terranes - a geochronological approach applied to the Rhodope terrane, N. Greece. 'Geoscience Africa 2004', The Birth and Growth of Continents, Abstract volume 1:384-385.

Liati, A., Gebauer, D. & Fanning, C.M. (2011). Geochronology of the Alpine UHP Rhodope zone: a review of isotopic ages and constraints on the geodynamic evolution. In: L.F. Dobrzhinetskaya, S.W. Faryad, S. Wallis, S. Cuthbert (Eds.), Ultrahigh-Pressure Metamorphism: 25 Years After The Discovery of Coesite and Diamond, Elsevier, London (2011), pp. 295-316.

Liati, A., Gebauer D. & Wysoczanski R. (2002). U-Pb SHRIMP-dating of zircon domains from UHP garnet-rich mafic rocks and late pegmatoids in the Rhodope zone (N Greece); evidence for early cretaceous crystallization and late cretaceous metamorphism. Chem Geol 184:281-299.

Liati, A., & Seidel, E. (1996). Metamorphic evolution and geochemistry of kyanite eclogites in central Rhodope, northern Greece. Contributions to Mineralogy and Petrology, 123(3), 293-307.

Lips, A.L.W., White, S.H. & Wijbrans, J.R. (2000). Middle-Late Alpine thermotectonic evolution of the southern Rhodope Massif, Greece. Geodinam Acta 13, 281-292.

Longerich, H.P., Jackson, S.E. & Günther D. (1996). Laser ablation-inductively coupled plasma mass spectrometric transient signal data acquisition and analyte concentration calculation. J. Anal. Atom. Spectrom., 11, 899-904.

Magganas, A., Sideris, C., Kokkinakis, A. (1991). Marginal basin-volcanic arc origin of metabasic rocks from the Circum-Rhodope Belt, Thrace, Greece. Mineralogy and Petrology 44, 235-252.

Meissner, R., & Mooney, W. (1998). Weakness of the lower continental crust: a condition for delamination, uplift, and escape. Tectonophysics, 296(1), 47-60.

Maltezou, F. & Brooks, M. (1989). A geophysical investigation of post-Alpine granites and Tertiary sedimentary basins in northern Greece. Journal of the Geological Society, 146(1), 53-59.

Marakis, G. (1969): Geochronology studies of some granites from Macedonia. Ann. Geol. Pays Hell., 21, 121-152.

Marchev, P., Arai, S., Ishida, Y., Shirasaka, M., & Downes, H. (2008). Trace element and isotopic composition of mafic and ultramafic cumulate xenoliths in alkaline basalts from the Eastern Rhodopes, Bulgaria: Inferences on deep processes under the metamorphic core complexes. In IOP Conference Series: Earth and Environmental Science, IOP Publishing, Vol. 2, No. 1, p. 012015.

Marchev, P., Arai, S., & Vaselli, O. (2006). Cumulate xenoliths in Oligocene alkaline basaltic and lamprophyric dykes from the eastern Rhodopes, Bulgaria: Evidence for the existence of layered plutons under the metamorphic core complexes. Geological Society of America Special Papers, 409, 237-258.

Marchev, P. & Filipov, P. (2012). First findings of Late Cretaceous magmatic rocks in the Pirin Mts. Bulgarian Geological Society, National conference, Geosciences 2012, Proceedings, p. 55-56.

Marchev, P., Georgiev, S., Raicheva, R., Peytcheva, I., von Quadt, A., Ovtcharova, M., & Bonev, N. (2013). Adakitic magmatism in post-collisional setting: An example from the Early-Middle Eocene Magmatic Belt in Southern Bulgaria and Northern Greece. Lithos, 180, 159-180.

Marchev, P., Harkovska, A., Pecskay, Z., Vaselli, O., Downes, H. (1997). Nature and age of the alkaline basaltic magmatism southeast of Krumovgrad, SE-Bulgaria. C. R. Acad. bulg. Sci. 50 (4), 77-80.

Marchev, P., Raicheva, R., Downes, H., Vaselli, O., Chiaradia, M. & Moritz, R. (2004). Compositional diversity of Eocene-Oligocene basaltic magmatism in the Eastern Rhodopes, SE Bulgaria: implications for genesis and tectonic setting. Tectonophysics 393, 301-328.

Marchev, P., Rogers, G., Conrey, R., Quick, J., Vaselli, O. & Raicheva, R. (1998a). Paleogene orogenic and alkaline basic magmas in the Rhodope zone: relationships, nature of magma sources, and role of crustal contamination. Acta Vulcanologica 10 (2), 217-232.

Marchev, P., Vaselli, O., Downes, H., Pinarelli, L., Ingram, G., Rogers, G. & Raicheva, R., (1998b). Petrology and geochemistry of alkaline basalts and lamprophyres: implications for the chemical composition of the upper mantle beneath the Eastern Rhodopes (Bulgaria). Acta Vulcanologica 10 (2), 233-242.

Marsh, B. D. (2006). Dynamics of magmatic systems. Elements, 2(5), 287-292.

Mavroudchiev, B., Nedyalkov, R., Eleftheriadis, G., Soldatos, T. & Christofides, G., (1993). Tertiary plutonic rocks from East Rhodope in Bulgaria and Greece. Bull. Geol. Soc. Greece 28, 643-660.

Meyer, W. (1968). Zur Altersstellung des Plutonismus im Südteil der Rila-Rhodope-Masse (Nordgriechenland). Geol Paleontol, 2, 173-192.

Meinhold, G., Kostopoulos, D., Reischmann, T., Frei, D., & BouDagher-Fadel, M. K. (2009). Geochemistry, provenance and stratigraphic age of metasedimentary rocks from the eastern Vardar suture zone, northern Greece.Palaeogeography, Palaeoclimatology, Palaeoecology, 277(3), 199-225.

Meinhold, G., Reischmann, T., Kostopoulos, D., Frei, D. & Larionov, A. N. (2010). Mineral chemical and geochronological constraints on the age and provenance of the eastern Circum-Rhodope Belt low-grade metasedimentary rocks, NE Greece. Sedimentary Geology, 229(4), 207-223.

Meinhold, G., & Kostopoulos, D. K. (2013). The Circum-Rhodope Belt, northern Greece: age, provenance, and tectonic setting. Tectonophysics, 595, 55-68.

Meyer, W., (1968). Zur Altersstellung des Plutonismus im Südteil der Rila-Rhodope-Masse (NordGriechenland). Geologie et Paläeontologie, 2, 173-192.

Menzies, M., & Murthy, V. R. (1980). Nd and Sr isotope geochemistry of hydrous mantle nodules and their host alkali basalts: implications for local heterogeneities in metasomatically veined mantle. Earth and Planetary Science Letters, 46(3), 323-334.

Michard, A., Gurriet, P., Soudant, M., & Albarede, F. (1985). Nd isotopes in French Phanerozoic shales: external versus. internal aspects of crustal evolution. Geochimica et Cosmochimica Acta, 49(2), 601-610.

Miller, D. M., Goldstein, S. L., & Langmuir, C. H. (1994). Cerium/lead and lead isotope ratios in arc magmas and the enrichment of lead in the continents. Nature, 368(6471), 514-520.

Moyen, J. F. (2009). High Sr/Y and La/Yb ratios: the meaning of the "adakitic signature". Lithos, 112(3), 556-574.

Mountrakis, D. (1983). Structural geology of the North Pelagonian zone s.l. and geotectonic evolution of the internal Hellenides. 'Habilitation' thesis, University of Thessaloniki (in Greek with English summary).

Mposkos, E. (1989). High-pressure metamorphism in gneisses and pelitic schists in East Rhodope zone (N Greece). Mineral Petrol 41, 337-351.

Mposkos, E.D. & Kostopoulos, D.K. (2001). Diamond, former coesite and supersilicic garnet in metasedimentary rocks from the Greek Rhodope: a new ultrahigh-pressure metamorphic province established. Earth Planet Sci Lett 192, 497-506.

Mposkos, E. & Liati, A. (1993). Metamorphic evolution of metapelites in the high pressure terrain of Rhodope, N. Greece. Can Mineral 31:401-424.

Mposkos, E., Liati, A., Katagas, Ch. & Arvanitides, N. (1990). Petrology of the metamorphic rocks of Western Rhodope, Drama area, N Greece. Geol Rhodopica 2, 127-142.

Nagel, T. J., Schmidt, S., Janák, M., Froitzheim, N., Jahn-Awe, S. & Georgiev, N. (2011). The exposed base of a collapsing wedge: the nestos shear zone (Rhodope Metamorphic Province, Greece). Tectonics, 30(4).

Pal'shin, I.G., Simov, S.D., Arakelyants, M.M., & Chernyshev, I.V. (1975). Absolute age of Alpine activations in Rhodope median massif, Bulgaria.International Geology Review, 17(10), 1161-1168.

Papadakis, A. N. (1965). The Serres-Drama pluton. PhD Thesis, Univ. of Thessaloniki. Sci. Ann. Fac. Phys. Math. Univ. Thessaloniki, 9, No 4, 130pp. (in Greek with English abastract).

Papadopoulos, C. & Kilias A. (1985). Altersbeziehungen zwischen Metamorfose und Deformation im Zentralen Teil des Serbomazedonischen Massiversus (Vertiskos Gebirge, Nord- Griechenland), Geol. Rundsch. 74, 77-85.

Papadopoulos, P., Arvanitides, N.D., Zanas, I. (1989). Some preliminary geological aspects on the Makri unit (phyllite series); peri-Rhodopian zone. Geologica Rhodopica 1, 34-42.

Papadopoulou, L., (2003). Mineral phase equilibria, crystallization conditions and evolution of the Maronia pluton, Thrace, Greece (Doctoral dissertation, Ph.D. thesis, University of Thessaloniki, 342pp (in Greek with English abstract).

Papadopoulou, L., Christofides, G., Koroneos, A., Bröcker, M., Soldatos, T. & Eleftheriadis, G. (2004). Evolution and origin of the Maronia pluton, Thrace, Greece. Bull. Geol. Soc. Greece, 36, 568-577.

Papanikolaou, D. & Panagopoulos, G. (1981). On the structural style of Southern Rhodope (Greece). Geol Balc 11, 13-22.

Papazachos, C. B. (1994). Structure of the crust and upper mantle in southeast Europe by inversion of seismic and gravimetric data. Ph.D. thesis, Aristotle Univercity of Thessaloniki, Greece.

Pearce, J.A., (1993). Role of the sub-continental lithosphere in magma genesis at active continental margins, in Hawkesworth, C.J., and Norry, M.J., eds., Continental basalts and mantle xenoliths: Cheshire, U.K., Shiva, p. 230-249.

Pearce, J. A. (1996). Sources and settings of granitic rocks. Episodes, 19(4), 120-125.

Pearce, J. A., Bender, J. F., De Long, S. E., Kidd, W. S. F., Low, P. J., Güner, Y., Saroglu, F., Yilmaz Y.,, Moorbath, S. & Mitchell, J. G. (1990). Genesis of collision volcanism in Eastern Anatolia, Turkey. Journal of Volcanology and Geothermal Research, 44(1), 189-229.

Pearce, J. A., Harris, N. B., & Tindle, A. G. (1984). Trace element discrimination diagrams for the tectonic interpretation of granitic rocks. Journal of petrology, 25(4), 956-983.

Pe-Piper, G., Christofides, G., & Eleftheriadis, G. (1998). Lead and neodymium isotopic composition of Tertiary igneous rocks of northern Greece and their regional significance. Acta Vulcanologica,10, 255-264.

Pe-Piper, G. & Piper, D. J. (2002).The igneous rocks of Greece. Gebr. Borntraeger, 562 pp.

Peccerillo, A. & Taylor, S. R. (1976). Geochemistry of Eocene calc-alkaline volcanic rocks from the Kastamonu area, northern Turkey. Contributions to mineralogy and petrology, 58(1), 63-81.

Perraki, M., Proyer, A., Mposkos, E., Kaindl, R. & Hoinkes, G. (2006). Raman micro-spectroscopy on diamond, graphite and other carbon polymorphs from the ultrahigh-pressure metamorphic Kimi Complex of the Rhodope Metamorphic Province, NE Greece. Earth Planet Sci Lett 241, 672-685.

Perugini, D., Poli, G., Christofides, G., & Eleftheriadis, G. (2003). Magma mixing in the Sithonia Plutonic Complex, Greece: evidence from mafic microgranular enclaves.Mineralogy and Petrology, 78(3-4), 173-200.

Petrelli, M., Poli, G., Perugini, D., & Peccerillo, A. (2005). Petrograph: a new software to visualize, model, and present geochemical data in igneous petrology. Geochemistry, Geophysics, Geosystems, 6(7).

Peytcheva, I., Von Quadt, A., Heinrich, C., Ivanov, Z., Kamenov, B., Kouzmanov, K. (2002). Evolution of magmatism and related ore formation in Central Srednogorie, Bulgaria: new insight from high-precision U–Pb zircon and rutile geochronology and isotope tracing. GEODE Study Center on Geodynamics and ore deposit evolution. Chaˆteau de Passie`res, near Grenoble 25-28 October 2002.

Plank, T., & Langmuir, C. H. (1998). The chemical composition of subducting sediment and its consequences for the crust and mantle. Chemical Geology, 145(3), 325-394.

Plank, T., (2005). Constraints from thorium/lanthanum on sediment recycling at subduction zones and the evolution of continents. Journal of Petrology 46, 921-944.

Platt, J. P., & England, P. C. (1994). Convective removal of lithosphere beneath mountain belts; thermal and mechanical consequences. American Journal of Science, 294(3), 307-336.

Popov, P. (1987). Tectonics of the Banat Srednogorie Rift. Tectonophysics 143, 209-216.

Reischmann, T., & Kostopoulos, D. (2002). Timing of UHPM in metasediments from the Rhodope Massif, N Greece. Geochim. Cosmochim. Acta, 66, A634.

Richards, J.R. & Kerrich, R. (2007). Special paper: adakite-like rocks: their diverse origins and questionable role in metallogenesis. Economic Geology 102 (4), 537-576.

Ricou, L.-E., Burg, J-P., Godfriaux, I. & Ivanov, Z. (1998). Rhodope and Vardar: the metamorphic and the olistostromic paired belts related to the cretaceous subduction under Europe. Geodin Acta 11, 285-309.

Rohrmeier, M. K., Von Quadt A., Driesner T., Heinrich C. A., Handler R., Ovtcharova M., Ivanov Z., Petrov P. & Peytcheva I. (2013). Post-orogenic extension and hydrothermal ore formation: High-precision geochronology of the Central Rhodopian metamorphic core complex (Bulgaria-Greece). Economic Geology, 108(4), 691-718.

Robertson, A. H. F., & Dixon, J. E. (1984). Introduction: aspects of the geological evolution of the Eastern Mediterranean. Geological Society, London, Special Publications, 17(1), 1-74.

Robertson, A. H. F., J. E. Dixon, S. Brown, A. Collins, A. Morris, E. Pickett, I. Sharp, and T. Ustaömer (1996). Alternative tectonic models for the Late Palaeozoic-Early Tertiary development of Tethys in the Eastern

Mediterranean region.Geological Society, London, Special Publications 105 (1), 239-263.

Sacks, P. E., & Secor, D. T. (1990). Delamination in collisional orogens. Geology, 18(10), 999-1002.

Schellart, W. P., & Moresi, L. (2013). A new driving mechanism for backarc extension and backarc shortening through slab sinking induced toroidal and poloidal mantle flow: results from dynamic subduction models with an overriding plate. Journal of Geophysical Research: Solid Earth, 118(6), 3221-3248.

Sergi, A. (1997). Mafic microgranular enclaves from the Xanthi pluton (Northern Greece): an example of mafic-felsic magma interaction. Mineralogy and Petrology, 61(1-4), 97-117.

Sharp, I. R., & Robertson, A. H. (2006). Tectonic-sedimentary evolution of the western margin of the Mesozoic Vardar Ocean: evidence from the Pelagonian and Almopias zones, northern Greece. Geological Society, London, Special Publications, 260(1), 373-412.

Sklavounos, S. (1981). The Paranesti granite. Mineralogy-Petrography. Ph.D. Thesis, University of Thessaloniki, Greece, 175 p. (in Greek with English abstract).

Schmidt, M. W., Vielzeuf, D. & Auzanneau, E. (2004). Melting and dissolution of subducting crust at high pressures: the key role of white mica. Earth Planet. Sci. Lett. 228, 65-84

Sokoutis, D., Brun, J. P., Van Den Driessche, J. & Pavlides, S. (1993). A major Oligo-Miocene detachment in southern Rhodope controlling north Aegean extension. Journal of the Geological Society, 150(2), 243-246.

Soldatos, T. (1985) Petrology and geochemistry of the Elatia pluton. Ph.D. Thesis, University of Thessaloniki, Greece, 303 p. (in Greek with English abstract).

Soldatos, T. & Christofides, G. (1986). Rb-Sr geochronology and origin of the Elatia Pluton, central Rhodope, North Greece. Geologica Balcanica, 16, 1, 15-23.

Soldatos, T., Koroneos, A., Christofides, G. & Del Moro, A. (2001b). Rb-Sr geochronology and origin of the Elatia Plutonite (Helenic Rhodope Massif,

N. Greece) constrained by new Sr isotopic data. Neues Jahrbuch für Mineralogie (Abh.), 176, 2, 179-209.

Soldatos, T., Koroneos, A., Del Moro, A. & Christofides, G. (2001a). Evolution of the Elatia plutonite (Hellenic Rhodope Massif, N. Greece). Chemie der Erde, 61, 92-116.

Soldatos, T., Koroneos, A., Kamenov, B.K., Peytcheva, I., von Quadt, A., Christofides, G., Zheng, X. & Sang, H. (2008). New U-Pb and Ar-Ar mineral ages for the Barutin-Buynovo-Elatia-Skaloti-Paranesti batholith (Bulgaria and Greece). Refinement of its debatable age. Geochem. Mineral. Petrol. 46, 85-102.

Soldatos, T., Poli, G., Christofides, G., Eleftheriadis, G., Koroneos, A. & Tommasini, S. (1998). Petrology and evolution of transitional alkaline-subalkaline granitoids from Vrondou (NE Greece): evidence for fractional crystallization and magma mixing. Acta Vulcanologica, 10, 319-330.

Spakman, W., Wortel, M.J.R., Vlaar, N.J. (1988). The Hellenic subduction zone: a tomographic image and its geodynamic implications. Geophys. Res. Lett. 15, 60-63.

Stalder, R., Foley, S. F., Brey, G. P., & Horn, I. (1998). Mineral-aqueous fluid partitioning of trace elements at 900-1200 C and 3.0-5.7 GPa: new experimental data for garnet, clinopyroxene, and rutile, and implications for mantle metasomatism. Geochimica et Cosmochimica Acta, 62(10), 1781-1801.

Streckeisen, A. & Le Maitre, R. W. (1979). A chemical approximation to the modal QAPF classification of the igneous rocks. Neues Jahrbuch für Mineralogie, Abhandlungen, 136, 169-206.

Sun, S. S. & McDonough, W. (1989). Chemical and isotopic systematics of oceanic basalts: implications for mantle composition and processes. Geological Society, London, Special Publications, 42(1), 313-345.

Su, Y. & Langmuir C.H. (2003). Global MORB chemistry compilation at the segment scale. Ph.D. Thesis, Department of Earth and Environmental Sciences, Columbia University.

Tatsumi, Y., and Eggins, S., (1995). Subduction zone magmatism: Boston, Blackwell, 211 pp.

Tatsumi, Y. (2001). Geochemical modeling of partial melting of subducting sediments and subsequent melt-mantle interaction: Generation of high-Mg andesites in the Setouchi volcanic belt, southwest Japan. Geology, 29(4), 323-326.

Tranos, M. & Lacombe, O. (2014). Late Cenozoic faulting in SW Bulgaria: Fault geometry, kinematics and driving stress regimes. Implications for late orogenic processes in the Hellenic hinterland. Journal of Geodynamics, 74, 32-55.

Tsokas, G. N., Christofides, G. C. & Papakonstantinou, C. (1996). A geophysical study of the granites and the sedimentary basins of the Xanthi area (N. Greece). pure and applied geophysics, 146(2), 365-392.

Turpaud, P. (2006). Characterisation of igneous terranes by zircon dating: implications for UHP relicts occurrences and suture identification in the Central Rhodope, Northern Greece. Ph.D. thesis, University of Mainz, Germany.

Turpaud, P., & Reischmann, T. (2010). Characterisation of igneous terranes by zircon dating: implications for UHP occurrences and suture identification in the Central Rhodope, northern Greece. International Journal of Earth Sciences,99(3), 567-591.

van Achterberg E, Ryan CG, Jackson SE, Griffin W (2001) Data reduction software for LA-ICPMS. In: Sylvester P (ed) Laser Ablation ICPMS in the earth science: principles and applications. Mineral Ass Canada 29, 239-243.

Verma, S. P., & Verma, S. K. (2013). First 15 probability-based multidimensional tectonic discrimination diagrams for intermediate magmas and their robustness against postemplacement compositional changes and petrogenetic processes. Turkish Journal of Earth Sciences, 22(6).

Vermeesch, P. (2006). Tectonic discrimination diagrams revisited. Geochemistry, Geophysics, Geosystems, 7(6).

Viquesnel, A. (1853), Résumé des observations géographiques et géologiques faites, en 1847, dans la Turquie d'Europe, Bull. Soc. géol. Fr., série 2(10), 454-475.

Vlahou, M. (2003). Tertiary volcanism of Samothraki Island and associated industrial minerals (K-feldspars, zeolites). Ph.D. thesis, Aristotle University of Thessaloniki, Greece, 367 p. (in Greek).

Vlahou, M., Christofides, G., Eleftheriadis, G., Pinarelli, L., and KassoliFournaraki, A., (2001). Major, trace element and Sr-isotope characterization of the Samothraki Tertiary volcanic rocks, NE Aegean, in Proceedings of the 9th Congress of the Geological Society of Greece, Athens: Bulletin of the Geological Society of Greece, 33 (3), 995-1002.

Vlahou, M., Christofides, G., Eleftheriadis, G., Pinarelli, L., & Koroneos, A. (2006). Tertiary volcanic rocks from Samothraki island (north Aegean, Greece): Sr and Nd isotope constraints on their evolution.Postcollisional Tectonics and Magmatism in the Mediterranean Region and Asia, 409, 283.

Vollmer, R. (1976). Rb-Sr and U-Th-Pb systematics of alkaline rocks: The alkaline rocks of Italy, Geochim. Cosmochim. Acta, 40, 283-295.

von Braun, E. (1968). Die mesozoischen Hüllgesteine der SE-Rhodopen in Westthrazien (Griechenland). Geologisches Jahrbuch 85, 565-584.

von Quadt, A., Moritz, R., Peytcheva, I. & Heinrich, C.A. (2005). 3: Geochronology and geodynamics of Late Cretaceous magmatism and Cu-Au mineralization in the Panagyurishte region of the Apuseni-Banat-Timok-Srednogorie belt, Bulgaria. Ore Geology Reviews 27, 95-126.

Wang, Y., Fan, W., Peng, T., Zhang, H., Guo, F. (2005). Nature of the Mesozoic lithospheric mantle and tectonic decoupling beneath the Dabie Orogen, central China: evidence from 40Ar/39Ar geochronology, elemental and Sr-Nd-Pb isotopic compositions of early Cretaceous mafic igneous rocks. Chem. Geol. 220, 165-189.

Wawrzenitz, N. & Mposkos, E., (1997). First evidence for Lower Cretaceous HP/HT-metamorphism in the Eastern Rhodope, North Aegean region, North-East Greece, Eur. J. Mineral. 9, 659-664.

Wyllie, P., J. (1984). Constraints imposed by experimental petrology on possible and impossible magma sources and products. Philos. Trans. Roy. Soc. A310, 439-456 (1984).

Wilson, M. (1989). Igneous Petrogenesis. London: Unwin Hyman (Ed).

Workman, R. K., & Hart, S. R. (2005). Major and trace element composition of the depleted MORB mantle (DMM). Earth and Planetary Science Letters, 231(1), 53-72.

Yanev, Y., Innocenti, F., Manetti, P. & Serri, G. (1995): Paleogene collision magmatism in Eastern Rhodopes (Bulgaria) - Western Thrace (Greece): Temporal migration, petrochemical zoning and geodynamic significance. - In: Proc. XV Congress of the Carpatho-Balkan Geological Association, Athens 4/2. pp. 578 - 583.

Yanev, Y. (1998). Petrology of the eastern Rhodopes Paleogene acid volcanics, Bulgaria. Acta Vulcanologica, 10, 265-278.

Yanev, Y. (2003). Mantle source of the Paleogene collision-related magmas of the Eastern Rhodopes (Bulgaria) and Western Thrace (Greece): Characteristics of the mafic magmatic rocks. N. Jb. Miner. Abh. 178, 131-151.

Zhao, Z. F., Dai, L. Q., & Zheng, Y. F. (2013). Postcollisional mafic igneous rocks record crust-mantle interaction during continental deep subduction. Nature, Scientific reports, 3.

Zindler, A., & Hart, S. (1986). Chemical geodynamics. Annual review of earth and planetary sciences, 14, 493-571.

APPENDICES

APPENDIX A -

Whole Rock Major and Trace Element Analyses

Elatia pluton											
	Enclaves		**Diorite**	**GRD**							
Sample	**PEL-1**	**PEL-3**	**PEL-4**	**A-06**	**A-10**	**A-23**	**D-05**	**D-08B**	**D-11A**	**DSK-09**	**DSK-14**
Type*	Enclave	Enclave	Diorite	GRD	GRD	GRD	GRD	GRD	GRD	GRD	GRD
Reference*	1	1	1	3	3	3	3	3	3	3	3
SiO_2	51.24	52.02	51.46	62.57	64.89	65.78	61.32	63.81	65.38	64.31	69.68
TiO_2	1.27	1.13	0.83	0.69	0.61	0.53	0.68	0.63	0.54	0.60	0.43
Al_2O_3	19.17	18.14	20.28	17.60	17.08	16.69	17.57	16.87	16.60	16.89	15.33
FeOtot	6.57	7.43	6.96	4.00	3.03	3.02	4.21	3.45	3.08	3.37	2.23
MnO	0.12	0.14	0.18	0.08	0.06	0.06	0.09	0.09	0.09	0.09	0.08
MgO	4.23	4.61	3.07	2.35	1.61	1.69	1.99	1.66	1.54	1.57	0.99
CaO	6.17	5.92	7.36	4.89	3.77	3.92	5.17	4.35	3.62	4.01	2.70
Na_2O	4.49	4.09	4.01	3.99	4.09	4.07	4.20	4.15	4.06	3.92	4.12
K_2O	2.83	3.02	3.04	2.06	2.54	2.52	2.23	2.81	3.18	3.09	2.77
P_2O_5	0.54	0.54	0.53	0.37	0.33	0.30	0.41	0.36	0.28	0.34	0.20
mg#	53.4	52.5	44.0	51.1	48.6	49.9	45.7	46.1	47.1	45.4	44.1
LOI	2.2	1.8	1.9	1.2	1.8	1.2	1.8	1.6	1.4	1.6	1.3
Sum	98.8	98.8	99.6	99.8	99.8	99.7	99.7	99.8	99.7	99.7	99.9
XRF											
Sc	15	16		9	6	8	11	13	8	7	6
V	162	169		65	61	50	84	67	53	61	42
Cr	1	37		36	31	30	36	32	29	29	25
Ni	15	45		18	13	9	18	14	15	12	6
Pb	8	11		10	15	10	9	14	15	14	17
Zr	285	274		284	216	217	296	246	243	253	193
Nb	26	16		25	13	20	11	22	18	17	15
U	2	2		4	5	5	1	2	4	8	6
Y	26	17		22	14	15	11	15	15	15	16
Th	18	11		16	19	14	18	15	13	17	18
Rb	106	148		86	178	88	100	107	114	102	114
Sr	871	677		715	376	589	835	658	613	732	422
Ba	663	609		635	596	564	659	788	909	921	316
ICP-MS											
Sc			10.9								
V	167.0	171.0	208.4								
Cr	1.1	36.8	18.5								
Ni	11.7	37.0									
Pb			17.8								
Zr			78.1								
Hf	6.3	6.7	1.9				5.6				
Nb	24.1	14.0	4.8								
Ta	1.20	0.70	0.46				0.60				
U	3.0	2.0	2.3				2.4				
Y	26.3	16.6	21.6				16.0			17.0	
Th	19.3	15.5	6.8				24.5				
Rb	109.4	152.6	98.6				93.0				
Cs	2.5	10.1	3.3				6.1				
Sr	857.7	674.9	1173.5								
Ba	696.0	600.0	728.4				640.0				
La	59.00	48.90	23.29				78.85			61.18	
Ce	120.60	94.40	52.95				135.94			107.69	
Pr	12.46	9.34	6.23				12.16			10.55	
Nd	46.00	33.10	29.62				44.19			40.35	
Sm	7.62	5.24	6.27				5.13			5.69	
Eu	1.72	1.03	1.50				1.19			1.24	
Gd	6.33	4.02	5.78				3.59			4.35	
Tb	0.91	0.60	0.71								
Dy	4.93	3.15	4.05				2.66			3.33	
Ho	0.91	0.59	0.83				0.58			0.69	
Er	2.58	1.67	2.22				1.76			1.80	

Tm	0.37	0.23	0.38		
Yb	2.35	1.47	2.05	1.28	
Lu	0.34	0.22	0.24	0.21	1.34
ΣREE	266.1	204.0	136.1		0.20
Eu/Eu*	0.7	0.7	0.7	0.8	0.7
(La/Lu)cn	18.0	23.1	9.9	39.0	31.8
(La/Sm)cn	4.9	5.9	2.3	9.7	6.8
(Gd/Yb)cn	2.2	2.2	2.3	2.3	2.6
(Tb/Lu)cn	1.8	1.9	2.0		

*Type: GRD= Granodiorites

**References: 1 Major & trace elements present study; 2 Major elements Soldatos et al. (2001a) & trace elements present study; 3 Major and trace elements Soldatos et al. (2001a); 4 Major & trace elements Jones et al. (1992)

Elatia pluton

	GRD										
Sample	**DSK-15**	**DSK-17**	**DSK-18**	**E-04**	**E-06**	**E-07**	**E-09**	**E-10**	**GBT.189**	**GBT.191**	**GBT.192**
Type*	GRD	GRD	GRD	GRD	GRD	GRD	GRD	GRD	GRD	GRD	GRD
Reference**	3	2	3	2	3	3	3	3	4	4	4
SiO_2	67.72	59.84	64.87	60.13	73.56	61.37	69.99	66.45	71.60	62.90	67.40
TiO_2	0.50	0.76	0.56	0.73	0.00	0.77	0.39	0.57	0.31	0.72	0.62
Al_2O_3	15.87	17.72	16.72	18.50	15.50	18.19	15.77	16.03	14.80	16.80	16.80
FeOtot	2.48	4.86	3.32	4.41	0.62	4.04	2.19	3.16	1.80	3.87	3.33
MnO	0.08	0.15	0.09	0.09	0.11	0.08	0.08	0.09	0.00	0.09	0.12
MgO	1.11	2.41	1.65	2.29	0.07	2.06	1.11	1.39	0.50	1.70	1.40
CaO	2.84	5.28	4.26	5.14	0.29	4.39	3.20	3.98	2.30	4.10	3.50
Na_2O	3.85	4.29	4.03	4.67	4.89	4.16	4.35	4.13	4.00	3.80	5.10
K_2O	3.60	1.89	2.68	2.67	4.38	2.44	1.80	2.52	4.02	2.83	2.40
P_2O_5	0.22	0.44	0.33	0.44	0.05	0.35	0.13	0.30	0.10	0.27	0.22
mg#	44.4	46.9	47.0	48.0	16.7	47.6	47.4	43.9	33.1	43.9	42.8
LOI	1.5	2.0	1.2	0.8	0.7	2.1	0.9	1.1			
Sum	99.8	99.6	99.7	99.8	100.1	100.0	99.9	99.8	99.4	97.1	100.9
XRF											
Sc	7	12	11	10	1	9	9	12		84	65
V	48		61	78	7	68	37	54	28	14	11
Cr	29	32	34	28	21	28	24	28	7	6	2
Ni	10	21	12	10	0	4	3	10	0		
Pb	20	9	9	10	21	11	22	18		213	180
Zr	203	285	242	344	56	300	223	234	184	21	28
Nb	19	18	11	25	27	24	14	19	5	6	5
U	5	3	3	4	9	2	1	4	6	23	22
Y	16	22	15	19	8	17	8	18	7	20	20
Th	14	14	12	15	5	17	4	14	19	119	170
Rb	135	117	128	112	337	83	90	101	143	538	475
Sr	476	791	689	821	49	758	433	556	304	535	497
Ba	722	414	1186	728	83	910	235	501	803		
ICP-MS											
Sc											
V		88.0									
Cr											
Ni											
Pb											
Zr		239.8		292.1						5.7	5.0
Hf		5.6	4.5	7.0					5.1		
Nb		16.3		17.5						1.28	1.99
Ta		1.50	1.10	1.20					0.20		
U		3.2	1.6	4.6							
Y		18.1	17.0	15.1							
Th		18.4	17.2	18.0							
Rb		85.7		105.5							
Cs		3.5	3.5	4.1							

Sr	762.0		817.7							
Ba	511.0		737.0							
La	60.70	47.17	70.50							
Ce	108.30	85.64	123.20							
Pr	10.80	8.74	11.86			8.68				
Nd	37.20	33.57	39.40					6.60		5.90
Sm	5.64	4.91	5.85			4.82	4.39	1.37		1.01
Eu	1.27	1.09	1.33			1.07	0.71			
Gd	4.76	3.73	4.79			3.78		0.69		0.63
Tb	0.65		0.62				0.31			
Dy	3.25	3.04	3.16			3.15				
Ho	0.58	0.67	0.60			0.81				
Er	1.68	1.70	1.62			1.83				
Tm	0.24		0.24					1.71		1.47
Yb	1.54	1.35	1.50			1.58	0.53	0.28		0.25
Lu	0.23	0.19	0.23			0.23	0.08			169.8
ΣREE	236.8		264.9			184.6				0.9
Eu/Eu*	0.7	0.7	0.7			0.7		18.4		18.9
(La/Lu)cn	27.4	25.8	31.8			19.9	50.6	4.7		4.9
(La/Sm)cn	6.8	6.0	7.6			5.8	5.6			
(Gd/Yb)cn	2.5	2.2	2.6			1.9		1.7		1.7
(Tb/Lu)cn	1.9	0.0	1.8				2.6			

*Type: GRD= Granodiorites

**References: 1 Major & trace elements present study; 2 Major elements Soldatos et al. (2001a) & trace elements present study; 3 Major and trace elements Soldatos et al. (2001a); 4 Major & trace elements Jones et al. (1992)

Elatia pluton

	GRD										
Sample	**GBT.19**	**I-11B**	**I-14A**	**I-16**	**M-10**	**PEL-**	**PS-01**	**PS-11**	**PS-12**	**PS-3**	**Z-12B**
Type*	GRD	GRD	GRD	GRD	GRD	GRD	GRD	GRD	GRD	GRD	GRD
Reference*	4	3	2	3	3	2	2	2	3	3	3
SiO_2	67.80	66.09	70.24	63.24	69.18	60.52	66.92	65.88	65.94	70.50	66.78
TiO_2	0.62	0.52	0.37	0.64	0.43	0.75	0.61	0.54	0.55	0.36	0.53
Al_2O_3	16.60	16.66	15.36	16.98	15.70	17.81	16.22	16.48	16.56	14.98	16.61
FeOtot	3.33	2.85	2.37	3.50	2.25	4.21	3.08	2.94	3.01	1.92	2.68
MnO	0.07	0.06	0.07	0.07	0.05	0.08	0.09	0.09	0.09	0.08	0.05
MgO	1.40	1.41	1.32	1.83	0.97	2.54	1.52	1.40	1.30	0.93	1.25
CaO	3.40	3.70	3.25	4.65	2.45	5.35	3.67	3.76	3.76	2.24	3.35
Na_2O	5.00	4.16	4.14	4.03	4.09	4.32	3.81	4.07	4.20	3.16	4.03
K_2O	2.35	3.26	1.80	2.83	3.73	2.14	2.41	3.26	2.86	4.84	3.18
P_2O_5	0.22	0.33	0.20	0.38	0.21	0.34	0.28	0.27	0.29	0.15	0.26
mg#	42.8	46.8	49.8	48.2	43.4	51.8	46.8	45.9	43.5	46.3	45.4
LOI		0.7	0.7	1.5	0.8	1.1	1.2	1.1	1.2	0.7	1.1
Sum	100.8	99.8	99.9	99.7	99.8	99.2	99.8	99.8	99.8	99.9	99.8
XRF											
Sc		9	7	21	9	10	13	10	10	7	10
V	71	47		58	36	100			49		30
Cr	10	27	27	37	26	2	29	29	28	27	29
Ni	4	5	3	17	6	18	9	9	10	6	4
Pb		14	14	12	22	7	31	16	16	32	17
Zr	195	237	139	241	176	283	224	218	250	167	213
Nb	17	19	13	25	15	18	22		20	12	16
U	3	2	4	4	8	2	2	5	3	2	6
Y	16	16	12	28	14	18	27	14	19	9	12
Th	25	19	14	15	29	15	13		19	8	19
Rb	103	127	152	120	171	73	111	117	118	132	121
Sr	514	558	413	547	431	773	526	555	582	473	530
Ba	505	794	467	670	532	643	599	675	685	987	591
ICP-MS											
Sc			25.0			94.0	54.0	64.0			

V						2.3				31.0
Cr						13.2				
Ni										
Pb			97.4				193.9	184.3		
Zr	5.5		2.8			6.0	5.2	4.7		
Hf			11.4			15.7	16.3	14.2		3.1
Nb	1.19		0.40			1.00	1.60	1.10		
Ta			5.2			3.3	2.8	3.0		0.90
U		21.0	10.6			16.6	21.9	14.1		2.8
Y		25.7	16.1			23.0	14.8	17.2		11.0
Th			138.4			77.8	92.8	106.2		12.0
Rb		2.2	11.0			3.1	2.8	2.5		
Cs			396.0			792.8	479.2	541.5		1.8
Sr			491.0			650.0	625.0	727.0		
Ba		23.20	23.80			69.60	39.10	41.40		
La		45.98	46.30			136.70	71.70	73.60		26.79
Ce		5.06	5.30			12.64	7.69	7.58		48.39
Pr		19.97	19.40			41.60	26.90	26.20		5.13
Nd	5.10	4.41	3.82			5.91	4.99	4.47		19.67
Sm	0.98	0.32	0.48			1.30	0.99	0.93		2.80
Eu		3.75	2.79			4.21	4.06	3.26		0.64
Gd	0.51		0.38			0.62	0.68	0.49		2.09
Tb		3.50	2.06			3.26	3.81	2.50		
Dy		0.67	0.34			0.59	0.75	0.51		1.93
Ho		1.75	0.86			1.70	2.21	1.40		0.48
Er			0.13			0.26	0.33	0.20		1.15
Tm	1.17	1.52	0.83			1.55	2.11	1.31		
Yb	0.21	0.21	0.12			0.23	0.33	0.19		1.10
Lu		110.3	106.6			280.2	165.7	164.0		0.17
ΣREE		0.2	0.4			0.8	0.7	0.7		
Eu/Eu*	26.0	11.5	20.6			31.4	12.3	22.6		0.8
(La/Lu)cn	6.5	3.3	3.9			7.4	4.9	5.8		16.4
(La/Sm)cn		2.0	2.7			2.2	1.6	2.0		6.0
(Gd/Yb)cn	1.6		2.2			1.8	1.4	1.8		1.5
(Tb/Lu)cn										

*Type: GRD= Granodiorites

**References: 1 Major & trace elements present study; 2 Major elements Soldatos et al. (2001a) & trace elements present study; 3 Major and trace elements Soldatos et al. (2001a); 4 Major & trace elements Jones et al. (1992)

Xanthi Plutonic Complex												
	MME											
Sample	**X-222**	**EX-207E**	**X-250E**	**X-119E**	**Xa84**	**Xa42B**	**Xa46A**	**Xa61**	**Xa46B**	**Xa46**	**Xa90**	**Xa11**
Type*	Enclave	Enclave	Enclave	Enclave	Enclave	Enclave	Enclave	Enclave	Enclave	Enclave	Enclave	Enclave
Reference**	1	1	1	1	4	4	4	4	4	4	4	4
SiO_2	53.03	56.11	56.62	57.65	55.79	57.42	58.08	58.32	58.74	59.05	59.13	59.73
TiO_2	1.10	0.89	0.90	0.74	1.11	0.77	0.85	0.66	0.86	0.84	0.99	0.79
$Al2O_3$	18.35	17.54	17.85	17.54	17.36	18.71	17.46	18.17	17.98	17.76	18.27	17.27
FeOtot	9.04	6.49	7.18	6.68	8.94	6.66	6.61	6.06	6.10	6.07	5.95	6.73
MnO	0.21	0.16	0.20	0.21	0.19	0.14	0.18	0.19	0.20	0.19	0.11	0.15
MgO	4.04	3.47	3.64	3.27	4.24	3.43	3.73	3.06	3.73	4.02	3.73	2.82
CaO	6.73	6.39	6.63	6.17	5.06	6.26	6.21	6.80	6.70	6.34	5.18	4.95
Na_2O	4.88	4.90	4.59	4.92	3.84	4.42	4.35	4.79	4.47	4.31	4.00	4.48
K_2O	1.55	1.82	1.66	2.02	2.20	1.16	1.51	1.08	0.23	0.44	1.73	2.02
P_2O_5	0.37	0.20	0.18	0.25	0.28	0.27	0.29	0.19	0.32	0.30	0.23	0.31
mg#	44.31	48.79	47.44	46.61	45.77	47.87	50.13	47.33	52.18	54.12	52.79	42.75
LOI	0.8	1.4	1.8	0.8								
Sum	100.1	99.4	101.3	100.2								
XRF												
Sc	43	19		25	21	19	22	18	18	16	15	15
V	220		172	166	151	101	157	137	108	111	114	137
Cr	39	21	6	33	13	4	16	4	10	8	14	6
Ni	6	3	2	2	7	6	5	4	4	4	4	21
Y	37	59	53	35	4	12	14	12	4	12	9	16
Zr	262	141	118	238	104	68	110	152	156	145	155	248
La	66	28	45	41	38	39	42	33	37	37	32	53
Nb	28	24	17	17								
Rb	134	88	109	96	230	100	243	59	109	111	161	210
Sr	432	423	360	361	362	412	350	434	430	408	382	384
Ba	360	426	326	259	710	442	623	286	432	428	601	474
ICP-MS												
V												
Pb	28.24	20.72	18.32	12.79								
Zr	179.48	141.00	162.62	177.28								
Hf	4.98	2.74	4.43	4.14								
Nb	19.50	24.29	18.64	11.43								
Ta	1.43	1.51	1.90	0.95								
U	7.23	6.16	6.18	6.20								
Y	28.72	59.00	47.21	26.77								
Th	14.27		15.22	22.41								
Rb	150.62	93.01	102.77	96.53								
Cs	5.78	1.91	3.96	3.32								
Sr	466.55	416.81	382.58	383.97								
Ba	423.04	459.52	347.40	349.57								
La	59.00	38.77	50.20	39.23								
Ce	109.93	89.62	109.92	77.19								
Pr	10.77	11.66	12.00	7.85								
Nd	43.60	45.36	52.37	31.43								
Sm	7.97	9.71	7.08	5.94								
Eu	1.44	1.62	1.51	1.12								
Gd	5.59	7.78	8.01	4.34								
Tb	0.85	1.29	1.24	0.64								
Dy	5.02	8.38	7.59	4.98								
Ho	0.95	1.49	1.51	0.80								
Er	2.86	4.45	4.72	2.72								
Tm	0.43	0.79	0.75	0.40								
Yb	3.00	4.52	4.36	2.21								
Lu	0.46	0.62	0.69	0.40								
ΣREE	671.5	671.5	669.5	730.0								
Eu/Eu*	0.6	0.6	0.6	0.6								

(La/Lu)cn	13.3	13.3	6.5	7.6
(La/Sm)cn	4.7	4.7	2.5	4.5
(Gd/Yb)cn	1.5	1.5	1.4	1.5
(Tb/Lu)cn	1.3	1.3	1.4	1.2

*Type: GRD= Granodiorites; LMzG= Leucomonzogabbros; MGb= Microgabbros; Mz= Monzonites; QMzd= Quartz monzodiorites; PLMz= Porphyrytic quartz leucomonzonites;
**References: 1 ICP-MS trace elements present study; 2 XRF trace and major elements Christofides (1977); 3 ICP-MS trace elements Christofides (1977); 4 Major & trace elements Sergi (1997)

Xanthi Plutonic Complex

	MME	Acid group										
Sample	**Xa7**	**X-156**	**X-147**	**X-83**	**X-165**	**X-210**	**X-300**	**X-41**	**X-254**	**X-601**	**X-270**	**X-250**
Type*	Enclave	GRD	GRD	GRD	GRD	GRD	GRD	GRD	GRD	GRD	GRD	GRD
Reference**	4	1,2	1,2	1,2	1,2	1,2	2	2	1,2	1,2	1,2	1,2
SiO_2	60.91	62.06	62.33	62.57	62.87	63.32	63.69	63.9	63.98	64.07	64.48	64.92
TiO_2	0.74	0.68	0.7	0.67	0.5	0.61	0.52	0.6	0.61	0.6	0.56	0.57
$Al2O_3$	17.42	16.77	16.46	16.17	16.37	16.04	16.55	16.08	16.02	16.27	15.82	15.91
FeOtot	5.48	5.06	5.02	4.91	4.33	4.38	4.37	4.43	4.19	4.17	4.28	4.02
MnO	0.14	0.12	0.12	0.11	0.09	0.09	0.09	0.11	0.1	0.09	0.10	0.09
MgO	2.52	2.17	2.06	2.1	1.9	1.95	1.94	1.88	1.85	1.76	1.75	1.71
CaO	5.31	4.77	4.56	4.33	4.79	4.17	4.44	4.12	4.04	4.33	4.24	4.02
Na_2O	4.79	3.65	3.47	3.29	3.32	3.39	3.4	3.65	3.3	3.56	3.41	3.33
K_2O	1.74	3.83	3.89	3.82	4.35	3.83	3.32	3.87	3.87	3.71	3.71	3.95
P_2O_5	0.34	0.24	0.25	0.14	0.26	0.13	0.14	0.2	0.12	0.17	0.17	0.11
mg#	45.05	43.33	42.23	43.23	43.89	44.22	44.14	43.07	44.01	42.94	42.13	43.10
LOI		0.84	0.62	0.98	0.73	0.91	0.92	0.68	0.97	0.6	0.8	0.9
Sum		100.2	99.5	99.1	99.5	98.8	99.4	99.5	99.1	99.3	99.3	99.5
XRF												
Sc	15		32		21	28	15	18	21	37		17
V	131	121	118	119	106			104				96
Cr	6	32	28	2	29	1	2	29				
Ni	8	2	3	1	3		1	3				
Y	28	39	38	49	27	31	24	35	45			20
Zr	204	324	351	214	296	178	122	288	161			158
La	81	43	42	35	39	30	24	34	33			28
Nb		31	24	13	19	11	6	25	12			9
Rb	130	136	168	168	129	147	86	157	164			164
Sr	416	431	439	456	683	407	576	397	443			410
Ba	386	648	651	806	882	832	1016	716	832	844	793	801
ICP-MS												
V			103			90			98			
Pb		20.30	32.00	21.48	25.84					21.16	21.97	24.49
Zr		253.86	267.40	229.28	170.60	221.90			186.90	231.17	221.87	200.79
Hf		6.24	7.70	5.83	3.85	6.30			5.50	6.42	5.87	5.09
Nb		17.35	17.10	16.08	9.51	13.80			12.60	14.63	12.17	15.69
Ta		1.62	1.30	1.32	1.43	1.20			1.00	1.00	0.95	1.15
U		8.87	7.90	6.38	4.00	8.30			7.30	9.59	6.14	9.68
Y		28.01	25.60	23.10	23.10	22.50			22.10	22.06	20.74	22.18
Th		35.75	39.40	34.85	19.38	34.20			23.70			35.72
Rb		146.54	169.40	158.09	150.13	163.50			162.90	169.68	151.82	183.87
Cs		3.59	6.40	4.97	4.01	3.30			4.00	3.97	3.99	7.15
Sr		458.09	475.10	355.32	747.38	453.20			459.90	465.72	459.04	400.05
Ba		733.52	672.00	660.02	1004.56	769.00			799.00	843.72	945.80	747.60
La		44.48	44.90	35.54	31.71	41.70			31.30	39.24	38.92	36.33
Ce		89.46	86.70	70.06	78.56	79.40			58.20	74.44	72.10	79.64
Pr		8.95	9.92	6.88	8.79	8.67			6.86	7.27	6.51	7.87
Nd		35.13	35.50	29.82	40.83	29.90			25.40	28.57	27.27	30.00
Sm		6.90	5.94	5.54	7.52	5.20			4.57	5.38	4.12	4.75
Eu		1.26	1.21	1.02	2.12	1.07			1.05	1.21	1.10	1.26

Gd	4.78	5.20	4.24	5.42	4.50	4.02	4.12	3.90	3.95
Tb	0.80	0.78	0.67	0.85	0.66	0.62	0.63	0.54	0.63
Dy	4.97	4.19	4.02	4.27	3.52	3.48	3.66	3.43	3.86
Ho	1.01	0.84	0.71	0.78	0.75	0.71	0.70	0.68	0.81
Er	2.53	2.42	2.22	2.10	2.16	1.97	1.95	2.12	2.07
Tm	0.44	0.42	0.34	0.32	0.37	0.35	0.35	0.34	0.39
Yb	3.01	2.44	2.18	1.78	2.33	2.10	2.25	2.12	3.13
Lu	0.53	0.39	0.33	0.36	0.37	0.32	0.36	0.36	0.44
ΣREE	559.9	549.1	444.4	509.6	491.9	398.7	440.1	438.2	474.4
Eu/Eu*	0.6	0.7	0.6	1.0	0.7	0.7	1.5	0.8	0.9
(La/Lu)cn	8.7	12.0	11.2	9.2	11.7	10.2	11.2	11.3	8.5
(La/Sm)cn	4.1	4.8	4.0	2.7	5.0	4.3	23.5	5.9	4.8
(Gd/Yb)cn	1.3	1.7	1.6	2.5	1.6	1.5	1.5	1.5	1.0
(Tb/Lu)cn	1.0	1.4	1.4	1.6	1.2	1.3	1.2	1.0	1.0

*Type: GRD= Granodiorites; LMzG= Leucomonzogabbros; MGb= Microgabbros; Mz= Monzonites; QMzd= Quartz monzodiorites; PLMz= Porphyrytic quartz leucomonzonites;
**References: 1 ICP-MS trace elements present study; 2 XRF trace and major elements Christofides (1977); 3 ICP-MS trace elements Christofides (1977); 4 Major & trace elements Sergi (1997)

Xanthi Plutonic Complex

	Acid group							Basic group				
Sample	**X-205**	**X-110**	**X-163**	**X-125**	**X-52**	**X-220**	**X-86**	**X-279**	**X-280**	**X-307**	**X-306**	**X-277**
Type*	GRD	GRD	GRD	GRD	GRD	GRD	GRD	LMzG	LMzG	LMzG	LMzG	MGb
Reference**	2	1,2	1,2	2	1,2	1,2	1,2	1,2	1,2	1,2	1,2	2,3
SiO_2	65.56	66.00	66.71	67.48	67.61	67.67	68.40	50.25	51.07	52.97	53.44	46.95
TiO_2	0.53	0.47	0.47	0.45	0.48	0.44	0.45	0.76	1.03	0.73	0.78	1.28
$Al2O_3$	15.80	15.44	15.80	15.42	15.43	14.88	15.56	20.99	19.36	22.82	20.89	18.44
FeOtot	3.73	3.78	3.99	3.47	3.42	3.46	3.20	5.79	7.27	5.47	5.98	10.02
MnO	0.09	0.06	0.07	0.08	0.07	0.07	0.07	0.10	0.12	0.11	0.10	0.18
MgO	1.64	1.48	1.61	1.32	1.22	1.23	1.26	2.93	3.48	2.71	2.71	5.91
CaO	3.73	3.81	3.48	3.22	2.71	2.98	3.02	8.68	8.42	7.02	7.98	11.31
Na_2O	3.40	3.94	3.57	3.55	3.16	3.47	3.21	3.56	3.35	3.71	3.78	2.88
K_2O	3.98	4.13	3.83	4.36	5.45	4.64	4.34	2.02	2.79	2.56	2.79	0.72
P_2O_5	0.11	0.19	0.20	0.14	0.15	0.15	0.10	0.40	0.48	0.43	0.40	0.24
mg#	43.90	41.10	41.85	40.37	38.86	38.75	41.20	47.43	46.03	46.88	44.66	51.25
LOI	0.8	0.6	0.8	0.6	0.6	0.6	0.5	2.1	1.6	0.9	0.9	0.8
Sum	99.4	99.9	100.6	100.0	100.3	99.6	100.1	97.5	99.0	99.4	99.8	98.7
XRF												
Sc	25	11	41	5	16						18	
V		75	81	73	73	66			238	151		
Cr		28	29	28	26	25		9	39	19	62	20
Ni		3	1	2	5	3		14	15		19	10
Y	48	27	24	30	48	42	29		33	23		
Zr	161	269	225	232	339	245	158		107	312	169	
La	41	37	41	49	55	42	15	39	46	31		19
Nb	11	20	12	18	42	34	14		8	13		
Rb	160	124	113	191	268	197	199		89	85	90	
Sr	393	515	456	323	261	322	309		913		1011	
Ba	754	1296	800	660	624	496	676	820	1659	1587	1740	565
ICP-MS												
V						59	65					
Pb		35.25	29.28		41.76	34.00		26.13	29.54	29.74	30.06	
Zr		162.33	132.49		322.07	177.10	206.70	123.91	149.13	148.50	109.75	
Hf		3.99	3.47		8.96	6.10	6.30	3.07	3.65	3.43	2.66	
Nb		11.48	10.21		33.78	23.10	16.30	7.72	10.62	9.89	7.53	6.00
Ta		1.38	1.54		3.83	2.50	1.90	0.62	0.88	0.67	0.72	
U		5.95	7.80		30.38	13.80	9.80	2.85	3.24	3.60	3.13	
Y		16.94	17.54		34.24	28.80	24.30	22.11	26.90	16.76	16.65	
Th		25.21	23.21		107.27	48.60	38.80	11.98	12.77	14.72	16.59	

Rb	139.76	164.29		338.06	203.20	200.40	59.75	90.05	91.98	85.95	
Cs	2.08	2.71		11.66	5.70	4.80	1.55	3.12	2.74	1.36	
Sr	548.55	537.24		303.51	353.60	338.50	1050.92	1002.13	883.03	992.78	816.00
Ba	1472.48	1091.30		630.27	516.00	639.00	786.10	1664.66	1586.85	1637.89	565.00
La	33.31	35.35		58.33	32.10	29.80	43.64	46.88	31.52	34.15	13.80
Ce	68.97	75.96		127.52	71.80	61.40	85.86	98.86	63.83	67.04	28.90
Pr	6.32	6.52		11.36	8.74	7.53	9.33	10.55	6.72	6.90	
Nd	24.13	23.01		43.05	31.40	27.60	39.80	45.60	29.26	28.53	20.80
Sm	3.89	4.72		7.67	5.69	5.11	6.88	8.17	5.34	4.74	
Eu	1.43	0.99		0.78	0.87	0.93	1.81	1.95	1.88	1.79	1.60
Gd	3.27	2.11		5.39	4.72	4.49	5.98	6.18	3.61	2.97	4.50
Tb	0.48	0.49		0.83	0.77	0.75	0.76	0.89	0.55	0.47	
Dy	2.99	2.34		5.45	4.23	3.95	4.34	4.90	3.04	3.11	3.69
Ho	0.63	0.48		1.01	0.89	0.80	0.77	0.96	0.62	0.59	0.70
Er	1.57	1.44		3.24	2.70	2.28	1.92	2.57	1.54	1.53	1.99
Tm	0.25	0.29		0.51	0.49	0.41	0.29	0.37	0.22	0.29	
Yb	1.45	1.82		3.22	3.27	2.39	1.70	2.26	1.45	1.12	1.68
Lu	0.28			0.51	0.53	0.38	0.28	0.34	0.22	0.24	0.24
ΣREE	395.9	394.5		692.5	477.5	422.0	548.2	620.3	409.1	414.4	
Eu/Eu*	1.2	0.8		0.4	0.5	0.6	0.8	0.8	1.2	1.4	1.0
(La/Lu)cn	12.4			11.9	6.3	8.1	16.0	14.5	15.0	14.6	
(La/Sm)cn	5.4	4.7		4.8	3.5	3.7	4.0	3.6	3.7	4.5	
(Gd/Yb)cn	1.8	0.9		1.4	1.2	1.5	2.8	2.2	2.0	2.1	
(Tb/Lu)cn	1.2			1.1	1.0	1.3	1.8	1.8	1.7	1.3	

*Type: GRD= Granodiorites; LMzG= Leucomonzogabbros; MGb= Microgabbros; Mz= Monzonites; QMzd= Quartz monzodiorites; PLMz= Porphyrytic quartz leucomonzonites;
**References: 1 ICP-MS trace elements present study; 2 XRF trace and major elements Christofides (1977); 3 ICP-MS trace elements Christofides (1977); 4 Major & trace elements Sergi (1997)

Xanthi Plutonic Complex												
	Basic group											
Sample	**X-28**	**X-N2**	**X-284**	**X-N3**	**X-N4**	**X-GAE-11**	**X-278**	**X-NG5**	**X-42**	**X-232 A**	**X-20**	**X-MZ**
Type*	MGb	MGb	MGb	MGb	MGb	MGb	MGb	MGb	Mz	Mz	Mz	Mz
Reference**	1,2	1,2	1,2	2	1,2	1,2	1,2	1,2	1,2	1,2	1,2	1,2
SiO_2	47.36	47.46	48.07	48.61	48.81	49.65	49.84	49.89	53.51	54.56	55.02	55.08
TiO_2	1.22	1.31	1.31	1.51	1.53	1.02	1.83	1.03	1.14	0.94	0.89	0.97
$Al2O_3$	17.94	19.23	19.67	18.26	18.40	18.41	21.27	18.03	15.57	18.23	17.46	15.34
FeOtot	10.83	9.11	10.38	10.55	10.59	8.97	7.99	9.89	8.64	6.80	5.94	7.07
MnO	0.20	0.19	0.16	0.02	0.19	0.17	0.15	0.20	0.18	0.13	0.11	0.13
MgO	5.93	5.88	5.21	5.86	5.90	5.61	4.29	6.72	5.48	3.27	3.71	4.20
CaO	10.47	11.12	10.68	10.57	10.39	10.28	9.96	9.07	7.93	6.29	5.93	6.64
Na_2O	2.58	3.07	3.14	3.32	3.33	3.12	3.15	3.01	3.32	3.52	3.16	2.94
K_2O	1.65	0.67	0.39	0.71	0.76	0.70	0.92	0.37	3.95	3.73	5.13	4.70
P_2O_5	0.34	0.52	0.33	0.33	0.34	0.30	0.22	0.25	0.73	0.33	0.42	0.56
mg#	49.39	53.47	47.22	49.75	49.81	52.70	48.92	54.76	53.06	46.13	52.67	51.41
LOI	1.3	0.1	0.4	0.1	0.1		0.5	0.2	0.7	1.4	1.0	0.6
Sum	99.8	98.6	99.7	99.8	100.3	98.2	100.2	98.6	101.1	99.2	98.7	98.2
XRF												
Sc	39				28				12	22	18	
V	335	334	281		330		227		207	196		
Cr	66	32	13	71	71		10		49	8	67	
Ni	12	2	9	18	19		7		15	9	35	
Y	31	26			24	20	20		40	23	24	27
Zr	232	205	216	44	209	42	57		438	205	367	377
La	26	31	17		17		15		46	45	61	
Nb	14	10			6		6		25	15	20	
Rb	58	6	3	8	9		19		196	193	285	
Sr	656			696	699	821	811		726	712	756	620
Ba	381	519	502	567	539	476	659	402	1142	1261	1805	1457
ICP-MS												

V			312				285			197		173	208
Pb	12.91	6.63			10.85			24.11	5.99	52.27	59.66		
Zr	138.59	53.75	44.00		54.51	39.50		72.78	22.91	307.20	279.93	507.10	393.40
Hf	3.84	1.52	1.40		1.58	1.40		1.50	0.82	8.40	7.14	13.30	11.30
Nb	8.68	3.24	3.00		3.55	2.50		4.64	1.08	18.80	19.82	30.50	26.90
Ta	0.70	0.17	0.20		0.24	0.10		0.41	0.06	1.40	1.23	2.10	1.90
U	1.71	0.19	0.20		0.20	0.40		0.51	0.13	10.00	7.73	19.80	14.20
Y	29.63	26.71	22.10		24.41	19.50		18.25	17.16	28.20	24.73	22.30	28.80
Th	10.29	0.90	0.90		0.97	1.70		1.45	0.87	31.90	27.34	68.00	48.70
Rb	57.93	8.47	4.10		8.97	9.80		20.52	3.13	187.30	201.75	286.00	284.70
Cs	1.93		0.30		0.93	0.30			0.87	6.90	5.53	14.50	11.20
Sr	744.91	944.11	882.20		798.36	854.10		885.60	991.69	733.40	708.10	796.00	657.90
Ba	500.66	600.11	450.00		548.23	492.00		638.62	300.34	1180.00	1212.11	1645.00	1502.00
La	24.85	21.16	19.00		19.65	19.60		19.45	17.46	45.30	39.96	55.60	51.70
Ce	52.34	45.10	41.60		40.55	40.10		42.03	37.16	90.70	82.93	107.60	106.70
Pr	6.60	5.54	5.74		4.98	5.30		4.76	4.49	11.14	8.63	12.54	13.10
Nd	30.61	27.24	26.30		24.31	22.80		22.03	22.61	42.50	36.47	45.70	49.80
Sm	6.96	6.03	5.15		5.80	4.51		4.58	4.77	7.41	6.69	7.34	8.78
Eu	1.72	1.59	1.84		1.77	1.61		1.52	1.90	1.66	1.89	1.50	1.61
Gd	6.48	5.13	4.77		4.88	4.40		4.16	3.81	6.31	5.58	5.77	6.71
Tb	0.87	0.86	0.76		0.84	0.70		0.60	0.61	0.91	0.76	0.78	0.95
Dy	5.67	5.25	3.97		4.87	3.50		3.19	3.27	4.64	4.75	3.98	5.00
Ho	1.09	0.95	0.82		0.97	0.71		0.76	0.61	0.96	0.87	0.75	0.95
Er	2.75	2.41	2.14		2.36	1.92		1.81	1.65	2.60	2.43	2.16	2.66
Tm	0.39	0.36	0.34		0.33	0.30		0.23	0.23	0.42	0.36	0.36	0.43
Yb	2.29	2.13	1.86		1.98	1.69		1.49	1.31	2.49	2.03	2.02	2.62
Lu	0.36	0.33	0.28		0.31	0.27		0.29	0.20	0.40	0.40	0.34	0.39
ΣREE	432.4	377.9	351.6		354.5	326.7		315.7	300.5	602.1	532.4	652.7	681.4
Eu/Eu*	0.8	0.9	1.1		1.0	1.1		1.0	1.3	0.7	0.9	0.7	0.6
(La/Lu)cn	7.2	6.6	7.0		6.5	7.5		7.1	9.3	11.8	10.3	17.0	13.8
(La/Sm)cn	2.2	2.2	2.3		2.1	2.7		2.7	2.3	3.8	3.8	4.8	3.7
(Gd/Yb)cn	2.3	1.9	2.1		2.0	2.1		2.2	2.4	2.0	2.2	2.3	2.1
(Tb/Lu)cn	1.7	1.8	1.8		1.8	1.8		1.4	2.1	1.5	1.3	1.6	1.7

*Type: GRD= Granodiorites; LMzG= Leucomonzogabbros; MGb= Microgabbros; Mz= Monzonites; QMzd= Quartz monzodiorites; PLMz= Porphyrytic quartz leucomonzonites;

**References: 1 ICP-MS trace elements present study; 2 XRF trace and major elements Christofides (1977); 3 ICP-MS trace elements Christofides (1977); 4 Major & trace elements Sergi (1997)

Xanthi Plutonic Complex

	Basic group											
Sample	**X-19**	**X-44**	**X-232**	**X-289**	**X-291**	**X-292**	**X-2**	**X-1**	**X-217**	**X-294**	**X-297**	**X-276**
Type*	Mz	Mz	Mz	Mz	Mz	Mz	QMzd	QMzd	QMzd	QMzd	QMzd	QMzd
Reference**	1,2	1,2	2	1,2	1,2	1,2	1	1	1,2	1,2	1,2	1,2
SiO_2	55.42	55.58	55.87	56.21	56.42	57.51	54.75	55.31	57.80	54.34	52.04	52.60
TiO_2	0.97	0.92	1.02	0.96	0.96	1.06	0.89	0.85	0.87	1.04	1.01	1.02
$Al2O_3$	17.36	18.06	15.81	16.37	17.20	17.27	18.14	18.34	17.85	16.51	17.23	19.00
FeOtot	7.35	6.04	6.29	6.53	6.90	5.59	7.44	7.07	5.65	8.12	8.20	8.06
MnO	0.14	0.12	0.11	0.12	0.13	0.09	0.16	0.17	0.13	0.17	0.16	0.17
MgO	3.51	3.59	4.51	3.88	3.25	3.36	3.60	3.61	2.57	4.83	4.84	4.14
CaO	6.47	6.00	5.51	5.77	6.14	4.87	7.36	6.85	5.31	8.19	8.51	8.28
Na_2O	3.72	2.74	3.00	3.19	3.28	3.39	3.35	3.41	4.10	2.96	3.49	3.76
K_2O	4.10	5.32	5.30	4.87	4.01	5.96	2.54	2.38	4.96	1.76	3.18	2.17
P_2O_5	0.45	0.58	0.43	0.42	0.30	0.45	0.34	0.28	0.42	0.26	0.49	0.29
mg#	45.96	51.44	56.09	51.41	45.62	51.72	46.29	47.63	44.80	51.46	51.26	47.78
LOI	0.6	0.8	1.3	1.2	0.9	0.6	1.0	0.9	0.7	0.5	0.3	0.1
Sum	100.1	99.7	99.1	99.5	99.5	100.2	99.6	99.1	100.4	98.7	99.4	99.6
XRF												
Sc		13	29	25	21				29	46	24	
V	169	231	178		191				150		236	221

Cr	92	114	119	72	17	78			33	59	78	23
Ni	40	36	59	34	9	40			8	19	23	
Y	40	36	33	31	29	26			42	34	31	30
Zr	595	428	371	321	210	533			470	237	349	291
La	42	50	82	58	39	83			53	22	42	32
Nb	40	35	31	20	17	33			37	10	22	13
Rb	282	207	358	268	202	415			211	84	101	56
Sr	769	565	504	652	658	516			588	593	903	
Ba	1668	1367	1194	1534	1148	1264			1244	473	1370	798
ICP-MS												
V											264	
Pb	42.00	63.46		61.64	38.45	70.74			37.81	13.98	41.00	24.43
Zr	292.80	285.05		412.16	330.05	472.28	147.75	168.47	387.75	343.16	180.70	170.83
Hf	7.34	7.00		10.48	7.86	12.33	4.03	4.09	9.70	7.99	5.20	4.03
Nb	25.21	28.42		26.30	22.07	46.12	9.08	9.23	26.25	8.79	14.10	8.89
Ta	1.82	1.42		2.15	1.95	3.26	0.57	0.65	2.07	0.66	0.90	0.56
U	14.28	8.59		12.73	13.49	22.38				2.13	3.60	1.53
Y	18.22	25.00		30.08	30.16	26.68	23.36	24.09	29.60	28.30	27.10	27.59
Th	45.88	33.68		48.08	40.11	87.00			45.77	9.80	14.50	7.61
Rb	284.02	256.01		252.57	193.85	388.39	83.75	86.60	232.32	84.52	108.60	52.08
Cs	10.19	10.26		8.68	9.08	17.17	2.69	1.66	5.70	5.78	2.50	1.62
Sr	852.90	536.23		658.54	678.18	515.46	752.98	613.40	631.27	577.07	1014.60	731.17
Ba	2045.35	1262.16		1528.78	1211.83	1195.98	783.47	792.71	1317.23	475.68	1317.00	753.08
La	41.34	40.88		55.09	48.42	71.32	38.39	31.66	51.15	22.77	45.70	29.83
Ce	90.51	83.28		114.52	99.92	143.20	80.63	65.85	108.38	47.03	91.80	62.12
Pr	9.04	8.97		12.47	10.66	13.77	8.78	7.01	11.33	5.36	11.39	7.12
Nd	37.12	38.96		52.63	45.17	56.77	36.38	29.04	47.07	25.26	44.20	31.99
Sm	6.55	7.64		9.92	9.23	9.35	6.75	5.54	8.99	5.58	8.04	5.37
Eu	1.61	1.88		1.68	1.77	1.48	1.83	1.54	1.77	1.62	1.94	1.68
Gd	4.92	4.87		6.51	6.76	4.71	4.83	4.54	6.27	4.90	6.47	5.66
Tb	0.62	0.78		1.01	0.91	0.89	0.71	0.75	0.92	0.85	0.93	0.87
Dy	3.43	4.70		5.65	5.30	4.63	4.16	4.60	5.72	5.02	4.79	5.01
Ho	0.61	0.88		1.07	1.01	0.93	0.81	0.81	1.03	0.96	0.93	0.97
Er	1.80	2.38		2.62	2.92	2.57	2.32	2.28	3.00	2.91	2.51	2.81
Tm	0.27	0.35		0.43	0.40	0.39	0.30	0.39	0.43	0.43	0.42	0.42
Yb	1.79	2.01		2.59	2.62	2.36	2.05	2.25	2.76	2.68	2.32	2.54
Lu	0.36	0.29		0.38	0.45	0.38	0.35	0.37	0.42	0.42	0.35	0.38
ΣREE	524.9	541.1		711.7	642.5	794.6	514.4	442.9	670.4	387.0	615.0	454.7
Eu/Eu*	0.8	0.9		0.6	0.7	0.6	0.9	0.9	0.7	0.9	0.8	0.9
(La/Lu)cn	12.0	14.4		15.1	11.1	19.3	11.3	9.0	12.6	5.7	13.6	8.2
(La/Sm)cn	4.0	3.4		3.5	3.3	4.8	3.6	3.6	3.6	2.6	3.6	3.5
(Gd/Yb)cn	2.2	2.0		2.0	2.1	1.6	1.9	1.6	1.8	1.5	2.3	1.8
(Tb/Lu)cn	1.2	1.8		1.8	1.4	1.6	1.4	1.4	1.5	1.4	1.8	1.6

*Type: GRD= Granodiorites; LMzG= Leucomonzogabbros; MGb= Microgabbros; Mz= Monzonites; QMzd= Quartz monzodiorites; PLMz= Porphyrytic quartz leucomonzonites;

**References: 1 ICP-MS trace elements present study; 2 XRF trace and major elements Christofides (1977); 3 ICP-MS trace elements Christofides (1977); 4 Major & trace elements Sergi (1997)

Xanthi Plutonic Complex									
	Basic group								
Sample	**X-296**	**X-282**	**X-P5**	**X-46**	**X-56**	**X-P4**	**X-P2**	**X-P1**	**X-P3**
Type*	QMzd	QMzd	QMzd	QMzd	QMzd	PLMz	PLMz	PLMz	PLMz
Reference**	1,2	1,2	2	1,2	1,2	2	1,2	2	1,2
SiO_2	53.01	53.86	54.60	55.05	55.86	59.31	60.07	60.46	60.92
TiO_2	0.99	1.01	1.07	1.10	0.92	0.88	0.86	0.83	0.85
$Al2O_3$	16.68	17.98	16.93	17.17	17.45	16.66	17.44	17.24	18.10
FeOtot	8.13	7.90	7.46	7.70	7.11	5.20	4.72	4.58	4.49
MnO	0.18	0.16	0.14	0.15	0.15	0.11	0.09	0.09	0.09
MgO	4.68	4.04	4.10	4.00	3.67	2.71	2.04	2.01	1.95

CaO	8.82	7.58	7.31	7.34	7.00	4.61	4.62	4.02	3.91
Na_2O	2.96	3.65	3.32	3.10	3.42	3.64	3.76	3.73	3.50
K_2O	2.42	2.92	3.67	3.29	3.28	5.20	5.63	5.70	5.85
P_2O_5	0.35	0.42	0.43	0.38	0.39	0.43	0.38	0.38	0.27
mg#	50.65	47.67	49.48	48.06	47.91	48.14	43.56	43.88	43.62
LOI	0.8	0.2	0.4	0.6	0.6	0.4	0.3	0.3	0.5
Sum	99.0	99.7	99.4	99.9	99.8	99.2	99.9	99.4	100.4
XRF									
Sc				-9	16			25	
V	221	214	205	219	191		106		
Cr	48	62	68	52	43	81	64	64	11
Ni	12	20	19	11	6	32	26	22	6
Y	33	28	40	35	34		43		31
Zr	148	332	399	380	365	407	525	476	373
La	43	46	51	49	47		56		58
Nb	13	12	27	26	19		41		22
Rb	108	74	143	121	116	324	364	365	328
Sr	737	794	699	656	648	616	676	661	593
Ba	979	1300	1330	996	979	1350	1327	1370	1464
ICP-MS									
V					195				
Pb	42.73	34.33		34.79	39.00		63.13		53.38
Zr	213.44	177.67		272.79	258.80		723.88		530.44
Hf	5.76	4.16		6.09	7.10		18.48		13.07
Nb	13.99	11.05		19.13	15.10		35.43		33.63
Ta	1.05	0.82		1.47	1.00		4.11		2.66
U	4.92	2.85		5.78	6.00		29.36		16.75
Y	30.13	23.61		27.52	28.40		41.24		29.59
Th	22.28	11.79		25.28	24.20		98.48		64.32
Rb	107.78	74.19		123.05	122.60		342.18		332.74
Cs	6.74	3.89		3.85	3.50		12.39		11.16
Sr	767.62	859.40		696.70	714.20		909.27		638.54
Ba	955.31	1370.09		1120.87	1058.00		2155.91		1548.86
La	43.94	38.50		45.04	48.10		89.00		60.55
Ce	88.67	80.63		91.95	95.60		181.45		117.49
Pr	9.86	8.39		9.65	11.49		18.23		11.97
Nd	42.33	36.28		40.76	43.00		71.10		49.98
Sm	7.52	6.13		7.99	7.50		12.82		9.54
Eu	1.73	1.62		1.74	1.66		1.46		1.40
Gd	6.23	5.28		5.37	6.32		8.77		5.96
Tb	0.98	0.77		0.81	0.94		1.25		0.92
Dy	5.36	4.33		4.77	4.78		7.33		4.78
Ho	1.04	0.78		0.93	0.99		1.42		1.00
Er	2.92	2.40		2.49	2.68		4.16		2.40
Tm	0.42	0.34		0.40	0.46		0.63		0.41
Yb	2.75	2.12		2.54	2.68		3.75		2.41
Lu	0.40	0.28		0.39	0.41		0.64		0.37
ΣREE	593.5	508.5		584.9	625.8		1045.0		708.2
Eu/Eu*	0.8	0.9		0.8	0.7		0.4		0.5
(La/Lu)cn	11.3	14.2		11.9	12.2		14.4		17.1
(La/Sm)cn	3.7	4.0		3.5	4.0		4.4		4.0
(Gd/Yb)cn	1.8	2.0		1.7	1.9		1.9		2.0
(Tb/Lu)cn	1.6	1.9		1.4	1.6		1.3		1.7

*Type: GRD= Granodiorites; LMzG= Leucomonzogabbros; MGb= Microgabbros; Mz= Monzonites; QMzd= Quartz monzodiorites; PLMz= Porphyrytic quartz leucomonzonites;

**References: 1 ICP-MS trace elements present study; 2 XRF trace and major elements Christofides (1977); 3 ICP-MS trace elements Christofides (1977); 4 Major & trace elements Sergi (1997)

	Vrondou pluton											
	GBDR											
Sample	**PVR-8**	**SB55**	**SB95**	**PVR-35**	**PVR-30**	**SB96**	**PVR-12**	**PVR-27**	**PVR-22**	**SB54**	**SB24**	**SB30**
Type*	GBDR	GBDR	GBDR	GBDR	GBDR	GBDR	GBDR	GBDR	GBDR	GBDR	GBDR	GBDR
Reference**	1	3	3	1	1	3	1	1	1	3	3	3
SiO_2	41.30	41.56	41.61	41.64	42.65	43.89	45.63	51.48	52.02	53.25	55.34	55.71
TiO_2	0.91	1.26	1.11	1.22	1.40	1.34	0.83	0.94	0.83	0.67	0.95	0.77
$Al2O_3$	18.09	18.13	17.73	17.89	16.76	17.18	14.11	18.58	18.16	18.56	17.36	17.97
FeOtot	13.17	12.37	13.95	13.28	13.68	14.04	9.29	9.29	6.78	8.33	8.12	7.08
MnO	0.17	0.20	0.17	0.19	0.16	0.16	0.16	0.18	0.10	0.33	0.16	0.22
MgO	8.39	8.40	7.02	6.66	6.92	7.02	6.77	3.56	3.79	3.27	3.51	3.71
CaO	53.16	54.75	47.28	47.19	47.41	47.12	56.48	40.56	49.88	41.16	43.52	48.27
Na_2O	13.75	15.01	14.38	13.74	14.04	11.88	19.74	8.73	8.49	7.98	7.78	7.03
K_2O	1.05	0.98	1.03	1.42	1.13	1.15	1.03	2.92	3.24	4.12	3.11	4.70
P_2O_5	0.25	0.24	0.35	0.41	0.33	0.50	0.21	1.69	3.62	1.29	1.77	1.44
mg#	0.07	0.09	0.24	0.14	0.07	0.24	0.09	0.25	0.26	0.41	0.39	0.24
LOI	1.0	1.0	1.2	1.5	1.0	1.4	0.8	1.0	1.6	1.3	1.1	0.8
Sum	98.2	99.2	98.8	98.1	98.1	98.8	98.7	98.6	98.9	99.5	99.6	99.7
XRF												
Sc	29			34	41		34	20	21			
V	310.2	427.5	405	377.9	361.2	375	185.9	198.9	96.6	217.1	163.1	167.5
Cr	46.5	89.4	43	5.7	48	48	19.9	14.5	149.4	12.8	13.1	16.6
Ni	50.6	78.1	38	31.8	27.6	26	35.7	5.2	91.7	6.5	1.2	2.4
Pb	0			0	3.7	7	1.4	0.5	18.6			
Zr	86.8	37.2	41	99.8	79.5	31	90.7	131.7	186.3	109	117.3	137.2
Nb	4.1	5.5	5	4.9	5.5	3	2.2	7.9	13.5	17.1	8	18
Y	10.5	11.2	14	20.2	19	13	12.4	22.6	21	40	25.5	19.7
Th	0.5	4.6	0	0	0	0	0.2	0.3	18.6	4.6	10.1	10.9
Rb	6	3.9	3	3.6	10.2	14	6.5	40.4	141.5	83.1	58.7	58.4
Sr	754.4	798.5	807	845.8	758.9	819	499.6	699.9	263.8	647.7	647.3	389.8
Ba	85.5	90.3	70	719.8	52.5	50	88	449.8	384.6	116.3	420.1	128
La	4.3	13.1	19	9	3.8	16	4.1	21.4	23.5	20.8	21.4	47.2
Ce	6.5	4	2	13.9	0	2	12.5	44	62.4	40.1	26	49.5
Nd	9.3			17.4	8.7		7	23.3	20			
ICP-MS												
Sc						30.30						
V	371			439	426	409.20	211	220	233			
Cr						17.05						
Ni	25.40			13.70	10.30	37.29	8.80	0.90	4.20			
Pb	2.20	5.70	7.00	2.40	3.90	4.68	1.50	2.20	1.20	13.60	11.00	15.10
Zr	24.20			31.90	13.90	12.67	55.70	149.40	110.30			
Hf	1.00			1.40	0.70	0.53	2.20	4.10	3.20			
Nb	1.60			3.00	2.00	1.91	0.70	5.00	5.20			
Ta	0.10			0.20	0.20	0.15	0.10	0.40	0.40			
U	0.20			0.40	0.60	0.50	0.40	1.60	1.80			
Y	9.70			19.90	18.70	13.58	10.10	22.60	23.00			
Th				0.50	0.90	0.75	0.80	5.30	7.40			
Rb	6.80			4.10	9.80	11.57	6.80	46.20	147.20			
Cs	0.60			0.10	0.30	0.38	0.20	0.70	3.00			
Sr	809.40			931.60	762.80	756.04	530.30	708.20	909.40			
Ba	70.00			651.00	41.00	43.51	66.00	476.00	490.00			
La	4.30		6.51	9.00	3.80	3.47	4.10	21.40	23.50			48.89
Ce	10.90		13.71	23.00	10.50	8.68	10.70	46.80	50.80			75.91
Pr	1.51			3.43	1.71	1.29	1.61	5.63	6.20			
Nd	6.80		11.04	17.30	9.90	7.82	8.20	23.60	25.30			27.57
Sm	1.82		3.32	4.01	3.07	2.68	1.99	4.80	5.23			7.53
Eu	0.63		0.78	1.22	0.90	0.87	0.60	1.40	1.40			0.89
Gd	1.85			4.10	3.66	2.46	1.99	4.61	4.63			
Tb	0.31		0.41	0.64	0.63	0.39	0.32	0.74	0.74			0.71
Dy	1.78			3.75	3.60	2.62	1.87	4.27	4.18			

Ho	0.37			0.76	0.71	0.53	0.39	0.87	0.80			
Er	1.01			2.17	1.94	1.41	1.11	2.43	2.38			
Tm	0.15			0.30	0.28	0.18	0.17	0.37	0.36			
Yb	0.96		1.46	1.93	1.65	1.42	1.12	2.36	2.28			2.93
Lu	0.15		0.24	0.29	0.23	0.15	0.20	0.35	0.33			0.49
ΣREE	32.5		37.5	71.9	42.6	34.0	34.4	119.6	128.1			164.9
Eu/Eu*	1.0			0.9	0.8	1.0	0.9	0.9	0.9			
(La/Lu)cn	3.0		2.8	3.2	1.7	2.4	2.1	6.4	7.4			10.4
(La/Sm)cn	1.5		1.2	1.4	0.8	0.8	1.3	2.8	2.8			4.1
(Gd/Yb)cn	1.6			1.7	1.8	1.4	1.4	1.6	1.6			
(Tb/Lu)cn	1.4		1.2	1.5	1.9	1.8	1.1	1.4	1.5			1.0

*Type: GBDR= Gabbrodiorites; MME= Mafic microgranular enclaves; MZ= Monzonites; QMZ= Quartz monzonites; QSY-GR= Quartz syenites and granites

**References: 1 Major & trace elements present study; 2 Major and trace elements Soldatos et al. (1998); 3 Trace elements Soldatos unpublished data; 4 Trace elements present study

Vrondou pluton

	GBDR	High-K MME										
Sample	**SB60**	**SB38X**	**PVR-32**	**K1X**	**SB70X**	**SB-88X**	**PVR-29**	**PVR-33**	**SB89X**	**SB90X**	**K3X**	**SB34X**
Type*	GBDR	High-K MME	High-K MME	High-K MME	High-K MME	High-K MME	High-K MME	High-K MME	High-K MME	High-K MME	High-K MME	High-K MME
Reference **	3	2,3	1	3	2,3	3	1	1	2,3	3	3	2,3
SiO_2	57.11	51.02	52.91	53.42	54.23	54.45	54.59	55.78	56.30	57.05	57.86	57.98
TiO_2	0.18	1.35	0.90	0.72	0.78	0.88	0.91	0.80	0.68	0.75	0.67	0.82
$Al2O_3$	21.67	5.50	17.56	12.75	16.07	17.35	17.20	17.31	17.02	16.84	17.03	15.86
FeOtot	3.69	7.71	7.57	7.87	7.15	6.02	6.85	6.15	5.98	6.43	5.77	5.35
MnO	0.20	0.43	0.23	0.36	0.19	0.15	0.17	0.15	0.14	0.15	0.16	0.14
MgO	0.69	8.88	4.28	4.99	4.57	3.40	4.10	3.01	2.80	2.64	2.51	3.50
CaO	25.00	67.23	50.19	53.03	53.24	50.16	51.62	46.60	45.47	42.23	43.65	53.80
Na_2O	9.65	17.45	7.48	10.36	6.90	6.25	7.18	6.27	6.35	5.68	5.78	5.66
K_2O	4.87	0.71	3.96	3.08	2.86	4.31	3.71	3.94	3.69	4.32	3.41	3.40
P_2O_5	0.81	3.09	3.06	4.91	5.48	3.59	3.18	4.52	5.10	4.33	4.91	5.79
mg#	0.35	1.48	0.20	0.30	0.29	0.47	0.29	0.32	0.50	0.40	0.43	0.43
LOI	0.5	1.5	0.7	0.8	1.0	0.9	0.7	0.7	0.9	0.9	1.1	0.5
Sum	99.7	99.2	98.8	99.5	99.5	97.7	98.9	98.9	99.4	99.5	99.6	99.4
XRF												
Sc			25				22	17				
V	99.8	158	185.3	162	121	156	183.7	147.4	147	153	179	127
Cr	3.1	114	21.9	183	127	24	41	24	22	16	10.3	77
Ni	0	48	10.3	34.9	35	8	10.2	8.7	14	8	8.9	29
Pb		8	11.2		25	19	17.1	12.4	34			32
Zr	87.1	185	153.9	140	167	222	193.2	182.4	243	183	184	238
Nb	10.3	75	9.7	14.7	12	16	14	18	16	15	16.9	23
Y	1.5	111	17.9	21	20	27	20.7	27.2	26	28	25	22
Th	17.5	39	4.2	9.3	5		12.2	11.9	23	20	16.7	28
Rb	23.4	133	160.6	245	287	141	150.6	171.6	263	234	238	303
Sr	1253.4	146	499.7	489	609	592	448.2	550.6	547	409	511	608
Ba	834.5	466	611.8	809	784	555	562.2	742.4	998	550	1068	1305
La	39.8	135	23.6	39	34	52	33.8	46.9	61	71	46	70
Ce	54.5	259	42.7	24	37		56.5	84.1	55	57	49	134
Nd			16.3				19.2	23.4				
ICP-MS												
Sc		32.88			20.43				11.64			15.03
V		179.3	214		156.0	194.05	215.00	173	176.19			157.77
Cr		106.3			114.6				16.57			68.66
Ni		24.61	3.70		36.85	15.03	4.80	3.20	17.12			16.84
Pb	14.10	11.92	5.40	25.00	17.22		5.30	6.80	23.53	30.00	26.00	23.78
Zr		201.2	147.30		181.1	230.43	203.90	212.50	218.08			228.73
Hf		7.69	3.90		4.13	5.35	5.90	6.00	5.20			6.34

Nb	65.84	8.60		12.57	14.82	12.40	16.50	15.25			24.91
Ta	5.04	0.40		0.54	0.72	0.60	1.20	0.87			1.22
U	13.39	5.50		2.47	3.68	5.40	5.00	5.26			9.82
Y	99.48	17.80		24.38	23.80	18.70	25.50	18.17			18.77
Th	50.35	6.70		7.76	12.73	12.70	15.50	15.87			23.73
Rb	119.7	164.60		262.1	123.91	155.20	179.20	245.26			313.71
Cs	1.39	2.40		3.28	1.38	4.30	2.30	4.00			4.84
Sr	145.1	525.20		551.8	538.17	447.70	559.10	455.22			575.14
Ba	326.4	590.00		722.7	526.61	546.00	746.00	949.47			1235.56
La	136.8	23.60		28.14	48.36	33.80	46.90	40.17	69.72	57.44	66.43
Ce	278.7	39.20		45.69	74.27	59.00	86.10	63.53	65.22	70.88	142.87
Pr	32.73	4.29		5.65	7.64	6.28	8.71	6.51			15.69
Nd	141.2	16.80		26.00	31.57	24.60	32.10	26.54	30.10	26.48	62.34
Sm	27.43	3.39		5.59	6.06	4.56	5.41	4.99	7.56	6.65	9.92
Eu	4.37	0.63		1.06	1.21	0.82	1.18	0.86	1.02	0.88	1.83
Gd	20.72	3.31		4.34	4.64	4.17	4.58	3.61			5.70
Tb	2.90	0.53		0.67	0.68	0.64	0.74	0.52	0.68	0.63	0.65
Dy	18.60	3.28		4.25	4.14	3.64	4.23	3.14			3.75
Ho	3.45	0.65		0.84	0.82	0.71	0.85	0.62			0.68
Er	9.85	1.90		2.49	2.40	1.99	2.59	1.79			1.79
Tm	1.33	0.28		0.36		0.30	0.40	0.26			0.24
Yb	10.19	1.79		3.13	2.77	1.92	2.61	2.16	2.14	2.40	1.92
Lu	1.31	0.30		0.42	0.39	0.29	0.43	0.28	0.38	0.40	0.25
ΣREE		689.8	100.0		128.6	185.3	142.7	196.8	155.0	176.8	165.8
Eu/Eu*		0.5	0.6		0.6	0.7	0.6	0.7	0.6		
(La/Lu)cn		10.8	8.2		7.0	12.8	12.1	11.3	15.0	19.1	14.9
(La/Sm)cn		3.1	4.4		3.2	5.0	4.7	5.5	5.1	5.8	5.4
(Gd/Yb)cn		1.6	1.5		1.1	1.4	1.8	1.4	1.3		
(Tb/Lu)cn		1.5	1.2		1.1	1.2	1.5	1.2	1.3	1.2	1.1

*Type: GBDR= Gabbrodiorites; MME= Mafic microgranular enclaves; MZ= Monzonites; QMZ= Quartz monzonites; QSY-GR= Quartz syenites and granites
**References: 1 Major & trace elements present study; 2 Major and trace elements Soldatos et al. (1998); 3 Trace elements Soldatos unpublished data; 4 Trace elements present study

Vrondou pluton												
	Low-K MME											
Sample	**TS29X**	**SB49X**	**PVR-31**	**SB50X**	**PVR-26**	**TS27X**	**PVR-13**	**SB-77X**	**PVR-25**	**SB65X**	**B7X**	**SB8**
Type*	Low-K MME	Low-K MME	Low-K MME	Low-K MME	Low-K MME	Low-K MME	Low-K MME	Low-K MME	Low-K MME	Low-K MME	Low-K MME	Low -K
Reference **	3	2,3	1	2,3	1	3,4	1	2,3	1	2,3	2,3	3
SiO_2	41.99	50.22	50.81	51.32	51.68	52.08	52.32	52.36	52.54	53.19	53.82	54.2
TiO_2	1.05	0.73	0.96	0.73	0.94	0.87	1.00	0.94	0.79	0.77	0.93	0.78
$Al2O_3$	21.36	18.70	18.05	19.76	18.87	18.25	18.47	17.80	18.31	18.33	18.08	17.3
FeOtot	9.85	8.40	9.06	8.19	9.08	8.48	8.39	6.51	7.91	7.65	8.02	7.76
MnO	0.17	0.30	0.20	0.25	0.19	0.26	0.29	0.18	0.34	0.26	0.35	0.20
MgO	6.74	5.42	3.94	3.81	3.47	4.37	3.27	3.73	3.85	4.29	3.19	3.70
CaO	54.94	53.49	43.65	45.33	40.51	47.88	40.99	50.53	46.45	49.98	41.46	45.9
Na_2O	16.63	8.19	8.84	8.26	8.87	8.88	7.77	7.53	8.11	7.69	8.00	7.65
K_2O	0.79	4.05	3.74	5.03	3.10	4.38	4.76	3.41	4.97	5.30	4.70	5.31
P_2O_5	0.10	1.30	1.79	1.03	1.51	0.75	1.07	2.52	0.81	0.72	1.14	1.00
mg#	0.07	0.19	0.38	0.27	0.25	0.21	0.22	0.53	0.20	0.22	0.28	0.32
LOI	0.7	1.6	0.9	0.4	0.7	1.1	1.2	1.2	1.1	0.7	1.1	1.0
Sum	99.4	99.1	98.7	99.1	98.7	99.6	98.8	96.7	98.9	99.1	99.6	99.3
XRF												
Sc			15		19		16		21			
V	442.4	179	188.9	207	205.6	194.6	180	154	225.7	137	215	164
Cr	67.2	21	16	20	14.7	15.3		16	18.4	19	11.8	14
Ni	22.5	15	4.8	5	2.8	4.5	4.6	4	10.5	6	2.6	
Pb		16		14	4.2		98.3	12	19.2	10	19	15

Zr	25.3	102	203.9	63	163	101.1	177.8	161	86.7	155	181	151
Nb	2.1	8	12.5	11	9.3	5.3	26.8	12	12.1	18	31	14
	4.5	28	30.1	32	28.5	12.4	37.5	27	28	36	47	25
Th	0	5	2.9	6	0.4	10.3	13.5		10.5	12	15.1	15
Rb	3.9	118	54.6	68	34	28	54.8	71	48.2	30	52	24
Sr	928.6	538	791.4	599	770.5	527.5	406.7	853	267.4	514	439	365
Ba	54	41	490.2	43	450.3	52.8	80.6	650	37.3	69	175	81
La	6.5	19	34.6	17	20.3	28.1	40.2	45	23.7	43	44	65
Ce	4	19	61.8	31	41.3	22.9	70.9		43.5	66	93	50
Nd			29.3		22.7		32.7		15.7		42.20667	
ICP-MS												
Sc		17.41		12.01						18.35	18.65	16.0
V		209.35	227.00	222.44	231.00	202.00	207.00	205.73	257.00	160.76	204.96	222.
Cr		20.06		10.51						25.25	13.18	16.5
Ni		18.18	2.10	14.31	0.60		1.60	8.75	3.30	16.53	11.28	12.2
Pb		7.25	4.00	9.42	4.10	14.70	109.50		2.20	7.53	11.52	12.3
Zr		83.47	165.60	48.65	127.40	60.70	179.30	157.29	91.20	126.19	186.70	159.
Hf		2.17	5.00	1.56	3.40	1.90	5.40	3.94	3.00	3.13	4.93	3.99
Nb		6.27	11.80	7.93	5.40	6.60	25.80	9.68	10.30	15.75	23.98	12.7
Ta		0.25	0.90	0.34	0.40	0.60	2.20	0.58	0.60	0.64	1.53	0.58
U		2.41	3.30	1.98	1.30	2.70	5.30	2.53	5.20	3.86	5.31	5.04
Y		15.58	34.00	20.92	25.80	12.30	41.40	26.82	30.40	22.02	36.57	19.9
Th		3.17	9.40	4.52	4.70	7.00	13.20	8.39	12.20	8.50	15.00	15.7
Rb		101.74	57.80	61.22	37.40	31.90	61.80	64.76	50.10	26.27	58.73	20.6
Cs		2.51	0.70	2.23	0.70	1.40	3.30	0.53	1.40	1.14	2.63	0.67
Sr		445.03	843.00	533.16	797.30	509.70	443.20	779.45	297.80	449.49	426.31	327.
Ba		26.98	475.00	23.25	447.00	37.00	81.00	620.71	31.00	31.64	80.99	49.4
La		16.51	34.60	19.88	20.30	30.40	40.20	33.89	23.70	39.43	42.62	50.8
Ce		35.42	80.80	46.33	50.00	46.60	109.30	63.26	55.40	75.48	91.50	67.5
Pr		3.90	9.63	5.23	6.33	4.21	12.29	7.52	6.52	7.19	10.20	6.19
Nd		16.52	39.30	22.35	26.10	14.80	42.40	34.48	26.20	26.84	35.88	22.6
Sm		3.22	7.36	4.66	5.76	2.32	7.65	6.88	4.99	4.64	7.87	4.32
Eu		0.83	1.91	1.14	1.64	0.84	2.13	1.75	1.21	1.23	2.34	0.95
Gd		2.63	6.42	3.74	5.23	2.18	6.44	5.60	4.61	3.57		3.49
Tb		0.39	1.05	0.56	0.82	0.34	1.08	0.80	0.75	0.54	0.94	0.49
Dy		2.48	5.96	3.67	4.54	1.89	6.48	5.02	4.48	3.46	6.21	3.42
Ho		0.52	1.19	0.71	0.94	0.41	1.39	0.96	0.94	0.77	1.22	0.65
Er		1.48	3.46	2.08	2.59	1.40	4.31	2.73	3.00	2.17	3.66	2.01
Tm		0.23	0.52	0.30	0.39	0.20	0.71		0.49	0.35	0.56	0.29
Yb		2.11	3.23	2.61	2.51	1.60	4.97	2.95	3.63	2.84	4.92	2.59
Lu		0.29	0.49	0.35	0.37	0.29	0.80	0.37	0.62	0.45	0.67	0.35
ΣREE			86.5	195.9	113.6	127.5	107.5	240.2	166.6	136.5	169.0	208.
Eu/Eu*			0.8	0.8	0.8	0.9	1.1	0.9	0.8	0.8	0.9	
(La/Lu)c			5.9	7.3	5.9	5.7	10.9	5.2	9.5	4.0	9.1	6.6
(La/Sm)c			3.2	3.0	2.7	2.2	8.2	3.3	3.1	3.0	5.3	3.4
(Gd/Yb)c			1.0	1.6	1.2	1.7	1.1	1.0	1.5	1.0	1.0	
(Tb/Lu)c			0.9	1.5	1.1	1.5	0.8	0.9	1.5	0.8	0.8	0.9

*Type: GBDR= Gabbrodiorites; MME= Mafic microgranular enclaves; MZ= Monzonites; QMZ= Quartz monzonites; QSY-GR= Quartz syenites and granites
**References: 1 Major & trace elements present study; 2 Major and trace elements Soldatos et al. (1998); 3 Trace elements Soldatos unpublished data; 4 Trace elements present study

Vrondou pluton												
	Low-K MME							**MZ**				
Sample	**SB29X**	**SB30X**	**SB58X**	**SB07X**	**PVR-28**	**SB69X**	**PVR-20**	**SB47**	**TS04**	**SB37**	**SB38**	**SB77**
Type*	Low-K MME	Low-K MME	Low-K MME	Low-K MME	Low-K MME	Low-K MME	Low-K MME	MZ	MZ	MZ	MZ	MZ
Reference **	3	3	3	3	1	3	1	2,3	3	3	2,3	3
SiO_2	54.75	54.95	55.13	55.78	56.26	57.02	57.45	55.33	55.72	56.22	56.41	56.58

TiO_2	0.65	0.70	0.75	0.72	0.74	0.75	0.57	1.03	0.91	0.60	0.60	0.63
$Al2O_3$	18.67	18.68	18.11	17.94	17.35	17.78	17.92	13.93	15.83	17.93	18.02	17.04
FeOtot	6.01	6.79	7.13	6.96	6.84	6.94	5.81	8.25	8.77	5.41	4.74	5.52
MnO	0.20	0.20	0.25	0.28	0.18	0.29	0.14	0.14	0.24	0.14	0.13	0.14
MgO	2.78	4.00	3.63	2.65	3.43	2.89	2.00	3.81	2.64	3.02	3.32	2.67
CaO	45.18	51.20	47.58	40.40	47.19	42.58	38.00	45.13	34.91	49.87	55.50	46.31
Na_2O	8.91	6.62	7.20	7.21	7.09	6.36	5.80	6.30	5.22	7.69	6.73	6.62
K_2O	4.03	4.92	4.50	4.67	3.98	4.25	4.95	1.37	3.48	3.47	3.74	3.55
P_2O_5	2.59	1.45	1.68	1.92	2.16	1.88	2.60	7.56	5.24	4.26	5.11	5.60
mg#	0.42	0.26	0.25	0.32	0.15	0.39	0.30	0.88	0.61	0.52	0.40	0.47
LOI	0.6	0.7	0.9	1.2	0.8	0.9	1.6	0.5	0.8	0.5	0.3	0.7
Sum	99.6	99.2	99.6	99.7	99.0	99.4	99.1	99.1	99.5	99.7	99.5	99.5
XRF												
Sc					16		6					
V	211.7	168	179.7	147	161	123.9	69.1	229	140.8	156.1	131	148
Cr	11.4	19	11.6	9.9	18	8.1	0	26	17.8	35.8	55	40
Ni	0	1	4.3	6	8.7	6.1	4.7	33	13.2	11.6	25	9
Pb		8			14.5		11.5	44			27	
Zr	107.5	140	127.9	202	129.7	136.8	133.9	259	404.5	182.3	186	156
Nb	14	15	16.2	15.9	10.9	14.7	11.8	18	25	11.3	12	10
Y	17.2	21	11.3	30	14.7	21.2	18.4	26	45.1	20.8	21	16
Th	15.5	11	6.2	13.3	8.3	11	11.7	30	22.6	17.1	23	18
Rb	82.1	59	77.3	61	78.8	139.7	153.8	386	180.4	192.9	233	195
Sr	791.1	375	426.6	532	388.1	439.4	406.8	704	1308.	776.9	722	723
Ba	538.7	122	185.8	278	622.1	186.7	949.8	1072	1626.	1355.	1281	1285
La	45.8	42	34.9	45	26.3	23.8	42.4	40	47.2	35.9	30	38
Ce	53	50	31.5	76	57.1	19.6	83.7	77	101.5	58.8	50	48
Nd					16.3		17.4					
ICP-MS												
Sc		19.85						29.84			9.98	
V		189.55			205.00		140.00	237.2			170.4	
Cr		13.66						19.23			47.21	
Ni		14.59			3.00		1.90	13.42			13.42	
Pb	19.10	8.17	10.00	30.00	9.50	11.70	14.30	30.73	36.90	19.10	23.86	22.00
Zr		144.67			140.80		148.80	266.7			182.3	
Hf		3.72			3.70		4.00	6.86			4.41	
Nb		15.64			9.90		11.40	17.72			14.68	
Ta		0.43			0.70		1.00	0.87			0.75	
U		7.25			7.10		9.90	10.85			7.09	
Y		14.33			13.60		25.00	27.73			17.18	
Th		8.86			8.80		27.20	29.67			20.21	
Rb		56.88			84.10		150.70	349.6			230.2	
Cs		0.38			1.50		1.80	5.31			3.79	
Sr		367.82			407.70		327.50	709.3			718.8	
Ba		100.21			620.00		426.00	1100.			1314.	
La		44.64		54.32	26.30		42.40	38.00	72.02	41.87	37.32	39.94
Ce		61.25		99.61	45.40		81.20	78.22	139.1	65.95	65.67	61.83
Pr		5.18			4.43		8.78	10.16			6.99	
Nd		17.96		33.93	14.80		32.70	49.24	61.80	26.15	29.60	26.15
Sm		3.16		7.36	2.76		5.63	10.67	14.28	6.34	5.57	6.29
Eu		0.73		1.50	0.81		1.02	2.15	2.54	1.14	1.35	1.18
Gd		2.13			2.46		4.63	7.24			3.63	
Tb		0.34		0.77	0.41		0.74	0.95	1.27	0.57	0.49	0.56
Dy		2.38			2.35		4.20	5.52			3.13	
Ho		0.52			0.47		0.87	0.98			0.59	
Er		1.58			1.39		2.52	2.72			1.68	
Tm		0.24			0.22		0.38	0.35			0.25	
Yb		2.06		3.66	1.55		2.57	2.68	3.74	2.02	1.98	1.93
Lu		0.31		0.60	0.27		0.40	0.34	0.53	0.35	0.26	0.35
ΣREE		142.5		201.8	103.6		188.0	209.2	295.4	144.4	158.5	138.2

Eu/Eu*	0.8			0.9		0.6	0.7	0.9	1.0	0.9	
(La/Lu)cn	14.8		9.4	10.1		11.0	11.5	14.1	12.4	15.2	11.9
(La/Sm)c	8.9		4.6	6.0		4.7	2.2	3.2	4.2	4.2	4.0
(Gd/Yb)c	0.8			1.3		1.5	2.2	0.0	0.0	1.5	
(Tb/Lu)c	0.7		0.9	1.0		1.3	1.9	1.6	1.1	1.3	1.1

*Type: GBDR= Gabbrodiorites; MME= Mafic microgranular enclaves; MZ= Monzonites; QMZ= Quartz monzonites; QSY-GR= Quartz syenites and granites

**References: 1 Major & trace elements present study; 2 Major and trace elements Soldatos et al. (1998); 3 Trace elements Soldatos unpublished data; 4 Trace elements present study

Vrondou pluton												
	MZ											
Sample	**SB35**	**SB36**	**SB39**	**SB33**	**SB74**	**K3**	**SB31**	**L3**	**SB70**	**SB71**	**SB93**	**SB86**
Type*	MZ	MZ	MZ	MZ	MZ	MZ	MZ	MZ	MZ	MZ	MZ	MZ
Reference**	3	3	3	3	2,3	3	3	3	2,3	2,3	2,3	3
SiO_2	58.01	58.02	58.57	58.95	59.00	59.29	59.40	59.79	60.43	60.84	61.09	61.41
TiO_2	0.57	0.58	0.47	0.58	0.48	0.67	0.55	0.73	0.47	0.45	0.56	0.52
$Al2O_3$	18.59	17.44	18.09	17.83	17.57	15.91	18.13	16.11	17.05	17.21	16.40	16.55
FeOtot	4.50	4.36	4.16	4.31	4.50	5.71	5.19	5.32	5.00	4.52	5.00	4.45
MnO	0.12	0.14	0.11	0.12	0.11	0.18	0.13	0.17	0.13	0.11	0.12	0.11
MgO	2.37	2.29	2.11	2.45	1.53	1.98	2.39	2.31	1.63	1.66	2.10	1.75
CaO	48.41	48.34	47.45	50.32	37.71	38.18	45.05	43.60	36.75	39.54	42.82	41.20
Na_2O	6.66	6.03	6.09	5.54	6.06	6.69	6.21	5.07	5.19	5.07	4.99	4.98
K_2O	3.68	3.97	3.66	3.83	4.19	3.90	2.62	3.70	3.36	3.84	3.49	3.95
P_2O_5	4.35	6.14	5.66	5.23	5.47	4.40	4.25	5.22	5.57	5.18	4.79	5.07
mg#	0.45	0.35	0.40	0.35	0.32	0.26	0.34	0.58	0.31	0.24	0.31	0.30
LOI	0.5	0.6	0.5	0.7	0.3	0.6	0.6	0.7	0.4	0.5	0.6	0.5
Sum	99.8	99.9	99.8	99.9	99.5	99.6	99.8	99.7	99.5	99.6	99.5	99.6
XRF												
Sc												
V	134.3	110.4	116.6	122.8	136	121	131.6	129	124	99	90	88
Cr	17.7	27.3	18.5	32.1	14	37	10.3	18.9	13	19	28	18
Ni	10.7	21.6	6.8	15.7	6	13	9.9	7.4	12	17	5	5
Pb					22				21	17	27	
Zr	93.4	173.2	150	208.9	176	188	160.7	341	251	271	206	184
Nb	8.4	29.7	11.2	11.3	18	16.6	15.2	22	20	19	14	16
Y	18.8	25	20.3	20.9	23	27	25.2	32	30	25	20	21
Th	11.4	22.2	13.8	7.7	22	20	18.2	24	31	26	21	21
Rb	159.6	310.7	229.4	238.5	203	151	199.6	153	251	233	184	167
Sr	801.5	583.8	702.6	572	770	610	713.1	1117	655	599	566	605
Ba	1597.7	984.9	1270.5	1084.8	1331	994	834.8	1294	746	802	1036	1090
La	23.1	56.9	26	36.5	54	37	37	54	41	51	53	53
Ce	47.1	78.1	52.8	49.6	68	52	52.6	110	84	66	62	65
Nd												
ICP-MS												
Sc					5.11				7.23	11.32	12.10	
V					132.14				113.60	105.75	107.92	
Cr					18.28				18.18	16.70	25.27	
Ni					11.47				17.13	13.59	15.64	
Pb	18.40	49.90	23.50	39.50	14.87	25.00	18.80	27.00	13.45	15.19	18.63	34.00
Zr					176.47				299.85	307.34	201.91	
Hf					3.54				7.14	7.45	4.85	
Nb					16.96				19.62	19.79	13.49	
Ta					1.01				1.66	1.53	0.83	
U					3.95				10.36	13.17	4.91	
Y					22.43				28.33	23.44	16.31	
Th					16.63				43.46	40.69	16.39	
Rb					170.29				218.60	225.67	150.32	
Cs					1.03				2.29	3.06	2.30	
Sr					680.66				606.17	531.15	481.49	

Ba					1269.45				711.25	748.39	986.61
La	40.71			40.58	43.49				46.69	48.87	36.76
Ce	62.03			65.60	71.14				76.71	82.90	60.64
Pr					8.19				8.50	8.61	6.25
Nd	23.57			24.03	32.53				35.67	34.59	25.65
Sm	6.33			5.78	5.61				6.52	5.88	4.50
Eu	1.08			1.12	1.27				1.19	1.07	1.03
Gd					4.36				4.96	4.43	3.43
Tb	0.55			0.49	0.63				0.67	0.62	0.48
Dy					3.63				4.40	3.91	2.83
Ho					0.73				0.90	0.78	0.54
Er					2.16				2.79	2.36	1.55
Tm					0.32				0.41	0.35	0.22
Yb	1.93			1.99	2.38				3.33	3.02	1.86
Lu	0.33			0.33	0.31				0.47	0.42	0.25
ΣREE	136.5			139.9	176.8				193.2	197.8	146.0
Eu/Eu*	0.9			1.0	0.8				0.6	0.6	0.8
(La/Lu)cn	12.8			12.8	14.6				10.2	12.0	15.2
(La/Sm)cn	4.0			4.4	4.9				4.5	5.2	5.1
(Gd/Yb)cn	0.0			0.0	1.5				1.2	1.2	1.5
(Tb/Lu)cn	1.1			1.0	1.4				1.0	1.0	1.3

*Type: GBDR= Gabbrodiorites; MME= Mafic microgranular enclaves; MZ= Monzonites; QMZ= Quartz monzonites; QSY-GR= Quartz syenites and granites

**References: 1 Major & trace elements present study; 2 Major and trace elements Soldatos et al. (1998); 3 Trace elements Soldatos unpublished data; 4 Trace elements present study

Vrondou pluton												
	MZ											
Sample	**SB73**	**SB07**	**BA1**	**SB42**	**SB32**	**SK7**	**SB82**	**SB91**	**K2**	**PVR-20H**	**K1**	**SB34**
Type*	MZ	MZ	MZ	MZ	MZ	MZ	MZ	MZ	MZ	MZ	MZ	MZ
Reference**	2,3	3	3	3	3	3	3	2,3	3	1	3	2,3
SiO_2	62.82	63.86	64.31	64.47	64.53	64.54	64.69	64.77	65.06	65.28	65.33	65.80
TiO_2	0.44	0.41	0.43	0.38	0.33	0.36	0.47	0.44	0.59	0.38	0.39	0.27
Al2O$_3$	16.31	16.28	15.94	16.63	17.76	16.42	15.93	15.91	13.24	16.11	16.29	17.57
FeOtot	3.75	4.03	3.57	3.14	2.71	3.46	2.86	3.48	4.29	3.37	3.18	2.44
MnO	0.11	0.14	0.14	0.10	0.09	0.14	0.08	0.10	0.14	0.09	0.12	0.07
MgO	1.48	0.87	1.37	1.57	0.74	0.35	1.57	1.48	1.11	1.41	1.29	0.92
CaO	41.26	27.76	40.60	47.15	32.74	15.28	49.44	43.13	31.55	42.74	41.92	40.20
Na_2O	4.43	4.83	4.82	4.47	3.33	4.07	4.97	4.45	5.12	4.13	4.12	2.58
K_2O	3.92	3.96	3.92	3.75	4.18	4.79	3.55	3.63	3.69	3.58	3.83	4.30
P_2O_5	5.42	4.73	4.61	4.63	5.53	4.88	4.78	4.68	5.66	4.17	4.61	5.25
mg#	0.25	0.16	0.20	0.21	0.19	0.10	0.21	0.24	0.14	0.14	0.17	0.12
LOI	0.7	0.4	0.5	0.5	0.5	0.6	0.6	0.4	0.6	0.7	0.5	0.4
Sum	99.7	99.6	99.8	99.9	99.9	99.7	99.7	99.6	99.7	99.4	99.8	99.7
XRF												
Sc										6		
V	87	52	77	84.6	25.2	61	83	60	61	205.8	87	31
Cr	21	1.7	6.4	10	8.2	5.8	19	16	8.2	0	6.3	7
Ni	12	0.4	6.4	6.6	8.8	2.9	9	6	6.1	8.4	5.1	13
Pb	19							28		0		28
Zr	166	224	187	151.5	411.7	197	164	150	187	162.6	162	401
Nb	15	12.1	16.6	15.1	29.3	12.7	11	14	2.7	8.3	14.7	22
Y	19	23	22	21.8	31.1	21	19	20	20	24.9	19.1	21
Th	20	13.3	18.4	16.2	80.6	27	19	23	22	1	19.4	68
Rb	210	165	202	200.9	272.8	187	159	207	200	140	222	267
Sr	532	634	487	467.6	477.5	504	438	429	395	855.6	461	449
Ba	951	1070	827	860.9	807.7	711	949	822	811	511.2	898	858
La	28	36	39	31.6	43.2	38	47	49	47	31.5	37	50
Ce	33	51	48	37.5	81.8	62	40	46	46	51.5	46	91

Nd										13.5		
ICP-MS												
Sc	5.80							8.31				-
V	95.86							83.56		82.00		44.72
Cr	24.25							30.62				21.43
Ni	15.84							12.14		1.30		-
Pb	14.18	23.00	23.00	23.90	33.80	26.00	29.00	16.63	28.00	4.40	23.00	30.45
Zr	176.93							139.54		137.70		376.75
Hf	4.25							3.47		4.10		8.06
Nb	14.26							13.53		8.80		23.91
Ta	0.92							0.87		1.10		1.26
U	5.90							5.95		12.20		19.79
Y	17.54							16.85		13.90		16.63
Th	25.36							19.27		31.10		59.49
Rb	198.00							180.47		155.50		293.66
Cs	1.54							1.99		1.70		5.39
Sr	458.71							328.05		428.10		367.00
Ba	922.92							724.82		994.00		724.57
La	37.00			43.91				36.03		31.50		42.62
Ce	59.77			72.82				61.51		55.20		73.46
Pr	6.13							6.02		5.23		7.02
Nd	24.98			22.41				22.30		17.40		26.51
Sm	4.43			5.80				4.07		2.78		4.06
Eu	0.97			0.93				0.89		0.79		0.95
Gd	3.34							3.24		2.26		2.96
Tb	0.49			0.57				0.42		0.39		0.46
Dy	3.09							2.83		2.14		2.76
Ho	0.56							0.54		0.45		0.53
Er	1.76							1.73		1.36		1.60
Tm	0.25							0.25		0.22		0.25
Yb	2.13			2.32				1.84		1.57		2.08
Lu	0.26			0.39				0.25		0.24		0.31
ΣREE	145.1			149.2				141.9		121.5		165.6
Eu/Eu*	0.7			0.9				0.7		0.9		0.8
(La/Lu)cn	15.0			11.7				14.9		13.6		14.3
(La/Sm)cn	5.3			4.8				5.6		7.1		6.6
(Gd/Yb)cn	1.3			0.0				1.4		1.2		1.1
(Tb/Lu)cn	1.3			1.0				1.1		1.1		1.0

*Type: GBDR= Gabbrodiorites; MME= Mafic microgranular enclaves; MZ= Monzonites; QMZ= Quartz monzonites; QSY-GR= Quartz syenites and granites
**References: 1 Major & trace elements present study; 2 Major and trace elements Soldatos et al. (1998); 3 Trace elements Soldatos unpublished data; 4 Trace elements present study

Vrondou pluton												
	QMZ											
Sample	**SB29**	**SK9**	**SB66**	**SK8**	**SB05**	**PVR-6**	**SB67**	**SB45**	**SB49**	**PVR-24**	**SB50**	**TS37**
Type*	QMZ	QMZ	QMZ	QMZ	QMZ	QMZ	QMZ	QMZ	QMZ	QMZ	QMZ	QMZ
Reference**	3	3	3	3	3	1	3	3	3	1	3,4	3
SiO_2	59.93	60.21	61.87	62.08	62.20	62.75	63.97	64.20	64.33	64.45	64.59	64.79
TiO_2	0.48	0.53	0.50	0.44	0.43	0.78	0.35	0.44	0.40	0.57	0.41	0.49
$Al2O_3$	17.25	18.02	17.10	17.68	16.59	16.56	17.29	16.36	16.21	15.54	16.62	16.40
FeOtot	4.86	4.78	4.56	4.02	4.41	4.66	3.10	3.67	3.61	4.00	3.60	3.70
MnO	0.13	0.16	0.15	0.15	0.18	0.10	0.13	0.13	0.13	0.08	0.13	0.11
MgO	2.18	1.58	1.96	1.29	1.44	2.38	0.97	1.31	1.32	3.56	1.33	1.93
CaO	44.43	37.06	43.38	36.36	36.80	47.64	35.83	38.86	39.46	61.30	39.67	48.18
Na_2O	5.44	6.33	5.66	5.34	5.45	4.31	4.94	5.10	5.10	4.04	5.13	4.74
K_2O	3.79	4.17	3.71	4.37	4.05	3.98	3.94	3.55	3.54	3.60	3.90	3.54
P_2O_5	4.96	3.13	3.48	3.55	3.88	2.98	4.59	4.16	4.24	2.31	3.57	3.57
mg#	0.28	0.20	0.17	0.18	0.26	0.19	0.17	0.20	0.19	0.20	0.14	0.19

LOI	0.5	0.6	0.6	0.7	0.5	0.5	0.4	0.7	0.8	0.9	0.4	0.4
Sum	99.8	99.7	99.7	99.8	99.3	99.2	99.8	99.8	99.8	99.3	99.8	99.8
XRF												
Sc						13				12		
V	136.2	92	114.3	84	79	110.4	78.7	74.4	80.9	119	73	76.9
Cr	15	4.8	17.6	5.1	8.1	0.3	16	9.4	10.3	0	6.2	13.9
Ni	6	3.4	2.2	5	5.7	8.9	3.1	5.4	3.5	5.4	3.1	4.3
Pb						15.4				24		
Zr	206.1	195	146.4	2.12	177	162.8	154.4	141.6	133.4	146	122.1	181.1
Nb	11	11.8	11.6	11.6	11.3	15.5	10.8	7.1	7.5	12.5	8.1	10.2
Y	20.5	25	20.1	24	23	19.7	14.8	20.9	21.2	23.4	18.4	18.4
Th	11.8	8.5	13.3	12.9	12.2	11.8	13.4	12.9	6	15.1	13.1	15.4
Rb	166.8	116	124.3	134	143	103.6	163.7	139.5	151.8	149.7	112.6	140.8
Sr	599.6	748	604.7	700	624	393.2	674.6	650.9	640.2	304.4	643.1	439.4
Ba	1331.2	969	671.9	1080	972	661.7	861.4	696.6	763.8	408.2	607.7	838.9
La	32	29	35.7	32	35	36.3	40.5	36.9	28.6	41	35.9	33.7
Ce	58.2	43	39.6	43	48	65.7	34.8	36.5	25.9	78.8	32.4	41.3
Nd						23.5				24.5		
ICP-MS												
Sc												
V						110.00				87.00	93.00	
Cr												
Ni						5.40				81.30		
Pb	15.10	19.7	18.5	20	21	1.1	18.1	29	25	2.3	26	20.5
Zr						184.20				175.8	145	
Hf						5.10				5.60	4.00	
Nb						14.30				11.90	7.80	
Ta						1.30				0.90	0.90	
U						4.10				4.10	4.40	
Y						20.40				17.80	18.80	
Th						12.40				22.30	14.40	
Rb						108.80				140.50	97.70	
Cs						1.30				5.50	1.60	
Sr						409.00				274.70	625.40	
Ba						708.00				354.00	512.00	
La				40.37		36.30				41.00	39.70	
Ce				66.57		78.40				92.60	65.40	
Pr						8.89				10.52	6.69	
Nd				26.78		32.90				39.70	24.40	
Sm				6.24		6.04				6.92	4.29	
Eu				1.15		1.41				1.00	1.09	
Gd						4.98				4.91	3.87	
Tb				0.64		0.76				0.70	0.55	
Dy						3.97				3.72	3.23	
Ho						0.73				0.64	0.67	
Er						1.93				1.72	2.03	
Tm						0.29				0.25	0.31	
Yb				2.54		1.89				1.65	2.04	
Lu				0.39		0.28				0.25	0.31	
ΣREE				144.7		178.8				205.6	154.6	
Eu/Eu*						0.8				0.5	0.8	
(La/Lu)cn				10.8		13.5				17.0	13.3	
(La/Sm)cn				4.1		3.8				3.7	5.8	
(Gd/Yb)cn						2.1				2.4	1.5	
(Tb/Lu)cn				1.11		1.84				1.90	1.21	

*Type: GBDR= Gabbrodiorites; MME= Mafic microgranular enclaves; MZ= Monzonites; QMZ= Quartz monzonites; QSY-GR= Quartz syenites and granites

**References: 1 Major & trace elements present study; 2 Major and trace elements Soldatos et al. (1998); 3 Trace elements Soldatos unpublished data; 4 Trace elements present study

Vrondou pluton												
	QMZ											**QSY-GR**
Sample	**TS35**	**B8**	**TS36**	**B7**	**L1**	**SB09**	**SB41**	**SK4**	**SB94**	**SB43**	**K2B**	**TS21**
Type*	QMZ	QMZ	QMZ	QMZ	QMZ	QMZ	QMZ	QMZ	QMZ	QMZ	QMZ	QSY-GR
Reference**	3	3	3	3	3	3	3	3	3	3	3	3
SiO_2	64.96	65.16	65.37	65.54	66.16	66.22	66.31	66.48	66.76	66.89	67.28	61.27
TiO_2	0.47	0.42	0.44	0.54	0.41	0.35	0.41	0.42	0.32	0.37	0.40	0.63
Al2O$_3$	16.66	16.09	16.73	13.98	16.02	16.06	16.35	15.59	16.14	16.39	15.71	15.60
FeOtot	3.69	3.60	3.34	4.75	3.76	3.02	2.84	3.60	2.89	3.04	2.99	4.77
MnO	0.11	0.14	0.11	0.18	0.13	0.12	0.10	0.13	0.10	0.10	0.08	0.14
MgO	1.80	1.35	1.67	1.16	1.26	0.88	1.49	1.32	0.86	1.24	1.08	2.18
CaO	46.47	40.06	47.13	30.30	37.37	34.20	48.31	39.52	34.67	42.11	39.13	44.88
Na_2O	4.35	4.75	4.28	4.67	4.42	4.12	3.99	4.70	4.24	4.43	3.47	4.45
K_2O	3.60	3.80	3.58	3.49	3.75	3.88	3.55	3.45	3.63	3.59	3.63	3.83
P_2O_5	3.43	3.81	3.71	4.28	2.93	4.45	4.13	3.35	3.94	3.18	4.29	5.79
mg#	0.17	0.16	0.16	0.15	0.14	0.14	0.22	0.15	0.17	0.16	0.12	0.49
LOI	0.6	0.5	0.5	0.9	0.8	0.6	0.5	0.6	0.6	0.5	0.8	0.7
Sum	99.8	99.8	99.9	99.7	99.8	99.8	99.9	99.8	99.7	99.9	99.8	99.8
XRF												
Sc												
V	67	66	71	71	97	46	67.7	76	40	77.7	60	115.6
Cr	12.1	5.3	12	2.2	8.8	3.3	11.7	7.9	21	11.9	4	21.8
Ni	5.7	6.1	9	4.5	2.5	2.9	4.3	0.8	2	4.1	3	12.2
Pb												
Zr	145.2	159	138.8	187	134	174	138.9	113	159	127.2	193	272
Nb	10.7	10.9	10.5	12.6	8.2	12.3	13.5	3.8	9	7.4	12.5	18.8
Y	21.3	22	18.5	25	21	23	22.2	16.3	14	18.3	19.8	29.7
Th	18.7	13.9	14.4	21	17.3	13.1	22.6	16.9	11	16.8	24	29.1
Rb	139.6	167	141.4	166	121	176	188.4	147	157	123	168	194.9
Sr	414.2	466	398	474	570	492	403.1	535	500	556.7	361	955.7
Ba	740.8	630	817	659	523	761	694.6	388	742	429.5	813	1101.6
La	29.7	28	33.4	37	28	25	30.1	27	32	22.3	36	51.4
Ce	38.9	26	25.4	59	34	43	45.2	22	45	31.5	36	110
Nd												
ICP-MS												
Sc												
V												
Cr												
Ni												
Pb	23.10	20.00	23.70	28.00	35.00	21.00	24.50	37.00	25.00	18.60	21.00	34.40
Zr												
Hf												
Nb												
Ta												
U												
Y												
Th												
Rb												
Cs												
Sr												
Ba												
La			37.57	57.01					35.37			77.30
Ce			55.44	75.97					50.92			129.74
Pr												
Nd			18.28	24.88					17.39			52.42

Sm	4.77	5.84	4.24	12.66
Eu	0.80	0.89	0.75	1.98
Gd				
Tb	0.48	0.55	0.41	1.04
Dy				
Ho				
Er				
Tm				
Yb	1.99	2.42	1.84	2.67
Lu	0.30	0.38	0.21	0.54
ΣREE	119.6	167.9	111.1	278.4
Eu/Eu*				0.8
(La/Lu)cn	13.0	15.6	17.5	14.9
(La/Sm)cn	5.0	6.1	5.2	3.8
(Gd/Yb)cn				0.0
(Tb/Lu)cn	1.09	0.98	1.33	1.31

*Type: GBDR= Gabbrodiorites; MME= Mafic microgranular enclaves; MZ= Monzonites; QMZ= Quartz monzonites; QSY-GR= Quartz syenites and granites

**References: 1 Major & trace elements present study; 2 Major and trace elements Soldatos et al. (1998); 3 Trace elements Soldatos unpublished data; 4 Trace elements present study

Vrondou pluton												
	QSY-GR											
Sample	**TS09**	**TS10**	**SB92**	**SB27**	**SB72**	**SK2**	**L2**	**SB83**	**L4**	**TS27**	**SB25**	**SB51**
Type*	QSY-GR	QSY-GR	QSY-GR	QSY-GR	QSY-GR	QSY-GR	QSY-GR	QSY-GR	QSY-GR	QSY-GR	QSY-GR	QSY-GR
Reference**	3	3	2,3	2,3	2,3	3	3	2,3	2,3	3	3	3
SiO_2	61.43	61.72	62.78	63.17	63.88	64.14	64.26	64.30	64.41	64.75	65.09	66.06
TiO_2	0.61	0.63	0.54	0.43	0.49	0.57	0.46	0.50	0.46	0.34	0.37	0.43
$Al2O_3$	16.34	17.00	16.22	17.14	16.07	12.99	16.80	16.04	15.76	17.39	16.97	15.65
FeOtot	4.58	4.58	4.48	3.65	4.19	5.33	3.57	4.04	4.11	3.05	3.10	3.17
MnO	0.14	0.15	0.12	0.10	0.10	0.18	0.12	0.10	0.15	0.09	0.12	0.12
MgO	1.79	0.30	1.87	1.83	1.42	1.30	1.22	1.58	1.32	1.06	1.40	1.20
CaO	41.07	10.45	42.67	47.16	37.68	30.31	37.87	41.05	36.38	38.22	44.59	40.25
Na_2O	4.30	4.49	4.78	4.03	4.55	6.01	3.47	4.36	5.22	4.69	4.60	3.40
K_2O	3.60	3.77	3.64	4.01	3.76	3.37	3.81	3.48	3.33	3.90	4.22	3.95
P_2O_5	5.98	5.99	4.23	4.71	4.30	4.52	4.72	4.47	4.17	3.87	3.40	5.14
mg#	0.40	0.36	0.23	0.20	0.18	0.18	0.42	0.19	0.19	0.15	0.17	0.30
LOI	0.6	0.8	0.8	0.3	0.6	1.0	1.0	0.5	0.6	0.4	0.4	0.5
Sum	99.8	99.8	99.7	99.6	99.6	99.6	99.8	99.6	99.8	99.7	99.8	99.9
XRF												
Sc				34								
V	102.9	97.5	77	73	79	73	77	67	77	55.8	57.9	59.6
Cr	11.2	12.1	21	13	17	8.4	24	28	7.2	5.7	6.5	14.2
Ni	4.4	6.4	9	11	10	2.2	9.2	5	3.6	4.1	6.7	8.2
Pb			25	19	15			24	25			
Zr	278.6	331.9	161	242	178	161	268	168	126	144.8	140.4	220
Nb	21.6	22.1	13	22	11	9	16.7	12	9.2	12	11.4	14.9
Y	30.7	28.2	20	33	26	21	25	20	17.7	22.7	22.1	23.6
Th	18.4	22.1	23	39	22	28	29	20	9.2	11.9	10.5	28
Rb	160.5	145.6	170	213	152	156	172	156	136	180.4	150.9	174.3
Sr	963.1	1050.7	432	474	455	818	854	411	762	616.2	482.6	794.5
Ba	1263.3	1218.4	793	654	658	659	1051	808	831	907.9	647.1	995.2
La	45.7	51.7	45	40	23	30	49	48	26	29.4	22	49.2
Ce	83.1	83	50	58	34	44	71	68	16	44.4	24.3	74.5
Nd				23								
ICP-MS												
Sc			12.31	6.31	9.15			6.66	11.02			
V			96.56	100.40	87.25			88.47	86.32			
Cr			22.08	18.95	15.33			26.26	21.74			

Ni			18.41	18.30	10.23			6.75	8.79			
Pb	35.20	39.80	13.51	12.82	9.54	32.00	28.00	14.99	15.09	18.90	15.70	34.20
Zr			188.25	285.98	175.03			148.43	145.06			
Hf			4.57	6.95	4.16			3.71	3.79			
Nb			11.90	23.58	11.50			10.91	7.70			
Ta			1.04	1.93	0.68			0.85	0.48			
U			5.35	13.58	6.33			5.22	3.53			
Y			20.88	27.51	20.80			13.99	17.40			
Th			23.60	48.77	19.29			17.08	15.29			
Rb			135.57	210.16	141.85			150.80	111.90			
Cs			1.37	2.01	0.79			1.60	1.79			
Sr			386.85	461.96	372.88			327.84	669.27			
Ba			766.13	655.46	603.25			728.03	641.15			
La	60.48		38.26	44.13	33.61			31.75	32.66			64.10
Ce	105.56		57.39	81.48	54.13			55.12	51.57			106.13
Pr			6.09	8.61	5.57			5.22	5.50			
Nd	45.54		25.27	33.87	22.19			19.62	23.03			39.65
Sm	11.19		4.78	6.42	4.10			3.40	4.50			9.71
Eu	1.74		0.99	1.19	0.90			0.81	1.06			1.50
Gd			3.92	4.81	3.47			2.68	3.51			
Tb	1.06		0.52	0.69	0.54			0.39	0.49			0.80
Dy			3.67	4.50	3.30			2.41	3.05			
Ho			0.67	0.90	0.70			0.45	0.62			
Er			2.06	2.90	2.08			1.42	1.82			
Tm			0.31	0.43	0.29			0.20	0.25			
Yb	3.00		2.37	3.42	2.63			1.63	2.03			2.42
Lu	0.50		0.33	0.44	0.36			0.24	0.27			0.42
ΣREE	229.1		146.6	193.8	133.9			125.4	130.4		0.0	224.7
Eu/Eu*	0.8		0.7	0.6	0.7			0.8	0.8			
(La/Lu)cn	12.6		12.2	10.3	9.8			13.9	12.6			15.9
(La/Sm)cn	3.4		5.0	4.3	5.2			5.9	4.6			4.2
(Gd/Yb)cn	0.0		1.3	1.1	1.1			1.3	1.4			
(Tb/Lu)cn	1.5		1.1	1.1	1.0			1.1	1.2			1.3

*Type: GBDR= Gabbrodiorites; MME= Mafic micrognular enclaves; MZ= Monzonites; QMZ= Quartz monzonites; QSY-GR= Quartz syenites and granites

**References: 1 Major & trace elements present study; 2 Major and trace elements Soldatos et al. (1998); 3 Trace elements Soldatos unpublished data; 4 Trace elements present study

Vrondou pluton

	QSY-GR											
Sample	**TS07**	**MP1**	**BA2**	**SB68**	**TS06**	**SB64**	**TS23**	**K3A**	**SB69**	**SB81**	**TS24**	**SB53**
Type*	QSY-GR	QSY-GR	QSY-GR	QSY-GR	QSY-GR	QSY-GR	QSY-GR	QSY-GR	QSY-GR	QSY-GR	QSY-GR	QSY-GR
Reference**	3	3	3	3	3	3	3	3	3	2,3	3	3
SiO_2	66.48	67.61	67.80	68.22	68.24	68.27	68.32	68.48	68.56	68.64	68.83	69.26
TiO_2	0.37	0.45	0.38	0.36	0.28	0.37	0.36	0.34	0.33	0.31	0.29	0.31
Al2O$_3$	16.32	13.55	14.23	15.75	16.19	15.61	15.90	15.14	15.41	15.18	16.04	15.07
FeOtot	3.21	3.43	2.77	2.84	3.27	2.95	2.76	2.79	2.69	2.62	2.22	2.28
MnO	0.12	0.12	0.09	0.12	0.07	0.13	0.10	0.09	0.12	0.08	0.07	0.10
MgO	1.18	0.65	0.90	0.99	0.43	1.07	0.99	0.89	0.91	0.68	0.77	0.66
CaO	39.56	25.22	36.69	38.32	18.99	39.24	38.98	36.25	37.58	31.65	38.20	34.05
Na_2O	3.98	3.18	3.82	3.85	2.00	3.94	2.95	3.01	3.83	2.66	2.36	2.69
K_2O	3.90	3.93	3.39	3.45	4.31	3.29	4.01	3.15	3.33	3.83	3.93	3.94
P_2O_5	3.47	5.97	5.61	3.52	4.30	3.43	3.57	5.17	4.05	5.05	4.81	4.97
mg#	0.14	0.17	0.14	0.14	0.10	0.19	0.32	0.13	0.14	0.15	0.18	0.19
LOI	0.7	0.7	0.7	0.5	0.5	0.5	0.5	0.6	0.4	0.5	0.3	0.4
Sum	99.8	99.7	99.8	99.7	99.7	99.7	99.8	99.8	99.7	99.7	99.8	99.9
XRF												
Sc												
V	61.3	46.3	47	52.9	13.3	61.1	51	69	50.9	34	40.4	37.1

Cr	14	3.3	2	12	8.7	7.9	11	5.4	19.3	13	9.4	7.7
Ni	1.9	8.2	3.9	0	2.2	1.8	5.7	5	0	1	2.6	3
Pb										19		
Zr	121.1	274.7	152	148.7	198	106.1	205.5	143	145.1	162	192.2	197.4
Nb	8.5	17.3	13.1	9.8	10.1	8.9	13.4	10.3	7.1	15	11.8	11.8
Y	14.8	24.1	21	13.3	14.9	12.4	21.1	18.6	11.2	19	18.1	19
Th	16.4	43.6	26	14.7	21	13.6	34.5	29	14.3	18	35.5	27.7
Rb	133.3	225.1	229	125.6	161.1	142.1	167.4	247	151.7	182	206.3	185.8
Sr	711.7	776.6	374	490.6	527.8	581.2	712.7	428	476.6	365	654	598.3
Ba	496.2	855.3	938	677.1	749	458.3	779.6	720	690.3	788	773	651.1
La	31	48.4	29	23.9	31.1	29.4	27.2	24	25.8	35	34.3	39.1
Ce	23.8	72.6	33	28.4	41.9	23.2	52.3	30	22.3	27	51.3	47
Nd												
ICP-MS												
Sc										7.03		
V										37.00		
Cr										19.04		
Ni										12.58		
Pb	34.70	35.60	24.00	21.00	53.90	21.40	26.70	25.00	21.90	11.61	32.10	38.60
Zr										145.47		
Hf										3.77		
Nb										12.12		
Ta										0.79		
U										6.43		
Y										14.99		
Th										20.59		
Rb										164.10		
Cs										2.33		
Sr										280.07		
Ba										697.00		
La				32.70						33.54		
Ce				54.01						56.10		
Pr										5.44		
Nd				19.51						19.82		
Sm				4.62						3.39		
Eu				0.92						0.75		
Gd										2.74		
Tb				0.49						0.37		
Dy										2.53		
Ho										0.49		
Er										1.40		
Tm										0.22		
Yb				2.03						1.92		
Lu				0.25						0.27		
ΣREE				114.5						129.0		
Eu/Eu*										0.7		
(La/Lu)cn				13.6						13.1		
(La/Sm)cn				4.5						6.2		
(Gd/Yb)cn										1.2		
(Tb/Lu)cn				1.3						0.9		

*Type: GBDR= Gabbrodiorites; MME= Mafic microgranular enclaves; MZ= Monzonites; QMZ= Quartz monzonites; QSY-GR= Quartz syenites and granites

**References: 1 Major & trace elements present study; 2 Major and trace elements Soldatos et al. (1998); 3 Trace elements Soldatos unpublished data; 4 Trace elements present study

Vrondou pluton												
	QSY-GR											
Sample	**L8**	**TS20**	**TS14**	**L9**	**TS26**	**TS17**	**SB02**	**SB04**	**TS12**	**SB03**	**L6**	**TS03**
Type*	QSY-GR	QSY-GR	QSY-GR	QSY-GR	QSY-GR	QSY-GR	QSY-GR	QSY-GR	QSY-GR	QSY-GR	QSY-GR	QSY-GR

Reference**	3	3	3	3	3	3	3	3	3,4	3	3	3
SiO_2	69.40	69.42	69.84	69.97	71.15	71.26	71.45	71.78	72.26	72.52	72.85	73.47
TiO_2	0.25	0.24	0.30	0.29	0.22	0.29	0.24	0.25	0.17	0.23	0.19	0.11
$Al2O_3$	16.39	15.30	15.43	12.72	15.08	14.93	15.36	14.82	14.91	14.87	14.53	14.68
FeOtot	2.17	2.27	2.04	2.75	2.06	1.61	1.77	1.81	1.17	1.33	1.41	1.04
MnO	0.08	0.10	0.08	0.16	0.07	0.08	0.08	0.08	0.07	0.06	0.07	0.04
MgO	0.45	0.76	0.78	0.48	0.74	0.43	0.51	0.35	0.27	0.32	0.35	0.16
CaO	26.96	37.32	40.57	23.73	39.04	32.24	33.96	25.65	29.17	29.94	30.73	21.48
Na_2O	2.90	3.29	2.45	3.87	2.87	2.45	1.86	1.30	1.91	1.60	2.13	1.66
K_2O	3.96	3.59	3.53	3.34	3.47	3.43	4.06	3.20	3.51	4.01	3.44	3.18
P_2O_5	3.43	4.37	4.78	5.63	3.63	4.79	3.79	5.45	5.27	4.32	4.38	5.22
mg#	0.12	0.11	0.11	0.10	0.08	0.09	0.11	0.08	0.05	0.07	0.06	0.05
LOI	0.7	0.5	0.6	0.5	0.5	0.6	0.7	0.8	0.4	0.6	0.5	0.4
Sum	99.9	99.9	99.9	99.8	99.8	99.9	99.9	99.9	100.0	99.9	99.9	100.0
XRF												
Sc												
V	13.5	36.3	23.3	20.3	29.7	13.3	20	9.7	13.3	12.1	12.4	13.3
Cr	10.5	9.8	14.1	5.1	4.4	12.7	2.5	2.1	4.9	0	1.5	5.9
Ni	4.2	2.1	6	2.9	1.8	6.7	4.6	4.8	0	4	3.2	0
Pb												
Zr	170	99.3	154.3	114	99	144	195	118	125.5	156	114	94.5
Nb	8.2	7.1	8.7	11.4	6.8	11	15	9.4	6.5	12	10.3	6.5
Y	19.9	14.7	16.5	15.7	14.8	19.2	16.6	19.7	12.5	17.5	16.7	15.5
Th	21	23.8	21.1	19.1	17.3	26.9	31	21	26.9	27	31	19.2
Rb	145	160.3	147.8	206	188.8	173.8	218	217	138.2	191	188	147.5
Sr	684	546.2	769.6	596	412.5	473	538	131	406.7	423	405	442.7
Ba	773	384.7	1359.6	550	373.8	929.1	696	577	910	640	807	788.1
La	27	20.9	34.5	17	14.6	47.2	42	21	30.4	33	34	22.8
Ce	43	12.6	46.3	8	14.7	71.6	57	33	26.7	35	46	10.1
Nd												
ICP-MS												
Sc												
V									11.00			
Cr												
Ni												
Pb	33.00	36.90	49.50	51.00	25.40	46.40	46.00	46.00	50.80	56.00	53.00	54.10
Zr									118.30			
Hf									3.40			
Nb									7.30			
Ta									1.00			
U									12.80			
Y									11.10			
Th									50.00			
Rb									136.30			
Cs									1.40			
Sr									435.10			
Ba									967.00			
La			49.98						34.90			
Ce			74.31						64.90			
Pr									6.11			
Nd			24.71						20.70			
Sm			5.67						3.09			
Eu			0.92						0.66			
Gd									2.37			
Tb			0.48						0.36			
Dy									1.80			
Ho									0.32			
Er									1.03			
Tm									0.16			
Yb			1.47						1.01			

Lu	0.24	0.18
ΣREE	157.8	137.6
Eu/Eu*	0.9	0.7
(La/Lu)cn	21.6	20.1
(La/Sm)cn	5.5	7.1
(Gd/Yb)cn	0.0	1.9
(Tb/Lu)cn	1.4	1.4

*Type: GBDR= Gabbrodiorites; MME= Mafic microgranular enclaves; MZ= Monzonites; QMZ= Quartz monzonites; QSY-GR= Quartz syenites and granites

**References: 1 Major & trace elements present study; 2 Major and trace elements Soldatos et al. (1998); 3 Trace elements Soldatos unpublished data; 4 Trace elements present study

Maronia pluton												
	Acid Group			Basic Group			Enclave	Intermediate Group				
Sample	**MP-90**	**MP-64**	**MP-68A**	**PMR-12**	**PMR-55P**	**MR-51**	**PMR-9A**	**MP-402**	**PMR-81**	**PMR-91**	**MP-08**	**MP-26**
Type*	Gr	Gr	Gr	Gb	Gb	Gb	Enclave	Mzg	Mzg	Mzg	Mzg	Mzg
Reference**	2,3	2,3	2,3	1,2	1,2	1,2	1,2	2,3	1,2	1,2	2,3	2,3
SiO_2	65.73	73.37	73.62	44.61	48.35	48.61	53.07	47.92	48.93	50.48	50.67	50.87
TiO_2	0.49	0.26	0.19	0.95	1.05	0.96	0.83	1.21	0.87	0.90	1.09	1.08
$Al2O_3$	14.62	14.19	13.94	13.89	16.98	15.41	16.02	15.44	16.17	15.06	17.80	16.74
FeOtot	3.71	1.67	1.73	10.93	9.24	8.61	8.24	8.48	8.95	8.30	10.56	9.58
MnO	0.06	0.02	0.02	0.18	0.16	0.17	0.25	0.21	0.17	0.16	0.19	0.16
MgO	1.89	0.59	0.70	9.33	5.87	7.08	5.15	7.87	6.95	6.28	4.56	5.42
CaO	3.46	1.52	0.94	14.10	10.12	11.16	7.27	11.24	11.47	10.11	8.57	9.47
Na_2O	2.36	2.50	2.93	1.22	2.24	2.04	3.57	2.18	2.24	2.31	2.82	2.34
K_2O	6.12	5.74	5.74	1.16	1.73	2.08	2.29	2.57	1.65	2.97	2.67	2.95
P_2O_5	0.22	0.10	0.15	0.91	0.68	0.69	0.27	0.80	0.73	0.63	0.48	0.59
mg#	47.57	38.65	41.85	60.32	53.09	59.43	52.68	62.30	58.04	57.42	43.46	50.19
LOI	1.7	1.9	0.8	1.1	2.1	1.8	1.8	0.6	0.5	1.3	0.8	0.2
Sum	100.3	101.9	100.7	98.4	98.5	98.6	98.8	98.5	98.6	98.5	100.2	99.4
XRF												
Sc	10	5	3	43	27	33	28		33	33	27	28
V	77	26	27	324	289	244	192	268	259	241	281	289
Cr	33	6	7	204	40	179	92	146	103	122	47	70
Ni				61	32	63	15		60	45		
Pb	34	26	38	5	4	9	19	20	12	16	24	26
Zr	312	207	114	137	143	154	137	112	163	197	267	129
Nb	25	19	11	8	7	10	19	9	10	8	17	13
U				2	0	6	4			4	2	
Y	26	21	17	22	22	24	40	25	24	23		28
Th				7	4	9	15	12	8	3		
Rb	312	274	253	53	79	95	119	96	76	121	108	107
Sr	399	189	246	723	893	782	367	731	727	859	731	711
Ba	954	592	557	376	730	871	468	774	568	2086	835	1235
La	44			24	25	36	38	30	36	32		
Ce	89			48	56	74	80	47	72	101		
Nd	40			33	31	38	47		41	40		
ICP-MS												
Sc												
V				378	354	270	205		298	280		
Cr												
Ni	19	8	10	38.8	19.6	32.4	6.6	45	35.8	26.8	33	40
Pb				8.2	5.3	7.6	9.7		4.3	7.7		
Zr				83.7	108	104.3	118.9		116.9	141.3		
Hf				3.4	3.7	3.8	3.7		4	4.8		
Nb				4.2	5.3	8.5	15.5		7.1	6.8		
Ta				0.4	0.4	0.6	1.3		0.5	0.4		
U	14.3			2.8	3.8	5.0	4.6		4.6	2.7		
Y				20.8	22.5	22.4	38		23.6	23.5		
Th				9.2	12.7	16.7	13.5		16.1	9.7		
Rb				55.5	83.6	95.2	119.2		78.1	126.9		
Cs				3.5	6.4	3.3	7		4.3	2.7		
Sr				748	920	798.2	381.8		761.2	908.1		
Ba				315	731	851	449		525	2111		
La	43.7			26.2	30.3	35.4	36.5		37.2	32.1		
Ce	89			62.8	68.9	78.2	86.7		83.5	71.9		
Pr	9.6			8.15	8.48	9.79	10.65		9.94	9.21		
Nd	40			35.2	35.3	40.1	41.9		41.8	39.5		
Sm	6.86			7.32	6.63	7.59	8.83		7.96	7.45		
Eu	1.09			1.65	1.81	1.59	1.49		1.83	1.77		

Gd	6.46		5.75	5.54	5.9	7.74		6.16	5.95
Tb	0.66		0.84	0.82	0.88	1.21		0.88	0.88
Dy	4.07		4.06	4.04	4.28	6.29		4.54	4.33
Ho	0.55		0.76	0.81	0.79	1.27		0.86	0.82
Er	2.03		2.01	2.2	2.24	3.73		2.32	2.41
Tm	0.25		0.28	0.31	0.32	0.58		0.32	0.36
Yb	1.88		1.81	1.89	2.02	4.09		2.11	2.09
Lu	0.24		0.25	0.3	0.3	0.65		0.31	0.31
ΣREE	206.4		157.1	167.3	189.4	211.6		199.7	179.1
Eu/Eu*	0.5		0.8	0.9	0.7	0.5		0.8	0.8
(La/Lu)cn	18.9		10.9	10.5	12.3	5.8		12.5	10.8
(La/Sm)cn	4.0		2.3	2.9	2.9	2.6		2.9	2.7
(Gd/Yb)cn	2.8		2.6	2.4	2.4	1.5		2.4	2.3
(Tb/Lu)cn	1.9		2.3	1.9	2.0	1.3		1.9	1.9

*Type: Gr= Granites; Gb= Gabbros; Mzg= Monzogranites; Mz= Monzonites; QMz= Quartz monzonites; QMzg= Quartz monzogranites

**References: 1 Trace elements present study; 2 Major elements Papadopoulou (2003) 3 Trace elements Papadopoulou (2003)

Maronia pluton

	Intermediate											
Sample	**PMR-66**	**PMR-5**	**PMR-92**	**PMR-13**	**PMR-93**	**MP-52**	**MP-60**	**PMR-3**	**MP-63**	**MP-06**	**MP-36**	**MP-70**
Type*	Mzg	Mzg	Mzg	Mzg	Mzg	Mzg	Mzg	Mzg	Mzg	Mzg	Mzg	Mzg
Reference**	1,2	1,2	1,2	1,2	1,2	2,3	2,3	1,2	2,3	2,3	2,3	2,3
SiO_2	50.97	51.02	51.05	51.08	51.37	51.41	51.64	51.97	52.06	52.10	52.25	52.46
TiO_2	0.94	0.93	0.90	0.92	0.95	0.97	1.02	0.97	0.92	0.95	0.93	0.77
$Al2O_3$	15.86	16.94	14.55	14.77	13.48	17.52	17.32	16.69	16.70	15.25	15.73	19.64
FeOtot	8.41	8.90	7.73	8.42	8.21	6.96	8.76	8.75	9.50	8.24	7.98	6.75
MnO	0.16	0.17	0.13	0.16	0.16	0.14	0.17	0.16	0.18	0.15	0.16	0.13
MgO	5.72	5.32	6.29	6.73	7.24	5.60	5.08	5.02	4.46	5.41	5.44	3.98
CaO	9.08	9.04	9.70	9.64	10.04	10.68	8.18	8.75	8.96	10.48	9.62	8.74
Na_2O	2.44	2.70	2.05	2.21	2.13	2.59	2.99	2.68	2.75	2.49	2.75	3.01
K_2O	3.02	2.63	3.65	3.07	3.34	2.29	2.87	2.66	2.32	3.31	2.84	2.56
P_2O_5	0.52	0.42	0.61	0.62	0.73	0.62	0.49	0.47	0.51	0.51	0.51	0.34
mg#	54.78	51.58	59.18	58.74	61.12	58.92	50.82	50.56	45.55	53.91	54.85	51.23
LOI	1.5	0.5	2.0	1.0	0.9	1.1	1.0	0.6	1.7	0.7	0.5	1.1
Sum	98.6	98.6	98.7	98.6	98.5	99.9	99.5	98.7	100.1	99.6	98.7	99.5
XRF												
Sc	27		32	31	34	70	69			69	71	56
V	235		248	211	230	214	252		283	248	246	199
Cr	76		153	147	217	149	49		43	132	101	60
Ni	43		44	55	60							
Pb	10		10	12	11	22	25		14	26	16	22
Zr	140		152	182	141	94	136		68	154	109	77
Nb	9		7	11	8	10	6		12	9	6	
U	6		1	5	3	9	12			7	7	6
Y	24		23	21	24				27			
Th	12		12	17	6		16			7		
Rb	120		136	149	130	102	126		110	167	135	98
Sr	664		665	627	640	939	812		1021	843	781	1062
Ba	1346		1390	1112	1746	668	527		996	1028	1408	1066
La	31		32	34	32	18	28		18	39	7	33
Ce	87		84	90	93	21	25		76	96	30	59
Nd	31		33	38	37	487	120		26	37	17	69
ICP-MS												
Sc		32.25						31.75				
V	272	257.50	263	252	257			249.94				
Cr		65.46						54.95				
Ni	21.7	55.72	24.9	30.2	29.8	49	25	56.36	19	53	40	19

Pb	4	22.59	5.3	6.4	3.2			26.46				
Zr	112.1	112.93	108.1	171.2	101			162.42				
Hf	3.6	3.54	3.9	5.3	3.6			4.72				
Nb	7.4	7.75	6.8	11	7.2			10.04				
Ta	0.5	0.74	0.5	0.8	0.4	4.19	0.00	0.66	9.98	7.66		3.34
U	5.3	4.76	3.1	6.2	2.6			4.27				
Y	22.4	22.14	22.5	22.8	24.5			29.02				
Th	19.1	16.87	11.1	18.5	9.1			21.15				
Rb	120	100.36	136.8	151.8	129.1			111.89				
Cs	4.7	4.13	2.6	4.7	2.8			3.73				
Sr	682	746.92	678.1	659.3	658.1			760.51				
Ba	1358	973.75	1388	1083	1658			1126.90				
La	33	30.52	31.7	37.7	32.7			37.66		33.1		
Ce	71.8	64.60	70.8	84.4	75.4			76.1		64		
Pr	8.54	7.20	8.88	9.96	9.55			8.57		7		
Nd	35.2	32.81	38.9	39.7	39.6			37.49		29		
Sm	6.86	6.06	7.26	7.56	7.74			7.93		4.83		
Eu	1.77	1.68	1.7	1.67	1.72			1.84		0.78		
Gd	5.6	5.03	5.85	5.88	6.38			5.38		4.74		
Tb	0.82	0.73	0.84	0.84	0.92			0.86		0.44		
Dy	4.07	4.07	4.32	4.23	4.7			5.17		2.58		
Ho	0.8	0.81	0.77	0.78	0.86			0.91		0.32		
Er	2.2	2.11	2.22	2.22	2.42			2.78		1.03		
Tm	0.32	0.34	0.32	0.31	0.35			0.44		0.12		
Yb	1.92	1.87	1.96	1.93	2.16			2.53		0.87		
Lu	0.3	0.29	0.31	0.3	0.32			0.35		0.11		
ΣREE	173.2	158.1	175.8	197.5	184.8			188.0		148.9		
Eu/Eu*	0.8	0.9	0.8	0.7	0.7			0.8		0.5		
(La/Lu)cn	11.4	11.1	10.6	13.1	10.6			11.2		31.3		
(La/Sm)cn	3.0	3.2	2.7	3.1	2.7			3.0		4.3		
(Gd/Yb)cn	2.4	2.2	2.4	2.5	2.4			1.7		4.4		
(Tb/Lu)cn	1.9	1.7	1.8	1.9	2.0			1.7		2.7		

*Type: Gr= Granites; Gb= Gabbros; Mzg= Monzogranites; Mz= Monzonites; QMz= Quartz monzonites; QMzg= Quartz monzogranites

**References: 1 Trace elements present study; 2 Major elements Papadopoulou (2003) 3 Trace elements Papadopoulou (2003)

Maronia pluton

	Intermediate											
Sample	**MP-102**	**MP-53**	**PMR-2**	**MP-38**	**MP-73**	**MP-11**	**MP-58**	**MP-34**	**MP-57**	**MP-67**	**MP-25**	**MP-37**
Type*	QMzg	Mz	Mz	Mz	Mz	Mz	Mzg	QMzg	Mzg	QMzg	Mz	QMzg
Reference**	2,3	1,2	1,2	2,3	2,3	2,3	2,3	2,3	2,3	2,3	2,3	2,3
SiO_2	53.52	53.69	53.91	54.11	54.20	54.38	54.50	54.55	54.57	54.69	54.80	54.97
TiO_2	0.92	1.01	0.93	0.97	0.94	0.91	0.89	1.02	0.88	0.96	0.93	0.90
$Al2O_3$	16.66	14.69	14.97	16.65	16.10	14.91	16.76	16.73	16.42	16.51	16.19	16.44
FeOtot	8.89	7.39	7.42	7.96	7.55	7.64	8.06	7.37	7.47	8.02	7.33	7.21
MnO	0.16	0.14	0.14	0.15	0.15	0.14	0.16	0.15	0.15	0.16	0.14	0.14
MgO	4.73	5.72	5.41	3.87	4.64	4.96	4.76	4.02	4.47	4.51	4.61	4.32
CaO	8.69	8.56	8.32	8.21	8.72	8.87	7.19	7.13	8.13	8.24	8.02	7.36
Na_2O	2.53	2.17	2.43	3.07	2.83	2.49	2.88	2.61	2.87	2.87	2.89	2.78
K_2O	3.03	5.08	4.33	3.81	3.86	4.15	3.41	3.70	3.70	2.94	3.72	3.56
P_2O_5	0.47	0.52	0.55	0.40	0.50	0.57	0.46	0.45	0.54	0.40	0.47	0.44
mg#	48.67	57.98	56.49	46.40	52.28	53.63	51.28	49.27	51.59	50.06	52.83	51.62
LOI	0.4	0.4	0.4	0.1	0.0	0.1	0.6	0.5	0.1	0.2	0.1	0.8
Sum	100.0	99.4	98.8	99.3	99.5	99.1	99.6	98.2	99.3	99.5	99.2	98.9
XRF												
Sc	28	67		78	12	56	53	64	-22	50	55	26
V	244			232	234	223	256	198	220	242	214	203
Cr	46	191		66	85	97	45	42	57	59	61	53

Ni												
Pb	36	24		24	23	28	29	21	19	23	17	24
Zr	169	79		197	214	173	103	153	147	131	236	208
Nb	16			4	10	5	3	2	9	2	12	5
U				14	4	5	10	6	10	8	12	10
Y	27							9				
Th				37	17	19	21	28	13	37	29	36
Rb	134	206		197	181	217	151	184	196	145	202	177
Sr	662	748		753	742	791	771	775	846	757	723	717
Ba	711	1712		955	1012	1860	952	1132	1411	740	1108	876
La		35		46	39	44	26	15	38	32	29	38
Ce		91		128	124	107	96	82	131	93	117	103
Nd		55		46	51	57	31	32	46	32	46	37
ICP-MS												
Sc			29.13									
V		213	215.31									
Cr			140.87									
Ni	37	62	60.45	20	43	35	28	23	32	26	32	30
Pb			30.84									
Zr		98.1	226.63									
Hf		3.3	6.19									
Nb		7.4	13.45									
Ta		0.6	0.99		16.12	0.61	2.33	4.00	2.52	5.39	0.32	1.76
U		2.8	5.91									
Y		19.3	24.02									
Th		9.2	23.82									
Rb		194.4	207.86									
Cs		3.1	5.12									
Sr		657.8	631.68									
Ba		1461	1345.36									
La		35.7	36.55		35.8							
Ce		77	78.87		82							
Pr		9.1	9.09		8.8							
Nd		36.5	40.63		40							
Sm		6.91	7.72		7.73							
Eu		1.49	1.75		1.64							
Gd		5.16	5.48		7.52							
Tb		0.75	0.76		0.76							
Dy		3.79	4.59		4.56							
Ho		0.75	0.85		0.65							
Er		1.88	2.29		2.18							
Tm		0.26	0.34		0.25							
Yb		1.74	2.31		1.84							
Lu		0.28	0.33		0.24							
ΣREE		181.3	191.6		194.0							
Eu/Eu*		0.7	0.8		0.6							
(La/Lu)cn		13.2	11.6		15.5							
(La/Sm)cn		3.2	3.0		2.9							
(Gd/Yb)cn		2.4	1.9		3.3							
(Tb/Lu)cn		1.8	1.6		2.2							

*Type: Gr= Granites; Gb= Gabbros; Mzg= Monzogranites; Mz= Monzonites; QMz= Quartz monzonites; QMzg= Quartz monzogranites

**References: 1 Trace elements present study; 2 Major elements Papadopoulou (2003) 3 Trace elements Papadopoulou (2003)

Maronia pluton												
	Intermediate											
Sample	**MP-14**	**MP-69**	**MP-56**	**MP-82**	**MP-403**	**MP-405**	**MP-03**	**MP-65**	**MP-62**	**PMR-1**	**MP-78**	**MP-94**
Type*	Mz	QMzg	QMzg	Mz	Mz	Mzg	Mz	QMz	QMzg	QMzg	QMz	QMz

Reference**	2,3	2,3	2,3	2,3	2,3	2,3	2,3	2,3	2,3	1,2	2,3	2,3
SiO_2	55.11	55.22	55.24	55.41	55.44	55.56	55.75	55.80	55.90	55.94	56.07	56.14
TiO_2	0.89	0.82	0.90	0.93	1.05	0.88	0.87	0.85	0.90	0.84	0.74	0.87
$Al2O_3$	15.00	16.13	16.49	15.69	16.64	16.28	16.27	15.98	16.60	15.21	16.07	16.19
FeOtot	6.81	7.83	7.26	7.05	7.03	7.16	7.29	6.90	6.88	6.96	7.25	7.26
MnO	0.13	0.16	0.15	0.14	0.17	0.17	0.14	0.13	0.14	0.13	0.13	0.12
MgO	4.76	4.43	4.40	4.38	4.54	4.83	4.12	4.56	4.04	5.21	3.78	4.11
CaO	8.66	7.07	7.17	7.02	6.61	7.25	5.94	7.93	6.82	7.64	6.57	6.62
Na_2O	2.51	2.92	2.84	2.63	3.08	3.00	3.08	2.78	2.90	2.67	3.00	2.52
K_2O	4.68	3.44	3.76	4.79	4.35	3.65	4.16	3.96	3.83	3.91	4.67	4.86
P_2O_5	0.51	0.46	0.46	0.53	0.45	0.33	0.45	0.39	0.45	0.45	0.50	0.53
mg#	55.47	50.19	51.93	52.54	53.51	54.59	50.18	54.09	51.11	57.17	48.16	50.21
LOI	0.5	1.1	1.0	0.2	0.9	1.1	1.4	0.2	0.6	0.4	0.4	0.3
Sum	99.6	99.6	99.6	98.8	100.3	100.2	99.5	99.5	99.1	99.3	99.2	99.5
XRF												
Sc	26	49		45			75	41	37		54	20
V	217	215	211	198	172	193	213	203	198		184	180
Cr	204	32	49	80	28	39	45	149	29		49	68
Ni												
Pb	53	21	23	19	33	28	18	28	24		27	39
Zr	223	171	191	181	270	169	226	210	176		240	289
Nb	8	10	8	10	18	13	5	2	8		6	19
U	17	14	16	4			15	17	10		15	
Y					29	24		1				24
Th	56	35	32	14	41	69	24	38	38		49	
Rb	278	193	208	266	173	157	192	215	209		248	252
Sr	637	739	694	773	623	689	752	618	692		725	596
Ba	1297	900	891	1341	834	909	973	1040	1042		1312	1409
La	20	49	31	30	44	34	35	50	31		24	
Ce	115	109	88	97	83	65	96	123	105		111	
Nd	115	38	79	45			31	53	47		44	
ICP-MS												
Sc										29.33		
V										190.26		
Cr										172.93		
Ni	40	22	27	33	21	22	35	50	26	55.53	23	37
Pb										26.78	27	39
Zr										211.82		
Hf										4.80		
Nb										10.96		
Ta	2.79	1.77								0.55		
U										4.95		
Y										24.67		
Th										19.60		
Rb										196.58		
Cs										4.64		
Sr										575.05		
Ba										1048.94		
La	36.9									34.86		
Ce	74									73.63		
Pr	8.6									7.94		
Nd	39									36.12		
Sm	7.37									7.59		
Eu	1.5									1.45		
Gd	7.15									4.71		
Tb	0.71									0.82		
Dy	4.05									4.51		
Ho	0.56									0.89		
Er	1.89									2.31		
Tm	0.23									0.39		

Yb	1.55	1.97
Lu	0.21	0.33
ΣREE	183.7	177.5
Eu/Eu*	0.6	0.7
(La/Lu)cn	18.3	11.1
(La/Sm)cn	3.1	2.9
(Gd/Yb)cn	3.7	1.9
(Tb/Lu)cn	2.3	1.7

*Type: Gr= Granites; Gb= Gabbros; Mzg= Monzogranites; Mz= Monzonites; QMz= Quartz monzonites; QMzg= Quartz monzogranites

**References: 1 Trace elements present study; 2 Major elements Papadopoulou (2003) 3 Trace elements Papadopoulou (2003)

Maronia pluton

	Intermediate										
Sample	**MP-88**	**PMR-4**	**MP-83**	**MP-89**	**MP-74**	**MP-32**	**MP-76**	**MP-97**	**MP-77**	**MP-98**	**MP-99**
Type*	QMz	QMz	QMz	Mz	QMzg	QMz	QMz	QMz	QMz	QMz	QMz
Reference**	2,3	1,2	2,3	2,3	2,3	2,3	2,3	2,3	2,3	2,3	2,3
SiO_2	56.16	56.19	56.27	56.47	56.53	56.53	57.11	57.11	57.53	57.77	58.09
TiO_2	0.86	0.87	0.86	0.93	0.84	0.90	0.82	0.86	0.93	0.86	0.74
$Al2O_3$	15.72	16.13	16.52	15.84	16.39	15.44	15.83	16.23	16.47	16.44	17.09
FeOtot	7.21	6.53	7.17	6.62	6.51	6.84	6.02	7.06	6.43	6.88	6.56
MnO	0.11	0.12	0.12	0.14	0.13	0.13	0.12	0.13	0.13	0.12	0.12
MgO	4.01	4.34	3.06	3.95	3.88	4.30	3.52	3.31	3.50	3.35	3.10
CaO	6.87	6.87	6.31	6.57	6.54	6.72	6.48	6.11	5.38	5.94	5.38
Na_2O	2.52	2.72	2.73	3.02	2.94	2.81	2.90	2.67	2.88	2.65	2.95
K_2O	5.11	4.36	4.78	4.42	3.88	4.63	4.74	4.91	4.49	4.94	5.01
P_2O_5	0.58	0.39	0.51	0.52	0.42	0.55	0.80	0.51	0.56	0.47	0.39
mg#	49.76	54.21	43.14	51.53	51.49	52.81	51.04	45.51	49.22	46.43	45.70
LOI	1.1	0.6	0.4	1.3	1.0	0.1	0.5	0.4	0.5	0.3	1.0
Sum	100.2	99.1	98.8	99.8	99.1	98.9	98.8	99.3	98.8	99.8	100.4
XRF											
Sc	21		17	23	11	53	45	16	61	17	17
V	182		182	188	191	207	186	169	194	162	139
Cr	64		24	52	69	116	154	33	52	50	28
Ni											
Pb	37		41	42	14	19	31	35	25	41	58
Zr	237		234	263	240	228	231	244	219	296	298
Nb	16		16	11	8	2	1	17	8	19	17
U				5	5	18	9		3		
Y	25		24	23				22		26	25
Th				21	24	30	41		31		
Rb	298		225	191	200	244	236	229	213	256	244
Sr	541		668	614	645	718	691	597	708	578	592
Ba	1292		1456	1254	1005	1691	1480	1237	1680	1188	1146
La				36	56	12	37		39	38	
Ce				74	117	141	141		112	79	
Nd				40	53	84	62		44	40	
ICP-MS											
Sc		23.77									
V		189.33									
Cr		77.78									
Ni	35	39.68	25	24	26	32	24	22	28	29	25
Pb	37	26.94									
Zr		192.63									
Hf		4.49									
Nb		13.60									
Ta		0.90		1.02	9.99	4.49	9.23		4.60		
U		5.94									
Y		22.63									

Th	22.83			
Rb	194.15			
Cs	5.42			
Sr	548.95			
Ba	942.64			
La	32.53	35.9	37.6	38.2
Ce	69.14	74	76	79
Pr	7.30	8.8	8.8	9.2
Nd	32.76	40	39	40
Sm	6.84	7.61	7.33	7.42
Eu	1.48	1.64	1.49	1.38
Gd	4.15	6.84	6.97	6.81
Tb	0.72	0.7	0.72	0.64
Dy	4.02	4.28	4.33	3.87
Ho	0.74	0.6	0.62	0.53
Er	2.21	2.07	2.14	1.84
Tm	0.32	0.25	0.25	0.21
Yb	1.93	1.74	1.9	1.56
Lu	0.29	0.24	0.25	0.21
ΣREE	164.4	184.7	187.4	190.9
Eu/Eu*	0.8	0.7	0.6	0.6
(La/Lu)cn	11.7	15.5	15.6	18.9
(La/Sm)cn	3.0	3.0	3.2	3.2
(Gd/Yb)cn	1.7	3.2	3.0	3.5
(Tb/Lu)cn	1.7	2.0	2.0	2.1

*Type: Gr= Granites; Gb= Gabbros; Mzg= Monzogranites; Mz= Monzonites; QMz= Quartz monzonites; QMzg= Quartz monzogranites

**References: 1 Trace elements present study; 2 Major elements Papadopoulou (2003) 3 Trace elements Papadopoulou (2003)

Maronia pluton			
	Intermediate		
Sample	**MP-100**	**MP-24**	**MP-404**
Type*	QMz	QMz	QMzg
Reference**	2,3	2,3	2,3
SiO_2	58.11	58.61	62.68
TiO_2	0.70	0.77	0.60
$Al2O_3$	16.98	15.39	15.76
FeOtot	6.40	5.74	5.21
MnO	0.12	0.12	0.14
MgO	2.83	4.30	2.84
CaO	5.58	5.49	4.89
Na_2O	3.06	2.85	3.10
K_2O	4.75	4.40	3.90
P_2O_5	0.40	0.47	0.29
mg#	44.08	57.16	49.28
LOI	0.5	0.4	0.8
Sum	99.4	98.5	100.2
XRF			
Sc	16	48	
V	139	157	110
Cr	25	136	15
Ni			
Pb	56	25	23
Zr	265	211	149
Nb	17	13	11
U		15	
Y	26		24
Th		41	25

Rb	230	263	157
Sr	649	596	504
Ba	1194	1100	726
La		33	29
Ce		96	39
Nd		53	
ICP-MS			
Sc			
V			
Cr			
Ni	26	45	11
Pb			
Zr			
Hf			
Nb			
Ta		3.72	
U			
Y			
Th			
Rb			
Cs			
Sr			
Ba			
La			
Ce			
Pr			
Nd			
Sm			
Eu			
Gd			
Tb			
Dy			
Ho			
Er			
Tm			
Yb			
Lu			
ΣREE			
Eu/Eu*			
(La/Lu)cn			
(La/Sm)cn			
(Gd/Yb)cn			
(Tb/Lu)cn			

*Type: Gr= Granites; Gb= Gabbros; Mzg= Monzogranites; Mz= Monzonites; QMz= Quartz monzonites; QMzg= Quartz monzogranites

**References: 1 Trace elements present study; 2 Major elements Papadopoulou (2003) 3 Trace elements Papadopoulou (2003)

Evros Volcanics

	PxBt Group											
Sample	**FA-1**	**FG-101**	**MAA-2**	**AK-7**	**FKP-30**	**MAA-1**	**MSR-11**	**PPT-1**	**MSR-12**	**PPT-3**	**CEP-16**	**MESTI-**
Type	And(Px)	And(Px)	And(Px)	And(Px)	And(Px)	And(Px)	And(Px)	And(Px)	And(Px)	And(Px)	And(Px)	And(Px)
Reference	1	3	1	3	1	1	1	2	1	2	1	1
SiO_2	54.30	55.53	56.26	56.89	57.49	57.90	57.92	58.39	58.61	58.84	58.90	58.90
TiO_2	0.74	0.90	0.68	0.76	0.70	0.54	0.57	0.63	0.62	0.79	0.91	0.86
$Al2O_3$	14.94	17.65	15.11	16.14	17.24	17.14	16.75	16.96	16.97	16.68	15.92	16.90
FeOtot	6.22	6.97	7.89	6.49	5.89	6.75	5.87	5.80	5.58	6.45	6.41	5.61
MnO	0.08	0.11	0.23	0.07	0.17	0.18	0.11	0.11	0.12	0.13	0.14	0.11
MgO	3.77	1.77	4.54	5.23	1.97	2.95	3.61	3.26	3.29	3.54	3.04	2.97
CaO	7.51	8.35	7.67	6.45	6.84	7.71	7.08	7.03	6.97	6.97	7.58	6.77
Na_2O	2.52	2.84	2.14	3.92	3.41	2.91	2.66	2.78	2.59	2.16	3.02	2.41

K_2O	2.96	2.10	2.74	2.20	2.50	2.02	1.92	1.90	2.05	1.82	2.33	2.19
P_2O_5	0.19	0.20	0.42	0.16	0.25	0.18	0.14	0.15	0.15	0.14	0.31	0.17
mg#	51.93	31.11	50.62	58.93	37.36	43.78	52.30	50.02	51.24	49.43	45.81	48.56
LOI	5.6	2.9	0.8	0.6	2.8	0.9	1.2	2.1	1.6	2.3	0.8	1.6
Sum	98.8	99.3	98.5	98.9	99.3	99.2	97.8	99.1	98.5	99.8	99.4	98.5
XRF												
Sc	25	23		21	16							
V	136	154	215	143	113	8			187			
Cr	72	47	42	57	46				31			
Ni	21	14	6	23	13							
Zr	188	187	98	161	199	135			106			
Nb	6	7	2	5	6	9			2			
Y	26	29	22	24	26	17			22			
Rb	157	184	147	80	143	197	139		109			
Sr	488	487	368	391	516	169	408		383			
Ba	533	534	472	624	596	448	438		565			
Ce	59	63		47	65							
Nd	27	34		26	30							
ICP-MS												
Sc			29.97			17.37		30.23	20.98	21.69	23.05	27.88
V		199	220	217		161		173.14	179	172.04	190	154.00
Cr			52.75			14.89		31.02	36.14	49.88	17.21	15.65
Ni		5.6	37.01	7.5		27.35			26.8	38.26	31.77	191.17
Pb		1.6	11.0	4.1		12.7		16.76	17	21.51	13	13
Zr		123.1	84.19	120		100.17		126.66	95.59	106.61	92.4	152.41
Hf		3.3	2.37	2.9		2.65		3.14	2.46	2.64	2.69	3.83
Nb		7.7	5.90	5.9		4.5		7.96	6.2	6.07	4.7	9.90
Ta		0.6	0.46	0.6		0.34		0.59	0.56	0.53	0.33	0.74
U		3.3	5.80	3		2.70		1.91	3	2.88	2.8	2.20
Y		21.27	18.62	20.1		23.68		24.46	18.39	19.37	24.10	35.16
Th		9.9	11.40	8.6		7.80		6.54	7.58	7.57	6.85	8.73
Rb		166.3	154.00	76.5		77.0		66.80	115	148.14	80	90
Cs		4.2	2.80	3.2		2.6		3.55	4.5	8.05	2.6	3.1
Sr		465.6	367.50	401.7		442.17		341.85	376.34	385.69	433.71	348.94
Ba		534.0	479.79	635.0		607.16		501.03	602.63	654.79	561.42	563.14
La		25.70	10.72	19.90		13.30		19.14	15.08	16.08	12.76	27.51
Ce		54.20	27.17	39.20		28.98		38.56	30.42	33.03	28.58	50.71
Pr		6.14	3.65	4.49		3.61		4.23	3.36	3.46	3.66	6.83
Nd		23.90	18.46	19.50		16.94		18.76	14.75	15.42	16.94	29.69
Sm		5.07	4.06	4.08		4.24		4.26	3.25	3.77	3.74	6.62
Eu		1.15	1.00	1.00		0.98		1.04	0.85	0.59	1.01	1.73
Gd		4.45	3.55	3.82		3.54		3.22	3.19	3.15	3.43	6.30
Tb		0.71	0.52	0.56		0.69		0.66	0.54	0.50	0.67	1.01
Dy		3.79	3.51	3.61		3.98		4.27	3.16	3.32	4.18	6.42
Ho		0.75	0.67	0.72		0.78		0.87	0.63	0.63	0.82	1.28
Er		2.36	1.91	2.29		2.42		2.39	1.92	2.00	2.25	3.53
Tm		0.32	0.26	0.32		0.40		0.35	0.32	0.34	0.39	0.55
Yb		2.06	1.44	2.18		2.21		2.09	1.72	1.94	2.44	3.35
Lu		0.34	0.31	0.33		0.39		0.35	0.30	0.26	0.40	0.52
ΣREE		377.7	242.1	305.8		269.7		306.4	245.7	253.4	266.6	464.0
Eu/Eu*		0.7	0.8	0.8		0.8		0.8	0.8	0.5	0.8	0.8
(La/Lu)cn		7.9	3.6	6.3		3.5		5.7	5.1	6.5	3.3	5.4
(La/Sm)cn		3.2	1.7	3.1		2.0		2.8	2.9	2.7	2.1	2.6
(Gd/Yb)cn		1.7	2.0	1.4		1.3		1.2	1.5	1.3	1.1	1.5
(Tb/Lu)cn		1.4	1.1	1.2		1.2		1.3	1.2	1.3	1.1	1.3

*Type: And(Px)= Pyroxene andesites; BasAnd= Basaltic andesites; TrAnd= Trachyandesites; TrDct= Trachydacites; Dct= Dacites; Rhy= Rhyolites

**References: 1 Major & trace elements Christofides et al (2004) and unpublished of the same author; 2 Major and trace elements present study; 3 Trace elements present study

Evros Volcanics												
	PxBt Group											
Sample	FLE-3	FKR-40	MES-3	FKP-31	FG-100	FP-5	FL13	FP-6	FL-12	FL-14	MAS-20	MAS-21
Type*	BasAnd	BasAnd	BasAnd	TrAnd	TrAnd	TrAnd	TrAnd	TrAnd	TrAnd	TrAnd	TrDct	TrDct
Reference**	3	3	1	1	1	1	1	1	1	1	1	1
SiO_2	53.87	54.98	55.77	55.12	56.68	57.29	57.64	58.18	59.39	59.99	63.81	64.10
TiO_2	0.81	0.74	0.84	0.76	0.79	0.69	0.77	0.74	0.69	0.69	0.49	0.52
$Al2O_3$	16.83	16.53	17.60	16.89	17.67	16.12	16.80	16.73	16.78	16.81	14.62	14.40
FeOtot	7.20	7.62	7.24	6.53	6.30	5.43	5.65	5.66	4.41	4.87	3.73	3.73
MnO	0.10	0.11	0.14	0.15	0.10	0.08	0.06	0.08	0.07	0.05	0.09	0.08
MgO	4.76	3.84	3.81	3.01	2.22	2.03	2.06	2.27	1.01	2.21	2.08	1.95
CaO	8.97	8.94	8.04	7.32	8.04	7.03	6.46	6.56	5.25	5.68	3.99	4.46
Na_2O	3.26	3.98	2.34	2.62	3.40	4.10	4.66	4.72	3.74	4.46	2.27	2.47
K_2O	0.99	1.21	1.33	3.33	2.93	2.99	1.77	2.06	3.50	2.55	5.29	5.09
P_2O_5	0.17	0.14	0.15	0.24	0.24	0.19	0.19	0.18	0.22	0.20	0.25	0.16
mg#	54.10	47.26	48.38	45.08	38.55	40.03	39.42	41.71	29.03	44.71	49.81	48.20
LOI	2.2	0.9	1.0	1.4	0.9	3.2	3.2	2.0	4.4	1.7	2.5	2.5
Sum	99.1	99.0	98.3	97.4	99.3	99.1	99.2	99.1	99.4	99.2	99.1	99.4
XRF												
Sc	36	25		16	19	16	22	18		15		
V	166	168		113	126	116	120	113	24	100	215	
Cr	92	34		46	41	68	55	71		45	42	
Ni	33	3		13	12	20	22	30	1	16	6	
Zr	146	148		199	193	192	203	194	115	199	98	
Nb	5	4		6	7	5	6	5	7	6	2	
Y	26	23		26	27	25	27	28	16	26	22	
Rb	83	45	259	143	112	121	163	206	302	130	147	259
Sr	390	458	514	516	489	437	553	423	83	408	368	514
Ba	595	481	825	596	507	590	910	623	451	584	472	825
Ce	44	41		65	60	52	60	76		64		
Nd	24	21		30	25	26	31	32		27		
ICP-MS												
Sc			26.18	17.53					9.79		12.54	
V	228	223	257	179					182		85	
Cr			28.22	36.09					15.27		64.79	
Ni	3.3	1.5		53.2							34.76	
Pb	5.2	1.8	10	16					20		31	
Zr	94.6	96.1	74.51	154.37					90.06		172.01	
Hf	2.6	2.5	2.07	3.69					2.22		4.56	
Nb	5.3	4.3	3.80	9.10					8.20		17.00	
Ta	0.5	0.5	0.30	0.75					0.36		1.50	
U	3.3	1.8	1.30	3.7					4.00		8.00	
Y	20.3	18.2	24.82	25.70					16.20		19.30	
Th	6.9	4.7	3.90	13.27					7.74		26.91	
Rb	71.9	41.39	43.00	123					96.00		209.00	
Cs	2.9	1.5	2.30	2.70					16.00		7.20	
Sr	353.9	466.2	355.07	527.15					308.03		452.25	
Ba	564	503	376.44	533.92					435.11		1130.10	
La	18.70	15.30	10.64	27.85					16.13		35.73	
Ce	36.40	30.80	23.24	55.27					33.11		70.48	
Pr	4.31	3.62	2.94	6.33					3.75		7.41	
Nd	17.30	13.90	13.03	26.50					16.00		27.89	
Sm	3.66	3.18	3.40	5.61					3.39		5.13	
Eu	0.94	0.89	1.10	1.50					1.53		1.20	
Gd	3.85	3.20	3.14	4.62					3.20		4.22	
Tb	0.62	0.55	0.61	0.80					0.49		0.56	
Dy	3.58	3.33	4.22	4.76					2.72		3.17	
Ho	0.79	0.69	0.84	0.93					0.60		0.60	
Er	2.33	1.93	2.45	2.38					1.54		1.90	

Tm	0.31	0.31	0.40	0.38					0.23		0.28
Yb	2.13	2.11	2.40	2.65					1.60		1.80
Lu	0.34	0.30	0.38	0.44					0.26		0.24
ΣREE	292.6	250.8	238.0	415.5					258.2		432.6
Eu/Eu*	0.8	0.8	1.0	0.9					1.4		0.8
(La/Lu)cn	5.7	5.3	2.9	6.5					6.4		15.3
(La/Sm)cn	3.2	3.0	2.0	3.1					3.0		4.4
(Gd/Yb)cn	1.5	1.2	1.1	1.4					1.6		1.9
(Tb/Lu)cn	1.2	1.2	1.1	1.2					1.3		1.6

*Type: And(Px)= Pyroxene andesites; BasAnd= Basaltic andesites; TrAnd= Trachyandesites; TrDct= Trachydacites; Dct= Dacites; Rhy= Rhyolites

**References: 1 Major & trace elements Christofides et al (2004) and unpublished of the same author; 2 Major and trace elements present study; 3 Trace elements present study

Evros Volcanics

	HblBt Group											
Sample	**AK-1**	**FK-32**	**FK-31**	**AK-4**	**MSR-13**	**FT-2**	**AK-3**	**AK-6**	**AK-8**	**CEP-14**	**FI-10**	**FK-30**
Type*	And	And	And	And	And	And	And	And	And	Dct	Dct	Dct
Reference**	1	1	1	1	1	1	1	1	1	1	1	1
SiO_2	58.08	59.56	60.40	60.62	60.73	61.16	61.27	62.25	62.95	64.83	65.70	66.79
TiO_2	0.46	0.53	0.51	0.49	0.53	0.59	0.49	0.43	0.52	0.50	0.50	0.50
$Al2O_3$	15.95	15.83	16.64	16.49	16.98	16.97	16.03	16.30	16.44	14.79	15.33	15.15
FeOtot	3.84	4.68	4.26	5.31	5.07	4.78	4.90	4.74	4.65	3.64	3.54	2.95
MnO	0.03	0.04	0.07	0.07	0.10	0.06	0.05	0.02	0.11	0.10	0.01	0.01
MgO	3.65	4.94	2.32	3.17	2.68	2.28	3.53	3.46	2.23	2.05	2.27	2.14
CaO	4.27	5.90	5.44	5.28	6.37	5.83	4.74	4.47	4.03	4.22	5.46	5.46
Na_2O	3.18	2.91	2.59	3.69	2.87	3.65	4.08	3.95	3.66	2.85	3.20	3.77
K_2O	2.79	1.82	2.88	2.14	1.96	2.36	2.19	2.11	2.52	5.11	2.07	1.97
P_2O_5	0.14	0.13	0.12	0.14	0.17	0.15	0.14	0.14	0.12	0.26	0.14	0.14
mg#	62.90	65.28	49.27	51.55	48.52	45.90	56.20	56.55	46.06	50.12	53.26	56.33
LOI	7.0	2.8	3.5	1.7	1.9	1.5	1.7	1.3	1.9	1.8	1.5	0.5
Sum	99.4	99.1	98.8	99.1	99.3	99.3	99.1	99.2	99.1	100.1	99.8	99.4
XRF												
Sc	17	18		16		13	16	17		5	16	17
V	77	88	112	90		71	83	76	102	18	70	75
Cr	32	39	4	36		33	35	33	4	25	37	39
Ni	8	15	9	1		7	6	3	15	3	9	8
Zr	273	140	123	138		145	134	132	127	133	131	136
Nb	8	8	4	6		6	5	7	2	9	6	7
Y	24	23	18	21		26	20	19	21	24	20	19
Rb	124	45	84	71	766	80	80	65	72	247	74	63
Sr	1099	263	260	325	398	314	296	326	415	223	258	251
Ba	499	442	461	506	68	572	470	470	701	453	445	443
Ce	55	50		46		45	43	39		73	41	47
Nd	18	17		21		26	15	15		25	14	11
ICP-MS												
Sc	12.35					17.27		10.53		11.88		
V	111					122		120		91		
Cr	25.46					13.71		11.96		54.55		
Ni										21.66		
Pb	18					16		11		31		
Zr	114.34					132.66		91.31		179.19		
Hf	2.68					3.60		2.45		4.55		
Nb	7.60					8.10		7.60		17.00		
Ta	0.74					0.67		0.68		1.48		
U	3.00					2.50		2.40		8.00		
Y	18.43					25.75		15.31		20.23		
Th	8.31					10.38		7.30		27.17		
Rb	88.00					92.00		60.00		218.00		

Cs	2.20					3.80		1.40		7.40		
Sr	317.59					375.42		297.86		486.43		
Ba	525.00					687.92		435.68		1316.58		
La	20.50					26.31		16.50		37.51		
Ce	40.69					50.27		33.45		72.36		
Pr	4.17					5.61		3.49		7.60		
Nd	16.94					22.54		13.97		28.48		
Sm	3.21					4.50		2.71		5.41		
Eu	0.87					1.10		0.89		1.25		
Gd	2.95					4.38		2.37		3.88		
Tb	0.57					0.70		0.40		0.62		
Dy	3.36					4.19		2.38		3.41		
Ho	0.63					0.82		0.47		0.59		
Er	1.80					2.45		1.54		1.90		
Tm	0.29					0.40		0.28		0.29		
Yb	1.63					2.75		1.53		2.05		
Lu	0.31					0.36		0.29		0.31		
ΣREE	284.8					373.0		236.1		449.4		
Eu/Eu*	0.8					0.7		1.1		0.8		
(La/Lu)cn	6.8					7.7		5.9		12.5		
(La/Sm)cn	4.0					3.7		3.8		4.4		
(Gd/Yb)cn	1.5					1.3		1.2		1.5		
(Tb/Lu)cn	1.2					1.3		0.9		1.3		

*Type: And(Px)= Pyroxene andesites; BasAnd= Basaltic andesites; TrAnd= Trachyandesites; TrDct= Trachydacites; Dct= Dacites; Rhy= Rhyolites

**References: 1 Major & trace elements Christofides et al (2004) and unpublished of the same author; 2 Major and trace elements present study; 3 Trace elements present study

Evros Volcanics

	HblBt Group											
Sample	**FLE-1**	**FT-1**	**CEP-17**	**FLK-5**	**FPL-1**	**CEP-18B**	**FF-200**	**CEP-19**	**CEP-6**	**FF-21**	**FLE-2**	**FL-11**
Type*	Dct	Dct	Rhy	Rhy	Rhy	Rhy	Rhy	Rhy	Rhy	Rhy	Rhy	Rhy
Reference**	1	1	1	1	1	1	1	1	1	1	1	1
SiO_2	68.23	68.79	68.03	69.22	71.09	71.18	71.23	71.29	71.36	71.36	71.54	71.97
TiO_2	0.53	0.55	0.46	0.23	0.25	0.22	0.21	0.23	0.26	0.26	0.44	0.21
$Al2O_3$	15.04	15.05	15.60	13.66	13.15	13.62	13.37	13.83	13.18	13.18	13.71	13.44
FeOtot	3.16	2.09	2.95	1.49	1.60	1.34	1.48	1.23	1.38	1.38	2.73	1.59
MnO	0.01	0.02	0.06	0.04	0.03	0.08	0.06	0.07	0.03	0.03	0.02	0.02
MgO	1.64	1.59	0.91	1.43	0.78	0.53	0.51	0.41	0.64	0.64	1.23	0.25
CaO	4.38	4.82	4.16	2.57	1.67	2.56	1.76	1.86	1.68	1.68	4.03	1.04
Na_2O	2.66	3.48	3.16	1.35	3.64	2.40	2.91	3.21	3.12	3.12	2.74	1.65
K_2O	3.01	2.38	3.02	3.70	4.20	3.04	4.32	4.34	4.57	4.57	2.65	8.02
P_2O_5	0.15	0.14	0.14	0.08	0.06	0.07	0.06	0.07	0.07	0.07	0.14	0.06
mg#	48.07	57.52	35.46	63.04	46.57	41.33	38.11	37.21	45.11	45.11	44.60	21.85
LOI	0.6	0.7	0.6	5.5	3.3	4.9	3.3	2.6	3.6	3.6	0.6	1.0
Sum	99.4	99.6	99.1	99.3	99.8	100.0	99.2	99.1	99.9	99.9	99.8	99.3
XRF												
Sc	15	5			18				5	5	12	
V	71	14		13	113		17		18	18	55	24
Cr	36	24		0	71		0		25	25	28	0
Ni	7	4		11	30		0		3	3	6	1
Zr	146	130		121	194		117		133	133	142	115
Nb	7	11		4	5		8		9	9	7	7
Y	22	24		16	28		21		24	24	22	16
Rb	110	227		220	206		225		247	247	91	302
Sr	293	154		1176	423		205		223	223	272	83
Ba	677	408		1053	623		401		453	453	615	451
Ce	52	64			76				73	73	55	
Nd	21	19			32				25	25	25	

ICP-MS					
Sc	12.64	15.00	8.62		8.27
V	105	92	21	20	23
Cr	14.01	20.00	16.61		15.01
Ni			25.59		
Pb	15	22	27	30	28
Zr	102.65	108.57	94.23	112.25	103.28
Hf	2.66	2.98	2.93	3.16	2.95
Nb	7.20	8.94	13.00	11.00	12.00
Ta	0.84	0.67	1.39	1.11	1.06
U	2.50	3.10	8.60	8.60	7.80
Y	19.27	17.87	15.52	17.13	17.32
Th	8.80	10.08	22.24	18.20	17.93
Rb	80.00	97.00	217.00	200.00	211.00
Cs	17.00	1.55	5.30	10.00	6.80
Sr	332.01	297.58	143.03	473.28	184.06
Ba	632.76	771.12	441.81	645.95	620.22
La	22.37	22.05	27.22	19.08	22.16
Ce	44.86	46.51	53.76	38.55	46.76
Pr	4.62	4.64	4.90	3.92	4.36
Nd	17.73	17.66	16.98	14.22	16.44
Sm	3.60	4.11	3.05	2.76	3.02
Eu	0.97	1.00	0.68	0.55	0.71
Gd	3.16	3.07	2.29	2.53	2.52
Tb	0.52	0.42	0.37	0.31	0.37
Dy	2.91	2.91	2.52	2.65	2.77
Ho	0.67	0.56	0.45	0.50	0.53
Er	1.75	1.81	1.43	1.45	1.53
Tm	0.27	0.30	0.28	0.29	0.23
Yb	1.65	1.73	1.91	1.82	1.80
Lu	0.32	0.29	0.26	0.31	0.26
ΣREE	302.8	303.6		252.4	282.1
Eu/Eu*	0.9	0.8		0.6	0.8
(La/Lu)cn	7.3	7.9		6.4	8.9
(La/Sm)cn	3.9	3.4		4.3	4.6
(Gd/Yb)cn	1.5	1.4		1.1	1.1
(Tb/Lu)cn	1.1	1.0		0.7	1.0

*Type: And(Px)= Pyroxene andesites; BasAnd= Basaltic andesites; TrAnd= Trachyandesites; TrDct= Trachydacites; Dct= Dacites; Rhy= Rhyolites

**References: 1 Major & trace elements Christofides et al (2004) and unpublished of the same author; 2 Major and trace elements present study; 3 Trace elements present study

Evros Volcanics				
	HblBt Group			
Sample	**FD-20**	**MA-1**	**FLK6**	**FLY-1**
Type*	Rhy	Rhy	Rhy	Rhy
Reference**	1	1	1	1
SiO_2	72.16	73.29	75.86	79.09
TiO_2	0.28	0.24	0.22	0.26
$Al2O_3$	13.41	13.31	12.47	10.63
FeOtot	1.48	1.23	0.90	1.09
MnO	0.02	0.01	0.02	0.02
MgO	0.98	0.13	0.52	0.84
CaO	2.32	0.52	1.04	1.28
Na_2O	1.63	2.71	3.80	2.89
K_2O	4.63	4.99	4.41	3.06
P_2O_5	0.07	0.06	0.02	0.08

mg#	54.20	15.82	50.48	57.97
LOI	3.0	1.5	0.8	1.0
Sum	99.9	98.0	100.1	100.2
XRF				
Sc	7		3	4
V	18	8	7	10
Cr	23	0	27	22
Ni	2		5	3
Zr	146	135	117	122
Nb	11	9	9	8
Y	27	17	25	20
Rb	168	197	176	123
Sr	327	169	122	176
Ba	430	448	778	641
Ce	53		62	47
Nd	24		28	14
ICP-MS				
Sc				
V				
Cr				
Ni				
Pb				
Zr				
Hf				
Nb				
Ta				
U				
Y				
Th				
Rb				
Cs				
Sr				
Ba				
La				
Ce				
Pr				
Nd				
Sm				
Eu				
Gd				
Tb				
Dy				
Ho				
Er				
Tm				
Yb				
Lu				
ΣREE				
Eu/Eu*				
(La/Lu)cn				
(La/Sm)cn				
(Gd/Yb)cn				
(Tb/Lu)cn				

*Type: And(Px)= Pyroxene andesites; BasAnd= Basaltic andesites; TrAnd= Trachyandesites; TrDct= Trachydacites; Dct= Dacites; Rhy= Rhyolites

**References: 1 Major & trace elements Christofides et al (2004) and unpublished of the same author; 2 Major and trace elements present study; 3 Trace elements present study

Samothraki Volcanics

	Old Group											
Sample	**LK-17**	**X-9**	**PSM-3**	**MT-117**	**LK-18**	**X-8**	**ZP-5**	**ZP-6**	**MAL-113**	**PSM-1**	**ZP-4**	**ZP-7**
Reference*	3	3	1	3	3	3	3	3	3	1	3	3
SiO_2	48.06	48.16	48.38	48.67	48.83	49.12	50.26	50.88	50.96	52.46	52.68	53.13
TiO_2	1.00	1.36	0.98	1.00	0.99	1.35	1.11	1.14	0.69	0.59	0.97	1.01
$Al2O_3$	14.97	16.17	18.25	18.04	15.23	16.18	17.31	17.39	12.85	14.64	17.28	17.79
FeOtot	5.60	6.29	9.01	6.66	5.97	6.21	4.27	3.86	4.99	5.72	5.43	4.58
MnO	0.17	0.03	0.17	0.13	0.17	0.21	0.19	0.25	0.57	0.16	0.12	0.17
MgO	6.32	3.49	5.02	2.21	5.95	3.83	4.80	5.07	0.97	3.03	3.91	4.10
CaO	9.68	11.69	5.81	8.83	9.61	10.95	7.33	6.91	10.61	9.20	6.07	4.53
Na_2O	4.10	3.96	3.55	5.95	4.76	3.94	5.23	5.01	4.10	2.98	6.07	6.19
K_2O	2.44	0.49	3.50	0.53	1.64	0.48	0.87	0.92	3.73	3.24	0.65	0.78
P_2O_5	0.27	0.30	0.21	0.25	0.22	0.30	0.23	0.24	0.43	0.15	0.32	0.19
mg#	66.80	49.71	49.82	37.16	63.95	52.36	66.72	70.06	25.71	48.54	56.17	61.46
LOI	4.3	4.7	4.6	4.9	3.0	4.2	4.2	3.6	9.4	7.7	3.9	4.4
Sum	96.9	96.7	99.5	97.2	96.4	96.8	95.8	95.3	99.3	99.9	97.4	96.9
XRF												
Sc			21		25		22	22		26	18	26
V	153	243			195	247	195	199			156	177
Cr	79	22		35	78	23	23	25			21	25
Ni	54	7		14	47	0	4	5	4		3	5
Zr	210	194			208	197	238	215			225	253
Nb	4	4			4	3	5	4			6	7
Rb		14			41	14	26	29			26	29
Sr	836	861			824	882	1214	929			633	1096
Ba	538	311		434	487	300	289	368	824		247	230
ICP-MS												
Sc	20	31				33						
V			233.74							154.31		
Cr			8.89							246.70		
Ni			21.40							65.70		
Pb			10.43	23.89		11.30			17.65	27.10		
Zr			105.03							146.62		
Hf			2.76	2.64					0.47	3.57		
Nb			4.07							6.80		
Ta			0.30	0.74					2.04	0.70		
U			0.54	2.73		1.24			1.67	5.55		
Y			29.29			32.40				22.20		
Th			4.09							19.81		
Rb			95.27							113.58		
Cs			62.53							6.20		
Sr		882	1497.98			861				823.13		
Ba			576.45							639.12		
La			15.86	25.27		19.00			32.68	28.82		
Ce		51.00	34.12	51.08		51.00			65.19	57.53		
Pr			4.16	6.16					8.22	6.01		
Nd			20.41	23.88		27.70			30.67	24.56		
Sm			4.91	4.74		6.73			6.10	4.99		
Eu			1.33	1.33		1.83			1.31	1.01		
Gd			4.61	3.97		6.39			5.67	3.97		
Tb			0.82	0.33		0.79			0.43	0.60		
Dy			4.98	3.57		4.97			3.84	3.58		
Ho			0.95	0.52		0.84			0.62	0.75		
Er			2.76	1.72		2.58			1.76	2.13		
Tm			0.45			0.33				0.40		
Yb			2.57	1.86		2.55			1.90	2.09		
Lu			0.41			0.31			0.13	0.33		
ΣREE			98.3	124.4		125.0			158.5	136.8		
Eu/Eu*			0.8			0.8			0.7	0.7		

(La/Lu)cn	4.0	6.4	26.1	9.1
(La/Sm)cn	2.0	1.8	3.4	3.6
(Gd/Yb)cn	1.4	2.0	2.4	1.5
(Tb/Lu)cn	1.4	1.7	2.2	1.2

*References: 1 Major and trace elements present study; 2 Major and XRF trace elements Vlachou (2003) and ICP-MS trace elements present study; 3 Major and trace elements Vlachou (2003)

Samothraki Volcanics

	Old Group											
Sample	**PSM-13**	**T-6**	**ZP-10**	**T-5**	**MBR-103**	**MAL-114**	**T-10**	**ZP-15**	**PSM-2**	**T-4**	**MT-125**	**ZP-2**
Reference*	1	3	3	3	3	3	3	2	1	3	3	3
SiO_2	55.37	55.47	55.64	56.24	56.31	57.15	57.18	57.26	57.32	57.84	59.15	59.53
TiO_2	0.84	0.70	0.64	0.75	0.57	0.92	0.67	0.57	0.90	0.73	0.71	0.60
$Al2O_3$	18.74	17.41	17.28	17.67	13.96	17.81	16.54	14.40	17.72	17.55	17.52	17.11
FeOtot	8.22	3.57	3.73	4.47	3.80	3.27	3.80	3.58	6.57	3.58	4.82	3.95
MnO	0.04	0.21	0.11	0.11	0.10	0.15	0.13	0.14	0.06	0.15	0.13	0.04
MgO	2.13	1.30	0.98	2.04	4.62	2.37	1.78	3.82	2.73	1.68	1.06	0.76
CaO	2.19	7.11	8.53	6.51	7.61	2.30	7.99	8.38	2.65	5.65	6.09	5.97
Na_2O	0.94	3.87	6.36	4.11	2.82	5.28	3.05	3.01	7.68	4.11	3.82	6.82
K_2O	2.20	3.39	0.73	3.60	2.80	4.79	2.45	2.93	0.45	4.00	3.59	0.50
P_2O_5	0.18	0.21	0.19	0.26	0.12	0.52	0.16	0.13	0.22	0.24	0.26	0.15
mg#	31.57	39.33	31.86	44.83	68.43	56.38	45.51	65.52	42.54	45.53	28.14	25.53
LOI	7.1	5.0	3.6	3.1	4.9	2.7	4.2	3.5	3.0	2.5	1.4	3.6
Sum	98.0	98.2	97.8	98.8	97.6	97.2	98.0	97.8	99.3	98.1	98.6	99.0
XRF												
Sc	25	15	17	12					25	13		18
V		109	95	114	150		124	151		112	134	112
Cr		22	29	20	243	1	34	219		21		30
Ni		7	6	0	50	1	4	44		3		7
Zr		245	338	252	142		221	140		246	195	212
Nb		5	18	8	6		6	7		9	7	8
Rb		123	17	122	105		90	114		129	131	14
Sr		545	1168	531	723		616	812		511	464	743
Ba		683	687	658	528	1359	643	509		733	656	168
ICP-MS												
Sc							21					
V	203.83							155	156.13			
Cr	55.21											
Ni	40.40											
Pb	165.05				23.66	29.52		21.20	14.50		22.30	
Zr	233.62								187.56			
Hf	5.99					2.07		3.8	4.83			
Nb	12.31							5.7	9.69			
Ta	0.86					0.33		0.5	0.87			
U	4.09				6.35	4.57		7.2	2.93		3.26	
Y	26.93							19.1	26.56		23.80	
Th	31.22				17.00			20.5	14.96		17.00	
Rb	74.28							100.3	12.88			
Cs	11.66							4	3.07			
Sr	540.24				757			641.6	596.70		485	
Ba	778.38							505	199.33			
La	56.13				28.57	43.53		29	30.64		31.00	
Ce	104.94				52.06	84.63		55.7	66.89		67.00	
Pr	11.06				6.06	10.96		6.14	7.25			
Nd	47.20				22.73	39.98		22.7	31.16		29.40	
Sm	9.32				4.02	8.21		4.3	5.92		6.00	
Eu	1.65				1.01	2.29		1.07	1.14		1.51	
Gd	6.05				4.42	8.23		3.72	5.30		5.37	
Tb	0.88				0.27	0.71		0.55	0.78		0.59	

Dy	5.07				2.95	4.42		3.33	4.74		3.74
Ho	0.94				0.36	0.83		0.71	0.89		0.61
Er	2.61				1.46	2.29		1.99	2.52		1.98
Tm	0.45							0.3	0.44		0.25
Yb	2.06				1.28	2.16		2.08	2.43		2.12
Lu	0.37					0.08		0.32	0.38		0.27
ΣREE	248.7				126.3	208.3		131.9	160.5		
Eu/Eu*	0.6				0.7	0.8		0.8	0.6		0.8
(La/Lu)cn	15.9				2.7	56.5		9.4	8.4		11.9
(La/Sm)cn	3.8				4.5	3.3		4.2	3.3		3.3
(Gd/Yb)cn	2.4				2.8	3.1		1.4	1.8		2.0
(Tb/Lu)cn	1.6				0.2	6.0		1.2	1.4		1.5

*References: 1 Major and trace elements present study; 2 Major and XRF trace elements Vlachou (2003) and ICP-MS trace elements present study; 3 Major and trace elements Vlachou (2003)

Samothraki Volcanics

	Old Group		Intermediate Group									
Sample	**MT-107**	**ZP-3**	**KP-2**	**MK-102**	**KP-6**	**KP-5**	**KP-8**	**KP-7**	**KP-3**	**MK-107**	**X-3**	**MX-110**
Reference*	3	3	3	2	3	3	3	3	3	3	3	3
SiO_2	59.74	61.22	52.02	52.65	54.82	55.42	56.46	56.71	57.10	59.38	60.29	61.01
TiO_2	0.65	0.62	0.83	0.82	0.55	0.54	0.61	0.52	0.51	0.50	0.68	0.71
$Al2O_3$	17.40	17.37	17.34	17.49	15.42	14.83	15.60	15.08	14.85	16.54	17.31	16.64
FeOtot	3.26	4.35	4.15	5.20	4.18	4.34	2.92	4.24	4.30	3.73	4.28	3.46
MnO	0.15	0.04	0.17	0.17	0.09	0.09	0.12	0.10	0.09	0.08	0.08	0.15
MgO	0.78	1.54	4.52	5.44	3.60	3.59	2.87	3.36	3.25	2.53	1.70	2.31
CaO	2.98	3.50	6.80	6.34	6.59	6.50	8.80	5.73	5.85	4.59	4.72	5.02
Na_2O	3.21	7.09	3.48	3.50	3.23	3.51	3.06	3.42	3.42	3.11	3.85	3.93
K_2O	7.21	0.49	3.61	3.26	3.11	2.91	2.32	3.16	3.07	3.83	4.04	3.59
P_2O_5	0.25	0.16	0.85	0.59	0.14	0.14	0.15	0.14	0.14	0.11	0.25	0.23
mg#	29.91	38.70	66.00	65.08	60.57	59.59	63.69	58.55	57.38	54.75	41.42	54.30
LOI	2.0	2.8	2.1	1.7	7.7	7.1	4.7	6.6	6.5	4.2	1.3	0.7
Sum	97.6	99.2	95.9	97.1	99.4	99.0	97.6	99.1	99.1	98.6	98.5	97.8
XRF												
Sc		19			24	21	20		21			
V		107	191	235	99	95	119	89	82	116	143	190
Cr	18	40	33	29	150	150	127	127	130	121	39	37
Ni	3	7	16	11	44	37	27	32	33	23	14	10
Zr		240	272	163	192	195	243	193	200	135	275	199
Nb		7	6	7	5	11	9	9	8	6	8	10
Rb		11	102	97	124	117	87	124	121	128	158	148
Sr		759	1180	1222	641	660	614	594	606	397	767	669
Ba	2152	106	1490	1526	600	611	607	607	40	595	779	759
ICP-MS												
Sc			18					20			22	
V				221								
Cr												
Ni				10.8								
Pb	46.07		21.90	45.43						57.70		20.90
Zr				152								
Hf				4.4								
Nb				6								
Ta				0.7								
U	3.93		2.90	4.7						8.56		4.31
Y			24.70	24.2								18.10
Th				14.1						15.00		22.00
Rb				87.1								
Cs				1.6								
Sr				1295.2						406		719
Ba				1477								

La	32.65	40.00	44.8	57.52	32.00
Ce	59.25	86.00	86.9	107.41	68.00
Pr	6.32		10.28	12.11	
Nd	22.90	39.60	39.6	40.71	27.70
Sm	4.32	8.12	7.89	6.09	5.51
Eu	1.09	2.06	1.81	1.67	1.17
Gd	7.68	7.18	6.77	7.75	4.85
Tb	0.16	0.70	0.91	0.29	0.49
Dy	2.55	4.08	4.55	2.61	2.97
Ho	0.28	0.61	0.82	0.27	0.45
Er	1.27	1.84	2.38	1.05	1.41
Tm		0.22	0.33		0.17
Yb	1.40	1.82	2.14	0.81	1.47
Lu		0.22	0.34		0.17
ΣREE	139.9	192.5	209.5	238.3	146.4
Eu/Eu*		0.8	0.7	0.7	0.7
(La/Lu)cn		18.9	13.7		19.6
(La/Sm)cn		3.1	3.6	5.9	3.7
(Gd/Yb)cn		3.2	2.6	7.7	2.7
(Tb/Lu)cn		2.2	1.8		2.0

*References: 1 Major and trace elements present study; 2 Major and XRF trace elements Vlachou (2003) and ICP-MS trace elements present study; 3 Major and trace elements Vlachou (2003)

Samothraki Volcanics

	Young Group											
Sample	**LK-20**	**PSM-8**	**AGP-9**	**MAGP-103**	**T-1**	**AGP-2**	**AGP-1**	**T-2**	**X-13**	**T-15**	**AGP-3**	**LK-19**
Reference*	3	1	3	3	3	3	3	3	3	3	3	3
SiO_2	55.51	57.24	57.59	58.19	58.60	58.65	58.96	60.06	60.29	61.00	61.04	61.48
TiO_2	0.76	0.84	0.73	0.63	0.75	0.67	0.70	0.83	0.68	0.72	0.68	0.73
$Al2O_3$	17.10	14.81	14.69	15.57	14.49	15.16	15.23	14.86	17.31	14.70	14.70	15.54
FeOtot	3.68	6.42	2.10	2.83	2.70	2.20	2.47	2.81	4.28	4.65	2.15	3.47
MnO	0.16	0.17	0.09	0.10	0.12	0.14	0.10	0.15	0.08	0.11	0.09	0.07
MgO	3.78	3.55	4.85	4.79	3.34	5.02	4.89	4.06	1.70	2.73	3.70	1.84
CaO	5.66	5.84	4.75	4.15	4.78	4.93	4.18	4.61	4.72	4.42	4.54	3.48
Na_2O	4.52	4.04	3.66	2.68	2.76	3.65	3.67	2.88	3.85	3.21	3.10	3.34
K_2O	3.26	3.27	3.50	4.26	4.72	4.00	4.15	4.76	4.04	4.87	3.73	4.20
P_2O_5	0.80	0.95	0.56	0.45	1.49	0.86	0.60	2.03	0.25	0.70	0.63	0.71
mg#	64.66	49.64	80.47	75.07	68.79	80.23	77.94	72.04	41.42	51.11	75.40	48.56
LOI	2.7	1.0	4.6	4.8	4.5	2.0	2.8	1.1	1.3	2.1	3.8	3.4
Sum	97.9	98.1	97.1	98.5	98.2	97.3	97.7	98.1	98.5	99.2	98.1	98.3
XRF												
Sc						15	13	13			16	11
V	76		100	116	48	55	100	45	78	100	87	81
Cr	47		112	76	32	104	103	39	13	12	34	44
Ni	20		74	32	24	64	65	27	3	11	15	10
Zr	341		509	350	521	572	494	534	166	445	470	501
Nb	35		26	19	11	14	26	13	10	20	16	25
Rb	157		143	164	168	154	165	171	161	168	123	164
Sr	983		1398	767	913	1267	1284	931	602	941	1304	1347
Ba	1790		4896	2727	2200	2124	2389	1785	1412	2872	2278	2310
ICP-MS												
Sc	22		17		17							
V		175.75										
Cr												
Ni												
Pb		38.39		67.16					44.50			
Zr		558.31										
Hf		13.24										
Nb		38.55										

Ta	2.26		
U	9.35	6.44	5.52
Y	48.06		9.70
Th	60.85	30.00	88.00
Rb	174.99		
Cs	3.61		
Sr	1510.53	833	
Ba	2014.11		
La	114.29	77.87	54.00
Ce	255.63	143.17	105.00
Pr	30.56	16.85	
Nd	132.32	61.46	37.20
Sm	22.50	8.71	5.97
Eu	4.89	2.48	1.35
Gd	14.19	12.98	4.88
Tb	1.79	0.61	0.41
Dy	8.55	3.83	2.30
Ho	1.45	0.46	0.30
Er	3.80	1.41	0.96
Tm	0.55		0.09
Yb	3.61	1.36	0.88
Lu	0.48		0.09
ΣREE	594.6	331.2	
Eu/Eu*	0.8	0.7	0.7
(La/Lu)cn	24.9		62.3
(La/Sm)cn	3.2	5.6	5.7
(Gd/Yb)cn	3.2	7.7	4.5
(Tb/Lu)cn	2.6		3.1

*References: 1 Major and trace elements present study; 2 Major and XRF trace elements Vlachou (2003) and ICP-MS trace elements present study; 3 Major and trace elements Vlachou (2003)

Samothraki Volcanics												
	Young Group											
Sample	**AGP-10**	**MT-106**	**MT-123**	**PSM-12**	**MT-118**	**LK-8**	**MLK-111**	**MK-111M**	**AGP-110**	**MT-124**	**LK-4**	**X-6**
Reference	3	3	3	1	3	3	3	3	3	3	3	3
SiO_2	62.55	62.88	63.06	63.10	63.18	63.43	63.44	63.57	63.64	63.70	63.75	64.20
TiO_2	0.47	0.71	0.72	0.37	0.75	0.78	0.57	0.68	0.58	0.69	0.57	0.45
$Al2O_3$	16.64	14.70	14.73	14.73	14.77	15.25	14.91	17.87	15.77	14.78	14.97	15.63
FeOtot	1.21	2.40	3.34	2.92	2.63	2.94	2.56	2.93	2.34	2.27	2.21	1.52
MnO	0.08	0.09	0.09	0.07	0.10	0.07	0.10	0.09	0.09	0.09	0.08	0.06
MgO	1.55	4.01	3.34	1.49	3.53	1.67	1.68	0.30	4.19	3.57	1.96	3.32
CaO	4.48	3.57	3.97	4.42	3.63	3.71	3.66	0.70	2.00	3.65	3.73	3.40
Na_2O	3.43	2.92	3.02	3.04	3.04	3.62	3.54	4.33	3.36	3.09	3.53	3.02
K_2O	3.18	4.72	4.65	3.34	4.83	5.02	4.06	6.88	4.16	4.73	4.42	3.48
P_2O_5	0.34	0.69	0.74	0.23	0.72	0.70	0.53	0.24	0.48	0.72	0.53	0.22
mg#	69.45	74.83	64.06	47.58	70.53	50.28	53.86	15.41	76.14	73.72	61.20	79.55
LOI	4.3	1.5	1.3	4.8	1.2	1.1	3.5	1.2	1.6	0.9	2.5	3.8
Sum	98.2	98.2	98.9	98.5	98.4	98.2	98.6	98.8	98.2	98.2	98.3	99.1
XRF												
Sc				18		15						13
V	60	105	103		103	98	104		79	101	82	61
Cr	21	11	13		8	126	19	0	15	9	26	34
Ni	7	8	8		9	25	4	6	5	5	9	8
Zr	331	421	416		462	514	348		319	403	459	258
Nb	9	17	16		18	21	19		14	15	19	7
Rb	124	165	159		162	236	152		149	160	181	172
Sr	1082	791	891		859	1372	1230		800	853	1387	654
Ba	1641	1934	1969		2079	1983	2742	13	2458	1979	2199	1087
ICP-MS												

Sc	10										17	
V				75.19								
Cr				23.98								
Ni				30.37								
Pb		46.51	58.39	72.88	31.90		77.80	37.64	64.24	36.50		
Zr				165.74								
Hf				3.73				4.82				
Nb				9.17								
Ta				1.14				0.77				
U		5.89	5.01	13.63	3.97		10.41	7.97	8.42	4.48		
Y				13.21	12.60					15.60		
Th		23.00	20.00	24.34	24.00		27.00		36.00	22.00		
Rb				220.77								
Cs				8.05								
Sr		791	980	642.01	859		1230		870	939		
Ba				1230.79								
La		77.63	74.07	50.13	68.00		99.19	71.66	75.19	78.00		
Ce		146.29	140.93	118.09	137.00		182.19	123.62	134.24	159.00		
Pr		16.67	16.34	9.97			20.63	15.42	14.11			
Nd		58.84	61.29	36.56	53.30		70.54	53.15	45.50	61.60		
Sm		8.94	8.31	5.84	8.46		9.73	8.62	7.61	9.96		
Eu		2.23	2.26	1.05	1.98		3.40	2.02	2.12	2.33		
Gd		10.04	10.09	3.44	6.99		14.69	9.66	10.28	8.29		
Tb		0.45	0.48	0.48	0.59		0.60	0.79	0.35	0.70		
Dy		3.97	3.85	2.33	3.23		4.57	5.51	3.49	3.85		
Ho		0.30	0.43	0.41	0.41		0.50	0.98	0.25	0.51		
Er		1.33	1.43	1.11	1.22		1.68	2.35	1.22	1.53		
Tm				0.20	0.12			0.18		0.16		
Yb		1.11	1.17	1.19	1.01		1.42	2.72	1.07	1.29		
Lu				0.22	0.11					0.13		
ΣREE		327.8	320.7	231.0			409.1	296.7	295.4			
Eu/Eu*				0.7	0.8				0.7	0.8		
(La/Lu)cn				23.3	64.2					62.3		
(La/Sm)cn				5.4	5.1				6.2	4.9		
(Gd/Yb)cn				2.3	5.6				7.8	5.2		
(Tb/Lu)cn				1.5	3.6					3.7		

*References: 1 Major and trace elements present study; 2 Major and XRF trace elements Vlachou (2003) and ICP-MS trace elements present study; 3 Major and trace elements Vlachou (2003)

Samothraki Volcanics

	Young Group											
Sample	**PSM-5**	**MAL-111**	**MLK-109**	**PSM-4**	**LK-2**	**LK-5**	**MAL-110**	**LK-1**	**X-1**	**MAL-105**	**MX-111**	**MX-113**
Reference*	1	3	3	1	3	3	3	3	3	3	3	3
SiO_2	64.49	65.06	65.65	66.06	66.72	66.92	67.14	67.25	67.36	67.42	67.63	67.72
TiO_2	0.47	0.40	0.51	0.43	0.70	0.74	0.41	0.77	0.45	0.41	0.39	0.39
$Al2O_3$	15.20	15.58	14.99	15.25	13.54	14.12	15.45	12.95	15.05	15.34	15.07	15.01
FeOtot	3.44	2.01	2.68	3.65	3.82	4.13	1.95	1.95	1.56	2.57	1.97	1.81
MnO	0.06	0.09	0.08	0.05	0.05	0.05	0.08	0.06	0.07	0.09	0.07	0.07
MgO	2.35	1.66	1.88	1.75	1.28	0.54	2.13	2.02	1.90	1.85	2.46	2.00
CaO	2.94	3.81	3.20	2.39	3.22	2.97	2.93	2.80	3.38	2.48	2.95	3.04
Na_2O	3.66	3.35	3.61	3.52	2.74	3.29	3.92	3.00	4.15	3.85	3.88	4.10
K_2O	4.35	3.56	4.37	4.03	4.16	4.18	3.78	4.56	3.43	3.66	3.49	3.54
P_2O_5	0.41	0.26	0.47	0.33	0.58	0.66	0.28	0.70	0.26	0.29	0.21	0.24
mg#	54.92	59.58	55.54	46.05	37.41	18.89	66.03	64.83	68.50	56.16	68.98	66.33
LOI	1.0	3.3	1.6	0.8	3.3	1.7	0.7	2.9	1.2	1.4	0.8	0.9
Sum	98.4	99.1	99.1	98.3	100.1	99.3	98.8	99.0	98.8	99.4	99.0	98.8
XRF												
Sc	18				8	15		12	12			
V		77	99		89	88	84	89	61	80	81	77

Cr		3	8		42	98	6	102	30	7	10	12
Ni		3	4		19	16	2	21	10	28	4	3
Zr		238	315		490	466	242	488	329	268	197	229
Nb		14	17		23	21	13	21	13	16	11	13
Rb		160	167		194	202	163	143	173	183	165	166
Sr		773	1332		1297	1228	1008	1262	935	997	778	914
Ba		1471	2408		2330	1845	1859	3016	1061	1708	1340	1439
ICP-MS												
Sc												
V	87.90			68.72								
Cr	64.91			33.63								
Ni	48.37			48.23								
Pb	47.35	62.23	81.56	26.72			68.9			66.48	68.10	61.36
Zr	410.66			379.30								
Hf	10.23			10.30			0.97			0.36		
Nb	21.43			21.52								
Ta	1.28			1.50			1.12			0.88		
U	8.23	12.17	12.64	9.75			5.19			7.93	8.56	9.94
Y	21.83			24.91								
Th	33.25	4.00	31.00	40.71			18			23	8.00	20.00
Rb	193.50			297.65								
Cs	4.05			17.79								
Sr	1053.69	773	1530	1099.61			1106			997	778	1005
Ba	2349.29			2223.36								
La	86.38	65.59	104.26	82.20			84.95				57.98	75.00
Ce	164.33	111.35	185.42	140.03			158.70				103.53	132.91
Pr	15.72	11.09	21.35	14.66			14.98				10.30	14.60
Nd	63.63	39.30	69.84	62.13			47.52			58.30	35.69	49.45
Sm	9.70	5.20	9.68	9.51			7.25			8.61	5.72	6.64
Eu	2.17	1.66	2.90	1.65			1.92				1.53	1.74
Gd	6.24	8.31	12.90	6.25			8.42				6.45	8.30
Tb	0.76	0.31	0.70	0.86			0.39				0.28	0.45
Dy	3.86	2.50	3.90	4.37			2.94				2.42	2.56
Ho	0.66	0.28	0.38	0.84			0.25				0.18	0.23
Er	1.84	1.33	1.47	2.12			1.10				0.91	0.90
Tm	0.33			0.41								
Yb	1.30	1.21	1.19	1.93			0.99				0.54	0.90
Lu	0.29			0.30								
ΣREE	357.2	248.1	414.0	327.3			329.4				225.5	293.7
Eu/Eu*	0.8			0.6								
(La/Lu)cn	30.7			28.1								
(La/Sm)cn	5.6			5.4								
(Gd/Yb)cn	3.9			2.6								
(Tb/Lu)cn	1.8			1.9								

*References: 1 Major and trace elements present study; 2 Major and XRF trace elements Vlachou (2003) and ICP-MS trace elements present study; 3 Major and trace elements Vlachou (2003)

Samothraki Volcanics				
	Young Group			
Sample	**MBR-105**	**MBR-101**	**LK-10**	**PSM-15**
Reference*	3	3	3	1
SiO_2	67.89	68.88	70.89	56.26
TiO_2	0.39	0.35	0.76	1.16
$Al2O_3$	15.11	15.11	13.32	10.73
FeOtot	2.09	2.02	1.33	5.09
MnO	0.08	0.06	0.07	0.21
MgO	2.21	1.78	1.19	7.57
CaO	2.34	2.32	1.82	5.02
Na_2O	4.34	4.17	3.15	0.71

K_2O	3.46	3.55	5.62	8.35
P_2O_5	0.21	0.22	0.76	0.84
mg#	65.35	61.04	61.42	72.59
LOI	0.9	0.9	0.6	2.7
Sum	99.0	99.4	99.5	98.6
XRF				
Sc				21
V	73	68	81	
Cr	12	6	71	
Ni	26	3	29	
Zr	203	211	388	
Nb	12	12	17	
Rb	155	170	267	
Sr	733	826	1036	
Ba	1347	1278	2164	
ICP-MS				
Sc				
V				133.27
Cr				418.84
Ni				292.09
Pb	55.85	31.50	46.80	24.94
Zr				901.49
Hf				26.16
Nb				20.92
Ta				1.44
U	8.28	5.06	5.50	12.63
Y		8.70	15.50	27.78
Th	18.00	24.00	96.00	36.96
Rb				389.09
Cs				4.32
Sr	733	880	1091	521.14
Ba				1839.41
La	60.11	51.00	68.00	84.79
Ce	106.63	100.00	144.00	189.82
Pr	11.77			20.41
Nd	40.74	34.40	58.50	89.07
Sm	6.12	5.48	9.19	14.33
Eu	1.68	1.22	2.01	3.37
Gd	7.35	4.72	7.16	10.10
Tb	0.34	0.36	0.59	1.26
Dy	2.90	1.98	3.11	5.81
Ho		0.25	0.40	0.92
Er	1.08	0.82	1.24	2.32
Tm		0.08		0.37
Yb	0.76	0.76	1.10	1.80
Lu		0.08	0.12	0.26
ΣREE	239.5			424.6
Eu/Eu*		0.7	0.7	0.8
(La/Lu)cn		66.2	58.9	34.2
(La/Sm)cn		5.9	4.7	3.7
(Gd/Yb)cn		5.0	5.3	4.5
(Tb/Lu)cn		3.1	3.3	3.3

*References: 1 Major and trace elements present study; 2 Major and XRF trace elements Vlachou (2003) and ICP-MS trace elements present study; 3 Major and trace elements Vlachou (2003)

CROV												
	Basic Group			Intermediate Group								
Sample	**KO-5**	**KA-23**	**KA-97**	**LY-69**	**KA-10**	**IAS-53**	**PKL-4**	**XE-3**	**PKL-13**	**KO-92**	**TS-67**	**PKL-2**
Type*	B	B	B	BAT	BAT	BAT	BAT	BAT	BAT	BAT	BAT	BAT
Reference**	1	1,2	1,2	1	1	1	3	1	3	1	1,2	3
SiO_2	48.86	49.98	50.74	52.88	53.02	54.56	55.85	55.89	56.10	56.36	56.80	58.96
TiO_2	1.23	1.15	1.20	1.17	1.13	0.89	0.98	0.89	0.94	0.98	0.93	0.78
$Al2O_3$	14.52	16.36	17.49	16.56	16.59	16.99	17.10	16.90	17.39	17.00	16.80	16.31
FeOtot	10.68	9.51	9.36	8.43	7.22	7.91	7.40	7.13	6.71	7.13	6.69	6.11
MnO	0.18	0.17	0.16	0.17	0.16	0.11	0.15	0.15	0.14	0.13	0.14	0.13
MgO	3.92	6.06	4.20	4.96	4.11	5.27	3.89	4.50	3.39	3.31	4.61	2.50
CaO	12.38	8.97	8.28	8.82	7.32	8.46	7.30	6.50	7.51	7.08	5.95	5.52
Na_2O	1.86	2.41	2.63	2.96	2.83	2.56	3.24	3.22	3.16	2.31	3.47	2.55
K_2O	1.67	2.23	3.21	2.64	3.38	2.19	2.70	2.64	0.79	3.15	2.54	2.38
P_2O_5	0.36	0.44	0.33	0.32	0.40	0.41	0.31	0.29	0.27	0.22	0.25	0.27
mg#	39.54	53.17	44.43	51.18	50.35	54.28	48.39	52.93	47.38	45.27	55.11	42.20
LOI	4.4	2.7	2.4	1.1	3.8	0.7	1.1	1.9	3.6	2.3	1.8	4.5
Sum	100.0	100.0	100.0	100.0	100.0	100.0	100.0	100.0	100.0	100.0	100.0	100.0
XRF												
Sc	31	25	25		23					28		
V												
Cr	49	26	4	43	35	51		33	28	25	31	
Ni	28	20	17	35	37	30		33	31	14	30	
Zr	209	280	146	201	237	185		229	235	338	240	
Nb	6	9	8	11	12	7		11	11	8	12	
Y	28	27	28	30	31	24		30	30	33	30	
Th	14	12	12						16			
Rb	49	78	114	68	88	74		70	91	134	72	
Sr	703	621	577	619	593	553		600	660	579	622	
Ba	556	502	762	791	883	576		830	692	744	869	
Nd												
ICP-MS												
Sc							25.48		21.49			17.87
V		318	257				186.19		158.01		162.0	142.29
Cr							40.84		34.64			58.72
Ni							55.89					45.30
Pb		5.2	7.3				18.58		18.43			29.70
Zr		120.0	144.0				194.86		183.40		183.2	210.70
Hf		3.5	4.2				4.55		4.34		4.3	5.37
Nb		6.7	7.4				10.70		9.06		7.9	10.76
Ta		0.4	0.6				0.91		0.63		0.5	0.85
U		2.1	2.6				3.12		2.14		2.2	3.50
Y		23.6	24.0				29.50		26.43		23.5	24.97
Th		7.4	8.9				12.37		9.64		9.5	15.32
Rb		78.4	105.7				82.02		58.96		71.5	75.18
Cs		1.3	1.2				1.39		53.22		1.0	1.23
Sr		595.1	585.7				553.98		930.29		664.9	812.99
Ba		494.0	711.0				770.23		716.57		779.0	1088.74
La	25.65	24.00	26.60				30.88		27.34		27.70	33.31
Ce	54.72	51.10	53.50				64.14		57.68		54.00	69.44
Pr	6.35	6.54	6.56				6.85		6.22		6.35	7.24
Nd	27.10	29.10	26.80				30.78		27.68		24.70	31.99
Sm	5.69	5.95	5.69				6.94		5.50		5.22	6.64
Eu	1.50	1.49	1.30				1.35		1.14		1.34	1.36
Gd	5.33	5.41	5.27				6.66		4.40		4.77	5.89
Tb		0.80	0.84				0.94		0.84		0.76	0.77
Dy	4.88	4.70	4.52				5.52		4.41		4.02	4.73
Ho	0.89	0.94	0.87				0.96		0.89		0.83	0.88
Er	2.49	2.52	2.41				2.78		2.56		2.35	2.40

Tm		0.36	0.35	0.44	0.37	0.34	0.40
Yb	2.36	2.15	2.30	2.86	2.09	2.25	2.65
Lu	0.35	0.32	0.35	0.40	0.41	0.34	0.37
ΣREE		140.9	83.9	161.5	141.5	135.0	168.1
Eu/Eu*	0.8	0.8	0.7	0.6	0.7	0.8	0.7
(La/Lu)cn	7.6	7.8	7.9	8.0	6.9	8.5	9.3
(La/Sm)cn	2.8	2.5	2.9	2.8	3.1	3.3	3.2
(Gd/Yb)cn	1.8	2.0	1.8	1.9	1.7	1.7	1.8
(Tb/Lu)cn		1.7	1.6	1.6	1.4	1.5	1.4

*Type: B=Basalts; BAT= Basalts, Andesites, Trachytes; RD= Rhyolites, Dacites

**References: 1 Major and trace elements Eleftheriadis (1995); 2 ICP-MS trace elements present study, XRF trace elements Eleftheriadis (1995) ; 3 Major and ICP-MS trace elements present study, XRF trace elements Eleftheriadis (1995)

CROV												
	Intermediate Group										**Felsic Group**	
Sample	**TS-66**	**LY-70**	**KA-15**	**PKL-5**	**PKL-10**	**PKL-3**	**PKL-11**	**PKL-1**	**PKL-12**	**PKL-8**	**PDP-4**	**LE-47**
Type*	BAT	BAT	BAT	BAT	BAT	BAT	BAT	BAT	BAT	BAT	RD	RD
Reference**	1,2	1	1	3	3	3	3	3	3	3	3	1
SiO_2	58.97	59.87	60.50	61.29	61.36	62.83	62.94	62.95	63.22	63.25	64.27	64.49
TiO_2	0.69	0.81	0.77	0.62	0.70	0.68	0.63	0.56	0.49	0.53	0.54	0.55
$Al2O_3$	16.78	16.49	16.74	15.55	17.30	17.07	17.52	16.32	17.27	16.37	15.63	15.87
FeOtot	4.73	5.38	5.11	5.10	4.76	4.44	4.31	4.21	3.83	3.64	4.09	4.17
MnO	0.13	0.13	0.10	0.10	0.13	0.12	0.09	0.09	0.09	0.08	0.15	0.11
MgO	3.33	2.94	2.91	2.83	1.76	1.01	1.23	1.70	1.44	1.34	1.42	1.53
CaO	4.12	5.26	4.72	4.72	4.50	3.38	3.93	3.52	3.74	2.62	4.29	4.18
Na_2O	3.30	4.01	2.73	3.44	3.84	4.22	3.85	3.50	3.30	3.69	3.45	3.59
K_2O	5.52	3.45	4.09	4.36	3.54	4.07	3.76	4.18	5.55	4.60	4.15	3.93
P_2O_5	0.36	0.36	0.26	0.38	0.30	0.24	0.27	0.24	0.21	0.19	0.17	0.19
mg#	55.64	49.33	50.36	49.70	39.71	28.91	33.72	41.76	40.10	39.64	38.23	39.53
LOI	2.1	1.3	2.1	1.6	1.8	1.9	1.4	2.7	0.9	3.6	1.8	1.4
Sum	100.0	100.0	100.0	100.0	100.0	100.0	100.0	100.0	100.0	100.0	100.0	100.0
XRF												
Sc							8					
V												
Cr	16	34	22		20		14		15		21	22
Ni	26	35	11		17		8		21		8	6
Zr	277	257	271		242		258		245		153	186
Nb	18	15	18		13		11		20		17	14
Y	33	32	42		34		25		34		31	26
Th		17					16					
Rb	187	202	163		127		135		168		197	207
Sr	684	433	489		463		496		608		347	357
Ba	2030	786	856		988		1005		1873		793	756
Nd												
ICP-MS												
Sc				27.40	16.85	16.92	17.59	14.32	17.18	25.66	24.11	
V	108.0			76.94	94.08	99.77	77.13	278.73	86.35	45.82	94.35	
Cr				97.46	24.40	25.95	24.61	19.30	37.23	16.55	33.94	
Ni				47.17	70.15	54.83	45.48	32.37		94.01	69.44	
Pb	25.6			34.08	22.90	27.64	24.37	56.73	44.28	30.71	39.18	
Zr	294.2			256.26	242.84	252.69	241.09	104.10	253.87	272.69	163.03	
Hf	7.1			6.60	5.52	5.65	5.12	2.29	5.23	6.13	3.33	
Nb	13.9			19.74	11.76	13.99	10.19	22.12	17.48	14.86	15.22	
Ta	1.1			1.73	0.93	1.24	0.81	0.68	1.81	1.34	1.15	
U	6.0			8.10	3.97	5.89	3.68	2.27	7.23	5.33	8.90	
Y	19.5			25.21	28.52	27.39	26.98	15.91	22.07	30.55	20.12	
Th	22.9			38.96	15.08	20.56	13.40	8.77	31.22	23.80	23.08	
Rb	71.5			157.51	131.58	149.42	138.88	258.14	194.29	215.40	237.67	

Cs	7.8			2.07	1.81	1.41	1.56	9.67	2.47	3.53	4.25
Sr	659.0			441.02	472.84	542.13	522.19	313.52	671.18	340.63	349.40
Ba	1845.0			2951.21	948.59	1099.16	1054.00	531.40	1837.78	969.45	821.23
La	43.60	38.21	50.28	49.90	36.26	38.44	35.41	24.90	57.79	39.41	34.33
Ce	81.70	79.80	88.61	93.47	72.31	79.00	72.61	50.28	123.77	76.19	73.39
Pr	9.17	9.50	10.78	9.88	7.42	7.74	7.67	5.38	11.04	7.65	6.59
Nd	35.20	40.49	44.81	43.97	31.21	33.25	31.95	23.82	39.60	32.98	25.61
Sm	6.17	7.41	7.65	8.33	5.90	6.53	5.79	4.39	8.49	5.54	4.87
Eu	1.55	1.41	1.63	1.48	1.20	1.25	1.23	2.19	1.25	1.28	1.11
Gd	5.06	6.14	6.52	5.36	5.31	5.54	4.64	3.45	4.71	4.34	3.84
Tb	0.70			0.85	0.79	0.78	0.72	0.51	0.76	0.76	0.53
Dy	3.94	5.43	5.72	4.79	5.05	5.00	4.85	3.11	4.10	4.71	3.43
Ho	0.76	1.13	1.21	0.79	0.90	0.87	0.90	0.52	0.70	0.91	0.70
Er	2.38	3.17	3.38	2.50	2.70	2.54	2.56	1.52	2.28	2.91	1.72
Tm	0.31			0.46	0.39	0.45	0.45	0.26	0.36	0.44	0.40
Yb	2.10	2.89	3.04	1.88	2.94	2.37	2.51	1.41	2.07	3.06	2.01
Lu	0.29	0.45	0.48	0.43	0.52	0.43	0.44	0.22	0.33	0.50	0.38
ΣREE	192.9			224.1	172.9	184.2	171.7	122.0	257.3	180.7	158.9
Eu/Eu*	0.8	0.6	0.7	0.6	0.6	0.6	0.7	1.7	0.6	0.8	0.8
(La/Lu)cn	15.6	8.8	10.9	12.0	7.2	9.2	8.4	11.8	18.3	8.2	9.3
(La/Sm)cn	4.4	3.2	4.1	3.8	3.9	3.7	3.8	3.6	4.3	4.5	4.4
(Gd/Yb)cn	1.9	1.7	1.7	2.3	1.5	1.9	1.5	2.0	1.8	1.1	1.5
(Tb/Lu)cn	1.6			1.3	1.0	1.2	1.1	1.6	1.6	1.0	0.9

*Type: B=Basalts; BAT= Basalts, Andesites, Trachytes; RD= Rhyolites, Dacites

**References: 1 Major and trace elements Eleftheriadis (1995); 2 ICP-MS trace elements present study, XRF trace elements Eleftheriadis (1995) ; 3 Major and ICP-MS trace elements present study, XRF trace elements Eleftheriadis (1995)

CROV

	Felsic Group											
Sample	**LE-48**	**L-4**	**PA-1**	**TRA-1**	**DIM-2**	**LIV-27**	**PDP-2**	**PKL-9**	**DIP-35**	**ZARK-1**	**PDP-3**	**PKL-1E**
Type*	RD	RD	RD	RD	RD	RD	RD	RD	RD	RD	RD	ENC
Reference**	1	1	1	1	1	1	3	3	1	1	3	3
SiO_2	65.06	66.83	67.60	70.11	70.33	70.35	70.92	70.99	71.27	72.32	76.02	51.15
TiO_2	0.55	0.52	0.38	0.34	0.39	0.34	0.32	0.34	0.37	0.22	0.18	1.13
$Al2O_3$	15.38	15.15	13.97	14.00	13.97	14.48	14.16	14.92	14.27	12.92	11.41	18.42
FeOtot	4.01	3.28	2.48	2.10	1.91	2.04	1.99	1.93	2.05	1.34	0.52	8.12
MnO	0.12	0.07	0.08	0.07	0.06	0.03	0.06	0.03	0.03	0.10	0.00	0.16
MgO	1.30	1.57	1.44	1.55	1.23	1.21	0.60	0.42	0.54	0.73	0.22	3.56
CaO	3.87	3.33	2.34	1.71	1.85	1.58	2.05	1.41	1.26	1.47	1.52	5.98
Na_2O	4.30	3.17	3.05	2.80	3.15	3.17	2.92	2.95	3.33	3.42	2.14	3.04
K_2O	4.04	4.14	4.43	4.60	4.37	4.57	4.71	5.25	5.84	3.79	3.32	3.51
P_2O_5	0.18	0.19	0.13	0.13	0.12	0.12	0.09	0.11	0.10	0.10	0.04	0.49
mg#	36.61	46.03	50.85	56.80	53.43	51.38	35.07	28.08	31.94	49.25	42.89	43.82
LOI	1.2	1.8	4.1	2.6	2.6	2.1	2.2	1.7	1.0	3.6	4.6	4.4
Sum	100.0	100.0	100.0	100.0	100.0	100.0	100.0	100.0	100.0	100.0	100.0	100.0
XRF												
Sc	10	13	7	9		5		8	8			
V												
Cr	18	14	3	4	3	4		12	5	1		
Ni	5	15	5	6	5	4		7	7	3		
Zr	197	229	142	131	126	150		138	145	121		
Nb	13	18	21	22	22	23		18	18	27		
Y	25	26	26	25	34	24		21	22	29		
Th								42				
Rb	211	224	221	402	257	292		265	339	440		
Sr	354	301	239	198	146	173		159	166	101		
Ba	772	787	619	611	669	579		637	583	414		
Nd												
ICP-MS												

Sc				18.16	20.77	21.35	29.40
V				46.52	38.31	26.69	81.67
Cr				21.91		38.80	70.20
Ni					75.73		102.49
Pb				52.24	38.31	53.22	29.67
Zr				136.22	183.21	82.04	335.72
Hf				3.90	5.82	2.32	8.07
Nb				21.20	20.80	11.08	13.23
Ta				2.23	2.66	1.41	2.45
U				11.59	8.79	13.73	12.33
Y				20.59	25.99	19.76	38.27
Th				29.20	35.25	12.38	47.60
Rb		194.80		377.44	292.85	251.51	148.86
Cs				6.18	4.79	41.04	1.89
Sr				187.32	185.56	608.11	842.66
Ba				600.63	762.58	892.07	2009.48
La	40.29	38.66	37.36	35.53	39.71	34.40	72.28
Ce	75.44	69.89	67.88	77.18	79.90	73.96	144.28
Pr	7.51	7.08	6.84	6.52	6.96	6.57	13.65
Nd	27.30	25.62	25.72	24.16	28.18	24.85	55.07
Sm	4.84	4.06	4.23	4.35	5.50	5.09	10.42
Eu	0.95	0.69	0.68	0.46	0.86	0.76	0.95
Gd	4.07	2.97	3.28	2.90	4.79	2.83	5.91
Tb				0.54	0.60	0.49	1.20
Dy	3.85	2.97	3.31	2.80	3.90	3.49	6.86
Ho	0.72	0.70	0.72	0.60	0.71	0.65	1.28
Er	2.07	1.98	2.12	1.81	2.17	1.89	3.83
Tm				0.33	0.48	0.34	0.75
Yb	2.29	2.09	2.30	2.19	2.73	1.76	3.47
Lu	0.35	0.34	0.36	0.31	0.60	0.52	0.51
ΣREE		157.1	154.8	159.7	177.1	157.6	320.5
Eu/Eu*	0.6	0.6	0.5	0.4	0.5	0.6	0.3
(La/Lu)cn	12.0	11.8	10.8	12.0	6.9	6.9	14.9
(La/Sm)cn	5.2	6.0	5.6	5.1	4.5	4.3	4.4
(Gd/Yb)cn	1.4	1.1	1.2	1.1	1.4	1.3	1.4
(Tb/Lu)cn				1.2	0.7	0.6	1.6

*Type: B=Basalts; BAT= Basalts, Andesites, Trachytes; RD= Rhyolites, Dacites

**References: 1 Major and trace elements Eleftheriadis (1995); 2 ICP-MS trace elements present study, XRF trace elements Eleftheriadis (1995) ; 3 Major and ICP-MS trace elements present study, XRF trace elements Eleftheriadis (1995)

APPENDIX B-

Bulk Sr, Nd and Pb Isotopic Compositions

Elatia pluton

Sample	Type	Reference*	Rb	Sr	$^{87}Rb/^{86}Sr$	87Sr/86Sr	2σ error	$^{87}Sr/^{86}Sr_i$	Sm	Nd	$^{147}Sm/^{144}Nd$	$^{143}Nd/^{144}Nd$	2σ error	$^{143}Nd/^{144}Nd_i$
PEL-1	Enclave	1	109.4	857.7	0.369	0.70630	0.000004	0.70600	7.62	46	0.100	0.51249	0.000004	0.51245
PEL-3	Enclave	1	152.6	674.9	0.654	0.70710	0.000004	0.70658	5.24	33.1	0.096	0.51246	0.000004	0.51243
PEL-4	Diorite	1	98.58	1173.53	0.243	0.70445	0.000004	0.70425	6.27	29.62	0.128	0.51269	0.000004	0.51264
E-04	GRD	1	105.5	817.7	0.373	0.70660	0.000003	0.70630	5.85	39.4	0.090	0.51246	0.000003	0.51242
PS-1	GRD	1	92.8	479.2	0.560	0.70677	0.000004	0.70633	4.99	26.9	0.112	0.51246	0.000004	0.51242
DSK-17	GRD	2	85.7	762.0	0.325	0.70642	0.000130	0.70616	5.64	37.2	0.092	0.51247	0.000003	0.51244
I-14A	GRD	2	138.4	396.0	1.011	0.70733	0.000020	0.70653	3.82	19.4	0.119	0.51236	0.000005	0.51232
PS-03	GRD	2	132.0	473.0	0.807	0.70685	0.000070	0.70621	3.1	28	0.067	0.51245	0.000003	0.51242
PS-11	GRD	2	106.2	541.5	0.567	0.70669	0.000020	0.70624	4.47	26.2	0.103	0.51245	0.000004	0.51241
D-5	GRD	2	96	809	0.342	0.70657	0.000270	0.70630						
I-11b	GRD	2	110.83	530.75	0.604	0.70669	0.000016	0.70621						
PS-9	GRD	2	94.72	533.30	0.514	0.70668	0.000018	0.70627						
D-10A	GR	1	231.9	115.8	5.796	0.71205	0.000140	0.70744	2.66	13.72	0.117	0.51236	0.000004	0.51231
DSK-20	GR	2	152	328	1.321	0.70871	0.000090	0.70766						
H-9	GR	2	153	123	3.592	0.71095	0.000060	0.70809						

*References: 1 Sr and Nd isotopic composition present study; 2 Sr isotopic composition Soldatos et al. (2001), Nd isotopic composition present study

Xanthi Plutonic Complex

Sample	Type	Rb	Sr	$^{87}Rb/^{86}Sr$	$^{87}Sr/^{86}Sr$	2σ error	$^{87}Sr/^{86}Sr_i$	Sm	Nd	$^{147}Sm/^{144}Nd$	$^{143}Nd/^{144}Nd$	2σ error	$^{143}Nd/^{144}Nd_i$	$^{208}Pb/^{204}Pb$	$^{207}Pb/^{204}Pb$	$^{206}Pb/^{204}Pb$
X-280	CGb	90.05	1002.13	0.090	0.70616	0.000003	0.70603	8.77	44.09	5.308	0.51252	0.000003	0.51250	38.876	15.665	18.688
X-GAE-1	CGb	38.2	836.8	0.046	0.70592	0.000004	0.70585	3.19	16.30	1.931	0.51254	0.000002	0.51251	38.824	15.663	18.690
X-NG1	Enclaves	4.04	1099.18	0.004	0.70581	0.000008	0.70581	6.41	26.25	3.880	0.51252	0.000007	0.51248	38.867	15.698	18.701
X-207E	Enclaves	93	417	0.223	0.70651	0.000004	0.70619	9.71	45.36	5.877	0.51252	0.000015	0.51238	38.899	15.666	18.793
X-147	GRD	169.4	475.1	0.357	0.70651	0.000007	0.70600	5.94	35.5	3.595	0.51249	0.000006	0.51238			
X-210	GRD	163.5	453.2	0.361	0.70665	0.000004	0.70613	5.20	29.9	3.147	0.51249	0.000004	0.51238	39.547	15.932	19.076
X-220	GRD	203.2	353.6	0.575	0.70693	0.000006	0.70611	5.69	31.4	3.444	0.51250	0.000006	0.51238			
X-254	GRD	162.9	459.9	0.354	0.70656	0.000004	0.70605	4.57	25.4	2.766	0.51250	0.000002	0.51239	38.931	15.668	18.786
X-86	GRD	200.4	338.5	0.592	0.70779		0.70694	5.11	27.6	3.093	0.51246	0.000002	0.51235	39.014	15.666	18.903
X-601	GRD	169.68	465.72	1.054	0.70656	0.000004	0.70604	5.38	28.57	0.114	0.51250	0.000005	0.51238	39.008	15.663	18.830
X-P3	LMzG	342.18	909.3	0.376	0.70851		0.70797	9.54	49.98	5.774	0.51241	0.000003	0.51239	39.041	15.686	18.772
X-28	MGb													38.907	15.687	18.785
X-222	MGb	150.62	466.55	0.323	0.70646	0.000003	0.70600	7.97	43.6	4.824	0.51250	0.000002	0.51238	38.923	15.661	18.781
X-277	MGb	9	816	0.011	0.70454		0.70452	4.90	20.8	2.966	0.51249	0.000013	0.51245			
X-GAE-11	MGb	9.8	854.1	0.011	0.70529	0.000006	0.70527	4.51	22.8	2.730	0.51258	0.000006	0.51255	38.810	15.669	18.688
X-N4	MGb	8.97	798.36	0.011	0.70593	0.000008	0.70592	5.80	24.31	3.511	0.51249	0.000013	0.51245	38.699	15.652	18.620
X-284	MGb	4.1	882.2	0.005	0.70608	0.000004	0.70607	5.15	26.30	3.117	0.51253	0.000002	0.51250			
X-20	Mz	286	796	0.359	0.70746		0.70694	7.34	45.70	4.443	0.51243	0.000002	0.51233	39.041	15.683	18.755
X-42	Mz	187.3	733.4	0.255	0.70674		0.70637	7.41	42.50	4.485	0.51249	0.000002	0.51238			
X-MZ	Mz	284.7	657.9	0.433	0.70796	0.000008	0.70734	10.17	53.28	6.156	0.51241	0.000005	0.51238			
X-MZ-501	PLMz	239	650	0.368	0.70817	0.000005	0.70743	8.78	49.80	0.107	0.51241	0.000006	0.51230			
X-294	QMzd													38.869	15.661	18.732
X-1	QMzd	91	621	0.147	0.70608	0.000004	0.70587	5.54	29.04	3.353	0.51253	0.000002	0.51251	39.100	15.708	18.845
X-297	QMzd	108.6	1014.6	0.107	0.70672	0.000009	0.70657	8.04	44.20	4.867	0.51250	0.000007	0.51248	38.225	15.668	18.683
X-56	QMzd	122.6	714.2	0.172	0.70674		0.70649	7.50	43.00	4.540	0.51250	0.000002	0.51248	38.933	15.673	18.687

Sr and Nd isotopes are from G. Christofides unpublished data

Vrondou pluton														
Sample	**Type**	**Reference***	**Rb**	**Sr**	**$^{87}Rb/^{86}Sr$**	**$^{87}Sr/^{86}Sr$**	**2σ error**	**$^{87}Sr/^{86}Sr_i$**	**Sm**	**Nd**	**$^{147}Sm/^{144}Nd$**	**$^{143}Nd/^{144}Nd$**	**2σ error**	**$^{143}Nd/^{144}Nd_i$**
PVR-12	GBDR	1	6.8	530.3	0.037	0.70531	0.000004	0.70529	1.99	8.2	0.147	0.51259	0.000003	0.51256
PVR-22	GBDR	1	6.8	534.3	0.037	0.70558	0.000003	0.70557	5.23	25.3	0.125	0.51254	0.000004	0.51252
PVR-30	GBDR	1	9.8	541.3	0.052	0.70537	0.000004	0.70534	3.07	9.9	0.188	0.51258	0.000004	0.51254
PVR-35	GBDR	1	4.1	545.3	0.022	0.70527	0.000003	0.70526	4.01	17.3	0.140	0.51261	0.000003	0.51258
PVR-8	GBDR	1	6.8	547.3	0.036	0.70514	0.000004	0.70512	1.82	6.8	0.162	0.51261	0.000003	0.51257
PVR-32	High-K MME	1	164.6	543.3	0.876	0.70650	0.000004	0.70613	3.39	16.8	0.122	0.51249	0.000003	0.51247
SB70X	High-K MME	1	262.18	551.89	1.374	0.70636	0.000004	0.70578	5.59	26.0	0.130	0.51249	0.000003	0.51247
PVR-13	Low-K MME	1	6.8	531.3	0.037	0.70680	0.000005	0.70679	7.65	42.4	0.109	0.51244	0.000004	0.51242
PVR-26	Low-K MME	1	37.4	537.3	0.201	0.70583	0.000004	0.70574	5.76	26.1	0.133	0.51251	0.000003	0.51248
TS27X	Low-K MME	1	31.9	509.7	0.181	0.70620	0.000004	0.70612	2.32	14.8	0.095	0.51248	0.000004	0.51246
CK77G	MZ	2	191.7	515.1	0.708	0.70765	0.000004	0.70719	5.194	27.471	0.117	0.51242	0.000020	0.51240
NKRS11GG	MZ	2	230.1	412.8	0.708	0.70779	0.000004	0.70710	3.123	38.550	0.116	0.51241	0.000018	0.51238
PVR-6	QMZ	1	108.8	409.0	0.770	0.71067	0.000004	0.71034	6.04	32.9	0.111	0.51228	0.000003	0.51225
SB50	QMZ	1	97.7	625.4	0.452	0.70630	0.000003	0.70611	4.29	24.4	0.106	0.51249	0.000004	0.51247
TS12	QSY-GR	1	136.3	435.1	0.906	0.70760	0.000004	0.70721	3.09	20.7	0.090	0.51239	0.000004	0.51238

*References: 1 Sr and Nd isotopic composition present study; 2 Sr and Nd isotopic composition Kolokotroni (1992)

Maronia pluton

Sample	Type	Reference*	Rb	Sr	$^{87}Rb/^{86}Sr$	$^{87}Sr/^{86}Sr$	2σ error	$^{87}Sr/^{86}Sr_i$	Sm	Nd	$^{147}Sm/^{144}Nd$	$^{143}Nd/^{144}Nd$	2σ error	$^{143}Nd/^{144}Nd_i$
PMR-9A	Enclave	2	119.2	381.8	0.903	0.70614	0.000019	0.70577	8.83	41.9	0.127	0.51260	0.000003	0.51257
PMR-12	Gb	1	55.5	748	0.215	0.70743	0.000011	0.70734	7.32	35.2	0.126	0.51245	0.000003	0.51243
PMR-55	Gb	1	83.6	920	0.263	0.70689	0.000005	0.70678	6.63	35.3	0.114	0.51247	0.000003	0.51245
MP-90	Gr	3	309.8	399.8	2.242	0.70814	0.000020	0.70722	6.86	40	0.104	0.51244	0.000042	0.51242
MP-89	Mz	2	189.4	603.1	0.909	0.70727	0.000026	0.70689	7.61	40	0.115	0.51247	0.000004	0.51245
MP-53	Mz	2	194.4	657.8	0.855	0.70750	0.000023	0.70714	6.91	36.50	0.114	0.51243	0.000004	0.51241
MP-73	Mz	2	177.9	645.7	0.797	0.70658	0.000025	0.70625	7.73	40	0.117	0.51253	0.000003	0.51251
MP-14	Mz	3	286.9	550.1	1.509	0.70780	0.000022	0.70718	7.37	39	0.114	0.51242	0.000043	0.51240
PMR-81	Mzg	1	78.1	761.2	0.297	0.70695	0.000020	0.70683	7.96	41.8	0.115	0.51246	0.000027	0.51244
PMR-5	Mzg	1	100.36	746.92	0.389	0.70619	0.000004	0.70603	6.06	32.81	0.112	0.51254	0.000005	0.51252
MP-98	QMz	3	228.2	525.6	1.256	0.70828	0.000018	0.70776	7.42	40	0.112	0.51242	0.000054	0.51240
MP-62	QMzg	3	153.3	703	0.631	0.70634	0.000021	0.70608	7.06	36.41	0.117	0.51251	0.000023	0.51249
MP-74	QMzg	3	175.7	653.6	0.778	0.70632	0.000016	0.70599	7.33	39	0.114	0.51250	0.000051	0.51248

*References: 1 Sr and Nd isotopic composition present study; 2 Nd isotopic composition present study, Sr isotopic composition Papadopoulou (2003); 3 Sr and Nd isotopic composition Papadopoulou (2003)

Evros volcanics

Sample	Type	Rb	Sr	$^{87}Rb/^{86}Sr$	$^{87}Sr/^{86}Sr$	$^{87}Sr/^{86}Sr_i$	Sm	Nd	$^{147}Sm/^{144}Nd$	$^{143}Nd/^{144}Nd$	$^{143}Nd/^{144}Nd_i$	$^{208}Pb/^{204}Pb$	$^{207}Pb/^{204}Pb$	$^{206}Pb/^{204}Pb$
AK-1	Andesite (Bt-Hbl)	88	317.59	0.802	0.70863	0.70829	3.21	16.94	0.115	0.51238	0.51236			
FT-2	Andesite (Bt-Hbl)	92	375.42	0.709	0.70802	0.70772	4.50	22.54	0.121	0.51238	0.51235	38.187	15.607	18.228
MSR-13	Andesite (Bt-Hbl)											38.800	15.664	18.751
CEP-16	Andesite (Px)	80	433.71	0.534	0.70602	0.70579	3.74	16.94	0.134	0.51262	0.51259	38.725	15.636	18.743
MAA-1	Andesite (Px)	77	442.17	0.504	0.70605	0.70584	4.24	16.94	0.151	0.51261	0.51258	38.802	15.659	18.768
AK-7	Andesite (Px)	76.5	401.70	0.551	0.70675	0.70652	4.08	19.5	0.127	0.51248	0.51245	38.905	15.697	18.821
FG-101 (20Ma)	Andesite (Px)	166.3	465.60	1.033	0.70661	0.70631	5.07	23.9	0.128	0.51250	0.51248	38.845	15.664	18.764
MES-3	Basaltic andesite	43	355.07	0.350	0.70592	0.70577	3.40	13.03	0.158	0.51263	0.51260	38.794	15.665	18.740
FKR-40	Basaltic andesite	41.39	466.20	0.257	0.70720	0.70709	3.18	13.9	0.138	0.51246	0.51243	38.845	15.683	18.718
FLE-3 (20Ma)	Basaltic andesite	71.9	353.90	0.588	0.70790	0.70773	3.66	17.3	0.128	0.51243	0.51242	38.805	15.659	18.785
FKP-31	Trachyandesite	123	527.15	0.675	0.70572	0.70543	5.61	26.5	0.128	0.51259	0.51256	38.701	15.652	18.722
FL-12	Trachyandesite	96	308.03	0.902	0.70608	0.70569	3.39	16.0	0.128	0.51256	0.51253	38.460	15.687	18.832
FL-14	Trachyandesite											41.288	16.705	19.898
MAS-20	Trachydacite	209	452.25	1.337	0.70801	0.70744	5.13	27.89	0.111	0.51245	0.51243	38.954	15.672	18.745
MAS-21	Trachydacite											38.962	15.676	18.751
FI-10	Dacite											38.957	15.750	18.963
FLE-1	Dacite											38.509	15.620	18.567
FF-21	Rhyolite											39.261	15.936	18.950
FLK-5	Rhyolite											38.876	15.670	18.826
FLE-2	Rhyolite											38.812	15.691	18.780

Pb Isotopes are from G. Christofides unpublished data

Samothraki volcanics											
Sample	**Type**	**Reference**	**Rb**	**Sr**	**$^{87}Rb/^{86}Sr$**	**$^{87}Sr/^{86}Sr$**	**$^{87}Sr/^{86}Sr_i$**	**Sm**	**Nd**	**$^{143}Nd/^{144}Nd$**	**$^{143}Nd/^{144}Nd_i$**
PSM-2	Old Series	1	12.88	596.70	0.0624	0.705455	0.70543	5.92	31.16	0.512495	0.512472
PSM-3	Old Series	1	95.27	1497.98	0.1840	0.705709	0.70563	4.91	20.41	0.512762	0.512733
MBR-103	Old Series	2	99	757	0.379	0.70514	0.70501	4.02	22.73	0.512705	0.51269
MT-125	Old Series	2	116	485	0.693	0.705459	0.70522	6	29.4	0.512671	0.51265
X-8	Old Series	2	14	861	0.047	0.705089	0.70507	6.73	27.7	0.512717	0.51269
X-9	Old Series	2	14	882	0.046	0.705097	0.70508			0.512754	0.51273
ZP-15	Old Series	2	114	612	0.538	0.705172	0.70503	4.95	24.7	0.512705	0.51269
MK-102	Intermediate Series	2	91	1279	0.205	0.706033	0.70603	7.55	36.5	0.512612	0.51260
MK-107	Intermediate Series	2	122	406	0.871	0.706207	0.70591	6.09	40.71	0.512607	0.51259
MX-110	Intermediate Series	2	143	719	0.575	0.706008	0.70581	5.51	27.7	0.51257	0.51256
LK-10	New Series	2	271	1091	0.718	0.709987	0.70978	9.19	58.5	0.512245	0.51223
MAGP-103	New Series	2	171	833	0.593	0.709615	0.70945	8.71	61.46	0.512241	0.51223
MAGP-110	New Series	2	150	870	0.500	0.709035	0.70890	7.27	45.5	0.512291	0.51228
MAL-105	New Series	2	183	997	0.530	0.709329	0.70918	8.61	58.3	0.512228	0.51222
MAL-110	New Series	2	167	1106	0.437	0.709353	0.70922	7.04	46.2	0.512266	0.51225
MAL-111	New Series	2	160	773	0.598	0.709312	0.70915	5.2	39.3	0.512272	0.51226
MBR-101	New Series	2	172	880	0.563	0.709415	0.70926	5.48	34.4	0.51226	0.51225
MBR-105	New Series	2	155	733	0.611	0.70926	0.70909	6.12	40.74	0.512269	0.51226
MLK-109	New Series	2	175	1530	0.331	0.709353	0.70926	10.51	68.4	0.512273	0.51226
MLK-111	New Series	2	152	1230	0.357	0.70946	0.70936	9.73	70.54	0.512265	0.51228
MT-106	New Series	2	165	791	0.603	0.708987	0.70882	8.94	58.84	0.512207	0.51220
MT-118	New Series	2	162	859	0.545	0.708906	0.70876	8.46	53.3	0.512293	0.51228
MT-123	New Series	2	164	980	0.484	0.708956	0.70881	8.31	61.29	0.512252	0.51224
MT-124	New Series	2	165	939	0.507	0.708973	0.70883	9.96	61.6	0.512303	0.51229
MX-113	New Series	2	169	1005	0.495	0.709426	0.70929	8.68	56.8	0.512196	0.51218
X-13	New Series	2	161	602	0.773	0.709479	0.70927	5.97	37.2	0.512236	0.51222

*References: 1 Sr and Nd isotopic composition present study; 2 Sr and Nd isotopic composition Vlchou et al. (2006)

CROV													
Sample	**Type**	**Rb**	**Sr**	**$^{87}Rb/^{86}Sr$**	**$^{87}Sr/^{86}Sr$**	**2σ error**	**$^{87}Sr/^{86}Sr_i$**	**Sm**	**Nd**	**$^{147}Sm/^{144}Nd$**	**$^{143}Nd/^{144}Nd$**	**2σ error**	**$^{143}Nd/^{144}Nd_i$**
KA-23	B	78.4	595.1	0.381	0.70665	0.000006	0.70649	5.95	29.1	0.124	0.51249	0.000004	0.51246
KA-97	B	105.7	585.7	0.522	0.70681	0.000004	0.70659	5.69	26.8	0.128	0.51247	0.000004	0.51245
PKL-3	BAT	149.42	542.13	0.797	0.70710	0.000003	0.70676	6.53	33.25	0.119	0.51246	0.000004	0.51244
TS-66	BAT	71.5	659	0.314	0.70761	0.000004	0.70748	6.17	35.2	0.106	0.51248	0.000004	0.51246
TS-67	BAT	71.5	664.9	0.311	0.70655	0.000004	0.70642	5.22	24.7	0.128	0.51246	0.000004	0.51244
PDP-2	RD	377.44	187.32	5.831	0.71021	0.000003	0.70772	4.35	24.16	0.109	0.51233	0.000004	0.51231
PKL-9	RD	292.85	185.56	4.567	0.71044	0.000004	0.70849	5.50	28.18	0.118	0.51233	0.000003	0.51231

This research has been co-financed by the European Union (European Social Fund – ESF) and Greek national funds through the Operational Program "Education and Lifelong Learning" of the National Strategic Reference Framework (NSRF) - Research Funding Program: Heracleitus II. Investing in knowledge society through the European Social Fund.